The Cenozoic evolution of the strike-slip Ecemiş Fault Zone and its implications for the mechanism of tectonic escape in Anatolia

Noah Jaffey

Thesis submitted for the degree of Doctor of Philosophy

University of Edinburgh

2001

This thesis is entirely my own work, except where indicated otherwise.

Noah Jaffey

Abstract

The mechanism by which crustal extrusion, or 'tectonic escape' functions remains poorly understood. Central Anatolia provides an example of extrusion where the kinematics of 'escape'-related strike-slip faults can be well-constrained. This study focuses on the Ecemiş Fault Zone, one of the main strike-slip fault systems involved in the Cenozoic westward extrusion of Anatolia. This study concentrates on the structure, sedimentology, geomorphology and subsidence history of the EFZ, to constrain the timing and offset on this fault zone, and thereby build a more comprehensive model of extrusion in the context of the regional geology.

Sedimentological data from Lutetian (Mid-Eocene) outcrops indicate that significant strike-slip occurred on the EFZ since the Mid-Eocene. Palaeocurrent and facies data establish that an inward-draining depocentre existed in the central EFZ during Late Oligocene – Early Miocene time, contemporaneously with regional crustal extension and unroofing of the nearby Niğde Core Complex. Sedimentological studies show that the present-day fault scarps of the EFZ were established during the latest Miocene – Early Pliocene, synchronous with the initiation of Anatolian extrusion. Subsidence curves indicate that the Late Oligocene – Early Miocene was a period of rapid subsidence rates in the Adana region (north of the Taurus Mountains) and that subsidence was more rapid in the EFZ area than in surrounding Cenozoic basins during this period. Rapid subsidence in the EFZ may have been associated with the formation of a pull-apart basin in the location of the EFZ. Slikenline data analysis indicate that the EFZ was undergoing sinistral trans-tension by at least Mid-Miocene time, and that this changed to dominantly E-W extension during the Quaternary. Slikenline data from the Çamardi area (northern EFZ) indicate that limited sinistral strike-slip has also occurred during the Quaternary, focused on a N-S striking small graben. Deformation patterns within the EFZ suggest that sinistral strike-slip faulting was active during the Middle Miocene. New $^{40}Ar/^{39}Ar$ radiometric dating in the Erciyes Basin (northern continuation of the EFZ) confirms that the fault zone was active during the Messinian and early Pleistocene. River and stream offsets suggest that at least 2.4 km of sinistral offset has occurred on the EFZ during the Quaternary. Structural and stratigraphic piercing points have previously been used to measure the total sinistral offset on the EFZ. These have been re-assessed and found to be inaccurate. The total offset on the EFZ is now constrained by a new piercing point, a Late Eocene north-vergent fold and thrust belt, which has been offset by 60±5 km across the EFZ.

The Ecemiş Fault Zone has a total offset comparable with that of the North Anatolian Fault Zone and larger than the East Anatolian Fault (both initiated during the Pliocene). It was active at least 7Ma prior to the start of extrusion along the two above faults. During its early history (Mid-Miocene), the EFZ accommodated variable N-S shortening between the eastern and western Taurides, related to regional collision. During extrusion (Pliocene and Quaternary) the EFZ changed from accommodating sinistral trans-tension, to accommodating dominantly E-W extension.

Acknowledgements

Firstly, my thanks go to Alastair Robertson, for his endless patience, encouragement and enthusiasm. Alastair is the best supervisor any young academic could wish for.

The 'Tethys Tag Team' have been a constant source of help, amusement and camaraderie during my time in Edinburgh. Thanks to Matt C., Theo and Matt "Hard-n-fast" – I'll miss those Turkish road adventures guys!

Many thanks to those who've kept me sane through the long field months. To Simon Hinchliffe, Hasan and Cavid Şafak (and their idyllic B&B), to Mehmet and the dogs for the company and the Pozanti boys – always disappointed that I never brought them their English wives.

Thanks go to Ulvican Ünlügenç for his kind help with logistics and to Hasan Çetin, Ali Koçyiğit and Cengiz Yetiş for their contributions to my understanding of Turkish geology. Also, thanks to Tobore Orife (Cardiff University) for spending so much time and effort helping me with the palaeostress program.

My academic development would have been sadly deficient without the many superb fieldtrips which I've had the opportunity to demonstrate on. Thanks go to Stuart Haszeldine, Hugh Sinclair and Simon Harley for their inspirational trips – I'll miss them. Others deserving of thanks are Rachel Flecker – for getting me enthused about Turkish geology in the first place, The Lost Sheep Mountaineering Club – for the many glorious mountain days and bothy nights, to Zoe Shipton for her boundless enthusiasm for clubbing, and to Bärbel Traub for brightening up my final months in Edinburgh.

Finally, thanks to my parents, Jane and Joel – for your constant support and care. I'll repay you by doing the same for my children one day.

Contents

List of Figures

Chapter 2

Chapter 3

Chapter 4

Chapter 5

Chapter 6

Chapter 7

Chapter 8

Chapter 9

Chapter 10

Chapter 11

Chapter 12

1 Introduction

1.1 Rationale

The relative importance of (i) crustal thickening, versus (ii) crustal extrusion in the accommodation of convergence between colliding continents is still widely debated (Searle *et al.* 1996, Tapponnier *et al.* 1990). In the India–Asia collision example attempts have been made to quantify the amounts of crustal shortening and the amounts of offset on extrusion-related strike-slip faults. Offsets and timing of faulting have been calculated for several of the important extrusion-related faults in the India-Asia collision zone (Searle 1996, Wang et al. 1998, Burchfiel et al. 1991). However, due to the relative inaccessibility of the terrain many extrusion-related faults remain poorly understood (e.g. Altyn Tagh fault) and a holistic understanding of how extrusion has developed has not yet been achieved.

In an attempt to better understand and quantify the process of extrusion during continental collision, the example of central Turkey (Anatolia) is used. Although on a much smaller scale than the India-Asia collision, the collision between Arabia (the northern peninsula of Gondwana during the Mesozoic) and Eurasia shows many similar features: (i) a north-moving indentor, (ii) the closure of an E-W trending Tethyan ocean, (iii) the accommodation of convergence by crustal thickening and by strike-slip faulting and (iv) the development of collisional and post-collisional processes over a similar timescale.

Previous work on extrusion within Turkey has focused largely on the dextral North Anatolian Fault and sinistral East Anatolian Fault. Whilst some work has been done on the offsets and timing of other strike-slip faults within Anatolia (Yetiş 1984, Koçyiğit & Beyhan 1998, Westaway *in press*) their offsets and timing remain controversial,

especially that of the Ecemiş Fault Zone, a NNE-SSW striking sinistral fault zone in central Anatolia. Through a multi-disciplinary examination of this fault zone and comparison with other significant faults in the region I aim to build a better understanding of how extrusion has developed during the Cenozoic in Turkey.

1.2 Aims

With the objective of better understanding the process and mechanism of extrusion in Turkey this thesis aims to answer the following questions:

- Is the Ecemiş Fault Zone a significant extrusion-related strike-slip fault?
- How has this fault zone evolved during the Cenozoic?
- What implications does this have to the process of tectonic escape in Turkey?

1.3 New contributions of this project

This thesis aims to utilise the following new lines of evidence from the Ecemiş Fault Zone (EFZ) and surrounding areas to fulfil the above aims:

- New palaeocurrent data and interpretation.
- New provenance work on EFZ sediments, to constrain timing of uplift and exhumation.
- The collection and interpretation of new structural data from the EFZ and surrounding rock units.
- New Slickenline data and interpretation.
- New determinations of palaeostress.
- New geochronology to better constrain the timing of faulting.
- The evaluation of published piercing points.

- New piercing points.
- A new proposed mechanism for the development of extrusion in Turkey.

Piercing points are defined as originally uninterrupted structural or stratigraphic entities which have been offset laterally by a strike-slip fault. These may include: other faults, dykes, localised igneous intrusions and extrusions and sedimentary features amongst other things. An agreement in the offset of several independent piercing points is usually necessary in order to unambiguously determine the lateral offset on a strike slip fault, as in the case of the Dead Sea Transform fault (Quennell, 1959).

1.4 Previous Work

A brief review of existing literature related to the Ecemiş Fault Zone is given here in chronological order. More detailed reference to previous work is made, where relevant, within each chapter.

A simplistic appreciation of the EFZ and surrounding structures can be gained from the 1:500,000 geological map of the Adana region (Fig. 2.4, Ternek 1962), which shows a strip of Cenozoic sediment following the course of the EFZ and the apparent offset of units in the adjacent Aladağ and Bolkardağ. The first detailed study of the stratigraphy and structure of the northern EFZ was carried out by Yetiş (1978, 1984), who defined six stratigraphic units within the Cenozoic (Fig. 3.2). He constrained the timing of activity on the fault zone as post-Palaeocene and pre-Lutetian (Mid Eocene), based on two adjacent Lutetian outcrops. He also constrained the total offset at 80±10km based on the offset of the boundary between two Mesozoic limestone units.

A major regional mapping project in the eastern Taurus Mountains undertaken by M.T.A. (Turkish Geological Survey) during the 1970s and 1980s resulted in a vast improvement in the understanding of units surrounding the EFZ. The geology of the

Aladağ (mountains east of the EFZ) was studied by Tekeli *et al.* (1984), who identified several NE-SW striking thrust faults which are truncated by the EFZ. The geology of the Bolkardağ (mountains west of the EFZ) was studied by Demirtaşli *et al.* (1984) who identified NE-SW striking (north-directed) thrust faults along the northern margin of the Bolkardağ, truncated by the EFZ.

Several local mapping and sedimentological projects have helped to better define the structure and stratigraphy of the EFZ during the 1990s. The Çamardi area was mapped by Kuscu (1992, Fig. 2.4 for location). A detailed facies study of the Oligo-Miocene sediments of the EFZ was carried out by Karedinizli & Kazanci (1993), who concluded that these sediments prograded from west to east and that their deposition was not controlled by the present-day faults of the EFZ. A useful structural and stratigraphic study of the Sulucaova-Kovali area (northernmost EFZ) was undertaken by Beyhan (1994). This study used aerial photographs to define fault outcrops in the EFZ for the first time, concluding that the EFZ is a complex braided strike-slip system in its northernmost extremity. The PhD thesis of Uçar (1997) resulted in the comprehensive lithological mapping of the southern EFZ (Kamisli – Camalan) and the definition of simple structures in the area. He concluded that deposition of Oligo-Miocene sediments was originally confined to within the EFZ.

Research groups from American universities began working in the area during the late 1990s when the geology, P-T-t and exhumation history of the Niğde Massif (a metamorphic body adjacent to the EFZ) was explored by Whitney & Dilek (1997, 1998). They found that major exhumation had occurred during the Oligocene and Miocene, affecting the evolution of the EFZ and interpreted the Niğde Massif as a core complex. Their most recent works re-interpret the Bolkar frontal thrust (Demirtaşli 1984) as a zone of normal faulting (Dilek & Whitney *in press*). Other American workers are currently studying the palaeoseismic record of the most recent faults within

the EFZ near Çamardi. They are using trenching and cosmogenic isotope exposure age dating of alluvial fan material (Mayer 1999) to date the last activity on the EFZ.

During the course of this PhD a major new study on the structure, geomorphology and seismicity of the EFZ has been published (Koçyiğit & Beyhan 1998). This work describes the EFZ as part of a larger Central Anatolian Fault Zone (CAFZ) which extends from Düzyayla, on the North Anatolian Fault in the north to Anamur on the Mediterranean coast in the south. They use aerial photographs extensively to interpret the location of faults. They constrain the total sinistral offset on the EFZ as 74km based on the offset of a south-directed thrust fault involving Permian over Triassic units. These findings have since been criticised by Westaway (1999) who questioned the accuracy of their seismic data and pointed out that their new piercing points contradict previous interpretations without referring to them. Westaway (1999) also criticised their use of aerial photographs to map fault segments without any field data to justify their interpretation. Koçyiğit & Beyhan (1999) replied, supplying geomorphological maps of the Çamardi area to back up their original claims that the EFZ is an active fault zone.

To date, the total offset and timing of activity on the EFZ remains controversial despite the debate described above. This is principally due to the lack of modern slickenline, palaeocurrent and GPS data on the fault zone and the lack of several convincing piercing points which agree. Previous workers, to date, have not attempted to integrate an understanding of the EFZ with the complete geological history of the area.

1.5 Fieldwork Methodology

This research uses structural, sedimentological, geomorphological and geochronological data, collected over 7 months of fieldwork in south-central Turkey. The main objectives of this data collection were:

1) A thorough description of lithological units within the EFZ and correlative units outwith the fault zone.
2) A three dimensional description of the structure of the EFZ.
3) The calculation of timing of activity and offset on the fault zone

The first objective was approached by measuring sedimentary logs in recognised type localities for each stratigraphic unit. In order to assess lateral facies changes and thickness changes, logs were taken along the fault zone (from N to S) and across it (from E to W) as well as in the adjacent Cenozoic Ulukisla and Karsanti Basins (Fig. 2.4 for location), where correlative sediments outcrop. Palaeocurrent data were taken systematically whilst logging. A total of 42 sedimentary logs were measured during the course of this study.

To fulfil the second objective I took a multi-disciplinary approach. In order to assess the kinematics of the fault zone through time, Slickenline and fault orientation data were collected whilst logging, and from fault scarps bounding the EFZ. To assess deformation associated with faulting during the Cenozoic, bedding orientation and fold vergence data were collected in fold belts within the EFZ and in the adjacent Aladağ and Bolkardağ. The mapping of alluvial fan structures and surfaces also proved very useful in defining the detailed geometry of the EFZ using both aerial photograph tracings (from the Turkish Geological Survey) and field mapping.

The final objective was tackled using two techniques. The timing of activity on the EFZ has been difficult to calculate in the past due to poor stratigraphic control on the age of the sediments and a lack of clear overlying relationships at fault exposures. In the northern EFZ, however, the fault zone passes through a volcanic province (the Central Anatolian Volcanic Province) and good overlying relationships can be observed, constraining the timing of faulting in this area. This work involved the collection and Ar^{40}/Ar^{39} radiometric dating of tuff and lava samples. The total sinistral offset on the

EFZ was calculated by mapping and collecting structural data from several possible piercing points to the E and W of the EFZ, and by critically assessing their viability as piercing points.

1.6 Thesis Structure

This thesis is divided into thirteen chapters. Following this introductory chapter (**Chapter 1**) the background to the theory of extrusion and the process of extrusion in Turkey is discussed in **Chapter 2**. **Chapter 3** deals with the published and new evidence for the stratigraphic units of the EFZ, establishing a formal stratigraphy which is used in the thesis. Following this, **Chapter 4** describes the sedimentological characteristics of each unit within the EFZ, firstly presenting, and then interpreting the different facies present using established models. Type sections of correlative units outside the EFZ are also described in order to assess spatial variation within each unit. **Chapter 5** then goes on to use simplified logs to construct subsidence profiles for the EFZ and adjacent Cenozoic basins. These subsidence curves are used to assess the timing of the creation of accommodation space and the implications for the timing of faulting are discussed. In order to better constrain the timing and extent of uplift and exhumation adjacent to the EFZ the provenance of the EFZ sediments is studied in **Chapter 6**. Conglomerate pebble, sand and mud grade material are quantitatively analysed to define sediment sources throughout the Cenozoic and the implications for fault development.

The structure of the EFZ is described and analysed in **Chapter 7**. This chapter deals with: (i) deformation both within and immediately outwith the EFZ, (ii) the analysis of Slickenline and fault orientation data to constrain the kinematics of faulting through

time, (iii) the calculation of palaeostress at key exposures and (iv) the assessment of the modern stress regime. Some of the most useful data with regard to identifying recent activity of the EFZ comes from the description of geomorphologic features along the fault zone. This is investigated in **Chapter 8**, where aerial photograph interpretation and mapping techniques are used to constrain the geometry and recent activity on the EFZ. **Chapter 9** attempts to better constrain the timing of faulting on the EFZ within the Erciyes Basin (Central Anatolian Volcanic Province, Fig. 2.4) using the $^{40}Ar/^{39}Ar$ radiometric dating of tuffs and lavas associated with faulting.

Chapter 10 attempts to draw together several lines of evidence to establish the total offset on the EFZ, critically assessing published piercing points and proposing new piercing points. **Chapter 11** then introduces vital geophysical evidence regarding the historical seismicity of the EFZ, local and regional published palaeomagnetic studies and recent results from GPS surveys which show relative crustal motion over a six year period. These diverse results are drawn together in a Discussion (**Chapter 12**) where the EFZ is compared with other significant strike-slip faults in the region and possible mechanisms for crustal extrusion in Turkey during the Cenozoic are assessed. Final conclusions are made in **Chapter 13**.

2 Regional Geological Setting

2.1 The Mediterranean and Tethys

The Eastern Mediterranean area forms part of the Alpine-Himalaya tectonic belt (Fig. 2.1). This broadly convergent tectonic regime was formed by the convergence of Africa (Gondwana) and Eurasia.

In Permo-Triassic times a westward-narrowing ocean basin, 'Palaeotethys' separated the two continents of Pangea (Şengör *et al.* 1984, Robertson & Dixon 1984). Closure of this ocean basin was accompanied by the opening of a series of small ocean basins in its wake, together forming the Mesozoic 'Neotethys' ocean (Fig. 2.2). Acceleration of north-south convergence between Gondwana and Eurasia during mid Cretaceous times (Smith & Spray 1984, Dewey *et al.* 1989) led to Neotethyan units in the Eastern Mediterranean becoming amalgamated with Eurasia, accompanied by the rotation of several microcontinental blocks (e.g. the Troodos microplate).

During Triassic times, a micro-continental block known as the Tauride block (Robertson & Dixon 1984) rifted away from the northern margin of Gondwana. The majority of this block was composed of passive margin material, formed by the opening of a northern Neotethyan ocean in Triassic times (Collins & Robertson 1998). Rapid convergence between Africa and Eurasia took place during the Cretaceous (Livermore & Smith 1984) and a north-dipping, intra-oceanic subduction zone developed between the Tauride block and the Eurasian margin (Lytwyn & Casey 1995), in a narrowing oceanic basin known as the 'Inner Tauride Ocean' (Görür *et al.* 1984, Şengör & Yilmaz 1981). The southward obduction of a series of ophiolites over the Tauride block occurred during the Latest Cretaceous (Lytwyn & Casey 1995, Parlak & Delaloye 1999) and was followed by the closure of the Inner Tauride Ocean during the Late Eocene.

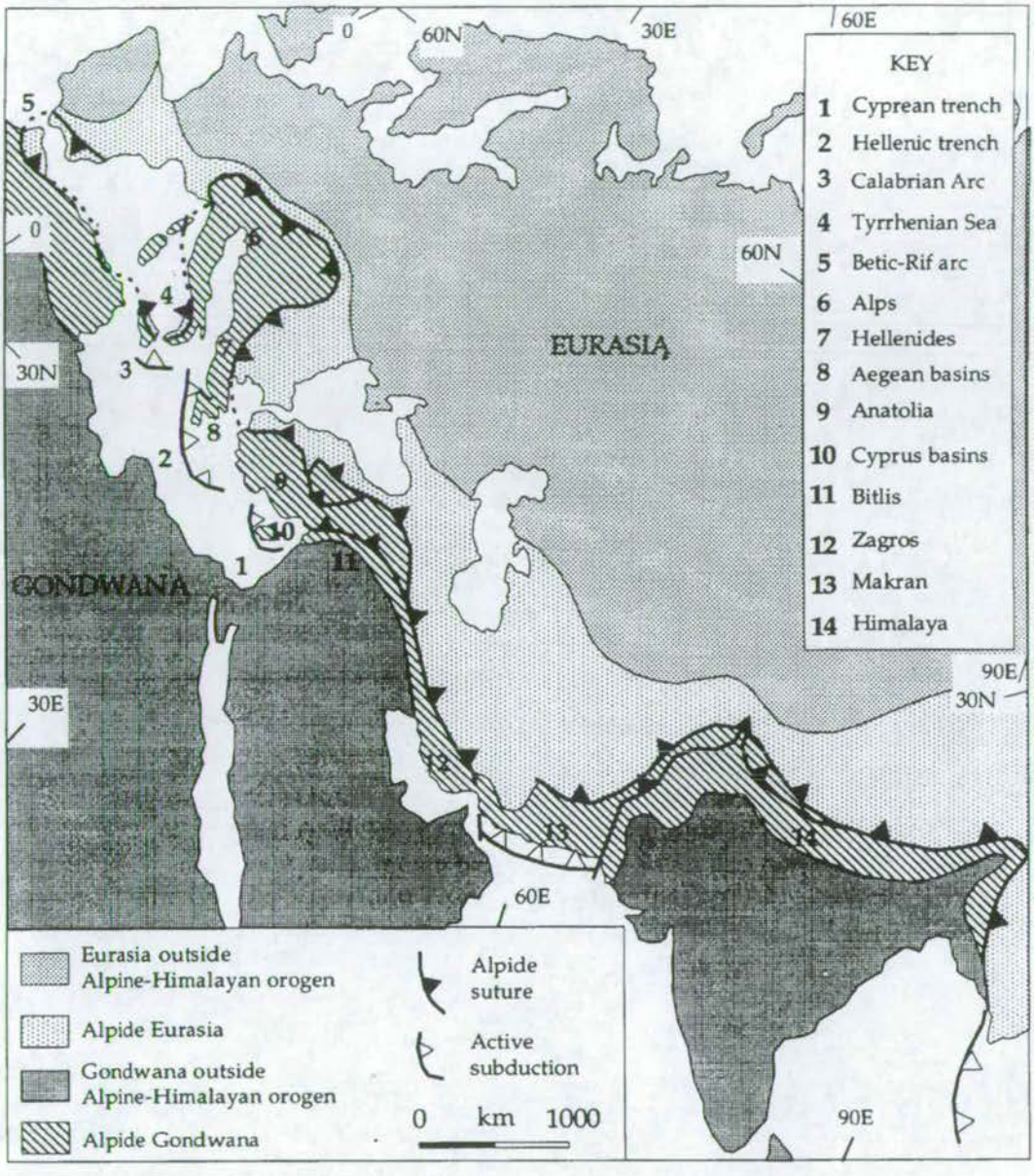

Figure 2.1 Tectonic map of the Himalayan-Alpine orogenic belt (after Payne 1989).

Continent-continent collision between the Arabian foreland and the Eurasian margin did not take place until the Middle Miocene (Dewey *et al.* 1986, Robertson 2000), when the Arabian foreland began to indent into the Eurasian margin. The western margin of the

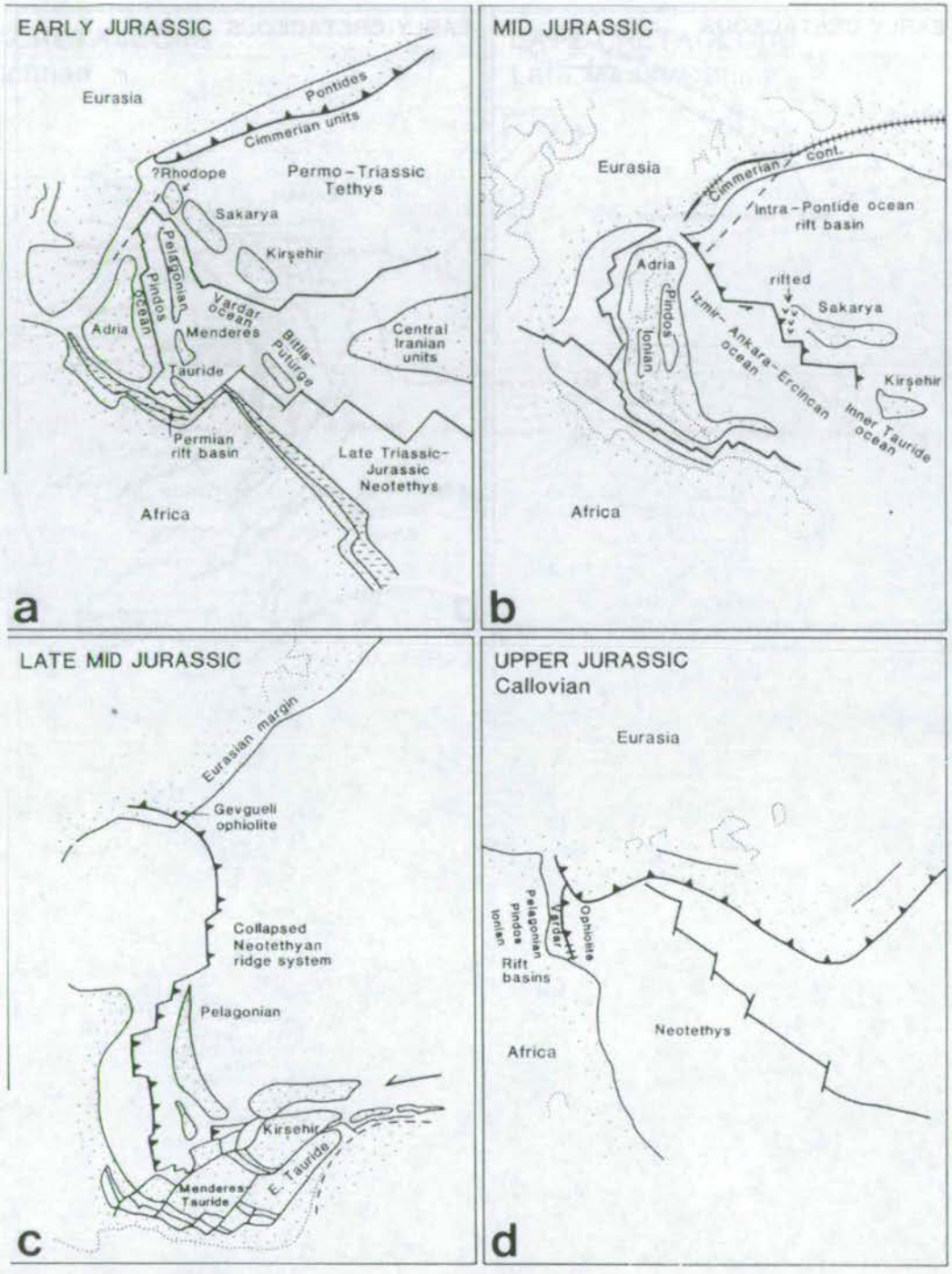

Figure 2.2 Alternative reconstructions of the Eastern Mediterranean Tethys Ocean in the Jurassic. **(a)** Alternative model of Robertson et al. 1991, **(b)** Model 3 - Sengör et al. 1984, **(c)** Model 1 - Robertson & Dixon 1984, **(d)** Model 2a - Dercourt et al. 1986. After Robertson *et al.* 1996.

Arabian block separated a pre-collisional setting in the easternmost Mediterranean from a collisional setting in southeastern Turkey (Robertson 2000). The region underwent crustal thickening, continental deformation and uplift during the Early Oligocene, causing a region-wide angular unconformity. The post collisional (Neo-tectonic) history of the study area is presented in Section 2.5.

2.2 *Present-day tectonic setting of the Eastern Mediterranean*

At present the Eastern Mediterranean region incorporates several diverse tectonic regimes (Fig. 2.3). Northeastward subduction of remaining Neotethyan oceanic crust continues along the Hellenic and Cyprus trench systems (Robertson & Grasso 1995). The collision of the Erastothenes seamount with the Cyprus Arc has caused uplift in Cyprus. Maximum uplift occurred during the latest Pliocene – Quaternary, and is presently more reduced (Robertson & Grasso 1995).

The easternmost Mediterranean is characterised by continental collision, which is accommodated by several regionally significant fault zones: (i) the south-vergent Zagros-Bitlis suture zone, (ii) the sinistral Dead Sea Fault Zone, (iii) the sinistral East Anatolian Fault Zone and (iv) the dextral North Anatolian Fault Zone (Fig. 2.3, Robertson 2000). The NAFZ and EAFZ currently accommodate the westward extrusion of Anatolia and their evolution is discussed in section 2.5. Active deformation is controlled by the interaction of the Anatolian block, moving west away from the collision of the Eurasian and Arabian plates, with the African plate which is moving north relative to Eurasia (Oral 1995).

Western Anatolia is currently experiencing N-S extension along several major graben systems, and through the exhumation of core complexes (Purvis 1998). This regime of

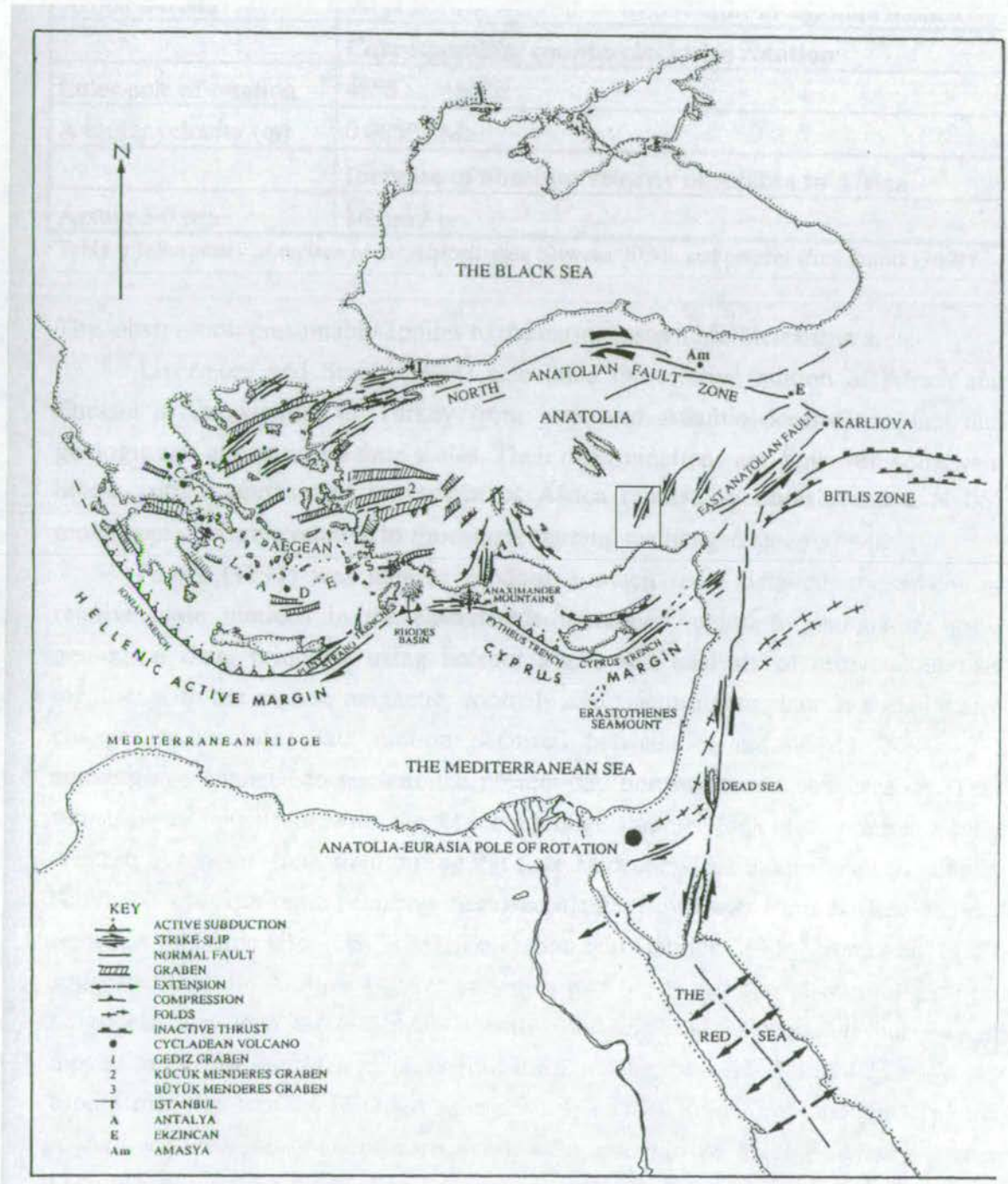

Figure 2.3 Map of the Eastern Mediterranean area showing the principal modern tectonic, or 'Neotectonic' features. After Glover 1996. Boxed area is the Ecemiş fault Zone study area.

extension began during the latest Oligocene – Early Miocene, and preceded the initiation of extrusion. The driving mechanism for N-S extension is currently believed to be a combination of (i) slab roll-back along the Hellenic arc and (ii) post-collisional orogenic collapse (Purvis 1998). The Isparta Angle region accommodated dextral shear between Central Anatolia and the Aegean region during the Late Miocene – Early Pliocene, but this changed to normal offset during the early Quaternary (Glover 1996).

2.3 Geology of south-central Anatolia

The Ecemiş Fault Zone dissects and lies adjacent to several distinct autochthonous and allochthonous geological units. These have been studied by many workers and it is useful to provide a brief description of the characteristics of each, in order to provide a context in which to view the EFZ.

2.3.1 Taurus Mountains

Forming the basement of the 'Tauride block' (see above), the Eastern Taurus mountain chain is divided by the EFZ into the western Bolkardağ and eastern Aladağ (Fig. 2.4b). Both of these units were originally formed during shallow-marine shelf carbonate sedimentation (Late Palaeozoic) on the northern continental margin of Gondwana (Tekeli *et al.* 1984). This passive margin underwent rifting and separation from the Gondwanian continent during the Mid-Triassic and after northward migration collided with the Pontides during the latest Palaeocene – earliest Eocene (Şengör & Yilmaz 1981). During latest Cretaceous both the Bolkardağ and Aladağ were locally tightly to isoclinally folded during the emplacement of overlying ophiolitic bodies, resulting in pervasive south-directed sheet-nappe structures (Tekeli *et al.* 1984). These original South-directed nappes have been subsequently folded in the Aladağ to produce the present structure (Fig. 2.5). The exposed Aladağ comprise Devonian to Cretaceous dolomites and limestones which have been subject to mild (sub-greenschist facies)

Figure 2.4 (a) Regional geological map of central-southern Turkey. (b) Geological map showing detail of the Ecemis Fault

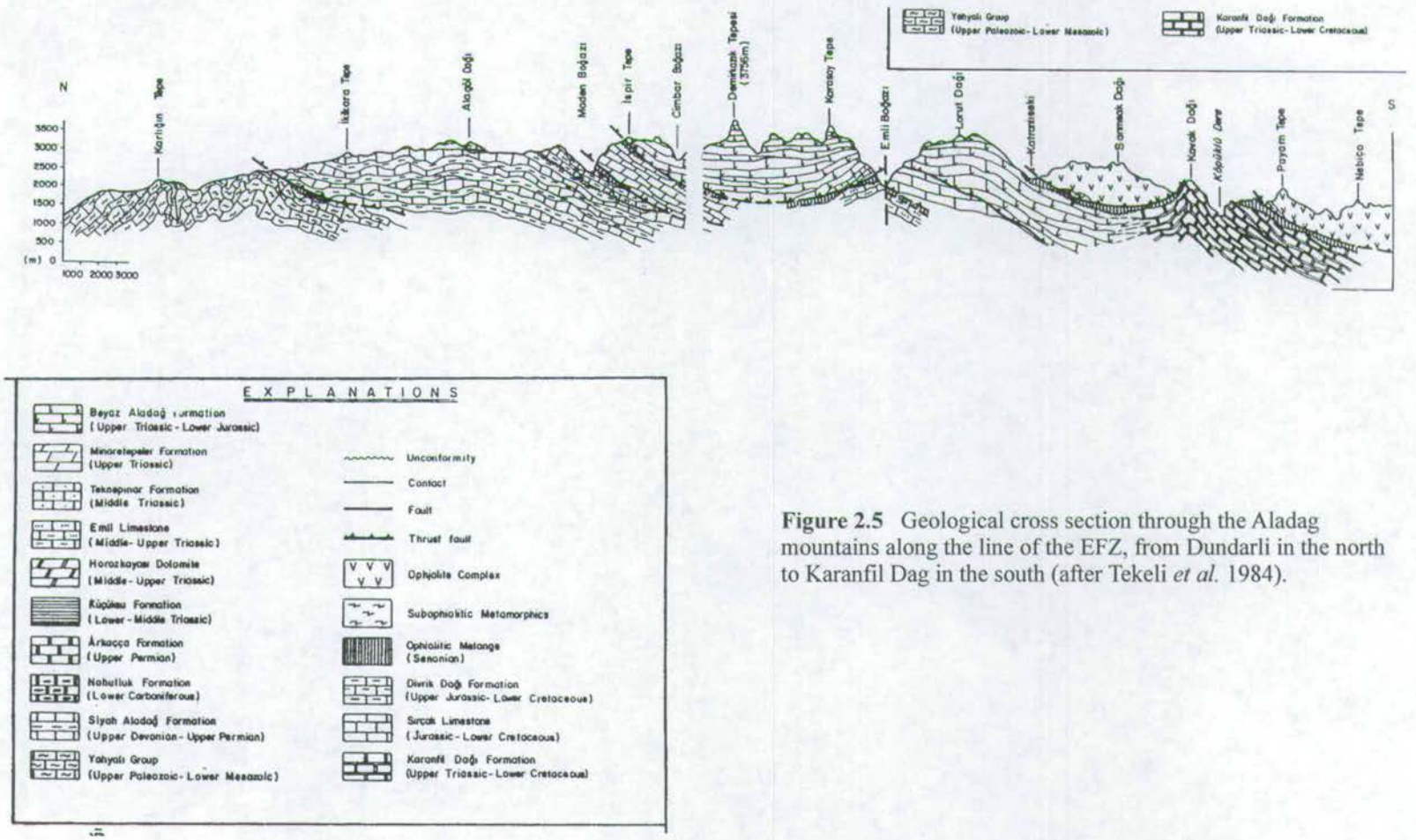

Figure 2.5 Geological cross section through the Aladag mountains along the line of the EFZ, from Dundarli in the north to Karanfil Dag in the south (after Tekeli *et al.* 1984).

burial metamorphism. The Bolkardağ mostly comprise a carbonate protolith with minor intercalations of pelitic and psammitic rocks (Demirtaşli *et al.* 1984). These were subject to much higher, lower amphibolite metamorphic facies. The reason for different metamorphic regimes across the EFZ is not well understood.

2.3.2 Niğde Massif

20-30km north of the Bolkardağ lies a roughly circular outcrop of high grade mid-crustal gneisses, marbles, quartzites and schists surrounded by Early Cenozoic sediments, named the Niğde Massif (Fig. 2.6 & 2.4b, Yetiş 1978, Göncüoğlu 1988). This body has been interpreted as a metamorphic core complex by Whitney & Dilek (1997). Originally a zone of thermally weakened continental crust, these rocks underwent burial to 5-6kbars (>700^{0}C) during crustal thickening (Whitney & Dilek 1998). P-T-t calculations indicate that this was followed by rapid exhumation and granite intrusion during the Early Miocene. Field mapping during this study has shown that the complex has a normal-faulted contact with pre-Miocene rocks, but an onlapping relationship with Miocene and younger rocks. The interpretation of this body as a core complex is still disputed by some Turkish workers (pers. com. I. Kuscu, M.C. Göncüoğlu 1998). These workers cite the presence of high grade metamorphic clasts from the Niğde Massif in overlying Lutetian (Mid-Eocene) sediments, as evidence for detachment faulting during the Eocene (rather than Oligo-Miocene, as proposed by Whitney & Dilek 1997). I. Kuscu (pers. com. 1998) also points out that the Niğde Massif has undergone a relatively small amount of unroofing compared to the Menderes Massif, in western Turkey (composed mainly of augen gneisses, Şengör *et al.* 1984b), thus he argues that the term 'core complex' is inaccurate.

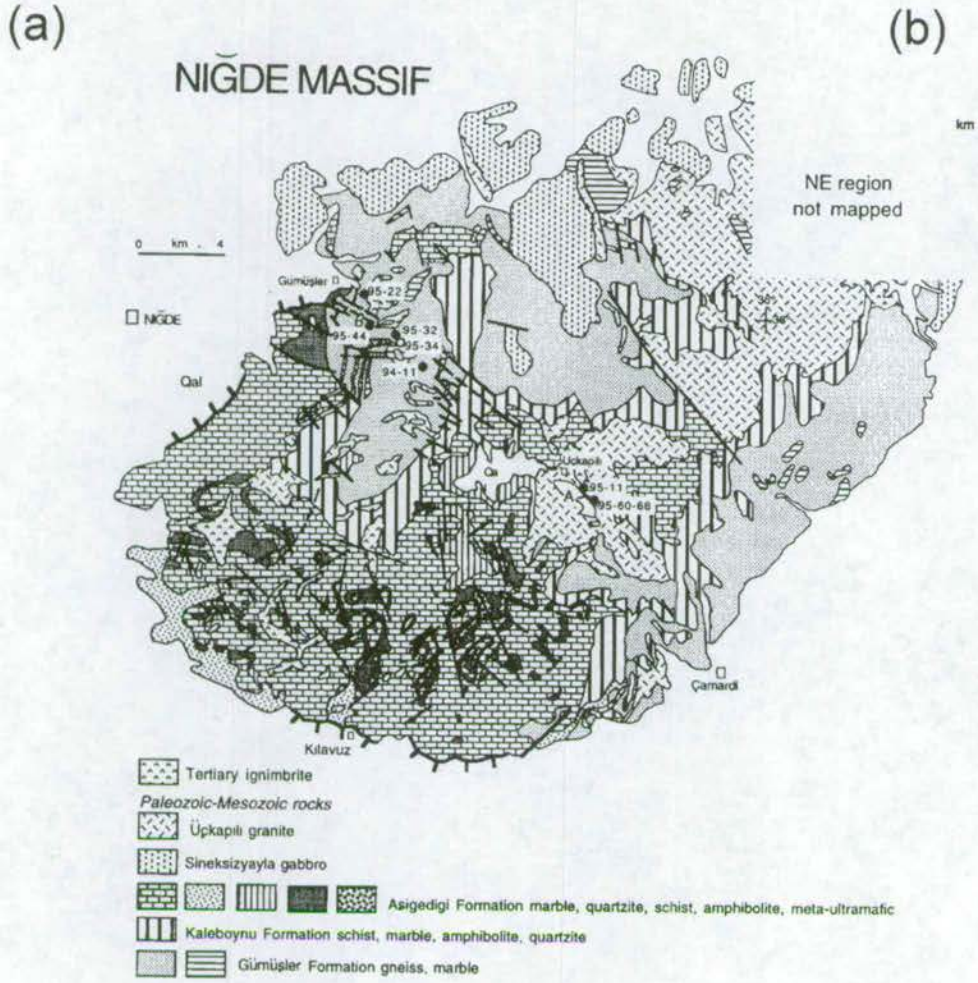

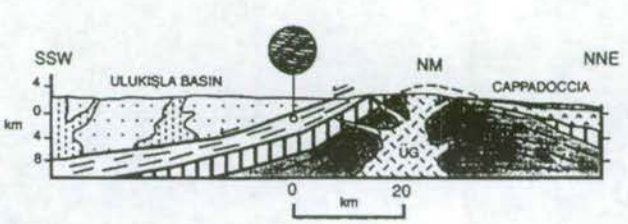

Figure 2.6 (a) Geological map of the Nigde Massif (Fig. 2.4b for location), after Whitney & Dilek 1998. Thick barbed line indicates mapped detachment fault. (b) Generalised geological cross section across the Nigde Massif and vicinity (no vertical exaggeration), after Whitney & Dilek 1997. Profile is parallel to stretching lineation in the massif.

2.3.3 Ophiolites

Several ophiolitic bodies are tectonically associated with the Tauride units in the EFZ area. These include the Pozanti-Karsanti (or Aladağ) ophiolite, which tectonically overlies the Aladağ, the Mersin ophiolite which lies directly to the south of the Bolkardağ, the Ali-Hoca ophiolite which has a faulted contact with the northern margin of the Bolkardağ and the Kiziltepe ophiolite which tectonically overlies the Bolkardağ (Fig. 2.4b). These ophiolitic bodies all tectonically overlie the Mesozoic Tauride platform carbonates and are commonly underlain by a Cenomanian melange (Dilek *et al.* 1999). These ophiolites mainly consist of tectonised mantle rocks, mafic-ultramafic cumulates and gabbros, and commonly lack sheeted dyke complexes and extrusive rocks (Dilek *et al.* 1999). Obduction of these ophiolites is believed to have begun during the Cenomanian (Mid Cretaceous, Parlak & Delaloye 1999) and to be completed by latest Cretaceous (~65Ma, Lytwyn & Casey 1995, Tekeli *et al.* 1984). The Pozanti-Karsanti, Alihoca and Kiziltepe ophiolites are believed to have originated from an 'Inner Tauride Ocean, between the Tauride platform and the Central Anatolian basement (Fig. 2.7, Görür *et al.* 1984). Obduction and emplacement trajectory was mainly from north to south (Lytwyn & Casey 1995, Tekeli *et al.* 1984), and was associated with the closure of this 'Inner Tauride Ocean' (Dilek *et al.* 1999). However, sub-ophiolitic fold vergence and thrust faults below the Mersin Ophiolite (south of the Taurus Mountains, Fig. 2.4) indicate that this ophiolitic body was emplaced from the SE towards the NW (Parlak *et al.* 1996).

2.3.4 Central Anatolian Volcanic Province (CAVP)

This volcanic region (Fig. 2.4a) represents Early Miocene to Quaternary volcanism related to the continental collision between the Afro-Arabian and Eurasian plates (Pasquare *et al.* 1988, Chapter 9). Volcanism is mostly of a calc-alkaline character and is considered to be divided into three main phases: (i) initial andesitic effusive activity

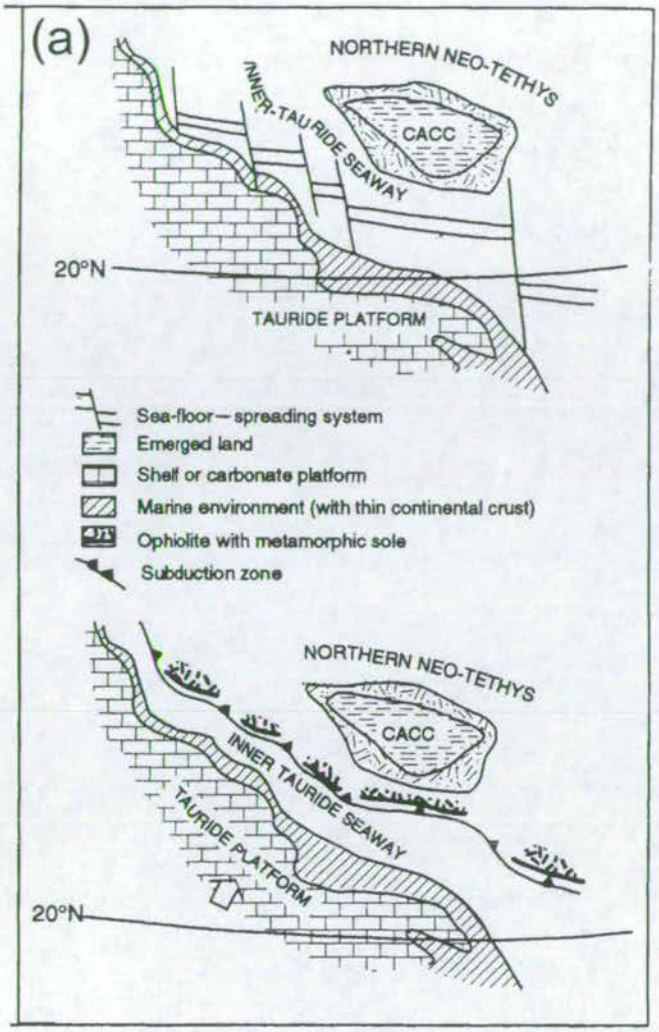

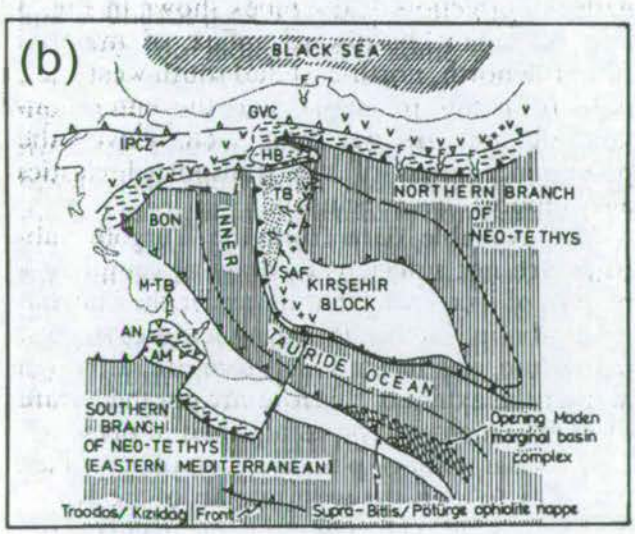

Figure 2.7 Two representations of the Inner Tauride Ocean: **(a)** The conversion of a sea-floor-spreading system into an active margin setting within a narrow Neotethyan seaway, following the onset of northward convergence of Africa-Arabia (convergence direction marked by arrow) in early Late Cretaceous time (after Dilek *et al.* 1999). CACC = Central Anatolian Crystalline Complex (Kirsehir Massif). **(b)** Palaeotectonic map of the Eastern Mediterranean during the Palaeocene, after Görür *et al.* 1984.

(Middle Miocene), (ii) the emplacement of a thick ignimbritic sequence (Mid - Late Miocene) and (iii) the development of andesitic-basaltic stratovolcanoes (Pliocene and Quaternary, Innocenti *et al.* 1975). It was pointed out that volcanic centres are located at the intersection of major faults with orientations similar to the EFZ and to the Tüzgölu faults (Toprak & Göncüoğlu 1993). The Erciyes (Sultansuz) Basin is a 50km long, 25km wide depression between Yayhali and Kayseri (Fig. 2.4a) which contains the Quaternary Erciyes stratovolcano (Innocenti 1975). This basin has recently be interpreted as a pull-apart basin associated with a releasing bend in the Central Anatolian Fault Zone (the northern continuation of the EFZ, Koçyiğit & Beyhan 1998, 1999).

2.3.5 Ulukisla Basin

A thick succession of Early Cenozoic sediments and volcanic rocks outcrops between the northern margin of the Bolkardağ and the Niğde Massif (Fig. 2.4b). These include basal submarine conglomerates, thick successions of turbidites and abyssal muds, submarine and sub-aerial extrusive volcanics, shallow marine shelf limestones and evaporites (Demirtaşli *et al.* 1984). These have been interpreted as the products of sedimentation and volcanism within a closing 'Inner Tauride Ocean' (Oktay 1982), which existed between the Bolkardağ and Kirsehir Massif during the Early Cenozoic (Fig. 2.7). Emergence and sub-aerial deposition occurred during the Oligocene and Miocene, and is now preserved in the Aktoprak Basin (Fig. 2.4b). Oligocene and Miocene subsidence in this area is possibly associated with the synchronous exhumation of the nearby Niğde Massif (Dilek & Whitney *in press*). The evolution of this area is currently the subject of a PhD study by Matthew Clark (Edinburgh University).

2.3.6 Karsanti Basin

This is an isolated intermontane basin located adjacent to, and NW of the Adana Basin (Fig. 2.4a). The basin is interpreted as being a precursor to the Adana Basin (Ünlugenç *et al.* 1993). The sediments of the Karsanti Basin are dated as Oligocene and are judged to be time-equivalents of Oligocene rocks within the EFZ and Ulukisla Basin (Chapter 3).

2.3.7 Adana Basin

One of the major Neogene basins of the Taurus belt, this basin contains up to $6000m^3$ of sediment, deposited from Burdigalian (Early Miocene) to recent (Fig. 2.4b, Yalcin & Görür 1984). It probably initially evolved as a result of intraplate extension associated with displacement around the Africa-Arabia-Anatolia plate triple junction (Aksu *et al.* 1992) but continued as a foreland basin during the Mid - Late Miocene and Pliocene. It is possible that the Taurus mountain range acted as a thrust load during this time (Williams *et al.* 1995). The basin underwent initial subsidence during the Burdigalian and Serravalian. This was followed by shallowing during the Tortonian and complete desiccation and evaporation during the Messinian. Normal marine conditions resumed during the Pliocene but relative sea level fell during the Quaternary, when terrestrial conditions prevailed in the main basin (Yalcin & Görür 1984). The genesis and age of the Adana Basin is similar to that of the Manavgat Basin further to the west (Antalya region). The Manavgat Basin formed as a result of flexural loading by the SE-thrusting Lycian Nappes (Flecker *et al.* 1995) during the Early Miocene.

2.4 The concept of extrusion (tectonic escape)

This section gives a literature review of the concept of extrusion since its conception.

2.4.1 Continental Collision

Continents originally form by the accretion of island arcs (Dewey & Windley 1981) and the obduction of oceanic material. Oceanic and hot spot material are not thought to contribute significant volumes of material to the continents (Burke & Şengör 1986) but island arcs, especially sediments from the accretionary wedge are thought to be major contributors. After formation, continents may then be modified by several processes which include:

- The creation of an Andean-type continental arc margin. This adds magmatic material and thickens the continental crust.
- Continental collision. May result in doubling of the crustal thickness by thrusting.
- Bombardment from space.
- Intracratonic hot spot volcanism.
- Rifting related volcanism.

Of these, continental collision is the most important in adding mass to continental bodies (Burke & Şengör 1986).

As two continental masses approach each other and collide it is thought that little suduction is possible due to the buoyancy and low shear strength of continental crustal material (McKenzie 1969). McKenzie (1972) argued that:

"after collision begins at continental promontories, convergence is accommodated by thickening of continental crust and the formation of small plates to consume oceanic lithosphere remaining in embayments."

Whilst studying the collision of the Arabian peninsula of Gondwana with Eurasia he envisaged the creation of small continental plates which moved away from the Eastern Turkey - Western Iran collision zone (Fig. 2.8, McKenzie 1972). He argued that this scenario would "avoid thickening the continental crust over much of Turkey by consuming the East Mediterranean sea floor instead." This marked the foundation of lateral escape and workers then applied McKenzie's theory to other parts of the world.

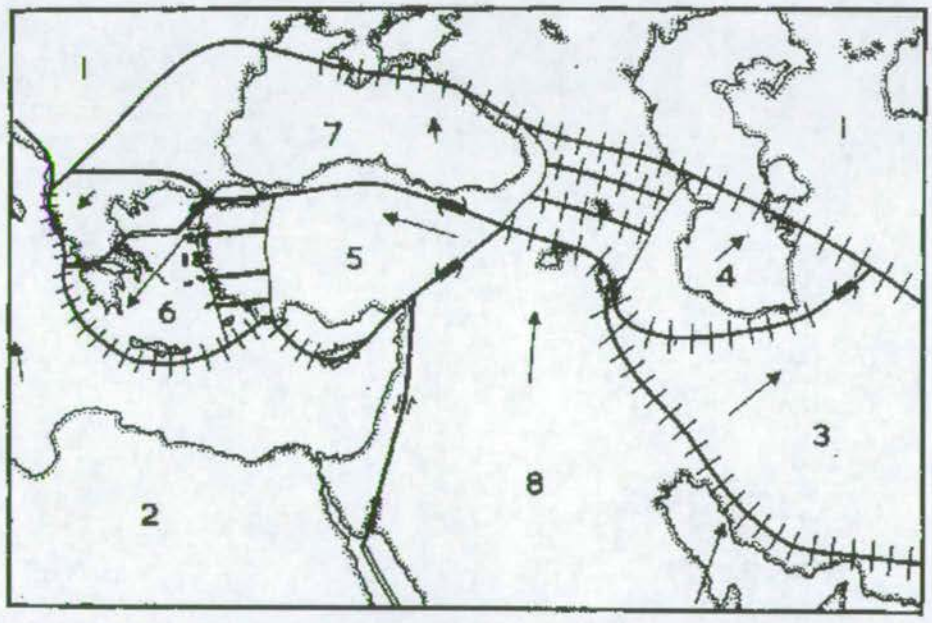

Figure 2.8 Sketch of plate boundaries and motions (after McKenzie 1972). Arrows show the directions of plate motion relative to Eurasia and their lengths are proportional to the magnitude of the relative velocity. Plates are assigned the following numbers: 1 Eurasian, 2 African, 3 Iranian, 4 South Caspian, 5 Turkish, 6 Aegean, 7 Black Sea and 8 Arabian.

2.4.2 Extrusion mechanisms

Molnar and Tapponnier (1975) carried out pioneering analogue modelling, using a rigid indentor and plastic (plasticine) recipient to model the India-Asia collision zone. These experiments resulted in wedges of the indented material being rotated and laterally extruded in several phases away from the loci of convergence, along slip lines (Fig. 2.9a). These slip lines were used by analogy to suggest large scale offsets on strike-slip faults in Indochina and Tibet (Fig. 2.9b). After several generations of such experiments Tapponnier *et al.* (1982) concluded that the India-Asia collision had proceeded via the following mechanism of progressive faulting and rotation:

1) Initial rotation of Indochina by 25 degrees clockwise.
2) Lateral extrusion of Indochina by 800km to the SE along the sinistral Red River Fault.
3) Migration of extrusion northward, activating the Altyn Tagh Fault.
4) Rotation of Indochina to a maximum of 40 degrees clockwise.

Later, Tapponnier *et al.* (1986) modified these conclusions, suggesting strike-slip fault displacements as high as 1000-1500km during polyphase extrusion. They argued that:

"underthrusting in the Himalayas now absorbs less than half of the total convergence between India and Asia, the rest being taken up primarily by strike slip faulting . . ."

The validity of these experiments was questioned by Şengör *et al.* (1985) and others, who argued that it was not valid to use instantaneous 2D models in homogeneous media to account for processes affecting 3D heterogeneous objects over tens of millions of years. There was heated debate over the driving forces behind extrusion during the 1980s, which separated into two camps:

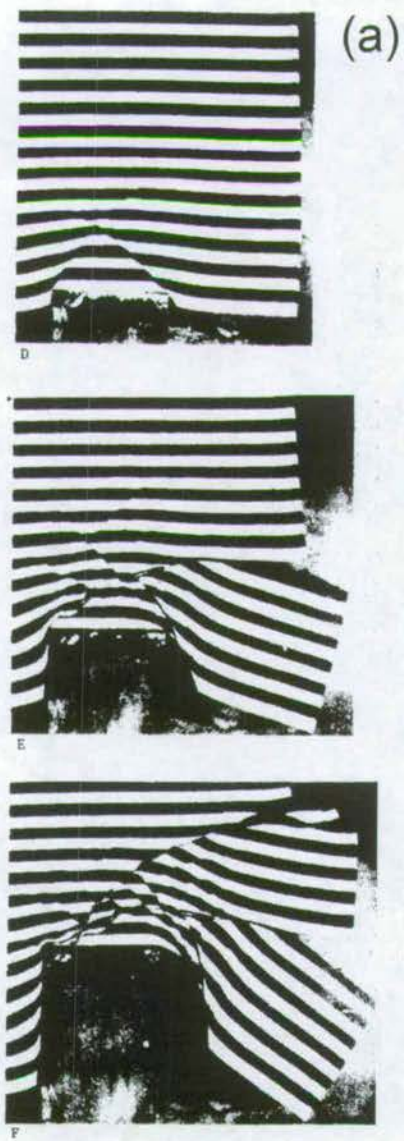

Figure 2.9a Three successive stages of indentation experiments on plasticine (after Tapponier *et al.* 1982). Indentor displacements for D = 1.2cm, for E = 3.5cm, for F = 6.3cm.

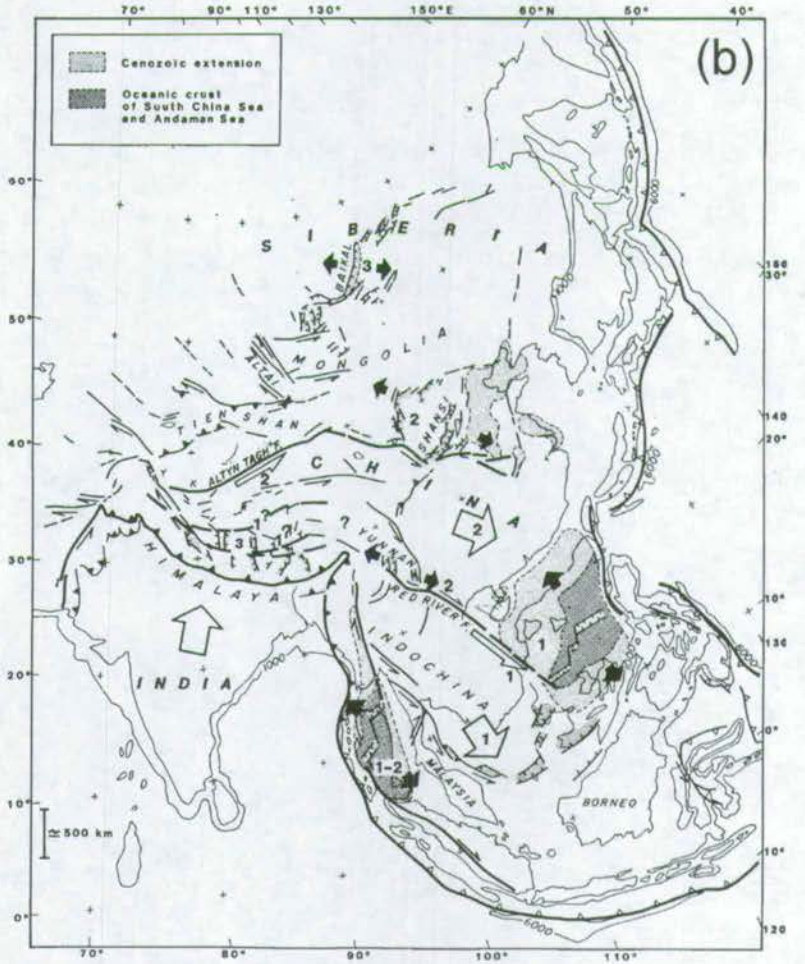

Figure 2.9b Schematic map of Cenozoic extrusion tectonics and large faults in eastern Asia (after Tapponnier *et al.* 1982). Heavy lines = major faults or plate boundaries, thin lines = lass important faults. Open barbs indicate subduction, sold barbs indicate intracontinental thrusts. White arrows represent qualitatively major block motions with respect to Siberia. Black arrows indicate direction of extrusion-related extension. Numbers refer to extrusion phases: 1 = 50-20Ma, 2 = 20-0Ma, 3 = most recent and future.

1) England & McKenzie (1982, 1983) used a viscous sheet over a fluid medium to model the extrusion process, concluding that differences in crustal thickness, formed by flow within the continental lithosphere (i.e. gravity) was the main driving force for lateral crustal motion.
2) Tapponnier *et al.* (1982) argued that forces applied at the boundaries of lithospheric wedges were the driving force.

Modern theorists believe that although boundary stresses are the cause of escape initiation, gravity is the driving force behind escape continuation (Mann 1997). The 'slab pull' of the dense oceanic crust at the unconstrained 'free face' is seen as the main driving force behind the lateral movement of continental crust.

Şengör *et al.* (1985) were of the opinion that the only way to test Molnar and Tapponnier's models and explore the process rigorously was to "undertake a detailed examination of the geology of regions where this process is now occurring". Şengör *et al.* (1985) suggested that the setting which would yield the most information on the evolution of escape would be basins formed during the internal deformation of escaping micro-plates. They argued that these basins may "preserve the only stratigraphic record of events associated with escape and thus allow us to study the critical temporal aspects of this process."

More recent work has focused on applying the concept of escape to zones of collision throughout the world. The Eastern Alps have been studied using similar plasticine experiments to Molnar & Tapponnier (1975) in order to interpret the structure of the Pannonian Basin and Carpathian mountains. Ratschbacher *et al.* (1991) concluded that Italy has acted as a rigid indentor into Europe, resulting in eastward movement of the Pannonian Basin toward the Carpathian Mountains, where confining stress is reduced (Fig. 2.10).

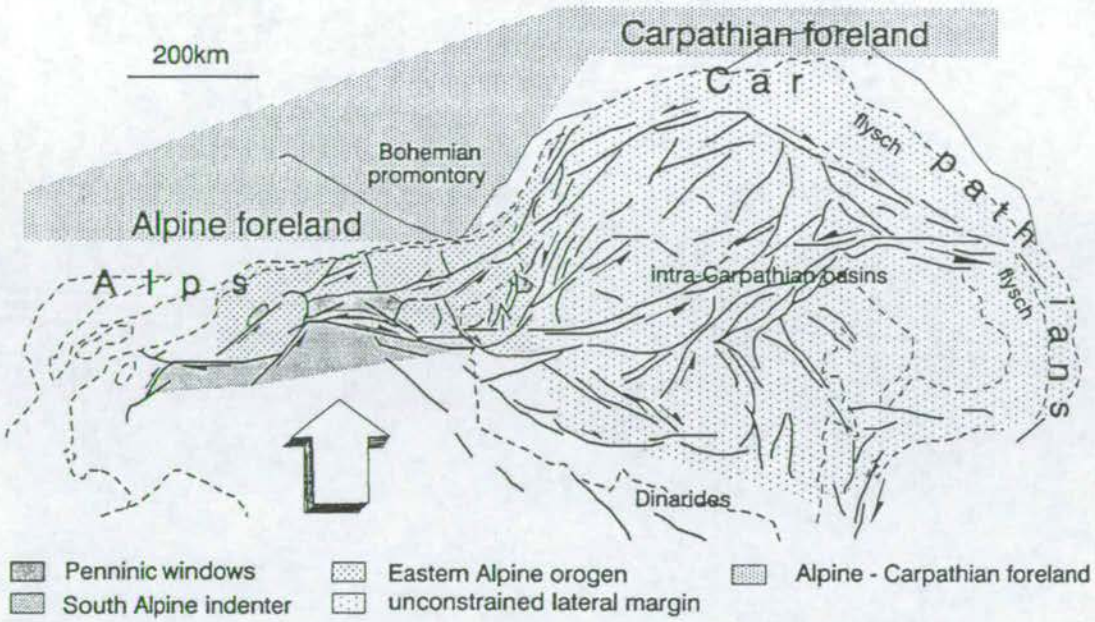

Figure 2.10 Sketch of the Alpine-Carpathian region showing Oligocene - Miocene lateral extrusion fault patterns in the eastern Alps and the intra-Carpathian (Pannonian) basins (after Ratsbacher *et al.* 1991).

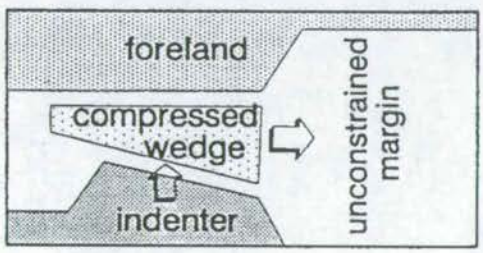

Some studies have focused on the sedimentary basins created and modified during transtension associated with lateral escape. Mann (1997) used the examples of the North Aegean Trough and Vienna Basin to show how maximum compressional stresses have rotated from collision-normal to a direction oblique to collision through time (Fig. 2.11). Mann (1997) drew attention to the fact that transtensional pull apart basins may be produced in active extrusion settings. He concluded that variations in transtensional styles may be more a factor of crustal age and thickness rather than the geometry and vectors of escaping microplates. Fodor (1995) exemplifies the modern approach to

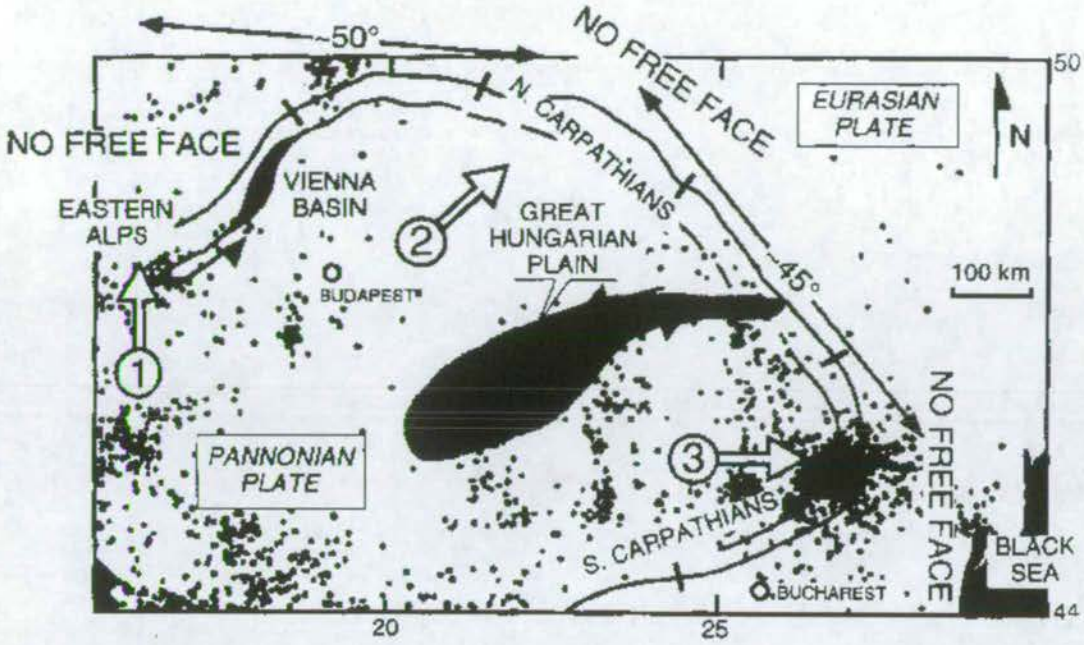

Figure 2.11 Simplified tectonic map of early Miocene to Recent plate boundaries between the Pannonian and Eurasian plates in eastern Europe (after Mann 1997). Arrow 1 indicates direction of northward early Miocene convergence between the escaping Pannonian and Eurasian plates; arrow 2 indicates middle to late Miocene northeastwards convergence direction and arrow 3 represents Pliocene - Pleistocene eastward convergence direction.

studying escape related basins in his study of the Vienna Basin (related to escape of the eastern Alps). Here he used a multi-disciplinary approach, using microtectonic, structural, stress-field, palaeomagnetic and sedimentological data to form a complete structural evolution of the extrusion-related basin. He concluded that the maximum compressive stress has rotated progressively counter-clockwise since initial collision, from collision-normal to collision-oblique.

The escape concept has been applied to the Australia-Banda arc collision zone, the collision between the Panama island arc and Colombia and also the Iapetus suture zone (Burke & Şengör 1986). However, the best studied and most cited area of tectonic escape is that of Anatolia.

2.5 Existing model of extrusion in Turkey

The Cenozoic geological history of Anatolia is generally divided into two phases: the Palaeotectonic (pre- continental collision) and Neotectonic (post- continental collision) periods, the division lying at Middle Miocene. The Neotectonic period is marked by crustal thickening, sub-aerial conditions throughout Turkey and the initiation of several strike-slip fault zones which allow the westward lateral extrusion of Anatolia away from the zone of collision. The main currently active strike-slip fault zones accommodating this extrusion are the North and East Anatolian Fault Zones.

2.5.1 Crustal Thickening

During the continental collision between Arabia and Eurasia, the south Eurasian crust was thickened substantially during the following processes (Tekeli *et al.* 1984, Lytwyn & Casey 1995, Whitney & Dilek 1997):

1) The emplacement of ophiolite nappes onto the Anatolide-Tauride platform during the latest Cretaceous (see 3.3 above).
2) Collision between the Tauride carbonate platform and Central Anatolian Crystalline Platform (Kirşehir Massif).
3) Imbrication and south-vergent deformation within the Tauride carbonate platform associated with ophiolite emplacement.
4) Further shortening associated with the terminal closure of Neotethys and continental collision between Arabia and Eurasia during the Middle Miocene.

This crustal thickening resulted in the burial of Tauride rocks to at least 5-6kbar (16-20km, $>700^0$C). This resulted in the formation of sillimanite-potassium feldspar gneiss during Barrovian metamorphism (Whitney & Dilek 1998).

2.5.2 Post-collisional extension

Studies from the Niğde Massif reveal that mid-crustal rocks were cooled and decompressed during rapid exhumation to <10km (<600^{0}C) during the Oligocene and Miocene (Whitney & Dilek 1998). These workers interpret this as part of a wider regional orogenic collapse, which was driven by:

1) The partial subduction of the Tauride carbonate platform beneath the CACC (Central Anatolian Crystalline Complex) during subduction of the Inner Tauride Ocean, resulting in isostatic rebound of the down-going plate (Fig. 2.12c & d).
2) Crustal over-thickening, resulting in exhumation of thermally weakened continental crust of the overriding plate (Fig. 2.12e & f).

Exhumation during the Oligo-Miocene was accommodated along the Bolkar frontal normal fault system and along low angle detachment surfaces surrounding the Niğde core complex (Dilek & Whitney *in press*, Fig. 2.12e & f). This exhumation was in its advanced stages by the Serravalian (12Ma). This model of Palaeocene partial subduction and Oligo-Miocene extension, especially the foreland basin origin of the Ulukişla Volcanics is controversial, and is the subject of current work by M.Clark (pers. com. 2000).

After crustal thickening and subsequent extension the continuing convergence between the Afro-Arabian and Eurasian plates was also accommodated by the formation of long strike-slip faults, and by the lateral extrusion of Anatolia along these faults, away from the zone of collision. The North and East Anatolian faults are considered to be the most important faults involved in this process, and their timing and offset is outlined below. Information on the Dead Sea Transform and the triple junction between the African, Arabian and Anatolian plates is also given.

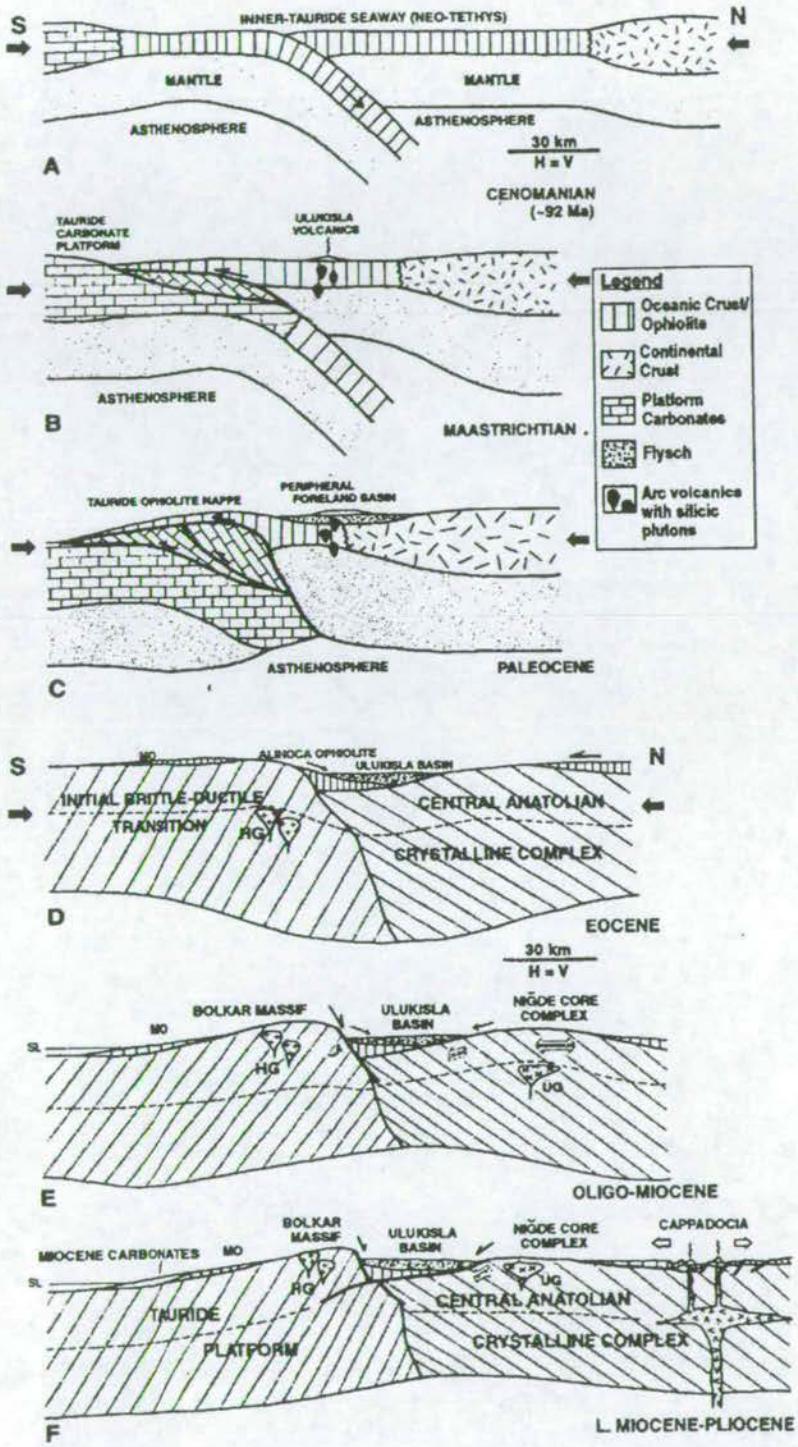

Figure 2.12 Sequential tectonic cartoon depicting the orogenic and post-orogenic evolution of south-central Turkey (after Dilek *et al.* In press). No vertical exaggeration. HG = Horoz Granite, UG = Uckapili granite, MO = Mersin ophiolite, SL = Sea level. Thick black arrows = compression, thick open arrows = extension, thick open half arrows = crustal exhumation in the core complex, half arrows = faults, wavy arrows = erosion and fluvial transport to sedimentary basins.

2.5.3 North Anatolian Fault Zone

The timing of initiation of the North Anatolian Fault Zone is fairly well established. Early estimates ranged from Early Cenozoic (Pavoni 1961) to between Burdigalian and Pliocene (Şengör 1979), but modern workers cite evidence from the Pontus Formation that the fault zone initiated as a wide shear zone toward the end of the Tortonian (7-8Ma) and that brittle slip began during the Early Pliocene at around 5Ma (Barka 1992, Barka & Hancock 1984, Westaway 1994).

The maximum dextral offset and slip rate on the fault zone is much more controversial. This is partly because the NAFZ runs along the line of the Intra-Pontide suture zone for much of its western length, and rock units on either side of the fault zone cannot be correlated as they are from originally different terranes. It is also partly due to the fact that much of the fault zone is obscured by volcanic cover. Early offset estimates were based on cross-fault zone correlations of Jurassic-Cretaceous units (350-400km, Pavoni 1961), and of the Anatolid/Taurid-Pontid suture zone (85±5km, Seymen 1975). The same feature was used by Bergougnan (1976) to infer 100-120km of total slip. Other early estimates included 60-80km based on the Gerede-Ilgaz region (Tokay 1973).

The 85±5km estimate of Seymen (1975) was widely quoted by Şengör (1979) and became accepted in the literature. Indeed, some recent workers have returned to this offset estimate, citing data from the Sea of Marmara pull apart basin (Armijo *et al.* 1999) and large scale river offsets (Westaway 1994). The 85±5km offset hypothesis predicts decreasing offset toward the east (only 50-60km offset E of 40^0E), and an average slip rate of 17mm/year (Westaway 1994).

Other workers however, have preferred lower total offset estimates: 25km based on the offset of Miocene sediments in the central NAFZ (Barka & Hancock 1984), 35±5km based on pull apart basin in Erzincan (Barka & Gülen 1989) and 30-40km based on

similar displaced Miocene sediments (Koçyiğit 1988). In a review paper, Barka (1992) concluded that displacement decreased from 40±5km in the east to 25±5km in the west, as opposed to Westaway (1994), who estimated 85±5km. At present there is still controversy over whether the maximum total offset is large (85±5km), or small (40±5km).

2.5.4 East Anatolian Fault Zone

The timing of first slip is generally accepted to be later than that of the North Anatolian Fault Zone. An initiation time of 2-3Ma (Late Pliocene) was suggested by Şaroğlu (1992). This was corroborated by Trifonov *et al.* (1994), who suggested an initiation age of 2Ma. Westaway (1994) initially argued for a 5Ma initiation age, synchronous with that of the NAFZ, but later changed his estimate to a 3Ma initiation age (Westaway 1996).

Estimates of total offset, although not as controversial as those for the NAFZ are still a matter of debate. They have included: 27km based on the offset of Mesozoic sediments NE of Hazar Lake (Arpat & Şaroğlu 1972), 13km based on the sinistral offset of the Euphrates gorge across the Hazar-Siro fault (Trifonov *et al.* 1994) and 21km based on the offset of Eocene units across the Hazar-Siro fault (Hempton 1984). A published total displacement of 20km based on the offset of Miocene structures on the Goksu fault (Perinçek & Çemen 1990) helped to establish 20-21km as the accepted total sinistral offset on the EAFZ. Westaway (1996) has since criticised the estimates of Hempton (1984), re-calculating the offset of his Eocene piercing point at 17km.

2.5.5 Malatya-Ovacik Fault Zone

This fault zone has only recently been interpreted. About 240km long, it splays SW from the NAFZ near Erzincan, follows the Ovacik valley and bends back to a SW

orientation near Arapkir before running under the Plio-Quaternary sediments of the Malatya basin.

The Malatya-Ovacik Fault Zone has been interpreted as currently active, and taking up present day distributed deformation within Anatolia (Koçyiğit & Beyhan 1998). Other workers (Westaway & Arger 1996, Westaway *in press*) propose initiation ~5Ma (synchronous with the NAFZ) and cessation of activity ~3Ma, during which time the MOFZ took up relative plate motion between Anatolian and Arabian plates. Westaway (in press) proposes that ~3Ma this plate boundary transferred from the MOFZ to the EAFZ. The evidence proposed for this is (i) current absence of seismicity on the MOFZ indicating that it is not currently active and (ii) no geomorphological evidence for recent slip. No positive evidence is proposed for a 5Ma initiation or 3Ma cessation of activity.

A total sinistral offset of ~30km is proposed based on ten separate piercing points (Westaway *in press*). These include the margins of the Mesozoic Munzur Group, the margins of basaltic volcanism, the length of the Ovacik pull-apart basin (25km) and apparent stream offsets.

2.5.6 Tüzgölu Fault Zone

The Tüzgölu fault zone is between 190 and 200km long and extends from north of Tüzgölu to south of Niğde (Fig. 2.4a) and is poorly understood compared to other neotectonic faults in central and eastern Anatolia. Early workers gave an initiation age of Miocene (Dellaloglu & Aksu 1984) but as the sediments of the Tüzgölu Basin were drilled and studied further, a picture of multiple re-activation developed.

A simple two phase model was proposed by Görür *et al.* (1984): (i) normal offset during the latest Cretaceous and (ii) dextral offset during the Neogene, based on unconformities within the Tüzgölu basin succession. This was later resolved into a three

phase model (Çemen *et al.* 1999): (i) normal faulting controlling initial Tüzgölu basin sedimentation during the Late Maastrichtian (latest Cretaceous), (ii) Re-activation as a dextral strike-slip fault during the Late Eocene and (iii) a second re-activation as a dextral transtensional fault zone during the Early Pliocene (neotectonic phase). Evidence for recent faulting includes faulting and deformation of Quaternary alluvial fans and cinder cones and dextral stream offsets. The quantification of total offset has not been attempted by any workers.

2.5.7 Dead Sea Transform

The Dead Sea Transform extends some 1000km from the Red Sea in the south to the East Anatolian Fault Zone in the north, and accommodates sinistral relative movement between the Arabian and African plates. Historical focal mechanism solutions show sinistral motion (Garfunkel & Ben-Avraham 1994).

Prior to its formation, N-S compression between the Arabian and Anatolian plates was accommodated by a belt of NE-SW striking folds across the Arabian platform (e.g. the Syrian Arc fold belt) and also by folding within SE Turkey (Aktaş & Robertson 1984). This deformation continued through the Late Cretaceous and Early Tertiary until the continental breakup of the Afro-Arabian plate during the Oligocene (25-30Ma), when the Red Sea was initiated as a new divergent plate boundary (Garfunkel & Ben-Avraham 1994).

The initiation of the Dead Sea Transform itself is dated at either 12-14Ma (Serravalian) or 18Ma, Burdigalian (based on the timing of the start of magmatic activity near Tiberias and the inception of the Dead Sea basin, Garfunkel & Ben-Avraham 1994). The sinistral offset of dike swarms aged at 20-25Ma also helps to constrain the timing of initiation.

A total offset of 105±5km has been calculated using several criteria (Quennell 1959, Freund 1965, Freund *et al.* 1970, Barov 1974) which include: matching all rock units of the platformal sedimentary cover and some units of basement complexes across the transform, correlating the Negev-Sinai shear belt and also 20-25Ma old dike swarm across the transform.

2.5.8 Triple Junction

The exact location and kinematics of the triple junction between the East Anatolian Fault (bounding Arabian and Anatolian plates), the Dead Sea Transform (bounding Arabian and African plates) and the Kyrenia-Misis fault (bounding Anatolian and African plates) are a matter of controversy. This is principally due to the fact that faults cropping out in this area have little topographic relief. Within this zone a complex history of transpression and transtension has been postulated (Karig & Kozlu 1990). It has been suggested that the first strike-slip movement occurred at the Oligocene – Miocene boundary, on the Engizec zone. This zone may have been transpressive during Latest Miocene – Early Pliocene (as the East Anatolian Fault began) and changed to transtensive during the Quaternary as lateral extrusion accelerated (Karig & Kozlu 1990). Recent work in the Misis area has thrown doubt on many of these early conclusions, pointing rather towards a history of: (i) Eocene initial continental collision-related compression, (ii) Late Miocene suture tightening and (iii) Pliocene strike-slip faulting (pers. com. A.Robertson 2000). In the Karamanmaraş area, the Bitlis frontal thrust fault is offset 25km sinistrally by the East Anatolian Fault Zone (Gülen *et al.* 1987), documenting a history of early N-S compression followed by later strike-slip and extrusion.

2.5.9 Bitlis Suture Zone

The area to the east of the Maraş triple junction is characterised by an E-W trending continental suture zone which has, and continues to, accommodate transpression between the African-Arabian and Eurasian plates (Kempler & Garfunkel 1991). This zone of compressional structures is known as the Bitlis-Zagros suture zone.

The suture zone has been divided into three E-W trending zones: (a) the deformed Arabian Platform, comprising an Early Cambrian to mid-Miocene sedimentary succession, (b) a zone of imbricated thrust slices and (c) a zone of nappes (Yilmaz 1993). In the Hazar Lake area (East Anatolian Fault, Figure 2.3), the suture zone has been divided into (from north to south): the Puturge Metamorphic Complex, the Maden melange and the Elazig Igneous Complex (Hempton 1985).

Structural and stratigraphic studies in the area generally agree that the suture zone has undergone three distinct periods of deformation; these being during the Latest Cretaceous, Mid to Late Eocene and Miocene (Yilmaz 1993, Hempton 1985, Aktaş & Robertson 1984). Deformation in the Palmyride fold and thrust belt (300km south of the suture zone) has been related to convergence along the Bitlis Suture Zone, and data from this area also indicates three periods of deformation, at similar times to that in the suture zone (Chaimov et al. 1992). The reasons for this deformation are more controversial, as is the timing of ocean closure and continental collision.

Workers agree that obduction of ophiolitic bodies, sourced from the remnants of the Neo-Tethys ocean, onto the Arabian Platform took place during the Campanian-Maastrichtian, which caused folding and metamorphism of the Arabian margin sediments (Hempton 1985). Controversy has arisen over the timing of continental collision, due in part to varying interpretations of the Maden Complex, part of the 'zone of nappes' in the suture zone (Yilmaz 1993). Original workers suggested that oblique closure of the Neo-Tethys Ocean took place during either the Middle Eocene, or Latest Cretaceous (Aktaş & Robertson 1984). This was contradicted by Yilmaz (1993), who

dated collision at Mid Eocene-Miocene, based on the interpretation of the Maden Complex as a marginal marine basin. Other workers have dated closure of the ocean at Mid to Late Eocene (Hempton 1985). Controversy still exists, but a closure age of Late Eocene is currently believed by most workers (Robertson 2000a). There is no data to suggest that the Neo-Tethyan ocean 'zipped shut' (i.e. diachronous continental collision), but data from northern India suggests that this is common in areas of indentor tectonics (Najman 2000).

The final period of deformation documented from the suture zone occurred after ocean closure, during the Mid to Late Miocene (Karig & Kozlu 1990, Hempton 1985, Yilmaz 1993, Aktaş & Robertson 1984). During this period, thrust imbricates in the suture zone were emplaced, during continued continental convergence, resulting in a 'tightening' of the suture (Hempton 1985). Local cross-cutting relationships show that the earliest extrusion-related strike-slip faults are younger than thrust faults and deformation associated with this last phase of deformation, and thus that extrusion (along the East Anatolian Fault, at least) began after Mid Miocene time (Gulen et al. 1987).

2.5.10 Neotectonic seismicity

A more detailed account of the seismicity of the Ecemis Fault Zone area is given in Chapter 11, but a summary is also given here. Works on the general seismicity of Turkey have largely focused on the Aegean region, North and East Anatolian Faults, portraying central Anatolia as a region of low seismicity (McKenzie 1970, McKenzie 1972, Rotstein 1984, Fig. 11.1). These works show that the EFZ area is much less seismically active than either the NAFZ or the EAFZ. The Harvard Centroid Moment Tensor (CMT) Catalogue is a catalogue of all earthquakes of moment magnitude 0-10, recorded using the moment tensor method (Dziewonski *et al.* 1981) since 1976. Data from this catalogue also shows that there has been no significant seismic activity in Central Anatolia (including the trace of the EFZ) since 1976 (Fig. 11.2).

A recent compilation of seismic data from 1907-1992, focusing on Central Anatolia (Fig. 11.3, Koçyiğit & Beyhan 1998) found that seismicity is concentrated on the Erciyes basin and NAFZ areas, with only one recorded earthquake on the line of the Ecemiş Fault Zone (magnitude 5.2 on 28/6/1944 at Hamidiye). The focal mechanism for this earthquake was not provided. Koçyiğit & Beyhan 1998 go on to infer the existence of a greater 'Central Anatolian Fault Zone' connecting the EFZ with the NE-SW striking Namrun fault zone, Sivas basin and Erciyes basin, based on this earthquake evidence, and field evidence.

2.5.11 Summary of current extrusion model

The existing model of extrusion is summarised below in chronological order:

Timing	Event
Late Cretaceous	Earliest evidence for closure of the Inner Tauride ocean.
latest Cretaceous	Obduction of ophiolitic nappes from N to S over the Tauride platform.
latest Cretaceous	South-directed deformation and thrusting of Tauride platform associated with ophiolite obduction.
Palaeocene- Eocene	Collision of Tauride carbonate platform with Central Anatolia Crystalline Complex.
Palaeocene- Eocene	Partial subduction of Tauride carbonate platform.
Palaeocene- Eocene	Crustal thickening
Oligocene-Miocene	Isostatic rebound of partially subducted Tauride platform
Oligocene-Miocene	Exhumation and uplift in the Taurus Mountains and Niğde area
Early or Middle Miocene	Initiation of the DSFZ as a strike-slip fault zone
Tortonian (Late Miocene)	Initiation of NAFZ as a shear zone

Early Pliocene	Initiation of the Maraş triple junction
Early Pliocene	Initiation of the NAFZ as a strike-slip fault zone
Late Pliocene	Initiation of the EAFZ as a strike-slip fault zone
Quaternary	Extrusion is active, as recorded in the change of regime at the triple junction.

3 Stratigraphy

3.1 Introduction

In order to constrain the temporal evolution of faulting and sedimentation in the Ecemiş Fault Zone (EFZ) the local and regional stratigraphy must be understood. This chapter describes stratigraphic schemes which have been developed by previous workers for the EFZ and nearby Ulukişla and Karsanti basins. The most relevant stratigraphic study for the EFZ is that of Yetiş (1978) which forms the backbone of the stratigraphy used in this thesis. Much of the Tertiary succession within the EFZ is of terrestrial origin and devoid of datable faunas; hence, fauna-rich time-equivalent sequences are also discussed from the Ulukişla and Karsanti basins, to the west and east of the study area, respectively (Fig. 3.1).

Figure 3.1 Location of Cenozoic sedimentary basins in the Adana region (south-central Turkey). Thick black lines represent faults, dashed line represents possible course of the EFZ south of Gulek.

3.2 *Existing Biostratigraphic Schemes – Summary and evaluation*

All published stratigraphic schemes were considered and calibrated to the timescale of Harland *et al.* (1990).

3.2.1 Ecemiş Fault Zone

The earliest stratigraphic review of the EFZ was carried out by Blumenthal (1956) as part of a regional synthesis of the geology of the Bolkar massif (Fig. 3.2a, Fig. 3.3b). This was followed by the PhD thesis of Yetiş (1978) who set up the first comprehensive stratigraphic scheme for the EFZ. He focused on the Çamardi area between Madenbogazi and Kamişli (Fig. 2.4), largely using foraminiferal and ostracod assemblages to define a stratigraphic scheme (Fig. 3.2 & 3.3a). This scheme recognised five major depositional units during the Tertiary: the Palaeocene Ulukişla Group (including the Çamardi Formation, Karadağ spilite and Mavras limestone), the Middle Eocene Kaleboynu Formation, the Oligocene Çukurbağ Formation (including the Korpinar gypsum member), the Miocene Burç Formation and the Quaternary Çatalca Formation. This scheme has been accepted and used by most succeeding workers, with slight variations.

Of these units, the Palaeocene age of the Çamardi Formation is based on assemblages of marine foraminifera such as: *Globigerina, Globorotalia, Planorbulina, Amphistegina, Rotalia, Cibicides* and others (Yetiş 1978, Fig. 3.3a). A Middle Eocene (Lutetian) age for the Kaleboynu Formation was established from assemblages of marine benthic foraminifera such as: *Nummulites, Assilina, Alveolina, Discocylina, Asterogerina* and others (Fig. 3.3a). A Miocene age was assigned to the Burç Formation based on assemblages of the freshwater ostracods *Heterocypris cf. Ponticum* Krstic and *Armiger cf. Crista* Linnaeus (Yetiş 1978, Fig. 3.3a). Ostracod assemblages are generally not as stratigraphically useful as

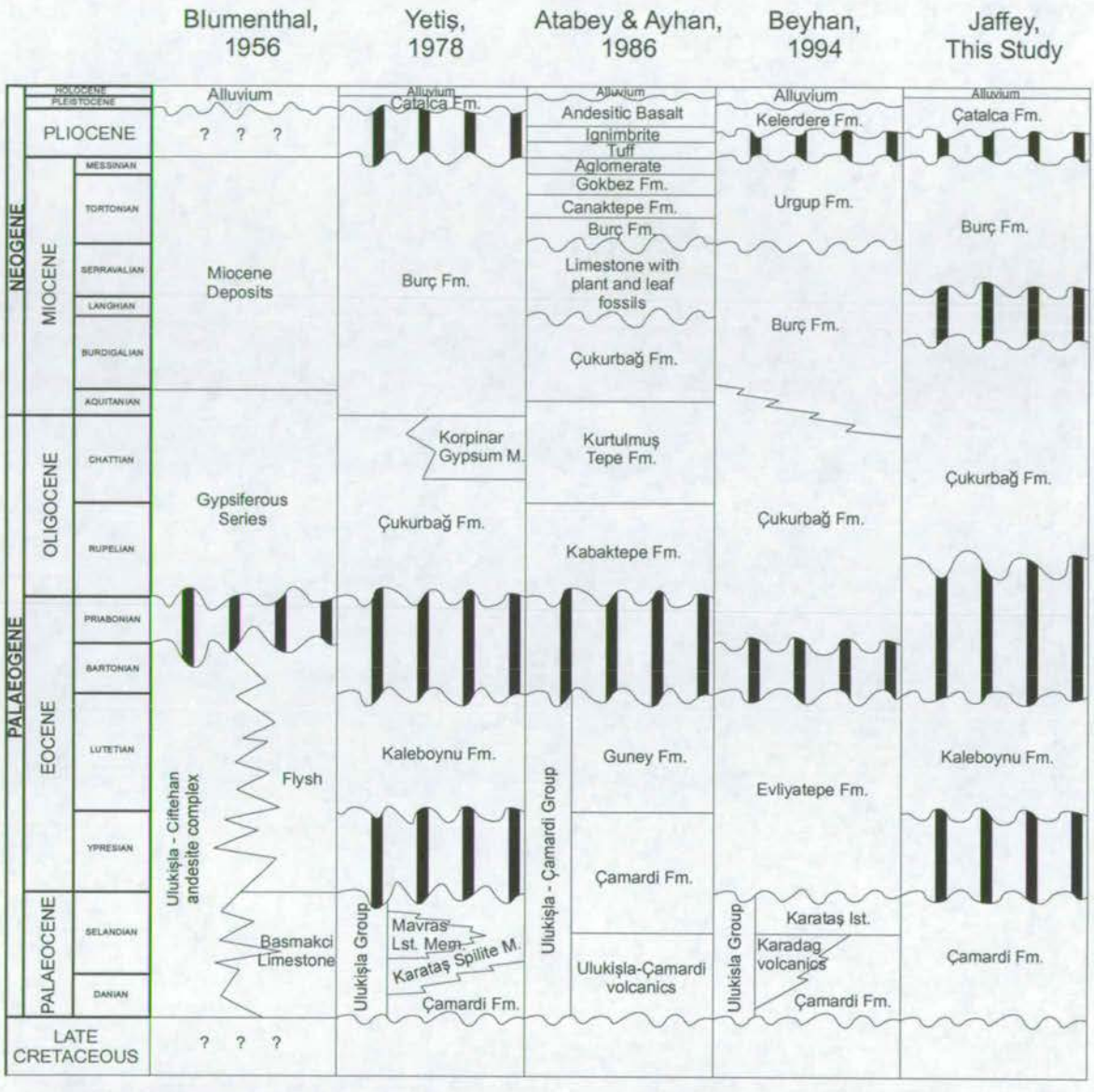

Figure 3.2 Comparison of stratigraphic schemes proposed for the Ecemiş Fault Zone (partly after Beyhan 1994).See text for discussion. Jagged lines represent interfingering relationships, areas of vertical stripes represent a hiatus in sedimentation, wavy lines represent unconformities.

foraminiferal ones as they typically have restricted ecological niches, hence are not geographically widespread and are less suitable for long-distance correlations (Brasier 1980). The broad Miocene age assigned to the Burc Formation by Yetiş

Formation	Fauna	Age	Reference
Catalca Formation.	No fossils		
Burc Formation.	Gastropod species: *Heterocypris cf. Ponticum* Krstic, *Armiger cf. Crista* Linnaeus.	Miocene	Yetis (1978)
Cukurbag Formation.	No fossils		
Kaleboynu Formation.	Microfossil species: *Nummulites, Assilina, Alviolina, Discocyclina, Asterogerina, Astrocyclina, Sphaerogypsina globsa, Gypsina, Lockhartia, Rotaliidae.*	Lutetian (Mid Eocene)	Yetis (1978)
Camardi Formation.	Microfossil species: *Globigerina, Globorotalia, Planorbulina, Amahistegina, Rotalia, Cibicides, Peneroplis, Kathina, Miscelanea, Lockhartia.*	Late Palaeocene	Yetis (1978)

Figure 3.3a Table of faunas used to construct biostratigraphic schemes for the Ecemiş Fault Zone.

Formation	Fauna	Age	Reference
Unnamed unit	No fossils	Miocene-Pliocene ?	Demirtaşli et al. (1984)
Aktoprak Formation	Gastropod species: *Planorbis* (Coretus) *mantelli*, *Planorbis* (Coretus) *cf. thiolleri*, *Limnae* (Stagnicola) *tschihatscheffi*, *Cyclostoma antiguum.*	Chattian (Late Oligocene) – Aquitanian (Early Miocene)	Blumenthal (1956)
	Ostracod species: *Neocyprideis williamsoniana*, *Candona* (Pseudocandona) *fertilis fertilis*, *Moenocypris forbesi*, *Zonocypris gökçeni n. sp.*, *Zonocypris kurtulmustepeensis n. sp.*, *Zonocypris ulukislaensis n. sp.*	Aquitanian (Early Miocene)	Nazik & Gokcen (1992)
Hasangazi Formation	Microfossil species: *Globorotalia cf. centralis, Discocyclina sp.*, *Gypsina mastalensis*, *Halkyarsia sp.*	Late Lutetian (Mid Eocene)	Demirtaşli et al. (1984)
Ulukişla Formation	Microfossil species: *Discocyclina sp.*, *Nummulites sp.*, *Vernevillina sp.*, *Asilina sp.*, *Operculina sp.*	Early – Mid Eocene	Demirtaşli et al. (1984)

Halkarpinar Formation	Microfossil species: *Globorotalia cf. pseudomonardi,* *Globorotalia valescoensis,* *Assilina cf. exponens,* *Discocyclina sp.,* *Distichoplax biserialis,* *Alevolina cf. triestina,* *Alveolina cf. globula,* *Nummulites sp.*	Mid Palaeocene – Early Eocene	Demirtaşli et al. (1984)
Guneydağ Formation	Microfossil species: *Missisipina sp.,* *Miscellanea miscella,* *Bolkarina aksarayi,* *Lacazina öztemüri,* *Fabularia donatae.*	Early Palaeocene	Demirtaşli et al. (1984)

Figure 3.3b Table of faunas used to construct biostratigraphic schemes for the Ulukişla Basin.

Formation	Fauna	Age	Author
Karsanti Formation	Foraminifera species: *Globigerina prbulloides* Blow, *Globegerina ampliapertura* Bolli, *Globigerina tripartita* Koch, *Gobigerina euapertura* Jenkins, *Globigerina ciperoensis angulisutaralis* Bolli.	Early Oligocene	Ünlügenç et al. (1993)
	Ostracod species: *Eucypris sp.,* *Novocypris sp.,* *Pseudocandona fertilis* Triebel, *Candona* (Lineocypris) sp., *Ilyocypris boehli* Tiebel, *Hemicyprideis helvetica* (Lienenklaus), *Vetustocytheridea sp.,* *Hemicyprideis montosa* (Jones & Sherborn), *Krithe sp.,* *Cytherura sp.,* *Echinocythereis sp.*	Mid Oligocene	Ünlügenç et al. (1993)

Figure 3.3c Table of faunas used to construct biostratigraphic schemes for the Karsanti Basin.

(1978) is questionable as the internal structures of freshwater ostracod fauna are usually not preserved, their carapaces are much less distinctive than those of marine

taxa and they are generally known to be more long ranging (Jones 1956). Ostracods are, however, excellent indicators of palaeo-environment, as their carapace morphology is very sensitive to changes in salinity and water energy (Brasier 1980).

The ages of the Çukurbağ and Çatalca Formations are inferred only, as these do not contain dateable fossils. Yetiş (1978) inferred an Oligocene age for the Çukurbağ Formation and a Quaternary age for the Çatalca Formation based on the ages of adjacent units. One must therefore look further afield, to the Ulukişla and Karsanti basins (Fig. 3.1) for dateable, time equivalent units.

More recently Atabey & Ayhan (1986) have constructed an independent stratigraphic scheme (Fig. 3.2). This work is inaccessible, being an internal report written for MTA (Turkish Geological Survey). However, it is unlikely that this contains additional relevant biostratigraphic results.

The most recent stratigraphic study of the Ecemiş Fault Zone is included in the Masters thesis of Beyhan (1994) on the Sulucaova-Kovali segment of the EFZ (Fig. 2.4 for location). He largely follows the scheme of Yetiş (1978), with the inclusion of Late Miocene volcanogenic tuffs (Fig. 3.2). Beyhan (1994) assigns a Pliocene age to the Çatalca Formation of Yetiş (1978), who originally described it as Quaternary. This new age is assigned only on the basis of the ages of adjacent units: the underlying Miocene Burç Formation and overlying Quaternary alluvium. Recent publications (Koçyiğit & Beyhan 1998) adopted a broader Pliocene – Quaternary time bracket for the Çatalca Formation, which is also adopted in this study. Recent attempts to further constrain the age of the Çatalca Formation, such as the use of cosmogenic isotopic techniques are described in section 8.6.2.

3.2.2 Ulukişla Basin

A comprehensive stratigraphy for the Bolkardağ and adjacent Ulukişla Basin was published by Demirtaşli *et al.* (1973, 1984, Fig. 3.4 & 3.3b). They separate the Tertiary rock record into six major units: the Lower Palaeocene Guneydağ Formation (marine limestones), the Upper Palaeocene Halkarpinar Formation (volcanics), the Lower Eocene Ulukişla Formation (volcaniclastic sediments), the Middle Eocene Hasangazi Formation (including marine limestones and evaporitic lake deposits), the Oligocene Aktoprak Formation (terrestrial red beds) and an unnamed Miocene-Pliocene terrestrial unit.

The Lower Tertiary succession of the Ulukişla Basin differs from that of the Ecemiş Fault Zone in that it is dominated by volcanic rocks and their detrital products. The Upper Tertiary terrestrial succession (Oligocene onwards) is, however, very similar to Upper Tertiary sediments within the Ecemiş Fault Zone. The Aktoprak Formation, described by Demirtaşli *et al.* (1984) is very similar to the Çukurbağ Formation of Yetiş (1978), both bearing gypsiferous beds at the base, showing red bed fluvial characteristics (section 4.4 & 4.5) and sharing an inferred Oligocene age. Blumenthal (1956) dates the Aktoprak Formation as Chattian (Late Oligocene) to Aquitanian (Earliest Miocene) using freshwater gastropod assemblages (Fig. 3.3b), which suggests a similar age for the Çukurbağ Formation of the EFZ. However, Tertiary freshwater gastropod assemblages generally have embryonic and immature shells, are long-ranging and are not considered good zonal fossils (Jones 1956). Demirtaşli *et al.* (1984) recognise an unconformity between the Oligocene Aktoprak Formation and Late Miocene – Pliocene units. The unnamed Miocene-Pliocene unit of Demirtaşli *et al.* (1984) remains undated but closely resembles the Miocene Burç Formation of Yetiş (1978), both Formations showing terrestrial characteristics and ostracod-rich, algal, lacustrine limestones (sections 4.7 & 4.8). I have therefore

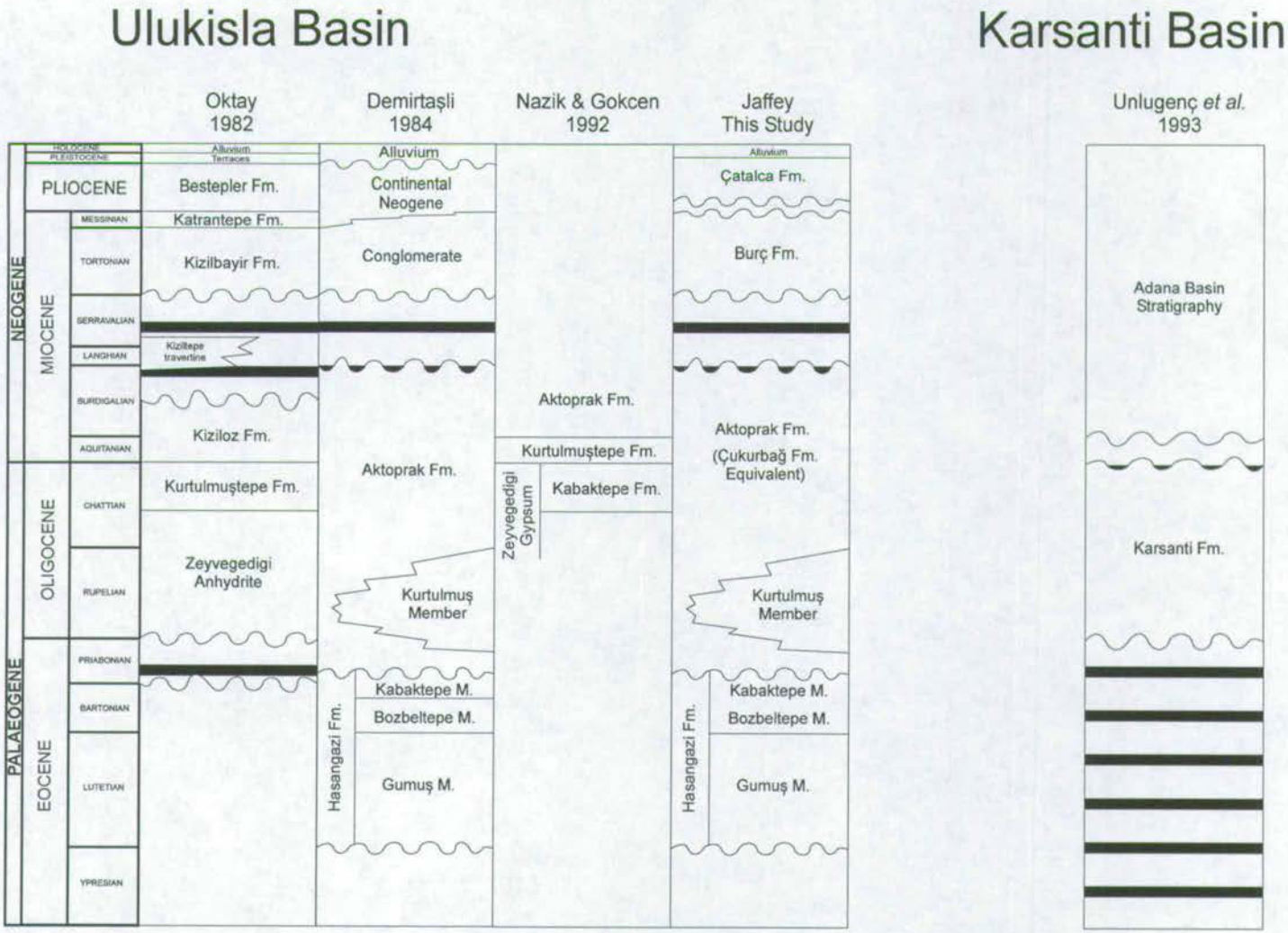

Figure 3.4 Comparison of stratigraphic schemes proposed for the Ulukisla Basin. See text for discussion. Jagged lines represent interfingering relationships, areas of vertical stripes represent a hiatus in sedimentation, wavy lines represent unconformities.

tentatively given the Miocene of the Ulukişla Basin the same temporal constraints as the Burç Formation of the EFZ.

A subsequent study of the Ulukişla area by Oktay (1982) resulted in a new stratigraphic framework for the Early Tertiary, and also in a new interpretation of the ages of Late Tertiary units (Fig. 3.4). Oktay (1982) interpreted the evaporitic Zeyvegedigi Formation as Oligocene based on unspecified fauna; this was previously interpreted as Middle to Late Eocene (Fig. 3.4, Demirtaşli *et al.* 1984). Oktay (1982) also re-interpreted the age of the Kiziloz Formation as Early Miocene, which was previously interpreted as Oligocene-Early Miocene by Demirtaşli *et al.* (1984). These re-interpretations have not been well justified by new fossil ages and I therefore use the results of Demirtaşli *et al.* (1984).

Later biostratigraphic work by Nazik & Gokcen (1992) on the basal Kurtulmus Member of the Aktoprak Formation suggested an Aquitanian age (earliest Miocene), based on assemblages of new freshwater ostracod species: *Zonocypris Ulukişlaensis, Zonocypris gokceni* and *Zonocypris kurtulmustepeensis* (Fig. 3.3b & 3.4). These findings have subsequently been criticised by A.Lord (pers. com. 1999) and H.Malz (pers. com. 1999), who point out that:

"The three Zonocypris species are all new . . . and therefore of no biostratigraphical value in isolation" (A.Lord, pers. com. 1999).

Dr H.Malz (pers. com. 1999) agrees that "the Aquitanian age determination of Nazik (1992) is not conclusive" and suggests that the species are more likely to be of Oligocene age, similar to species such as: *Neocyprideis williamsoniana, Candona (Pseudocandona) fertilis fertilis* and *Moenocypris forbesi*. Nazik now accepts (pers. com. 1999) that the ostracod assemblages used may in fact be long-ranging.

The age of the Aktoprak Formation remains poorly constrained. The age of the basal contact is constrained as post-latest Eocene (it lies above the Kabaktepe Member of Demirtaşli et al. 1984), and the upper contact is constrained as pre-Middle Miocene (it lies below the base of the Mio-Pliocene unit). I have adopted an age range of Late Oligocene to Early Miocene based on the gastropod assemblage ages of Blumenthal (1956) (Fig. 3.3b), and on the comments of A.Lord and H.Malz (above). This conforms with ages given to the Çukurbağ Formation by recent workers (Karadinizli & Kazanci 1993, Koçyiğit & Beyhan 1998).

The Aktoprak Formation is lithologically similar to the Çukurbağ Formation of the Ecemiş Fault Zone and may help to better constrain the age of this poorly dated unit. Unlike the Aktoprak Formation, the basal contact of the Çukurbağ Formation is a high-relief angular unconformity with the underlying Eocene sediments. It therefore seems likely that the base of the Çukurbağ Formation was marked by a hiatus in sedimentation during the Early Oligocene and that sedimentation resumed during the Mid- or late Oligocene (Fig. 3.2). The Çukurbağ Formation is given the same upper temporal constraints as the Aktoprak Formation.

3.2.3 Karsanti Basin

This is currently an intermontane basin situated to the east of the Ecemiş Fault Zone (Fig. 3.1) which drains into the Adana Basin. Work by Ünlügenç *et al.* (1993) has dated the basin fill (Karsanti Formation) as Oligocene based on fresh-water and marine ostracod assemblages and planktic foraminifera assemblages (Fig. 3.3c). These ostracod and foraminifera-bearing sediments rest conformably above a succession of conglomeratic and sandy redbeds which are very similar in facies to the Çukurbağ Formation of Yetiş (1978) (sections 4.4 & 4.6). A tentative lithostratigraphic correlation can be made between these two units, which are at present separated by the Aladağ Mountains, based on the similarity of facies and

spatial proximity, and because ages derived by Ünlügenç *et al.* (1993) for the Karsanti basin (Oligocene) are similar to those of the Çukurbağ Formation and Aktoprak Formation discussed above.

3.3 Existing Radiometric Ages

The existing stratigraphic schemes of the Ecemiş Fault Zone rely mostly on biostratigraphic data. However, K/Ar techniques have been used to obtain radiometric ages of tuffs and lavas of the Central Anatolian Volcanic Province, through which the EFZ runs (Erciyes Basin area, Fig. 3.5). K/Ar dating (Innocenti *et al.* 1975) has revealed that calkalkaline volcanic activity in this area dates from Late Miocene until prehistoric times. This radiometric dating is outlined in Fig. 3.6 and described in detail in Section 9.2. Additional K/Ar dating of volcanic products of the Central Anatolian Volcanic Province was carried out by Besang *et al.* (1977), Batum (1978) and Ercan *et al.* (1990), but these are included in Turkish Petroleum Company and MTA (Turkish Geological Survey) reports, and are not accessible.

New $^{40}Ar/^{39}Ar$ radiometric dating of tuffs and lavas within the Erciyes Basin was carried out during this study to establish the timing of faulting on the EFZ in this area. These results are described fully in Chapter 9.

3.4 Formal Stratigraphy of the Ecemiş Fault Zone

The stratigraphy of the EFZ is now summarised by integrating all of the lithostratigraphic, biostratigraphic and radiometric data into a N-S stratigraphic cross section along the EFZ (Fig. 3.7). The time constraints of each formation are largely based on Yetis (1978) apart from the timing of the Çukurbağ Formation, which is based on that of the Aktoprak Formation of the Ulukişla Basin. A new hiatus in

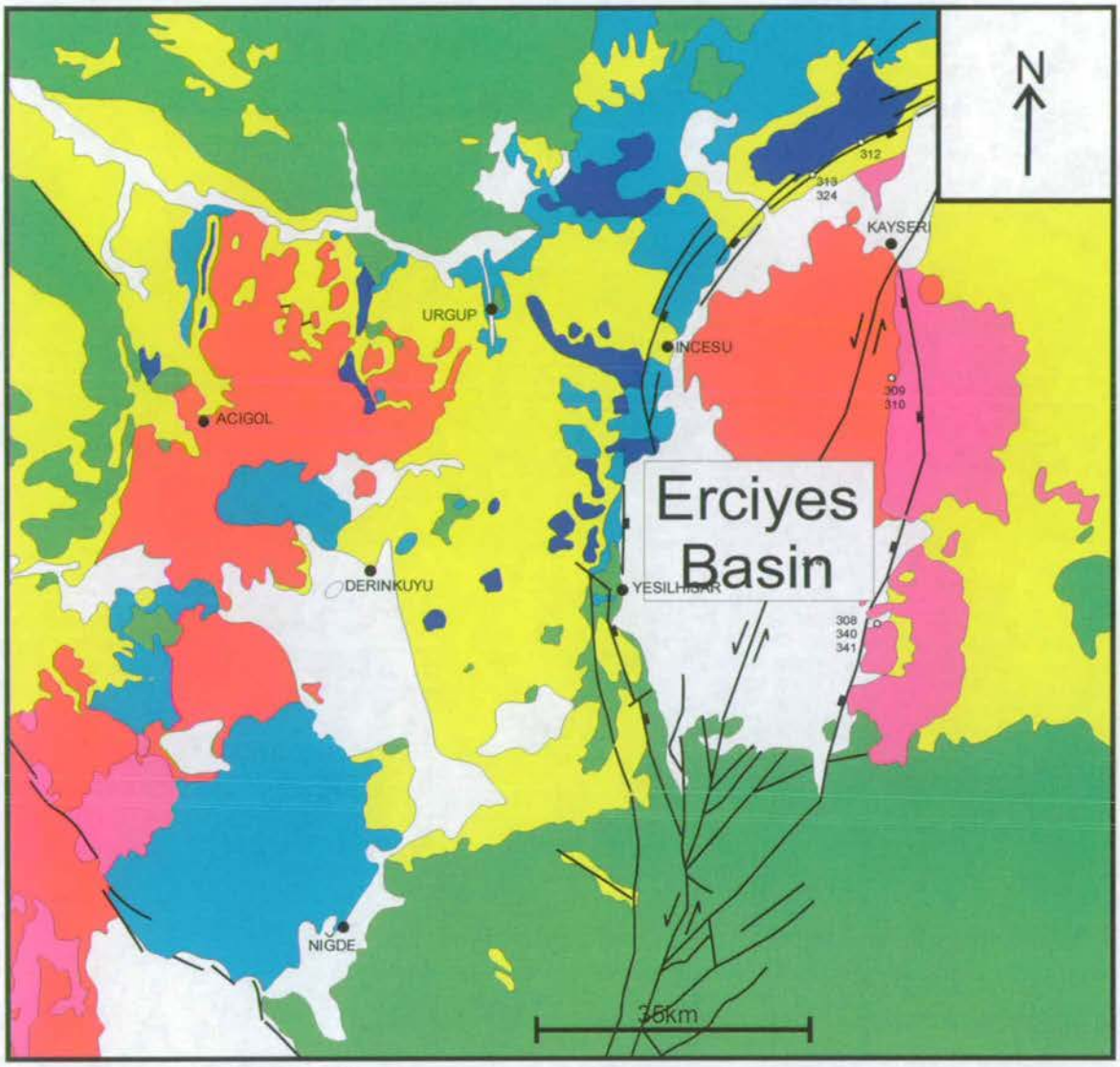

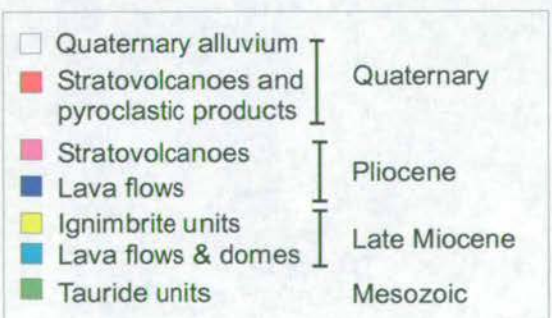

Figure 3.5 Geological map of the Erciyes Basin, Central Anatolian Volcanic Province (see Fig. 2.4 for wider location) showing the location of major faults (after Pasquare *et al.* 1988). Numbered circles represent samples collected during this study. Lines with boxes indicate normal faults, boxes on the downthrown side. Strike-slip faults are indicated by bi-divergent arrows.

Sample	Stratigraphic Unit	Rock Type	K/Ar Age (Ma)
KY1	Akkoy Fm.	Rhyolitic Ignimbrite	8.5±0.2
KY4	-	Andesitic lava	5.0±0.3
U60	-	Andesitic lava	5.1±0.1
U64	-	Andesitic lava	5.0±0.3
U78	-	Andesitic lava	5.5±0.2
U79	Valibaba Tepe Fm.	Ignimbrite	2.7±0.1
U83	-	Dacitic lava	0.9±0.2
U84	-	Andesitic lava	0.3±0.1
U115	Valibaba Tepe	Ignimbrite	2.8±0.1

Figure 3.6 Radiometric ages found from samples from the Erciyes Basin, Central Anatolian Volcanic Province (after Innocenti *et al.* 1975). These have been used to construct the geological map (Fig. 3.5).

sedimentation was added between the Çukurbağ Formation and Burç Formation due to the angular unconformity seen between these two units (Fig. 4.24), although the duration of his hiatus is not known. Due to the deformed nature of the sediments of the EFZ it is usually not possible to follow the same stratigraphic bed from east to west across the EFZ and therefore an E-W stratigraphic cross section was not constructed.

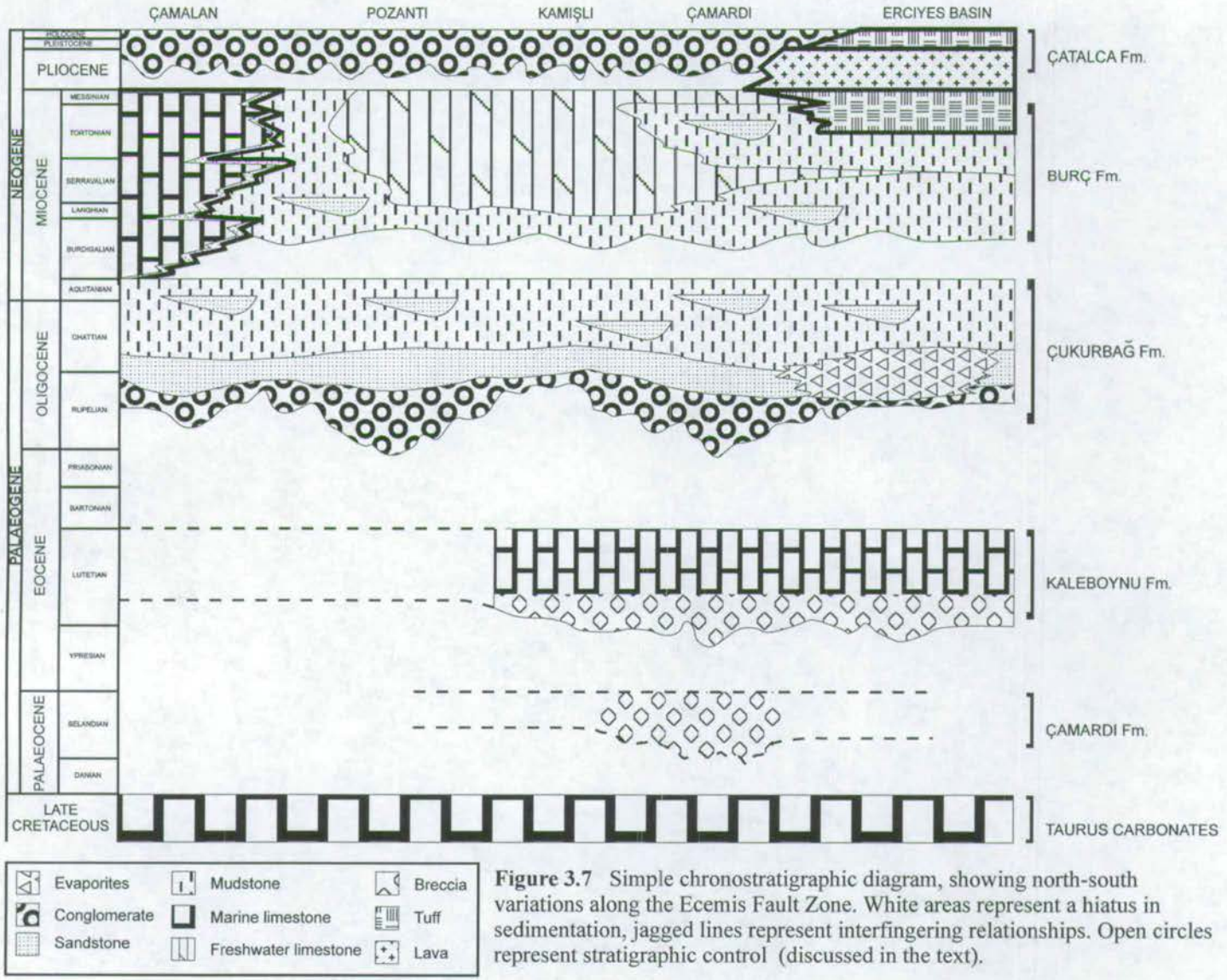

Figure 3.7 Simple chronostratigraphic diagram, showing north-south variations along the Ecemis Fault Zone. White areas represent a hiatus in sedimentation, jagged lines represent interfingering relationships. Open circles represent stratigraphic control (discussed in the text).

4 Sedimentology

4.1 Introduction

This chapter discusses the sedimentary characteristics of the post-Palaeocene stratigraphic units, as defined in the previous chapter. Sedimentological information is instructive, e.g. in locating ancient depocentres, estimating palaeo- slope gradients and in revealing the nature of regional uplift and faulting. Sedimentological data are presented below, from each Formation (section 4.3), including:

(i) A field description of each succession at its type section.
(ii) A field description of other important sections, where necessary.
(iii) A representative log of the type section.
(iv) An account of the associated flora and fauna.
(v) Palaeocurrent data.

In the second half of the chapter (section 4.4) the data are used to interpret the environment of deposition by providing:

(vi) A systematic breakdown of the depositional facies within each formation.
(vii) An interpretation of the environment of deposition of each facies, based on established models and examples.
(viii) Description of lateral facies changes within each formation, including a log correlation panel where appropriate.
(ix) A summary of palaeo-environments for each formation.

4.2 Previous Work

Sedimentological analysis of the Cenozoic rocks of the Ecemiş Fault Zone has been carried out by previous workers. These include a study of Yetiş (1978) who set up the first biostratigraphic framework for the area (Section 3.2.1, Fig. 3.2). He divided the post-Palaeocene stratigraphy into four formations: the Middle Eocene Kaleboynu Formation, Oligocene Çukurbağ Formation, Miocene Burç Formation and the Quaternary Çatalca Formation (Fig. 3.2). This division was retained here with some changes, as discussed in Section 3.2.1. Yetiş (1978) described the overall sedimentary succession but did not discuss lateral variations or provide palaeocurrent data. Karadenizli & Kazanci (1993) focused on the Oligocene – Early Miocene Çukurbağ Formation, by dividing it into facies associations and examining lateral facies variation, from Kamişli in the north, to Gülek in the south (Fig. 2.4). They concluded that the Oligo-Miocene basin was not confined by the Ecemiş Fault Zone and that sediment was mainly sourced from the Ulukişla Basin to the west.

This chapter aims to test existing conclusions and to provide new sedimentological data and interpretations for all of the post-Palaeocene units within the Ecemiş Fault Zone. New palaeocurrent data will be included to help constrain the palaeotopography and drainage pattern for each unit.

4.3 Sedimentological Data

4.3.1 Middle Eocene Kaleboynu Formation

This Formation has very limited outcrops within the fault zone. The first is at Evliya Tepe, a hill 3km NNE of Çamardi, in the central EFZ, where 140m of succession crop out (Fig. 4.1). The second is at Kaleboynu Tepe, a small hill 17km NE of Çamardi, high on the southern side of Madenboğazi stream. At this locality only 15-20m of succession is exposed (Fig. 4.1).

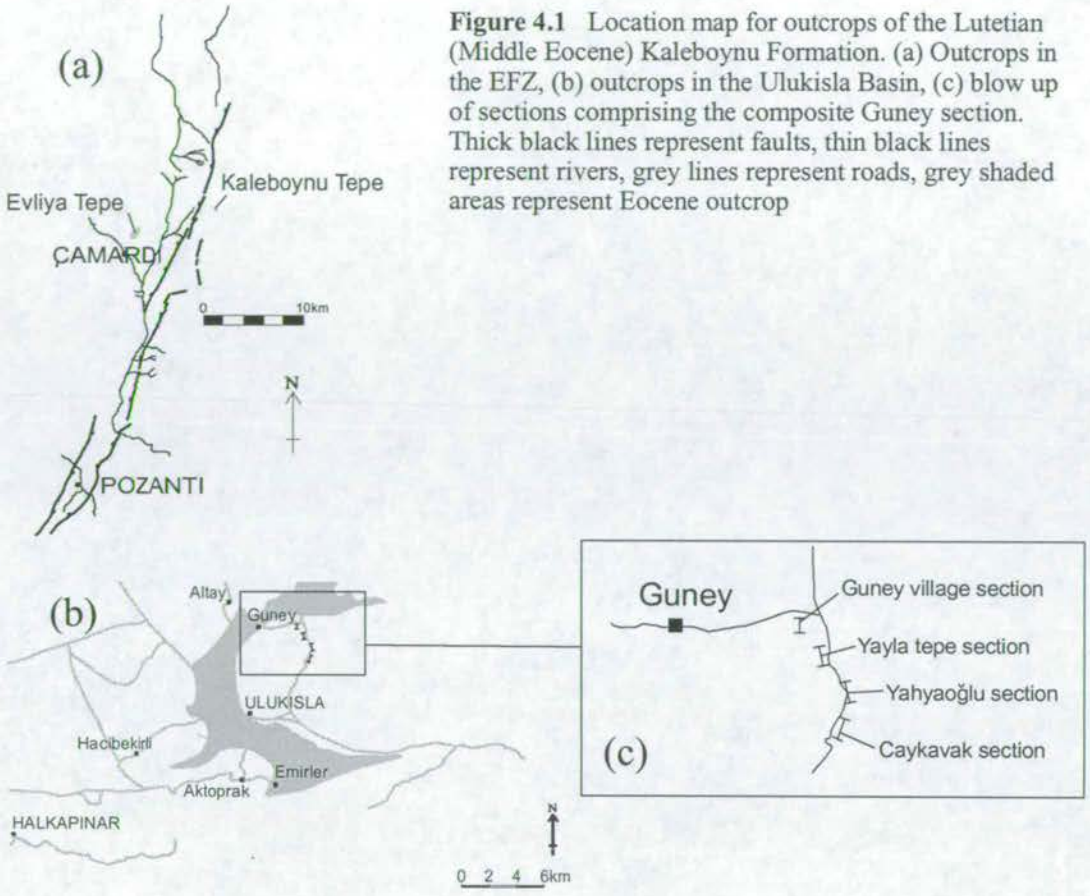

Figure 4.1 Location map for outcrops of the Lutetian (Middle Eocene) Kaleboynu Formation. (a) Outcrops in the EFZ, (b) outcrops in the Ulukisla Basin, (c) blow up of sections comprising the composite Guney section. Thick black lines represent faults, thin black lines represent rivers, grey lines represent roads, grey shaded areas represent Eocene outcrop

4.3.1.1 Evliya Tepe

On the western slopes of Evliya Tepe, rocks of the Niğde Metamorphic Complex, the Palaeocene Çamardi Formation and the Lutetian Kaleboynu Formation crop out. Figure 4.2 shows a complete log of the Evliya Tepe succession, which has the following characteristics:

Base-25m

The base of the section is marked by an angular unconformity of 27^0 (Fig. 4.3) which brings Kaleboynu Formation rocks into contact with steeper dipping Çamardi Formation (Upper Oligocene –Lower Miocene red beds) rocks beneath. Basal

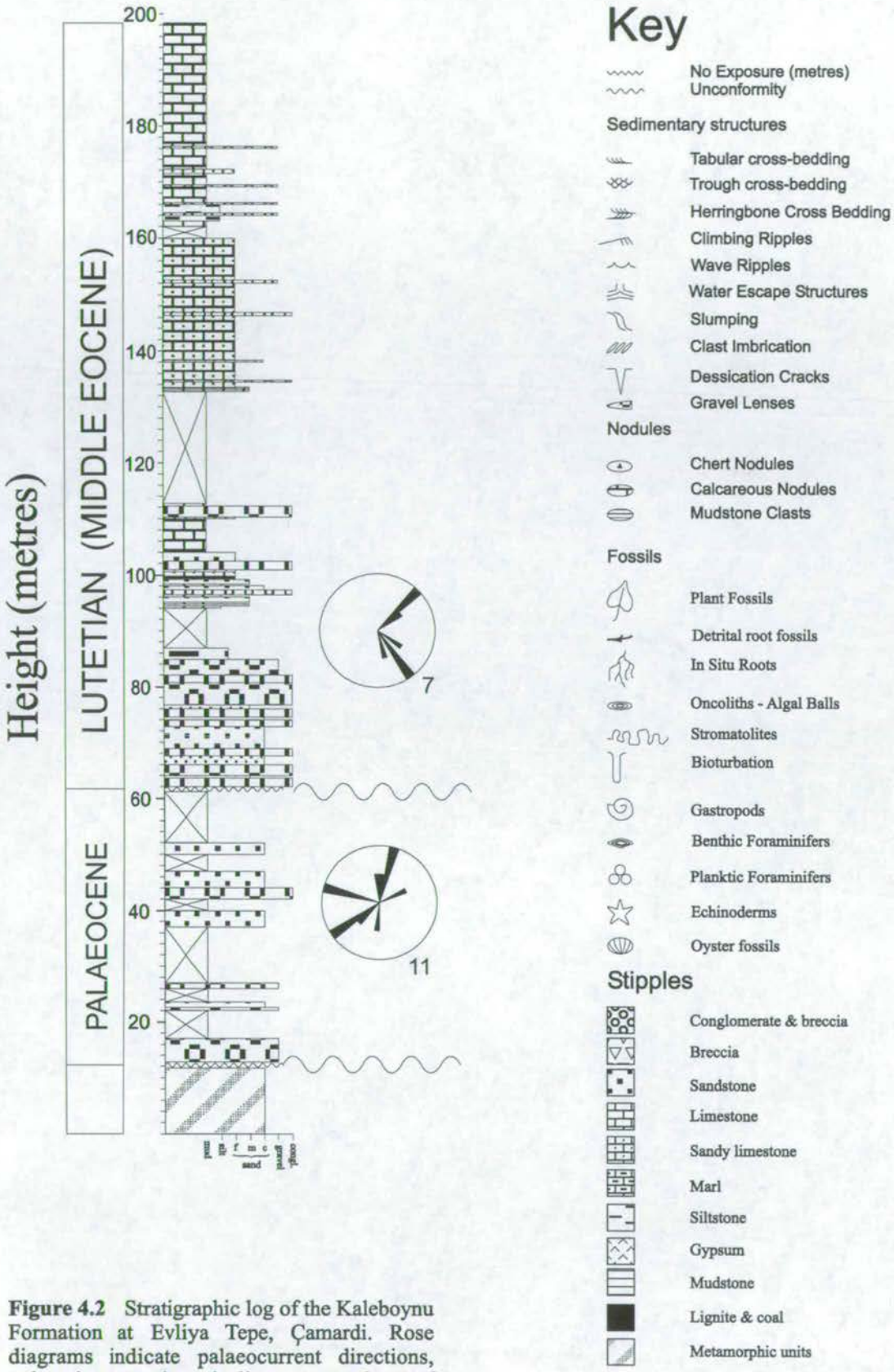

Figure 4.2 Stratigraphic log of the Kaleboynu Formation at Evliya Tepe, Çamardi. Rose diagrams indicate palaeocurrent directions, subscript number indicates number of palaeocurrent data points.

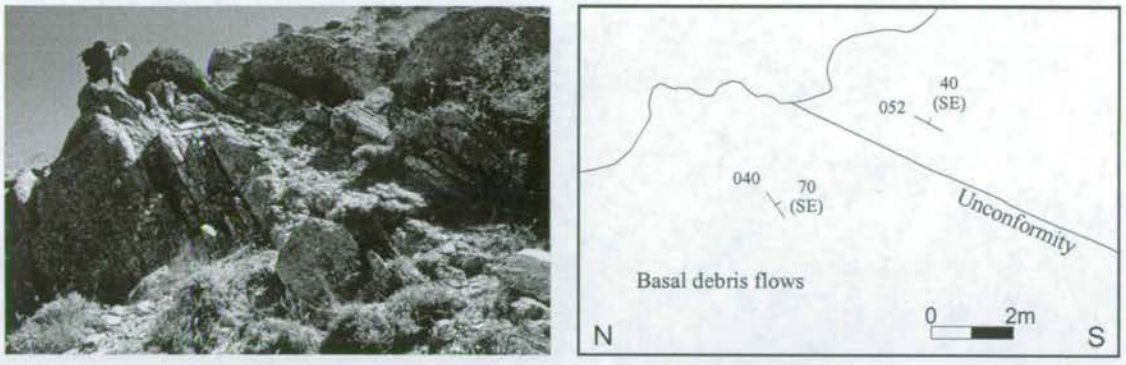

Figure 4.3 Sketch of angular unconformity within the Kaleboynu Formation at Evliya Tepe (location Fig. 4.1). Right hand sketch picks out angular discordance between basal debris flow deposits and upper marine sediments.

conglomerates mark the start of the succession, containing angular pebble to cobble sized clasts, composed of quartz, schist and Nummulitic limestone. These conglomerates are interbedded with coarse to fine sandstones of similar composition, which contain unidirectional flute cast structures. In places the conglomerates are very angular and texturally immature, incorporating complete and fragmented *Nummulites*. This conglomeratic facies passes upwards into flaggy, fine-grained sandstones, which contain 2-3cm wide *Rhizocorallium*-type trace fossils (Fig. 4.4a) and slump structures.

34-52m

Sediments change rapidly up-section, to centimetre-scale interbedding of: (i) Well sorted, texturally mature, fine-grained arkosic sandstones with unidirectional cross bedding (Fig. 4.4b & c), (ii) Unfossiliferous dark grey marls and (iii) Dark grey *Nummulites*-bearing micritic limestones (Fig. 4.7a).

75-138m

This section comprises a continued interbedding of fine sandstones and mudstones, with an increasing abundance of burrow bioturbation and symmetrical ripple lamination up-section. The proportion of micritic limestone increases upwards until sandstones disappear altogether. Micritic limestone deposition is sporadically interrupted by thin

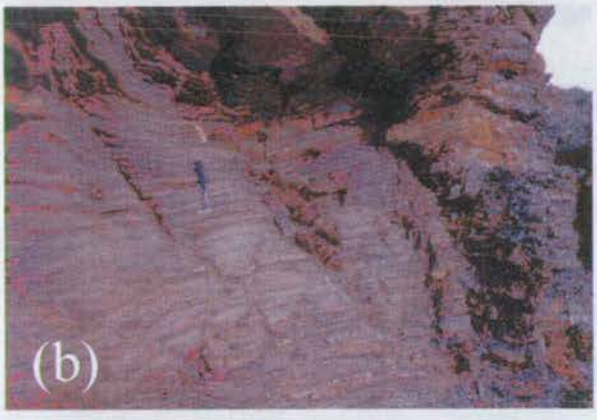

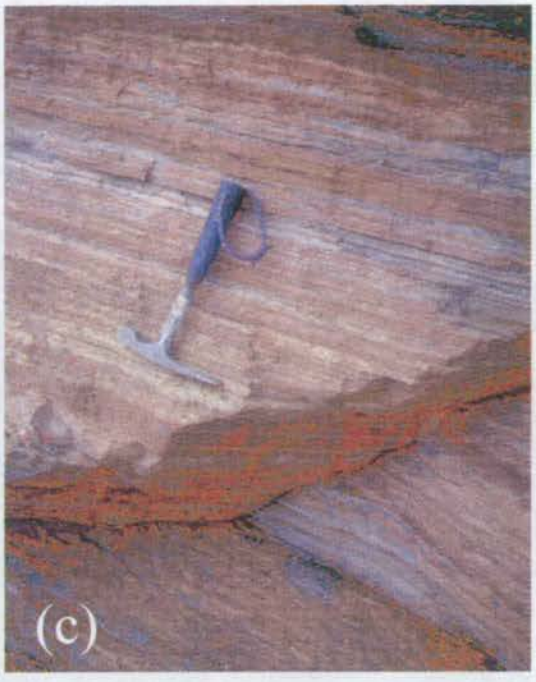

Figure 4.4 (a) Trace fossil on a bedding plane within the Kaleboynu Formation at Evliya Tepe (~100m on Evliya Tepe log, Fig. 4.2). The trace fossil resembles Rhizocorallium. (b) & (c) Cyclical sedimentation mid-way through the Evliya Tepe section. Interbedded fine grained sandstones, micritic limestones and siltstones. (d) Assemblage of benthic foraminifera within the Kaleboynu Formation at Kaleboynu Tepe (~96m on log, Fig. 4.6). (e) Matrix supported conglomerate at the top of the Kaleboynu Tepe section (~240m on Kaleboynu Tepe log, Fig. 4.6).

(2-5cm thick) schist-bearing gravel deposits with erosive bases, which scour into underlying limestones.

4.3.1.2 Kaleboynu Tepe

To the east of the Ecemiş Fault Zone at Kaleboynu Tepe there is another outcrop of Eocene rocks. Due to the emphasis placed on these two outcrops by Yetiş (1984) for dating the movement on the Ecemiş Fault Zone, this outcrop is also described. Figure 4.5 is a complete log of the succession at Kaleboynu Tepe.

Base-10m

The base of the section is marked by a 15-20^0 angular unconformity which brings Kaleboynu Formation rocks into contact with steeper dipping Mesozoic limestones beneath (Fig. 4.6). Basal sediments are massive, micritic limestones containing small (<1cm diameter) benthic and planktic foraminifers.

10-20m

The section is interrupted by a 20^0 angular unconformity (Fig. 4.6). Above this sandy limestones were deposited, containing large and abundant benthic foraminifera (Fig. 4.4d) including *Nummulites* and *Assilina*. These beds lack any evidence for current or wave activity.

110-200m

The next exposed unit comprises coarse, haematite-rich conglomerates, gravels and coarse-grained sandstones. The contact between this unit and the underlying limestones is not exposed. Conglomerate clasts are composed of serpentinised peridotite (65%), gabbro (20%), red chert (10%) and Nummulitic limestone (5%). Clasts are dominantly well rounded and matrix supported (Fig. 4.4e). Sediments are generally texturally

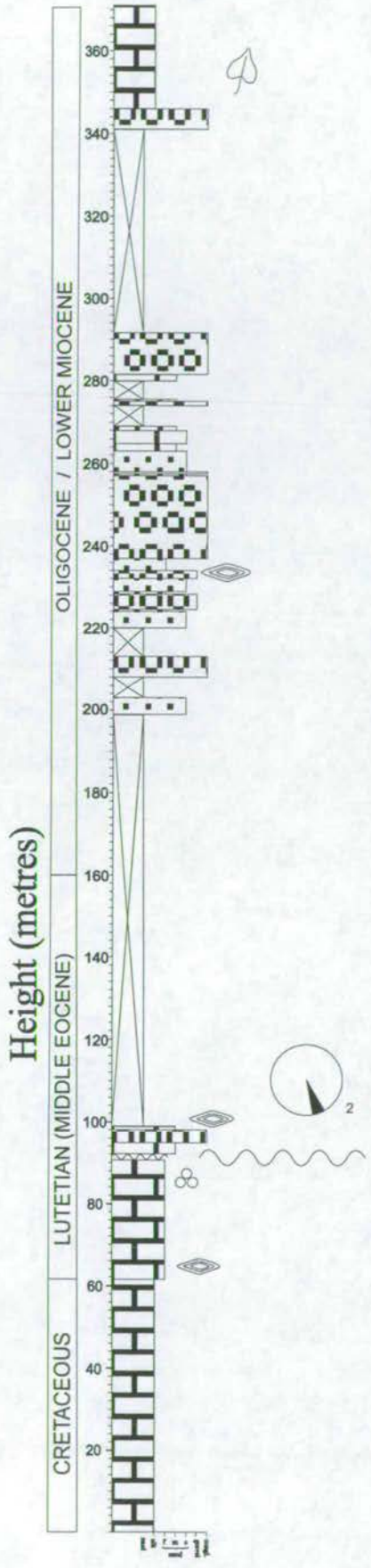

Figure 4.5 Stratigraphic log of the Kaleboynu Formation at Kaleboynu Tepe. See Fig. 4.2 for key to symbols, see Fig. 4.1 for location of section. Rose diagrams indicate palaeocurrent directions, subscript number indicates number of palaeocurrent data points.

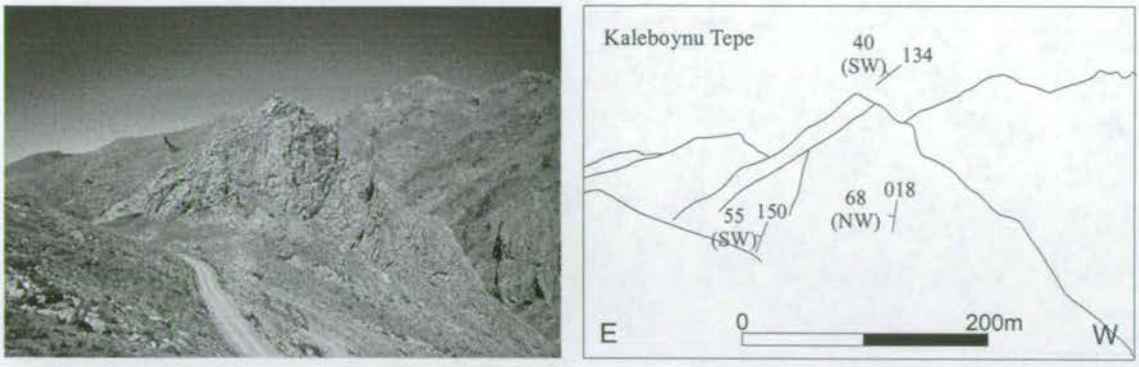

Figure 4.6 Sketch of Kaleboynu Tepe looking north (location Fig. 4.1). Right-hand sketch picks out two angular unconformities within the Eocene succession.

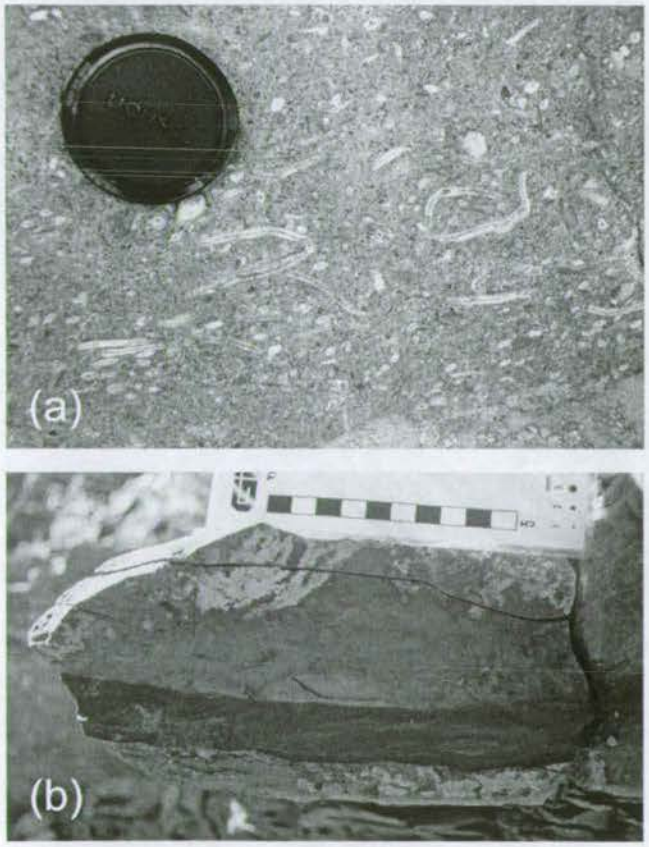

Figure 4.7 (a) Assemblage of benthic foraminifers within the Kaleboynu Formation at Evliya Tepe (~140m on log, Fig. 4.2). (b) Planar cross-bedding within the Kaleboynu Formation at Guney (~2.6m on log, Fig. 4.9).

immature, being poorly sorted (size range 1mm-15cm) with little internal structure. This unit may represent the base of the Oligo-Miocene Çukurbağ Formation.

4.3.1.3 Fauna

Benthic foraminifera identified within the Kaleboynu Formation include: *Nummulites, Assilina, Alveolina, Discocyclina, Asterogerina, Asterocyclina, Sphaerogypsina globosa, Gypsina, Lockhartia* and *Rotaliidae* (Fig. 4.7a, Yetiş 1978). The species *Assilina 'exponense', Nummulites pelfuratus and Nummulites stiatus* have been identified from the Kaleboynu Tepe exposure and are diagnostic of a Lutetian age and a shallow marine environment (N. Avsar, pers. com. 1997).

4.3.1.4 Palaeocurrents

Palaeocurrent indicators found in this formation include the avalanche face orientation of asymmetrical ripples and groove casts. Rose diagrams of palaeocurrent data (Fig. 4.8a), taken from the Evliya Tepe succession, show generally west-directed flow during the Eocene (with a component of N-directed flow). Palaeocurrent indicators from the Kaleboynu Tepe succession are rare, but indicate flow toward the SSE. Indicators there were more problematic, pebble imbrication being the only form available.

4.3.2 Age Equivalent Sediments; The Bozbeltepe Member, Ulukişla Basin

The stratigraphy and sedimentology of the Ulukişla Basin (2.2, Fig. 3.4) have been studied by Demirtaşli *et al.* (1984). They identified a succession of Lutetian age overlying the Eocene volcanogenic Ulukişla Formation. This is named the Bozbeltepe Member (stratigraphy table Fig. 3.4); the thickest succession is seen in the Guney village area, 10km N of Ulukişla (Fig. 4.1b).

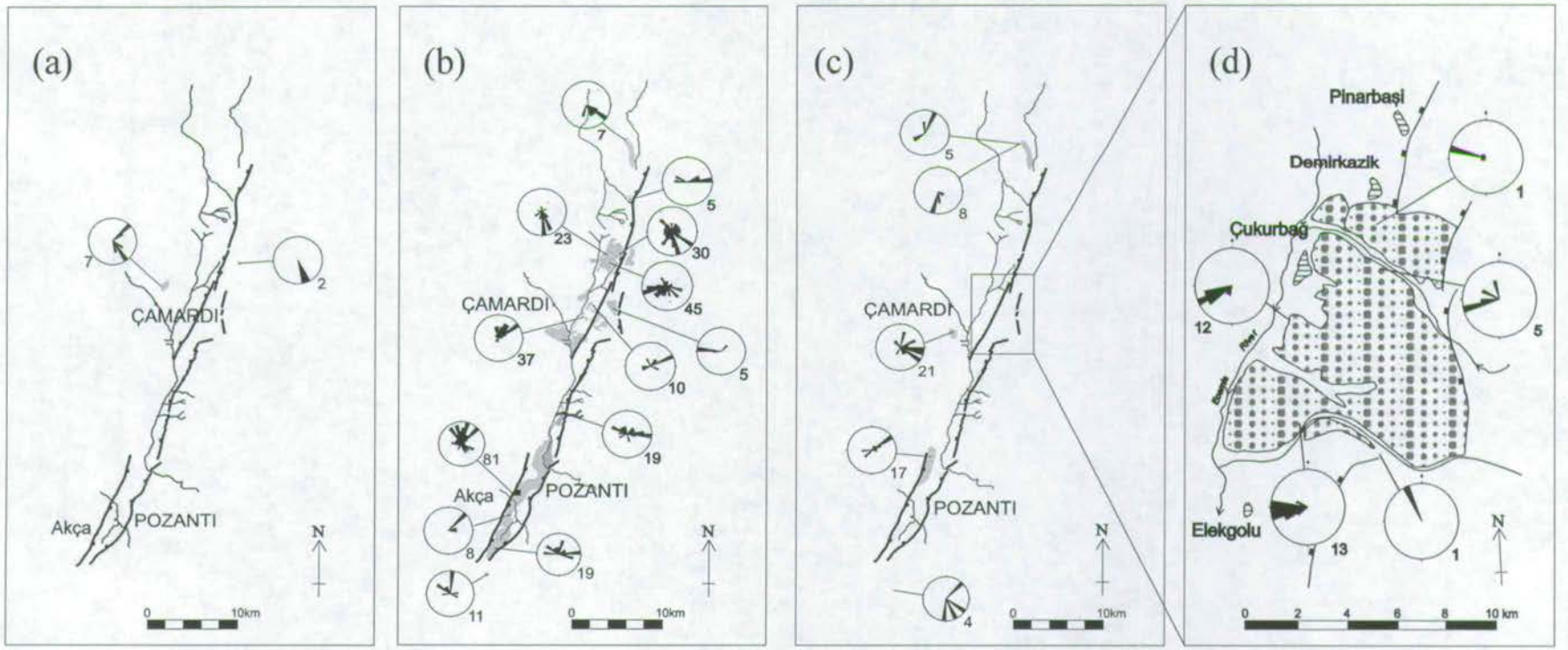

Figure 4.8 Palaeocurrent data for (a) the Middle Eocene Kaleboynu Formation, (b) the Oligo-Miocene Çukurbağ Formation, (c) the Late Miocene Burç Formation an (d) the Plio-Quaternary Çatalca Formation of the EFZ. Rose diagrams represent palaeocurrents, subscript numbers indicate number of palaeocurrent datapoints. Thick black lines represent faults, thin black lines represent rivers, grey shaded areas represent outcrop extent.

4.3.2.1 Composite Guney Section

The Guney section comprises four outcrops correlated to produce a composite section. These outcrops are seen on a N-S transect through the Guney area, 10km N of Ulukişla (Fig. 4.1b). These are the basal Caykavak section (6km NE of Ulukişla), the Yahyaoğlu section (7km NE of Ulukişla), the Yayla Tepe section (8km NNE of Ulukişla) and the uppermost Guney village section (9km NNE of Ulukişla). The total thickness of the succession was established by Demirtaşli *et al.* (1984) at 400m.

This unit is being studied in more detail by Matthew Clark (Edinburgh University PhD student) and, therefore, only a brief discussion is given here, for comparison with the Ecemiş Fault Zone Eocene succession. A representative log of the Guney village part of this composite section is shown in Fig. 4.9, but the entire composite section is described below:

Caykavak section (28m)

The basal contact is conformable, with iron-rich mudstones resting on basaltic pillow lavas of the Ulukişla Formation The basal sediments comprise matrix-supported gravels and conglomerates derived from the underlying basalts and volcaniclastic sandstones. Conglomerate clasts are angular and poorly sorted with a muddy or sandy matrix; they lack any coherent internal structure. Higher in the succession deposition changes to interbedded volcanogenic sandstones, mudstones and white tuffaceous beds.

Yahyaoglu section (13m)

This section comprises interbedded (2-3cm scale) micritic grey limestone, green marly siltstones and fine-grained, mica-rich, planar cross-bedded sandstones. Low-angle disconformities are seen between beds.

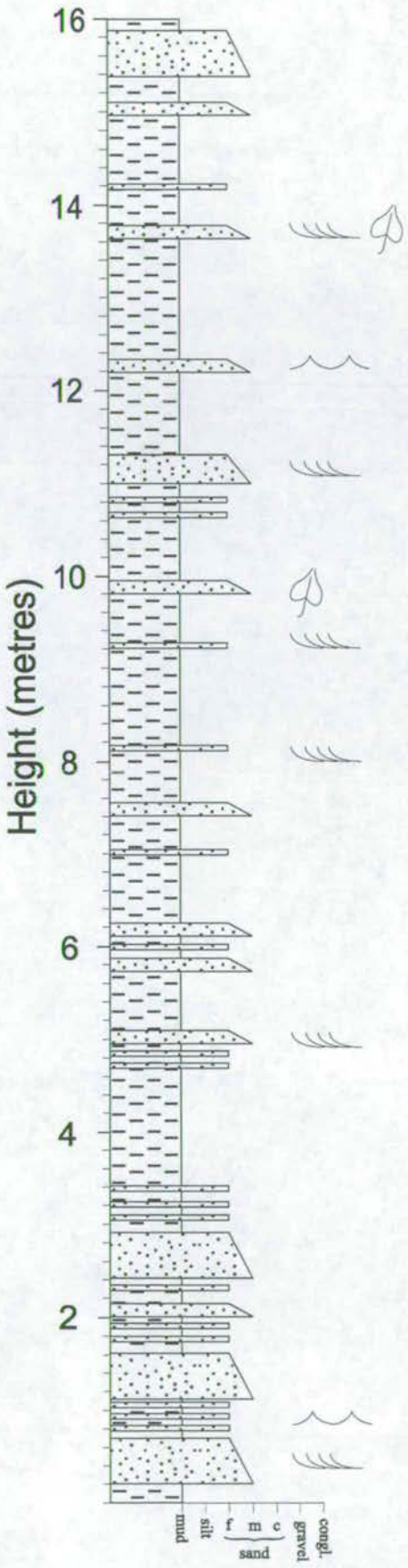

Figure 4.9 Stratigraphic log of the Kaleboynu Formation at Guney village. See Fig. 4.2 for key to symbols, see Fig. 4.1 for location.

Yayla Tepe section (6m)

Similar deposition continued with interbedded (2-10cm scale) brown, fine grained, feldspathic sandstones and dark grey mudstones. Grading is seen within the sandstones as well as large scale (20-30cm wavelength) symmetrical wave ripple marks, flute and groove marks. Mudstones are relatively organic rich.

Guney Village section (16m)

Deposition is dominated by organic-rich mud with interbeds of planar-cross-bedded, graded sandstones (2-10cm thick beds). Sandstones display symmetrical wave ripples, planar 'shooting flow' lamination (linear sedimentary structures on bedding planes which indicate very rapid, upper flow regimes), and plant debris. Sedimentation is cyclical, dividing into 4-5m packets with the following characteristics (Fig. 4.7b):

Base
10-40cm dark grey, organic-rich siltstones and mudstones
7-15cm Planar cross-bedded sandstones.
20-35cm Siltstones grading to mudstones upwards.
10-20cm Planar cross bedded, coarse to fine sandstones.
Top

4.3.2.2 Fauna

Demirtaşli *et al.* (1984) have identified several microfossil species from the Bozbeltepe Member, including the planktonic foraminifera *Globorotalia cf. centralis,* and the benthic foraminifera *Discocyclina sp. Gypsina mastalensis* and *Halkyardia sp.* which they have dated at Late Lutetian (Middle Eocene).

4.3.2.3 Palaeocurrents

Palaeoflow was measured at two localities using the orientation of avalanche faces on asymmetrical crossbedding in sandstones and (rare) groove marks (Fig. 4.10a). Results show that submarine flow was generally toward the north, away from the volcanic outcrops of the Ulukişla Formation.

4.3.3 Late Oligocene - Early Miocene Çukurbağ Formation

This Formation crops out widely within the Ecemiş Fault Zone (Fig. 4.11a). The thickest and best preserved deposits are found in the Pozanti-Alpu area (southern EFZ), in the Elekgölü-Çukurbağ area (central EFZ) and east of Bademdere village (northern EFZ, 15km NE of Çamardi, location Fig. 4.11a). Two reference sections have been chosen due to the lateral variation in facies along the fault zone; these are the Bademdere section (15km NE of Çamardi) and the Alpu section (2km N of Pozanti, location Fig. 4.11a).

4.3.3.1 Composite Bademdere Section

The composite Bademdere succession comprises three outcrops which can be laterally correlated along strike. These are the basal section at Testideresi Tepe (280m), the Kovali River section (128m) and the uppermost section at Bulanlik River (140m). These local sections are separated by areas of non exposure such that the total section thickness (calculated using trigonometry) is ~1000m. This thickness calculation should be considered a maximum, as measured beds are slightly folded (Change of $5\text{-}10^0$ through the succession). This is the thickest succession of Oligo-Miocene sediments outcropping in the Ecemiş Fault Zone. A log of the entire Badembere composite section is shown in Fig. 4.12. The composite section is described below:

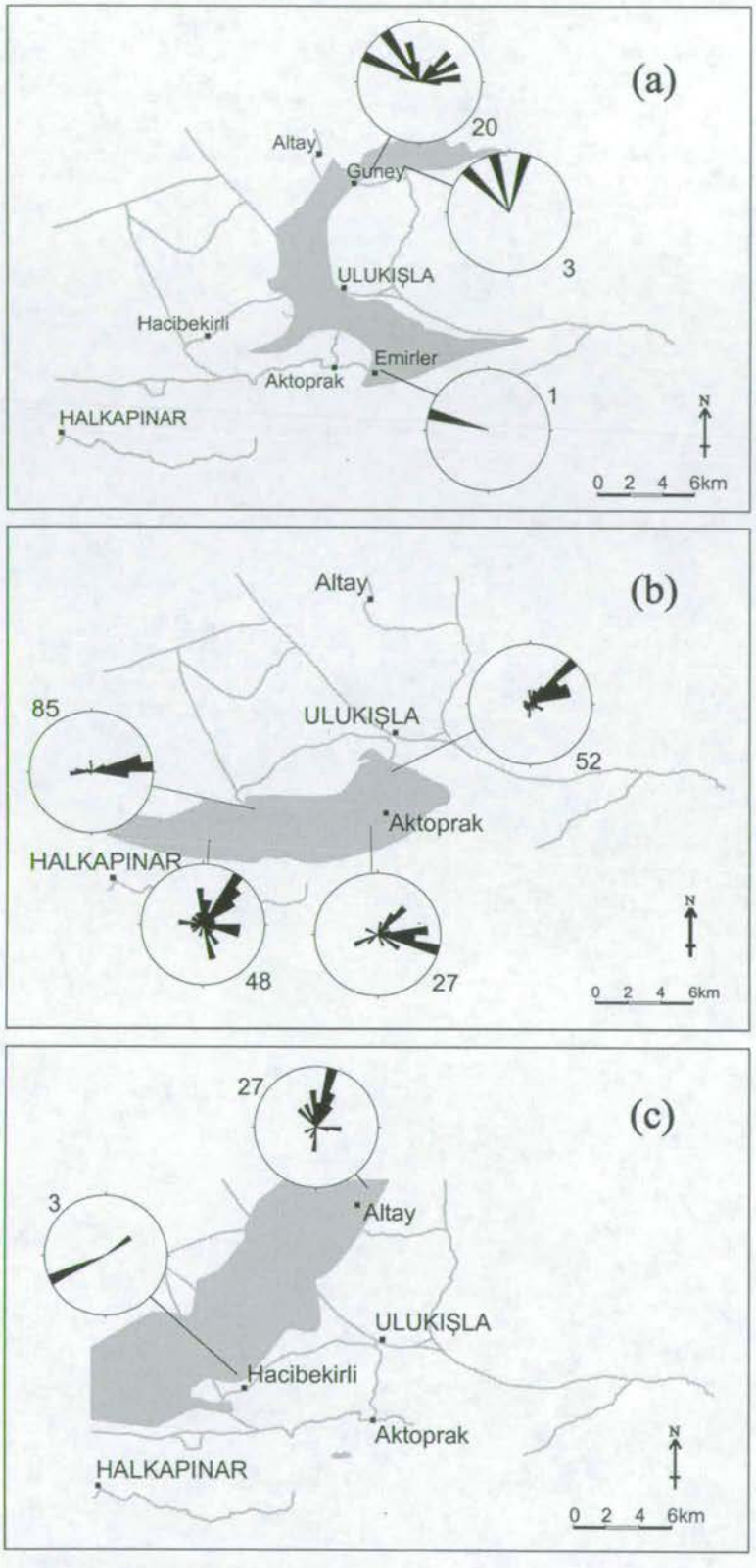

Figure 4.10 Palaeocurrent data for: (a) the Middle Eocene Kaleboynu Formation, (b) the Oligo-Miocene Çukurbağ Formation and (c) the Late Miocene Burç Formation of the Ulukişla Basin. Rose diagrams represent palaeocurrents, subscript numbers indicate number of palaeocurrent datapoints. Grey lines represent roads, grey shaded areas represent outcrop extent.

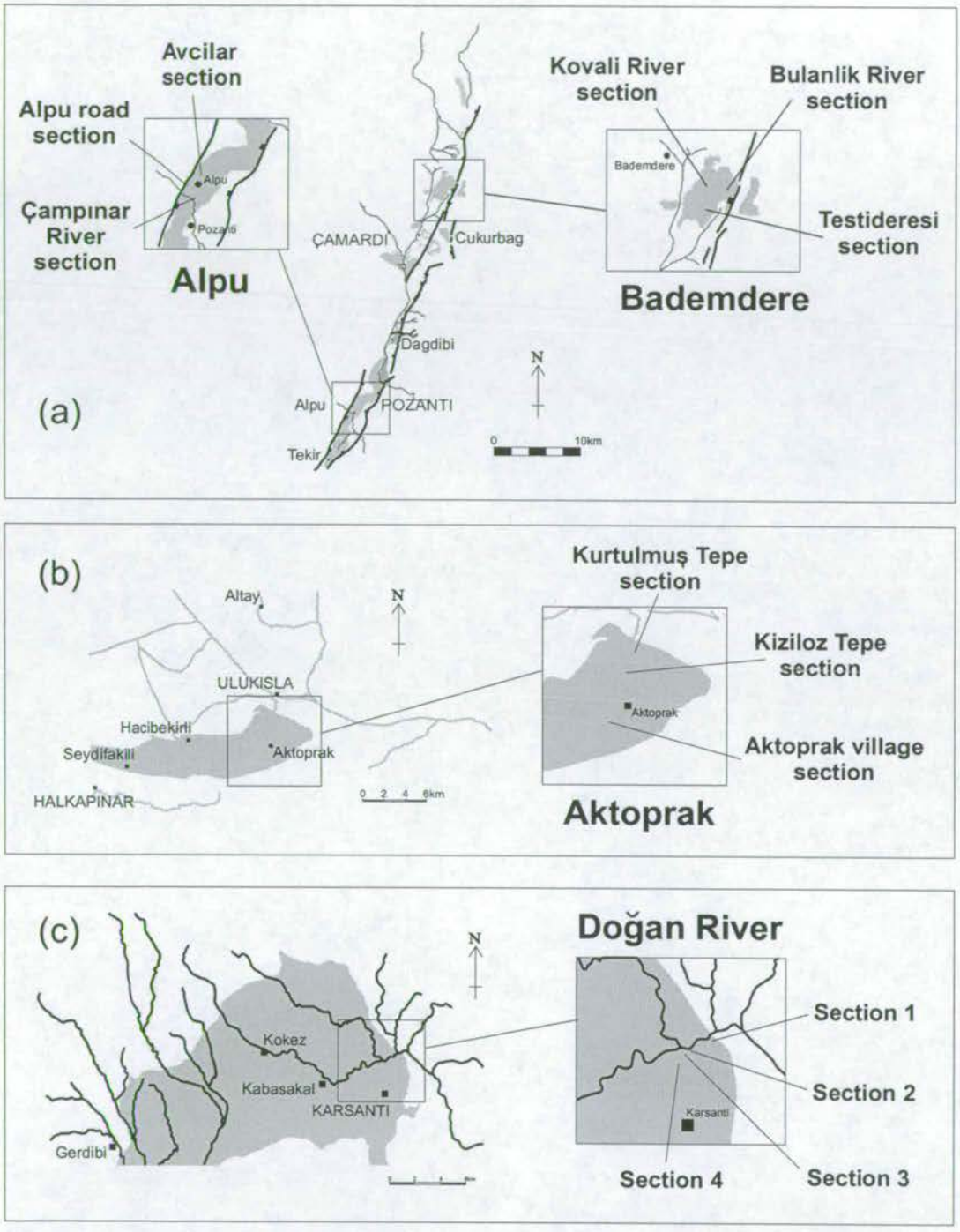

Figure 4.11 Location maps for logged sections in: (a) the Ecemiş Fault Zone, showing the composite Bademdere and Alpu sections and their component sections (b) the Ulukişla Basin, showing the composite Aktoprak section and its component sections, and (c) the Karsanti Basin, showing the composite Doğan River section and its component sections. See Fig. 2.4 for location of these basins. Thick black lines represent faults, thin black lines represent rivers, grey lines represent roads. Grey shaded areas represent outcrop extent of Oligo-Miocene rocks.

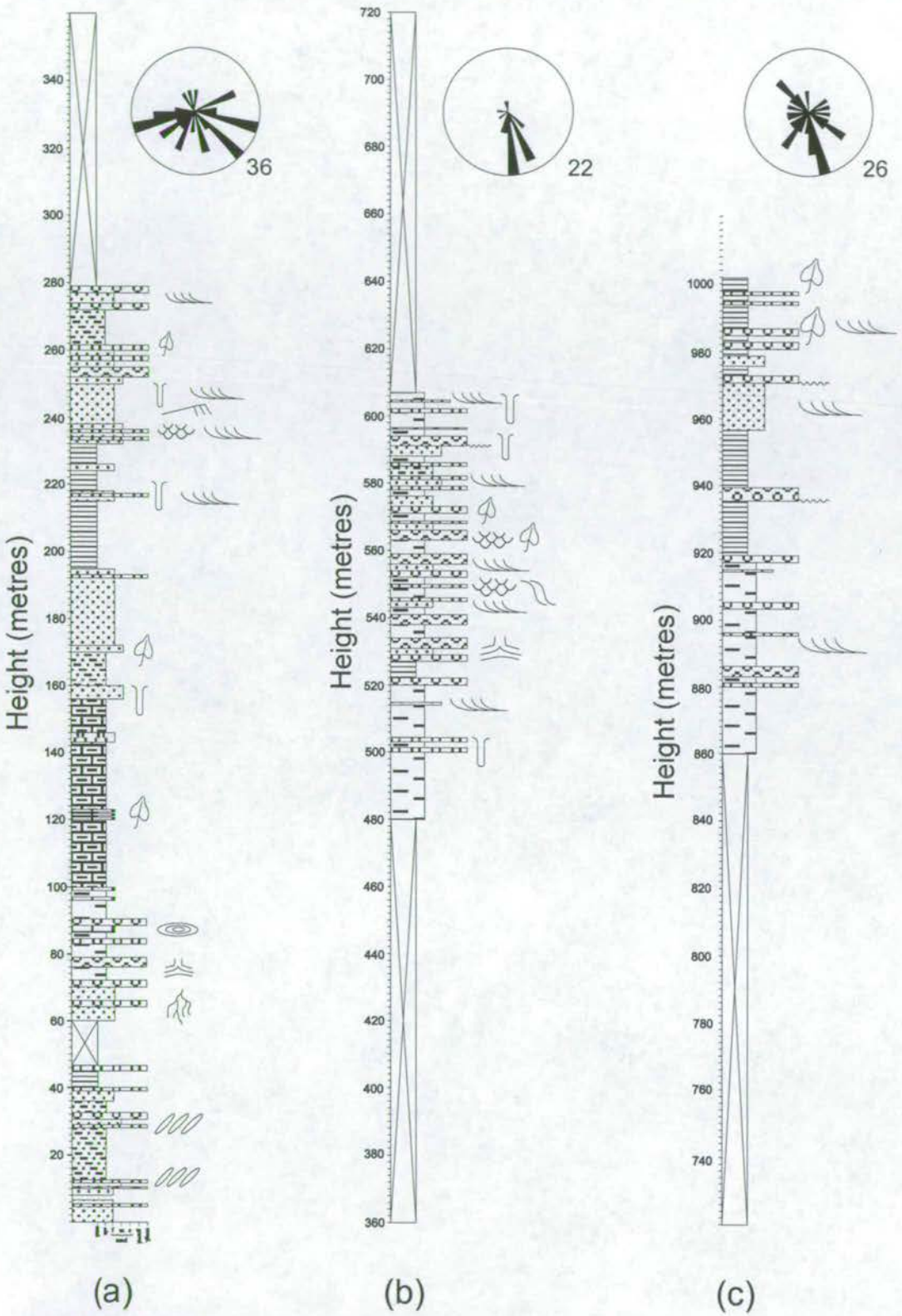

Figure 4.12 Stratigraphic log of the Çukurbağ Formation at Bademdere. This composite section comprises: (a) the lower Testideresi Tepe section, (b) the middle Kovali River section and (c) the upper Bulanlik River section. See Fig. 4.2 for key to symbols and Fig. 4.11 for locations of sections. Rose diagrams represent grouped palaeocurrent data for each section, subscripts indicate number of palaeocurrent datapoints.

Testideresi Tepe section (Base-280m)

The lowermost rocks comprise interbedded: (i) iron-rich marls (carbonate mud) containing root fossils, vertical burrows and spherical carbonate nodules and (ii) matrix-supported conglomerates containing well rounded and well-sorted clasts of limestone, which incise into underlying marls. 1-2m thick algal mats are seen above these beds, containing discontinuous algal lamination, encrusted plant stems and other plant debris. The algal mats pass upwards into interbedded (10-50cm-thick) calcareous mudstones, micritic limestones (containing leaf fossils) and silty, low grade coals. Overlying the coals is a 3-4m thick interval of mixed selenite gypsum and anhydrite breccia. The Selenite and anhydrite are brecciated into 3-5cm diameter laths; this brecciation appears to be depositional, as there are no collapse structures in overlying strata.

Above this evaporite layer the character of deposition changes to interbeds of:

(i) Well-sorted, texturally mature, red sandstones containing trough and planar cross-bedding. These sandstone bodies are thin (50cm-1m) and are laterally continuous over 20-30m (Fig. 4.13a).

(ii) 2-3m thick gravel and conglomerate bodies containing sub-rounded to angular clasts, with some angular blocks, as large as 80cm diameter. Conglomerates are often well imbricated (Fig. 4.13b) and are dominated by limestone clasts. These bodies are laterally confined to <10m and incise into underlying mudstones, their bases often bearing scour marks and groove casts.

(iii) Red marls and siltstones which contain leaf and root fossils.

Kovali River section (480-608m)

This outcrop is entirely comprised of interbeds of:

(i) Gravel and conglomerate bodies with a lensoid geometry (1-15m wide, 2-3m deep, Fig. 4.13c) and erosive bases which incise into underlying mudstones (Fig. 4.13d). Conglomerate clasts range from 1-20cm in diameter, are matrix-supported, well

Sheet-like braided fluvial sandstone bodies (Facies 2C) and channel-filling conglomerates (Facies 2B) within the Testideresi section.

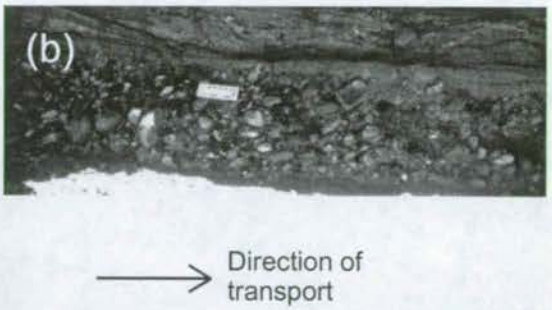

Imbrication in fluvial conglomerates within the Testideresi section (facies 2B).

Gravel and conglomerate bodies with lensoid geometries and erosive bases (Facies 2B), which incise into underlying mudstones. Kovali River section, Bademdere.

Erosive base to channel-filling conglomerate body (Facies 2B). Kovali River section, Bademdere.

Lensoid gravel and coarse sandstone bodies which incise into underlying mudstones (Facies 2C). Gravel bodies extend laterally over 10-30m and contain planar and trough-crossbedding.

Figure 4.13 Features of the Oligo-Miocene Çukurbağ Formation at Bademdere (Fig. 4.11 for location).

rounded and poorly sorted. Clasts are dominated by gabbro and basalt and are generally well imbricated in the direction of flow.

(ii) Less confined (2-50cm thick) sheet-like bodies of medium to coarse-grained sandstone, extending laterally up to 20m. Sandstones contain planar and restricted trough-crossbedding.

(iii) Iron stained, parallel laminated siltstones and calcareous mudstones containing leaf fossils, root fossils and vertical burrows. Slumping is common within the these beds, especially directly below the erosive bases of conglomerate bodies.

There is a general increase in the abundance and thickness of conglomerate units towards the top of the section.

Bulanlik River section (860-1000m)

The uppermost part of the Bademdere section displays similar facies to the Kovali section with interbeds of:

(i) Lensoid (0.5-1m thick) gravel and coarse sandstone bodies which incise into underlying mudstones (Fig. 4.13e). Gravel bodies extend laterally over 10-30m and contain planar and trough-crossbedding. Clasts are matrix-supported and are dominated by limestone.

(ii) Iron-rich laminated siltstones and calcareous mudstones containing root fossils, leaf fossils and slump structures.

This section contains a greater proportion of mud and a lower proportion of conglomerate than the underlying sections.

4.3.3.2 Composite Alpu Section

The composite Alpu section comprises three outcrops which can be seen on the road between Alpu and Pozanti (Fig. 4.11a). These are the basal Campinar River section (1.5km S of Alpu village), the Alpu roadcut section and the Avcilar section (3km NE of Alpu village). These sections are separated by areas of no exposure such that the total section thickness (calculated using trigonometry) is ~800m. Again, this is a maximum estimate due to the minor folding of the succession in this area (5-10^0 change in bedding

angle). A complete log of the Alpu section is shown in Fig. 4.14, and is described below.

Campinar River section (Base-140m)

This basal section is dominated by coarse (0.5-7cm diameter) conglomerates and gravels with clast-supported, poorly sorted, well-rounded clasts. Conglomerate bodies are vertically stacked, incise into one-another and are laterally continuous for up to 50m (Fig. 4.15a & b). Conglomerate bodies are often vertically separated by coarse sandstones which display slump structures, planar and trough cross bedding and rare desiccation cracks. This is the coarsest facies of the Oligo-Miocene Çukurbağ Formation seen within the Ecemiş Fault Zone.

Alpu Road section (240-340m)

This section is marked by a decrease in the proportion of conglomerate, with lensoid conglomerate bodies (up to 9m thick) separated by sandstone and mudstone deposition. Sand bodies have a sheet-like geometry (10-50cm thick) and are laterally continuous over 30-40m.

Avcilar section (370-580m)

The basal third of this section is characterised by interbeds of:

(i) Coarse trough-cross-bedded and planar-cross-bedded sandstone bodies, which are generally thin (under 50cm thickness) and laterally continuous over 5-10m.

(ii) Lensoid gravel and conglomerate bodies with erosive bases (Fig. 4.15c) outcrop every 6-8m vertically through the section. Conglomerate bodies are thinner than in the previous sections with a greater proportion of sand and siltstones. Gravel and conglomerate bodies are continuous over 10-20m and interfinger laterally with coarse sandstones (Fig. 4.15d).

(iii) Grey, fine-grained silty sandstone. These contain slump structures and root fossils.

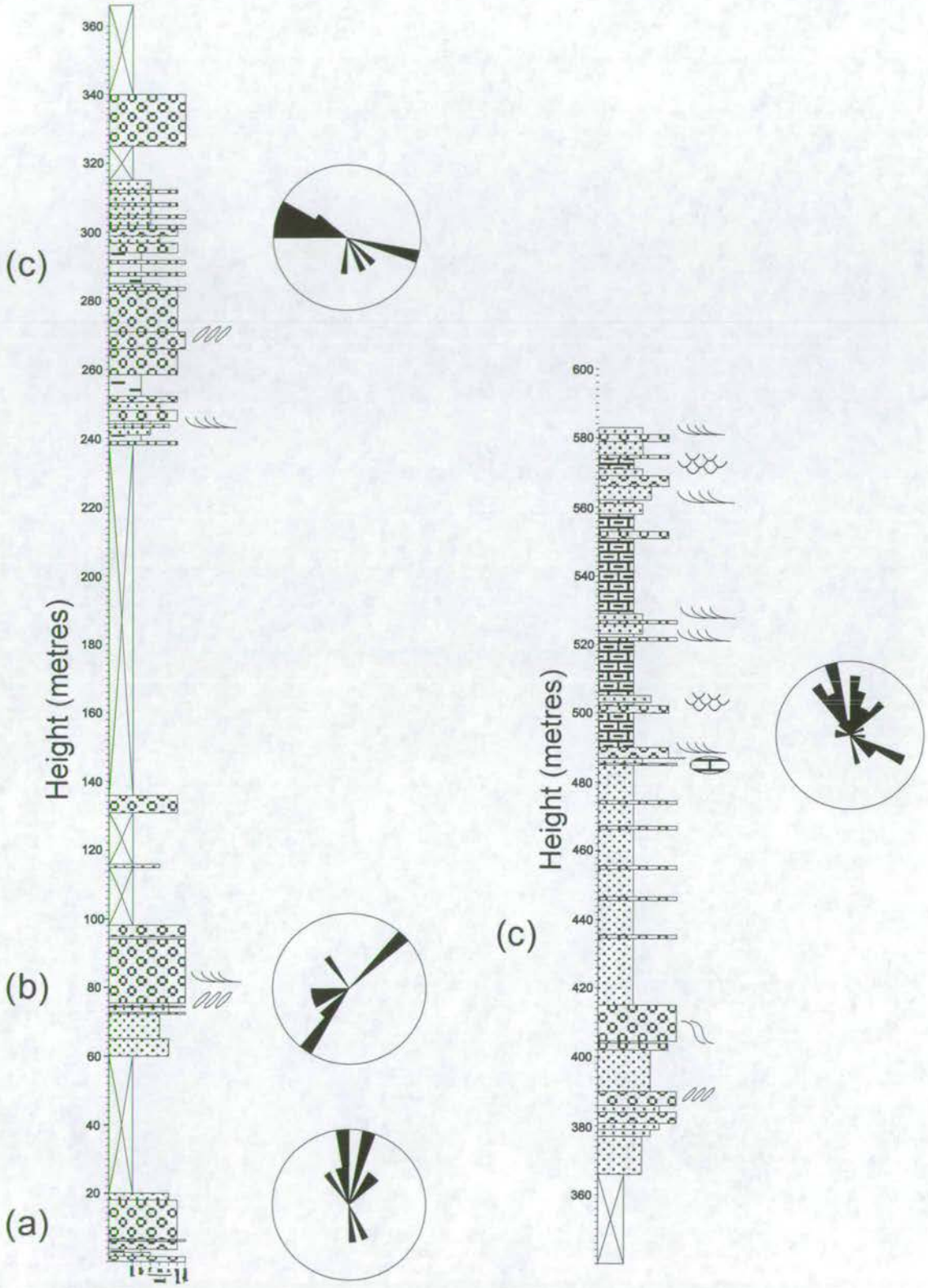

Figure 4.14 Stratigraphic log of the Çukurbağ Formation at Alpu. This composite section comprises: (a) the lower Çampinar River section, (b) the middle Alpu road section and (c) the upper Avcilar section. See Fig. 4.2 for key to symbols and Fig. 4.11 for locations of sections. Rose diagrams represent grouped palaeocurrent data for each section.

Conglomerate bodies are vertically stacked, incise into one-another and are laterally continuous for up to 50m (Facies 2C). Campinar section, Alpu.

Lensoid gravel and conglomerate bodies with erosive bases (Facies 2C). Avcilar section, Alpu.

Gravel and conglomerate bodies (Facies 2C) laterally interfinger with coarse sandstones (Facies 2B). Avcilar section, Alpu.

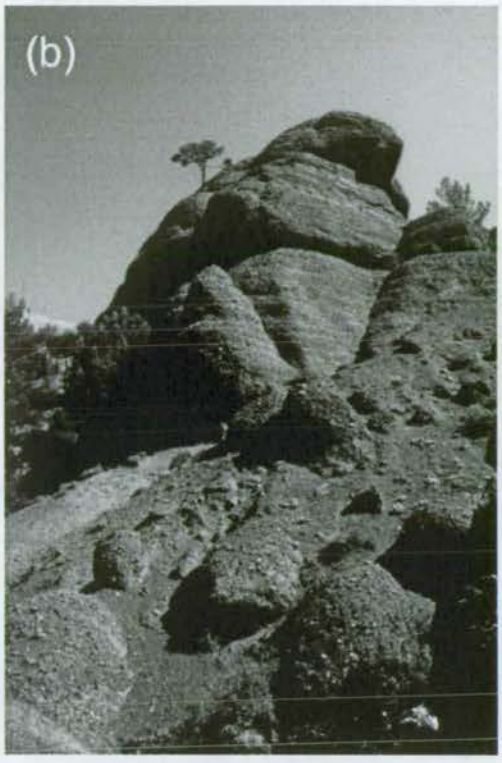

Conglomerate bodies are vertically stacked, incise into one-another and are laterally continuous for up to 50m (Facies 2C). Campinar section, Alpu.

Figure 4.15 Features of the Oligo-Miocene Cukurbag Formation at Alpu (Fig. 4.11 for location).

4.3.3.3 Flora and Fauna

No fauna have been found within the barren terrestrial Çukurbağ Formation. Leaf fossils are pervasive throughout the succession, preserved in siltstone and mudstone units. These have a long, blade-like shape similar to the modern-day willow. These plant fossils may have future potential for dating.

4.3.3.4 Palaeocurrents

Abundant asymmetrical ripple lamination, planar and trough cross-bedding and groove marks in the sandstone units of the Çukurbağ Formation allow the collection of accurate and abundant palaeocurrent data. Palaeocurrent indicators used include the orientation of the avalanche faces of planar cross beds, groove marks and pebble imbrication. Palaeocurrent data from all of the outcrops of the Oligo-Miocene Çukurbağ Formation (Fig. 4.8b) reveals the following trends: In the south of the EFZ (Gülek to Pozanti) flow was generally toward the north. In the central area (Dagdibi) palaeoflow was from the east and west. In the Çamardi area palaeoflow appears to have been inwards towards a depocentre in the Çukurbağ-Bademdere area. Palaeoflow in the north of the area (Hacibeyli) was south to southeast-directed. This palaeocurrent pattern is interpreted as a large inward draining, closed basin with palaeo-highs to the south, north, east and west of the present-day Ecemiş Fault Zone, and depocentres in the Dagdibi and Bademdere areas (Fig. 4.8b). The exact morphology of the palaeo-basin (i.e. the orientation of the basin axis) cannot be easily constrained as much of the Çukurbağ Formation has been uplifted and removed by the present-day fault scarps of the EFZ.

Vertical variation in palaeocurrents at both Bademdere and Alpu (Fig. 4.12 & 4.14) indicate that palaeoflow direction remains roughly similar throughout the Çukurbağ Formation. The Bademdere succession maintains a consistent south directed palaeoflow and the Alpu succession a north directed palaeoflow.

4.3.4 Age Equivalent Sediments; The Oligo-Miocene Aktoprak Basin, Ulukişla

The stratigraphy and sedimentology of the Ulukişla Basin (Location Fig. 2.4) have been studied by Demirtaşli *et al.* (1984) and Oktay (1982). In both studies a succession of Oligocene to Early Miocene terrestrial red beds was recognised. This unconformably overlies the intensely deformed Early Tertiary volcanic and volcaniclastic succession of the Ulukişla Basin and is unconformably overlain by a Late Miocene succession. The Oligo-Miocene unit was named the Aktoprak basin (Demirtaşli *et al.* 1984) and has a minimum E-W extent of 34km and a minimum N-S extent of 5-8km (present outcrop extent). The thickest succession is seen on a N-S transect through Aktoprak village in the east of the basin (Fig. 4.11b). In contrast to the EFZ faulting of the succession is minimal, allowing more effective lateral correlation and estimation of thickness.

4.3.4.1 The Composite Aktoprak Section

The composite Aktoprak section comprises three outcrops which can be seen on the road between Ulukişla and Aktoprak (Fig. 4.11b). These are the basal Kurtulmus Tepe section (3km S of Ulukişla), the Kiziloz Tepe section (5km S of Ulukişla) and the Aktoprak Village section (1km SW of Aktoprak village, Fig. 4.11b). These three exposures are separated by areas of no exposure such that the total section thickness (calculated by trigonometry) is ~900m. A complete log of the Aktoprak composite section is shown in Fig. 4.16.

Kurtulmus Tepe section (Base-450m)

The section rests unconformably on the highly deformed and brecciated Kabak Tepe evaporitic Formation (Fig. 3.4, Demirtaşli *et al.* 1984). The section begins with a thick (~300m) succession of interbedded (50-70cm interbeds):

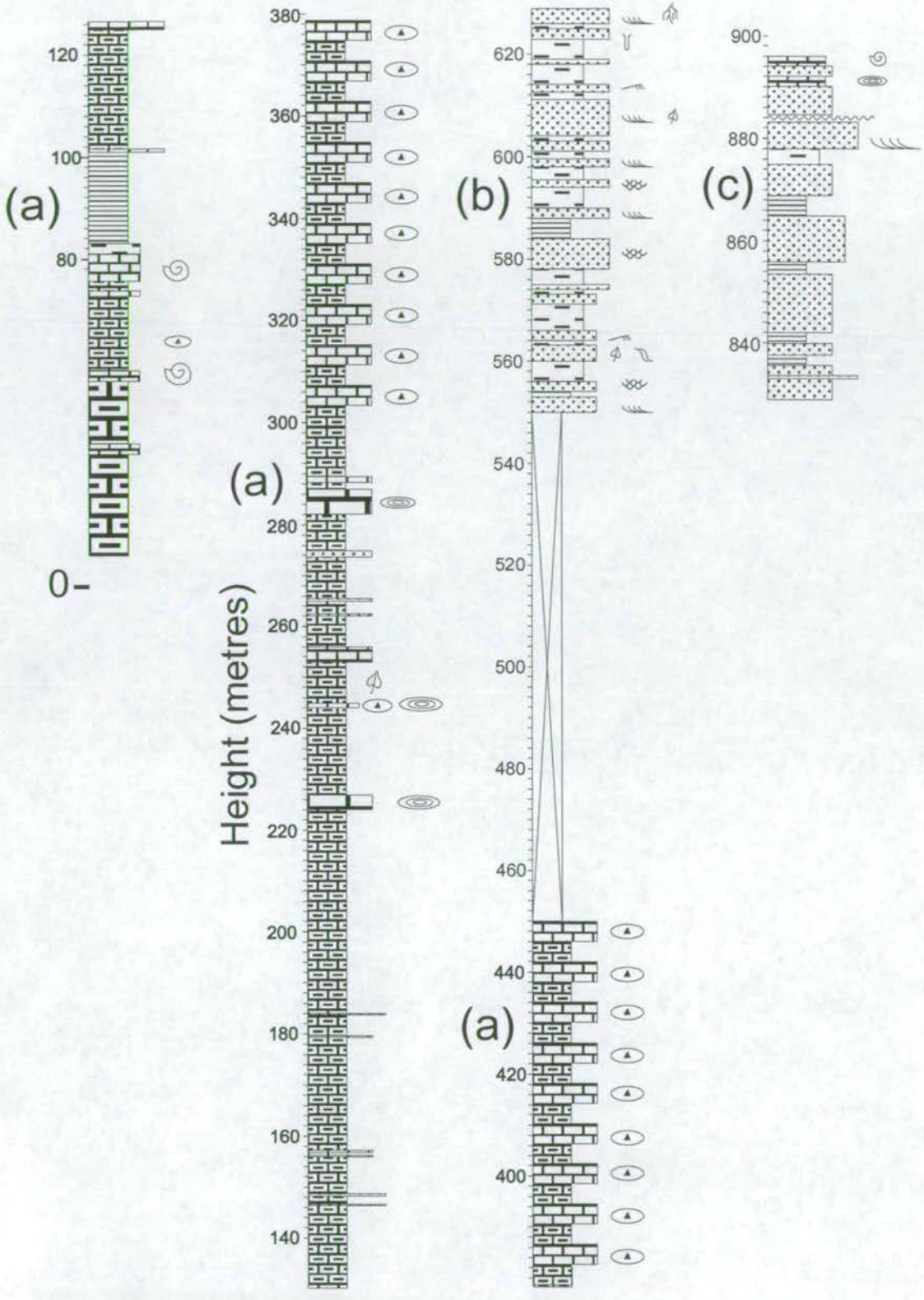

Figure 4.16 Stratigraphic log of the Çukurbağ Formation at Aktoprak (Ulukişla Basin). This composite section comprises: (a) the lower Kurtulmuş section, (b) the middle Kiziloz Tepe section and (c) the upper Aktoprak village section (see Fig. 11b for locations, see Fig. 4.2 for key to symbols).

(i) Light coloured, finely laminated marl (calcareous mudstone) containing rare gastropod shells and broken leaf fossils. Light and dark coloured laminations resemble varve deposits.

(ii) Thin (up to 1m thick) finely laminated, chalky limestones, rich in gastropods and ostracods, also containing wave ripple lamination.

The upper 150m of the section is characterised by an increase in the proportion of limestone. Limestone beds become thicker (up to 2m) and chert nodules (Fig. 4.17a) and stromatolitic beds (Fig. 4.17b) become common. The best preserved ostracod assemblages are found within the upper part of the section. A transition to sandstone deposition is seen at the very top of the section.

Kiziloz Tepe section (550-630m)

This section comprises (2-3m thick) interbeds of:

(i) Haematite-rich, coarse, tabular sandstone bodies (1-2m thick) extending laterally for 30-40m and lensoid bodies (confined laterally to 1-2m) which incise into underlying mudstones and siltstones. These sandstone bodies contain planar and trough cross-bedding (Fig. 4.17c & d), basal groove marks and mudstone rip-up clasts. 'Shooting flow' lineation was also observed on bedding planes.

(ii) Haematite-rich, laminated calcareous siltstones and mustones containing plant debris, root fossils, water-escape and slump structures.

Aktoprak Village section (830-900m)

This section displays similar (20-40cm thick) interbeds of:

(i) Medium – fine-grained tabular sandstone bodies, which exhibit planar and trough-crossbedding. Sand bodies are thinner and less coarse than at Kiziloz Tepe. Towards the top of the section lunate ripples are observed within the sand bodies.

(ii) Laminated mudstones and siltstones containing plant fossils, water escape structures, slump structures and vertical burrows.

Secondary chert nodules, replacing stromatolites in limestones (Facies 2G) of the the Kurtulmuş section, Aktoprak.

Stromatolitic beds within limestones (Facies 2G) of the Kurtulmuş section, Aktoprak. One metre staff for scale.

Trough cross-bedding within braided river sandstones (Facies 2B) in the Kiziloz Tepe section, Aktoprak. Palaeoflow was perpendicular to the photograph.

Planar cross-bedding within braided river sandstones (Facies 2B) in the Kiziloz Tepe section, Aktoprak. Palaeoflow was from left to right.

Figure 4.17 Features of the Oligo-Miocene Çukurbağ Formation at Aktoprak, Ulukişla Basin (Fig. 4.11 for location).

4.3.4.2 Flora and Fauna

Gastropod fauna collected from the Kurtulmus Tepe section are dated as Chattian (Late Oligocene) to Aquitanian (Earliest Miocene) by Blumenthal (1956). More recently, freshwater Ostracod assemblages from the Kurtulmus Tepe section were identified and dated as Aquitanian (Earliest Miocene) by Nazik & Gokcen (1992). As discussed in section 3.2.2, these ages are open to question, as the assemblages may also be of Late Oligocene age. Plant fossils are fragmented have not been investigated for dating purposes.

4.3.4.3 Palaeocurrents

Palaeoflow was measured at four sections in the Aktoprak Basin (Fig. 4.10b) principally using the orientation of avalanche faces on planar cross-bedding. Flow was consistently towards the E and NE in all outcrops.

4.3.5 Age Equivalent sediments; The Oligocene Karsanti Basin

The stratigraphy and sedimentology of the Karsanti Basin (Fig. 2.4) were studied by Ünlügenç *et al.* (1983). They described a succession of Oligocene sediments, unconformably overlying the Pozanti-Karsanti ophiolite and unconformably overlain by an Early Miocene succession above. During this study additional logging was carried out to test for any similarity with the Çukurbağ Formation of the EFZ and to assess regional facies trends. The Karsanti Basin has a minimum E-W extent of 20-25km and a minimum N-S extent of 13-16km (present outcrop). The thickest succession is seen at the Doğan River type section, 2.5km N of Karsanti (also known as Aladağ, Fig. 4.11c).

4.3.5.1 The Composite Doğan River Section

The composite Doğan River section comprises four outcrops which can be seen on the road between the Doğan River and Karsanti town (Fig. 4.11c). These are section 1 (at the bridge over the Doğan River, 2.5km N of Karsanti), the section 2 (on the southern bank of the Doğan River, 2km NNW of Karsanti), the section 3 (on the steep road from Karsanti town to the Doğan River, 1.5km NNW of Karsanti) and section 4 (at Karsanti town). These four exposures are separated by areas of no exposure such that the total section thickness (calculated by trigonometry) is ~360m. This method is valid as the Karsanti succession has suffered only minimal folding and faulting. A log of the Doğan River composite section is shown in Fig. 4.18.

Section 1 (Base-186m)

The succession lies unconformably on the Cretaceous Pozanti-Karsanti Ophiolite and begins with ~150m of interbedded conglomerate and gravel bodies and red, sandy siltstones. Conglomerate bodies are tabular and laterally continuous over at least 20-30m (Fig. 4.19d). Conglomerate clasts are initially poorly sorted and supported by a muddy matrix (Fig. 4.19a), but up succession they become better sorted and clast supported. The lower part of the section displays multiple internal angular discordances. In the upper part of the section the geometry of the conglomerate bodies changes to discrete, conglomerate-filled lenses (2-5m wide, 1-2m thick) which incise into red mudstones which outcrop alongside.

Higher in the section the conglomerates sequentially give way to: (i) organic-rich sandstones, bearing basal groove marks (Fig. 4.19e) (ii) a discontinuous low reflectivity coal seam, (iii) micritic limestone rich in plant fossil debris and Gastropods and (iv) Gastropod-rich micritic limestone without plant debris (Fig. 4.19f).

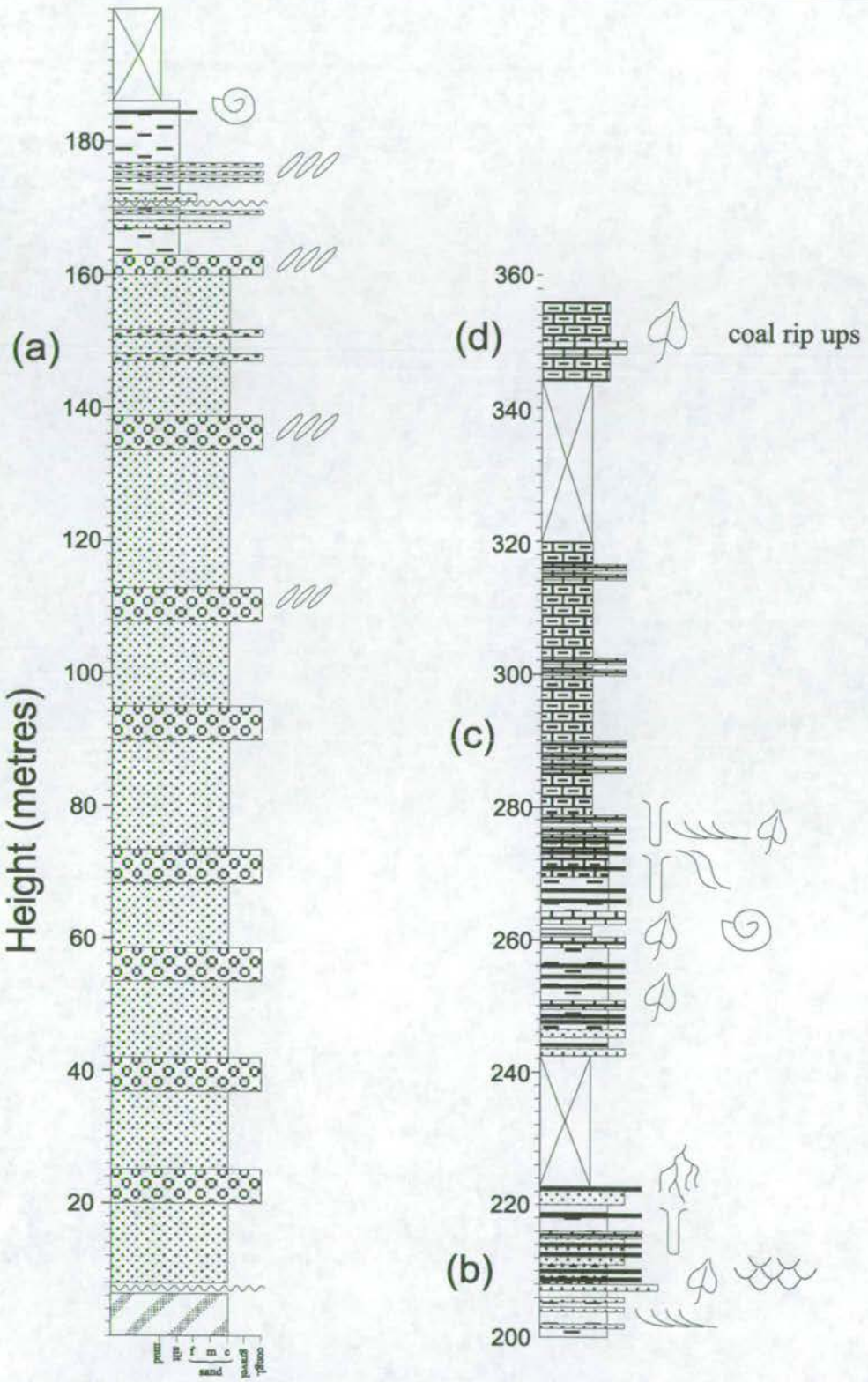

Figure 4.18 Stratigraphic log of the Çukurbağ Formation (Karsanti Formation of Ünlügenç *et al.* 1993) at Doğan River, Karsanti. This composite section comprises **(a)** the lower Section 1 at the bridge over Doğan River, **(b)** Section 2 on the southern bank of Doğan River, **(c)** Section 3 and **(d)** Section 4 on the road between Doğan River and Karsanti. See Fig. 4.2 for key to symbols and Fig. 4.11c for location of sections.

Poorly sorted, matrix-supported conglomerate clasts within continental debris flow deposits (Facies 2H). Section 1, Doğan River section,

Calcareous septarian nodules within floodplain siltstones (Facies 2A). Section 4, Doğan River section.

Calcareous concretions, replacing fossil root systems within floodplain siltstones (Facies 2A). Section 4, Doğan River section.

Tabular conglomerate bodies, part of the basal debris flow unit (Facies 2H). Section 1, Doğan River section.

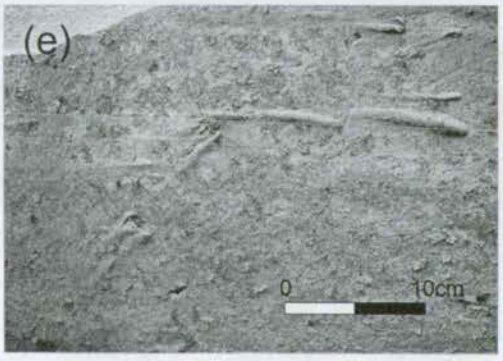

Basal groove marks in braided river sandstones (Facies 2B), Section 1, Doğan River section.

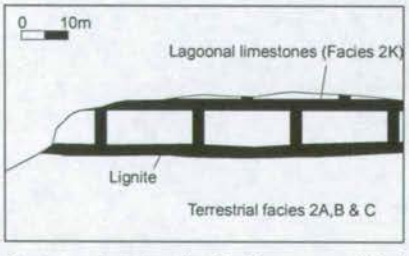

Gastropod-rich, micritic limestones (Facies 2K) and underlying lignite seam (Facies 2J). Section 1, Doğan River section.

Figure 4.19 Features of the Oligo-Miocene Çukrbağ Formation (Karsanti Formation of Ünlügenç *et al.* 1993) at Doğan River, Karsanti Basin (see Fig. 4.11 for location).

Section 2 (200-220m)

This section comprises 1m-thick interbeds of:

(i) Lensoid-shaped, fine-grained sandstone bodies containing planar and trough-cross-bedding.

(ii) Thin (<50cm) Gastropod-bearing, bioturbated micritic limestones, which are laterally continuous over large distances (>50m).

(iii) Organic-rich mudstones containing vertical burrows, root fossils and other plant fragments.

Section 3 (242-320m)

This section (>20m) comprises interbedded micritic limestones and organic-rich mudstones (20-30cm scale interbeds). Limestones are laterally continuous over the scale of the outcrop (>50m) and contain abundant leaf fossils (often very well preserved, see following section), ostracod assemblages and horizontal burrow marks. Limestones are interbedded with well laminated sediments which consist of a (thicker) silt layer followed by a (thinner) organic-rich mud layer, in cyclical repetition (1-2cm scale).

Section 4 (345-360m)

This section is characterised by deposition of rhythmite mudstones, interbedded with thin micritic limestones. Well preserved plant fossils are abundant (described below in Section 4.3.5.2). The uppermost part of the succession is marked by a return to dominance by sandstone and gravel bodies. These contain septarian calcareous nodules (Fig. 4.19b) and fossil root systems which have become the focus for calcareous concretion during diagenesis (Fig. 4.19c).

4.3.5.2 Flora and Fauna

Ünlügenç *et al.* (1993) identify several species of marine ostracods and planktic foraminifers and date them as Oligocene. These are listed in Fig. 3.3c.

Two types of fossil leaf were documented from Section 3:

(1) A long (20-30cm) and thin (<1cm) leaf resembling that of the modern day willow (*Salix sp.* various, Fig. 4.21a). This has multiple (~10) veins running parallel to the sides of the leaf.

(2) A smaller leaf (5cm by 2cm) resembling that from the modern day Birch (*Betula sp.*, Fig. 4.21b). Veins bifurcate from a central canal to form the common V pattern.

4.3.5.3 Palaeocurrents

Palaeoflow was measured at seven sections in the Karsanti Basin (Fig. 4.20), using the orientation of avalanche faces on planar cross-bedding and the imbrication of the long axis of pebbles in conglomeratic beds. Results show that the Karsanti Basin was an inward-draining basin during the Oligocene.

4.3.6 Upper Miocene Burç Formation

This unit has a restricted outcrop within the Ecemiş Fault Zone. The thickest and best preserved deposits are found at Burç (central EFZ, 5km S of Çamardi, Fig. 4.22a). There are also substantial Late Miocene deposits at Kamişli, Akca and Gülek, further south within the EFZ (Fig. 4.22a). Two reference sections are described here in order to illustrate lateral facies changes: the 140m-thick Burç section (1km SE of Burç village in the centre-north of the EFZ) and the 490m-thick Gülek section (at Gülek town in the south of the EFZ, Fig. 4.22a).

4.3.6.1 The Burç Section

A log of the Burç succession is shown in Fig. 4.23. An angular unconformity of 30^0 is seen at the base of the succession at its contact with the Çukurbağ Formation (Fig. 4.24). The basal part of the section is characterised by interbedded (0.5-1m scale)

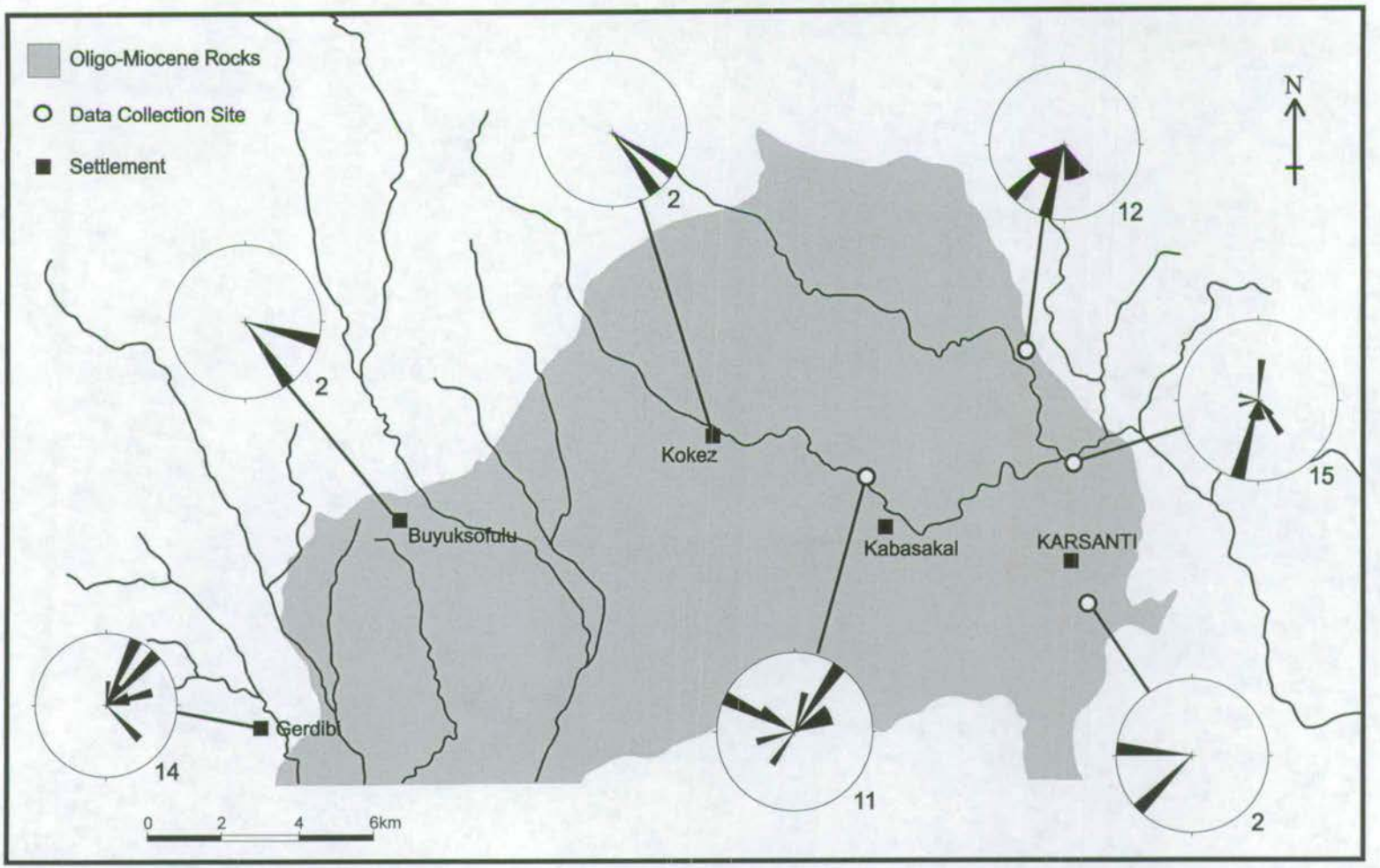

Figure 4.20 Palaeocurrent data for the Oligo-Miocene Çukurbağ Formation (Karsanti Formation of Ünlügenç *et al.* 1993) of the Karsanti Basin. Rose diagrams represent palaeocurrent directions, subscript numbers indicate number of palaeocurrent datapoints. Black lines represent rivers.

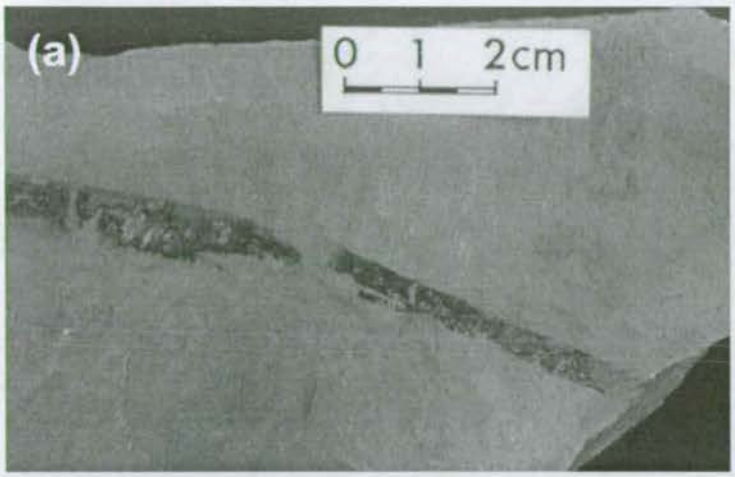

Figure 4.21a A long (20-30cm) and thin (<1cm) leaf fossil, resembling that of the modern day Spider plant or Bullrush. Preserved within calcareous mudstones of the Çukurbağ Fm. (Karsanti Fm.), Karsanti Basin. This has multiple (~10) veins running parallel to the sides of the leaf.

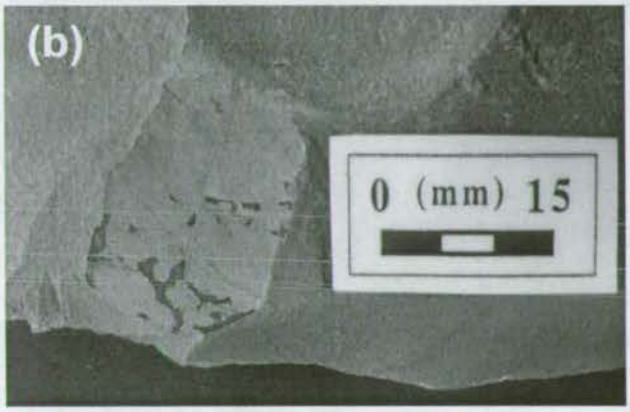

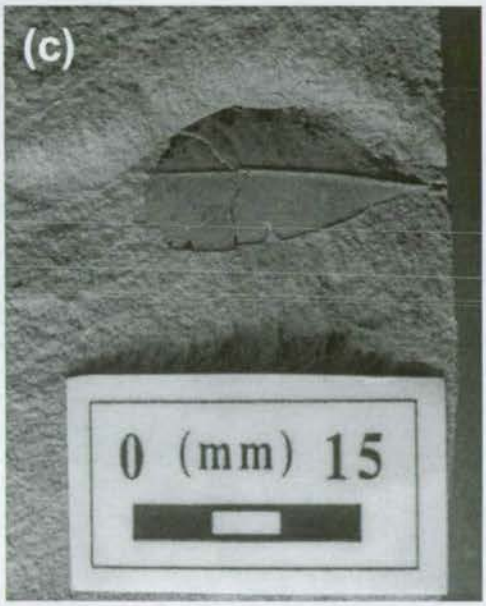

Figure 4.21b-e Broadleaf fossils (5cm by 2cm) resembling those from the modern day Birch, preserved within calcareous mudstones of the Çukurbağ Fm. (Karsanti Fm.). Veins bifurcate from a central canal to make the common V pattern.

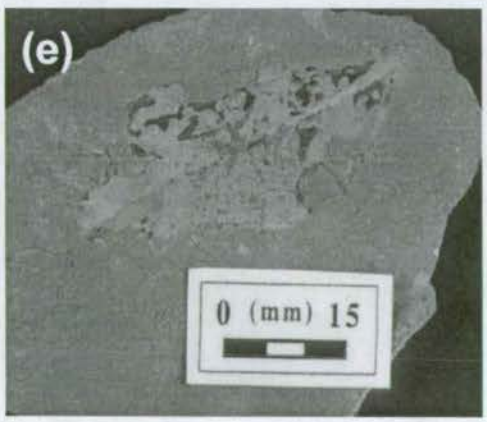

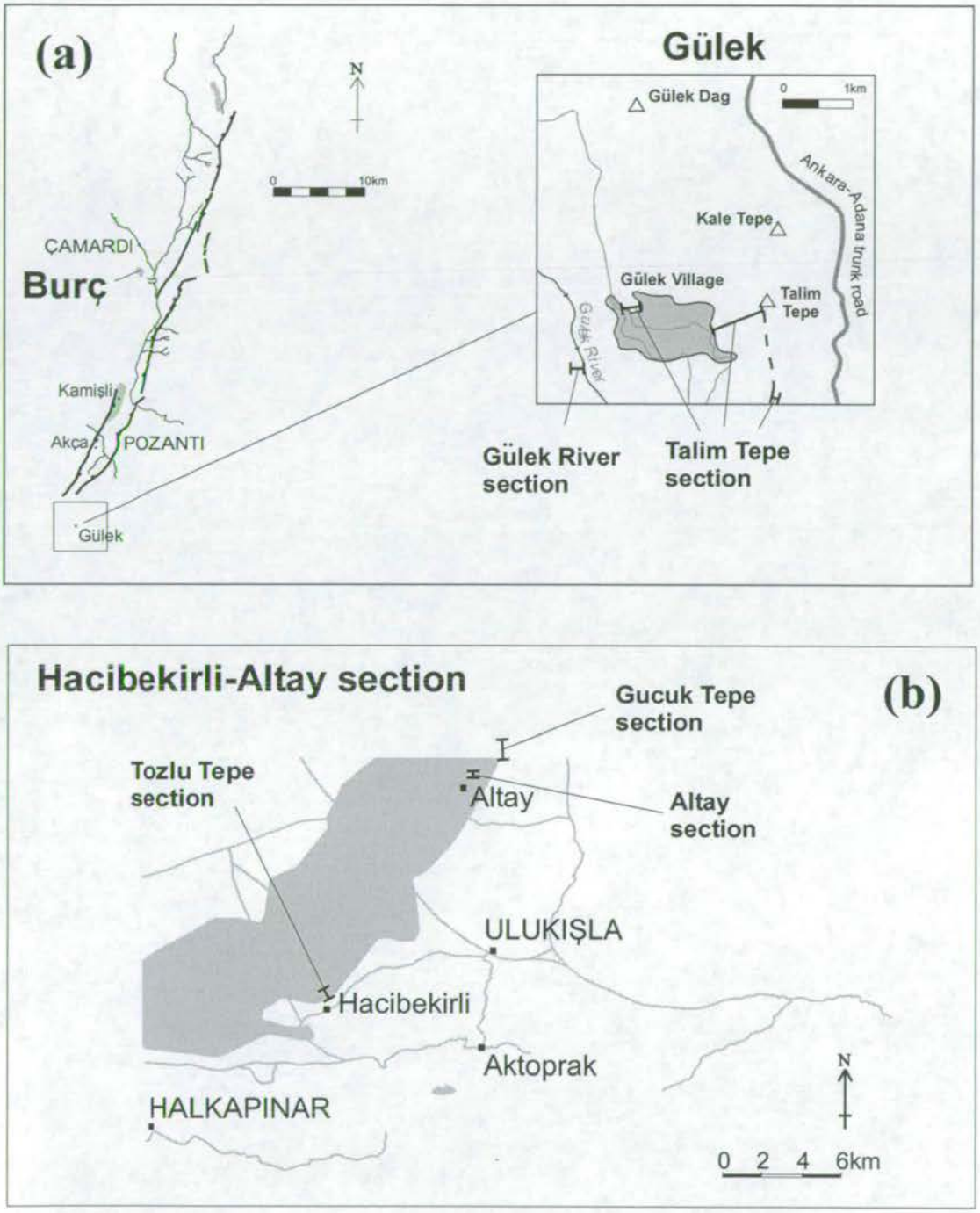

Figure 4.22 Location map for logged sections of the Late Miocene Burç Formation in: **(a)** the Ecemiş Fault Zone, showing the Burç and composite Gülek sections and **(b)** the Ulukişla Basin, showing the composite Hacibekirli-Altay section. See Fig. 2.4 for the location of these basins. Thick black lines represent faults, thin black lines represent rivers, grey lines represent roads. Grey shaded areas represent outcrop extent of Burç Formation rocks.

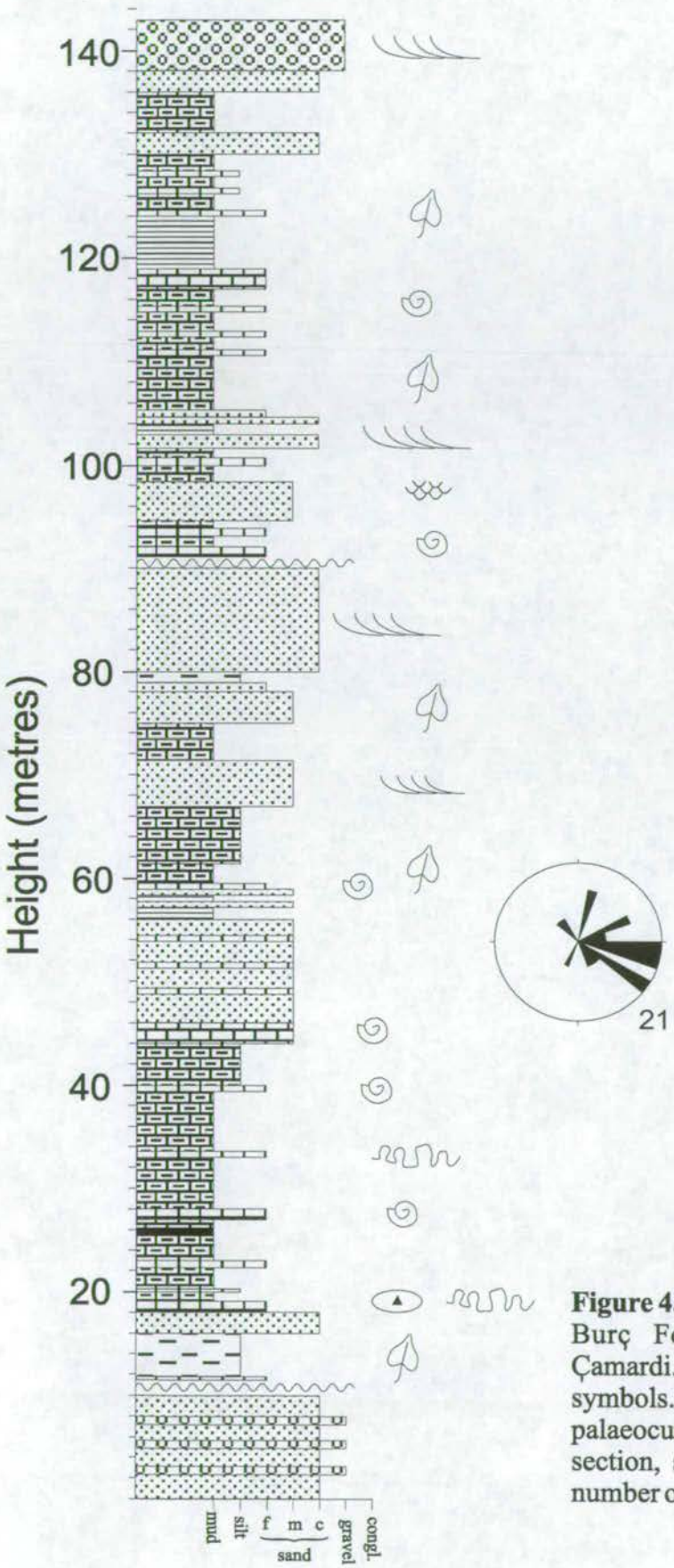

Figure 4.23 Stratigraphic log of the Burç Formation at Burç, near Çamardi. See Fig. 4.2 for key to symbols. Rose diagram represents palaeocurent directions for entire section, subscript number indicates number of palaeocurrent datapoints.

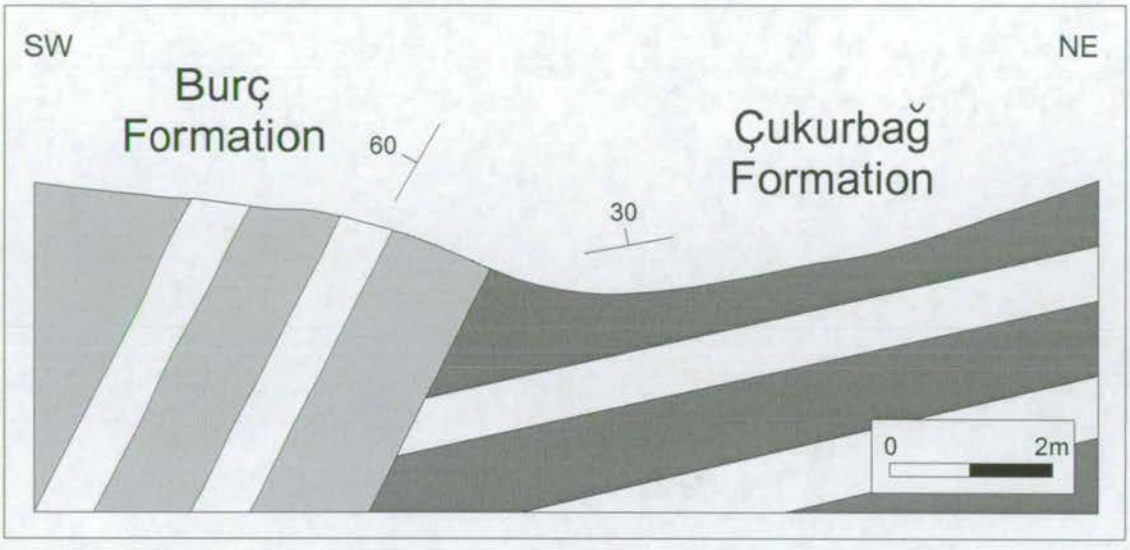

Figure 4.24 Sketch of the angular unconformity between the Burç Formation and the Çukurbağ Formation at Burç village (Map reference M33b3 - 755833).

organic-rich siltstones and micritic limestones. Limestones contain abundant Gastropods, plant fragments (e.g. leaf fossils). Some limestone beds contain discontinuous algal lamination with humped (bioherm) structures. A low reflectivity coal seam also outcrops in the lower part of the section.

At 45m there is an increase in sandstone deposition. These sandstones crop out in isolated bodies, which are laterally continuous over 6-7m and display internal 2-3m scale planar cross-bedding (Fig. 4.25). Sand grains are texturally and chemically mature (quartz rich). There is an internal angular discordance in the succession at 90m, after which deposition returns to interbedded siltstones and micritic limestones, containing Gastropods, leaf fossils and other plant debris.

4.3.6.2 The Composite Gülek Section

The composite Gülek section is situated in the far south of the EFZ and comprises two outcrops which can be seen both above and below the road between Camalan and Gülek (Fig. 4.46): these are the basal Gülek River section (1km SW of Gülek) and the Talim

Tabular foresets which prograde across the lensoid sandstone outcrop. These are interpreted as lateral accretion surfaces in a point bar deposit associated with a meandering river (Facies 3C).

Lateral accretion surfaces in a point bar deposit associated with a meandering river (Facies 3C).

Sketch of the geometry of a sandstone body in the Burc section (80-90m on Burc log, Fig. 4.23). The sandstone body is laterally continuous over 25m and incises into underlying siltstones. It contains internal tabular foresets which prograde from W to E.

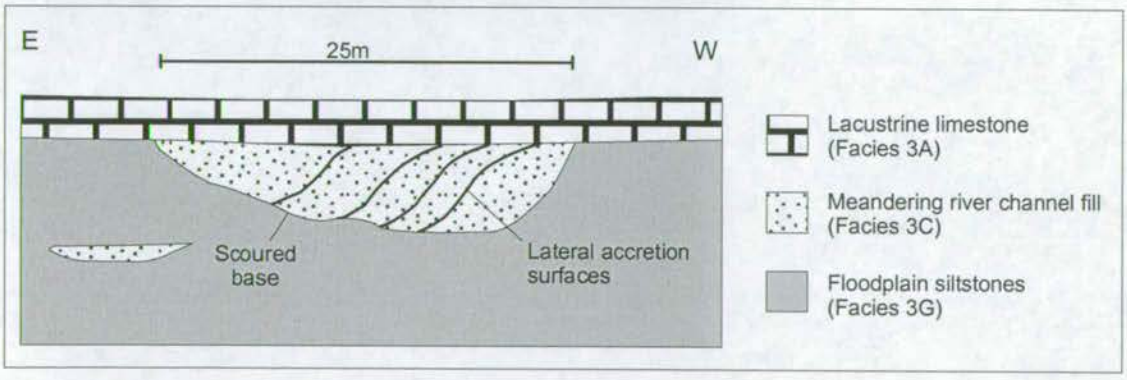

Figure 4.25 Geometry and internal features of a large sandstone body within the Burç Formation at Burç village.

Tepe section (0.5km ENE of Gülek, Fig. 4.22a). These two exposures are separated by areas of no exposure such that the total estimated section thickness is ~490m. A complete log of the composite Gülek section is shown in Fig. 4.26.

Gülek River section (Base-70m)

A thick conglomerate body marks the base of the exposure. This is a 20-30m thick unit of matrix-supported conglomerate containing well rounded and sorted large pebbles to small cobbles. The conglomerate is laterally extensive over the width of the outcrop (>20m). These conglomerates pass upwards into interbedded: (i) green, fine-grained, cross-bedded sandstones, (ii) Haematite-rich, calcareous mudstones (1-2cm thick) and (iii) 2-7m thick conglomerate and gravel lenses which incise (from 20-100cm) into underlying sandstones and mudstones.

Talim Tepe section (270-488m)

After 200m of non exposure the character of deposition changes to interbedded (1-2m thick) white micritic limestone and red/green calcareous siltstones with occasional (1m thick) lensoid conglomerate bodies with erosive bases. The limestones contain abundant oncolites (spheres with concentric layers of algae encrusting around a nucleus) and plant stems and other plant debris with substantial algal encrustations (Fig. 4.27c). Calcareous siltstones contain abundant calcareous concretions and root fossils.

At ~300m from the base of the section, an erosional contact cuts down at least 15m into the underlying succession. This is overlain by a thick (70-100m) conglomerate body, which consists of lens-shaped conglomerate bodies incising into- and separated vertically by red calcareous siltstones. The conglomerate bodies are clast supported, 2-10m thick, and pinch out laterally to the NW and SE over 10-30m. Clasts are sub-rounded and poorly sorted.

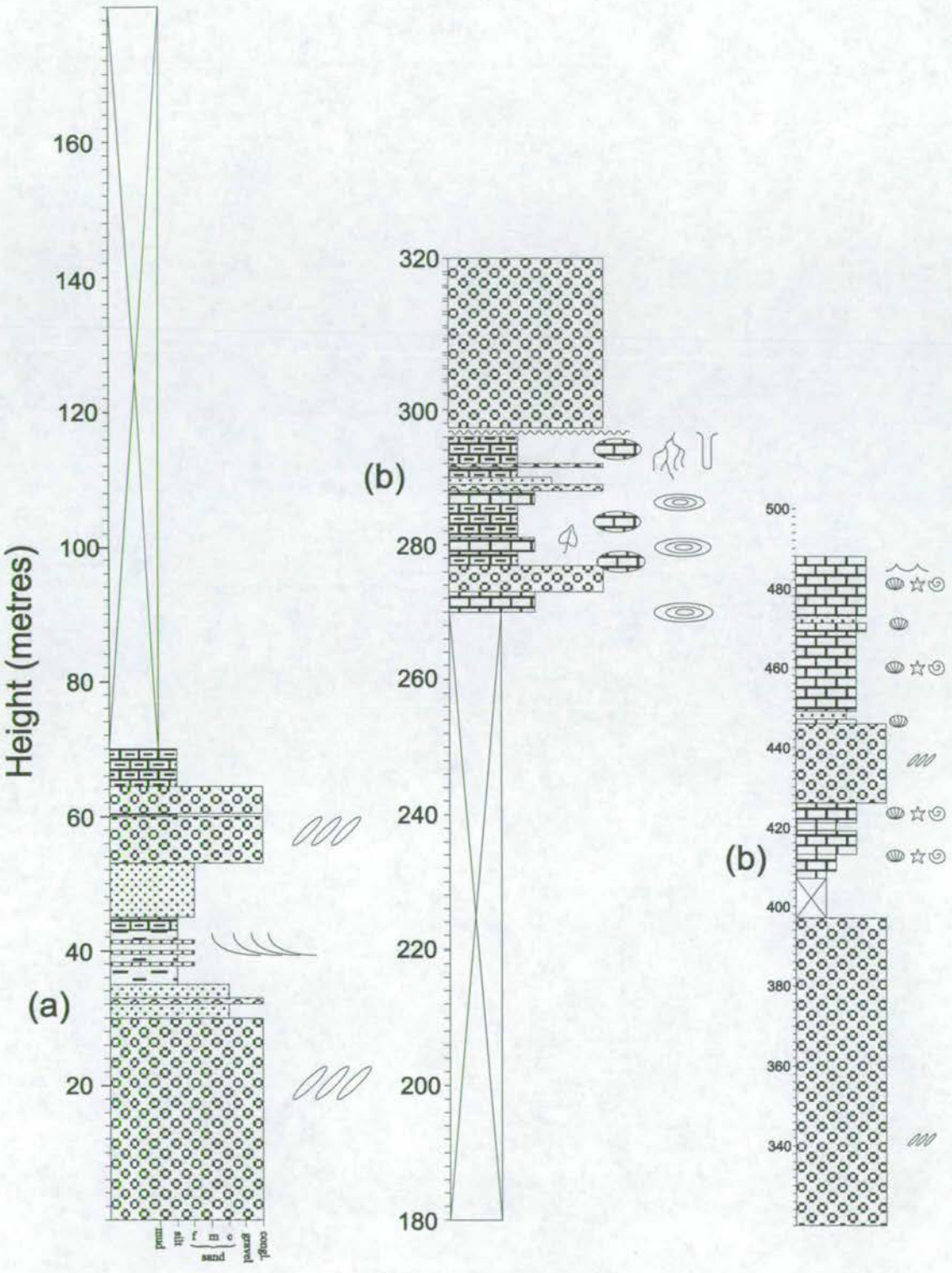

Figure 4.26 Stratigraphic log of the Burç Formation at Gülek. This composite section comprises: (a) the lower Gülek River section and (b) the upper Talim Tepe section (see Fig. 4.22a for location, see Fig. 4.2 for key to symbols).

Echinoid and oyster fossils from shallow marine limestones (Facies 3I), Talim Tepe section, Gülek.

2m high tabular foresets in shallow marine bioclastic limestones (Facies 3I), Talim Tepe section, Gülek.

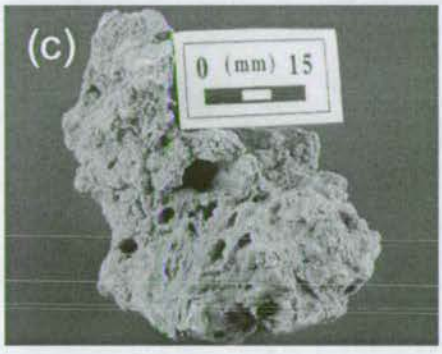

Cold water algal tufa deposits (Facies 3H) encrusting plant stems and other plant material in concentric layers. Talim Tepe section, Gülek.

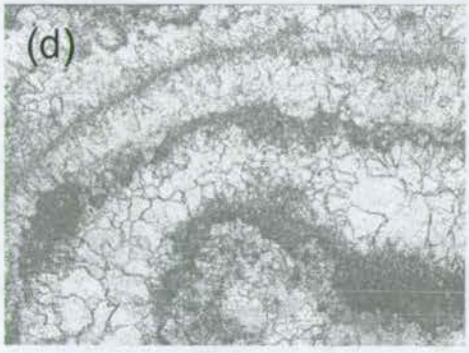

Phomicrograph of cold water algal tufa, showing concentric algal growth rings and calcite spar filling early cavities . Talim Tepe section, Gülek.

Tabular cross-bedding within braided river sandstones (facies 3E). Tozlu Tepe section, Hacibekirli.

Vertical fissure within red calcareous mudstones (floodplain, facies 3F). Fissures taper downward and are filled by overlying sandstone. Gucuk Tepe section,

Figure 4.27 Features of the Late Miocene Burç Formation at Gülek (EFZ),

Above this conglomerate complex the first marine fauna are found. Deposition switched to dominantly well-cemented micritic limestone, containing abundant echinoid tests, oyster shells, pecten shells, crinoid ossicles, *Turritella* Gastropod shells and ostracod assemblages (Fig. 4.27a). These are interbedded with well-sorted sandstones, bearing symmetrical ripple lamination. Limestone deposition is interrupted sporadically by a 15-20m thick, well-rounded conglomerate body which has incised into the limestones. The highest part of the Gülek section is characterised by oyster beds and bioclastic limestones which contain large scale (2m high) planar foresets (Fig. 4.27b).

4.3.6.3 Flora and Fauna

Yetiş (1987) identified several species of freshwater ostracod in the limestones of the Burç Formation, at Burç, which include *Heterocypris cf. Ponticus* KRSTIC and *Armiger cf. Crista* LINNAEUS (Fig. 3.3a). He dated these assemblages at Miocene. The limestones seen at the top of the Gülek section (basal deposits of the Adana basin) are well dated as Burdigalian (Early Miocene) by Yalcin & Görür (1984), using extensive assemblages of marine benthic and planktic foraminifers.

4.3.6.4 Palaeocurrents

Palaeoflow was measured at five sections in the Ecemiş Fault Zone area (Fig. 4.8c), using the orientation of avalanche faces on planar and cross-bedding. Outcrops are limited but results show that flow was toward the E in the centre of the EFZ (Burç and Kamişli), and to both N and S in the north of the EFZ (Hacibeyli area). In the far south of the EFZ (Gülek) flow was toward the S and SE.

4.3.7 Age Equivalent Sediments: The Late Miocene of the Ulukişla Basin

Demirtaşli *et al.* (1984) recognised a succession of undeformed Miocene-Pliocene aerial fluvial and lacustrine limestones which unconformably overlie the deformed Oligo-Miocene Aktoprak Basin sediments. This succession was un-named and extends N and E from Ulukişla as far as the Tuzgölü basin. The thickest succession close to the EFZ is seen between Hacibekirli and Altay (Fig. 4.22b).

4.3.7.1 The Composite Hacibekirli-Altay Section

The composite Hacibekirli-Altay section comprises three outcrops which can be seen on a SW-NE transect through the Ulukişla Basin between Hacibekirli and Altay villages (Fig. 4.22b). These are the basal Tozlu Tepe section (1km NE of Hacibekirli village), the Altay section (0.25km N of Altay village) and the Gucuk Tepe section (1km NNE of Altay village). These three exposures are separated by areas of non exposure such that the total section thickness (calculated using trigonometry) is ~340m. The lack of faulting and deformation in this succession means that this estimate is an accurate one. A complete log of the Hacibekirli-Altay composite section is shown in Fig. 4.28.

Tozlu Tepe section (Base-50m)

This comprises interbedding of:

(i) Haematite-rich calcareous mudstones (marls).

(ii) Thin (<1m thick) micritic limestones containing Gastropod shells and detrital plant fragments.

(iii) Lens-shaped, texturally-mature gravels and coarse-grained, planar-cross-bedded sandstone bodies. The section is topped by a 2-3m thick accumulation of porous algal tufa with oncolites and stromatolites encrusting plant stems and leaves.

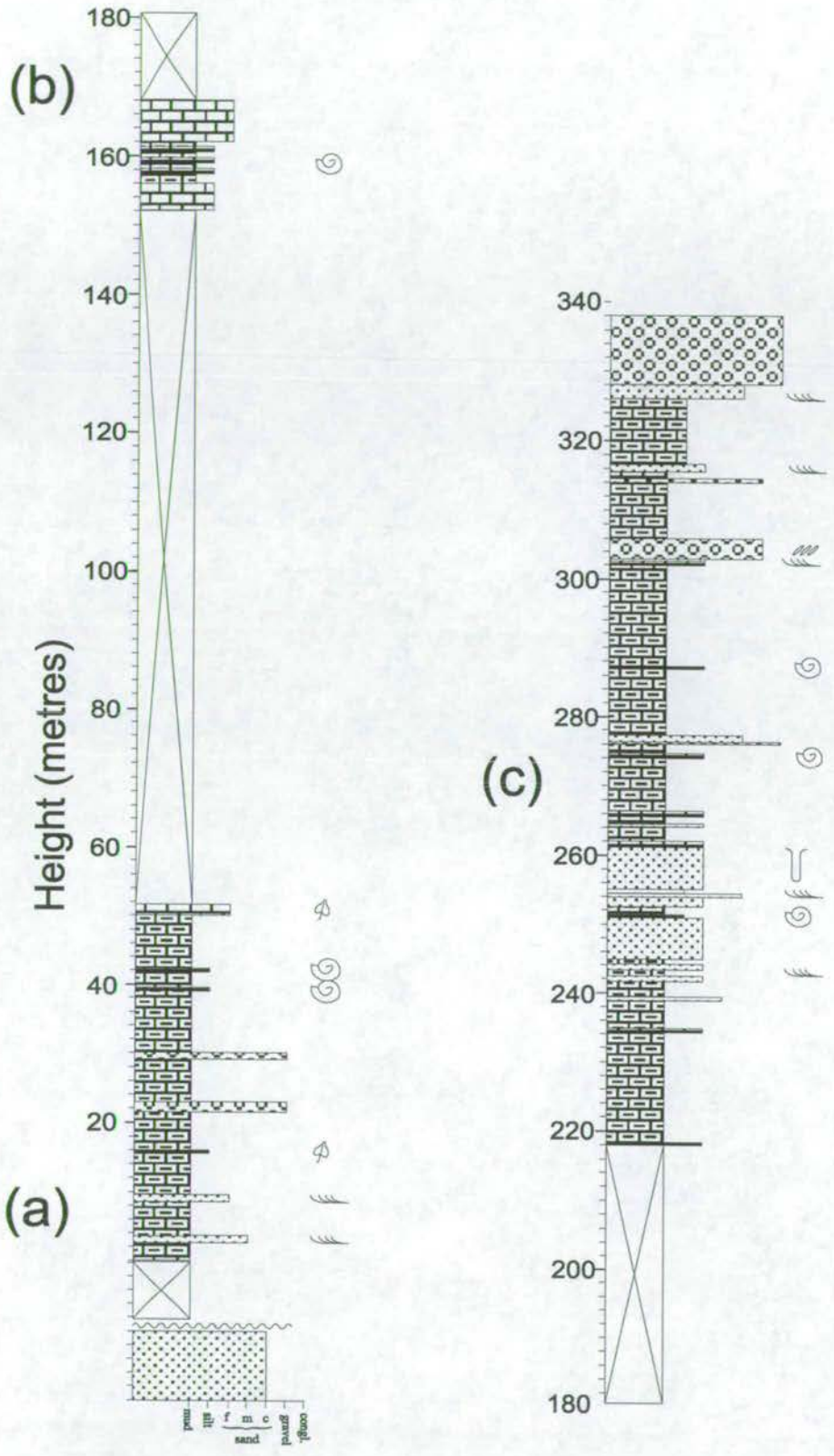

Figure 4.28 Stratigraphic log of the Burç Formation at Hacibekirli and Altay, Ulukişla Basin. This composite section comprises: **(a)** the lower Tozlu Tepe section (Hacibekirli), **(b)** the middle Altay section and **(c)** the upper Gücuk Tepe section. See Fig. 22b for location of sections and Fig. 4.2 for key to symbols).

The section is topped by a (1-2m thick) bed of encrusting limestone. Cavities remain in the shape of plant stems and leaves, surrounded by concentric layers of limestone (Fig. 4.27d).

Altay section (152-168m)

Deposition is similar to that at Tozlu Tepe with (10cm thick) interbeds of Gastropod-bearing micritic limestone and organic-rich marls. Plant stem fossils and other plant debris are preserved within the chalky limestone.

Gucuk Tepe section (218-338m)

This section is marked by a change to clastic-dominated deposition. The lower part of the succession is dominated by interbedded:

(i) Red calcareous mudstones. Slump structures, water escape structures, vertical burrows and calcareous concretions are common within the marls. Fissures which taper downward were also observed at several localities, filled by overlying sandstone (Fig. 4.27f).

(ii) Fine- to coarse-grained sandstones and occasional gravel intervals. These contain planar and trough cross-bedding (Fig. 4.27e) and climbing ripples.

(iii) Thin (20-30cm) micritic limestones containing Gastropod shells.

Towards the top of the section, conglomerate bodies become more frequent (2-3m thick, 10-20m long, lens-shaped bodies), culminating in a conglomerate body 10m thick. The conglomerates are clast supported and well imbricated, with well-rounded and well-sorted clasts. They are normally graded from a coarse base.

4.3.7.2 Flora and Fauna

Gastropod species have not been classified or dated. Leaf fossils are poorly preserved and fragmented (although abundant) and are likely to be long-ranging (Black 1970) and hence not useful for dating purposes. A Late Miocene age is inferred by comparison with the Burç Formation in the EFZ. Both units lie unconformably above the Oligo-Miocene Çukurbağ Formation and share similar facies. Both units bear micritic limestones with abundant gastropod and ostracod assemblages (unlike the underlying Çukurbağ Formation or the overlying Çatalca Formation) and also encrusting tufa.

4.3.7.3 Palaeocurrents

Palaeoflow was measured at two sections in the Ulukişla Basin (Fig. 4.10c), using the orientation of avalanche faces on planar cross-bedding and imbrication of the long axis of pebbles in conglomerates. Outcrops are very limited, but results show that flow was generally towards the north (Altay area); data from the Hacibekirli area are not considered reliable as there are only three datapoints. If Demirtaşli *et al.* (1984) are correct in their argument that these rocks form the base of the Quaternary Tuzgölü basin (outside the study area, Fig. 2.4), then northward transport would reflect flow toward the basin depocentre.

4.3.8 Pliocene - Quaternary Çatalca Formation

This unit crops out widely within the Ecemiş Fault Zone (Fig. 4.29, Enclosure 1). The thickest and best preserved deposits are found 10km E of Çamardi (Fig. 4.29a) where they outcrop as a thick fan-shaped complex. There are also substantial Plio-Quaternary deposits in the Pozanti – Tekir area and at Horoz (Fig. 4.29b), where they crop out as

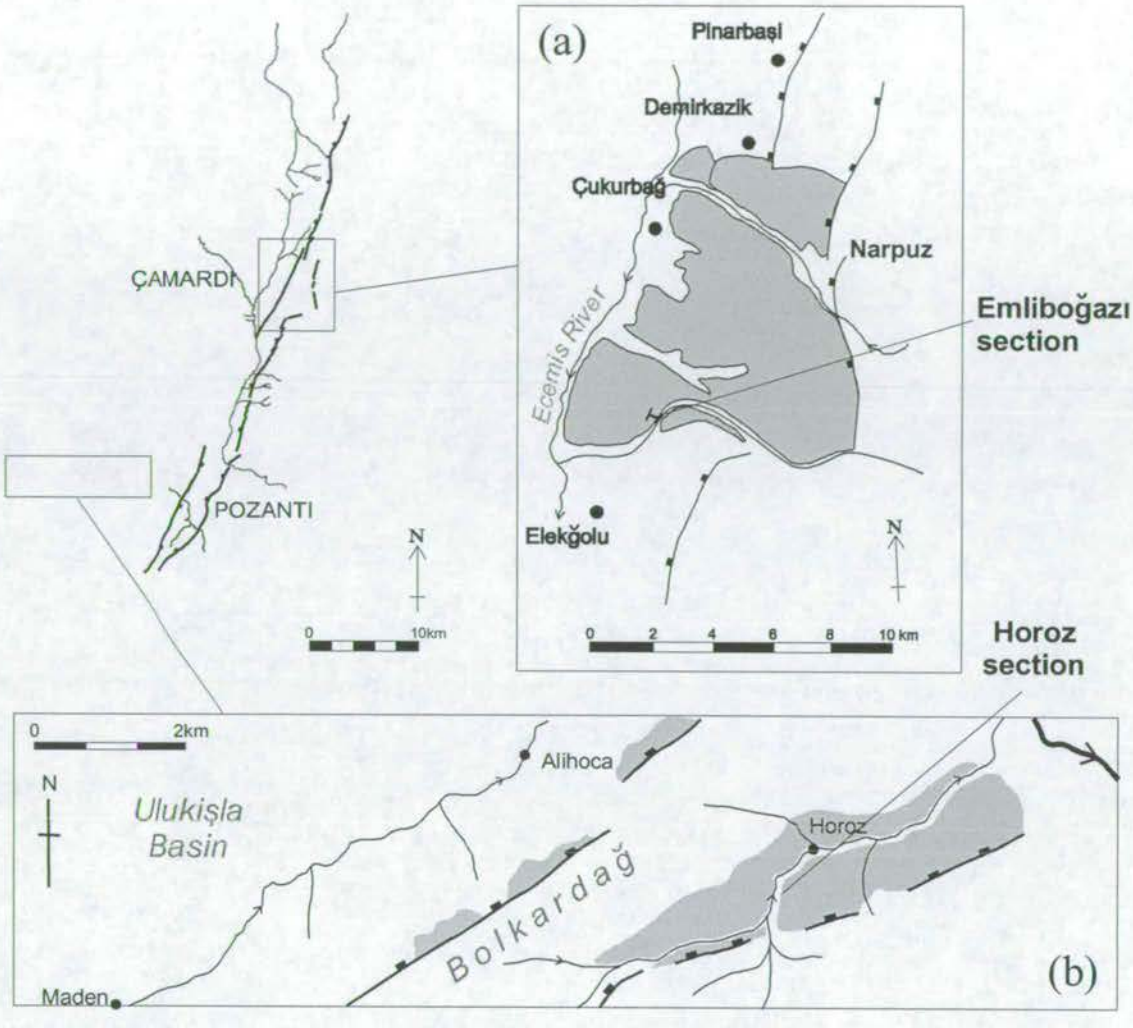

Figure 4.29 Location maps for logged sections of the Plio-Quaternary Çatalca Formation in: (a) the Ecemiş Fault Zone, showing the Elekğolu section and (b) the Horoz area, showing the Horoz section. See Fig. 2.4 for location of these areas. Thick black lines represent faults, thin black lines represent rivers, grey shaded areas indicate outcrop extent of Plio-Quaternary Çatalca Formation rocks.

the eroded remnants of fan-shaped bodies. The Plio-Quaternary succession at Emliboğazi is taken as the type section, where ~70m of section crop out (3km NE of Elekgölü village, Fig. 4.29a).

4.3.8.1 The Emliboğazi Section

A log of the Emliboğazi section is shown in Fig. 4.30a.

Base-10m

The base of the Çatalca Formation is an angular unconformity with up to 5m of relief This angular unconformity cuts into steeply dipping Oligo-Miocene Çukurbağ Formation rocks and bringing them into contact with horizontally bedded Çatalca Formation. The basal 10m of the Çatalca Formation is a massive, matrix-supported, unsorted, chaotic mega-breccia (Fig. 4.31a). Clasts are angular blocks (1-2m diameter) composed of ophiolite-derived material, supported by a matrix of angular pebbles, coarse sand and mud.

10-70m

The upper succession is marked by an abrupt change to clast-supported conglomerates with well-sorted and rounded clasts (0.5-15cm in diameter). Pebble beds are normally graded (1-2m thick) and clasts are uniformly well imbricated in the direction of transport (Fig. 4.31b). The composition of the clasts is 95-99% grey micritic limestone sourced from the nearby Aladağ Mountains. The conglomerates are well cemented by a calcite cement.

4.3.8.2 Age Determination

As yet no dateable fossils has been found in the conglomerates of the Çatalca Formation Beyhan (1994) reported that wood fragments have been discovered, but that they were not suitable for C^{14} dating. I conducted a pilot study into cosmogenic isotopic exposure age dating of the upper surface of the fan complex, but the limestone composition, expense and time required for analysis of results ruled out further work during the course of this study. A Pliocene – Quaternary age was assigned to this formation based

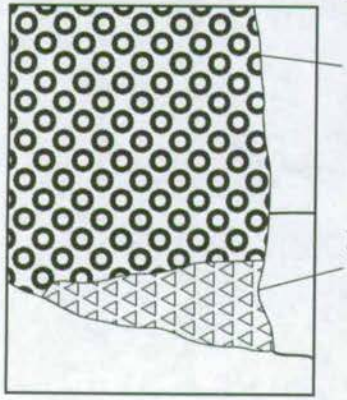

Outcrop of Çatalca Formation at Emliboğazi,

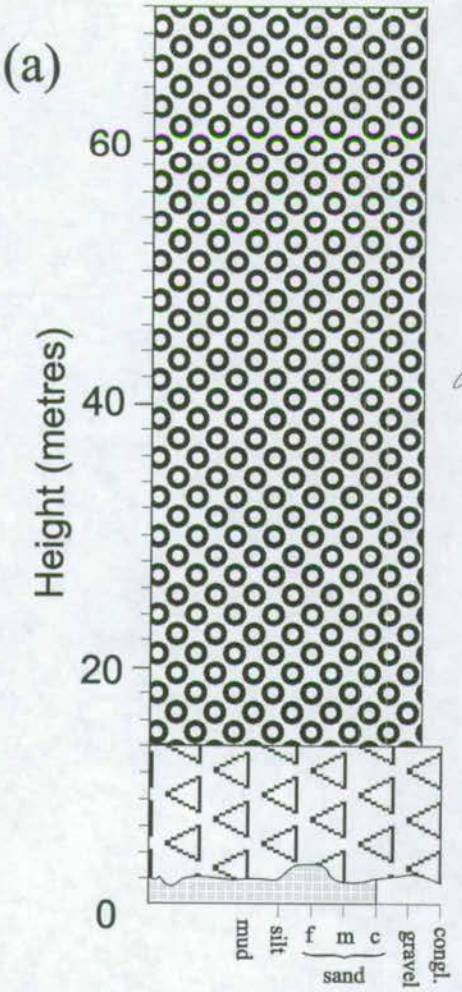

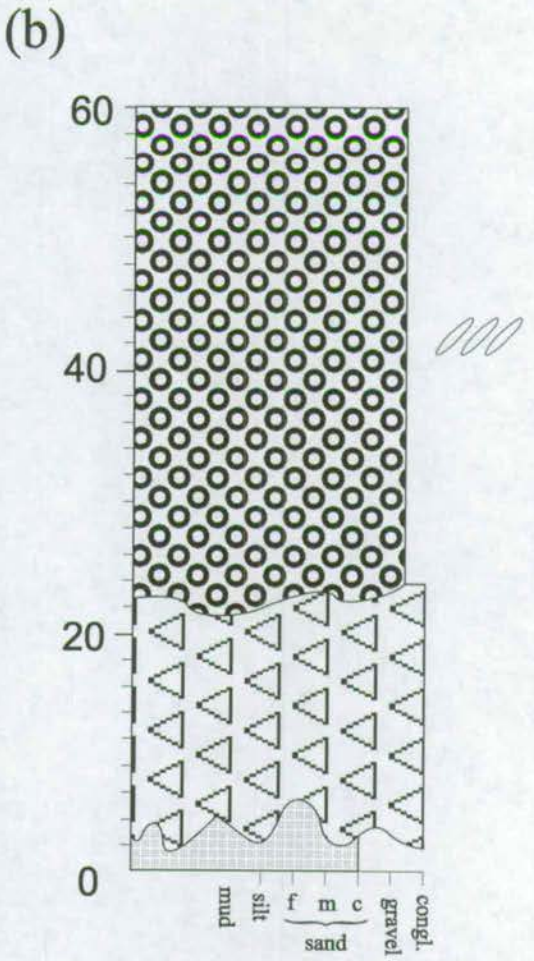

Figure 4.30 Stratigraphic logs for the Çatalca Formation at (a) Emliboğazi, Elekğolu (EFZ) and (b) Horoz (easternmost Bolkardağ). See Fig. 4.29 for location of logged sections, see Fig. 4.2 for key to symbols.

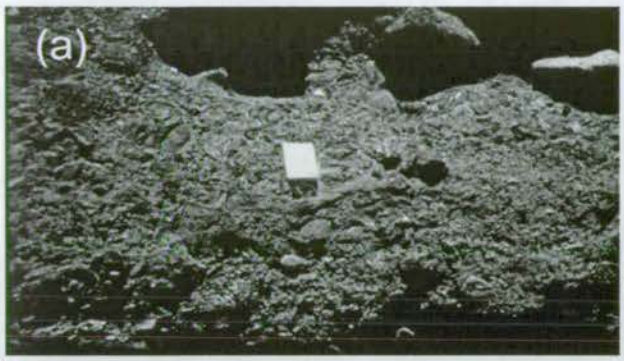

Massive, matrix-supported, unsorted, mega-breccia. Clasts are angular blocks composed of ophiolite-derived material, supported by a matrix of angular pebbles, coarse sand and mud. Facies 4A, Emliboğazi section (basal 10m).

Clast-supported conglomerates with well sorted and rounded clasts. Pebble beds are normally graded (1-2m thick) and clasts are uniformly well imbricated in the direction of transport. Emliboğazi section.

Angular unconformity with 1-5m of relief, bringing Plio-Quaternary rocks in contact with the underlying crystalline Bolkar Group. Horoz section (base).

Well sorted, normally graded, clast-supported pebbly conglomerates and well sorted cobble-bearing conglomerates. Horoz section.

Figure 4.31 Features of the Pliocene - Quaternary Çatalca Formation at Emliboğazi (EFZ) and Horoz (easternmost Bolkardağ). See Fig. 4.29 for location.

on the lower limit of Late Miocene (Burç Formation age) and the well cemented nature of much of the alluvial material which suggests an early Quaternary, or older age.

Work is also currently being carried out by Prof. Larry Meyer (Miami University, Ohio, USA) to use ^{36}Cl cosmogenic isotopes to date the exposure age of the upper surface of the fan complex and also to trench the fan across active fault strands in order to study microstructures and palaeoseismicity; results have not yet been published.

4.3.8.3 Palaeocurrents

Palaeoflow was measured at five locations on the Çamardi fan (Fig. 4.8d), using the orientation of the long axis of imbricated pebbles in conglomerates. Results show that flow was generally westwards, away from present-day fault scarps. The number of data collection points is inadequate to determine categorically whether the Çatalca Formation was sourced from a point or a line source; however the lack of a radial palaeoflow pattern indicates that either a line source or multiple point sources were active during the Plio-Quaternary.

Near the present Ecemiş River (1km SW of Çukurbağ) palaeoflow was diverted towards the SW, suggesting that drainage from the alluvial fans might have been diverted by a palaeo-Ecemiş River at the distal termination of the fans (Fig. 4.8d).

4.3.9 Age Equivalent Sediments; The Plio-Quaternary of the Bolkardağ

Similar Pliocene - Quaternary material outcrops in the high valleys of the Bolkardağ (W of the EFZ) such as in the Ali Hoca - Maden valley and Horoz valley (Fig. 4.29). The

outcrops in the upper Horoz valley are especially thick and well preserved and are described here.

4.3.9.1 The Horoz Section

The section described is exposed on the southern bank of the Horoz River, 1km SW of Horoz village (Fig. 4.29). A complete log of the Horoz section is shown in Fig. 4.30b.

Base-20m

The base of the Plio-Quaternary unit is defined by an angular unconformity with 1-5m of relief. This brings Plio-Quaternary rocks in contact with the crystalline Bolkar Group (Demirtaşli et al 1984). The basal 20m of the section are composed of unsorted, chaotic, matrix-supported breccia (5cm-1m diameter blocks). Clasts are composed of Bolkar Group crystalline limestone, ophiolitic material, granite and schist (Fig. 4.31c).

20-40m

Deposition changed rapidly to interbedded (1-3m scale) well sorted, normally graded, clast-supported pebbly conglomerates and well sorted cobble-bearing conglomerates (Fig. 4.31d). Clasts are moderately well rounded and the sandy matrix is well cemented by calcite. Clasts are dominantly composed of Bolkar Group limestone (99%) with a minor ophiolite-derived input; they are well imbricated.

4.3.9.2 Age Determination

No dateable fossils have been collected from these outcrops or from similar rocks elsewhere in the Bolkar Mountains. They are assigned a Pliocene – Quaternary age, based on their extreme similarity to the Çatalca Formation of the EFZ, their state of cementation and their stratigraphic position above all other units.

4.3.9.3 Palaeocurrents

Palaeoflow from the Plio-Quaternary unit was measured at four localities in the Horoz valley (Fig. 4.32), using the orientation of the long axis of imbricated pebbles in conglomerates. Results show that palaeoflow was NW directed in localities close to interpreted normal fault scarps (i.e. away from the footwall of scarps), and NE-directed (axial to the Horoz valley) in localities >1km away from fault scarps.

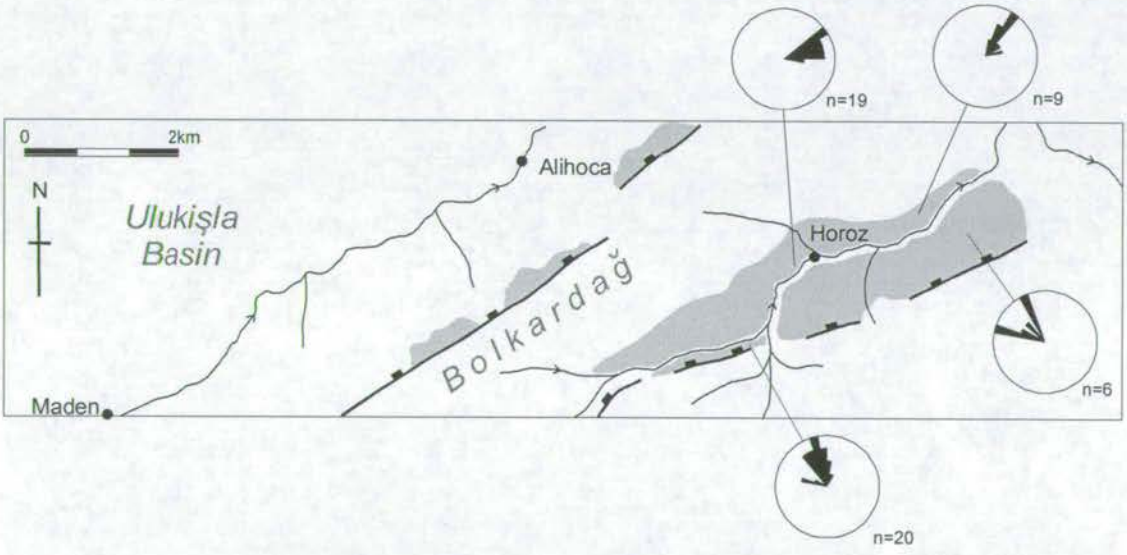

Figure 4.32 Palaeocurrent data for the Plio-Quaternary Çatalca Formation at Horoz (see Fig. 4.29 for location). Rose diagrams indicate palaeocurrent direction, subscript numbers indicate number of palaeocurrent datapoints. Thick black lines represent faults, thin black lines represent rivers, grey shaded areas represent Çatalca Formation outcrop extent.

4.4 Facies Interpretation

4.4.1 Interpretation of the Kaleboynu Formation

4.4.1.1 The Evliya Tepe section (Fig. 4.2)

The following facies were identified:

Facies 1A

The base of the section comprises texturally immature, chaotic, matrix supported, breccias, with clasts in the pebble to cobble size range. They are interpreted as debris flows, due to their matrix-supported nature, the lack of any grading or imbrication and the angular nature of the clasts (Fig. 4.33). Due to their close association with the marine facies 1B, these are interpreted as submarine debris flows (Fig. 4.33). Such submarine debris flows are commonly associated with turbidity currents (Nemec & Steel 1984) but the lack of other turbidite structures and the close association of the debris flow deposits with the shallow marine facies 1B suggest a shallow-marine origin. Submarine debris flows have been documented from very low gradient slopes in shallow marine settings (Pickering *et al.* 1989, Lowe 1976). Provenance indicates possible sources from either the underlying Palaeocene Çamardi Formation (Kuscu 1992) or the Nigde Metamorphic Complex (Fig. 2.4), which contains both schist-bearing and granitic bodies (Whitney & Dilek 1997). In general, subaqueous debris flows transport smaller clasts than subaerial flows (Pickering *et al.* 1989), and this can be seen when comparing facies 1A (subaqueous) with facies 2H (subaerial).

Facies 1B

Interbedded with the debris flows are laterally continuous texturally mature sandstones, bearing *Rhizocorallium*-like trace fossils (Fig. 4.34) and small scale convolute bedding structures in strata directly beneath the debris flows. The trace fossils suggest a near-shore submarine environment of deposition, and convolute bedding is due to the loading of water-rich sediment by the rapidly deposited debris flows.

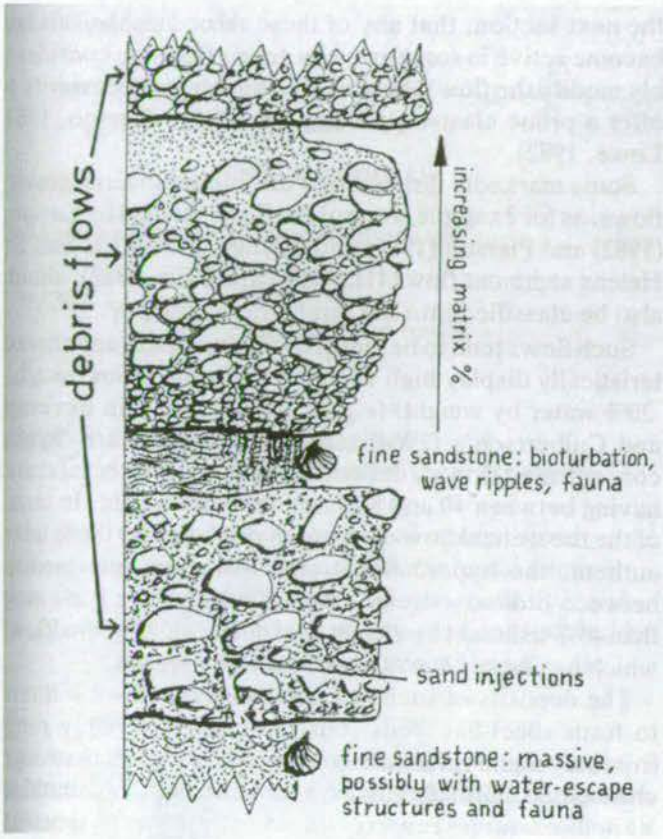

Figure 4.33 Some typical features of subaqueous mass-flow deposits (after Nemec & Steel 1984). These features are present in Facies 1A of the Evliya Tepe section.

The central and upper parts of the section are characterised by the interbedding of three facies. These are:

Facies 1C

Texturally mature, fine-grained, arkosic sandstone, containing wave ripples. These are interpreted as near shore (above wave-base) sandstones.

Facies 1D

Dark grey micritic limestones containing the large benthic foraminifera *Nummulites* and *Assilina* (Fig. 4.7).

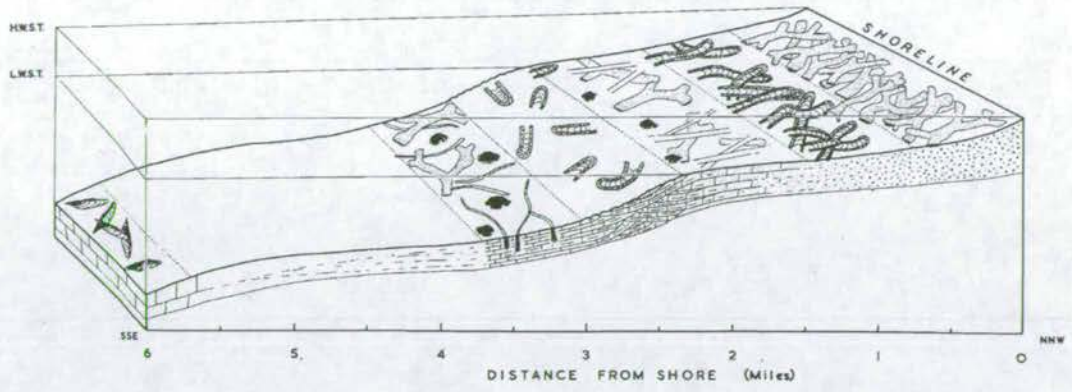

Figure 4.34 Suggested bathymetric zonation of the endobenthos in shallow-water limestones from the Bajocian Scarborough Beds of the Yorkshire coast. Horizontal scale is accurate, vertical and lateral scales are diagramatic (after Farrow 1966).

Benthic Foraminiferal palaeoecology

Assemblages of benthic (bottom dwelling) foraminifera are commonly used to interpret depositional setting. Factors influencing the type and form of foraminifera present include: light intensity, water energy, temperature, salinity and water depth (Hallock & Glen 1986). In general, small, robust, thick-shelled foraminifers are found in shallow marine conditions with high energy, high light intensity and abundant nutrients. Large, flat, thin-shelled foraminifers are, by contrast, found in conditions of lower energy, lower light intensity and fewer nutrients (Hottinger 1983). The presence of giant rotaline foraminifers (such as those present at Evliya Tepe and Kalenboynu Tepe) indicate normal salinity marine conditions, and low water energy (i.e. well below wave-base, Hallock & Glen 1986). A block diagram indicating typical water depths for nummulitic foraminifers is shown in Fig. 4.35 (Sinclair *et al.* 1998) and suggests that the large *Nummulites*, such as those found in the Kaleboynu Formation were deposited in water depths below the storm wave-base (suggested depth of 50-100m, but could be shallower if the coast was not subject to regular storms).

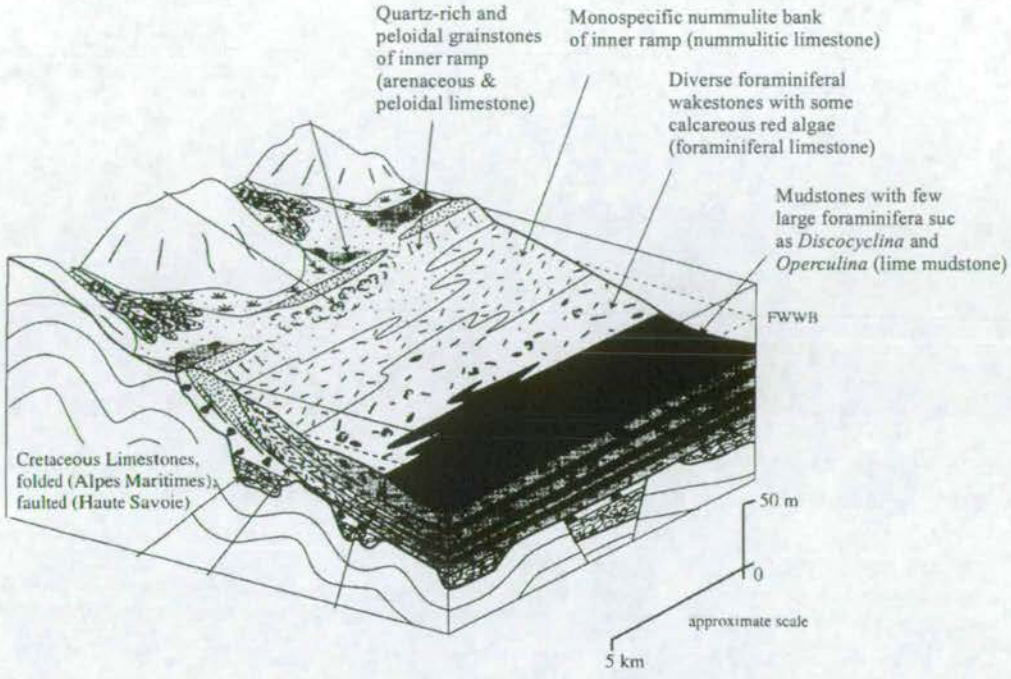

Figure 4.35 Block diagram of the depositional environments of the Nummulitic Limestones of the French Alpine foreland basin (after Sinclair *et al.* 1998). This represents a wave-dominated carbonate ramp with minor strorm activity.

Facies 1E

Dark grey calcareous mudstone (marl). The close association with marine limestones suggests a marine origin. I interpret these as being deposited in slightly deeper water away from clastic input, possibly on the middle or outer shelf.

Facies 1F

The deposition of foraminiferal micritic limestone was regularly interrupted by thin gravel beds. These have erosional bases and a similar composition to the clasts found in the debris flows of facies 1A. Such gravels are characteristic of storm beds. During storms, the lower wave-base entrains and transports more coarse material than during quiescent periods, resulting in the transport of gravelly material further across the

continental shelf. A model for storm deposit occurrence is given in Fig. 4.36 (Aigner & Reineck 1982).

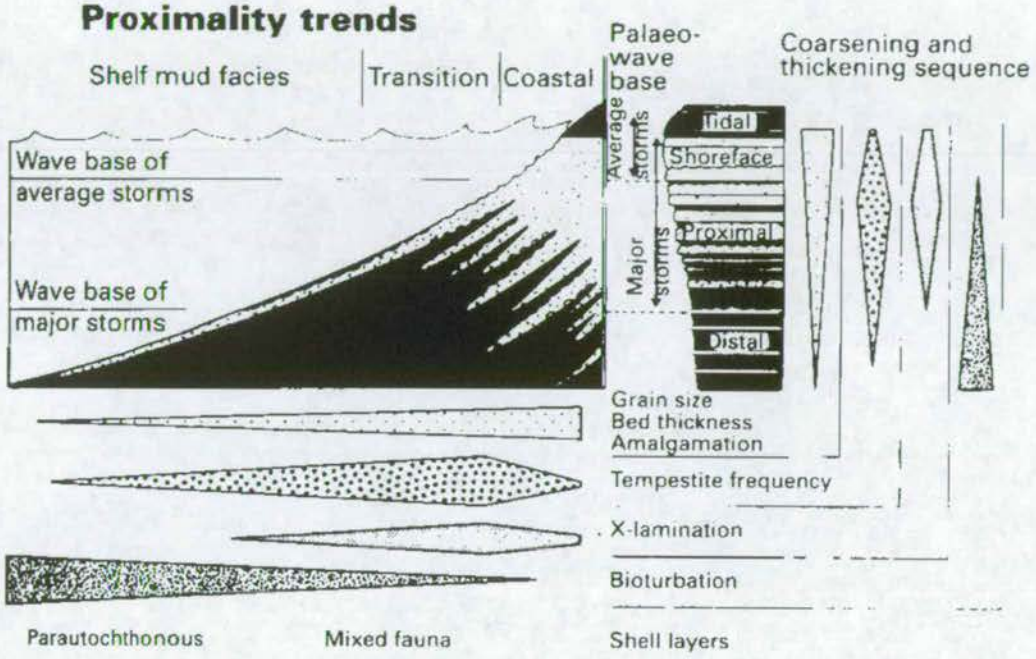

Figure 4.36 Proximal-distal trends in modern shelf stormdeposits based on German Bight (southeast North Sea). After Aigner & Reineck 1982.

Evliya Tepe section: overview

The cause of debris flow mobilisation during the Mid-Eocene is poorly constrained, but may be due to: (i) local tectonic uplift of the adjacent Niğde Massif and associated earthquake activity or (ii) unstable steep depositional slopes in a shallow-marine environment. The remainder of the succession is transgressive, developing from a near-shore to an open shelf environment, periodically affected by storm deposits.

4.4.1.2 The Kaleboynu Tepe succession (Fig. 4.5)

The underlying Early Cretaceous succession comprises micritic limestones, which contain the planktic foraminifera *Kilianina sp., Kurnubia sp.* and *Pfenderina sp.* (Tekeli

et al. 1984), which indicate an open-shelf environment of deposition (Boudagher *et al.* 1997). A period of uplift tilted these limestones and formed an erosional unconformity between Lower Cretaceous and Eocene rocks. Any Palaeocene deposits at this locality have been entirely removed. The Eocene succession is composed of the following facies:

Facies 1G

Dark grey micritic limestones characterise the base of the section. The dominance of small planktic foraminifera within these limestones, and the absence of benthic forms suggest that they were deposited in an open-marine shelf environment (>100m water depth; Boudagher *et al.* 1997).

Facies 1D (variation)

Unconformably overlying facies 1G is a succession of sandy to silty limestones, bearing abundant and diverse benthic foraminifera (Fig. 4.4d, section 4.3.3). These are similar to the species identified in facies 1D and are indicative of a shallow, warm (>15^{0}C), marine shelf setting, below wave-base (see 'benthic foraminifera palaeoecology', above for discussion).

Facies 1H

The top of the section is characterised by a thick succession of matrix-supported, texturally immature conglomerates. Lithified clasts of the underlying foraminiferal limestone are incorporated into these conglomerates, indicating that the Eocene succession was lithified, uplifted, eroded and re-worked into the overlying conglomeratic units. The conglomerates are tentatively interpreted as terrestrial debris flows due to the Iron-rich (red) nature of the silty matrix, the lack of coeval marine fossils and the lack of sorting in the sediment, but a submarine origin is not ruled out. They are very similar to those found at the base of the Çukurbağ Formation at the Doğan River section (facies 2H).

Yetiş (1978) inferred that this upper 100m-thick succession of coarse conglomerates and sandstones are of Eocene age, based on the *Nummulites* foraminifera present. I believe, however, that this upper succession is more likely to belong to the Oligo-Miocene Çukurbağ Formation as:

(i) A 20^0 angular unconformity exists between demonstrably Eocene limestones and the overlying conglomerates.

(ii) Foraminifera found within the overlying conglomerates are broken and detrital.

(iii) The haematite-rich nature, and ophiolite-derived composition of the conglomerates is extremely similar to the facies found within the Oligo-Miocene Çukurbağ Formation elsewhere in the Ecemiş Fault Zone.

The Kaleboynu Tepe succession represents a regressive trend, shallowing upwards from open shelf to terrestrial depositional environments. The presence of two angular unconformities (with 20^0 changes in bedding angle) within the succession suggests that the area experienced repeated tectonic uplift during throughout the Mid-Eocene.

4.4.1.3 Lateral Facies Changes within the EFZ

Establishing trends in facies is difficult due to (i) the existence of only two Eocene outcrops and (ii) the cutting out of much of the succession at Kaleboynu Tepe beneath erosional unconformities. However, it appears that the two Eocene outcrops are fundamentally different in several respects. The western outcrop (Evliya Tepe, Fig. 4.2) is a transgressive succession, deepening upwards from a shallow to an open marine shelf environment. The eastern outcrop (Kaleboynu Tepe, Fig. 4.5) is regressive (shallowing upwards) and is also affected by uplift phases and consequent erosional unconformities during the Eocene which are not present at Evliya Tepe. Palaeocurrents (Fig. 4.8) also reveal opposing flow directions: West and north directed at Evliya Tepe and SSE directed at Kaleboynu Tepe.

These observations are not consistent with the two exposures being deposited in close proximity to each other. Rather they suggest that the two outcrops originated in widely divergent settings and may have been brought together after the Eocene by strike-slip faulting (see Section 10.2.1)

4.4.1.4 The Guney succession (Fig. 4.9)

The lowermost Caykavak section (Fig. 4.1b) is composed of the following facies:

Facies 1I

Iron-rich mudstones directly overlie the pillow lavas of the Ulukişla Group. These are interpreted as deep sea sediments, deposited from suspended fines.

Facies 1A (variation)

Much of the basal part of the Guney section is composed of thin (0.5-1m) matrix-supported, texturally immature, conglomerates composed of volcanic material. These are interpreted as submarine debris flows, similar to those found at the base of the Evliya Tepe section (facies 1A). The occurrence of planktic foraminifers throughout this succession (Fig. 3.3b) defines it as submarine.

Facies 1J

White, siliceous, clay layers are present within the basal succession. These are interpreted as submarine bentonites (de-vitrified tuffs) due to their silica-rich composition and close association with foraminiferal mudstones (Facies 1K). The association of facies 1A and 1J suggests a palaeo-environment close to an oceanic volcanic centre (Fig. 4.37, Sigurdsson *et al.* 1980). Eruptions and associated seismic activity triggered submarine slumps and debris flows (facies 1A) and between such

events, pyroclastic ash entered the hydrosphere and settled out as submarine tuff layers (facies 1J).

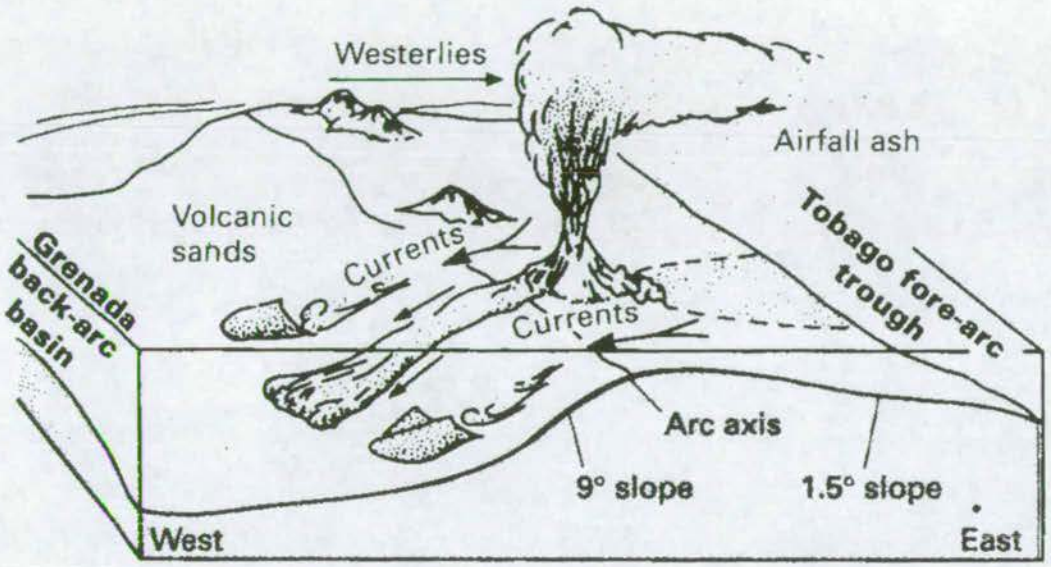

Figure 4.37 Schematic diagram of the Lesser Antilles volcanic arc to show the distribution of volcaniclastic deposits within forearc and backarc basins (after Sigurdsson et al. 1980).

Facies 1K

The upper part of the Guney section is characterised by the cyclical deposition of fine-grained feldspathic sandstones and foraminifer-bearing, organic-rich mudstones. The sandstones contain evidence for repeated uni-directional currents (tabular cross-bedding and groove marks, Fig. 4.7b) and periods of low flow (normally graded siltstones and mudstones). These sandstones have previously been interpreted as turbidites (Demirtaşli *et al.* 1984), but the intermittent presence of wave ripple lamination indicates an above-wave-base setting; therefore a classical deep-marine turbidite interpretation cannot be valid. I suggest instead a shallow-marine shelf environment affected by periodic

offshore currents. Such currents may have been the result of (i) storm events (Fig. 4.36), (ii) unstable, steep depositional slopes in the coastal area or (iii) seismically triggering slumps (Fig. 4.37). Considering the association with volcanic and volcanogenic facies (above), an eruption- or seismic-related trigger is considered most likely.

Facies 1L

Interbedded with facies 1K are thin (0.5-1m) organic-rich mudstones and siltstones, which contain planktonic foraminifera (Fig. 3.3b). The presence of the planktonic foraminifera, *Globorotalia* suggests an open-shelf setting (Boudagher-Fadel *et al.* 1997), with fines being deposited during periods of low clastic input.

4.4.1.5 Summary of Eocene sedimentation

The Eocene sediments of the Guney area represent a dissimilar association of facies to those of the Ecemiş Fault Zone. Whereas the EFZ outcrops are mainly micritic limestone- dominated and bear shallow-shelf benthic foraminifer assemblages, those of the Ulukişla basin are dominated by mudstone and sandstone, and planktic foraminifer assemblages, suggesting generally deeper water deposition. The combined palaeocurrent data (Fig. 4.8a & 4.10a) indicate a submarine depocentre to the north of Guney and to the west of Evliya Tepe (in the Niğde area) during the Lutetian. A block diagram representation of probable palaeoenvironments during the Lutetian is given in Figure 4.38.

4.4.1.6 Ancient and modern analogs of the Kaleboynu Formation

The Mid-Eocene (Lutetian) was a period of sea-level highstand throughout the Tethyan region (Haq *et al.* 1987). This highstand resulted in clastic sediment starvation in many of the existing basins along the Tethyan belt, and the preferential deposition of carbonates in the shallow marine environment. The Eocene Nummulitic Limestones of

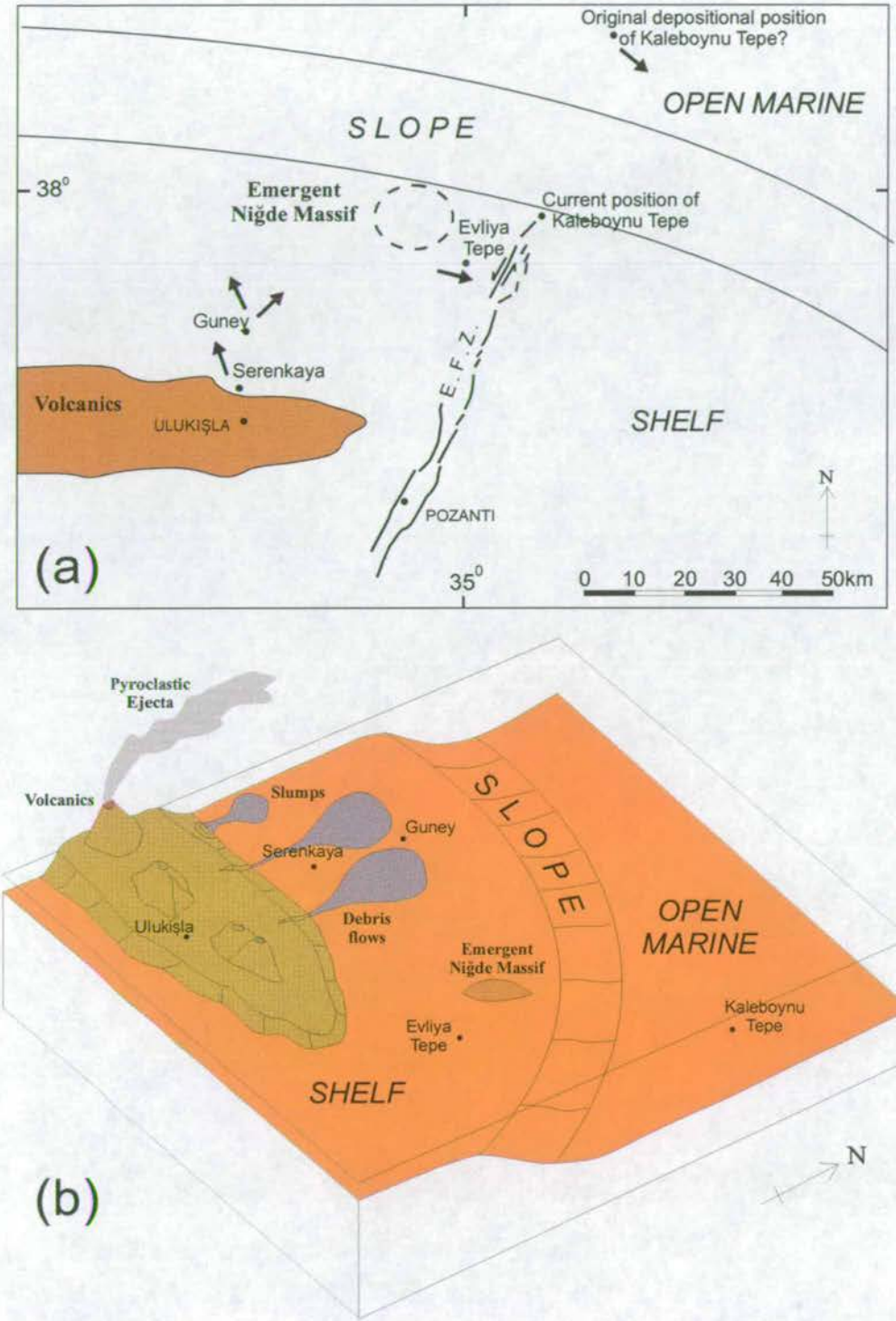

Figure 4.38 (a) Map of Middle Eocene palaeo-environments, based on sedimentological data. Black dots represent current positions of settlements, black arrows represent simplified palaeocurrent data. (b) Block diagram of Middle Eocene palaeo-environments based on sedimentological data. Vertical and horizontal scales are not accurate.

the Haute Savoie (external chains of the French Alps) are typical of the foraminiferal carbonates deposited during this period. These packstones and grainstones were deposited on a low energy, wave-dominated, carbonate ramp, situated on the cratonic margin of the Alpine foreland basin (Sinclair *et al.* 1998). The limestones are characterised by monospecific accumulations of *Nummulites*, and the facies represent the development of nummulite shoals or banks in an inner ramp setting close to fair weather wave base (Fig. 4.35). These deposits differ from the Kaleboynu Formation in that they are monospecific, but the clastic-starved, foreland basin setting is similar to present hypotheses regarding the Eocene closure of the Inner Tauride Ocean (Dilek *et al.* 1999, Demirtaşli *et al.* 1984).

Similar Nummulitic Limestones can be found at the opposite end of the Tethyan suture zone, in the Indus Group sediments of Ladakh, India. These are of Early Eocene (Ypresian) age and contain the Nummulites species: *Miliola*, *Biloculinella* and *Orbitoididae* (Van Haver 1984). The packstones record a sea level highstand and deposition on an inner, carbonate ramp setting, with Nummulites shoals accumulating at approximately mean fair weather wave base (Sinclair & Jaffey *in press*). Pebble layers with sharp bases are present within the limestones, composed of clasts of underlying units, and these have been interpreted as the result of episodic storm influence. These pebble layers bear a close similarity to those found in the Kaleboynu Formation at Evliya Tepe (Section 4.3.1.1).

The modern equivalent of the depositional environment of the Nummulitic Limestones of the Middle Eocene are carbonate ramps. These are low-angled, generally homoclinal (but with subtle slope geometries) slopes, especially dominant at times when reef-constructing organisms were absent or inhibited (Burchette & Wright 1992). The zone of greatest organic carbonate production is in the 'inner-ramp' setting; fair-weather wave base to normal storm wave base. Carbonate ramps are best developed where subsidence is flexural and gradients are slight over large areas, as in foreland and

cratonic interior basins, and along passive margins (Burchette & Wright 1992). An example of a modern day carbonate ramp is the Trucial Coast of the South Arabian Gulf (foreland basin setting), which includes oolitic barriers and beaches, lagoon, sabkha, muddy mid- and outer-ramp facies, with a maximum water depth of ~100m (Purser & Evans 1975).

4.4.2 Interpretation of the Çukurbağ Formation

4.4.2.1 The Bademdere section (Fig. 4.12)

Four distinct facies associations were recognised within the composite Bademdere succession:

Facies 2A

The first facies comprises laterally continuous (>50m) bodies of red, calcareous siltstones and mudstones. These rocks frequently contain *in situ* leaf and root fossils, calcareous nodules and some bioturbation in the form of vertical burrows. This association is interpreted as a terrestrial floodplain facies with zones of caliche-type calcareous nodules indicating the start of pedogenesis. Floodplain sedimentation is mainly the result of the deposition of suspended fines during floods, with grain size generally diminishing distally, away from river channels (Guccione 1993).

Facies 2B

The second facies comprises laterally discontinuous (2-5m wide, up to 2m thick) lens-shaped bodies of conglomerate and gravel. These bodies generally have erosive bases and conformable top surfaces, and are internally well imbricated in one direction. The uni-directional palaeocurrents, lensoid geometry and close association with terrestrial mudstones (facies 2A) and braided river sandstones (facies 2C) indicates that these rocks represent a river channel-filling facies (Fig. 4.39; Ramos & Sopena 1983).

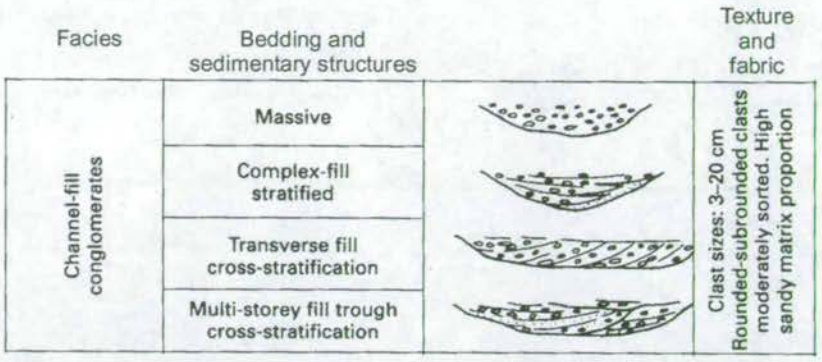

Figure 4.39 Part of a classification for conglomerate alluvial facies. The facies are defined on the basis of texture, structures and the shape of the units (after Ramos & Sopeña 1983).

Facies 2C

Closely associated with the channel fill, but much more laterally continuous are texturally mature red sandstones (Facies 2C). These are laterally continuous, sheet-like bodies (>20m wide) which connect outcrops of the conglomerate facies along the same horizon. They are characterised by restricted areas of trough cross-bedding separated by wider zones of tabular cross-bedding. Areas of trough cross-bedding are interpreted as channels, and areas of parallel cross-bedding are interpreted as point bars. The presence of multiple channels and point bars over a laterally extensive area suggest that this is an ancient sandy braided-river environment (Boggs 1987). This facies closely resemble the braided-river deposits of the Helvetiafellet Formation in the Lower Cretaceous of Spitzbergen (Fig. 4.40; Nemec 1992). The sandstones interfinger with the floodplain mudstone facies, when furthest from the conglomerate filled channels.

Facies 2D

The final facies comprises a succession of closely associated algal mat deposits, micritic limestones, thin, low reflectivity coals and gypsum (Selenite) evaporites. The presence of microbial mat without bioherm structures, associated marine fauna or tidal current indicators suggests a lake setting. Well preserved leaf fossils in the micritic limestones

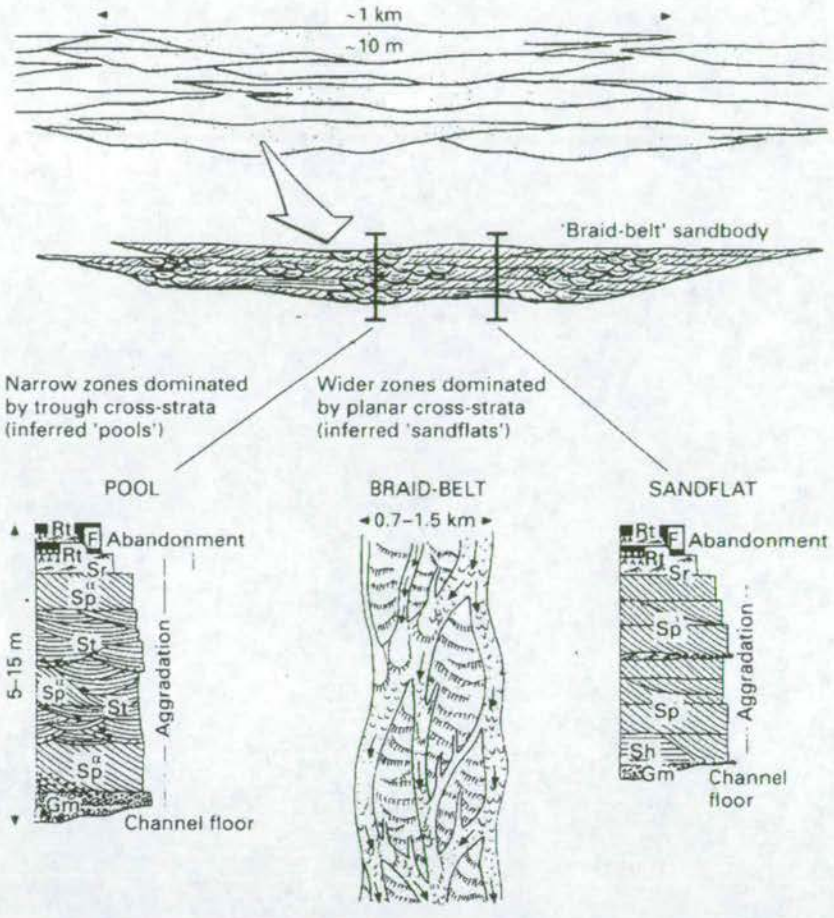

Figure 4.40 Geometry and internal organisation of channel Sandbodies of inferred low sinuosity, braided river origin in The Helvetiafjellet Formation, Lower Cretaceous, Spitzbergen (after Nemec 1992).

indicate that this water was poorly aerated, again consistent with a lake setting. The transition upwards to coals and then evaporitic beds suggests the gradual desiccation of this water body and colonisation by swamp and later playa conditions. These deposits bear a close resemblance to hypothetical successions from the margin of a saline evaporitic lake basin (Fig. 4.41; Kendall 1984).

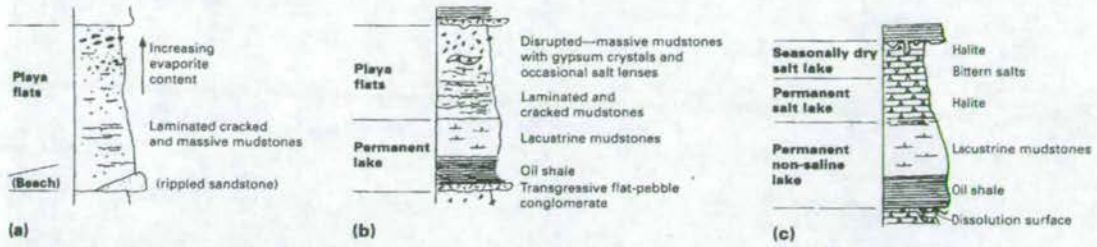

Figure 4.41 Hypothetical cycles from the margin (a) to centre (c) of a saline lake basin, showing sedimentary responses to increasing aridity and consequent shrinkage and evaporitive concentration of the lake (after Kendall 1984).

Bademdere section overview

The composite Bademdere section shows a transition from lacustrine conditions through a phase of desiccation (Testideresi section) to a terrestrial braid-plain setting (Kovali section and Bulanlik section).

4.4.2.2 The Alpu section (Fig. 4.14)

Facies 2E

The base of the composite Alpu section is characterised by clast supported, well imbricated, laterally continuous conglomerate bodies (Facies 2E). Their clast-supported nature indicates stream flow rather than debris flow transport, and their lateral continuity suggests a sheet flood, rather than channel transport mechanism. These deposits are interpreted as the upper part of a fluvial braided fan, similar to that of the outwash fan near the Scott Glacier, Alaska (Fig. 4.42, Boothroyd 1972). Higher up the succession laterally continuous sand bodies start to dominate, with similar characteristics to Facies 2C above. These are interpreted as braided river sand bars and channel fills.

The Alpu road section and Avcilar section contain similar facies associations to those found in the majority of the Bademdere section. Facies 2A (floodplain), 2B

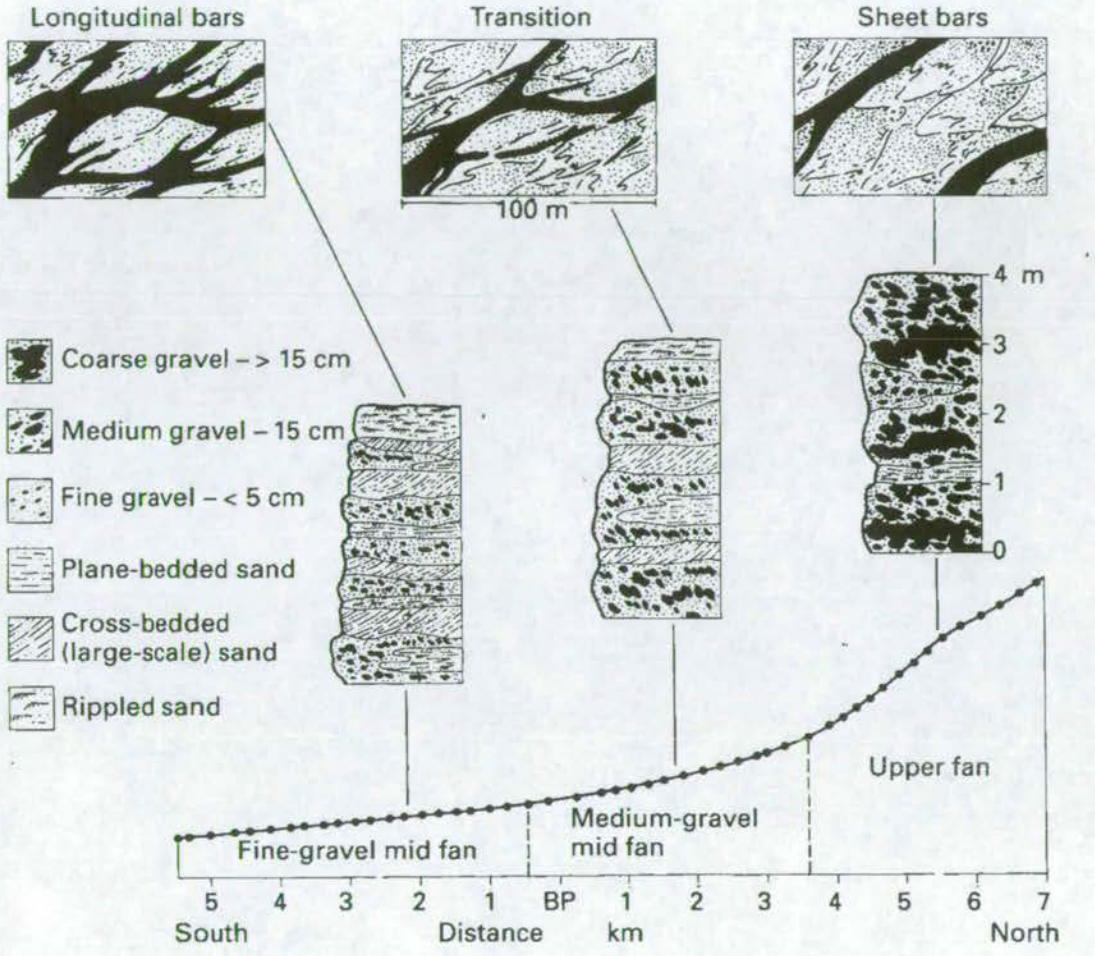

Figure 4.42 Changes in gradient, bar type and internal structure along an alluvial fan in front of the Scott Glacier, Alaska (after Boothroyd 1972).

(conglomerate channel fill) and 2C (braided river sandstones) are closely associated throughout the remainder of the section. The Alpu section represents a transition from a high-energy alluvial fan environment to a lower energy braided river environment.

4.4.2.3 Lateral Facies Changes within the EFZ

Any correlation of logged sections in the terrestrial Çukurbağ Formation is problematic in view of the lack of dateable fauna and marker horizons; hence, there is no

recognisable internal stratigraphy. Fig. 4.43 is an attempt to correlate these sections using changes in clast type within the fluvial conglomerates and gravels. A gradual change from ophiolite related (gabbro and chert dominated, 6.2.6) to carbonate sourced (limestone dominated, 6.2.1) conglomerate clasts is seen half way through the Bademdere section and also in other sections throughout the EFZ (6.3.3). The Formation is bounded by a lacustrine and evaporitic member at the base (best seen in the Testideresi section at Bademdere) and an angular unconformity at the top (with the Late Miocene Burç Formation).

The upper alluvial fan facies (facies 2E) is present at the base of the Çukurbağ Formation throughout the EFZ but is thickest at Pozanti, Alpu and Dagdibi. The braided river facies (association of facies 2A, 2B and 2C) is most prevalent in the upper parts of the Bademdere and Alpu areas. These are areas of maximum thickness of the Çukurbağ Formation and have been interpreted as depocentres from palaeocurrent patterns.

4.4.2.4 Was the Oligo-Miocene basin bounded by the present Ecemiş Fault Zone?

Palaeocurrent evidence suggests that the Oligo-Miocene Çukurbağ Formation was deposited in an inward-draining basin with depocentres near Bademdere and Alpu (Fig. 4.8b). Koçyiğit & Beyhan (1999) believe that Oligo-Miocene deposition was controlled by the present-day bounding faults, citing the unpublished PhD thesis of Uçar (1997). However, Karadenizli (1991) argues that present-day bounding faults were not present during Oligo-Miocene deposition and that sediment was sourced from the west. To test these conflicting hypotheses I examined exposures of the Çukurbağ Formation where they abut against the bounding faults of the Ecemiş Fault Zone. The following observations were made:

(i) Relatively fine-grained floodplain facies (facies 2A) are often seen abutting the main bounding faults. At Akça village (Fig. 4.44) conglomerate-filled channels in an

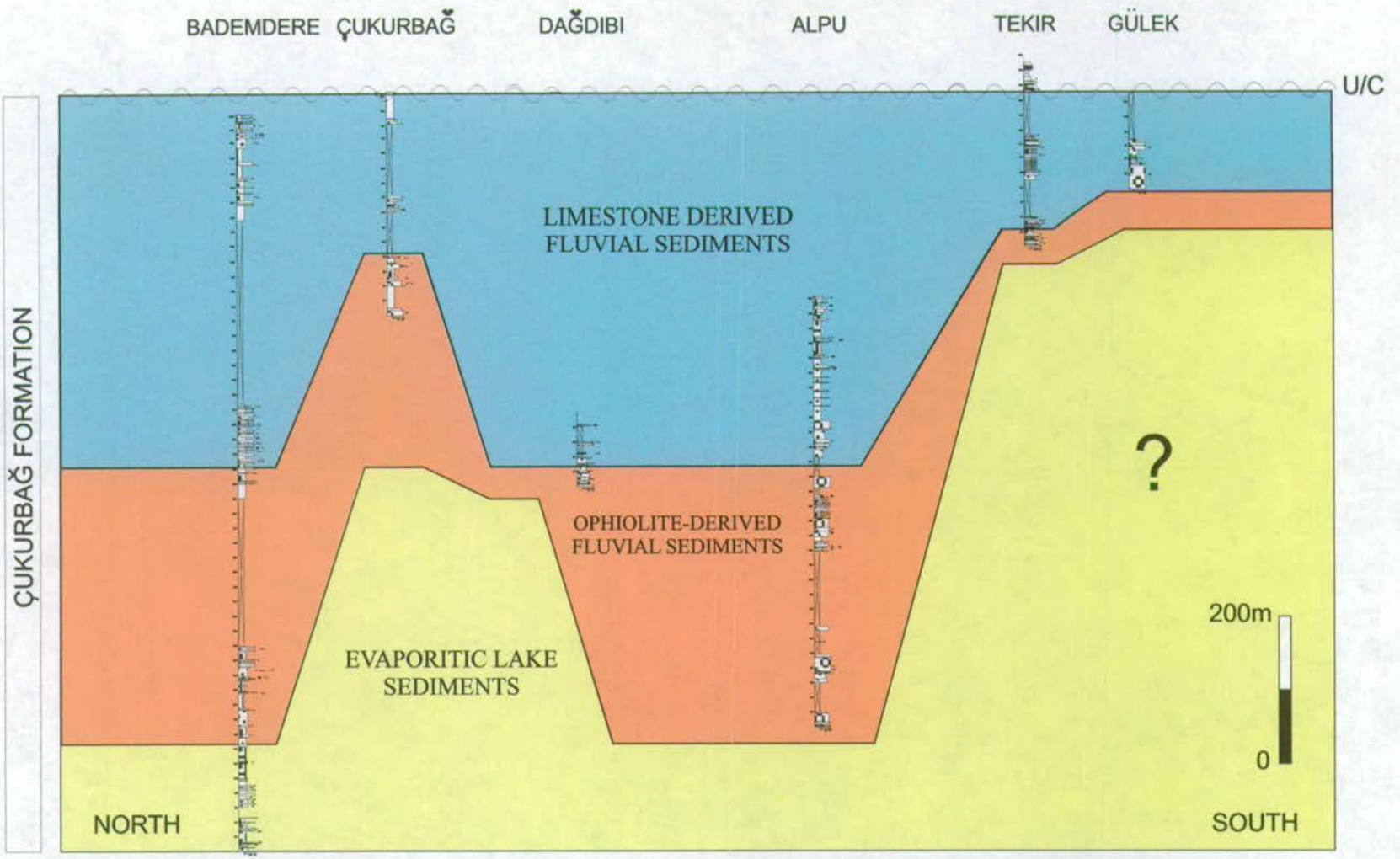

Figure 4.43 Log correlation for measured sections of the Çukurbağ Formation within the EFZ. Correlations are mainly based on the Çukurbağ Fm.-Burç Fm. unconformity, but also on the basal lake and swamp facies and changes in conglomerateclast lithology. Vertical scale is acurate, horizontal scale is not. Location of sections is shown in Fig. 4.11a.

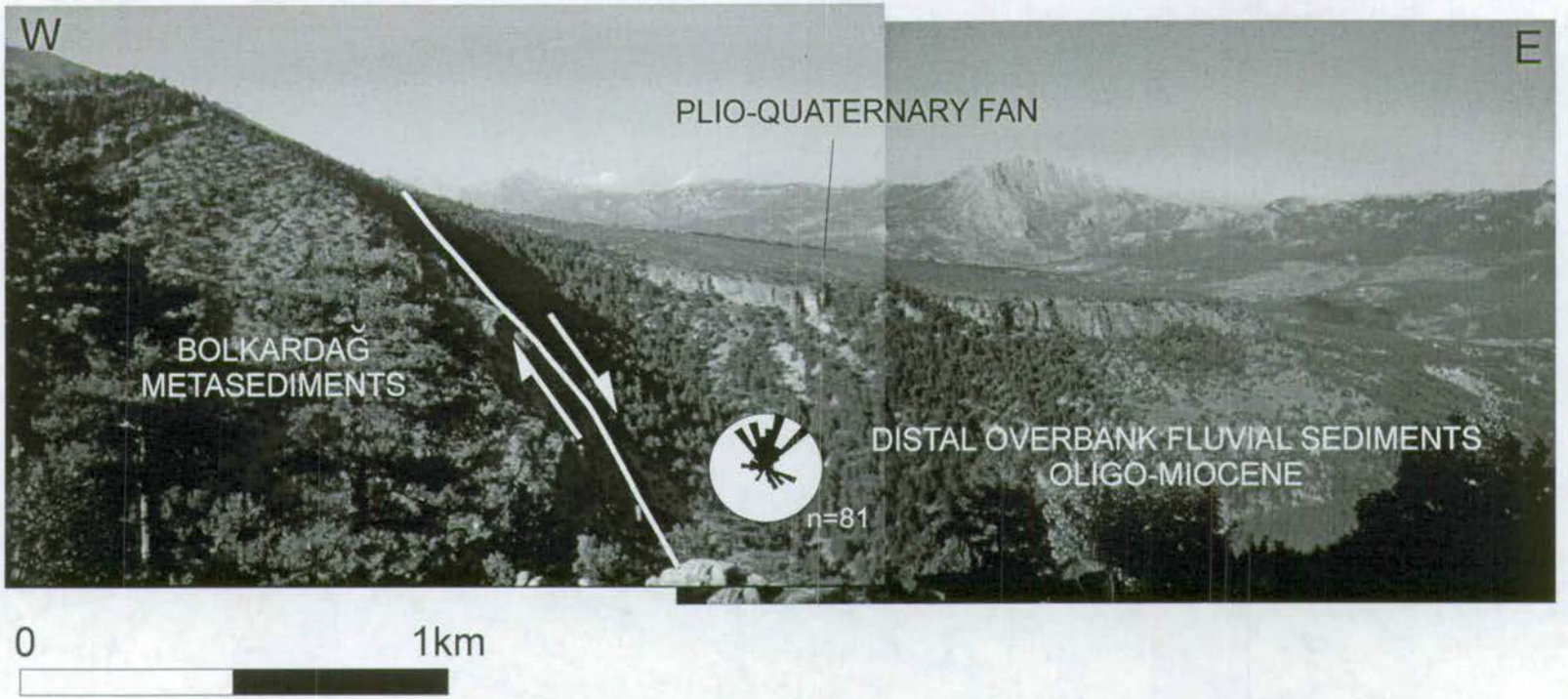

Figure 4.44 Palaeoflow is axial to the EFZ (N-directed) directly adjacent to fault scarps in many locations. Low-energy mudstones (Facies 2A) are also seen directly adjacent to fault scarps. Akça, near Pozanti. Rose diagram represents palaeoflow direction in hangingwall sediments (N is at the top). Subscript number indicates number of palaeocurrent datapoints.

(overbank) mud-dominated succession are seen directly adjacent to the main fault scarp with palaeoflow toward the N, axial to the fault zone (Fig. 4.44). If the fault was active during sedimentation then coarser, more proximal sediment would be expected, with palaeoflow directly away from the scarps. What we see, however, is the presence of fine-grained terrestrial mudstones and siltstones adjacent to the bounding fault scarp with no consistent change in sediment grade away from the scarp. The same relationship can be seen all the way along the fault zone, especially at Alpu, Tekir and Bademdere (Fig. 4.11a).

(ii) From the palaeocurrent data (Fig. 4.8b) it is clear that palaeoflow is frequently axial along the fault zone (N or S directed). Axial flow is seen in basal sediments close to main fault as well as those further up the succession.

(iii) In an attempt to study facies variations across the fault zone (E-W trends) I compared two outcrops of the Çukurbağ Formation at Bademdere (Fig. 4.11a): the Kovali River section (west, Fig. 4.12b) and the Bulanlik River section (east, Fig. 4.12c). Although not exact time equivalent sections, these are the nearest to time-equivalents available in the Çukurbağ Formation of the EFZ, given its deformed nature. Facies trend from higher energy furthest from the bounding fault (deeper conglomerate-filling channels at Kovali River section) to lower energy facies adjacent to the bounding fault (floodplain dominated succession at Bulanlik River section). This is the opposite of what would be expected if these sediments were sourced from present-day fault scarps.

From the above observations it is concluded that the deposition of the Oligo-Miocene Çukurbağ Formation was not controlled by the bounding faults of the Ecemiş Fault Zone as seen today. It is concluded that the Oligo-Miocene terrestrial basin was originally more extensive to the east and west than the present EFZ and that much of the original succession has been removed by uplift and erosion in the footwalls of later

faults. Although having a wider lateral extent, this Oligo-Miocene terrestrial basin was centered on the present-day EFZ.

4.4.2.5 The Aktoprak section (Fig. 4.16)

The composite Aktoprak section comprises four distinct facies associations:

Facies 2F

Facies 2F is found at the base of the Aktoprak section. It comprises a thick succession of micritic limestones and rhythmite-like calcareous mudstones which contain freshwater gastropod and ostracod body fossils (Fig. 3.3b). 'Rhythmites' are defined as rhythmically bedded deposits of mudstones and siltstones, often characteristic of lacustrine sedimentation (Jackson 1997). The fauna and 'rhythmite' nature of the sediments indicate that these rocks were deposited in a standing body of freshwater. Rhythmites are the most characteristic lacustrine facies (Reading, 1978) and here they may represent varves (de Geer 1912); however, due to a lack of temporal constraint on sedimentation rate, the duration of each lamination cannot be determined. Leaf fossil debris and wave ripple lamination suggest that deposition took place near to the lake margin.

Facies 2G

This comprises a succession of interbedded stromatolitic algal mats (laterally continuous over at least 20m) and calcareous mudstones. Associated freshwater ostracod assemblages indicate that these algal mats grew in a lake margin environment. Facies 2G is found directly overlying facies 2F. Based on the example of Littlefield Lake, Michigan (Fig. 4.45, Murphey & Wilkinson 1980) gastropod- and ostracod-rich mud (Facies 2F) is generally found in deeper lake water than that of algal mat development (Facies 2G).

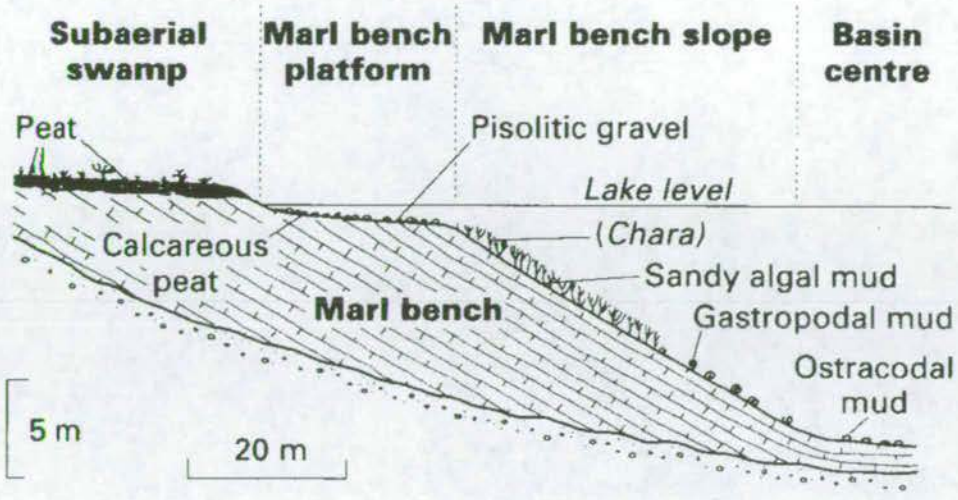

Figure 4.45 Typical cross-section through the margin of Littlefield Lake, Michigan, showing the morphology of the marl bench and the distribution of modern facies (after Murphy & Wilkinson 1980).

The upper part of the Aktoprak section is characterised by Facies 2A (floodplain siltstones) and 2C (braided river sandstones). Facies 2C in this area contains groove marks and parallel lamination on bedding surfaces, indicating rapid current flow.

Aktoprak section overview

The section as a whole displays a transition from open freshwater lake facies, to algal lake margin, into terrestrial braided-river fluvial conditions. Within the terrestrial succession the erosive nature and grain size of sandstone bodies decreases up section, indicating a decrease in depositional energy and possibly lower slope gradients.

4.4.2.6 Lateral Facies Changes within the Aktoprak Basin

Correlation of sections in the Aktoprak Basin is aided by the presence of the basal non-marine limestones (named the Kurtulmus Member by Demirtaşli *et al.* 1984). A correlation of measured sections from west to east in the Aktoprak Basin is shown in

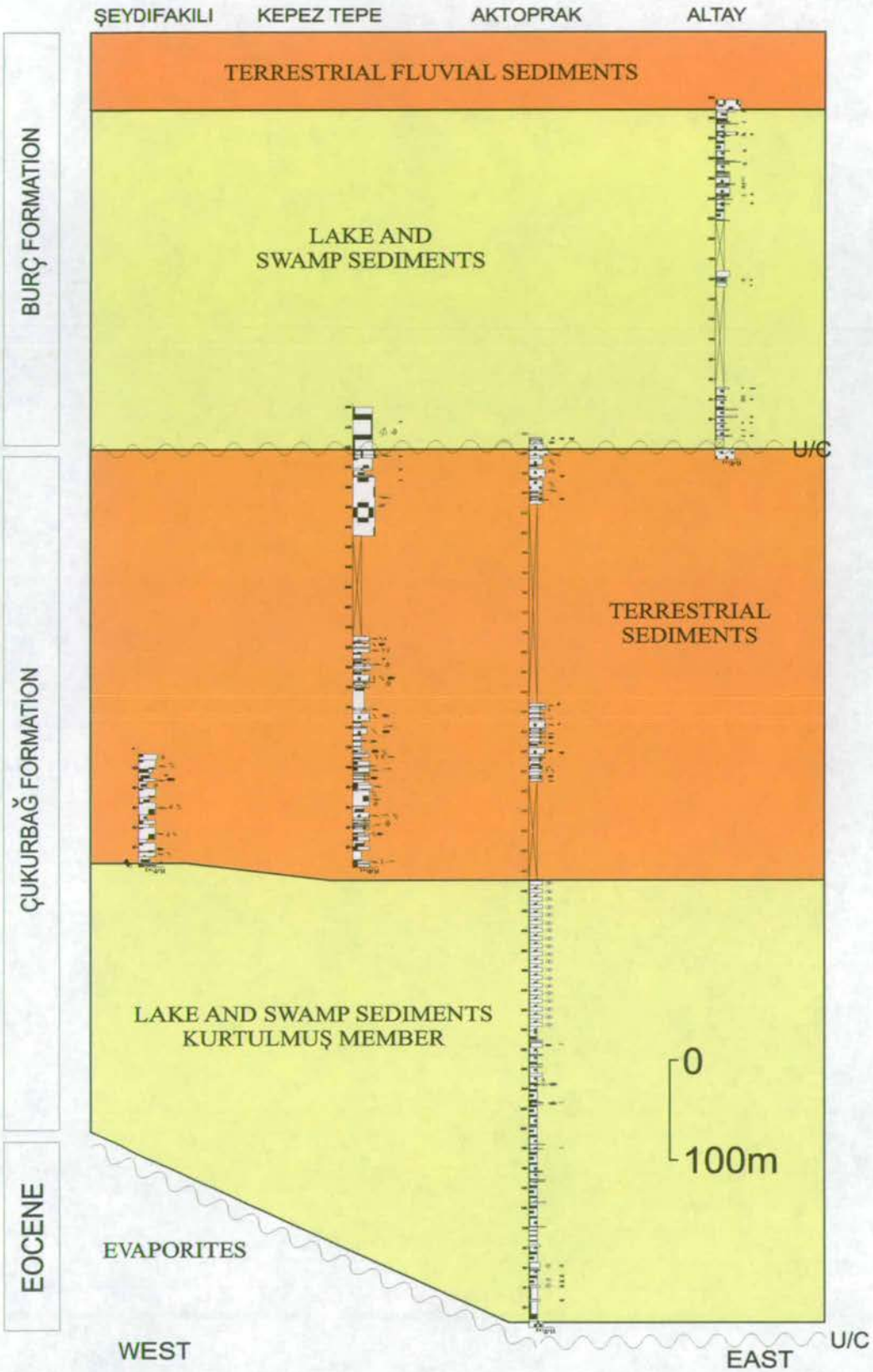

Figure 4.46 Log correlation for measured sections of the Çukurbağ Formation within the Ulukişla Basin. Correlations are mainly based on the Çukurbağ Fm.-Burç Fm. unconformity, but also on the basal lake and swamp facies. Vertical scale is accurate, horizontal scale is not. See Fig. 4.11b for locations of sections.

Fig. 4.46. A general trend of sedimentary transport from the west to the east can be inferred from the decreasing thickness and grain size of sand and gravel bodies and the increasing proportion of floodplain siltstones and mudstones (facies 2A) toward the east. This is also supported by palaeocurrent data throughout the Aktoprak Basin (Fig. 4.10b).

4.4.2.7 The Doğan River section (Fig. 4.18)

The following facies were identified from the Doğan River section:

Facies 2H

The basal 100m of the section comprises 5-10m thick conglomerate sheets with erosional bases and highly texturally immature clasts, which are supported by a silty to sandy matrix. These are interpreted as large continental debris flow deposits, based on their matrix-supported nature, overall wedge-shaped geometry in cross section (thickest at basin margins) and close association with other continental facies. Such debris flows are commonly found in the upper parts of alluvial fan complexes (Fig. 4.47, Spearing 1974). Conglomerates are interbedded with red siltstones containing root fossils (facies 2A).

Facies 2I

Sand bodies containing trough and planar cross-bedding are seen in association with facies 2A (floodplain siltstones). These have concave-up bases and flat tops and have a lateral extent of 2-5m. Point bar structures were not identified and there is rapid switching from one channel to another, so a meandering river interpretation is suspect. It seems more likely that these sandstone bodies represent the distal part of a braided river system (considering its association with facies 2C).

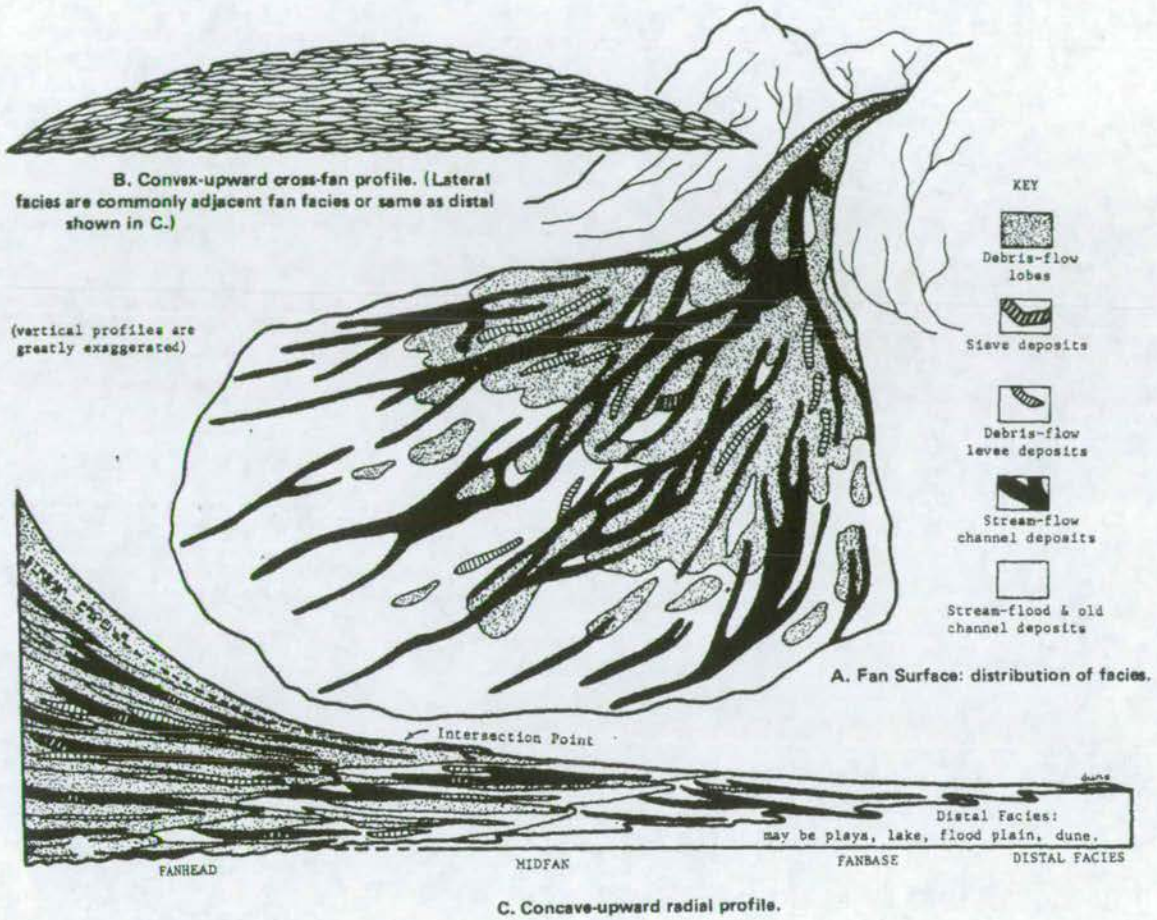

Figure 4.47 Typical surface features and cross-sectional profiles of alluvial fans. (a) fan surface, (b) profile across the fan, (c) longitudinal profile (after Spearing 1974).

Facies 2J

Laterally discontinuous coal stringers outcrop in association with facies 2A (floodplain siltstones) and facies 2I (distal braided-river sandstones). These are interpreted as river bank swamp deposits (Fig. 4.48, McCabe 1984).

Facies 2K

The central part of the Doğan River section is characterised by laterally continuous micritic limestones containing marine gastropod, foraminifera and ostracod fauna (Fig. 3.3c). These have been interpreted as lagoonal facies by Ünlügenç *et al.* (1993);

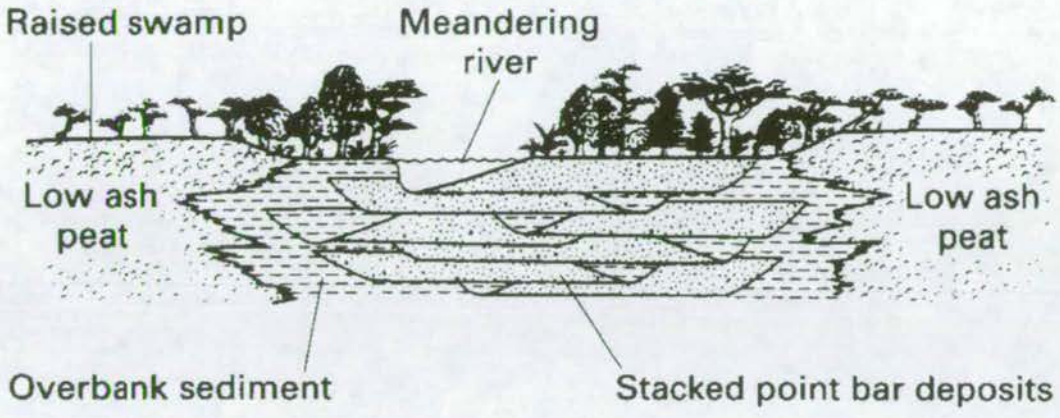

Figure 4.48 A model for the fluvial deposition in an area of raised swamps. The elevated swamp inhibits overbank flooding, prevents avulsion, and results in strip-like coal deposits adjacent to fluvial channel-filling sandstones (after McCabe 1984).

however, this interpretation is not uncontroversial. The presence of planktic foraminifera and lack of benthic foraminifera indicates open marine conditions (water depth >100m). There is a lack of tidal palaeocurrent indicators, barrier island sands, and bioturbation, all of which are expected in a lagoonal environment (Fig. 4.49, Reinson 1984). However, the close association of these limestones with facies 2I and 2J (terrestrial) and the presence of detrital plant material indicates that a marginal marine lagoonal interpretation is more likely. The global sea level curves of Haq *et al.* (1987) highlight a significant sea level rise at the base of the Oligocene (~35Ma) and a significant sea level fall during the Mid-Oligocene (~31Ma), with high relative sea levels during the Early Oligocene. Biostratigraphic work (Fig. 3.3c) points towards an Early Oligocene age for these sediments and they are therefore likely to have been affected by these high relative sea-levels.

Facies 2L

Closely associated with the lagoon limestones are beds of organic-rich siltstones and mudstones. These contain vertical (*Skolithos*-like) burrows, root and leaf fossils. The

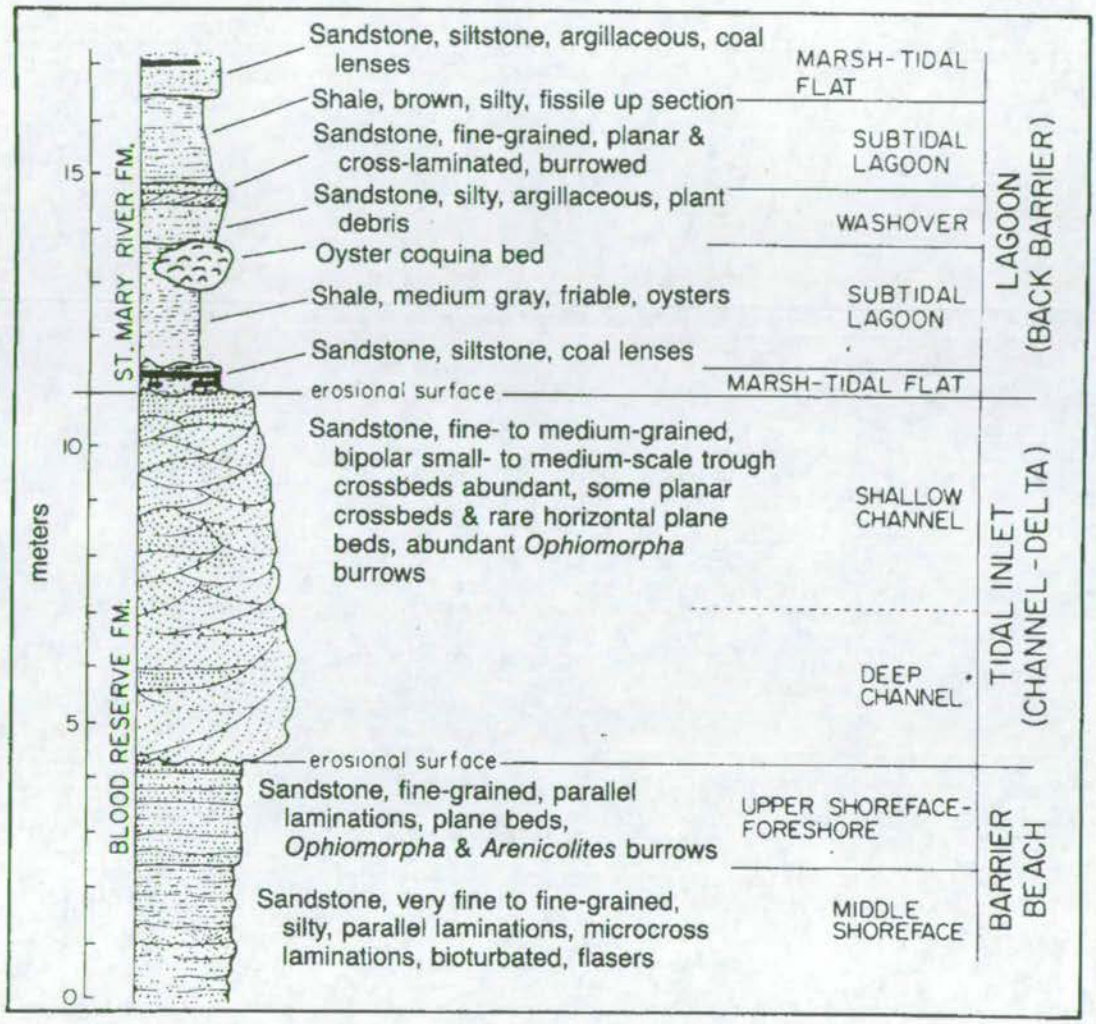

Figure 4.49 Typical stratigraphic section from a lagoon environment. Composite stratigraphic section of Cretaceous formations in southern Alberta, Canada. Back barrier lagoonal deposits of the St. Mary River Formation overlie tidal-inlet and tidal-delta deposits of the Blood Reserve Formation (after Reinson 1984).

willow leaf fossils suggest a well irrigated environment with abundant freshwater drainage. They are interpreted as swamp, or lake-margin deposits on the periphery of the lagoon.

The upper part of the Doğan section is dominated by calcareous siltstone-mudstone rhythmites, which contain exceptionally well preserved leaf fossils (Fig. 4.21a & b) and

freshwater ostracod assemblages. The quality of leaf preservation suggests that leaves were deposited in a substrate where oxygen and aerobic bacteria were excluded (Black 1970), and hence an environment with low rates of circulation, such as a lowland swamp or lake. The interpretation of an open lake facies by Ünlügenç *et al.* (1993) is in agreement with the above evidence.

Overview of the Doğan River Section

The Doğan River section begins with continental debris flow deposits, deposited on steep slopes. This passes upwards into braided-river deposits, then to a distal braided-river plain setting, colonised by swamps. The landscape was submerged mid-way through the succession, resulting in a shallow lagoon environment. Subsequent sea level changes or tectonic uplift have resulted in the restoration of non-marine conditions, dominated by lacustrine deposition.

4.4.2.8 Lateral Facies Changes within the Karsanti Basin

A correlation of logged sections from west to east across the Karsanti Basin is shown in Fig. 4.50. High-energy debris flows (facies 2H) and braided river deposits (facies 2C, Section 4.4.2.1), were found at all localities at the margins of the basin as basal sediments. Toward the centre of the basin (Kabaskal) a new marginal marine facies is seen (facies 2L), with interbedded wave-rippled sandstones and oyster assemblages. I infer from this and palaeocurrent evidence (Fig. 4.20) that the basin depocentre was located in the Kabaskal area (location Fig. 4.20) during the Oligocene, and that this area saw the incursion of fully marine conditions for a short period. The margins of the basin appear to have only experienced marine conditions for a short period of time, with lake facies dominating in the upper part of the succession.

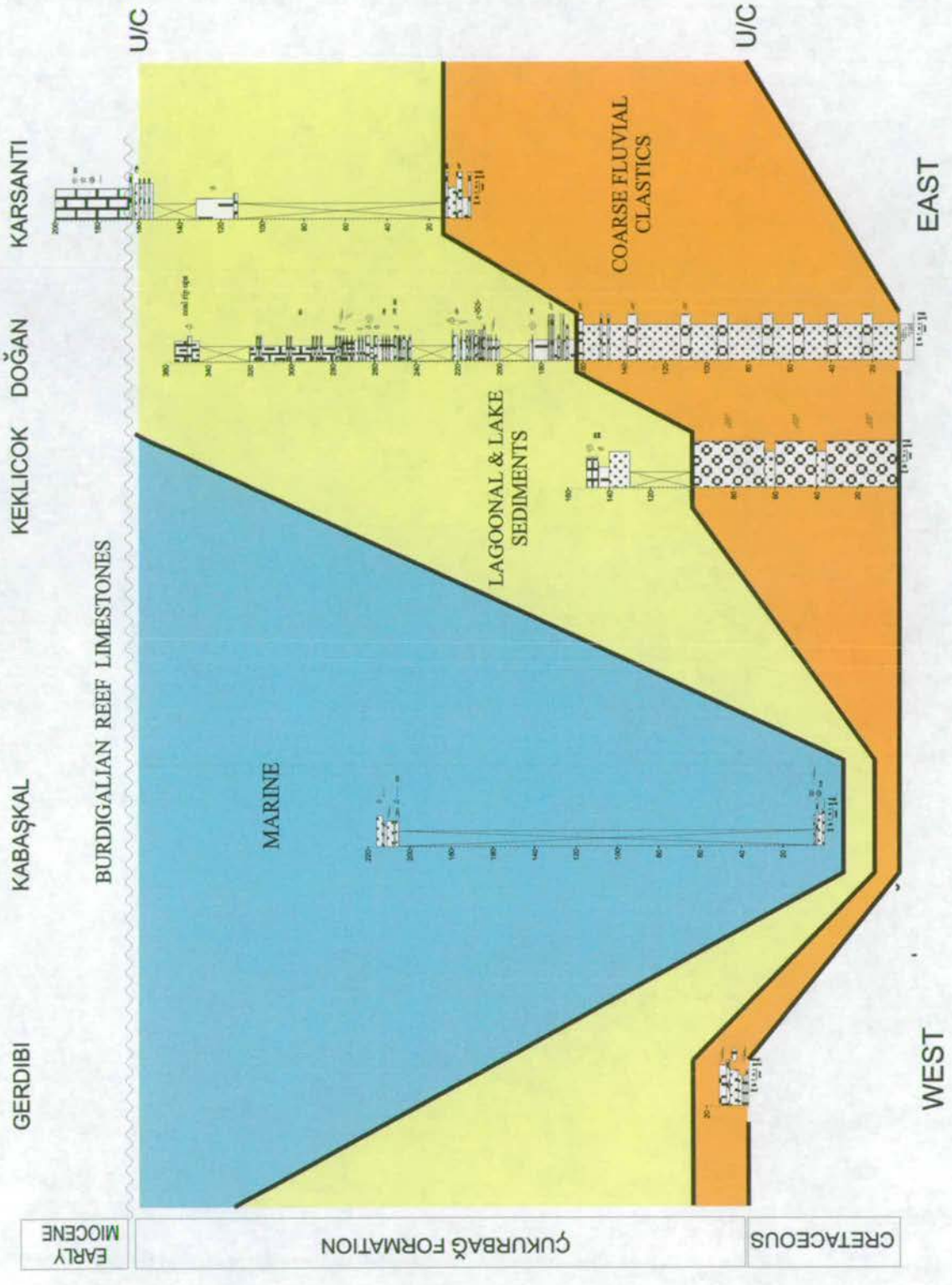

Figure 4.50 Log correlation for measured sections of the Cukurbag Formation within the Karsanti Basin. Correlations are mainly based on the basal clastic unit, but also on the lake and lagoon facies. Vertical scale is accurate, horizontal scale is not. See Fig. 4.11c for locations of sections.

4.4.2.9 Summary of Oligo-Miocene sedimentation

A block diagram representation of sedimentation during the Oligo-Miocene is given in Figure 4.51. Palaeocurrent data (Fig.s 4.8b, 4.10b & 4.20) indicates that sedimentation was divided into two continental basins: the inward-draining Karsanti Basin and the larger Ulukişla-EFZ Basin, which had its depocentre in the central EFZ. The basal sediments of the Çukurbağ Formation in the EFZ and Karsanti Basin are coarse debris flows and alluvial fanglomerates, indicating that significant topographic highs existed at the basin margins. Kaleboynu Formation facies data indicates these topographic highs were not present during the Middle Eocene, and the Haq *et al.* (1987) curve indicates that the Early Oligocene was a period of high sea levels, which excludes fluvial rejuvenation as a controlling factor on basal Çukurbağ Formation sedimentation. Data from subsidence curves show that the Early Oligocene was a time of zero subsidence (Fig. 5.12), therefore a period of tectonic uplift across the Taurus Mountains during the Early Oligocene is implied as the dominant factor controlling the deposition of the basal Çukurbağ Formation. Palaeocurrent data and relationships at the present boundaries of the EFZ indicate that the Çukurbağ Formation was not shed from, or influenced by present-day fault scarps.

Freshwater lake conditions were established in the Ulukişla Basin during the Late Oligocene – Early Miocene. In the EFZ, evaporitic lakes existed in low-lying areas, with braided rivers draining into them. The Karsanti Basin appears to have been at a lower topographic level than the Ulukişla-EFZ Basin during this period, and experienced lagoon and shallow-marine conditions. Freshwater lakes also existed at the margins of this basin.

The Early Miocene (upper part of the Çukurbağ Formation) of the entire area was dominated by braided river and floodplain sedimentation, with little evidence for the continued existence of freshwater or evaporitic lakes.

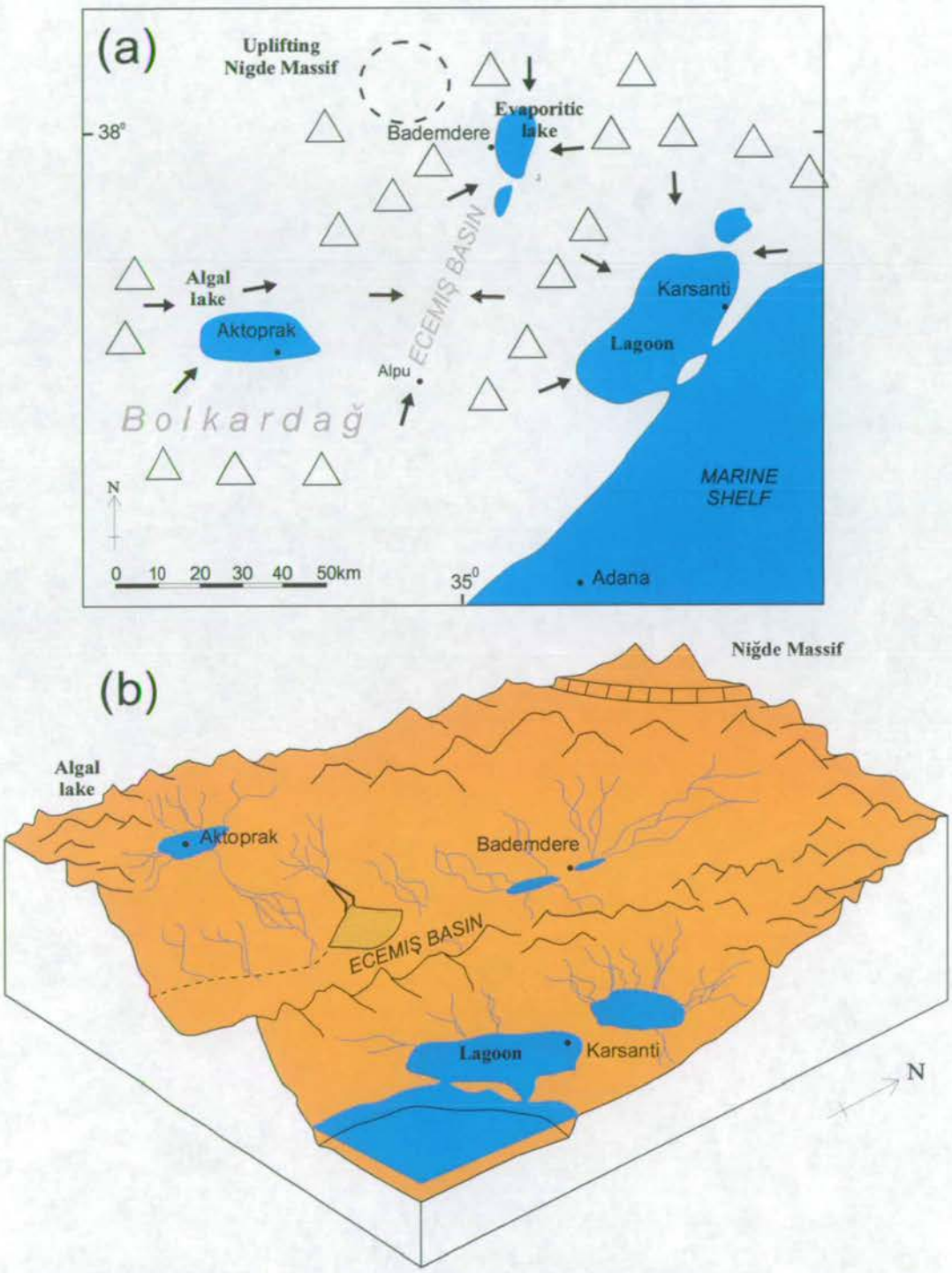

Figure 4.51 (a) Map of Late Oligocene - Early Miocene (Çukurbağ Formation) palaeo-environments, based on sedimentological data. Black dots represent current positions of settlements, black arrows represent simplified palaeocurrent data, triangles represent topographic highs. (b) Block diagram of Late Oligocene - Early Miocene (Çukurbağ Formation) palaeo-environments based on sedimentological data. Vertical and horizontal scales are not accurate.

4.4.2.10 Ancient and modern analogs of the Çukurbağ Formation

The phenomena of coarse clastic sedimentation in areas of active extension has been widely documented. In western Turkey this process is recorded in the Latest Oligocene – Early Miocene (21-15Ma) Dagdere and Tepeköy Formations of the Gördes and Selendi Basins. These Formations comprise continental red-beds which have been interpreted as alluvial fan, terrestrial debris flow and sheet flood deposits (Purvis 1998). Alluvial fans and debris flows were deposited during detachment faulting along the northern margin of the Menderes Metamorphic Massif; this passes upwards into braided river stream and alluvial plain facies, which was deposited during Late Miocene slope re-equilibration, after faulting had ceased (Purvis 1998). This succession is similar that of the Çukurbağ Formation; the base of both Formations is characterised by alluvial fan and debris flow deposits, passing upwards into braided river and alluvial floodplain facies. The trigger for sedimentation is also similar; post-collisional extension ('orogenic collapse'), resulting in the exhumation of metamorphic complexes (Cf. the Niğde Massif and Menderes Massifs).

Another useful analog for the Çukurbağ Formation can be found in the Lower Miocene Clews Formation (Mojave Desert, California). Syn-extensional continental deposits were controlled by west-facing half-graben. The initial stages of sedimentation were characterised by a closed drainage pattern, with marginal sheetflood-dominated alluvial fans and central lakes (Fillmore 1993). This is similar to the depositional environment envisaged for the basal sediments of the Çukurbağ Formation in the EFZ. Initial lacustrine sedimentation is interpreted as reflecting the development of a flexural sag basin in the hangingwall (Fig. 4.52a). Subsequently coarse conglomerates and breccias prograded across the basin, and this is interpreted as a response to normal faulting, antithetic to the low angle detachment fault (Fig.4.52b). There is not enough data available from the Çukurbağ Formation to infer the existence of such antithetic faults, but the general sedimentary succession is similar.

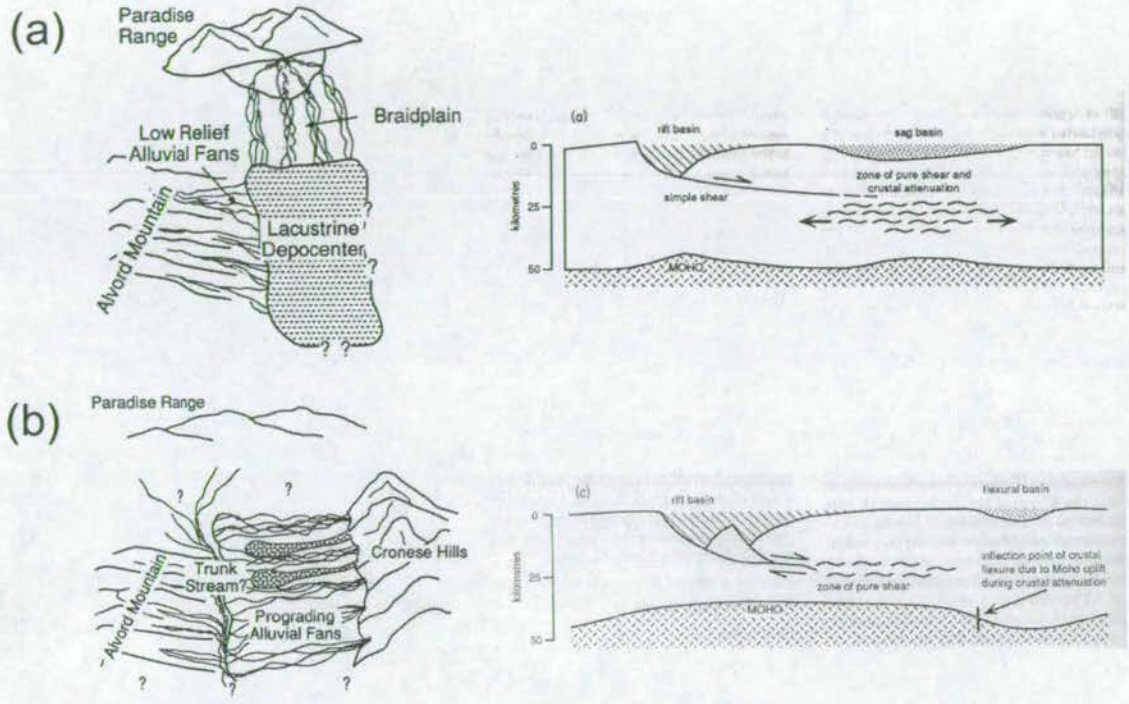

Figure 4.52 Palaogeogeraphy and depositional systems (left) and crustal model for basin development (right) in the Clews Formation of Alvord Mountain, Central Mojave Desert, California (after Fillmore 1993). **(a)** lacustrine deposition in a supra-detachment sag basin, **(b)** subsequent alluvial fan and braided stream deposition in a supra-detachment rift basin.

A modern-day example of strike-slip within a zone of crustal-scale extension is the Mormon Point supra-detachment basin (Death Valley, California), in the southern part of the Basin and Range Province (Burchfiel *et al.* 1995). This area has undergone intra-continental extension for at least ~15Myr, and Death Valley has formed a dextral pull-apart structure since the Early Pliocene (~5Ma). The combination of these processes has resulted in an asymmetric basin, which has filled with alluvial fanglomerates, braided stream conglomerates and sandstones, lacustrine limestones and evaporites during the Late Cenozoic.

4.4.3 Interpretation of the Late Miocene Burç Formation

4.4.3.1 The Burç section (Fig. 4.23)

Facies 3A

The majority of the Burç section is comprised of silty limestones which contain plant fragments, freshwater gastropod and ostracod assemblages (Fig. 3.3a). These are often rhythmically laminated (similar to facies 2F) and are interpreted as open lacustrine deposits.

Facies 3B

Closely associated with these are biohermed stromatolite beds and discontinuous low quality, silty coals. These are interpreted as lake margin facies algal mats and swamps (cf. facies 2D). This was also the interpretation made by Yetiş (1978).

Facies 3C

A 2m-thick sand body crops out, 45m from the base of the section, which is laterally continuous over 6-7m. It is characterised by 50cm-thick tabular foresets which prograde at 90^0 to the direction of flow (Fig. 4.25). These are interpreted as lateral accretion surfaces in a point bar deposit (Bernard & Major 1963, Leeder 1999). The geometry and internal structures of the sand body suggest that it represents a meandering river channel (Fig. 4.53).

The Burç section is dominated by rocks of open lacustrine (facies 3A) and marginal lacustrine (facies 3B) origin. There is also evidence for terrestrial conditions midway through the section where the distal sediments of a meandering river system are preserved.

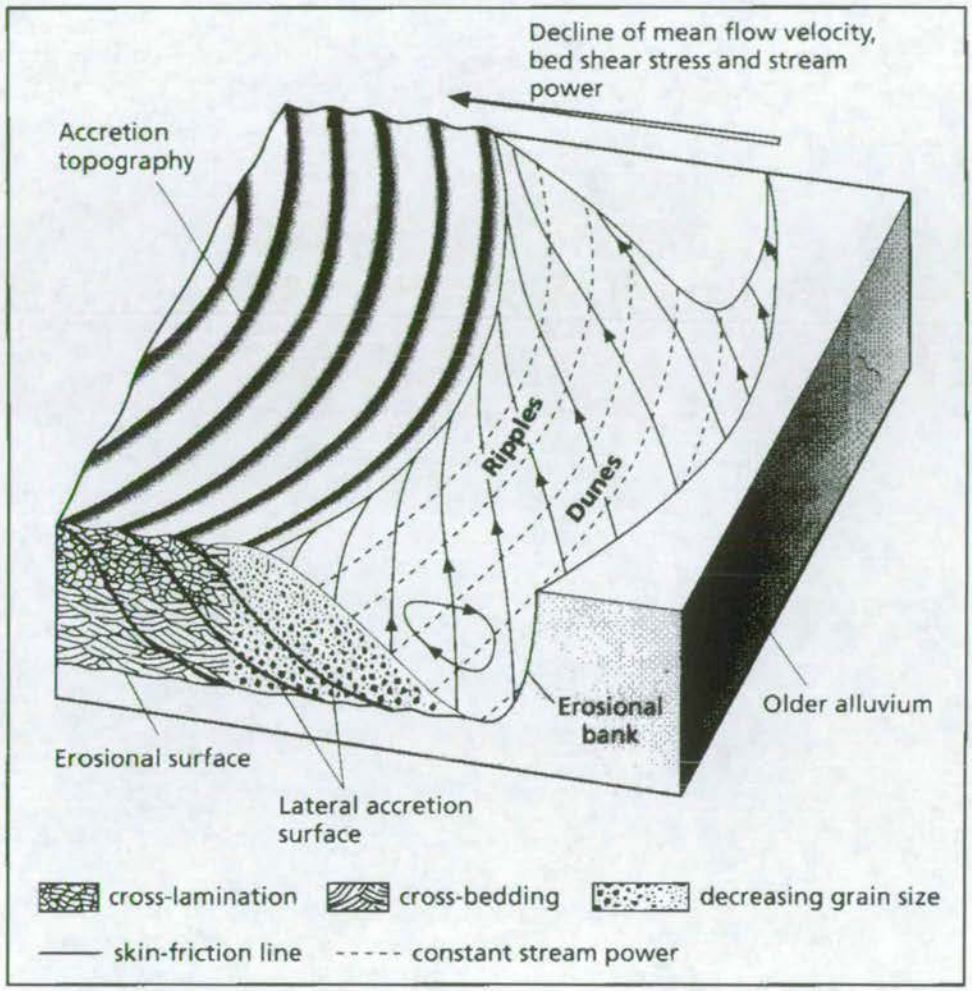

Figure 4.53 Helical flow in a meander bend causing regular changes in grain size, bedforms and sedimentary structures in the deposits of the accretionary point bar (after Leeder 1999).

4.4.3.2 The Gülek section (4.26)

Facies 3D

The thick (20-30m) basal conglomerates are texturally mature, clast supported and laterally continuous over at least 20m. These are interpreted as sheet-flood deposits in

the upper part of an alluvial fan (similar to facies 2E), which result in the vertical stacking of laterally continuous coarse conglomerates (Fig. 4.42; Boothroyd 1972).

Facies 3E

Above the coarse conglomerates deposition is dominated by laterally continuous, coarse, sandstone bodies which contain trough- and tabular cross-bedding and scour into underlying sediments. These are interpreted as braided river sandstones, similar to those of facies 2C (Fig. 4.40).

Facies 3F

Braided river sandstones are closely associated with red siltstones and mudstones which bear root fossils. This is similar to the previously identified floodplain facies (facies 2A).

Facies 3G

In the central part of the Gülek section calcareous siltstones outcrop, bearing abundant calcareous nodules and root fossils. These are interpreted as caliche palaeosols (Machette 1985), which record arid or sub-humid conditions where evaporative loss exceeded the supply of water to the surface by rainfall or flooding (Reading 1978).

Facies 3H

Interbedded with the caliches are white crystalline limestones which encrust plant stems and other plant material in concentric layers (Fig. 4.27c). These layers contain discontinuous algal lamination are interpreted as cold water algal tufa deposits (see below). The limestone also forms as concentric balls which are interpreted as oncolites. Oncolites form by the accretion of successive layers of blue-green algae around a nucleus in an agitated sub-aqueous environment (Burne & Moore 1987). These rocks differ from facies 3B (algal lake margin) in that algae is preserved as oncolites, rather than as stromatolites.

Tufa

The terms travertine and tufa are both used to describe $CaCO_3$ deposited from solutions of calcium bicarbonate. A classification scheme based on the processes and environments of deposition of these deposits is shown in Fig. 4.54 (Glover 1996). This shows that Tufa is mainly precipitated from cold water springs with the aid of algae, whereas travertine is associated with hot springs and with bacterial or non-biogenic precipitation. Tufa deposits commonly form around the mouths of cold springs bearing $CaCO_3$-supersaturated water and are commonly associated with lacustrine environments (Shearman *et al.* 1989). Groundwater-fed tufas and travertines can also provide palaeoclimate information (Evans 1999). Holocene tufas are characteristically found in humid, temperate climates, whereas tufa growth is slowed by cold conditions, and semi-arid conditions (such as those during the Oligo-Miocene of the EFZ) can rarely maintain the high water tables necessary for sustained tufa deposition (Pedley 1990).

The Mediterranean area is ideally suited for tufa deposition, having significant quantities of carbonate basement and a temperate, humid climate with marked seasonality (the most favourable climate for tufa precipitation, Glover 1996). Tufa depositional environments can include: the barrage/lake system, the waterfall system, lacustrine and paludal (marsh) system, fluvial and slope systems. The close association of the Gülek tufas with caliche palaeosols and varved lacustrine limestones, and the encrusted plant material suggests a lake margin (paludal) setting (Fig. 4.55).

Facies 3I

The upper part of the section is dominated by sandy to silty bioclastic limestone (the Karaisali Formation of Yalcin & Görür 1984). These contain wave ripple lamination and the body fossils of echinoids, pecten, marine gastropods and crinoid ossicles, which have been dated as Burdigalian (Yalcin & Görür 1984). These limestones are interpreted as being deposited in a littoral to shallow marine shelf environment.

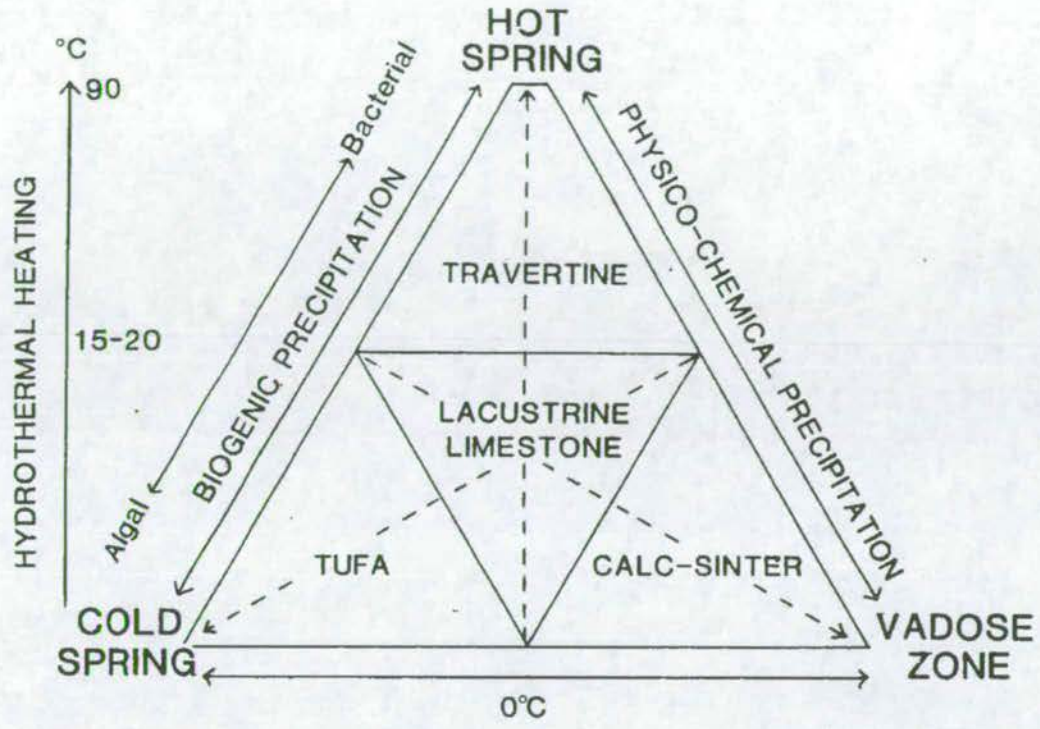

Figure 4.54 Classification of terrestrial carbonates. The corners of the triangle represent environments of deposition. Terrestrial carbonate types are shown by the four fields within the triangle and processes controlling precipitation are represented by the edges of the triangle and the dotted lines perpendicular to them. A quantitative representation of the hydrothermal heating line is given on the left (after Glover 1996).

Facies 3J

Several thin (15-20cm thick) conglomerate and gravel sheets are interbedded with the bioclastic limestones (facies 3H). These have erosive bases and are composed of texturally mature, well-rounded clasts, indicating that they are not sourced from the immediately local environment. These conglomerate bodies are interpreted as the distal part of gravel-rich submarine fan deposits (Prior & Bornhold 1988), issuing into the shallow marine zone. Submarine fans may be associated with fault activity on the EFZ taking place during the Burdigalian (Section 7.2.5).

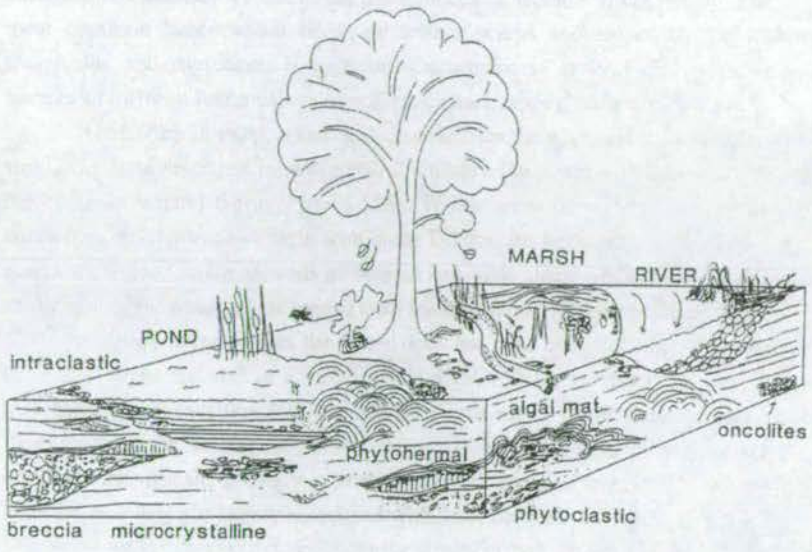

Figure 4.55 Model for tufa deposition in the lacustrine and paludal (marsh) system, showing the associated flora and fauna of the complex paludal system and its association with the deeper lacustrine microcrystalline carbonates (after Glover 1996 and Ordóñez & García del Cura 1983).

Gülek section overview

The Gülek section began in the terrestrial environment passing from basal alluvial fan conglomerates up into braided river sediments. Higher up the section (Tali Tepe) the succession is characterised by algal lake margin and caliche sedimentation. This was interrupted by another phase of alluvial fan deposition which marked the start of the Burdigalian marine transgression. Alluvial fans remained active during the transgression, shedding fan conglomerates onto the shallow marine shelf.

Due to the relationship of the Burdigalian limestones (Early Miocene) resting unconformably on inferred Burç Formation rocks, the age of the Burç Formation here must be revised to earliest Miocene (Fig. 4.56) rather than simply Miocene as previously inferred by Yetiş (1978). It is likely that the majority of the Burç Formation has been cut out by Burdigalian erosion.

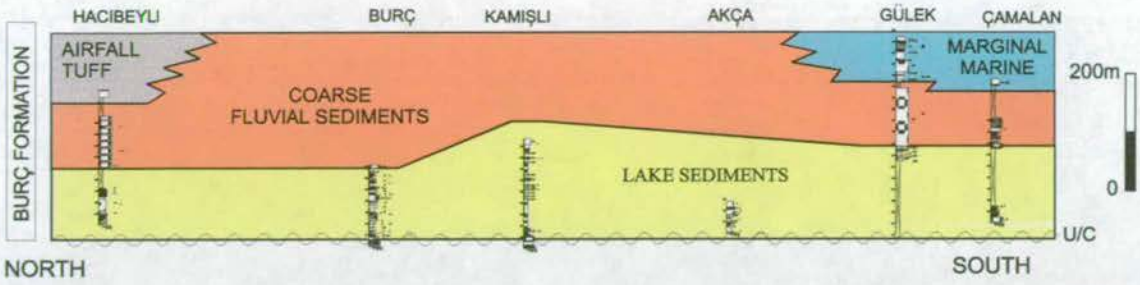

Figure 4.56 Log correlation for measured sections of the Burç Formation within the EFZ. Correlations are mainly based on the Çukurbağ Fm.-Burç Fm. unconformity, but also on the top of the lake facies. Vertical scale is accurate, horizontal scale is not. See Fig. 4.22a for locations of sections.

4.4.3.3 Lateral Facies Changes in the Late Miocene of the EFZ

A log correlation panel for outcrops of the Late Miocene Burç Formation is shown in Fig. 4.56. Correlations are made using the unconformable basal contact with the Çukurbağ Formation. Shallow lake and lake margin deposition is seen along the entire length of the EFZ during the Early-Late Miocene. From Tekir southwards the Burç Formation succession was influenced by marine incursions in its upper part. From Hacibeyli northwards the Ürgüp Formation unconformably overlies the Burc Formation, which includes airfall tuffs in its upper part (Fig. 4.56). These airfall tuffs are not part of the Ecemiş Fault Zone (*sensu stricto*, as defined by Yetiş 1978), but are discussed further in Chapter 9. They have been identified as airfall tuffs by Pasquare (1968) and Beyhan (1994).

The palaeocurrent history in the south of the EFZ reveals that there is an important change from N-directed flow during the Oligo-Miocene (Çukurbağ Formation) to S- and SE-directed flow during the Miocene (Burç Formation). This switch is approximately synchronous with the first marginal marine deposits at Gülek and Camalan. Marine conditions did not reach as far as Tekir where lacustrine marls and algal mats were prevalent; this suggests that a coastal barrier existed between Gülek and Tekir during the Early Miocene, with areas south of Gülek experiencing marine conditions.

4.4.3.4 The Hacibekirli-Altay section (Fig. 4.28)

The rocks of the Tozlu Tepe section are characterised by four facies. These include:

Facies 3F

Red calcareous siltstones and mudstones containing root fossils. These are interpreted as floodplain sediments.

Facies 3K

White micritic limestones bearing gastropod shells. These fauna have not been identified as freshwater or marine, but the lack of other marine fauna and structures suggests that the limestones were deposited under freshwater conditions. They closely resemble the lacustrine facies (facies 2F) identified in the Aktoprak section.

Facies 3H (variation)

A bed of white, finely crystalline limestone which formed in concentric layers around plant stems and other plant material. This is found in close association with the freshwater limestone described above (facies 3J). The thickness of this unit is laterally variable, from 2m to 0.5m. It is interpreted as a tufa deposit similar to those described in the Gülek section (facies 3H). Again, the close association with lacustrine facies and the encrustation of abundant plant stems and leaves suggests a lake margin paludal (marsh) environment of deposition (Fig. 4.55).

The upper part of the Hacibekirli-Altay section comprises further gastropod-bearing limestones (identified previously as lacustrine facies, 3K) and red, root-bearing siltstones (floodplain facies, 3F). The uppermost part of the Gucuk Tepe section is characterised by an interbedding of braided river sandstones (facies 3E) and alluvial fan conglomerates (facies 3D).

Hacibekirli-Altay section: overview

The basal and middle parts of the succession are characterised by open lacustrine and lake margin sedimentation. The upper part of the section is marked by an increase in depositional energy and a possible increase in slope gradients, resulting in braided river and alluvial fan sedimentation.

4.4.3.5 Lateral Facies Changes in the Late Miocene of the Ulukişla Basin

The section described was the only measured section of Late Miocene rocks in the Ulukişla Basin; thus, analysis of lateral facies change is necessarily limited. At Hacibekirli, the thickness of the tufa increases from 2m (N) to 44m (S) at the top of Kepez Tepe (1km S of Hacibekirli, Fig. 4.22b), suggesting that there was a lacustrine depocentre to the S of the current southern limit of exposure at Hacibekirli. The Ulukişla Basin has acted as a sub basin to the larger Tüzgölu Basin throughout the Cenozoic.

4.4.3.6 Summary of Late Miocene sedimentation

A representative block diagram of sedimentation during the Late Miocene is given in Figure 4.57. The dominant facies throughout the Late Miocene of the EFZ and the Ulukişla Basin was open lake or lake margin facies. The change from continental red-bed deposition during the Late Oligo – Early Miocene, to lacustrine-dominated deposition during the Late Miocene was possibly a result of the change from a more arid Mediterranean climate to a generally wetter and more humid one. This change has been documented between the Tortonian and Messinian in northeastern Africa (Griffin 1999) and it is likely that these results are also valid for southern Turkey during the same period.

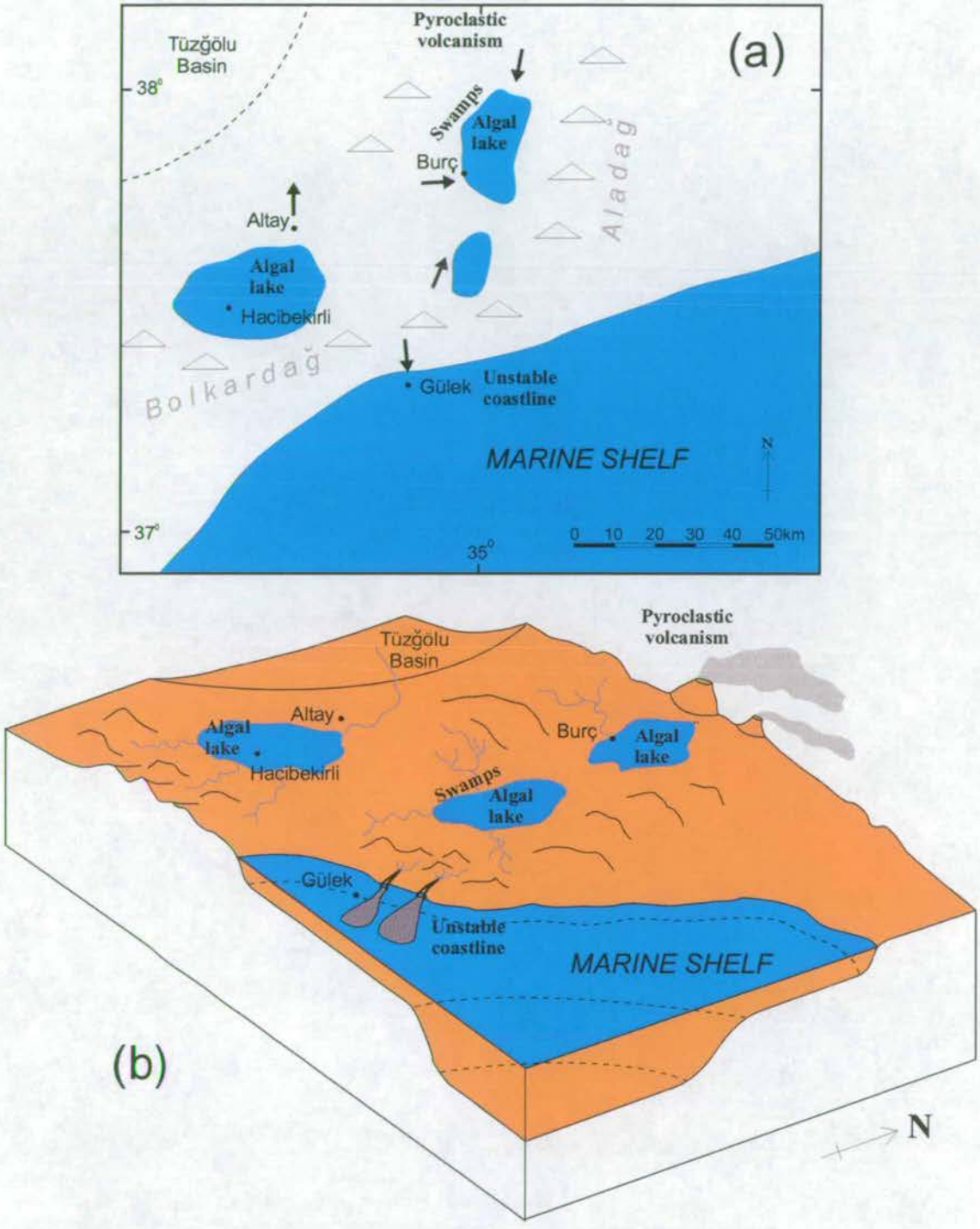

Figure 4.57 (a) Map of Late Miocene (Burç Formation) palaeo-environments, based on sedimentological data. Black dots represent current positions of settlements, black arrows represent simplified palaeocurrent data, triangles topographic highs. (b) Block diagram of Late Miocene (Burç Formation) palaeo-environments based on sedimentological data. Vertical and horizontal scales are not accurate.

The influence of meandering rivers is seen in the central Burç section, suggesting that topographic gradients were low and that the steep slopes of the Oligo-Miocene had been largely removed. There is no sedimentological evidence for the existence of large fault scarps along the EFZ during this period. Towards the end of the Late Miocene (top of the Burç Formation) lacustrine conditions were superseded by braided river and alluvial fan facies in the Ulukişla Basin, but this did not affect the EFZ. In the south of the EFZ a coastal watershed developed in the Tekir area (Fig. 4.8c & 4.57), dividing lacustrine conditions to the north from coastal and shallow marine conditions to the south. During the end of the Late Miocene the northern extremity of the EFZ was affected by pyroclastic tuff deposition, sourced from the Central Anatolian Volcanic Province (Pasquare 1968; Fig. 2.4).

4.4.3.7 Ancient and modern analogs of the Burç Formation

The tufa and lacustrine carbonates of the Gülek and Hacibekirli-Altay sections (this study) have many analogs in the Neogene rock record of Turkey. One such analog is the Late Pliocene – Early Pleistocene Antalya Tufa of the Isparta Angle (southern Turkey) where cold, freshwater carbonate deposition took place in a complex lacustrine, paludal (marsh) and fluvial environment (Glover 1996). As discussed in Section 4.4.3.2 (above) tufa deposition requires the presence of cold water springs and algae, as well as a large hinterland area of carbonate basement. Oncoidal tufa is believed to be deposited in quiet fluvial or lacustrine environments, and is commonly associated with freshwater ostrocod assemblages (Nickel 1983). Stromatolites in the Antalya Tufa predominantly grow in nearshore environments and shallow water (up to ~10m), and require relatively calm conditions (Eggleston & Dean 1976). All of the above facies are also found within the Burç Formation, and similar depositional environments are envisaged.

A useful modern-day analog of the Burç Formation carbonates are the tufas, oncolites and stromatolites of Central Spain (especially the tufa deposits of the Tajuña River,

Mundo River and Dulce River). Several types of tufa have been documented here, including: (a) spring and waterfall carbonates, which form wedge-shaped tufa buildups, and (b) water flow (fluvial) carbonates, which form encrustation tufa on plants (Ordóñez & García del Cura 1983). The water flow facies described from this example include: Vertical tube facies, crossed tube facies, detrital tufa facies, stromatolites and oncolites. All of these facies are present in the Burç Formation at Gulek and Kamisli (central EFZ), therefore a dominantly fluvial environment is envisaged as the most likely for the deposition of the Burç Formation carbonates.

4.4.4 Interpretation of the Pliocene – Quaternary Çatalca Formation

4.4.4.1 The Emlibogazi section (Fig. 4.30a)

Facies 4A

The basal 10m of the section is composed of unsorted, angular blocks of ophiolite-derived material supported by a matrix of unsorted sand, silt and mud. The body is laterally continuous over at least 30m, has a sheet-like geometry and scours deeply into the underlying succession. It is interpreted as a thick debris flow deposit, similar to that described at the base of the Doğan River section (facies 2H). Terrestrial debris flows are found in the upper and middle parts of alluvial fans (Fig. 4.47), which commonly develop in arid settings in response to local tectonic activity (Hubert & Filipov 1989).

Facies 4B

The upper 60m is composed of texturally mature, normally graded, well- imbricated, clast supported conglomerates, which lack erosive bases. These are interpreted as alluvial fan conglomerates, based on the grade and structure of the sediment, on the palaeocurrent dispersion pattern (Fig. 4.8d) and on the present-day fan morphology of the conglomerate body (Fig. 8.2, Enclosure 2). The Çatalca Formation has also been interpreted as alluvial fan material by Yetiş (1978) and by Beyhan (1994), who named it

the Keledere Formation. These conglomerates are similar to those described at the base of the Gülek section (facies 3D) and the base of the Alpu section (facies 2E). They are generally found on the middle and lower parts of the alluvial fan system (Fig. 4.42, Boothroyd 1972).

I infer that these flows originated from, and were controlled by, the main fault scarps as seen today, based on palaeocurrent evidence (Fig. 4.8d) and the fact that there are no similar Pliocene – Quaternary deposits east of these scarps. The transition from facies 4A to 4B may indicate a decrease in local slope gradients as the main scarp has eroded.

At present the Ecemis River incises into the toe of the Çamardi alluvial fan complex (Fig. 4.58a, Enclosure 1). Palaeocurrent data from this area indicate that at the western edge of the Çamardi alluvial fan complex, palaeoflow changes from W / NW-directed to SW-directed. This may be a result of toe-cutting of the fan system during the Plio-Quaternary by a palaeo-Ecemis river. Similar toe cutting of alluvial fans has been attributed to the migration of axial rivers toward the footwall block of a half graben, associated with normal fault movement and consequent basin tilting (Mack & Leeder 1999).

4.4.4.2 Lateral Facies Changes within the Çatalca Formation of the EFZ

At Elekgölü (Fig. 4.29) the Çatalca Formation was seen to thicken from 30m on the east side of the Emli gorge to 70m on the west side. At Narpuz (Fig. 4.29), the Çatalca Formation is also seen to thicken from 20m at the scarp to 50m, 1km further west. Westwards thickening is not compatible with a normal wedge-shaped alluvial fan (Fig. 4.47), which is normally thickest closest to the source area. This wide variation in the thickness of facies 4A and 4B may be due to the alluvial fan material filling an initially non-planar topography.

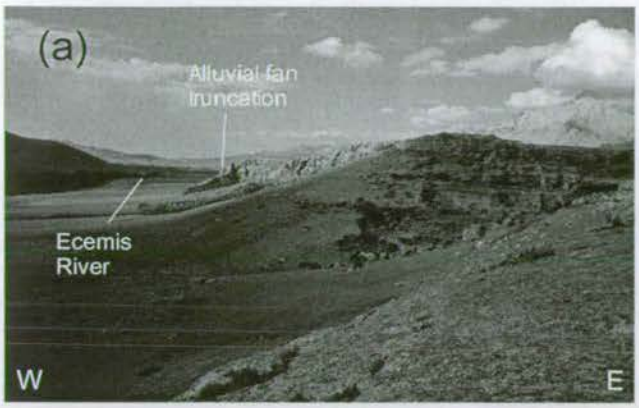

Toe-cutting of the Çamardi alluvial fan complex by the Ecemiş River at Çukurbağ (Enclosure 1 for location).

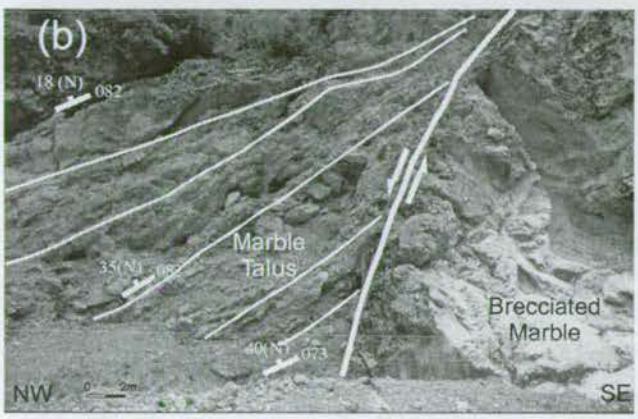

A NE-SW striking, N-dipping normal fault in the Horoz valley. The deposition of the Horoz conglomerates has been influenced by these normal faults; Plio-Quaternary units fan away from, and become more distal rapidly away from footwall Bolkar Group limestone outcrops.

Normal fault block topography of the upper Horoz valley. Footwall 'highs' stand out as ridges, Plio-Quaternary fanglomerates fill the hangingwall 'lows'.

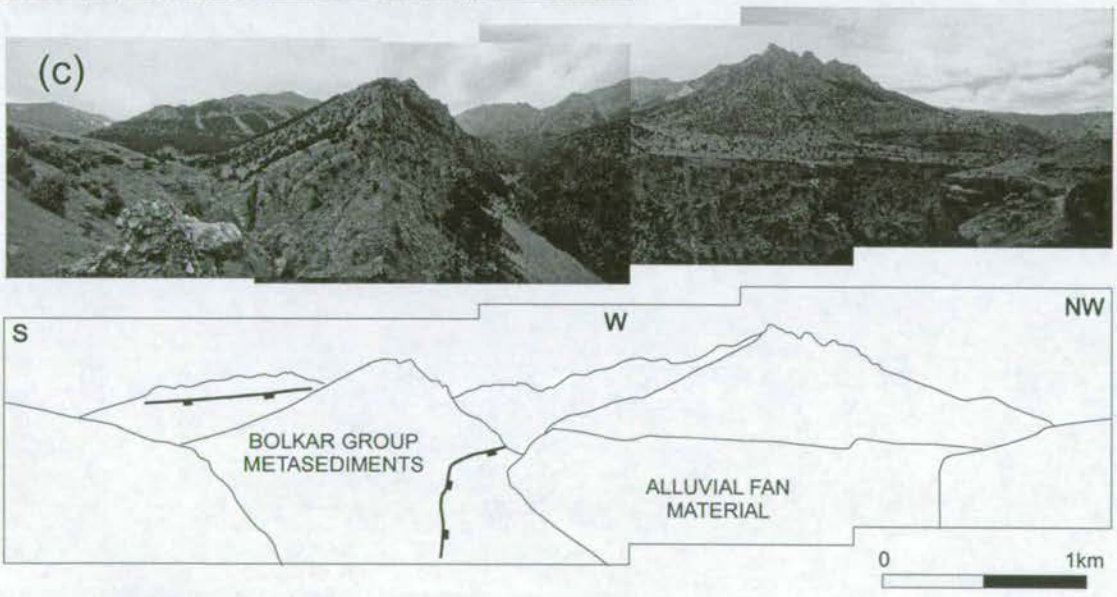

Figure 4.58 Features of the Plio-Quaternary Çatalca Formation at Çamardi and Horoz. For locations see Fig. 4.29.

4.4.4.3 The Horoz section (Fig. 4.30b)

The basal 20m of unsorted, matrix-supported breccia is very similar to facies 4A described above, and is interpreted as a debris flow deposit. These have been derived from various sources, including the Bolkar Group, local ophiolites (Alihoca ophiolite, Fig. 2.4) and local granites (Horoz granite, Fig. 2.4).

The upper 20m are composed of well sorted and texturally mature conglomerates, which are normally graded and well imbricated. These are very similar to facies 4B described above, and are interpreted as alluvial fan conglomerates. Palaeocurrent data (Fig. 4.32) indicate that the deposition of the Horoz alluvial fans was heavily influenced by local E-W trending normal fault scarps. They also suggest a scenario of initial transport of material away from fault scarps (NW), and flow being diverted axially (NE) once it was over 1km from fault scarps (Fig. 4.32).

4.4.4.4 Lateral Facies Changes in Plio-Quaternary at Horoz

The presence of E-W striking, N-dipping normal fault scarps has been suggested along the Horoz and Alihoca - Maden valleys from Oligocene until Pliocene times (Dilek & Whitney *in press*). During this study, NE-SW striking, N-dipping normal fault scarps have also been identified in the Horoz valley, which have influenced conglomerate deposition patterns (Fig. 4.32, Fig. 4.58). The inference that deposition of the Horoz conglomerates has been influenced by E-W striking normal faults is based on (i) field relations where Plio-Quaternary units become more distal, and fan away from Bolkar limestone outcrops (Fig. 4.58b), (ii) palaeocurrent data (Fig. 4.32) and (iii) from the normal-fault-block topography of the upper Horoz valley (Fig. 4.56c).

Two phases of alluvial fan (facies 4B) deposition are seen at the NE end of the Horoz valley. Here the underlying older generation (relatively flat lying) is truncated by a

steeply bedded (25-35^0) more texturally immature, younger generation of fanglomerates. This could be cause either by (i) Plio-Quaternary movement on normal faults bounding the Horoz valley, or (ii) down-cutting of the Horoz river to a new base level, thereby incising into the first generation of alluvial fans and cannibalizing them. The first explanation seems less likely as second generation fans are not seen ubiquitously along the Horoz valley or elsewhere in the Bolkaradag. The second explanation is preferred as incision is also seen within the Çatalca Formation near Çamardi (discussed further in Chapter 8), which is part of the same drainage system (Enclosure 1).

4.4.4.5 Summary of Plio-Quaternary sedimentation

A representative block diagram of sedimentation during the Pliocene-Quaternary is given in Figure 4.59. Palaeocurrent data indicate that deposition was controlled by present day fault scarps in the EFZ and was influenced by fault scarps in the Bolkardağ (Horoz area). This is consistent with the interpretation of a system of westward-building alluvial fans. The basal debris flows (seen throughout the EFZ) indicate a direct response to fault scarp creation, whereas the overlying alluvial fanglomerates were the result of continued alluvial fan development as fault scarps were eroded. It seems probable that a phase of N-S and E-W oriented normal faulting (and consequent accommodation space creation) occurred in the EFZ-Bolkardağ area during the Early Pliocene.

4.4.4.6 Ancient and modern analogs of the Çatalca Formation

Several conglomeratic units have been documented from the Pliocene and Pleistocene rock record of the Eastern Mediterranean. In southern Cyprus, the Fanglomerate Group was deposited as a result of the Pleistocene unroofing of the Troodos ophiolite (Poole & Robertson 1998). The Fanglomerate Group comprises high-energy coarse alluvial fans,

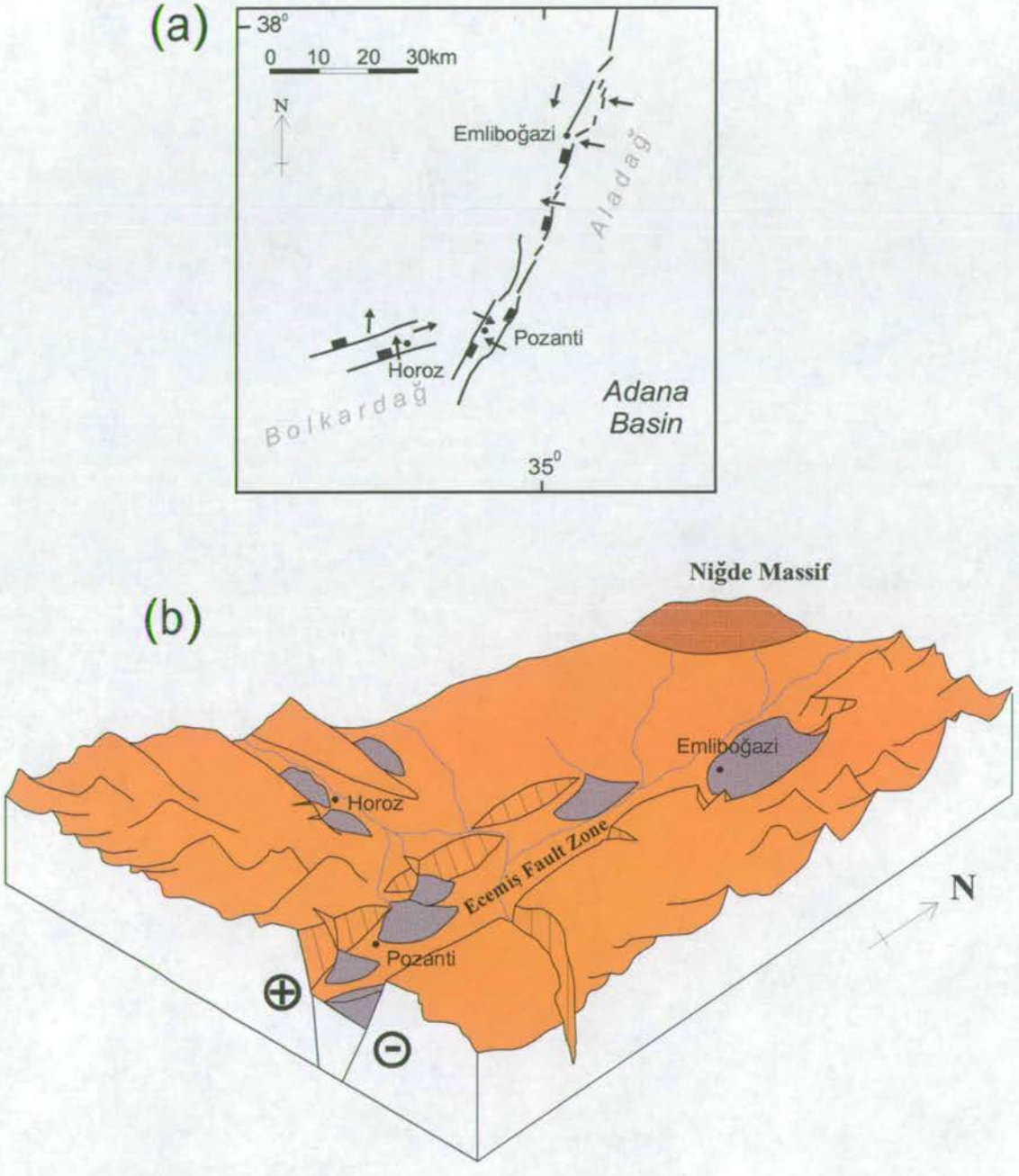

Figure 4.59 (a) Map of Pliocene - Quaternary (Çatalca Formation) palaeo-environments, based on sedimentological data. Black dots represent current positions of settlements, black arrows represent simplified palaeocurrent data, thick black lines are faults with rectangles on the downthrown side. (b) Block diagram of Pliocene - Quaternary (Çatalca Formation) palaeo-environments based on sedimentological data. Vertical and horizontal scales are not accurate.

channel fans, braided stream and floodplain deposits, and outcrops in a near-radial dispersal pattern away from the centre of the Troodos ophiolite (Mt. Olympos). Tectonic uplift of the ophiolite during the Pleistocene has lead to fanglomerate deposition on progressively lower topographic levels (Poole & Robertson 1998), resulting in a number of fan terraces. These have been correlated with (dateable) littoral marine terraces to constrain the rate of uplift of the ophiolite. The uplift mechanism for terrace formation seen here is in contrast to the climatic mechanism envisaged for the formation of the fan terraces of the Ecemiş Fault Zone.

Another useful analog for the Çatalca Formation is the Early Pliocene Kemer Fanglomerate of the Isparta Angle (southern Turkey). This crops out as a series of small, coarse-grained fan deltas, deposited adjacent to scarps of the western Taurides (Glover 1996). Two distinct facies have been identified: (i) a Clast-supported conglomerates composed of well-sorted, angular-subangular clasts, interpreted as steep alluvial fan deposits; (ii) Extremely poorly sorted, matrix-supported conglomerates, interpreted as debris flow deposits. These two facies have also been identified in the Emliboğazi section (Section 4.4.4.1 above).

A useful modern analog of the Camardi fan complex is the Warm Spring Canyon alluvial fan of Death Valley, California. Sedimentation on this alluvial fan is primarily controlled by the 'North Death Valley Fault Zone' half-graben structure. The alluvial fan is dominantly composed of debris-flow deposits, but these are interstratified with clast-supported sheet flood deposits (Blair 1999). The surface of the fan can be divided into the uplifted, older deposits (comprising the upper and medial parts of the fan) and an incised channel, which dissects and bypasses the older fan surface (Fig. 60a-d; Blair 1999). This is directly comparable to the uppermost surface and incised terraces of the Çamardi fan. As at Çamardi, the Warm Spring Canyon alluvial fan is incised to several levels (Fig. 61) and these incised terraces have been backfilled with poorly sorted pebble-cobble gravel sediments (Blair 1999). The incised channel has been offset

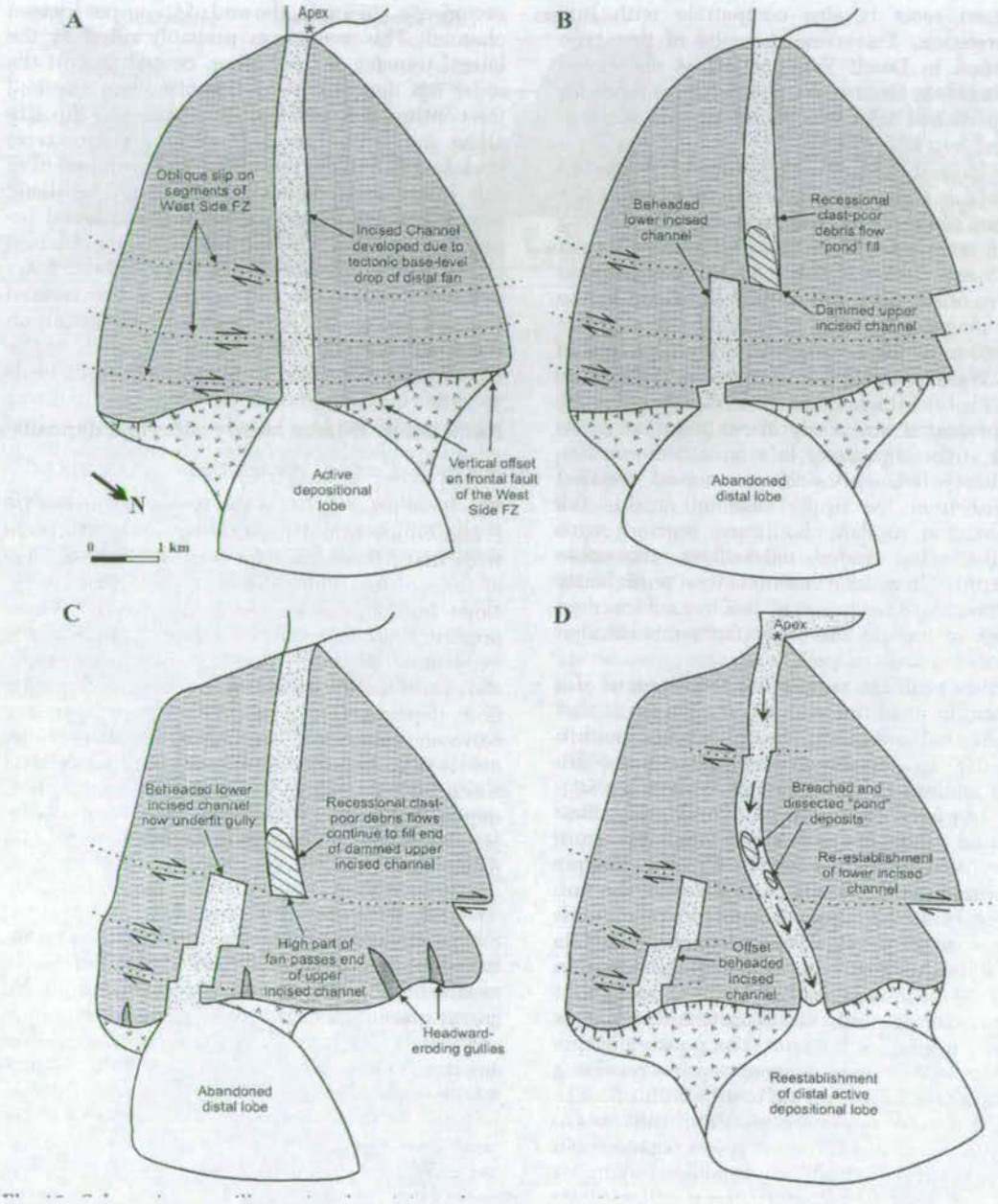

Figure 4.60 Schematic maps of the Warm Spring Canyon alluvial fan, illustrating the effects of dextral strike-slip faulting on sedimentation (after Blair 1999). **(a)** Oblique slip fault motion causes uplift of old fan deposits and the development of an incised channel. **(b)** Dextral strike-slip along a mid-fan cross-fault beheads the lower incised-channel segment. **(c)** Strike-slip faulting continues, moving the abandoned distal lobe to the margins of the fan. **(d)** A breach develops in the blocked incised channel and a new incised channel is established, providing sediment to a new distal lobe.

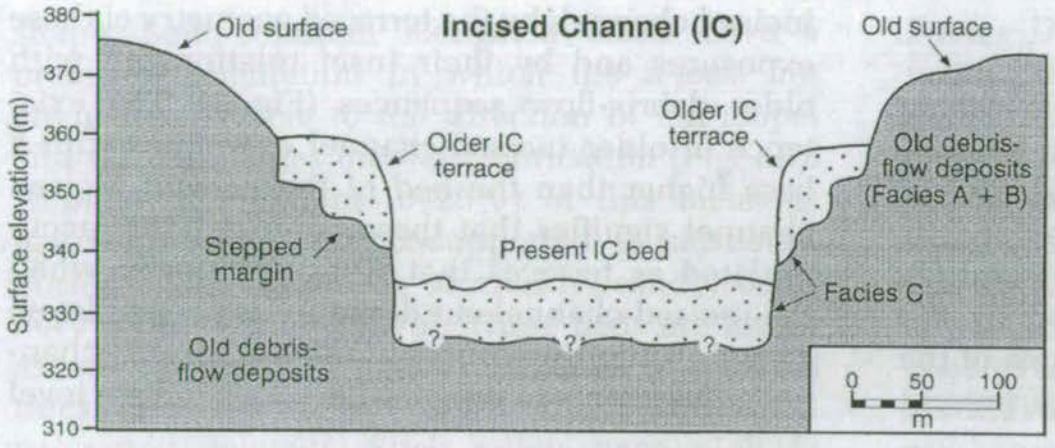

Figure 4.61 Topographic profile and facies cross section of the proximal incised channel, Warm Spring Canyon alluvial fan, Death Valley, California (after Blair 1999). This illustrates the relationship between incised channel deposits and older debris-flow deposits. Vertical exaggeration = 4.3x

several times by a dextral strike-slip fault which cuts across the fan, perpendicular to the drainage direction (Fig. 60b). Strike-slip offset of the incised channel (and its active distal lobe) has resulted in the abandonment of old distal lobes and the re-establishment of new ones further to the northwest (Fig. 60d). It is possible that the same process has taken place on the Çamardi fan; see Section 8.4 for further discussion.

4.5 Conclusions

4.5.1 Eocene Kaleboynu Formation

- Marine conditions prevailed throughout the region during the Middle Eocene. The presence of large benthic foraminifera at outcrops in the EFZ indicate that this area was in an aerated, tropical, shallow shelf setting during the Lutetian. Different facies of deposition and the dominance of planktonic foraminifers in the Ulukişla Basin indicate that this area was in an open marine or outer shelf setting.
- Palaeocurrent data indicate that a submarine depocentre existed in the Niğde area.

- The composition of basal debris flows at Evliya Tepe indicate that the Niğde Massif existed as a topographic high during the Lutetian (Middle Eocene).
- Opposing palaeocurrents and widely divergent stratigraphies in adjacent Lutetian outcrops in the EFZ suggest that these outcrops originated further apart and were brought together by post-Lutetian strike-slip faulting.

4.5.2 Oligo-Miocene Çukurbağ Formation

- Palaeocurrent data indicate that two continental basins existed in this area during the Oligo-Miocene: the inward-draining Karsanti Basin and the larger Ulukişla-EFZ Basin, which had its depocentre in the central EFZ. It is unlikely that present-day fault scarps existed during this period.
- Significant topographic highs existed along the margins of these basins. It is likely that these highs came into existence during the Early Oligocene, when there was a hiatus in sedimentation across the area. Basal debris flows (Doğan River section) and alluvial fanglomerates (Alpu section) within the Çukurbağ Formation were shed from these palaeo-highs.
- Freshwater lake conditions were established in the Ulukişla Basin during the Late Oligocene (lower part of the Çukurbağ Formation). In the EFZ, evaporitic playa lakes existed in low-lying areas, with braided rivers draining into them. The change from evaporitic playa lake conditions (EFZ) and open lacustrine conditions (Ulukişla Basin) to a continental braid plain setting during the early Miocene (upper part of the Çukurbağ Formation) may be a result of: (i) local tectonic uplift or (ii) climatic change leading to an increase in aridity.
- The Karsanti Basin was at a lower topographic level than the Ulukişla-EFZ Basin during this period, and was invaded by shallow marine conditions during the Oligocene.

4.5.3 Late Miocene Burç Formation

- The dominant facies throughout the Late Miocene of the EFZ and the Ulukişla Basin was open lake or algal lake margin facies, briefly interrupted by meandering river and swamp conditions. The change from continental red-bed deposition during the Oligo-Miocene to lacustrine-dominated deposition during the Late Miocene was probably a result of the change from a more arid climate to a generally wetter and more humid one.
- There is no sedimentological evidence for the existence of large fault scarps along the EFZ during this period.
- Palaeocurrent data indicate that the inward-draining Ulukişla-EFZ Basin no longer existed. Instead, a new drainage divide was established at Tekir (southern EFZ), dividing south-directed flow to the Mediterranean from north-directed flow into the EFZ.
- Towards the end of the Late Miocene (top of the Burç Formation) lacustrine conditions were superseded by braided river and alluvial fan facies in the Ulukişla Basin, but this did not affect the EFZ.
- During the Messinian (Latest Miocene) the northern extremity of the EFZ was affected by pyroclastic tuff deposition, sourced from the Central Anatolian Volcanic Province.

4.5.4 Pliocene – Quaternary Çatalca Formation

- Palaeocurrent data indicates that deposition was controlled by present day fault scarps in the EFZ and was influenced by fault scarps in the Bolkardağ (Horoz area).
- The basal debris flows (seen throughout the EFZ) indicate an immediate response to fault scarp creation, whereas the overlying alluvial fanglomerates were the result of continued alluvial fan development as fault scarps were eroded.

- A phase of N-S and (limited) E-W oriented normal faulting (and consequent accommodation space creation) occurred in the EFZ-Bolkardağ area during the Early Pliocene.
- The Çatalca Formation has a variable thickness, controlled by pre-existing topography, distance from source and alluvial fan morphology.

5 Subsidence History

5.1 Rationale

The construction of subsidence curves for logged sections both within and outwith the Ecemiş Fault Zone is a useful tool for the study of the timing and amount of subsidence in an area. By the use of this technique I aim to compare subsidence rates and total subsidence between the Ecemiş area and nearby Ulukişla and Adana basins, thereby inferring whether or not the EFZ has undergone a subsidence history consistent with that of other nearby Cenozoic basins. By comparison with known subsidence profiles I also aim to make comments regarding the nature of the tectonic setting of basins in the Ecemiş area.

5.2 Theory

5.2.1 What causes subsidence?

The three main accepted mechanisms which cause subsidence within the earth's crust are: (i) lithospheric stretching, (ii) flexural loading and (iii) strike-slip faulting.

5.2.1.1 Lithospheric Stretching-related subsidence (after Turner 1998)

Several models have been proposed to explain how stretching affects the lithosphere. The simplest approach was the model of uniform lithospheric stretching (McKenzie 1978). In this model the entire lithosphere is stretched, instantaneously, by a factor termed beta (Fig. 5.1). Stretching is accommodated by large scale normal faulting of the brittle upper crust and ductile creep in the lower crust and mantle. As the lithosphere is stretched, and thereby thinned, hot asthenospheric mantle rises passively to replace it. This passive upwelling of hot asthenospheric mantle generates a thermal anomaly, which induces uplift. However, the replacement of relatively light crust by denser

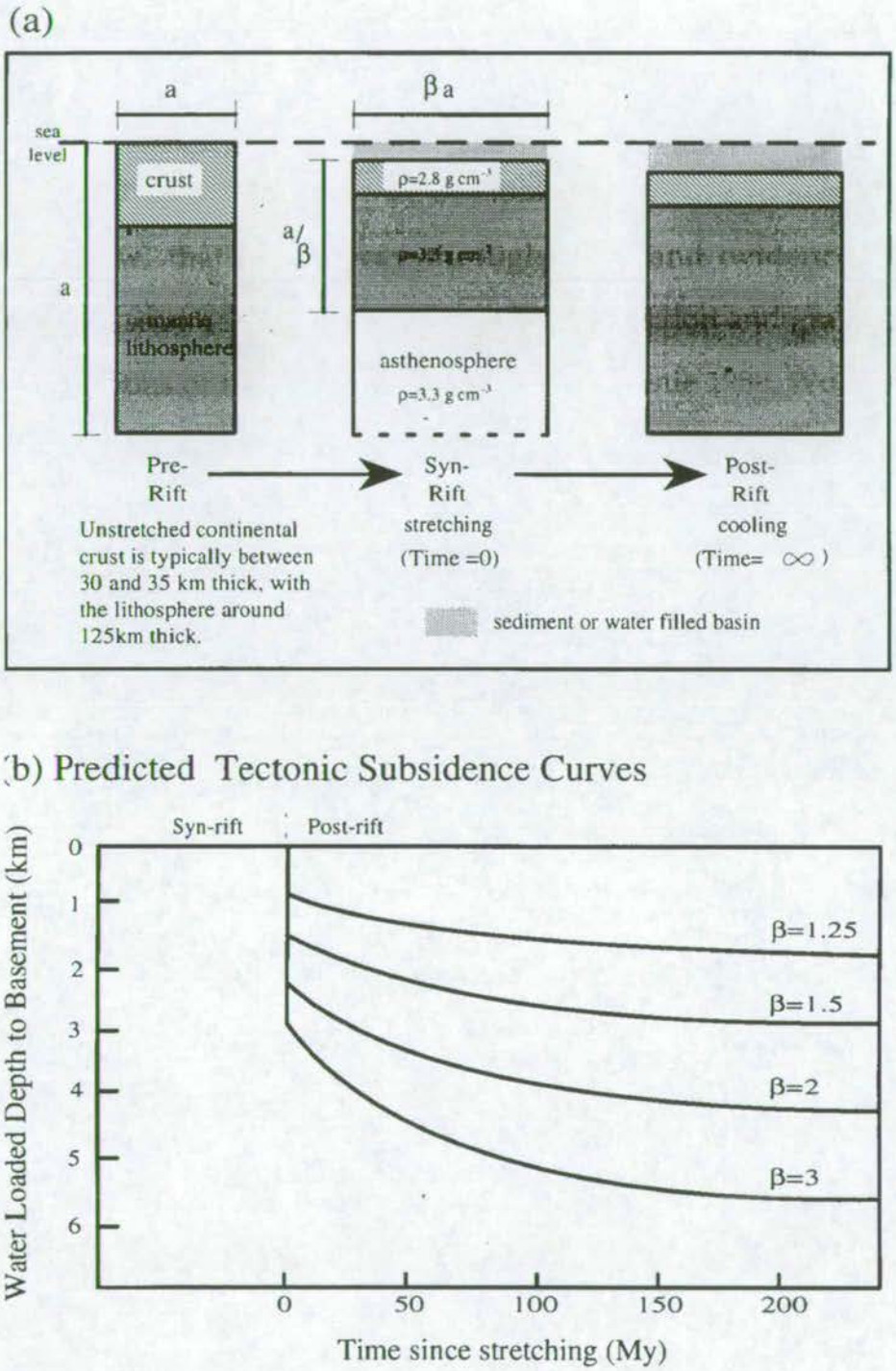

Figure 5.1 Uniform lithospheric stretching model (after McKenzie 1978 and Turner 1998). (a) progression of pre-rift to post-rift. (b) examples of hypothetical subsidence profiles with different beta (stretching) factors.

mantle induces subsidence. Whether net uplift or subsidence results depends on (i) the amount of stretching (β factor) and (ii) the pre-stretched ratio of lithospheric to crustal thickness. Net subsidence is predicted, except for unusually thin crust (McKenzie 1978). Once stretching has ceased, the lithosphere cools, returning to an equilibrium state. This cooling causes the density of the lithosphere to increase, and drives the post-rift phase of thermal subsidence which then proceeds at an exponentially decreasing rate.

This translates to a two-phase subsidence profile: (i) initial rapid subsidence associated with large scale faulting (up to 38% of total subsidence, Allan *et al.* 1986), and (ii) exponentially decreasing subsidence caused by thermal contraction (associated with lithospheric cooling) and sediment loading. This results in a typically concave-upward subsidence profile.

This simple model has been subsequently improved to allow for: (i) non-instantaneous stretching of the lithosphere (finite duration stretching model, Cochran 1983) and (ii) the effect of sediment blanketing (insulation) and radiogenic heat production on the cooling rate and subsidence rate of post-rift basins (Beaumont *et al.* 1982)

An important alternative to the uniform lithospheric stretching model is the simple shear model of Wernicke (1985), based on evidence from the Basin and Range (western USA). He suggested that lithospheric extension was accommodated by large scale simple shear along a detachment which may penetrate the whole lithosphere (Fig. 5.2). Quantitative treatments of this model (Issler *et al.* 1989) predicts some extremely complicated subsidence patterns and histories for individual sites within the basin (Fig. 5.2).

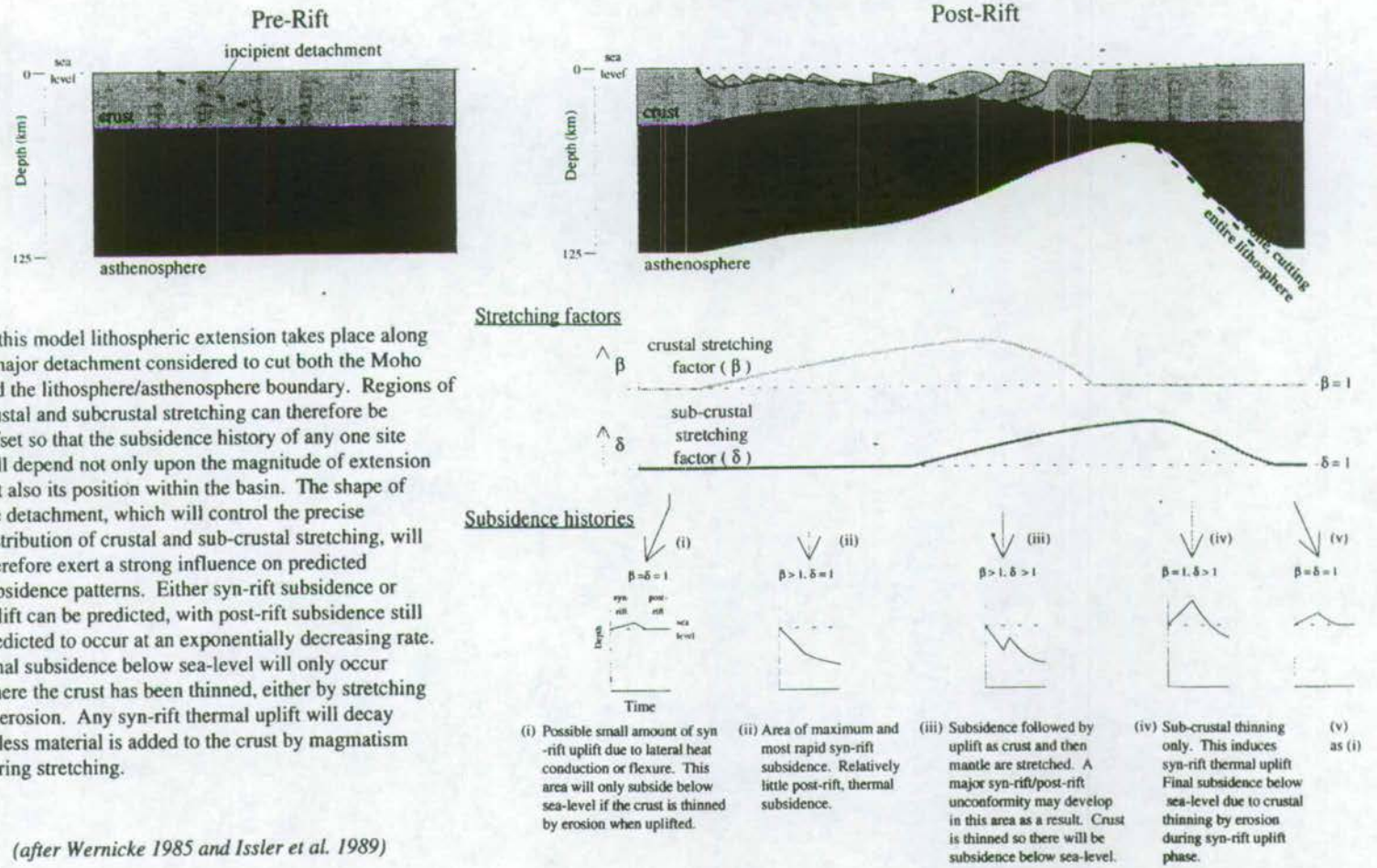

In this model lithospheric extension takes place along a major detachment considered to cut both the Moho and the lithosphere/asthenosphere boundary. Regions of crustal and subcrustal stretching can therefore be offset so that the subsidence history of any one site will depend not only upon the magnitude of extension but also its position within the basin. The shape of the detachment, which will control the precise distribution of crustal and sub-crustal stretching, will therefore exert a strong influence on predicted subsidence patterns. Either syn-rift subsidence or uplift can be predicted, with post-rift subsidence still predicted to occur at an exponentially decreasing rate. Final subsidence below sea-level will only occur where the crust has been thinned, either by stretching or erosion. Any syn-rift thermal uplift will decay unless material is added to the crust by magmatism during stretching.

(after Wernicke 1985 and Issler et al. 1989)

Figure 5.2 The simple shear stretching model of lithospheric extension (after Wernicke 1985, Issler *et al.* 1989 and Turner 1998)

5.2.1.2 Flexural loading-related subsidence

Foreland basins and ocean trenches are formed by the deflection of the lithosphere by an applied force (Allen & Allen 1990). This force is often in the form of a mountain chain (load) which has been transported over another section of lithospheric crust by large scale reverse faulting. The wavelength of the deflection in the loaded plate (hence the size of the basin) is dependent on the flexural rigidity of the loaded plate.

Subsidence curves from foreland basin sediments generally have a relatively gradual onset (as the thrust load approaches), with subsidence accelerating with time, resulting in a convex-upward subsidence profile (Fig. 5.3, Allen *et al.* 1986). Because the depocentre (point of maximum subsidence) migrates over time, there are strong temporal and spatial changes in subsidence rates throughout the foreland basin. Comparing subsidence profiles from a rift-sag basin (North Sea) and a foreland basin (Alpine Molasse Basin), it becomes clear that the subsidence rate in foreland basins is an order of magnitude higher than those in rift-sag basins (Fig. 5.4a). Some foreland basin subsidence profiles may be confused with the initial extensional part of the profile from a rift-sag basin with highly stretched continental lithosphere (both having high subsidence rates), but as the rift-sag basin moves into its thermal subsidence phase, the distinction becomes clear (Fig. 5.4b).

5.2.1.3 Strike-slip faulting – related subsidence (after Allen & Allen 1990)

Basins associated with strike-slip deformation are generally small and complex compared to rifts, passive margins and foreland basins, and mechanical models of their evolution have been slow to appear. Basins in strike-slip zones form in areas of localised extension caused by the geometry and kinematic history of the fault configuration, or in areas of net shortening, where flexural loading may drive subsidence. Characteristically, a strike-slip related basin may experience both extension

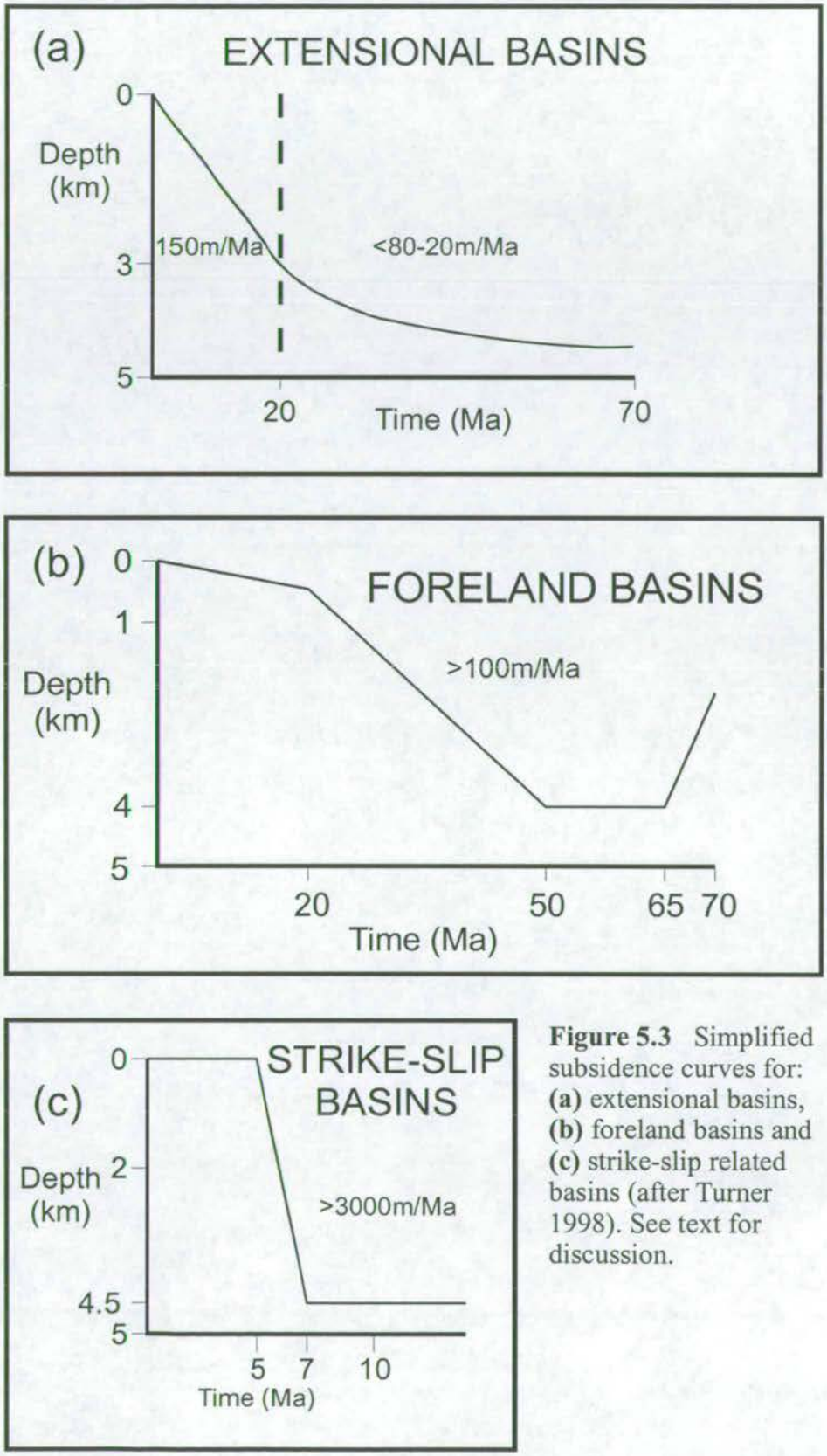

Figure 5.3 Simplified subsidence curves for: **(a)** extensional basins, **(b)** foreland basins and **(c)** strike-slip related basins (after Turner 1998). See text for discussion.

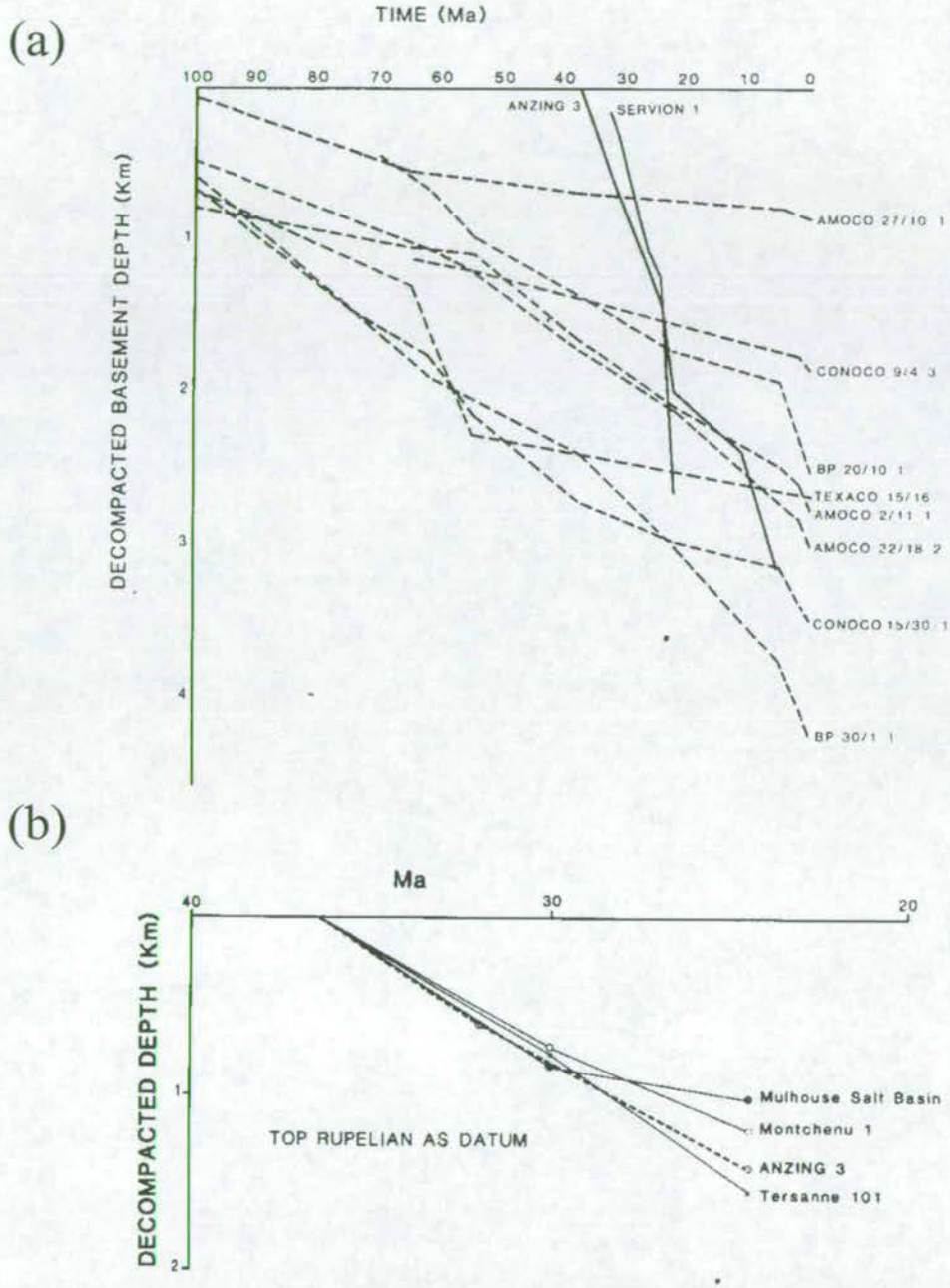

Figure 5.4 **(a)** A comparison of subsidence profiles for the north Alpine foreland basin (Anzing 3 & Servion 1) and selected wells from the North Sea (the remainder of the curves). After Allen et al. 1986. The curves from the Alpine foreland basin have much greater sedimentation rates than those from the North Sea. **(b)** Decompacted subsidence curves from the Alpine Molasse basin (Anzing 3), south Rhine graben (Mulhouse salt basin) and Valence basin (Tersanne 1 and Montchenu 1), showing the similarity between the initial stages of extensional fault - controlled subsidence and foreland basin subsidence (after Allen et al. 1986).

and shortening during its life span, or one part of a basin may experience shortening while the other part is undergoing extension. Strike-slip basins are therefore very much tectonic-driven and there is little evidence for substantial thermally-driven subsidence. Subsidence rates are commonly extremely high, but subsidence may be relatively short lived. This results in a subsidence curve with distinct 'steps', or short periods of rapid subsidence, followed by, and preceded by low subsidence periods (Fig. 5.5, Pitman & Andrews 1985).

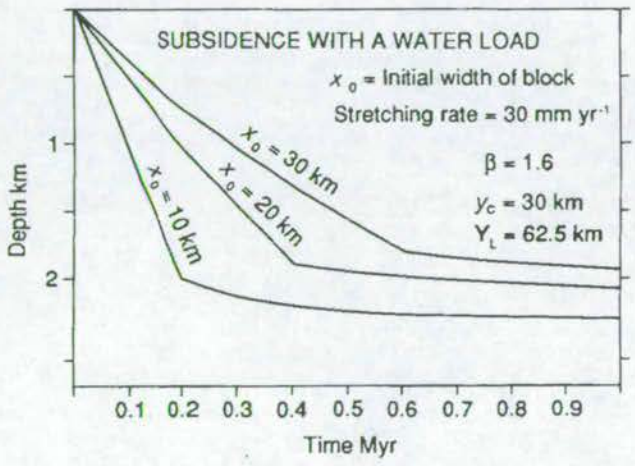

Figure 5.5 Subsdence as a function of time for strike-slip associated basins experiencing lateral heat loss in addition to vertical conduction (after Pitman & Andrew 1985). Three subsidence curves are shown for three initial widths of zones of stretching (10km, 20km and 30km) for a point in the centre of the basin. The initial steep segment of the curve represents subsidence due to lateral heat loss as well as crustal stretching. The flatter later segment represents subsidence due to the remaining thermal contraction.

Subsidence in strike-slip zones tends to occur where strike-slip is accompanied by a component of divergence. This might result from a bend or overstep in the fault trace, resulting in a 'pull apart basin' (Fig. 5.6, Burchfiel & Stewart 1966), or through extension at the boundaries of rotating blocks within a strike-slip zone (Fig. 5.7, Nicholson *et al.* 1985). Well documented examples of pull apart basins include the Dead Sea Basin and Arava Fault trough on the Arabia-Sinia (Levant) plate boundary zone (Garfunkel 1981). Rotating-block boundary basins have been documented from the intersection of the San Andreas and San Jacinto faults, California (Nicholson *et al.* 1985).

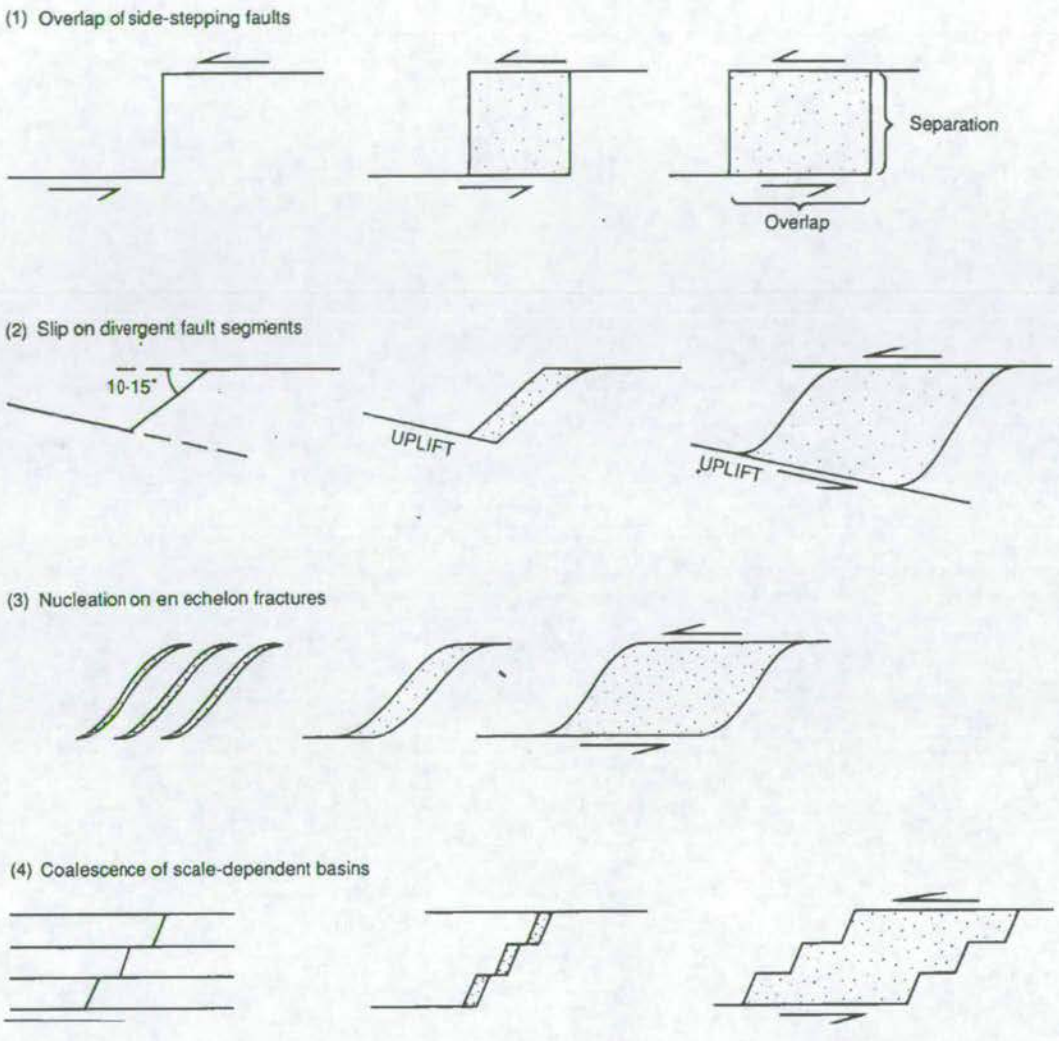

Figure 5.6 Models of pull-apart basin development (after Mann et al. 1983 and Allen & Allen 1990).

5.2.2 Previous interpretations of subsidence driving mechanisms

The Adana Basin (Fig. 3.1) has a significant history of previous sedimentological investigation. The original interpretation was that this basin formed as a result of the incompatibility problems at an intracontinental FFF triple junction, where the Dead Sea Fault Zone meets the East Anatolian Fault Zone (Şengör *et al.* 1980, Yalçin & Görür

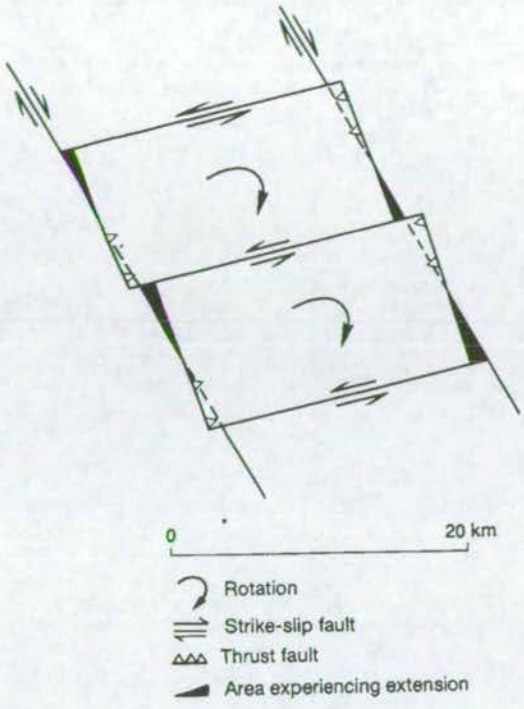

Figure 5.7 Model for the rotation of blocks of the San Andreas and San Jacinto faults, California (after Nicholson *et al.* 1985). Rotation causes overlaps (small reverse faults) and gaps (small normal faults) to form along the main bounding right-lateral faults. The areas of extension may become sedimentary basins.

1984), i.e. subsidence was associated with strike-slip. More recent interpretations have used seismic reflection profiles to image the Adana Basin. A blind, south-directed thrust fault has been interpreted along the northern edge of the Adana Basin (Fig. 5.8, Williams *et al.* 1995), and the Taurus mountains have been interpreted as a thrust load, causing flexural subsidence in the Adana 'foreland' Basin. They argue that the Adana Basin initiated in the Early-Mid Miocene as a foreland basin but has subsequently been affected by extensional faulting (Williams *et al.* 1995) and strike-slip faulting. The interpretation of the Adana Basin as a foreland basin is not uncontroversial, as the thrust fault carrying the Taurus belt 'load' does not outcrop, not even in the EFZ where one would expect Miocene sediments to be deformed and faulted during load emplacement.

The Karsanti Basin was a precursor to the Adana Basin. Sedimentation was controlled by large scale half grabens, connected to deep seated faults (Fig. 5.9, Williams *et al.*

(a)

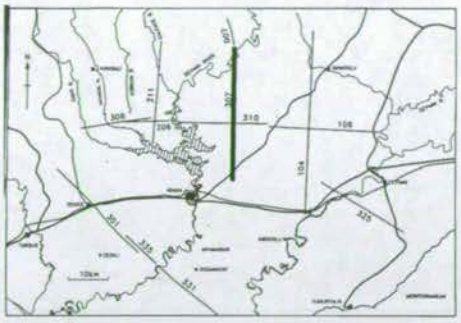

Figure 5.8 **(a)** Location map of the Adana Basin, showing seismic line in (b) (heavy line), **(b)** Seismic reflection profile and interpretation (after Williams *et al.* 1995). Blind south-directed thrust fault is interpreted one third from the right.

(b)

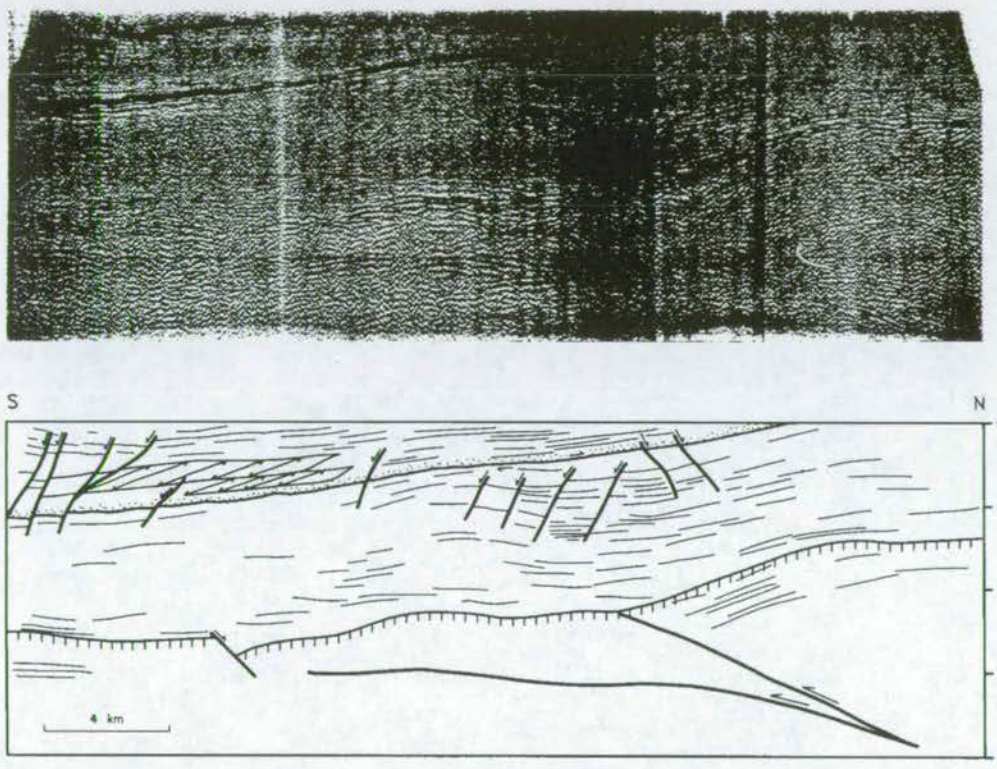

1995) during the Late Oligocene. The interpretation is of simple extension, without the influence of flexure or strike-slip.

Little has been published concerning the driving mechanism for subsidence in the Uluki°la Basin and EFZ. The history of the Uluki°la Basin is complex (see 2.3.5) and is currently the subject of a PhD study by Matthew Clark (Edinburgh University). The Uluki°la Basin has been interpreted as a fore-arc basin (Oktay 1982) and a foreland

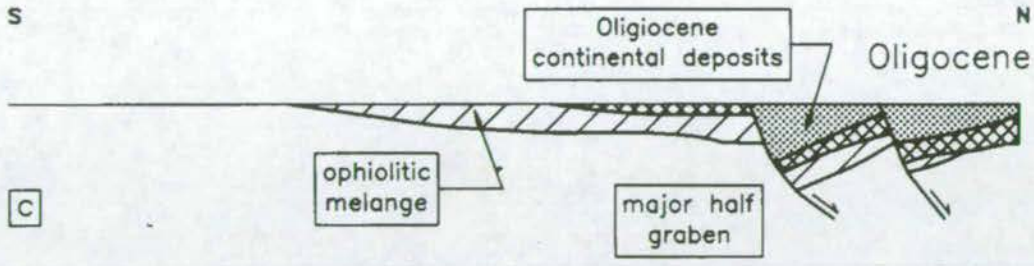

Figure 5.9 Diagramatic cross section through the Karsanti Basin (after Williams *et al.* 1995). Late Oligocene extensional faulting in the north of the Adana region and deposition of continental sediments (Karsanti and Gildirli Formations).

basin, affected by the north-directed thrusting of the Tauride belt (Demirtaşli *et al.* 1984).

5.2.3 Backstripping

Backstripping is the technique used to calculate observed tectonic subsidence curves. Total decompaction subsidence is calculated using the approach described by Steckler and Watts (1978). The stratigraphic section preserved at each site is split up into a number of layers, dated using published foraminiferal or ostracod biostratigraphy (Chapter 3). Each of these layers is assigned a bulk lithology and the water depth of deposition for sediments at the top and bottom of the layer is estimated using facies, fossil and trace fossil evidence (Fig. 5.10). Unconformities are treated as periods of zero deposition, and assigned a nominal thickness. These layers are then removed (backstripped) sequentially to reconstruct the total subsidence history of the site. Layers are decompacted using standard porosity-depth relationships determined by Sclater and Christie (1980) (Fig. 5.11) and then 'unloaded'. All curves are plotted using the timescale of Harland *et al.* (1989). See Turner 1998 for more information.

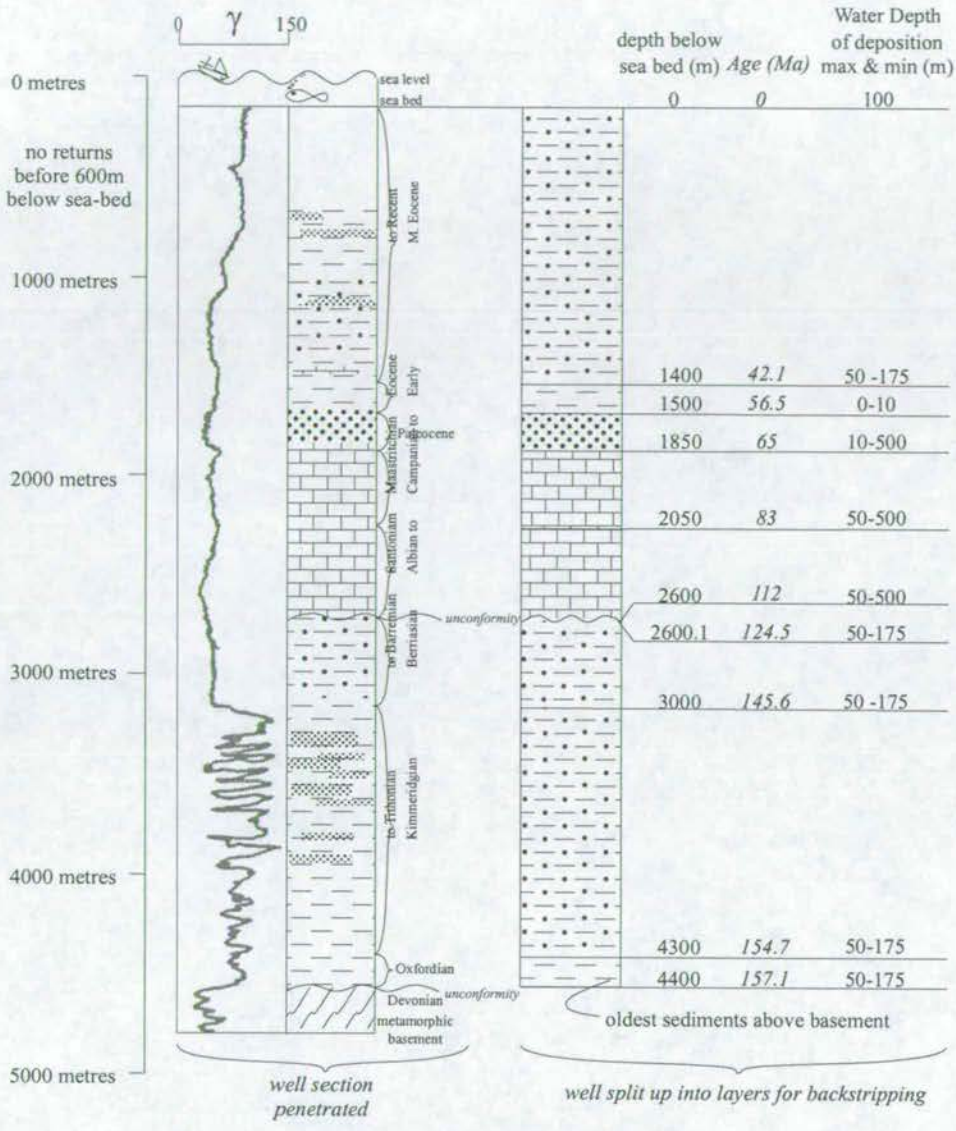

Well X - somewhere in the North Sea

Lithologies	
	sand
	silt
	shale
	limestone/chalk

Figure 5.10 Backstripping data preparation (after Turner 1998). Before a well can be backstripped the preserved stratigraphic succession must be simplified and split up into a number of layers ready for input to the backstripping calculations. The age, depth below sea-bed (or an alternative datum level) and water depth of deposition for the top of each layer are assessed and each layer is assigned a bulk lithology. Although not shown in the diagram above, in this study the water depth of deposition for the base of each layer is also included. The age, depth below sea-bed and water depth of deposition of the oldest sediments sitting on basement are also required.

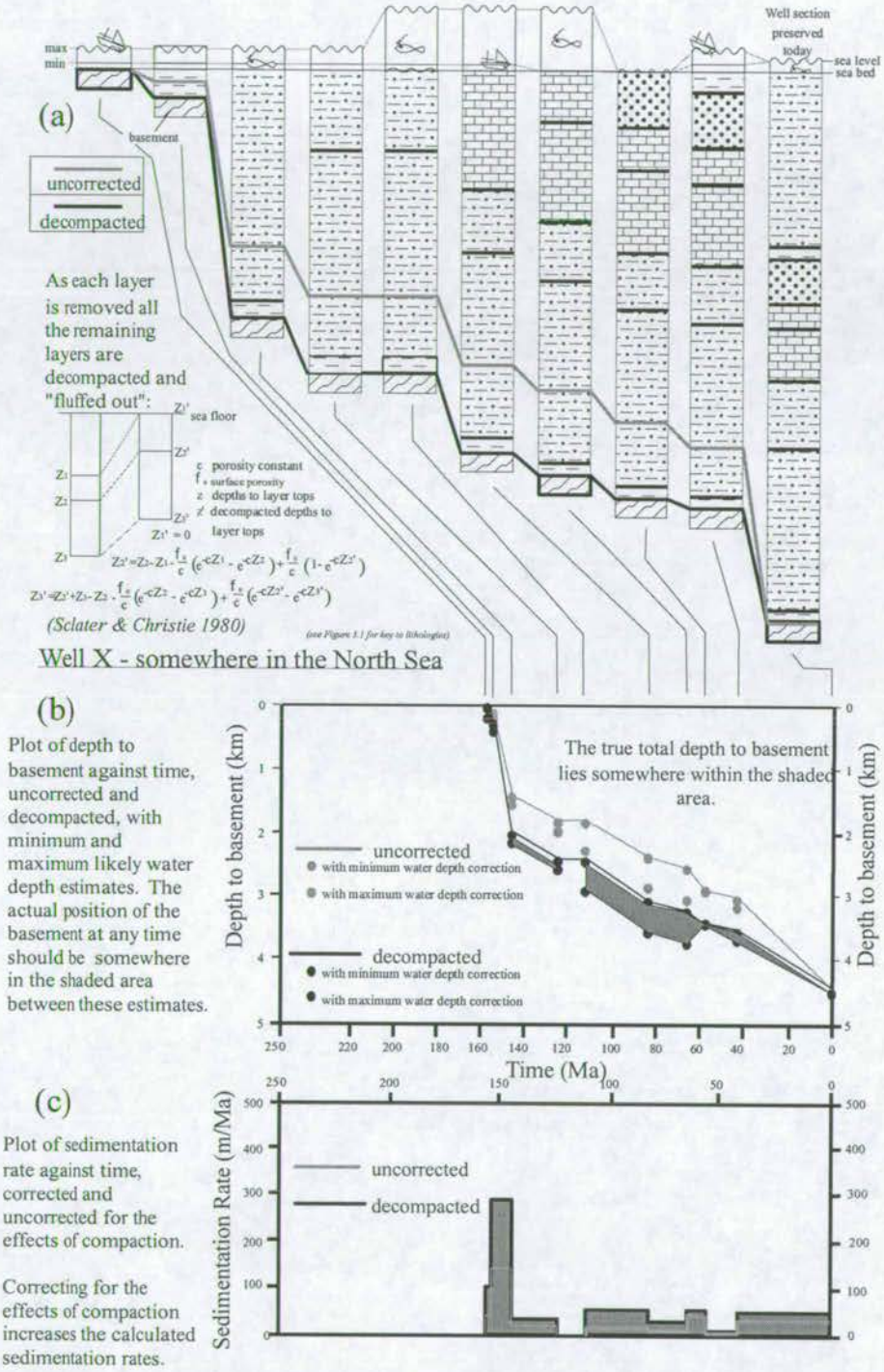

Figure 5.11 Decompaction procedure (after Turner 1998). **(a)** Graphic decompaction. **(b)** Explanation of the subsidence curve, showing uncorrected and decompacted depth to basement. **(c)** Explanation of sedimentation rate graph (part of program output).

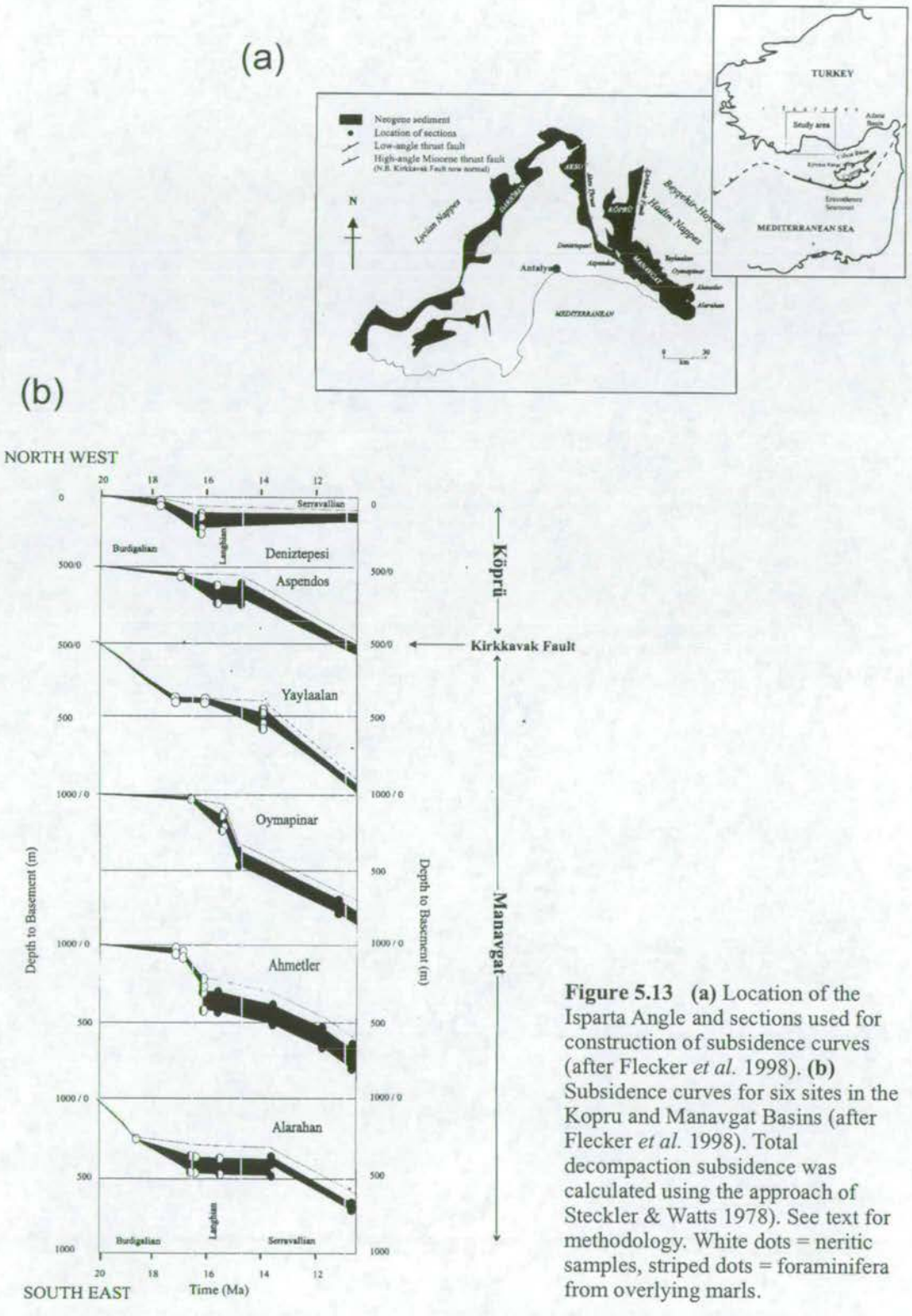

Figure 5.13 **(a)** Location of the Isparta Angle and sections used for construction of subsidence curves (after Flecker *et al.* 1998). **(b)** Subsidence curves for six sites in the Kopru and Manavgat Basins (after Flecker *et al.* 1998). Total decompaction subsidence was calculated using the approach of Steckler & Watts 1978). See text for methodology. White dots = neritic samples, striped dots = foraminifera from overlying marls.

5.3 Methodology

Simplified composite logs were constructed for the post-Palaeocene stratigraphy of the Ecemiş Fault Zone, Ulukişla, Karsanti and Adana Basins. These utilised logging carried out during this study, apart from that of the Adana Basin which was taken from Yalçin & Görür (1984). Appendix 1 displays the simplified logs.

These logs were used as input for the backstripping programme developed by Jon Turner (1998) which sequentially decompacts and unloads each specified unit. Input information included: age of each unit, thickness of unit, water depth at top and bottom contact and general composition (silt, shale, sand, limestone or volcanic) of the unit. This results in an output display of sedimentation rate (lower bar scale) and depth to basin floor (central line graph). A single line indicates subsidence without water depth correction; a shaded area is subsidence with minimum and maximum water depth corrections. The program does no account for periods of uplift and erosion, hence the initial results (Figure 5.12a) show the base of the basins as being well below sea level, whereas in fact they are near or above sea level. In Figure 5.12b, I have attempted to account for periods of erosion during the Early Oligocene, Middle Miocene and earliest Pliocene (see Chapter 4 for evidence for uplift during these times). I have done this by raising the last part of the curve to the level of the current basin floor, and adjusting earlier sections of the curve according to sedimentological and palaeontological indicators of elevation.

5.4 Results

The following comments are made from Fig. 5.12a, the output of the subsidence program of Turner (1998). These curves do not show the effects of uplift and erosion, enabling an easier comparison with the idealised curves of Figure 5.3. It should be borne in mind, however, that these curves do not represent the true subsidence history of

these basins (this is better illustrated in Figure 5.12b). The constraint on the amount of uplift is poor, but estimates have been made based on Palaeontological and sedimentological palaeoenvironment indicators.

5.4.1 Mid- to Late Eocene

The Eocene was a period of relatively high sea levels (i.e. or low topography), low subsidence rates and low sedimentation rates (max 20m/Ma) in the Ecemiş Fault Zone. This is based on the exposures of the Kaleboyu Formation at Evliya Tepe (Appendix 1). However, the upper part of the succession is not exposed and therefore the total thickness (and thus inferred subsidence rate) may be an underestimate. Sedimentation and subsidence were more active in the Ulukişla Basin than in the EFZ during this time (50-250m/Ma).

5.4.2 Early Oligocene

The Early Oligocene was marked by a hiatus in subsidence and sedimentation in the Ecemiş and Ulukişla Basins (quantity of total uplift is estimated in Figure 5.12b). Biostratigraphic control on the exact timing of this hiatus is poor and it may be shorter than displayed. By contrast, in the Karsanti Basin, subsidence and sedimentation were taking place at moderate rates (50-100m/Ma).

5.4.3 Late Oligocene to Early Miocene

During the earliest Miocene the Ecemiş, Ulukişla and Karsanti Basins experienced maximum subsidence rates. The subsidence related to the formation of the Aktoprak basin (Ulukişla Basin) resulted in especially high sedimentation rates (max. 810m/Ma). A pronounced 'step' is seen in the Ecemiş Basin subsidence profile at this time (Figure 5.12a), with a less pronounced step in the Ulukişla Basin profile. The Middle Miocene

is marked by a further period of uplift and erosion, which is more pronounced in the Ecemiş area than in the Ulukişla Basin (Figure 5.12b).

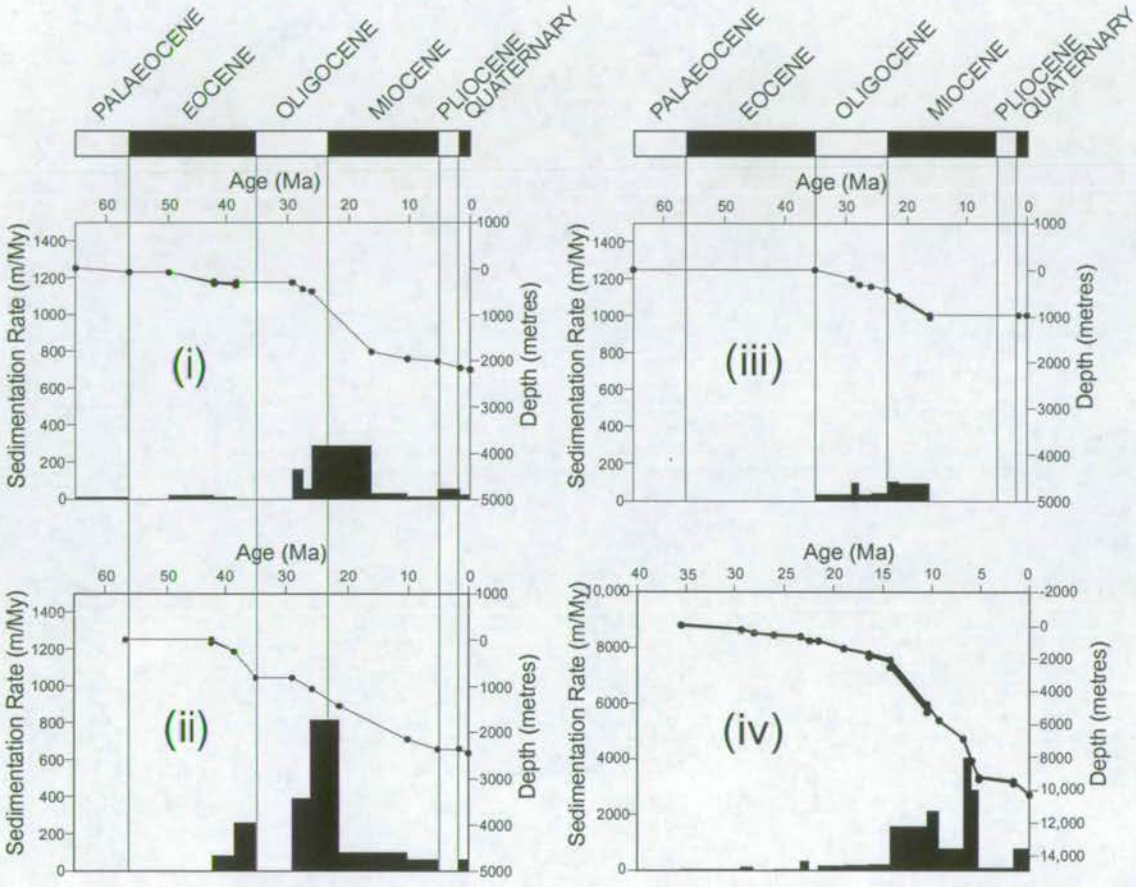

Fig. 5.12a Subsidence history plots generated from composite logs in four basins (see Fig. 3.1 for basin locations). **(i)** Ecemis Fault Zone composite log, **(ii)** Ulukisla Basin composite log, **(iii)** Karsanti Basin composite log and **(iv)** Adana Basin composite log. The Oligo-Miocene unit of the Ecemis Fault Zone has poor time constraints, thus curves should be seen as rough indicators of rapid vs. slow sedimentation and subsidence. Total decompaction subsidence was calculated using the approach of Steckler and Watts (1978). See text for methodology. Data displayed include sedimentation rates (lower bar scale), depth to basin floor (central line graph).

5.4.4 Late Miocene

The Late Miocene saw a slowing of subsidence and sedimentation rates in the Ecemiş and Ulukişla Basins, while those in the Adana Basin increased. The Adana Basin experienced its maximum subsidence rate during the Late Miocene. There was a final

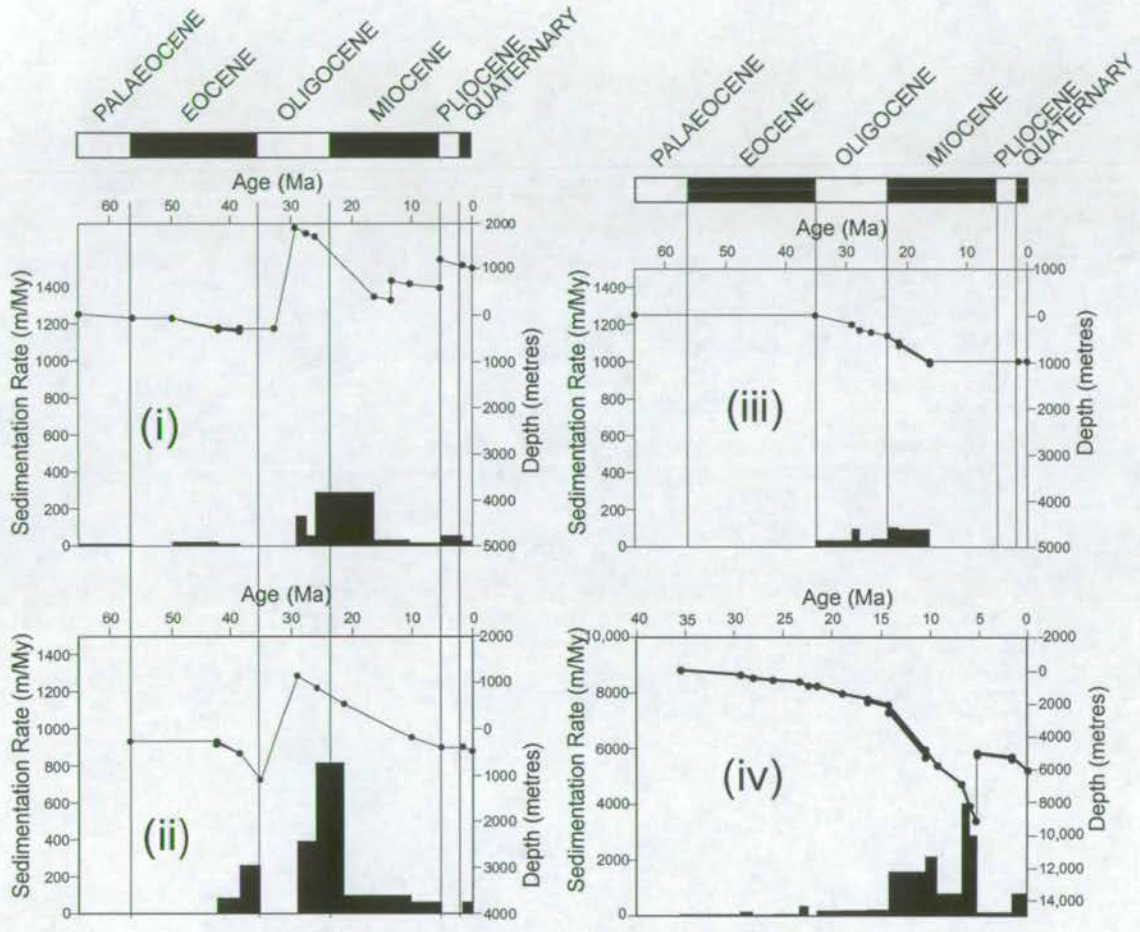

Fig. 5.12b Subsidence history plots generated from composite logs in four basins (see Fig. 3.1 for basin locations). **(i)** Ecemis Fault Zone composite log, **(ii)** Ulukisla Basin composite log, **(iii)** Karsanti Basin composite log and **(iv)** Adana Basin composite log. The Oligo-Miocene unit of the Ecemis Fault Zone has poor time constraints, thus curves should be seen as rough indicators of rapid vs. slow sedimentation and subsidence. Total decompaction subsidence was calculated using the approach of Steckler and Watts (1978). See text for methodology. Data displayed include sedimentation rates (lower bar scale), depth to basin floor (central line graph).

period of uplift and erosion during the earliest Pliocene which affected the Ecemiş area and the Adana Basin (Figure 5.12b)

5.4.5 Pliocene to Quaternary

The Pliocene and Lower Quaternary period then saw a second phase of relative subsidence in the Ecemiş Fault Zone area. During this period local subsidence occurred, in the hanging-walls of new normal and oblique fault scarps (Chapter 4), this subsidence should not be seen as a region-wide phenomena.

5.5 Interpretation

5.5.1 General shape of subsidence profiles

Generalised subsidence curves for basins in different tectonic settings are shown in Fig. 5.3, based on well established subsidence models (5.2.1 above). Notably, extensional basins have a concave-up subsidence curve with subsidence rates decreasing after an initial burst, foreland basins have a convex-up subsidence curve and strike slip 'pull-apart' basins have a distinct step in their subsidence profile, reflecting very rapid pulses of subsidence.

In general terms, the Adana Basin has a convex-up subsidence curve and closely resembles the foreland basin model (Fig. 5.12a-iv, 5.12b-iv), in agreement with published interpretations (Williams *et al.* 1995). The Karsanti Basin profile is also convex-up and resembles the start of a foreland basin profile (Fig. 5.12a-iii). When added to the Adana Basin profile (Fig. 5.12a-iv), it appears that the Karsanti Basin may be the first effects of flexure in the larger scale foreland basin setting.

The Ulukişla subsidence curve has a multiply stepped shape. Initial subsidence (Eocene) follows an exponentially increasing subsidence trend (convex-up), typical of foreland

basin settings. However, later stages show exponentially decreasing subsidence (concave-up), suggesting a rift-basin setting (Fig. 5.12a-ii, 5.12b-ii). This is compatible with other findings in this study (Chapter 7), which show that thrust loading and flexure occurred during the Late Eocene. The Ulukişla Basin profile suggests that the effects of flexure ceased at the end of the Eocene and that the basin behaved as a rift basin from the Late Oligocene onward.

The Ecemiş Fault Zone has a pronounced step in its subsidence curve (Fig. 5.12a-i) and I interpret this very rapid and short-lived subsidence as being consistent with subsidence within a strike slip basin (see 5.2.1.3 above).

5.5.2 Implications for regional tectonics

The Eocene appears to have been a period of shallow marine deposition with subsidence focused mainly in the Ulukişla Basin. During the Oligocene there was a regional uplift event and cessation of subsidence, except in the Karsanti Basin where sedimentation continued. Following this during the Early Miocene, rapid subsidence resumed with sudden increases in subsidence and sedimentation in the Ecemiş and Ulukişla Basins. This is consistent with the initiation of a strike-slip basin in the Ecemiş area during this time. During the Late Miocene subsidence slowed in the Ulukişla and Ecemiş Basins and increased in the southerly Adana Basin. The Pliocene and Quaternary have seen a resumption of subsidence within the Ecemiş Fault Zone without a similar resumption in the Ulukişla and Adana Basins. This subsidence was local only, focused in the hanging-walls of new faults which became active in the EFZ during the Plio-Quaternary (see section 4.9).

Subsidence analysis has also been carried out in the Miocene Aksu, Köprü and Manavgat Basins of the Isparta Angle (Fig. 5.13a, Flecker *et al.* 1998). In this area subsidence was initiated during the Burdigalian (Early Miocene), and was partially a

result of thrust loading by the Lycian Nappes from the NW. This is similar to the initiation of the Adana Basin, as interpreted by Williams *et al.* (1995), i.e. the result of thrust loading of the Tauride belt during the Early Miocene. However, subsidence profiles from the Aksu, Köprü and Manavgat Basins do not show the characteristics of foreland basins (Fig. 5.13b), but rather are the results of extensional faulting (Flecker *et al.* 1998).

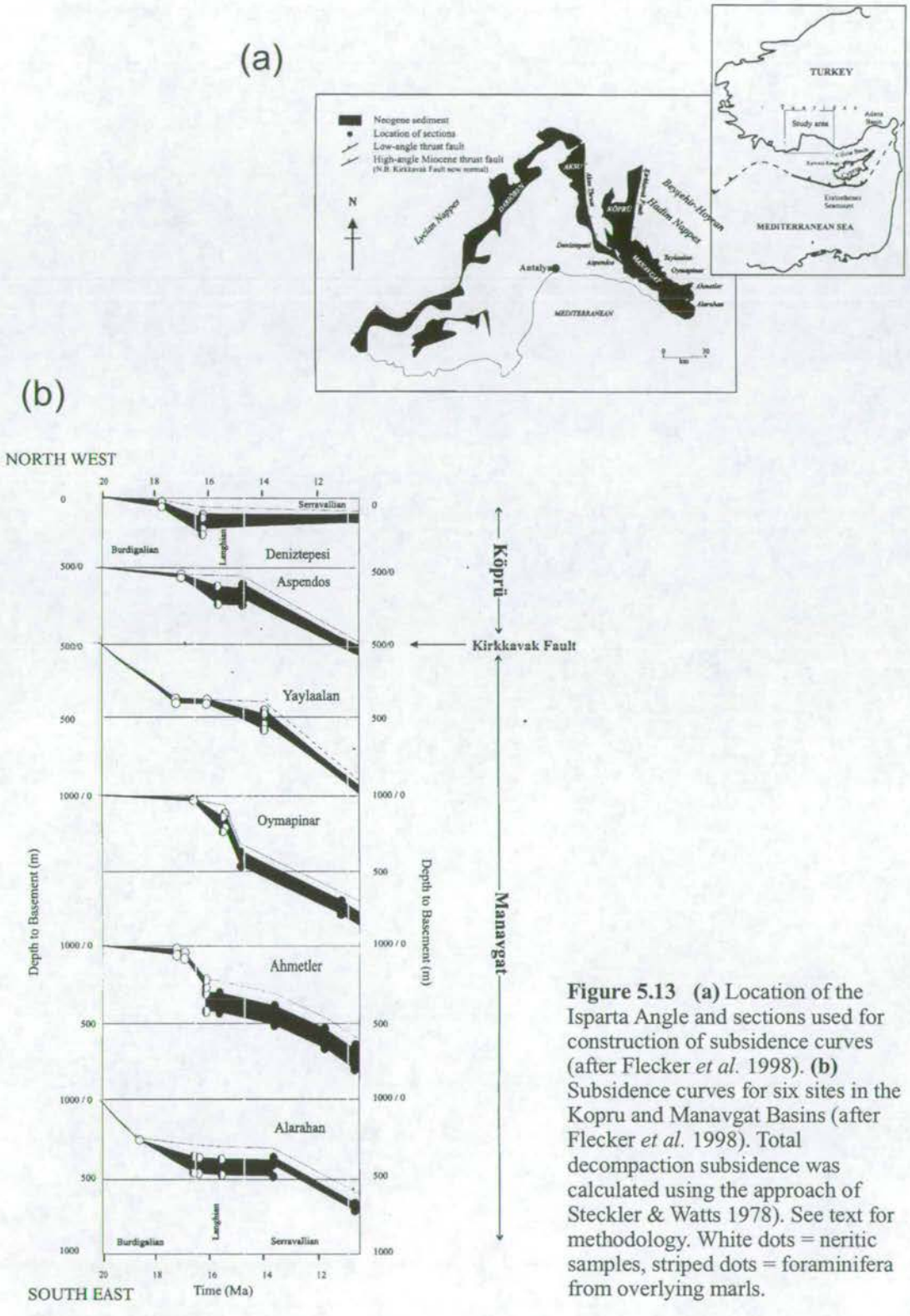

Figure 5.13 **(a)** Location of the Isparta Angle and sections used for construction of subsidence curves (after Flecker *et al.* 1998). **(b)** Subsidence curves for six sites in the Kopru and Manavgat Basins (after Flecker *et al.* 1998). Total decompaction subsidence was calculated using the approach of Steckler & Watts 1978). See text for methodology. White dots = neritic samples, striped dots = foraminifera from overlying marls.

6 Provenance

6.1 Introduction

A study of the composition and provenance of Cenozoic sedimentary rocks within the EFZ and adjacent Cenozoic basins can shed light on the uplift and exhumation history of the Taurus Mountains in the area. More specifically, provenance data can help to identify the location of sediment sources along the EFZ and how these may have migrated through time. The main aims of this chapter are: (i) to infer the timing of regional uplift and (ii) elucidate the implications of changing sediment input for the evolution of the EFZ.

Provenance trends are assessed using sedimentary rocks with a wide spectrum of grain sizes. Firstly, changes in the clast type found in fluvial conglomerates are measured, to determine the source areas of proximal fluvial sediments. Secondly, point count data from fluvial and lacustrine sandstones are used to identify and quantify changes in sandstone provenance. Lastly, terrestrial mudstones (interpreted as fluvial overbank deposits) are analysed using an X-ray fluorescence technique, using immobile elements as markers for source rock types.

6.2 Potential Sediment Sources

An examination of a regional geological map (Fig. 2.4) reveals possible local and regional sources for Cenozoic sediments (Fig 6.1):

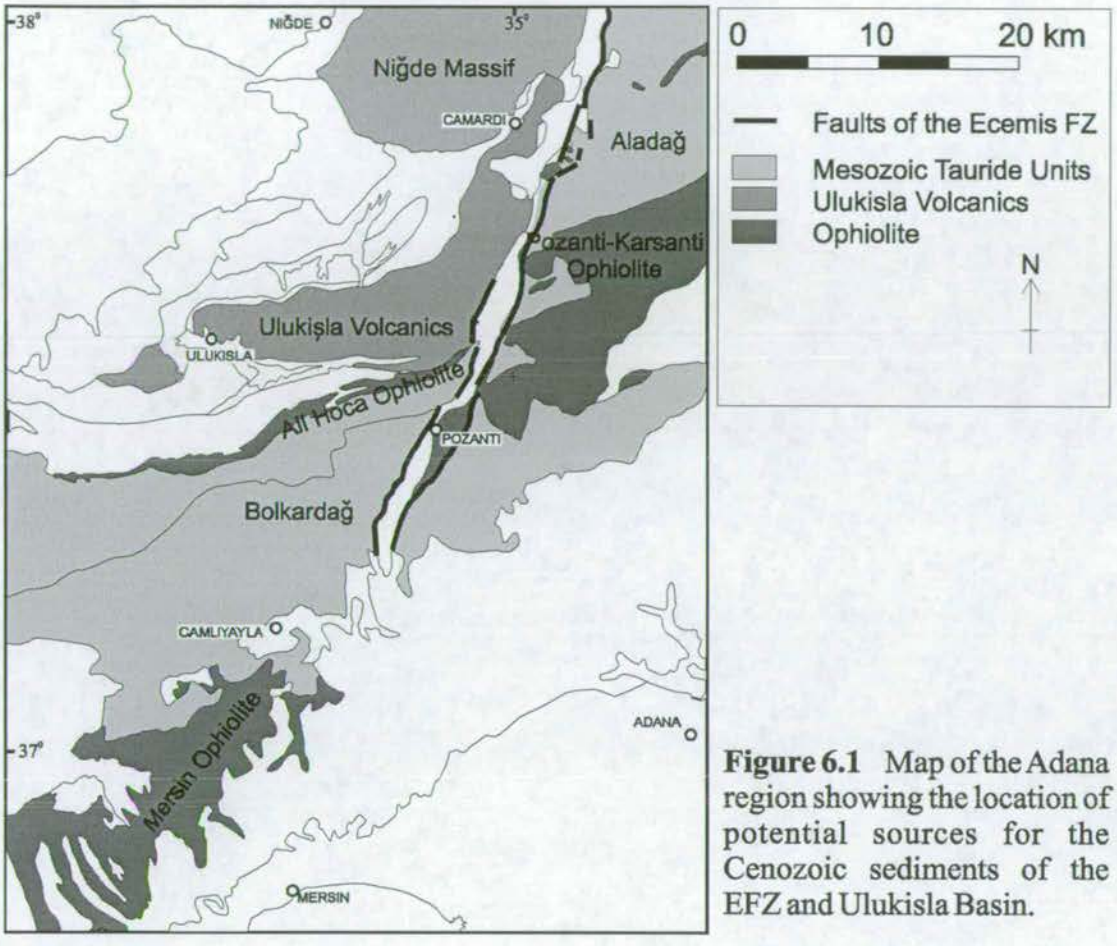

Figure 6.1 Map of the Adana region showing the location of potential sources for the Cenozoic sediments of the EFZ and Ulukisla Basin.

6.2.1 Aladağ Tauride carbonates

These comprise the high mountains bounding the EFZ to the east. In this area the deepest Tauride carbonate rocks at the surface are at lower greenschist facies or lower grade of metamorphism (Tekeli *et al.* 1984), with original sedimentary structures and fossils still visible. The unit most likely to contribute to the sediments of the EFZ is the Late Triassic – Early Jurassic Beyaz Aladağ Formation (Tekeli *et al.* 1984). This comprises micritic dolomites and dolomitic limestones, with abundant calcareous algae and a megalodont fauna. Characteristic detrital grains and clasts likely to be derived from this source include micritic limestone, dolomite and calcite vein material.

6.2.2 Bolkardağ Tauride metasediments and carbonates

To the west of the EFZ the Tauride carbonate platform is currently exhumed to a much deeper level, exposing upper greenschist to amphibolite grade meta-pelites and carbonates (Dilek & Whitney in press). There is also a blueschist facies overprint along the northern edge of the Bolkardağ, and this has been attributed to the partial subduction and subsequent isostatic rebound of this part of the Bolkardağ during the Miocene (age of uplift based on apatite fisson track ages of 23.6±1.2Ma from the Horoz granite, Dilek *et al.* 1997). It is therefore reasonable to infer that prior to the Miocene, material shed from the Bolkardağ would have been of a lower metamorphic grade. Typical detrital clasts and grains shed from this source include: mica schists, phyllites, slates and marble.

6.2.3 Niğde Massif

This range of mountains to the NW of the EFZ has been interpreted as a partially unroofed metamorphic core complex (Whitney & Dilek 1998). Tauride platform carbonate material has been exhumed such that the lower metamorphic grades have been removed and up to granulite facies rocks (max. 5-6kbar, $>700^{0}$C) are currently exposed. The complex includes not only highly metamorphosed carbonates but also meta-ophiolite. The Uçkapili Granite is intruded into the centre of the massif and is a quartz, plagioclase, K-feldspar, biotite and muscovite granite (Whitney & Dilek 1998). Characteristic detrital clasts being shed from the Niğde Massif include: gneiss, garnet-mica schist, 2-feldspar granite, marble, quartzite, amphibolite, meta-basites and meta-cherts. Sediments sourced from this area are expected to be especially rich in quartz and micas.

6.2.4 Horoz granite

The Horoz pluton intrudes into the Bolkardağ marble (Fig. 2.4), forming a contact aureole of hornblende-hornfels facies rocks. The pluton itself is composed of two main rock types: medium-grained hornblende-biotite granodiorite and fine-medium-grained biotite granodiorite (Çevikbaş *et al.* 1995). The mineralogy of these 'HB granites' includes: quartz + plagioclase + albite + orthoclase + biotite + hornblende. Clasts derived from this body are characteristically composed of hornblende-rich granite.

6.2.5 Ulukişla Volcanics

The volcanogenic Ulukişla Formation outcrops to the west of the EFZ and comprises andesitic pillow lavas, tuffs, agglomerates and volcanic breccias intercalated with minor amount of sandstones, shales and limestones (Demirtaşli *et al.* 1984). Sediments sourced from this area are expected to be rich in basaltic lithoclasts, K-feldspar, plagioclase and pyroxenes.

6.2.6 Pozanti-Karsanti ophiolite & Alihoca ophiolite

The Pozanti-Karsanti ophiolite is tectonically emplaced over the Mesozoic Aladağ carbonate platform and includes a metamorphic sole, hartzburgite tectonites, dike swarms, ultramafic cumulates and layered gabbros (Lytwyn & Casey 1995). The thin metamorphic sole is mainly composed of hornblende and plagioclase-bearing amphibolitic metabasite. Hartzburgitic tectonites have almost completely been altered to serpentinite. Dyke swarms are of doloritic to gabbroic composition. The Alihoca ophiolite is mainly a tectonic melange and is composed of blocks of gabbro, serpentinite, crystalline limestone and dolorites cut by aplite dykes (Demirtaşli *et al.* 1984). Sediments sourced from these ophiolitic rocks are expected to be rich in ophiolitic clasts such as basalt, dolorite, gabbros and serpentinised hartzburgites.

Detrital grains may include: plagioclase, hornblende, serpentinite, pyroxenes and heavy minerals such as chromite.

6.2.7 Intraclastic Cenozoic sediments

Lithologies generated during the Oligo-Miocene and Late Miocene include foraminiferal limestones, different compositions of terrestrial sandstones and mudstones, stromatolitic and oncolitic limestones and lignite (Chapter 4). All of these may have been eroded and reworked into Oligo-Miocene and Late Miocene units.

6.3 Conglomerate Clast Type Variation

6.3.1 Rationale

Conglomerate clast type can be used as a general indicator of spatial and temporal (up section) variation in source rock type. This is useful within the Oligo-Miocene Çukurbağ alluvial to fluvial terrestrial unit where conglomerate packages are ubiquitous. The Late Miocene and Eocene units are less conglomerate rich, such that sandstone petrography becomes a more useful method of evaluating provenance.

The aim is to plot clast type abundance against measured logs (Enclosure 1), to compare N to S variations along the EFZ. Temporal (up section) clast type variations through the Oligo-Miocene are also assessed.

6.3.2 Methodology

During the course of sedimentary logging at twelve localities along the EFZ, conglomerate clast types were identified and populations measured. In each case a $1m^2$ vertical section was chosen and all clasts with C-axis length of over 1cm were identified and counted; size fractions were not separated. Percentages were then calculated and

plotted as graphical logs (Enclosure 1). Within the Oligo-Miocene Çukurbağ Formation four localities included a significant abundance of conglomerate for graphic display: Bademdere, Çukurbağ, Alpu and Tekir (Enclosure 1, from N to S). Within the Late Miocene Burç Formation two localities were used: Burç and Gulek (Enclosure 1).

6.3.3 Results

Palaeocene Çamardi Formation

This unit outcrops unconformably above the Niğde Massif high-grade metamorphic rocks at Evliya Tepe, Çamardi. It contains polycrystalline quartz-, schist- and marble - bearing gravels and conglomerates. The only local source for such clasts is the local Niğde Massif.

Oligo-Miocene Çukurbağ Formation

In general conglomerates of this unit contain a larger proportion of ophiolite-derived clasts (i.e. gabbro and radiolarian chert) than those of the overlying Burç Formation Ophiolite-derived clasts are most abundant in the south of the EFZ (Tekir and Alpu sections) and also toward the base of the unit. Mesozoic limestone clasts are more abundant in the north of the EFZ (Bademdere section) and toward the top of the unit. Volcanic clasts (andesite and rhyolite) are most abundant in the centre of the EFZ (Çukurbağ), and are of only minor importance outside this area.

Late Miocene Burç Formation

Conglomerates of this unit are dominated by Mesozoic micritic and recrystallised limestones, with the proportion of limestone clasts increasing up-section. Intraclastic Late Miocene chalk and mudstone clasts are also present, as well as clasts of granite (Burç section) and mica schist (Gulek section). Neither schist nor granite clasts are seen within the Çukurbağ Formation

6.4 Sandstone Petrography

6.4.1 Rationale

Sandstone petrography and point counting provide a more quantitative assessment of how source areas change through time. Material is better sorted than in a conglomerate and grain sampling strategy is more rigorous, point counting providing a statistically random method of sampling sand grains. Triplots of Quartz-Feldspars-Lithics and other sandstone constituents can usefully discriminate source changes spatially and through time.

6.4.2 Methodology

Four suites of sandstones were analysed using standard point counting techniques (Dickinson & Suczek 1979). The suites represent: (i) the northern EFZ (Bademdere and Burç sections), (ii) the southern EFZ (Alpu, Kamişli and Gülek sections), (iii) the western Ulukişla Basin (Kepez Tepe and Altay sections) and (iv) the eastern Ulukişla Basin (Aktoprak section). Suites comprise varying numbers of samples depending on the stratigraphic thickness of the unit involved. Samples were point counted using 300 grain identifications per thin section. Results are tabulated in Appendix 2. Undulosity (gradual extinction of quartz grains associated with metamorphism) was evaluated during point counting and quartz grains were separated into non-undulose, undulose and poly-crystalline (as defined by Basu *et al.* 1975).

6.4.3 Framework Grains

The sandstones studied are mainly lithic arenites. Framework grains are briefly described below:

6.4.3.1 Quartz

Mono-crystalline, non-undulose quartz (Qm, 2-17% of all framework grains) and undulose quartz (Qu, 1-17%) are present throughout all sandstone suites. Poly-crystalline quartz being much less common.

Trends

Undulosity trends (proportions of Qu to Qm) for the EFZ and Ulukişla Basin are shown in Fig. 6.2. The EFZ suites indicate two pulses of Qu release in both north and south. In the north of the EFZ (Fig. 6.2a) quartz undulosity starts low (first three samples) and rapidly increases, giving a two-peak distribution. The south EFZ suite (Fig. 6.2b) shows a similar two-pulse Qu peak but has fewer data-points. In the western Ulukişla Basin (Fig. 6.2c), quartz undulosity begins high and gradually decreases up-section. The eastern Ulukişla Basin suite (Fig. 6.2d) shows an increase and finally a slight decrease, but only has four data-points.

6.4.3.2 Feldspar

K-feldspar (K) and plagioclase (P) are present in varying amounts throughout the suites. K-feldspar is the more abundant, mainly as altered orthoclase but with a very small proportion of microcline. K-Feldspars are sourced from plutonic rocks such as the Niğde Massif and Horoz granites and from the Ulukişla volcanics. Plagioclase is less abundant, being present as individual laths or (rarely) larger euhedral crystals. These are partly sourced from the basalts of the Pozanti-Karsanti and Alihoca ophiolites and are easily chemically weathered to kaolinite in the fluvial profile.

Trends

Plots of total abundance of feldspars and the relative abundances of K-feldspar and plagioclase (Fig. 6.3) show the following trends. The northern EFZ (Fig. 6.3a) and eastern Ulukişla Basin (Figs. 6.3d) have a relatively low abundance of total feldspars (max. 12-14% of all framework grains) and feldspar abundance increases up section. In

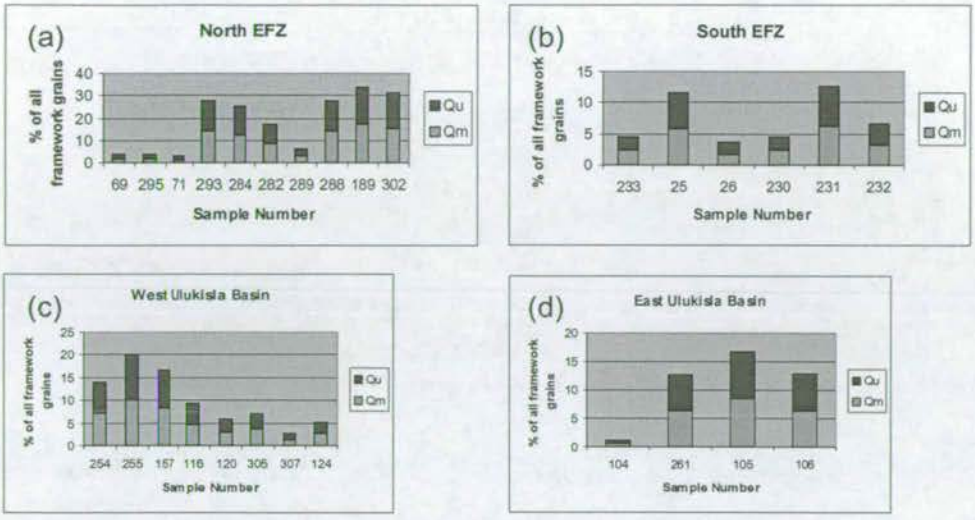

Figure 6.2 Plot showing variation in the abundance of undulose quartz (Qu) and non-undulose quartz (Qm) up-section in: **(a)** north EFZ suite of sandstones, **(b)** south EFZ suite of sandstones, **(c)** west Ulukişla Basin suite of sandstones and **(d)** east Ulukişla Basin suite of sandstones. Samples numbers are arranged with base of section to the left and top of section to the right. Abundances are shown as a percentage of total framework grains, counted using standard point counting techniques (Dickinson & Suczec 1979).

the northern EFZ this increase is in two pulses. The southern EFZ (fig. 6.3b) and western Ulukişla Basin (Fig. 6.3c) have a higher abundance of total feldspars (max. 20-26% of all framework grains) and feldspar abundance decreases up section (with the exclusion of a single K-feldspar peak in the W. Ulukişla curve).

Interpretation

Trends in total feldspar abundance are very similar to those in undulose quartz for the same suite of rocks (except in the southern EFZ dataset). This indicates that both feldspars and undulose quartz may have the same source in this area.

6.4.3.3 Lithic Fragments

Lithic-carbonate (Llst), lithic-sandstone (Lsst) and lithic-igneous (Lign) grains occur in varying proportions throughout the rock suites. Micas (Mc) and chert (Ct) have been counted separately. Llst grains are usually dominant, consisting of micritic limestone

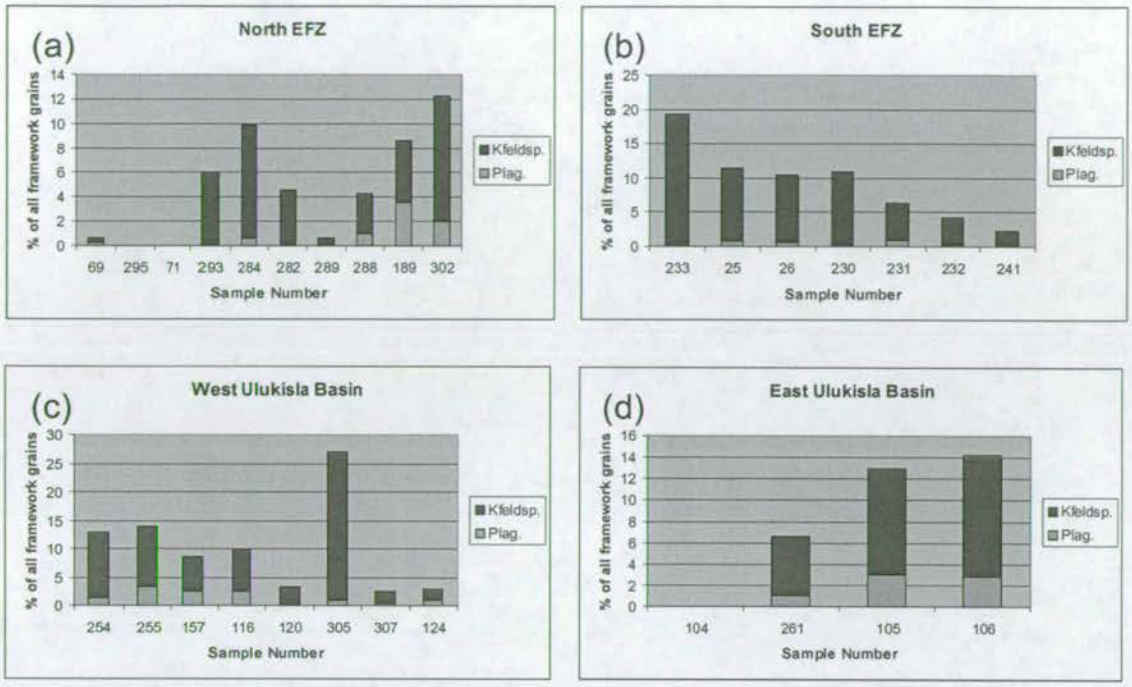

Figure 6.3 Plot showing variation in the abundance of plagioclas feldspar (Plag.) and potassium feldspar (Kfeldsp.) up-section in: **(a)** north EFZ suite of sandstones, **(b)** south EFZ suite of sandstones, **(c)** west Ulukişla Basin suite of sandstones and **(d)** east Ulukişla Basin suite of sandstones. Samples numbers are arranged with base of section to the left and top of section to the right. Abundances are shown as a percentage of total framework grains, counted using standard point counting techniques (Dickinson & Suczec 1979).

(from the Cenozoic succession) and larger calcite grains from the recrystallised limestones located within the Mesozoic stratigraphy of the Aladağ and Bolkardağ. Lsst grains are rare and consist of calc-arenites from the Cenozoic succession. Lign grains comprise: (i) de-vitrified (formerly glassy) tholeiitic basalt, (ii) serpentinite, (iii) gabbro and (iv) augite. These are mainly derived from ophiolitic material. Mc (micas) are undifferentiated biotites and muscovites. Ct (chert) comprises both un-recrystallised radiolarian chert and re-crystallised granular chert.

Trends

Plots of the abundance of lithic fragments against time (Fig. 6.4) reveal similar trends to those found from feldspars. In the northern EFZ (Fig. 6.4a) and eastern Ulukişla Basin (Fig. 6.4d) Llst abundance is high but decreases up section. Lign and chert (ophiolite)

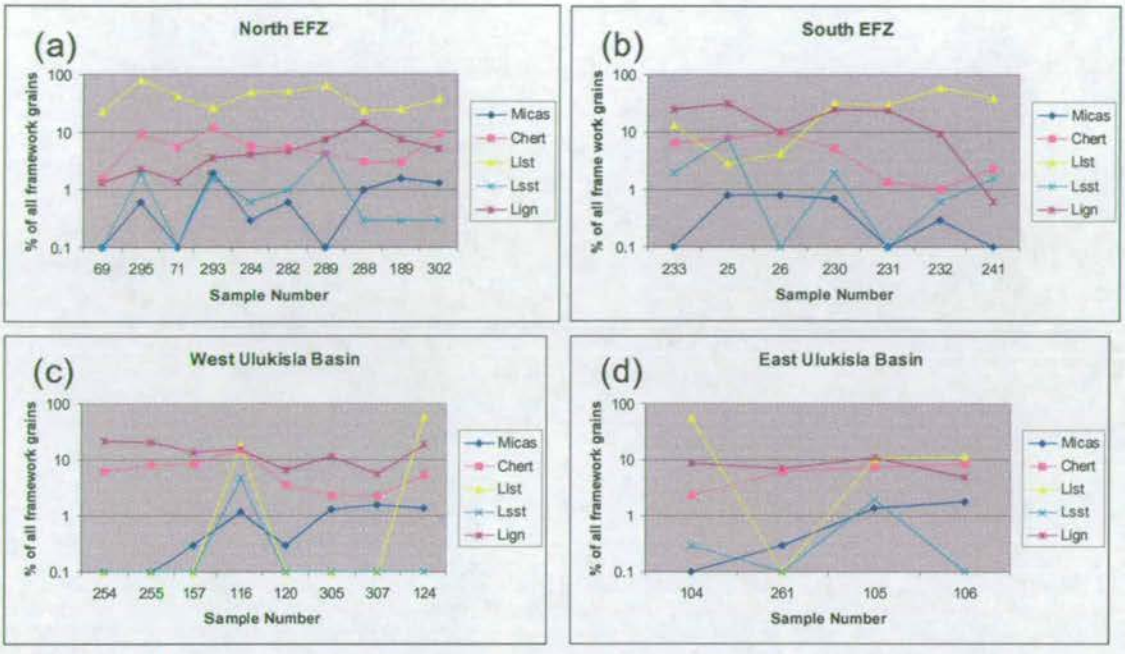

Figure 6.4 Plot showing variation in the abundance of different lithic fragments up-section in: **(a)** north EFZ suite of sandstones, **(b)** south EFZ suite of sandstones, **(c)** west Ulukisla Basin suite of sandstones and **(d)** east Ulukisla Basin suite of sandstones. Sample numbers are arranged with section base to the left and section top to the right. Abundances are shown as a percentage of total framework grains, counted using standard point counting techniques (Dickinson & Suczec 1979). Llst = limestone grains, Lsst = sandstone grains, Lign = igneous grains.

abundance is constant or increases in the same suites. In the southern EFZ (Fig. 6.4b) and western Ulukişla Basin (Fig. 6.4c) Llst abundance is lower and increases up section. The abundance of Lign and chert (ophiolite-derived) decreases up section. Mica abundance increases up section in all suites except the southern EFZ where it decreases slightly. Mica abundance increase follows a similar pattern in the western and eastern Ulukişla Basin. Ophiolite-derived material is generally low in K, and does not contain K-bearing micas (biotite). It is more likely that micas are derived from the pelites of the Bolkardağ and Niğde Massif, or from the Horoz or Uçkapili (Niğde Massif) granites.

Interpretation

These trends, and those of feldspar abundance, suggest that the northern EFZ and eastern Ulukişla Basin share a provenance history of decreasing (or constant) Mesozoic

Tauride carbonate influence and increasing ophiolitic influence with time. Conversely, the southern EFZ and western Ulukişla Basin share a pattern of increasing Mesozoic Tauride carbonate influence and decreasing ophiolitic influence with time. Increasing mica abundance in the northern areas may reflect the unroofing and erosion of deeper Tauride schists and/or granites (Uçkapili and Horoz granites).

6.4.4 QFL & Source Discrimination Triplots

Triangular diagrams were constructed to plot variations in Q (total quartz), F (total feldspars) and L (total lithics) in four suites of rocks (Fig. 6.5). This is useful in identifying trends in sediment maturity and provenance (Dickinson & Suczec 1979). Additionally, source discrimination triangular diagrams were constructed to identify trends in source area (Fig. 6.6). The three apices are: Taurus source (Llst), Niğde source (total quartz + micas) and ophiolite source (Lign + chert).

North Ecemiş Suite (Bademdere + Burç)

This suite of 11 samples shows a trend from lithic-dominated at the base of the Çukurbağ Formation to more quartz-rich at the top of the Burç Fm (QFL triplot, Fig. 6.5a). This corresponds to an increase in grain rounding, sorting and general textural maturity up section. This maturity change is most pronounced between the Burç sandstones (Late Miocene) and the Bademdere (Oligo-Miocene) suite. The north Ecemiş suite shows very little feldspathic influence.

When lithic constituents are separated in the 'source discrimination triplot' (Fig. 6.6a) a trend from Llst-rich at the base of the Çukurbağ Formation (Fig. 6.7a) to more quartz- and mica-rich at the top of the Burç Formation (Fig. 6.7b) is seen. The input from ophiolitic sources is relatively small.

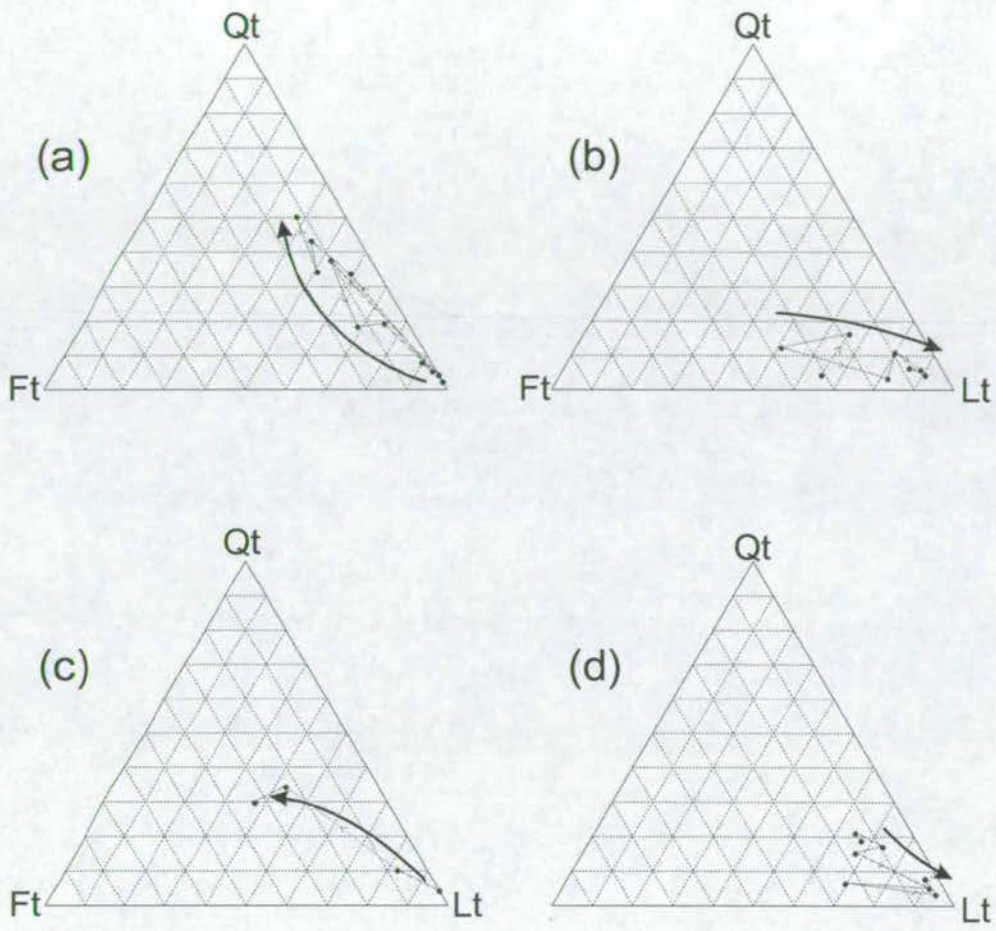

Figure 6.5 Triangular plots showing variations in the abundances of total quartz (Qt), total feldspars (Ft) and total lithic fragments (Lt) in four suites of sandstones: **(a)** north EFZ (Bademdere + Burç sections), **(b)** south EFZ (Alpu + Gülek sections), **(c)** east Ulukişla Basin (Emirler + Aktoprak sections) and **(d)** west Ulukilşa Basin (Kepez Tepe + Altay sections). Thin lines and arrows represent path from base to top of section, thick black arrows represent general trends. Abundances were calculated using standard point counting techniques (Dickinson & Suczec 1979).

South Ecemiş Suite (Alpu + Gülek)

A QFL triplot for this suite shows a trend from a shared feldspar-lithics influence to a clear lithic dominance (Fig. 6.5b). This corresponds to a trend from coarse, poorly sorted, angular-subrounded grains at the base of the Çukurbağ Formation to very fine-medium grained, well rounded, calcareous sandstone at the top of the Burç Formation There is very little quartz influence.

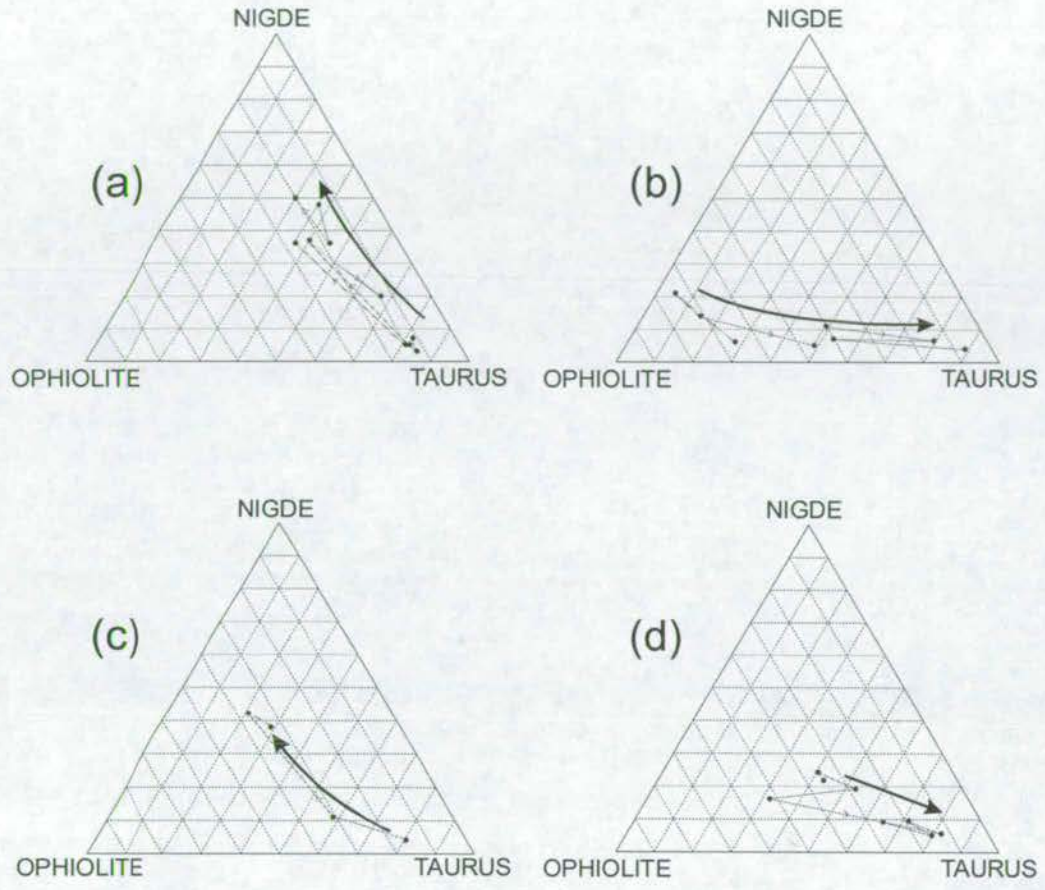

Figure 6.6 Triangular plots which group mineral abundances to show variations in source area. Nigde = qtz + micas, Ophiolite = Lign + chert, Taurus = Llst. Trends are shown for four suites of sandstones: **(a)** north EFZ (Bademdere + Burç sections), **(b)** south EFZ (Alpu + Gülek sections), **(c)** east Ulukişla Basin (Emirler + Aktoprak sections) and **(d)** west Ulukilşa Basin (Kepez Tepe + Altay sections). Thin lines and arrows represent path from base to top of the suite, thick black arrows represent general trends. Abundances were calculated using standard point counting techniques (Dickinson & Suczec 1979).

A source discrimination triplot is more revealing (Fig. 6.6b) and shows a trend from Lign+chert (ophiolitic) dominance and the base of the Çukurbağ Formation (Fig. 6.7c) to Llst (Tauride) dominance at the top of the Burç Formation (Fig. 6.7d). Plutonic (quartz + mica) influence is low.

Photomicrograph of a quartz-rich sandstone from the top of the Burc section, Burc Fm. Slide shows three grains of quartz. One undergoing undulose extinction (XPL 4 x magnification).

Photomicrograph of a sandstone from the top of the Gulek section (Burc Fm.). Slide shows several grains of calcite and micritic limestone (XPL 10 x magnification).

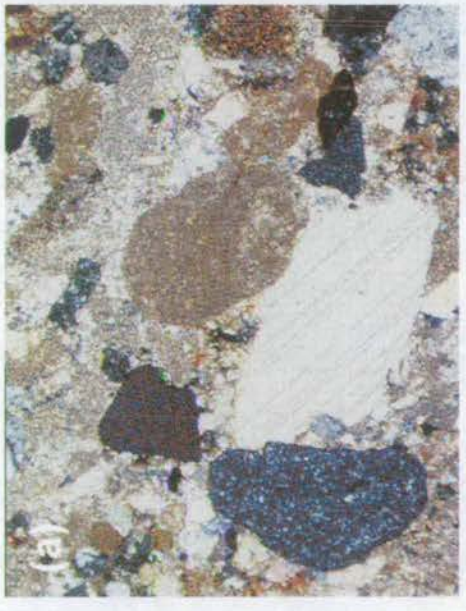

Photomicrograph of a carbonate-rich sandstone from the base of the Bademdere section, Cukurbag Fm. Slide shows grains of calcite (centre base) and micritic limestone (centre right). XPL 10 x

Photomicrograph of a sandstone from the base of the Alpu section (Cukurbag Fm.). Slide shows a grain of sepentinite surrounded by calcite cement (XPL 10 x magnification).

Figure 6.7 Photomicrographs froim sandstones of the Çukurbag and Burç Formations, showing changes in mineralogy and textural maturity.

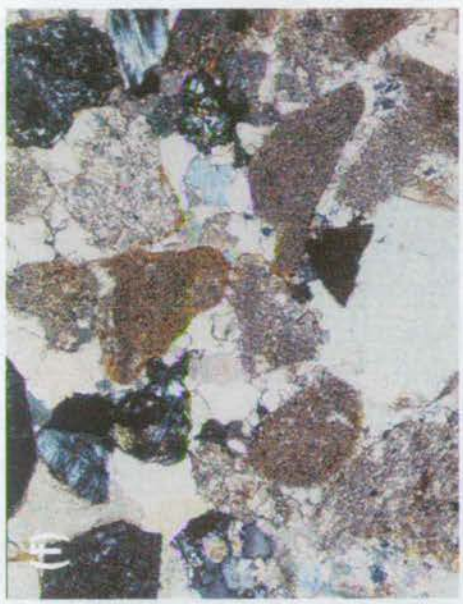

Photomicrograph of a sandstone from the Hacibekirli-Altay section (Burc Fm. of the western Ulukilsa Basin). Slide shows multiple grains of calcite and micritic limestone. XPL 4 x magnification.

Photomicrograph of a sandstone from the top of the Aktoprak section (Cukurbag Fm. of the eastern Ulukilsa Basin). Slide shows grains of quartz (upper left) and serpentinite (lower right). XPL 10 x magnification.

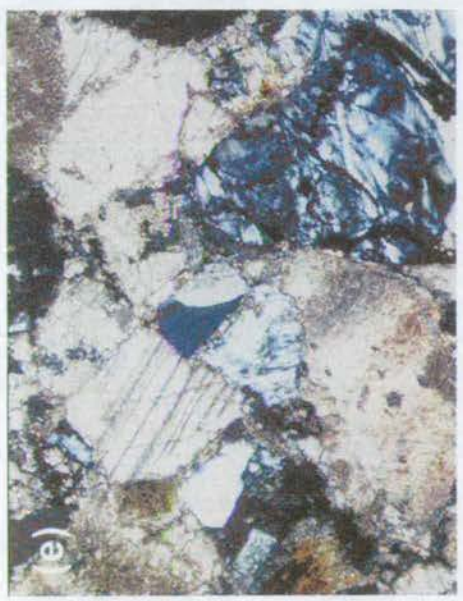

Photomicrograph of a sandstone from the Kepez Tepe section (Cukurbag Fm. of the western Ulukilsa Basin). Slide shows grains of calcite (upper left) and serpentinite (lower right). XPL 10 x magnification.

Photomicrograph of a sandstone from the very base of the Aktoprak section (Cukurbag Fm. of the eastern Ulukilsa Basin). Slide shows grains of calcite (upper left) and micritic limestone (right). XPL 10 x magnification.

Figure 6.7 Photomicrographs froim sandstones of the Cukrbag and Burc Formations, showing changes in mineralogy and textural maturity.

West Ulukişla Suite (Kepez Tepe + Altay)

A QFL triplot (Fig. 6.5c) shows that this suite separates into two subgroups, the lithic-influenced Kepez Tepe section (Çukurbağ Formation) and the lithics-dominated Altay section (Burç Formation). This separation is picked out better in the source discrimination triplot (Fig. 6.6c), where the Çukurbağ Formation rocks show a mixture of ophiolitic and Tauride influence (Fig. 6.7e), whereas the Burç Formation rocks are influenced by a Tauride source solely (Fig. 6.7f). Ophiolite input appears to have shut off during the Middle Miocene.

The Middle Miocene is marked by a change from coarse, angular, poorly sorted, texturally immature sandstones and gravels (Çukurbağ Formation) to finer grained, better sorted, sub-rounded sand grains, interbedded with oncolitic limestones, stromatolites and mudstones (Burç Formation). As in the southern EFZ, plutonic grains (quartz and micas) do not play an important role.

East Ulukişla Suite (Emirler + Aktoprak)

This is a much smaller suite than the preceding ones and includes only the Çukurbağ Formation. A QFL triplot (Fig. 6.5d) indicates a trend from lithics-dominated at the base of the Çukurbağ Formation to a mixture of feldspar, lithics and quartz influence at the top of the Çukurbağ Formation. The source discrimination triplot (Fig. 6.6d) reveals a trend of Llst dominance at the base (Fig. 6.7g) to mixed ophiolitic and plutonic influence at the top of the Çukurbağ Formation (Fig. 6.7h). This basal Çukurbağ Formation trend is not seen in the West Ulukişla suite as the Kepez Tepe section does not penetrate as far down as the Eocene – Oligocene boundary (as here).

These trends closely resemble those seen in the northern Ecemiş suite. The petrography shows a change up section from basal marble-dominated, angular, poorly sorted breccias and conglomerates into medium-fine grained, well sorted sub-angular ophiolite-derived sandstones.

6.4.5 Summary of Sandstone petrography results

The northern EFZ and eastern Ulukişla Basin sediments have progressed from an original limestone (Taurus) influence (Çukurbağ Formation) to an increased influence of quartz and micas, accompanied by an increase in textural maturity up-section (Burç Formation). There is little ophiolite influence to the sediments in these areas.

The southern EFZ and western Ulukişla Basin sediments have progressed from an original ophiolitic influence (Çukurbağ Formation) to a limestone (Tauride) influence up-section (Burç Formation).

6.5 Mudstone Geochemistry

6.5.1 Geochemical analysis of provenance – Rationale

The geochemistry of mudstones can help to indicate the tectonic setting and provenance of sediments and is particularly useful when sediments are fine grained. The concentration of certain incompatible trace elements (such as La, Sc, Th, Zr and V) in an unknown mudstone can be used to determine likely source rock if the geochemical composition of that source rock is known (Bhatia 1983, Bhatia & Crook 1986).

Tectonic discrimination models have been devised using the major element ratios K_2O/Na_2O and Al_2O_3/SiO_2 to determine between: (i) passive continental margin (high Si, high K/Na), (ii) active continental margin (high Si, intermediate to low K/Na) and (iii) ocean island arc (low Si, variable K/Na, Fig. 6.8, Roser & Korsch 1986).

However, several effects have been identified by Wronkieicz & Condie (1987) which are detrimental to geochemical techniques being used for provenance determination. These should be recognised and assessed before provenance work is commenced:

Grain size effect

Hydraulic sorting influences the chemical composition of grains in a given sample. It is, therefore, best to compare samples of a similar grain size. Finer grain sizes are better mixed and provide better samples.

Samples taken during this study are all of mud grain size.

Adsorption effect

Clays can adsorb Rare Earth Elements and metals from seawater, especially when sedimentation rates are very low (e.g. manganese nodules). Analysis of REEs should therefore account for this.

REEs are not used in this study.

Diagenesis and metamorphism

Large Ion Lithofiles (LILEs) and some major elements may be redistributed during both processes. REEs and HFSEs are the least susceptible to this redistribution.

Samples taken during this study have been buried to a maximum if 1km and have not undergone the lowest stages of metamorphism (i.e. diagenetic grade only).

Source area weathering

This has an important influence on Alkali and Alkali Earth elements. For instance Cs, Rb and Ba can be fixed in the weathering profile and become concentrated, whereas Na, Ca and Sr are leached from the profile.

These elements are not used as provenance tracers in this study.

6.5.2 Sampling Strategy

Geochemical analysis of seven potential source rocks, three modern mudstones and twenty unknowns from the Cenozoic units of the EFZ were determined using the X-ray fluorescence technique (see Fitton *et al.* 1984 and Appendix 3 for procedures).

Potential source rocks which were sampled include: Uçkapili Marble, granite and schist (all from within the Niğde Massif), Akca limestone (Bolkardağ) and Yayhali limestone (Aladağ). Data from Lytwyn & Casey (1995) was used for the geochemistry of the Pozanti-Karsanti ophiolite.

Three modern mudstones were sampled in order to characterise modern river mudstones with known provenance and compare with the unknowns. These were from within the Niğde Massif, from Horoz (Bolkardağ) and Madenboğazi (Aladağ).

Twenty unknowns were sampled during sedimentary logging and correspond (as closely as possible) to the suites used during sandstone petrography. There are three suites of mudstones: northern EFZ Çukurbağ Formation (Bademdere, 8 samples), northern EFZ Burç Formation (Burç, 4 samples) and eastern Ulukişla Basin (Aktoprak, 8 samples).

X-Ray Fluorescence techniques and results are described in Appendix 3.

6.5.3 K_2O / Na_2O vs. SiO_2 diagram (Fig. 6.8)

Elemental analysis results (Appendix 3) were used to separate the potential sources and modern muds into source 'fields' using the K_2O/Na_2O–SiO_2 discrimination plot (Roser & Korsch 1986). The K_2O/Na_2O ratios of seven potential source rocks and three modern mudstones were plotted against SiO_2 values (Fig. 6.8a).

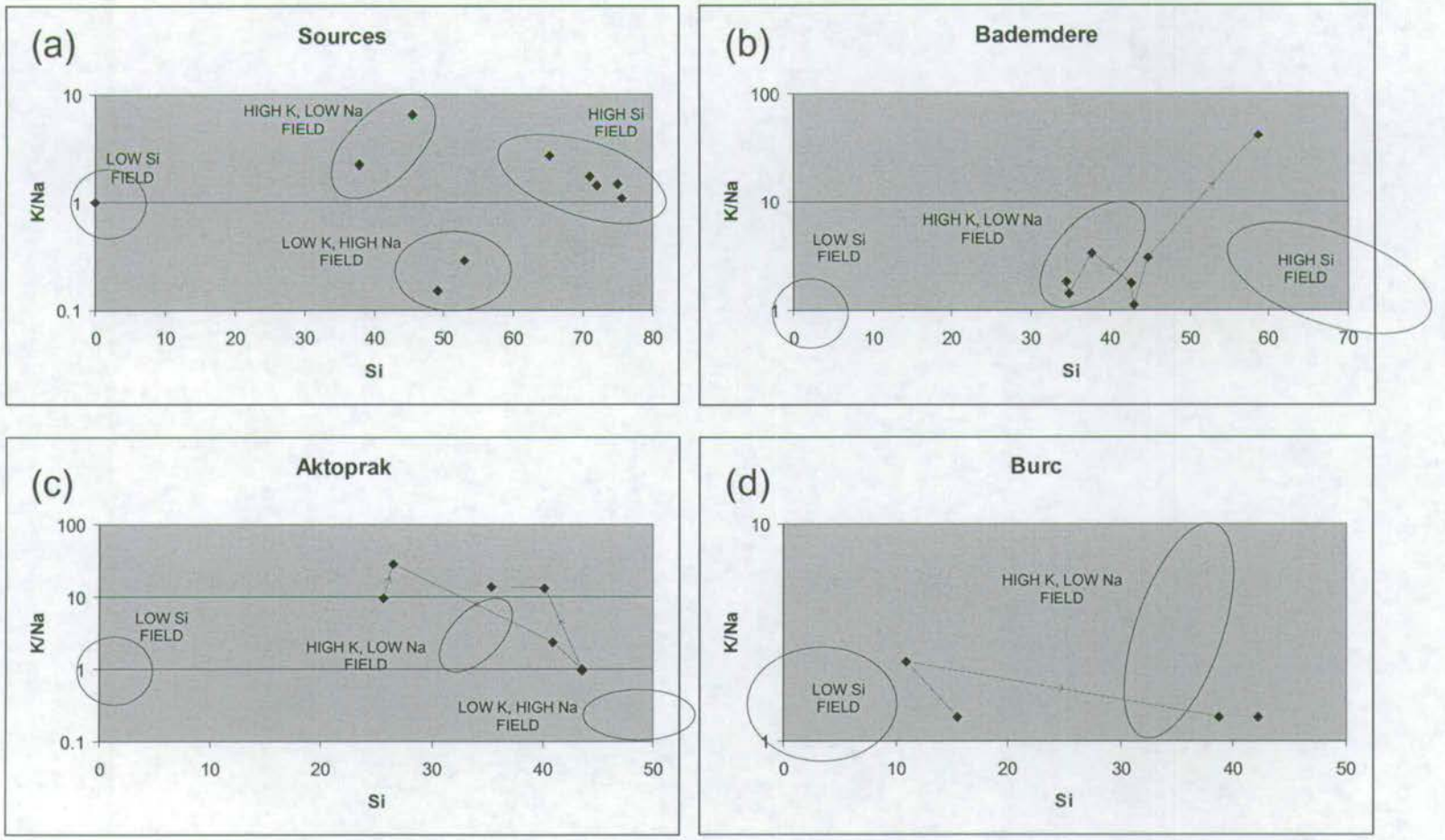

Figure 6.8 Plot of K/Na against Si, to discriminate between sediment source areas (modified from Roser & Korsch 1986). Ratios and abundances are taken from XRF elemental analyses (Appendix 4). **(a)** Potential source areas, **(b)** Bademdere suite of mudstones, northern EFZ, **(c)** Aktoprak suite of mudstones, eastern Ulukisla Basin, **(d)** Burc suite of mudstones, northern EFZ. Thin lines and arrows represent path from the base to the top of the mudstone suite.

Potential source rocks separate into four distinct fields (Fig. 6.8a): (i) Granites, schists and modern alluvial mud from the Niğde Massif plot into a high Si field, (ii) ophiolitic rocks (data from Lytwyn & Casey 1995) plot into a low K, high Na field, (iii) modern alluvial mud from the Taurus Mountains (Aladağ and Bolkardağ) plot into a high K, low Na field and (iv) marble from the Niğde Massif plots into a low Si field.

Samples from the Oligo-Miocene Bademdere suite mainly plot in the high K, Low Na field, changing from low to higher Si content up-section (Fig. 6.8b). Samples higher in the section plot into the high Si field.

Samples from the Oligo-Miocene Aktoprak suite (eastern Ulukişla Basin) show a similar trend (Fig. 6.8c). The suite begins in the high K, low Na field, moves toward the Low K, high Na field and finally migrates toward the high Si field, increasing in Si up section.

Samples from the Late Miocene Burç suite begin close to the low Si field and migrate into the high K, low Na field, increasing in Si content up section (Fig. 6.8d).

6.5.4 Multi-element diagram normalised to NASC (Fig. 6.9)

Multi-element diagrams can be used to examine the distribution of major and trace elements in mudstones. Multi-element plots compare a range of elements from potential sources and the three mudstone suites (Bademdere, Aktoprak and Burç) normalised to average North American Shale Composite (Gromet *et al.* 1984). A plot developed by McCann (1991) is used here (Fig. 6.9). Elements are arranged such that those elements mainly derived from acidic source rocks (e.g. Niğde and Horoz granites) plot on the left side of the diagram, whilst those derived from basic and ultrabasic rocks (e.g. ophiolites in this area) plot on the right.

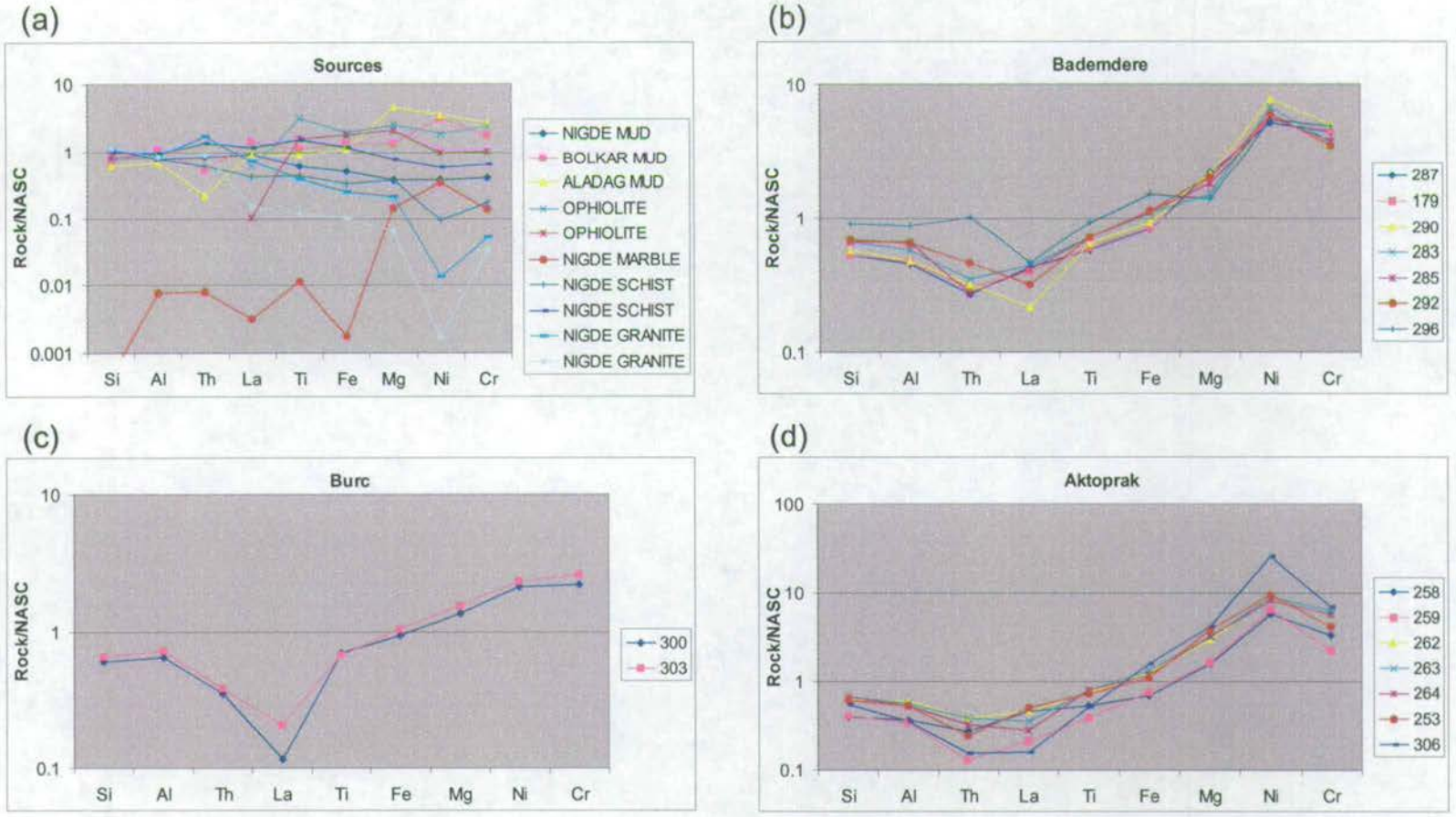

Figure 6.9 Multi-element plot of selected major and minor elements, showing 'acidic elements' (elements associated with acidic rock types) on the left and 'basic elements' (those associated with basic rocks) on the right (modified from McCann 1991). Abundances are taken from XRF elemental analyses (Appendix 4). **(a)** Potential source areas, **(b)** Bademdere suite of mudstones, northern EFZ, **(c)** Aktoprak suite of mudstones, eastern Ulukisla Basin, **(d)** Burc suite of mudstones, northern EFZ. In the keys to the suites of unknown mudstones (b-d), base of section is to the top of the column, top of section is to the base of the column.

Potential source rocks show a wide diversity of 'basic' and 'acidic' elements (Fig. 6.9a). Modern mud samples from the Bolkardağ and Aladağ and ophiolitic clasts are enriched in Mg, Ni and Cr (basic elements), whereas Niğde granites and schists are depleted in these elements relative to NASC. The enrichment of Aladağ mud in Mg, Ni and Cr is due to its sampling site being in a river draining the Madenbogazi ophiolite outcrop and chromite mine. There is very little enrichment in 'acidic elements', Niğde granites and schists are slightly enriched in Si relative to NASC.

Mudstones from the Bademdere suite (Fig. 6.9b) are generally enriched in 'basic elements' (Ni and Cr). Mudrocks become less enriched in Ni and Cr and more enriched in Si, Al and Th up-section.

Samples from the Burç suite (Fig. 6.9c) have lower concentrations of 'basic elements' than those of the underlying Bademdere suite. However, there is no enrichment in 'acidic elements' relative to NASC.

The Aktoprak suite (Fig. 6.9d) is highly enriched in the 'basic elements' Ni and Cr and this enrichment increases consistently up section. The suite is depleted in 'acidic elements' relative to NASC.

6.5.5 Al – Ca – Cr+Ni triplot (Fig. 6.10)

This triplot uses the concentrations of characteristic single or combined major and trace elements to discriminate simply between three potential source rocks (Fig. 6.10a). These being: (i) Tauride limestone (Ca), (ii) Niğde Massif granites and schists (Al) and ophiolitic source material (Cr + Ni *100). Sampled source rocks separate into an Al-rich field (Niğde granites and schists), a central intermediate Al-Ca field (ophiolitic rocks) and a Ca-rich field (Bolkardağ and Aladağ muds).

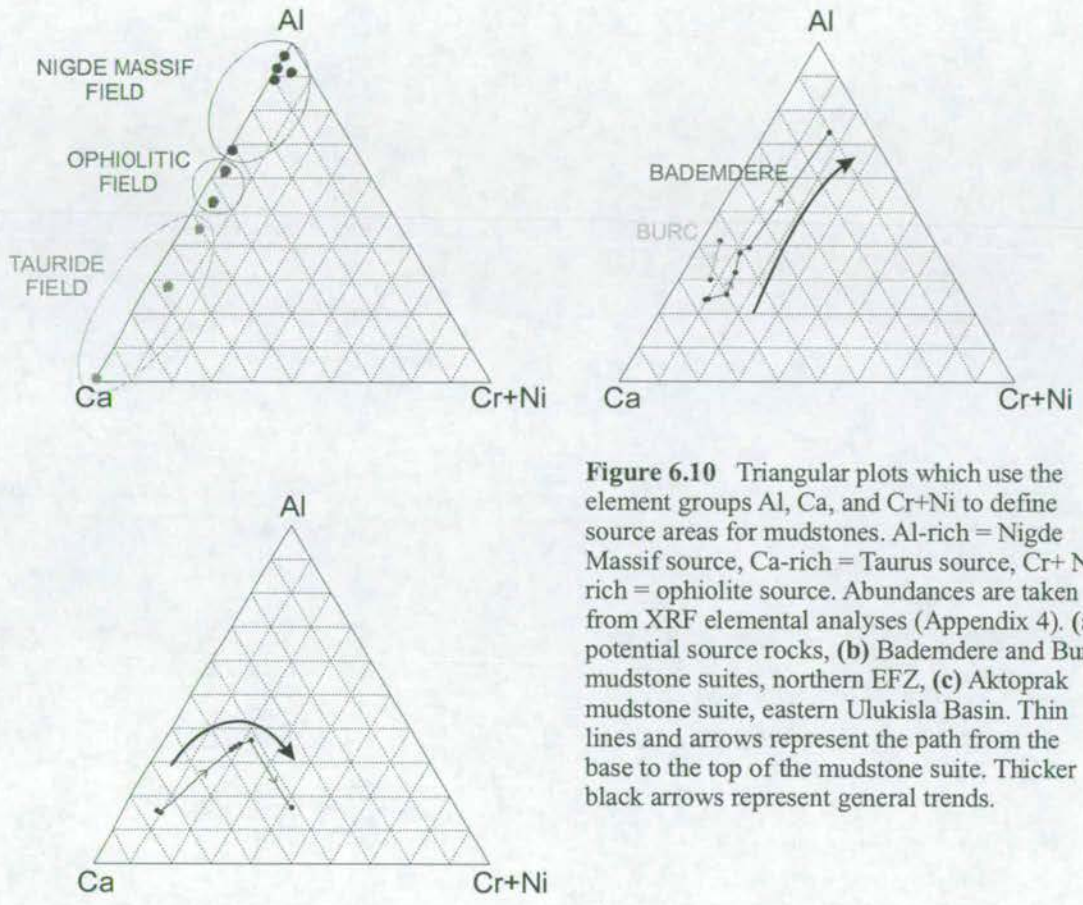

Figure 6.10 Triangular plots which use the element groups Al, Ca, and Cr+Ni to define source areas for mudstones. Al-rich = Nigde Massif source, Ca-rich = Taurus source, Cr+ Ni-rich = ophiolite source. Abundances are taken from XRF elemental analyses (Appendix 4). **(a)** potential source rocks, **(b)** Bademdere and Burc mudstone suites, northern EFZ, **(c)** Aktoprak mudstone suite, eastern Ulukisla Basin. Thin lines and arrows represent the path from the base to the top of the mudstone suite. Thicker black arrows represent general trends.

The Oligo-Miocene Bademdere suite exhibits a trend from the high Ca field into the high Al field up-section (Fig. 6.10b). The Late Miocene Burç mudstones lie mainly in the high Ca field. The Oligo-Miocene Aktoprak mudstone suite (Fig. 6.10c) is generally less Al-rich and exhibits a trend from the high Ca field toward a more Cr + Ni-rich composition up-section.

6.6 Interpretation and conclusions

6.6.1 Conglomerate Provenance

The composition of the conglomerates of the Palaeocene Çamardi Formation indicate that the nearby Niğde Massif was partially exhumed at this time, providing a source for mica-schist clasts. This is contrary to Whitney & Dilek (1997), who argue that the first appearance of detrital material from the massif occurs in the Middle to Late Miocene. The Eocene succession provides little in the conglomerate size range.

The Oligocene appears to have been the main period of orogenic uplift in the area, maximum conglomerate thicknesses being deposited during the Late Oligocene. High energy alluvial fan and braided river facies are found at the base of the Çukurbağ Formation throughout the EFZ, suggesting steep erosional slopes. The Pozanti-Karsanti ophiolite tectonically overlies the Mesozoic Tauride carbonate units; therefore, it is expected that ophiolitic clasts should be the first to be eroded and to be prevalent in the basal units of the Çukurbağ Formation. The increasing abundance of limestone clasts up-section reflects the removal of ophiolite and increased exposure of Tauride limestones through the Late Oligocene and Early Miocene. The Pozanti-Karsanti ophiolite appears to have been initially thickest in the south of the EFZ, where the first conglomerates are ophiolite-derived, but was much thinner (or perhaps missing altogether) in the northern EFZ. Conglomerates of the central EFZ are dominated by the Ulukişla volcanics which were providing sediment from the eastern Ulukişla Basin (see palaeocurrents during Oligo-Miocene, Figs. 4.10b & 4.8b). No schist or granite clasts are present in the Oligo-Miocene Çukurbağ Formation, suggesting that the Niğde Massif and Horoz granites were not exposed at this time.

The Late Miocene (Burç Formation) conglomerates have a much lower ophiolite component and are dominated by Tauride limestones, suggesting that most of the

Pozanti-Karsanti ophiolite had been removed by that time. The occurrence of granite clasts at Burç indicates that the Niğde Massif may have been unroofed to a significant degree by the Late Miocene. The occurrence of mica schist clasts at Gülek indicates that the Bolkardağ had been uplifted to a degree similar to today, where medium to high grade carbonates and pelites are exposed (Demirtaşli *et al.* 1984).

6.6.2 Sandstone Provenance

Sandstones show compositional changes from N to S and E to W through the area. In the northern EFZ (Bademdere and Burç sections) sands change up section from Tauride limestone-rich (Oligo-Miocene) to more quartz and mica-rich (Late Miocene), also increasing in textural maturity up-section. This may reflect one (or all) of several factors: (i) decreasing slope angles, (ii) increased storage and recycling of sediment within the basin and (iii) increased sediment input from the Niğde Massif during the Early Miocene. Ophiolitic grains are not important constituents in the sandstones of the northern EFZ and it is assumed that ophiolite thickness was low or non existent in the north of the EFZ during the Oligo-Miocene.

In the southern EFZ (Alpu and Gulek sections) sandstones change from ophiolite-derived to Tauride limestone-derived up section. This is the expected transition from a source area stratigraphy of limestone overlain by ophiolite. The lack of quartz in the southern EFZ suggests that the Niğde and Horoz granites were never adjacent to this part of the fault zone.

The Oligo-Miocene succession of the Ulukişla Basin began with a short initial input of Bolkardağ limestone and then evolved into an ophiolite-derived composition in both the east and the west. Late Miocene sandstones are dominantly Taurus limestone-derived and palaeocurrents indicate that these are sourced from the Bolkardağ (Fig. 4.10c). They are also finer and more texturally mature, suggesting lower slopes and a lower energy of

deposition. Lacustrine stromatolites and micritic limestones also suggest that the climate was wetter and that inward-draining basins developed during this time.

Overall, the northern EFZ and eastern Ulukişla Basin appear to have been adjacent to the highest, most exhumed parts of the Taurus in the region during the Oligo-Miocene. This is reflected in the initially thinner ophiolite and the unroofing of the Taurus to a deep crustal level where gneiss and granite were exposed and reworked as detrital grains into nearby Cenozoic basins. The southern EFZ and western Ulukişla Basin appear to have been adjacent to areas with a lower amount of exhumation; deep crustal source rocks are lacking and the ophiolites remained thicker, playing a more important role in the Cenozoic basin sandstones of these areas.

6.6.3 Mudstone provenance

Sampled mudstones were deposited as terrestrial, overbank, floodplain muds (Facies 2A, section 4.4.2.1). Geochemical results reveal similar trends to those found using sandstone petrography. The Oligo-Miocene mudstones of the northern EFZ change up-section from a Tauride limestone-influence (Fig. 6.10b, high K, low Na field) to being increasingly Si-rich and dominated by Niğde Massif detritus (high Si field). Late Miocene mudstones in the same area show a renewed Tauride influence (Fig. 6.10d, high K, low Na field), probably due to uplift of the Aladağ during the Middle Miocene. Mudstones of the eastern Ulukişla Basin (Aktoprak section) are limestone-rich at the base (Fig. 6.10c, high K, low Na field), migrate toward an ophiolite influence (low K, high Na) and finally move toward the high Si field (Niğde influence) at the top. These results agree with sandstone petrography conclusions.

6.6.4 Implications for the evolution of the EFZ

The Niğde Massif was partially unroofed during the Palaeocene and Eocene and influenced the upper part of the Oligo-Miocene succession. The massif was not exhumed to current, mid-crustal level until the Middle Miocene.

Sandstone petrography and mudstone geochemistry results suggest that large ophiolitic bodies existed adjacent to the southern EFZ and Ulukişla Basin during the Late Oligocene – Early Miocene, acting as sediment sources for these basins (Fig. 6.11a). Ophiolites were thickest in the southern EFZ and thinner / non-existent in the northern EFZ during this time. Uplift of the Bolkardağ and Niğde Massif was also occurring during the Oligo-Miocene, and these acted as sources of Tauride limestone to the EFZ (Fig. 6.11a).

During the Late Miocene, ophiolite bodies had become less important as sediment sources, and may have reduced in size relative to the Oligo-Miocene (Fig. 6.11b). The Niğde Massif had been exhumed to a degree where deep crustal rocks (gneiss, schist and granite) were exposed, being eroded and acting as sediment sources to the northern EFZ (Fig. 6.11b). The Bolkardağ had also been exhumed, so that schists and phyllites were exposed, supplying detrital clasts to the southern EFZ. The Bolkardağ also acted as a source of Tauride limestone to the southern EFZ and Ulukişla Basin during the Late Miocene.

Conglomerate clast data (Chapter 4) indicate that Plio-Quaternary sediments (primarily alluvial fan material) are derived from the uplifted footwalls of nearby fault scarps, which supplied initially ophiolite-derived material and later, Tauride limestone and meta-sediment detritus to the whole of the EFZ (Fig. 6.11c). The Çatalca Formation contains no significant contribution from the deep crustal rocks of the Niğde Massif.

Strike-slip offset can be quantified using point sedimentary sources, by tracking the spatial extent of their detrital products on the opposing side of the fault. The only potential unique point sources are the Uçkapili (Niğde Massif) granite and the Horoz granite. However, considering the sinistral offset of the EFZ, their ancient erosional products are likely to outcrop to the NE of the study area. This area is now largely covered by the Miocene – Recent volcanic products of the Central Anatolian Volcanic Province (Fig. 2.4), obscuring any evidence for migration of these point sources. The use of these point sources also assumes that they have remained at their current crustal level throughout strike-slip, which is unlikely considering the uplift and exhumation documented in this area.

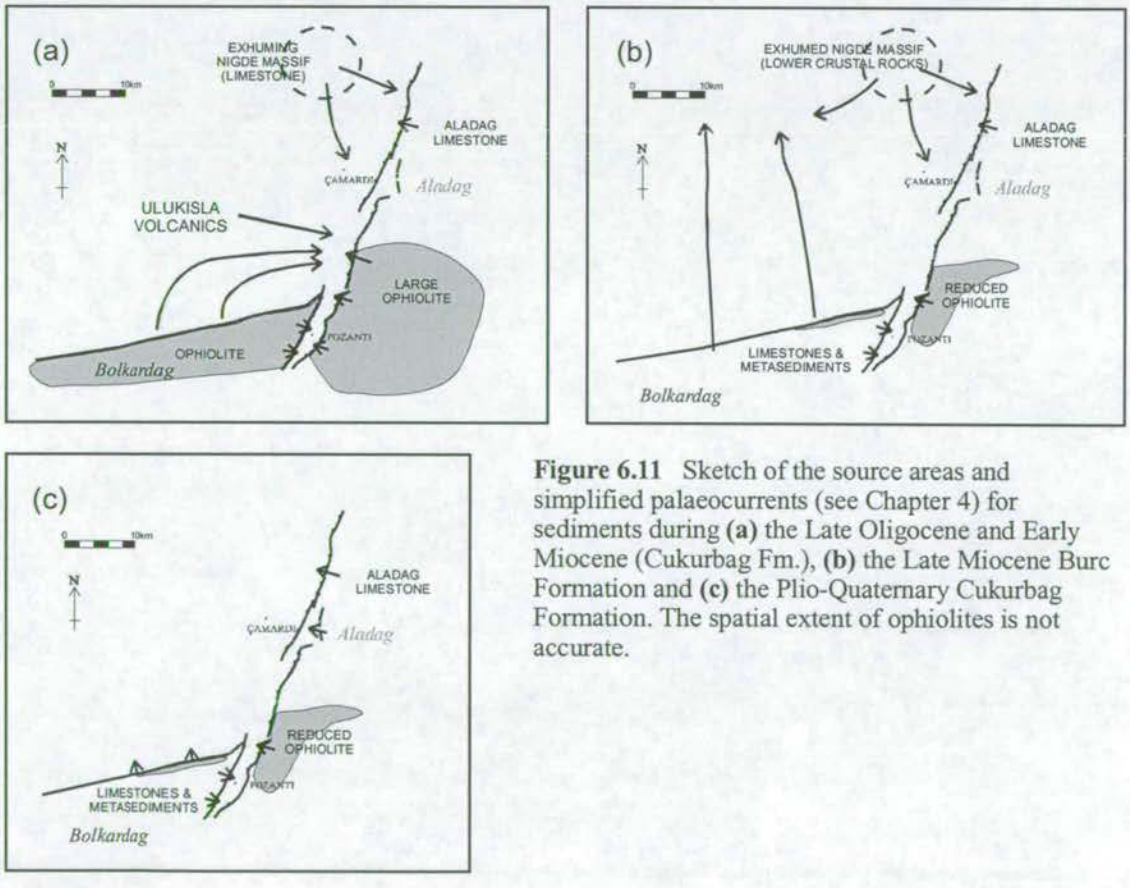

Figure 6.11 Sketch of the source areas and simplified palaeocurrents (see Chapter 4) for sediments during **(a)** the Late Oligocene and Early Miocene (Cukurbag Fm.), **(b)** the Late Miocene Burc Formation and **(c)** the Plio-Quaternary Cukurbag Formation. The spatial extent of ophiolites is not accurate.

7 Structure

7.1 Introduction

The aim in this chapter is to describe and interpret the structural characteristics of the Mesozoic and Tertiary stratigraphic units within the Ecemiş Fault Zone and nearby Taurus Mountains. This new structural data will be used to generate a thorough interpretation of the structural evolution of the Ecemiş area, and to constrain the timing and nature of strike-slip on the Ecemiş Fault Zone more accurately than in previous studies.

The chapter will be divided into the following sections: (i) Deformation and associated kinematic indicators, (ii) Fault and slickenline data, (iii) Palaeostress and (iv) Modern stress.

7.2 Previous Work

Previous structural studies of the Ecemiş Fault Zone and surrounding areas have been based on simple structural mapping (Demirtaşli *et al.* 1984, Tekeli *et al.* 1984, Yetiş & Demirkol 1984). Uçar (1997) constructed a structural map of the southern EFZ, showing faults within Mesozoic Tauride units adjacent to the EFZ (Fig. 7.1). He also constructed a strain ellipse for the area, which he used to explain the orientation of normal and reverse faults within the Aladağ and Bolkardağ.

Koçyiğit & Beyhan (1998) constructed more detailed structural maps of the entire EFZ (Fig. 7.2a), using aerial photographs and field mapping to locate fault segments. Their maps show linear structures (faults), but do not indicate the sense of movement on the majority of these faults. They were later criticised by Westaway (1999) for inferring

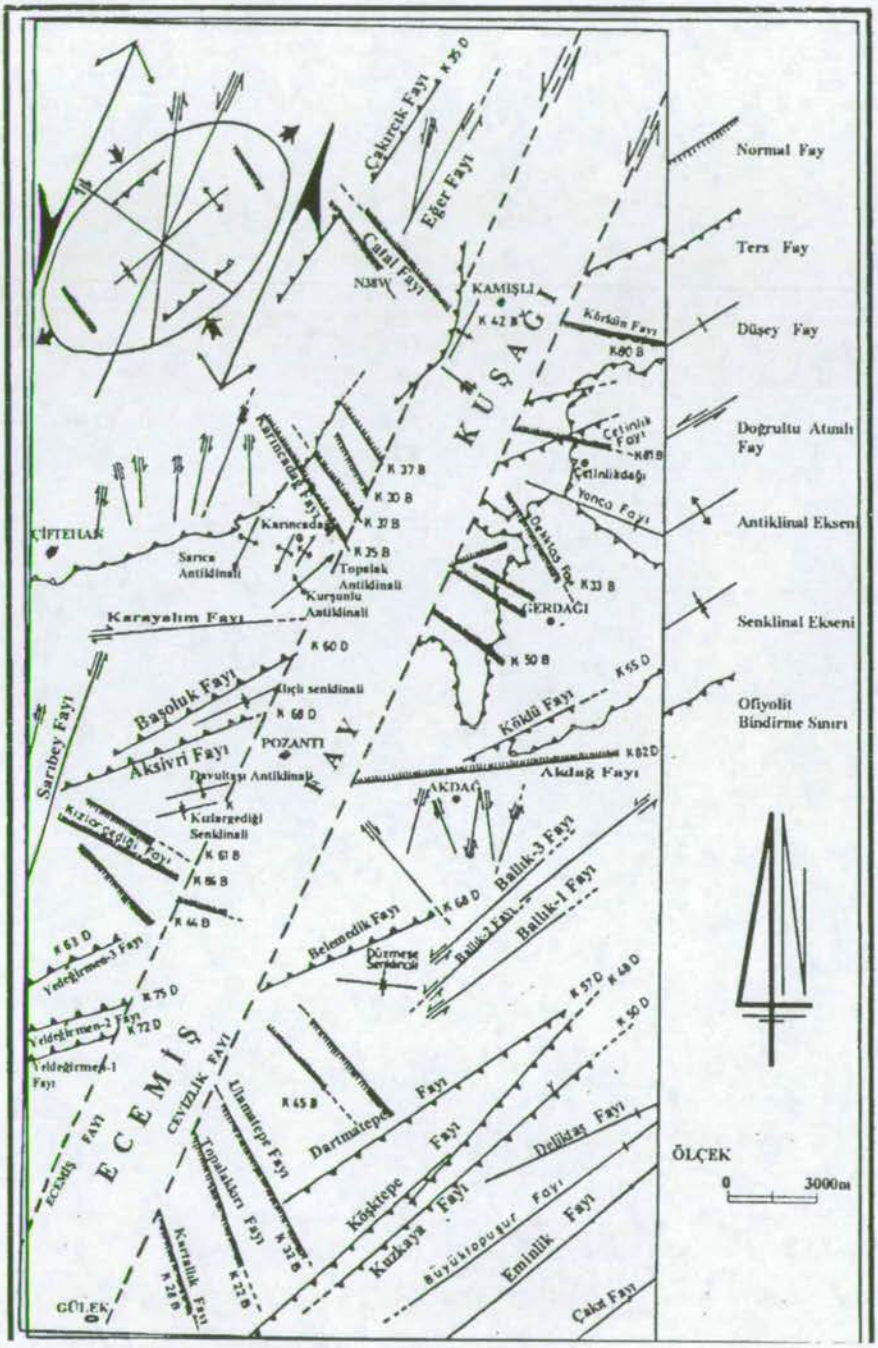

Figure 7.1 Structural geology map of the southern EFZ (Gulek to Kamisli), after Ucar 1997. Faults are mapped a simple lines and arelabelled in Turkish. Normal Fay = normal fault, Ters Fay = reverse fault, Duseu Fau = vertical fault with unknown displacement, Dogrultu Atimili Fay = strike-slip fault, Antiklinal Ekseni = anticlinal fold axis, Senklinal Ekseni = synclinal fold axis, Ofiolit Bindirme Sinari = thrust fault at the base of an ophiolite body. Strain ellipse in top right corner is based on mapped faults within the Aladag and Bolkardag adjacent to the EFZ.

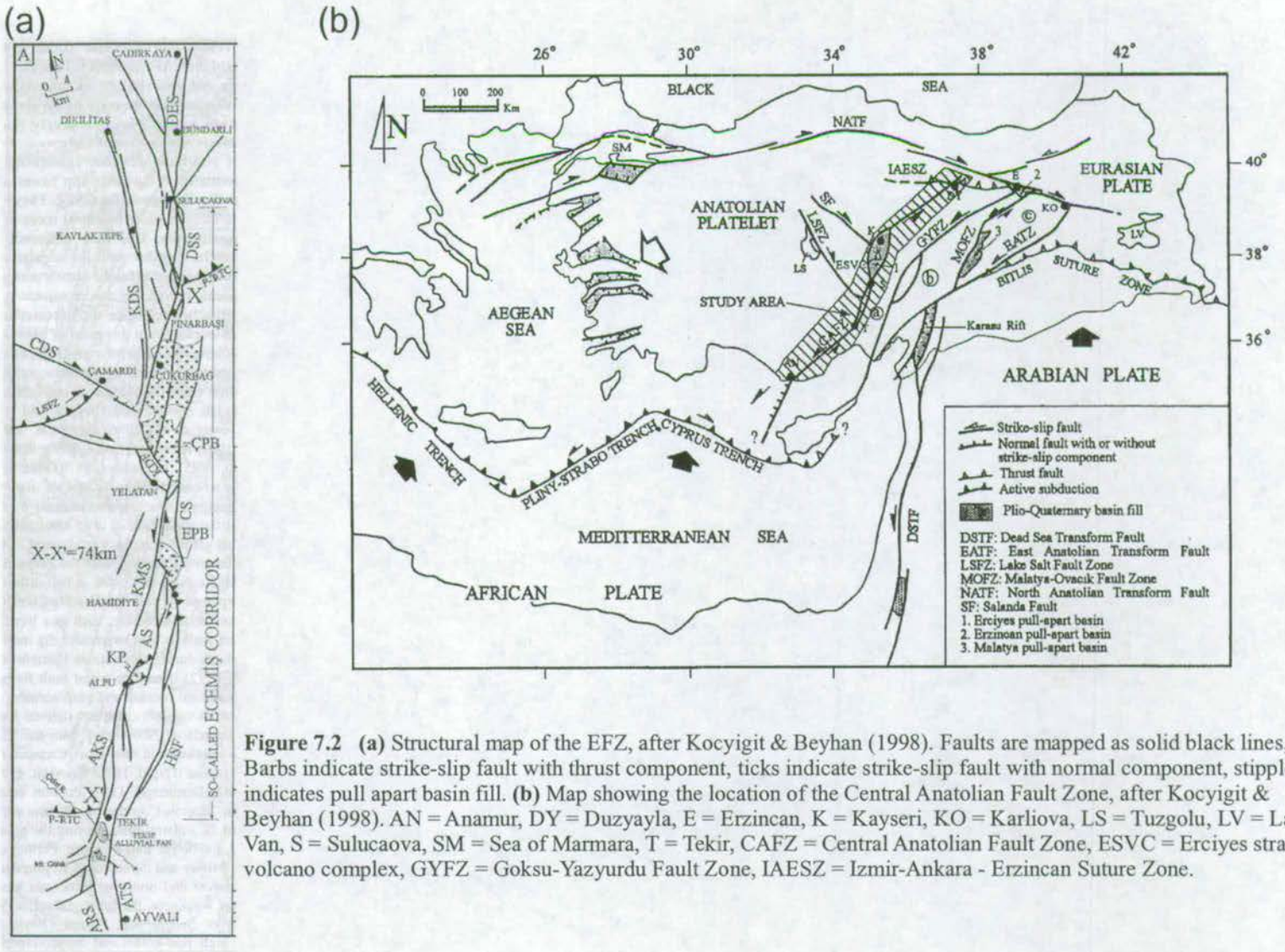

Figure 7.2 **(a)** Structural map of the EFZ, after Kocyigit & Beyhan (1998). Faults are mapped as solid black lines, Barbs indicate strike-slip fault with thrust component, ticks indicate strike-slip fault with normal component, stipple indicates pull apart basin fill. **(b)** Map showing the location of the Central Anatolian Fault Zone, after Kocyigit & Beyhan (1998). AN = Anamur, DY = Duzyayla, E = Erzincan, K = Kayseri, KO = Karliova, LS = Tuzgolu, LV = Lake Van, S = Sulucaova, SM = Sea of Marmara, T = Tekir, CAFZ = Central Anatolian Fault Zone, ESVC = Erciyes strato-volcano complex, GYFZ = Goksu-Yazyurdu Fault Zone, IAESZ = Izmir-Ankara - Erzincan Suture Zone.

fault segments which did not exist and for ignoring previously published fault segments. Koçyiğit & Beyhan (1998) proposed that the EFZ is part of an Early Pliocene, intra-continental fault zone (the Central Anatolian Fault Zone) which has re-activated the older EFZ, and which runs from Duzyayla, near the North Anatolian Fault Zone to Anamur on the Mediterranean coast (Fig. 7.2b). This theory is still very controversial and this work chooses to focus on the older and better exposed EFZ, rather than the larger CAFZ.

As yet, no analysis of deformation by stereographic projection in either the Taurus Mountains or EFZ has been attempted. No collection or quantitative analysis of fault orientation or slickenline data have previously been carried out.

7.3 Deformation

7.3.1 Methodology

During the course of field investigations, bed orientation data was collected from units of Permian to Quaternary age in the vicinity of the Ecemiş Fault Zone and from Cenozoic units of the Ulukişla Basin and the Karsanti Basin. Measurements were taken at 50-100m intervals (or much closer) whilst constructing structural maps of the EFZ, such that a representative sample of bed orientations for each unit was collected. This resulted in good coverage of the Cenozoic rocks of the EFZ, Ulukişla Basin and Karsanti Basin, and more localised coverage of the northern margin of the Bolkardağ and the margins of the Aladağ (adjacent to the EFZ). Due to the steepness of many of the scarps adjacent to the EFZ, structural data from margins of the Taurus Mountains could not be collected from the entire length of the EFZ. Bedding orientation data was plotted on stereographic projections by rock unit (i.e. by age).

7.3.2 General Results

From the differences seen between deformation trends in different rock units, it became apparent that several deformation phases have affected this area.

In the Mesozoic units on the margins of the EFZ, fold and thrust zones were observed with vergence in two opposing directions. It has been possible to determine that these two deformation phases were of different ages, using local stratigraphic relationships. Cenozoic units within the EFZ are folded with a different orientation to deformation within the Mesozoic units. Each deformation phase is dealt with in chronological order, including stereographic evidence for deformation, kinematic data and evidence for the age of deformation.

7.3.3 Late Cretaceous Deformation

SE-directed folding and thrust faulting was observed to be pervasive throughout the Bolkardağ and Aladağ along the margins of the EFZ (Fig. 7.3). At Hamidiye and Madenboğazi this deformation was found to be closely associated with the base of the Late Cretaceous Pozanti-Karsanti Ophiolite, which has been tectonically emplaced from N to S over the Aladağ Mountains (Lytwyn & Casey 1995). Indeed ophiolitic material has been incorporated into SE-directed thrust faults at Madenboğazi and Hamidiye (Tekeli *et al.* 1984). For evidence of the age of deformation, see section 7.3.3.4 below.

7.3.3.1 Deformation and vergence at Tekir

Koçyiğit & Beyhan (1998) infer a major south-directed thrust fault in the Bolkardağ in the Tekir area (location Fig. 7.3). During this study bed orientations were measured which show that a fold train exists, associated with a S-vergent thrust fault in this area.

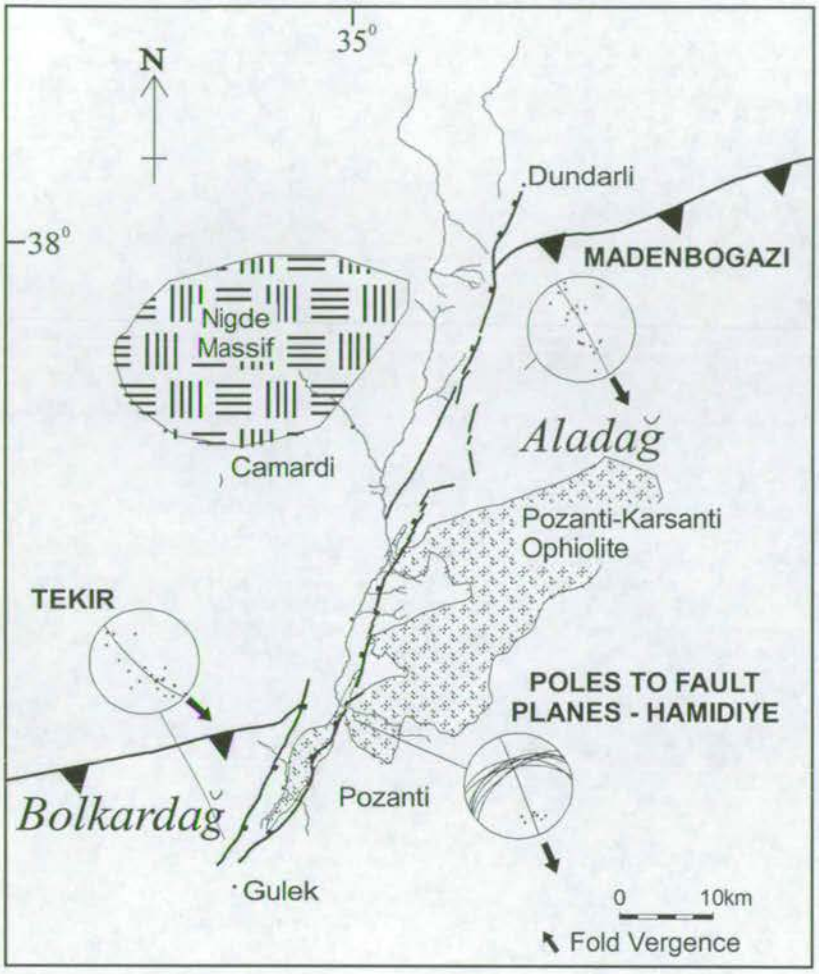

Fig. 7.3 Late Cretaceous deformation of Mesozoic Tauride units. Stereoplots show poles to bedding planes (dots), fold profile planes (great circles) and fold vergence (solid arrow). The faults of the current EFZ (thick black lines) and rivers (thin lines) are shown for location purposes only.

The fold profile plane strikes NW-SE (Fig. 7.4) and fold vergence indicates tectonic transport toward the SE.

7.3.3.2 Deformation and vergence at Madenboğazi

A N-directed (S-dipping) thrust fault has been inferred within the Aladağ Mountains in the upper reaches of the Madenboğazi river (a disused mining area 2km E of the EFZ, location Fig. 7.3) by Tekeli *et al.* (1984). After structural investigation a large scale S-dipping fault was observed (Fig. 7.5). Fold profile planes above and below this fault

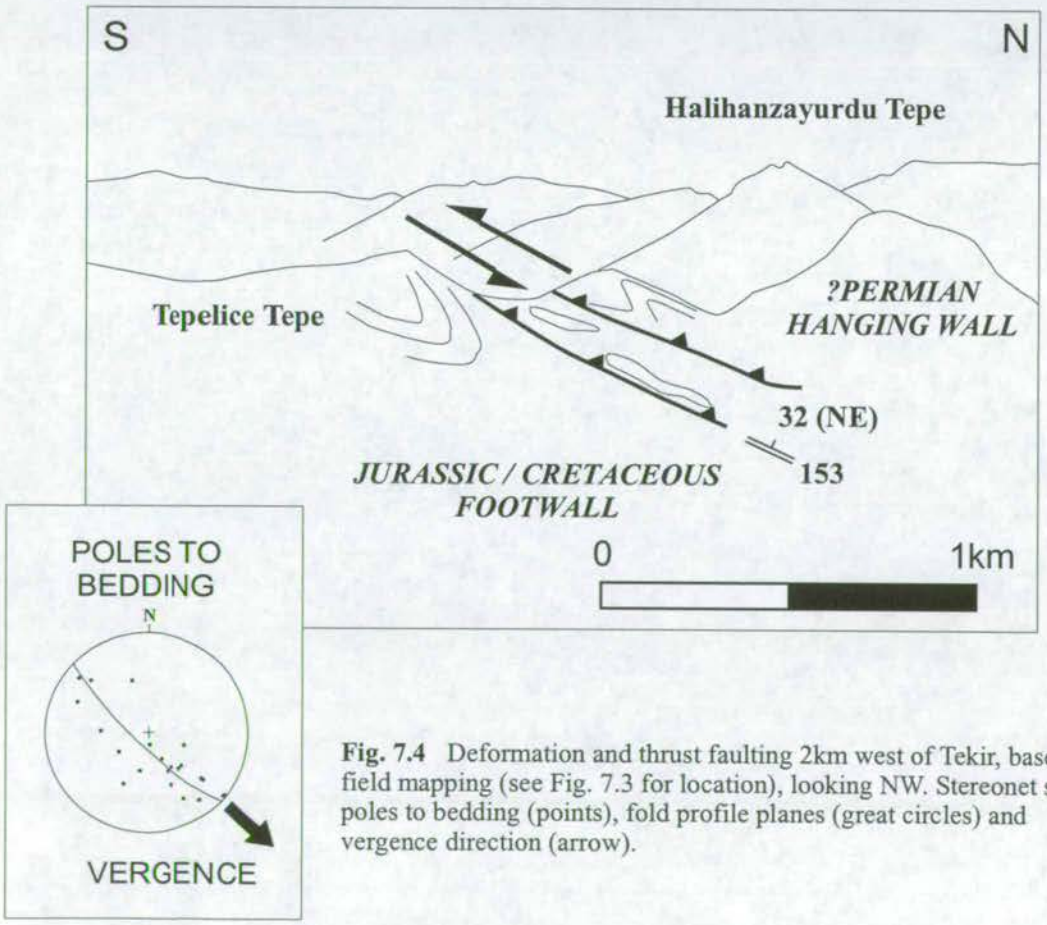

Fig. 7.4 Deformation and thrust faulting 2km west of Tekir, based on field mapping (see Fig. 7.3 for location), looking NW. Stereonet shows poles to bedding (points), fold profile planes (great circles) and vergence direction (arrow).

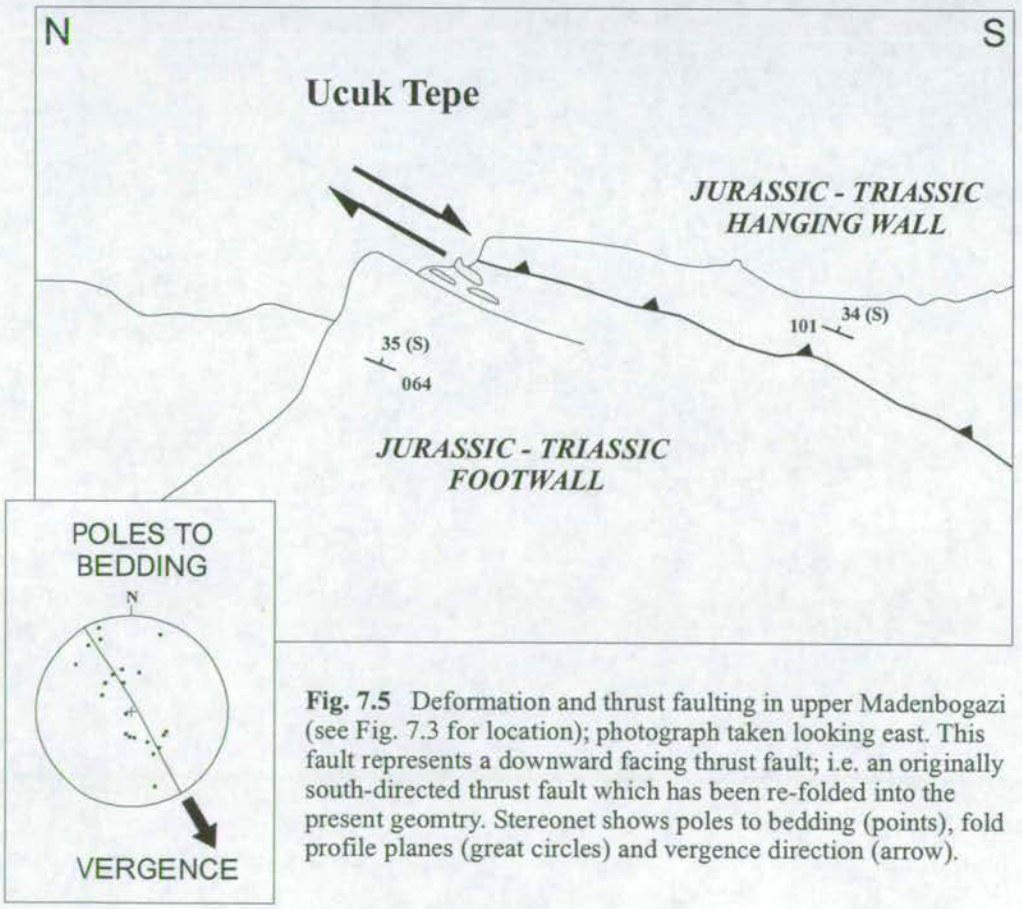

Fig. 7.5 Deformation and thrust faulting in upper Madenbogazi (see Fig. 7.3 for location); photograph taken looking east. This fault represents a downward facing thrust fault; i.e. an originally south-directed thrust fault which has been re-folded into the present geomtry. Stereonet shows poles to bedding (points), fold profile planes (great circles) and vergence direction (arrow).

strike NW-SE, and available vergence data (Fig. 7.6) indicate tectonic transport towards the SE and not towards the NW as Tekeli *et al.* (1984) originally indicated. The Madenboğazi structure is interpreted as a downward-facing (S-dipping, SE-directed) thrust fault. The downward facing geometry may be a result of folding during later compression.

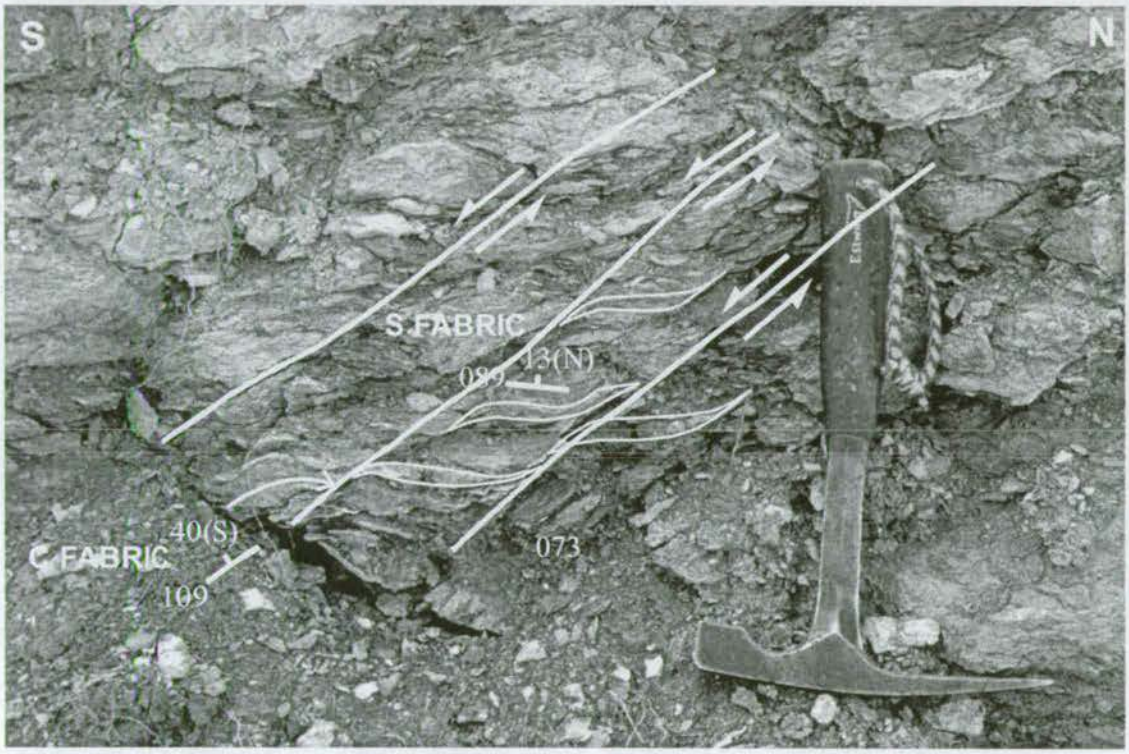

Figure 7.6 Shear structures (S-C fabrics) associated with thrust faulting at Madenbogazi (location Fig. 7.3) indicate tectonic transport towards the SE. The large scale structure is a downward-facing (S-dipping, SE-directed) thrust fault.

7.3.3.3 Deformation and vergence at Hamidiye

2km SE of the village of Hamidiye the contact between the base of the Pozanti-Karsanti Ophiolite and the Mesozoic carbonate units of the Aladağ outcrops (location Fig. 7.3). A zone of intense folding, thrust faulting and shearing was observed at this contact with pervasive S-C fabrics indicating top to the SE vergence (Fig. 7.7).

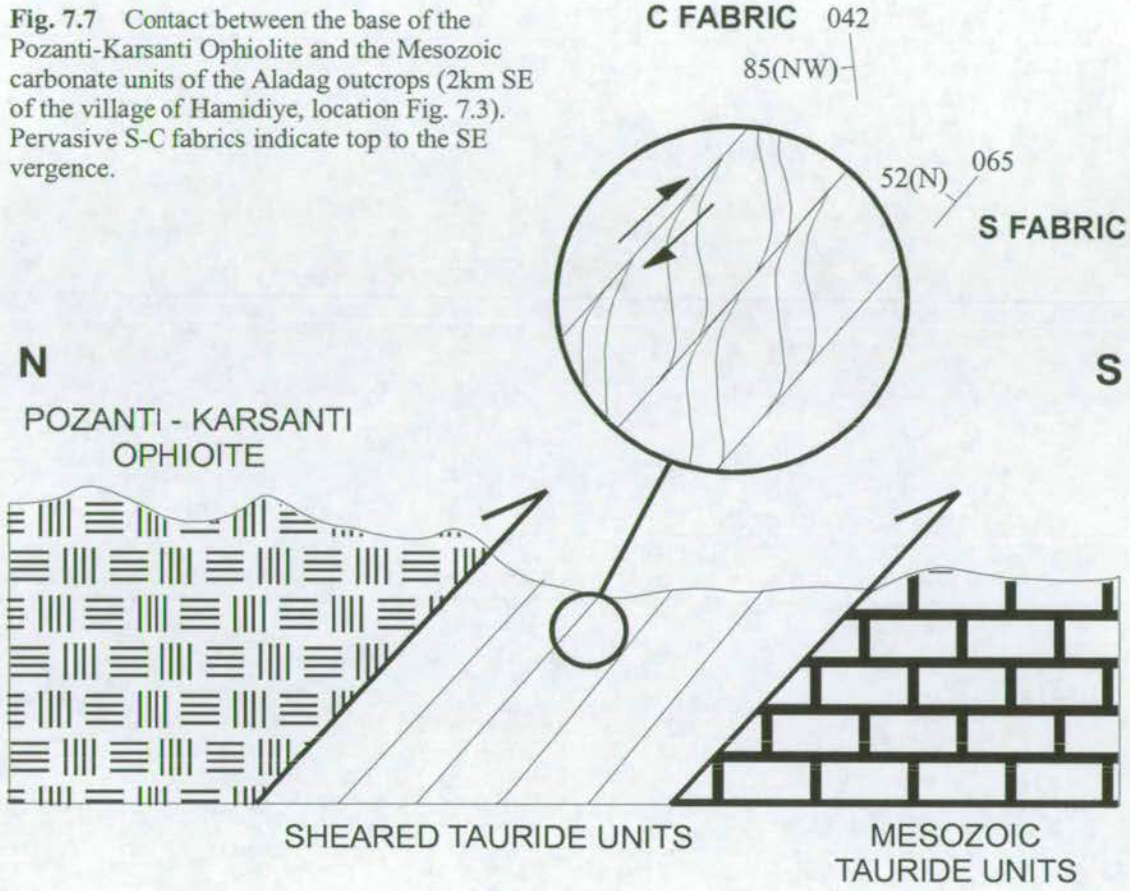

Fig. 7.7 Contact between the base of the Pozanti-Karsanti Ophiolite and the Mesozoic carbonate units of the Aladag outcrops (2km SE of the village of Hamidiye, location Fig. 7.3). Pervasive S-C fabrics indicate top to the SE vergence.

7.3.3.4 Evidence for the timing of deformation

Due to the close association between the SE-directed deformation zones and the base of the Pozanti-Karsanti Ophiolite, they are interpreted as being generated during ophiolite emplacement. Initial ridge detachment of the Pozanti-Karsanti Ophiolite is dated at 94Ma (Cenomanian) by Thuizat *et al.* (1981) using K-Ar dating of the metamorphic sole, and final obduction onto the Aladağ from N to S has been dated at approximately 65Ma (Cretaceous-Palaeocene boundary) by Lytwyn & Casey (1995), based on Palaeocene sediment cover relationships. Palaeocene turbiditic sediments directly overlying the Pozanti-Karsanti ophiolite at Akdağ (2km E of Pozanti) are undeformed

relative to the ophiolite and underlying Tauride units. Therefore the SE-directed deformation is interpreted as being generated during obduction (latest Cretaceous).

7.3.4 Late Eocene Deformation

NW-directed folding and thrust faulting was observed along the northern margin of both the Bolkardağ and Aladağ mountains (Fig. 7.8). This was found to be confined to a narrow (1-3km wide) fold and thrust belt and to mark the most northern extent of the Bolkardağ and Aladağ.

7.3.4.1 North Bolkardağ deformation and vergence

Along the northern margin of the Bolkardağ a train of mountain-scale, NW-vergent recumbent folds was observed above a south-dipping thrust fault. Bedding plane orientations and vergence were measured within the Mesozoic units of the Bolkardağ at three localities: at Karagol (west), Deliktas valley (centre) and Maden (east). Data were plotted as poles to bedding planes on equal area stereonets and profile planes to these folds were calculated (Fig. 7.8). Plots show that fold profile planes (plotted as great circles) uniformly strike NW-SE and that fold limbs become progressively more isoclinal (the fold tightens) toward the east. Fold vergence at each of these outcrops indicate tectonic transport toward the NW (Fig. 7.9)

7.3.4.2 Uçukkaya-Sulucaova deformation and vergence

To the east of the Ecemiş Fault Zone several structural lineaments were mapped by Tekeli *et al.* (1984). The most northerly of these is a N-directed thrust fault at Uçukkaya Tepe which joins the EFZ just south of Sulucaova village. Bedding data were gathered from two localities in the Aladağ Mountains close to this inferred thrust: at Uçukkaya

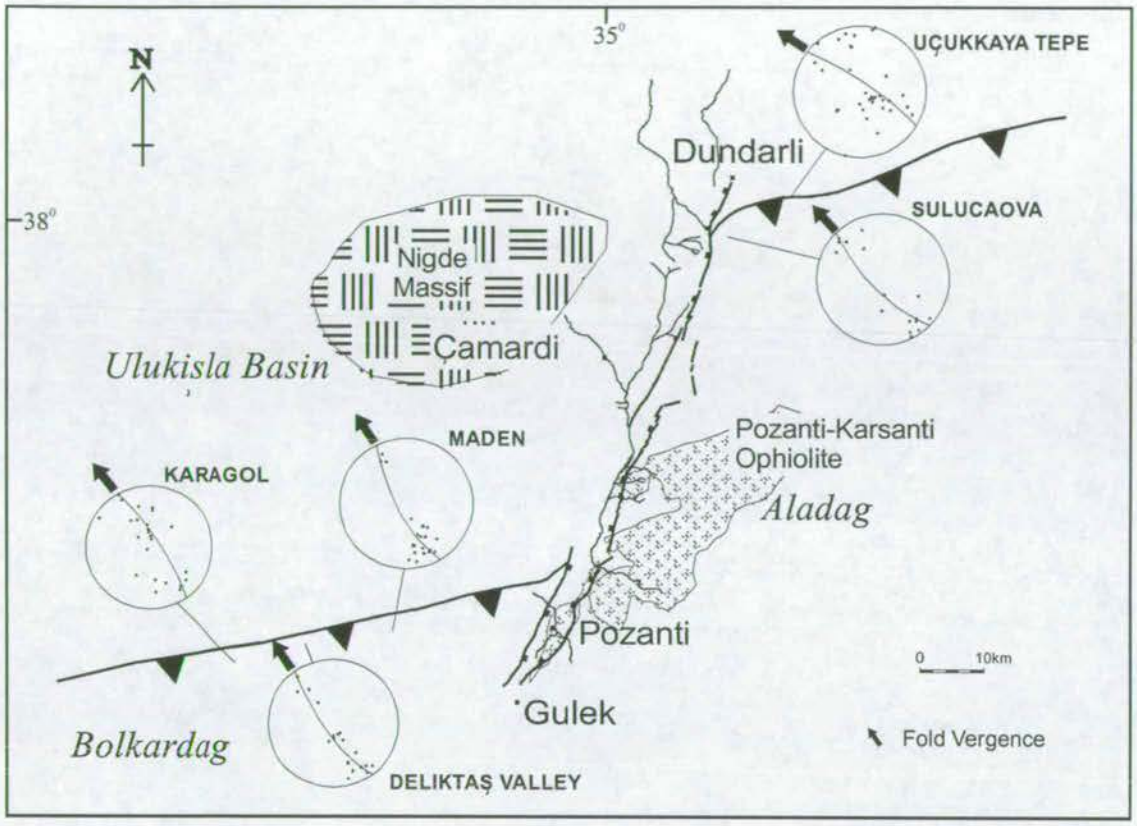

Fig. 7.8 Late Eocene fold and thrust belt along the northern margin of the Bolkardag and Aladag. Stereoplots show poles to bedding planes (dots), fold profile planes (great circles) and fold vergence (solid arrow). Thrust faults are shown by triangles on the overriding plate. Faults of the current EFZ (thick black lines) and rivers (thin lines) are shown for location purposes only.

Tepe and Sulucaova (location Fig. 7.8). Stereographic projections of poles to bedding planes show that fold profile planes strike NW-SE (Fig. 7.10); fold vergences indicate tectonic transport towards the NW (Fig. 7.10).

7.3.4.3 Evidence for timing of deformation

The cessation of NW-directed folding and thrusting is well constrained at Maden (N margin of the Bolkardağ), where undeformed Oligocene conglomerates drape

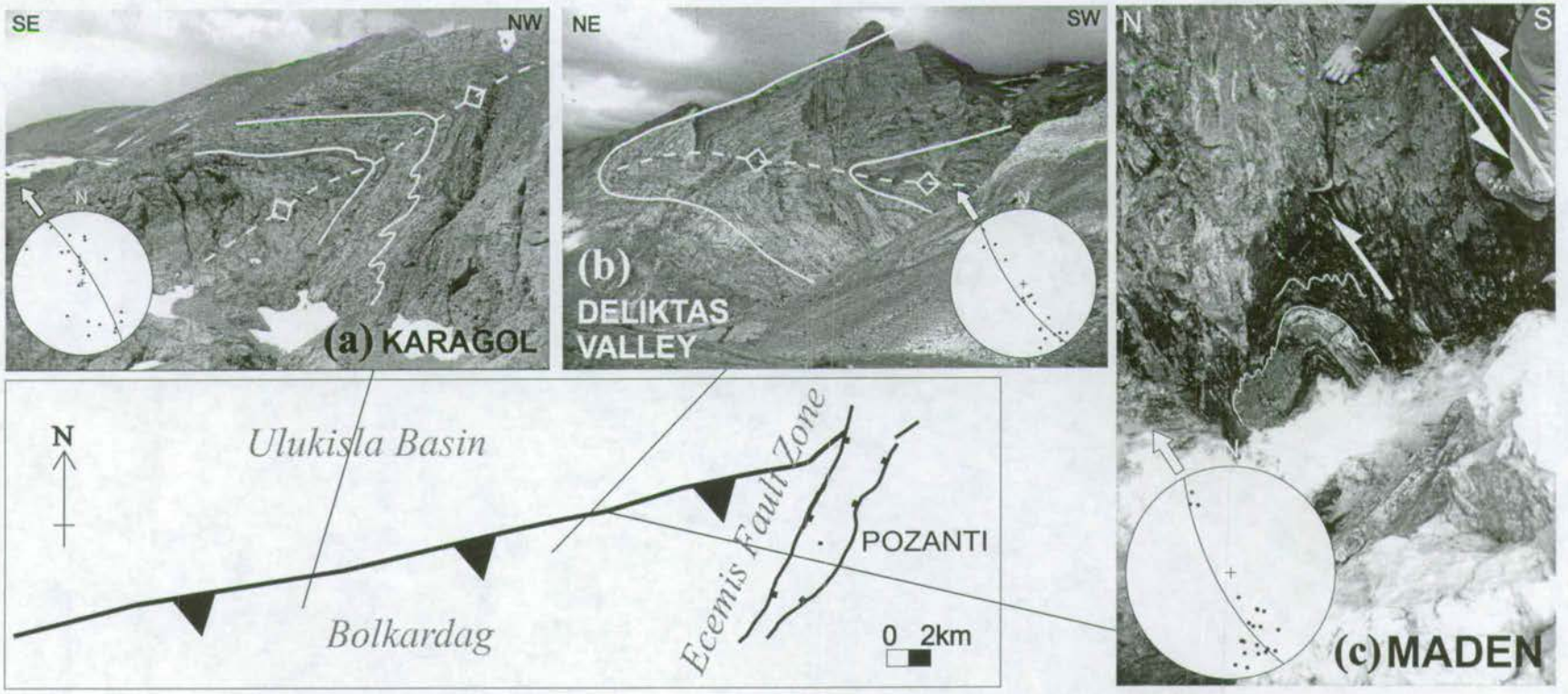

Fig. 7.9 Photographs of the Bolkar (north-directed) fold and thrust system. **(a)** North-vergent recumbent folding at Karagol, **(b)** North-vergent recumbent folding at Deliktas Valley (1km SW of Maden village), **(c)** North-vergent thrust fault contact at Maden village with associated ductile deformation. Stereonets show poles to bedding (points), fold profile planes (great circles) and vergence direction (arrow).

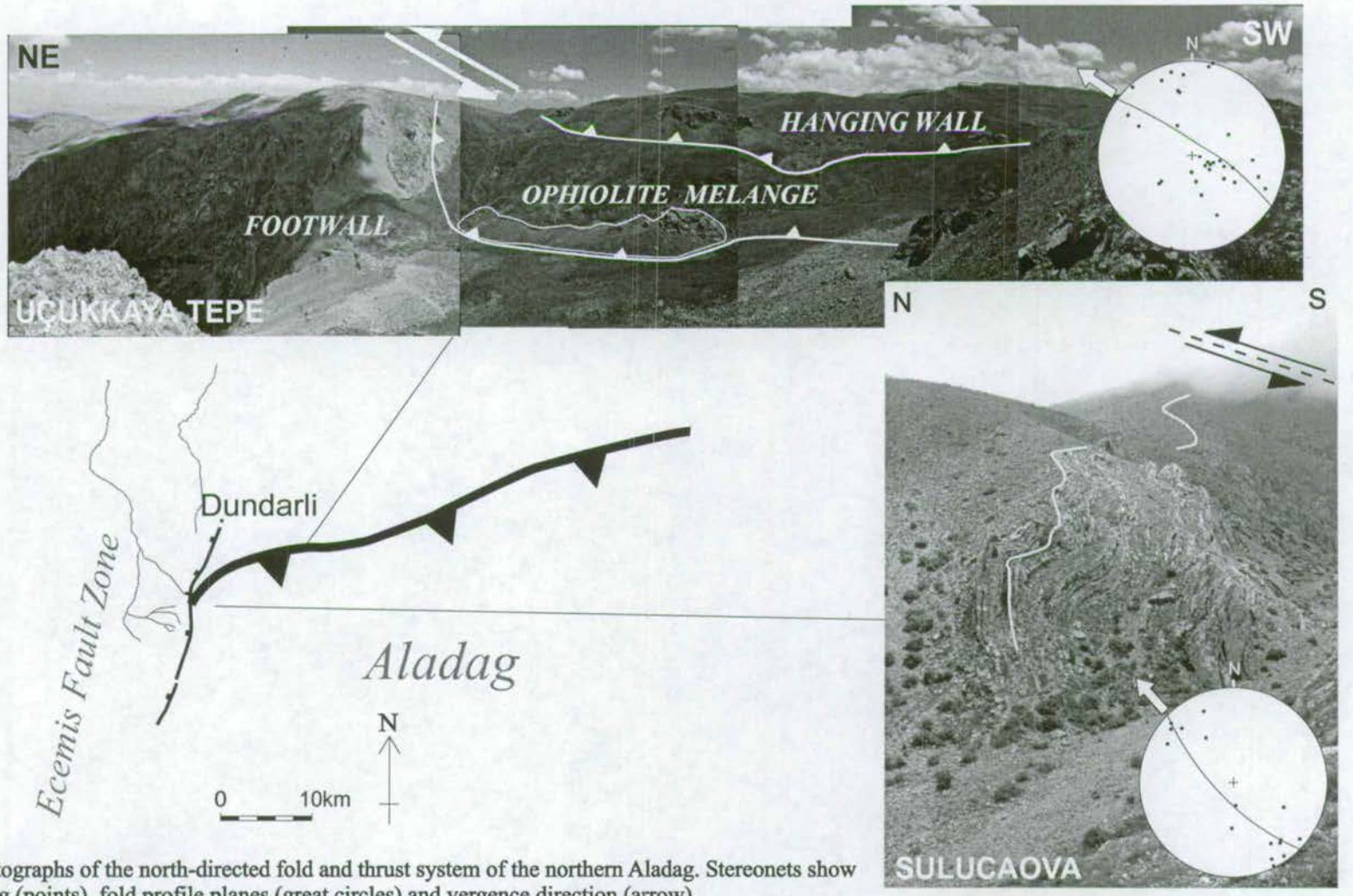

Fig. 7.10 Photographs of the north-directed fold and thrust system of the northern Aladag. Stereonets show poles to bedding (points), fold profile planes (great circles) and vergence direction (arrow).

unconformably over both the NW-directed thrust fault and overlying folded Mesozoic carbonate units (Fig. 7.11). This draping unit is the Oligocene Delimahmutlu Formation of Demirtaşli *et al.* (1984).

Deformation in the Ulukişla Basin to the north also helps to constrain the timing of NW-directed deformation along the northern margin of the Bolkardağ. Structural data collected by Matthew Clark (pers. com. 2000, Fig. 7.12) suggests that Palaeocene to Late Eocene units within the Ulukişla Basin are tightly deformed relative to the overlying Oligocene-Miocene Aktoprak Basin sediments. This suggests that the majority of N-S compression within the Ulukişla basin occurred during the latest Eocene and before Oligocene time.

There are no similar constraints on the timing of deformation along the northern margin of the Aladağ. However, due to the presence of similar hangingwall units, similar thrust fault geometries, similar fold profile planes and similar vergence in the northern Aladağ and Bolkardağ margins it is inferred that the two deformation zones were generated synchronously and possibly adjacent to one another.

7.3.5 Middle Miocene Deformation

Within the EFZ the preserved Cenozoic sediments have undergone varying degrees of deformation. Structural mapping shows that the Oligo-Miocene Çukurbağ Formation is highly deformed relative to the overlying (relatively undeformed) Late Miocene Burç Formation. Stereographic projections of poles to bedding planes for folds within the Oligo-Miocene redbeds (Fig. 7.13) reveal that in the north and centre of the EFZ fold profile planes strike NW-SE. This changes to a NE-SW strike in the south of the EFZ, perhaps due to the proximity of the Namrun Segment bend in the orientation of the EFZ (Koçyiğit & Beyhan 1998, Fig. 7.2b). These folds do not show any preferential vergence.

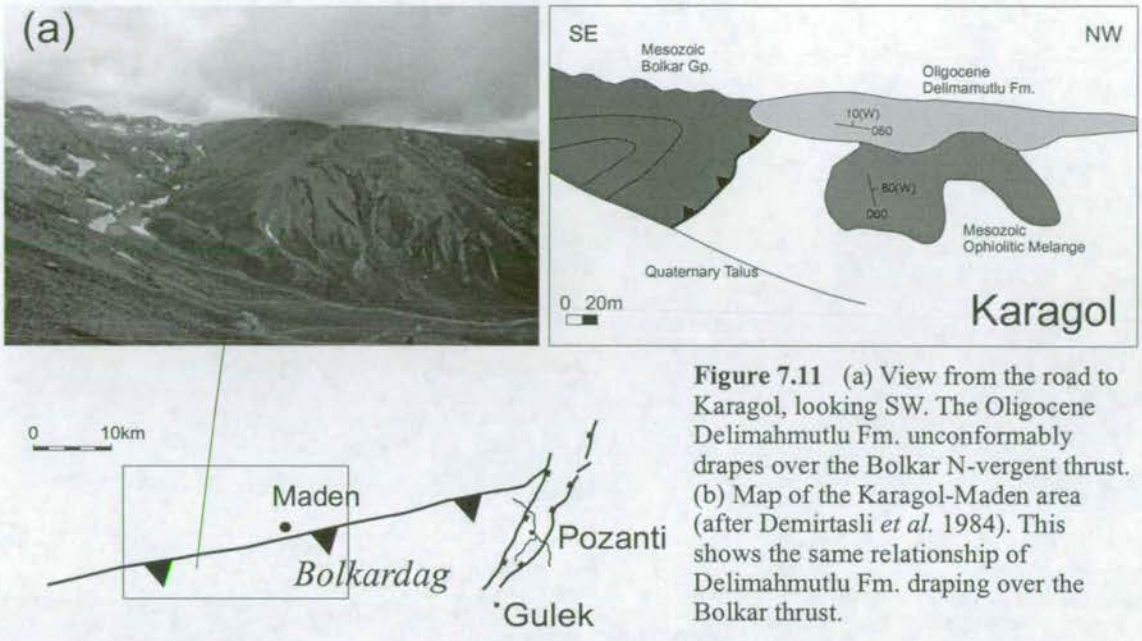

Figure 7.11 (a) View from the road to Karagol, looking SW. The Oligocene Delimahmutlu Fm. unconformably drapes over the Bolkar N-vergent thrust. (b) Map of the Karagol-Maden area (after Demirtasli *et al.* 1984). This shows the same relationship of Delimahmutlu Fm. draping over the Bolkar thrust.

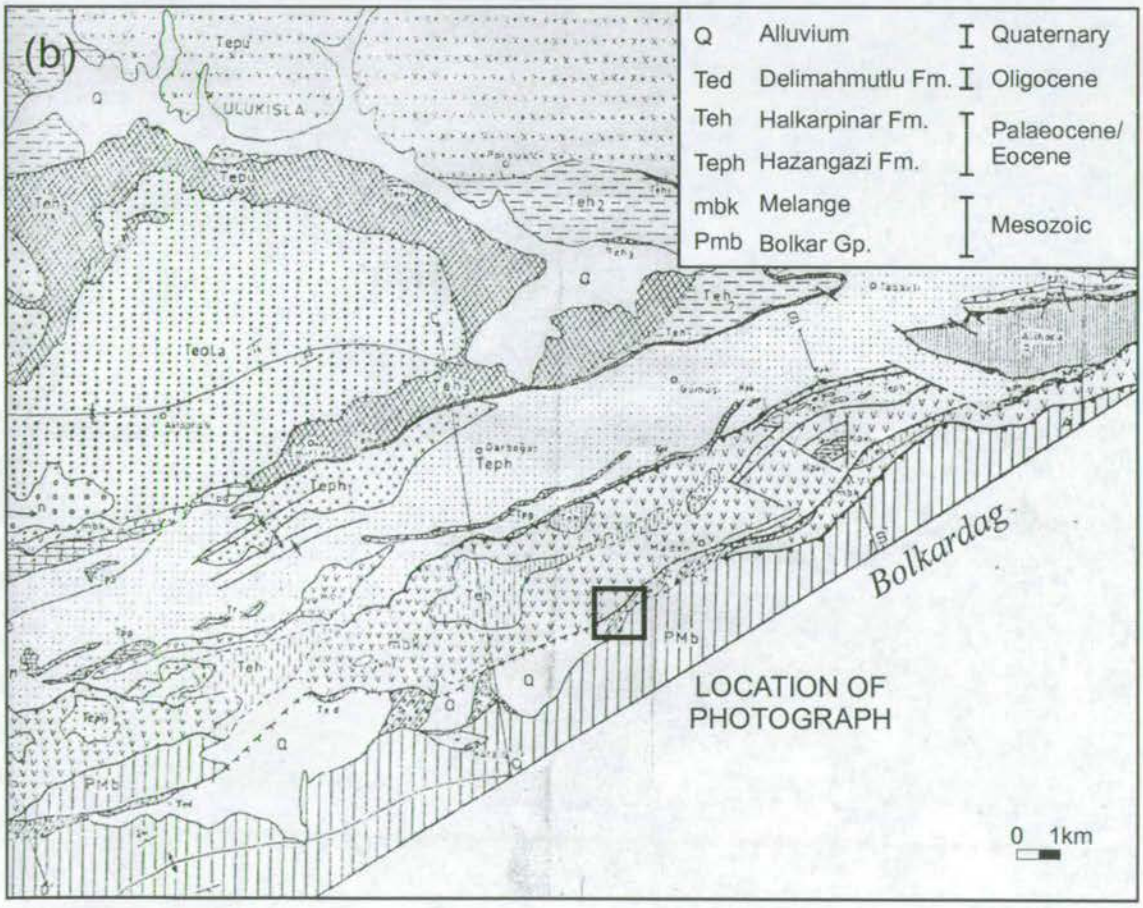

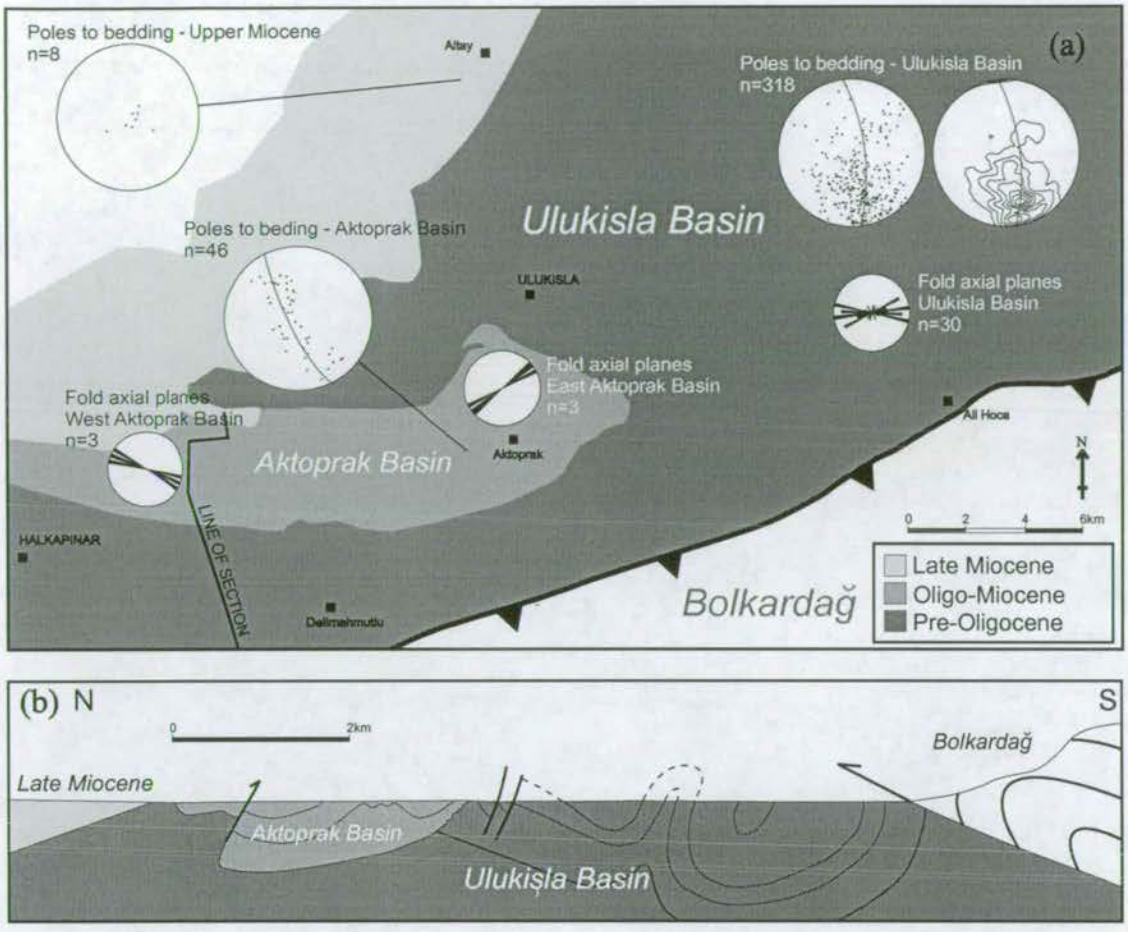

Fig. 7.12 **(a)** Deformation in the Ulukisla Basin (including data from Clark 2000) Aktoprak Basin (Oligo-Miocene) and Late Miocene units are separated from Early Cenozoic units. Stereonets shows poles to bedding (points) and fold profile planes (great circles). Rose diagrams show orientation of fold axial planes. **(b)** Cross section from north to south across the Aktoprak Basin and Bolkar frontal thrust system.

Additionally, it was observed that deformation within the Çukurbağ Formation increases in intensity toward the main fault scarps of the EFZ. This is seen especially clearly at Narpuz, east of Çamardi (Fig. 7.14) where Oligo-Miocene sediments close to the bounding fault scarps are tightly folded, with folds verging away from the fault scarp. This phenomenon is closely associated with localised west-vergent recumbent folding within the Mesozoic Aladağ units at Madenboğazi (Fig. 7.14). This folding only

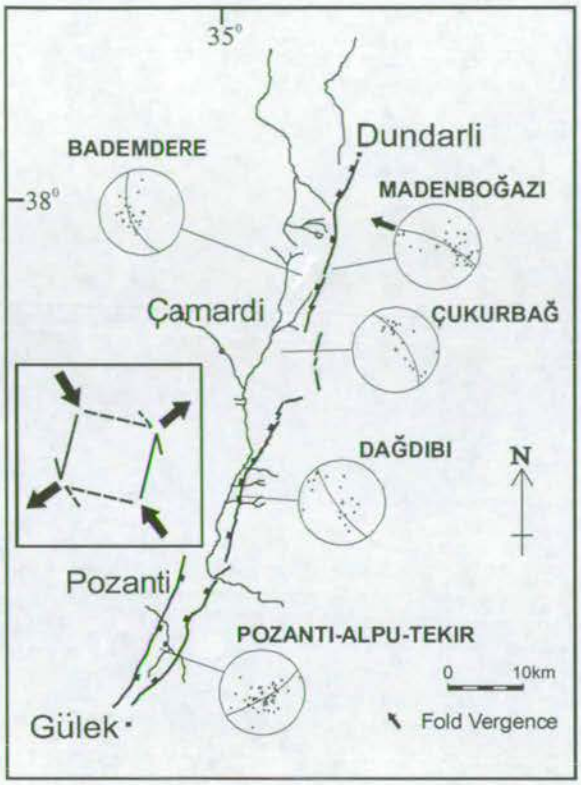

Fig. 7.13 Middle Miocene age folding within the Oligo-Miocene sediments of the EFZ. Stereoplots show poles to bedding planes (dots), fold profile planes (great circles) and fold vergence (solid arrow). Faults of the current EFZ (thick black lines) and rivers (thin lines) are shown for location purposes only. Inset indicates proposed orientations (in plan view) of maximum compressive stress (inward facing arrows) and minimum compressive stress (outward facing arrows) during sinistral strike-slip (slip vector represented by solid half arrows). See text for discussion.

affects an area under 1km from the main fault scarp. The association between similar, localised folding in the Aladağ and adjacent Çukurbağ Formation (Fig. 7.14), and the lack of such fold association in the Burç Formation suggests that localised compression occurred along the EFZ during the Middle Miocene, causing local intense folding in adjacent Mesozoic and Oligo-Miocene units. This may possibly be associated with the location of a strike-slip restraining bend (Fig. 7.15).

7.3.5.1 Evidence for the cause and timing of deformation

Comparison of deformation within the Oligo-Miocene of the EFZ (Fig. 7.13, 7.14) and the Ulukişla Basin (Fig. 7.12) indicates that deformation is much more intense in the EFZ, but that regional compression was affecting the entire region.

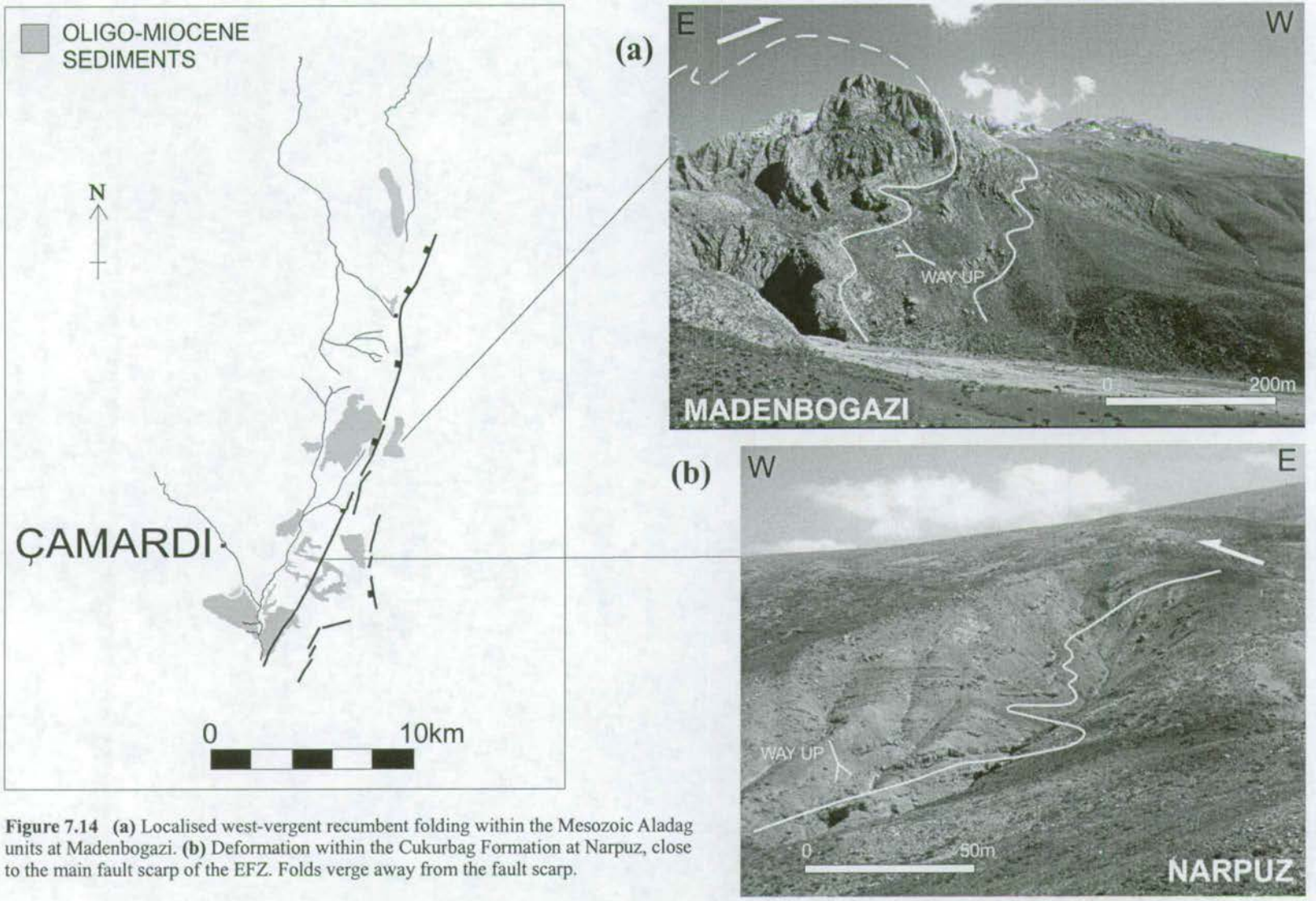

Figure 7.14 **(a)** Localised west-vergent recumbent folding within the Mesozoic Aladag units at Madenbogazi. **(b)** Deformation within the Cukurbag Formation at Narpuz, close to the main fault scarp of the EFZ. Folds verge away from the fault scarp.

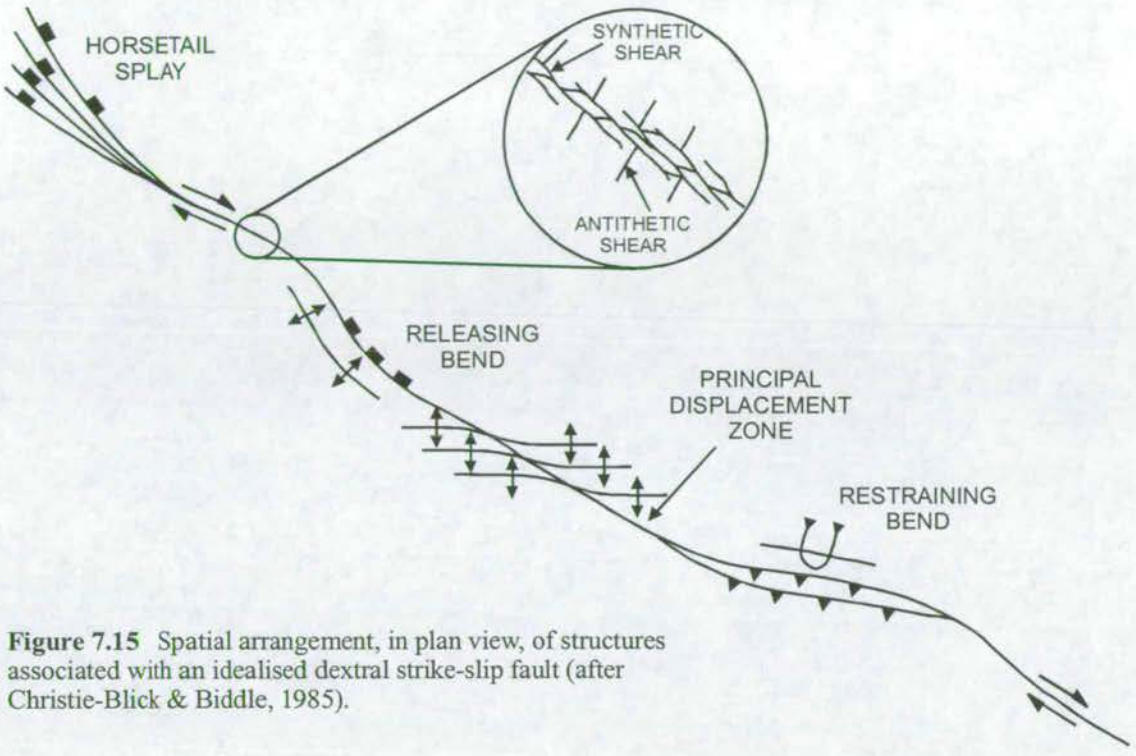

Figure 7.15 Spatial arrangement, in plan view, of structures associated with an idealised dextral strike-slip fault (after Christie-Blick & Biddle, 1985).

Folding within the Oligo-Miocene redbeds of the EFZ has previously been interpreted as the result of E-W compression due to the reactivation of the Ecemiş Fault Zone as a west-directed thrust fault (Koçyiğit & Beyhan 1999). However, NW-SE striking fold profile planes (observed in the Oligo-Miocene redbeds in this study) are not compatible with pure E-W compression, neither is there any evidence for W-directed thrust faulting along the Ecemiş Fault Zone. Instead, it is proposed here that sinistral strike slip faulting on the EFZ during the Middle Miocene may have resulted in NW-SE striking fold profile planes (Fig. 7.13 inset), with a NW-SE oriented σ^1 produced during pure left lateral strike-slip, as shown in a strain ellipse (Fig. 7.16). It is probable that the deformation pattern found within the Çukurbağ Formation of the EFZ is a result of the combination of localised sinistral strike-slip and regional compression, which has affected all of the surrounding Cenozoic basins.

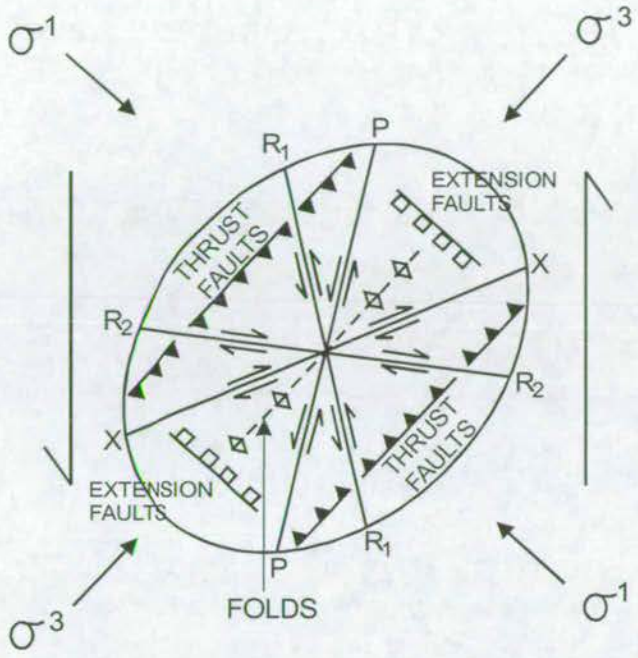

Figure 7.16 Regional strain ellipse associated with a strike-slip fault system (after McClay 1987). The Reidel shear faults are the synthetic R_1 and antithetic R_2 systems (in most cases displacements are minor on these faults). In some systems synthetic P and antithetic X shears may also develop. Folds and contraction (thrust) faults are developed at 90^0 to Sigma 1, whereas extension (normal) faults are developed 90^0 to Sigma 3.

A Middle Miocene age is inferred for this deformation phase as it is seen to affect the Late Oligocene – Early Miocene Çukurbağ Formation (Fig. 7.13) but not the relatively undeformed overlying Late Miocene Burç Formation. The angular unconformity between the two Formations is documented in Fig. 4.24.

7.3.6 Cross Sections

Two cross sections have been constructed across the strike of the Ecemiş Fault Zone. These were taken in the Çamardi area in the north of the EFZ (Figure 7.16b) and in the Tekir/Pozanti area in the south (7.16c). The northern section runs from Evliya Tepe in the NW to Emler Tepe in the SE and contains small dog-legs in the Çukurbağ Village area. The southern section runs from 1km N of Akça in the NW to north of Akdağ in the south, and contains a 5km dog-leg. Dog-legs were included in order to position the sections across locations of best exposure. The NE-SW oriented parts of the sections are

not shown. Fault trajectories are extrapolated up to 1500m below the surface, but there is no subsurface data to substantiate this. Both northern and southern sections illustrate local deformation in the footwall of the bounding faults (see section 7.3.5 above) and also the angular unconformity between the Çukurbağ Formation and Burç Formation.

When comparing these sections to those from idealised trans-tensional faults (Hardy *et al.* 1985, Figure 7.16d), the following similarities were found:

- EFZ fault geometries are compatible with the upper part of a negative flower structure.
- Faults present have mostly normal separation on successive profiles.
- The fault zone is flanked by en-echelon faults, with normal separation.

When comparing the EFZ sections with an idealised strike-slip fault zone (Christie-Blick & Biddle 1985, Figure 7.16e), the following similarities were found:

- The fault zone involved basement rocks (deeper Tauride carbonates) and contrasts basement types across the fault zone.
- Both normal and reverse separation faults are found in the same profile (these may be of different age in the EFZ case).

In general, the fault geometries and structural characteristics of the EFZ appear to be similar to those of idealised strike-slip fault zones.

7.4 Fault and Slickenline data

7.4.1 Methodology

The orientation of fault slip faces and of slickenlines on these faults was recorded in Eocene – Recent units of the Ecemiş Fault Zone with the aim of assessing whether different aged units display different fault populations, and if so, how these populations change through time. There was no rigid sampling strategy; data was gathered from all observed slip faces during the course of structural mapping, from metre scale to

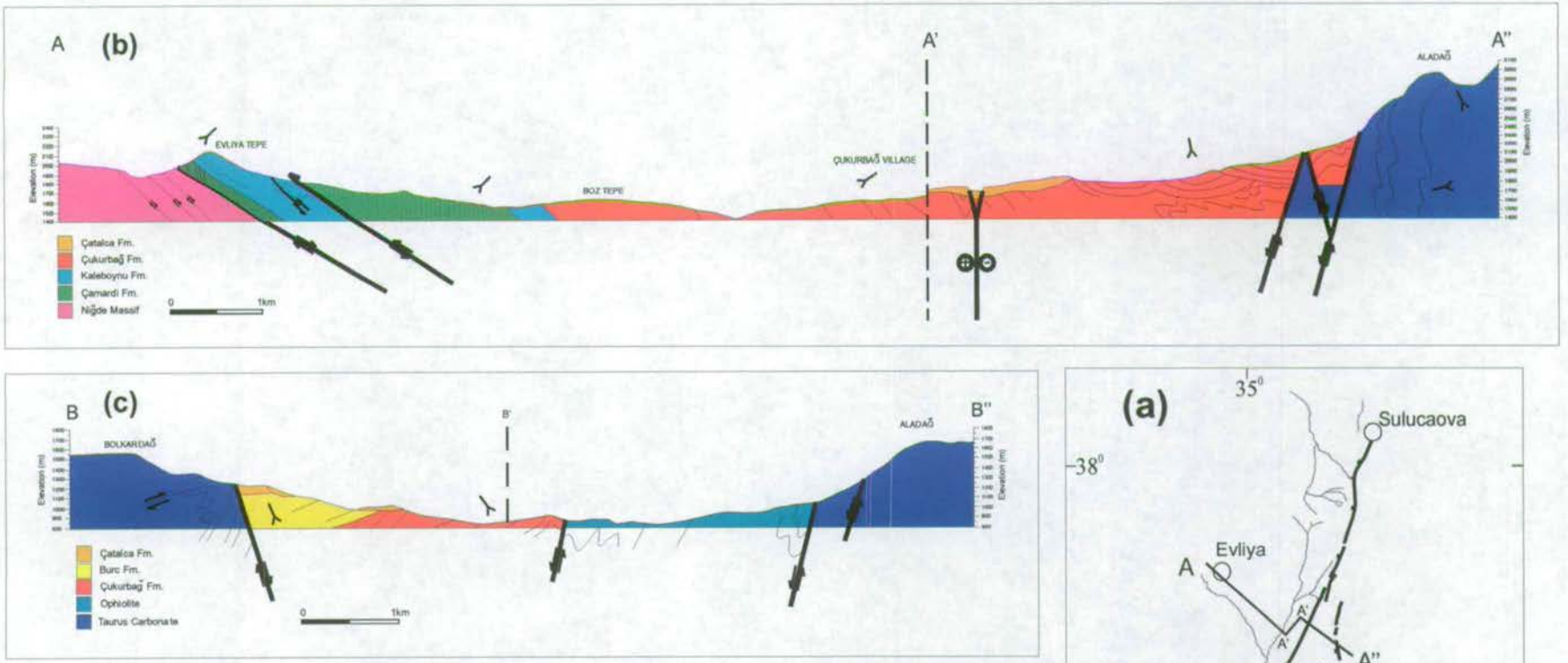

Fig. 7.16 Cross sections across the Ecemis fault Zone: **(a)** Location of cross sections and dog-legs **(b)** Northern cross section in the Camardi area A-A"**(c)** Southern cross section in the Pozanti area, B-B".

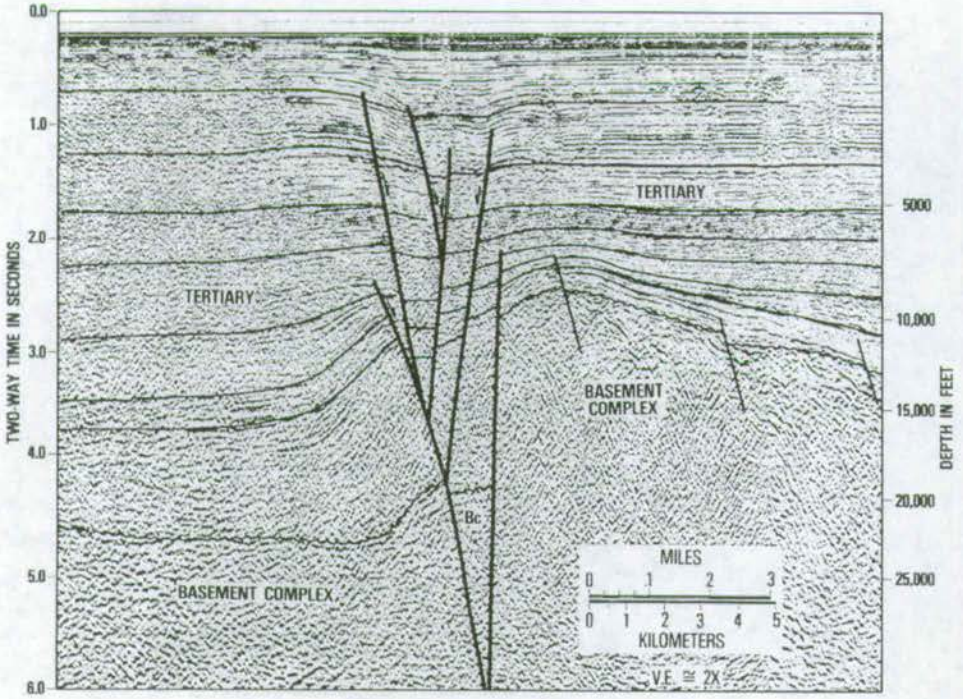

Figure 7.16d Seismic profile across a major divergent wrench fault zone in the Bering Sea (after Harding et al. 1985).

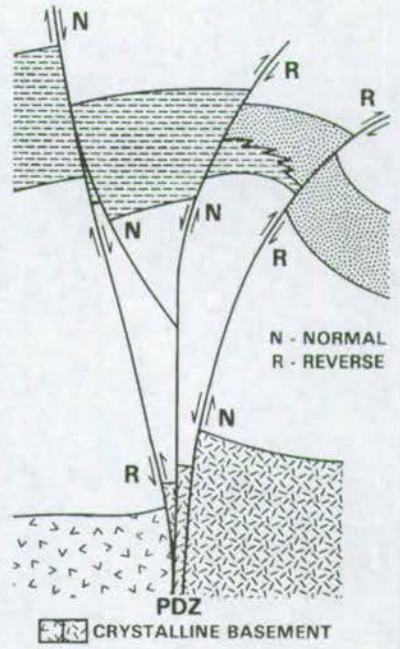

MAJOR CHARACTERISTICS

- BASEMENT - INVOLVED
- PDZ SUB-VERTICAL AT DEPTH
- UPWARD DIVERGING & REJOINING SPLAYS

JUXTAPOSED ROCKS

- CONTRASTING BASEMENT TYPE
- ABRUPT VARIATIONS IN THICKNESS & FACIES IN A SINGLE STRATIGRAPHIC UNIT

SEPARATION IN ONE PROFILE

- NORMAL- & REVERSE-SEPARATION FAULTS IN SAME PROFILE
- VARIABLE MAGNITUDE & SENSE OF SEPARATION FOR DIFFERENT HORIZONS OFFSET BY THE SAME FAULT

SUCCESSIVE PROFILES

- INCONSISTENT DIP DIRECTION ON A SINGLE FAULT
- VARIABLE MAGNITUDE & SENSE OF SEPARATION FOR A GIVEN HORIZON ON A SINGLE FAULT
- VARIABLE PROPORTIONS OF NORMAL- & REVERSE-SEPARATION FAULTS

TIME-STRATIGRAPHIC UNIT WITH VARIABLE SEDIMENTARY FACIES

Figure 7.16e The major characteristics, in transverse profile, of an idealised strike-slip fault. After Christie-Blick & Biddle, 1985.

centimetre scale. It was later realised that separating and removing smaller scale faults would have been beneficial, thereby removing a part of the 'noise' element. This was not possible in retrospect, however, as the scale of slip faces was not measured during data collection.

Fault orientations were potted on stereographic projections as (i) contoured poles to fault planes and (ii) as rose diagrams indicating fault strike. Data were separated primarily by rock unit (i.e. by age) in order to identify temporal changes in fault populations. Older units are likely to display more complex fault populations than younger ones due to overprinting by subsequent fault phases; therefore, results are presented in reverse chronological order. It should be born in mind that fault populations in Late Miocene rocks are likely to display Latest Miocene and Plio-Quaternary fault signatures, and that fault populations in Eocene rocks can display an even more complex overprint. Hence data clarity is reduced with increasing age.

Data was separated secondarily by sense of slip and also by locality in order to identify spatial and sense-of-slip trends through time.

7.4.2 Results & Interpretation

7.4.2.1 Faulting within the Plio-Quaternary Çatalca Formation

Faulting within this unit was only observed in Plio-Quaterary exposures east of Çamardi. Fig. 7.17 presents data from the Narpuz Gorge area, where contoured poles to fault planes and fault strike rose diagrams indicate the exclusive presence of N-S striking normal faults. Offset is difficult to measure in the conglomeratic Plio-Quaternary alluvial fan material but slickenlines were used where present.

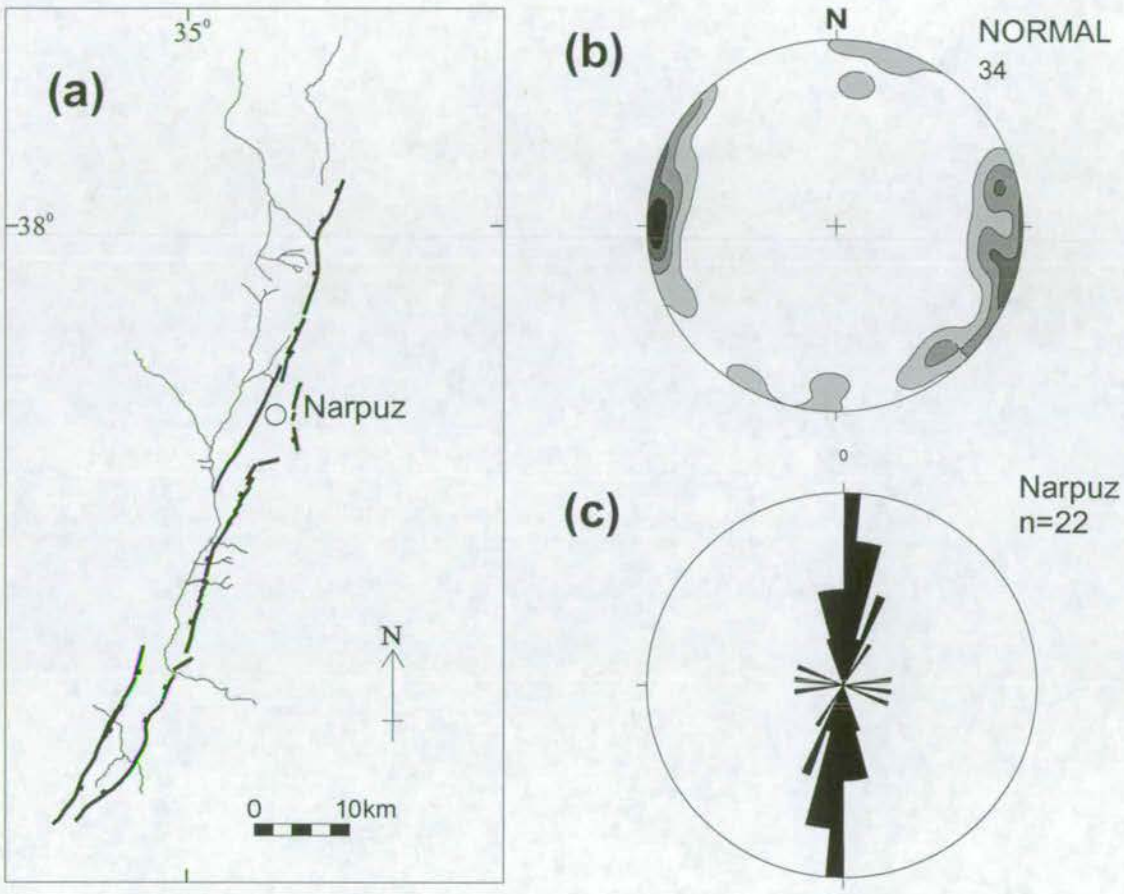

Fig. 7.17 Graphic display of faults within the Plio-Quaternary rocks of the Narpuz area (east of Camardi). **(a)** Location of data collection site **(b)** Stereonet showing poles to fault planes (contoured), **(c)** Rose diagram showing strike of faults. All recorded faults have a normal slip sense.

Interpretation:

From the limited data available it appears that Plio-Quaternary alluvial fans at Çamardi have been exclusively affected by E-W extension. From this, and the fact that all Plio-Quaternary material in the EFZ area is closely associated with normal fault scarps, it is inferred that the Plio-Quaternary period was dominated by E-W extension.

7.4.2.2 Faulting within the Late Miocene Burç Formation

Data were collected from five areas along the EFZ (Fig. 7.18). Rose diagrams reveal that faults within this unit have a dominant NE-SW strike in the north (Çadirkaya, Hacibeyli and Burç) and NW-SE in the south of the EFZ (Kamişli and Camalan).

Contoured poles to fault planes reveal that overall, NE-SW striking normal and (to a lesser extent) NE-SW striking sinistral faults are dominant in Burç Formation rocks. NW-SE striking dextral faults are also significant. Reverse faults are less significant and do not show a preferred orientation.

Further examination of slip sense data reveals that sinistral slip is dominant in the north of the EFZ (Çadirkaya, Hacibeyli and Burç); dextral and normal slip are dominant in the central area (Kamişli), and normal slip dominates in the south (Çamalan, Fig. 7.18).

Interpretation:
The Late Miocene Burç Formation is the youngest unit to contain a significant population of strike-slip faults. NE-SW striking normal and sinistral faults in the north of the EFZ suggest that this area was subject to sinistral transtension from Late Miocene to ?Earliest Pliocene period. During the same period the Kamişli area (Fig. 7.18) was affected by NW-SE striking dextral faulting. This is likely to be the result of dextral NW-SE striking Reidel shears (Fig. 7.16) associated with the dominant sinistral regime. It is unlikely that these are associated with the dextral Tuzgolu Fault (Fig. 2.4), as this fault does not intersect the EFZ at any point.

7.4.2.3 Faulting within the Oligo-Miocene Çukurbağ Formation

Data were collected from ten areas along the EFZ. Rose diagrams indicate that the north of the EFZ (Bademdere, Çukurbağ, Elekgolu and Yelatan) is dominated by NE-SW to

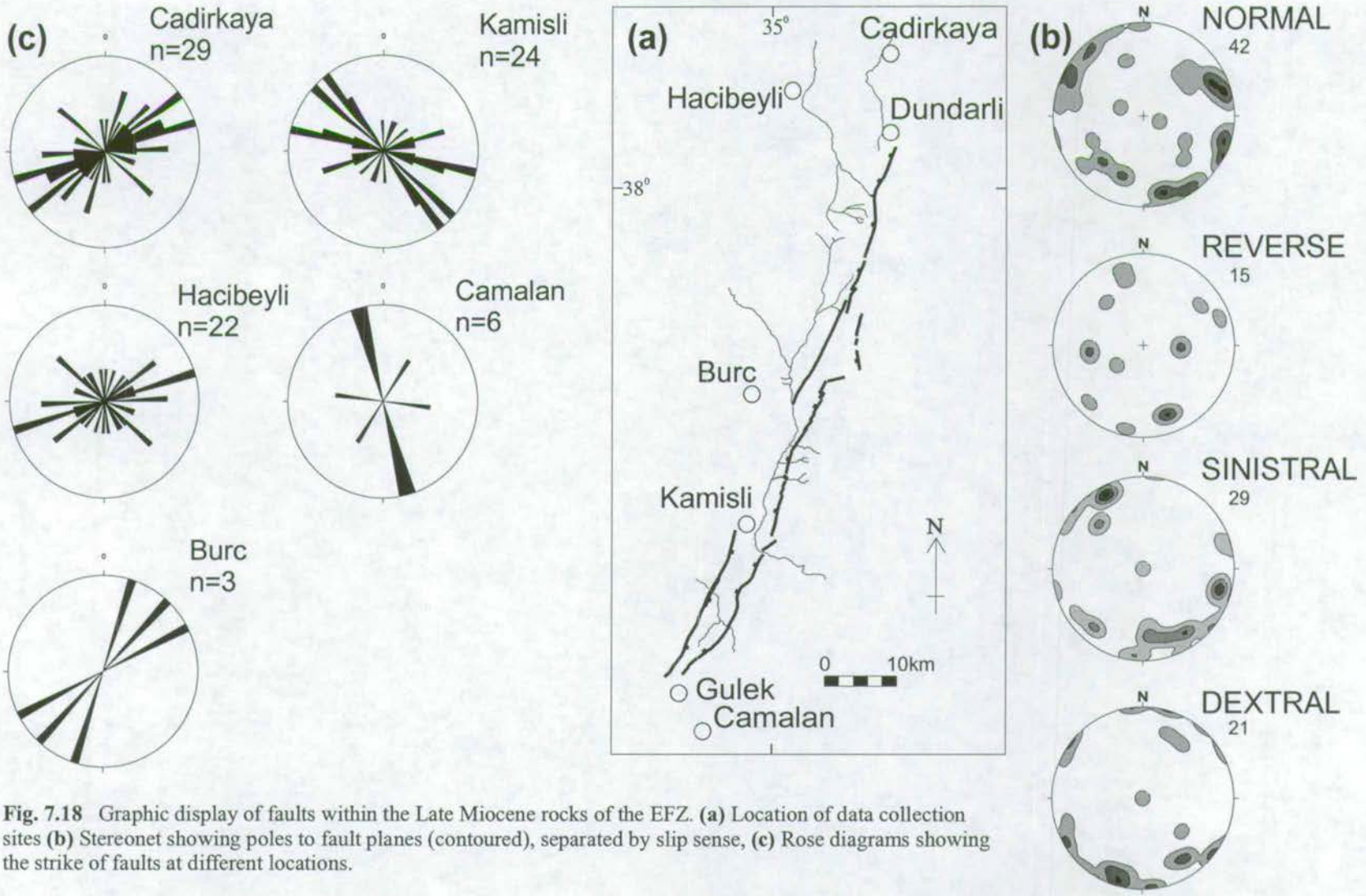

Fig. 7.18 Graphic display of faults within the Late Miocene rocks of the EFZ. **(a)** Location of data collection sites **(b)** Stereonet showing poles to fault planes (contoured), separated by slip sense, **(c)** Rose diagrams showing the strike of faults at different locations.

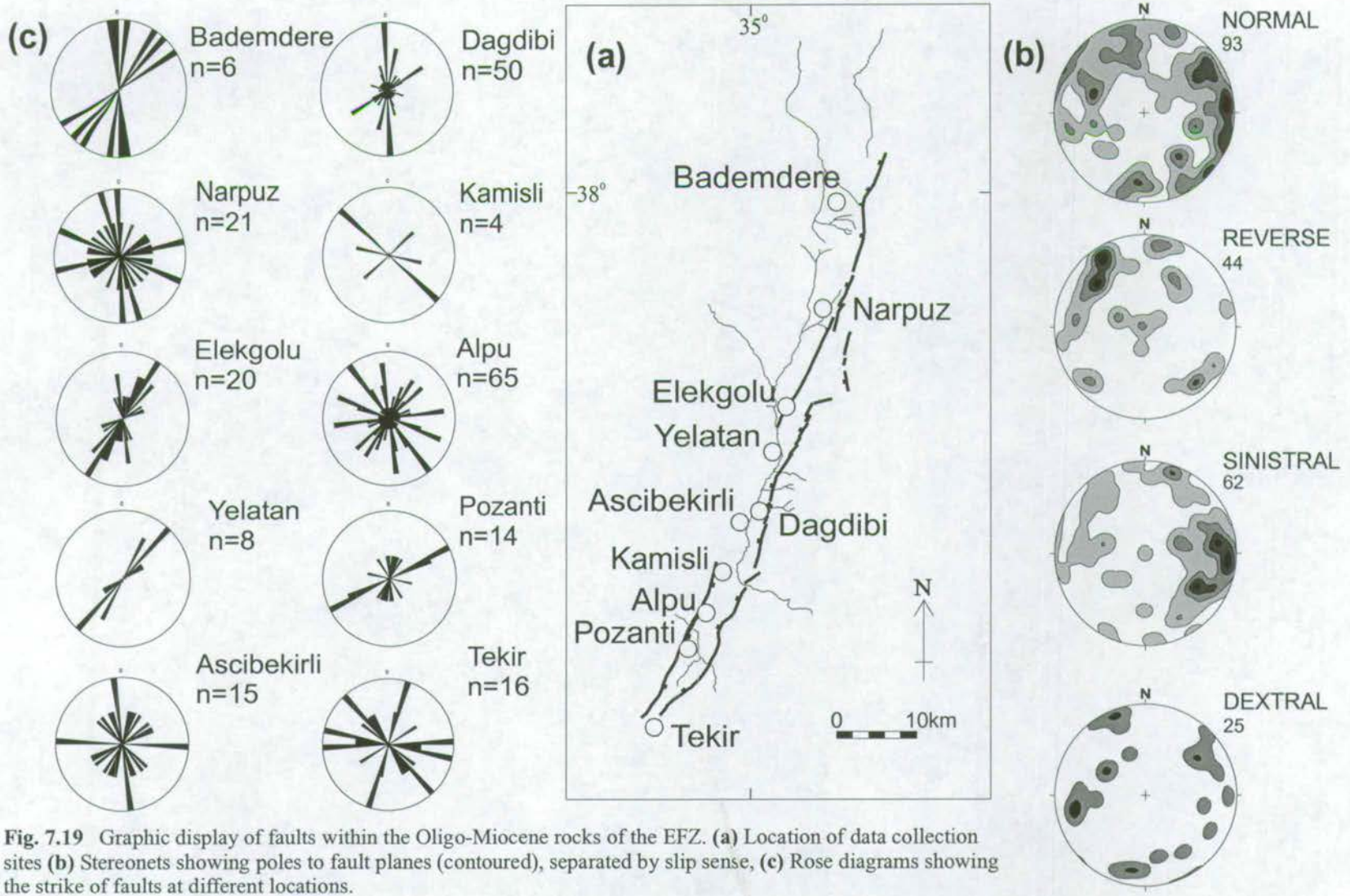

Fig. 7.19 Graphic display of faults within the Oligo-Miocene rocks of the EFZ. **(a)** Location of data collection sites **(b)** Stereonets showing poles to fault planes (contoured), separated by slip sense, **(c)** Rose diagrams showing the strike of faults at different locations.

N-S striking normal and sinistral faults (Fig. 7.19). The south of the EFZ (Dağdibi, Kamişli, Alpu, Pozanti, and Tekir) is dominated by normal faulting with various orientations, mostly either N-S or E-W striking.

Contoured poles to fault planes reveal (i) the overall continued dominance of NE-SW to N-S striking normal and sinistral faulting and (ii) a 'new' component of E-W striking normal faulting. Reverse slip faults are of local significance only but are well clustered, with NW-directed transport. Dextral slip faults are less common and are have a poor clustering.

At Elekgolu a well-grouped population of sinistral faults was observed within the Çukurbağ Formation. These faults directly underlie a 'small graben' structure in the overlying Plio-Quaternary Çatalca Formation, along which several modern rivers are offset sinistrally (section 8.3.3).

Interpretation:

It is not possible from the above data to tell whether the dominance of NE-SW striking normal and sinistral faults is due to (i) sinistral transtension during the Late Miocene which has overprinted these older rocks or (ii) continued sinistral transtension during the Oligo-Miocene. Continued sinistral transtension during the Late Oligocene – Early Miocene cannot be discounted.

Reverse faults are concentrated at Yelatan (central EFZ) where the fault zone (as a graben) is at its narrowest, 1-2km wide. The presence of reverse faults nearby at Hamidiye and Alpu has also been documented by Koçyiğit & Beyhan (1998), suggesting that these may be the sites of strike-slip restraining bends.

Normal faulting with a N-S and E-W strike is dominant in the fault population. It is suggested that this was a period of extensive normal faulting throughout the region

(agreeing with Oligo-Miocene exhumation of the Bolkardağ and Niğde Massif, Whitney & Dilek 1998, Dilek & Whitney in press).

The Elekgolu fault population (below the 'small graben') is interpreted as the result of Plio-Quaternary sinistral faulting which has affected the alluvial fan geomorphology and penetrated the underlying Çukurbağ Formation.

7.4.2.4 Faulting within the Middle Eocene Kaleboynu Formation

Eocene exposures are sparse, data could only be collected in five areas (Fig. 7.20). Rose diagrams reveal very variable fault strikes. NE-directed reverse faulting is dominant to the east of the EFZ (Sulucaova and Kaleboynu Tepe), whereas NW-directed reverse faulting is dominant to the west (Evliya Tepe).

Contoured poles to fault planes reveal that strike-slip faulting is of little significance within this unit and that normal and reverse faulting are of equal significance.

Interpretation:

Little meaningful interpretation can be made due to the high probability of overprinting during post-Eocene periods. The good clustering of NW-directed reverse faults at Evliya Tepe and NE-directed reverse faults at Sulucaova, and the fact that they differ from fault populations in younger units in the same area suggest that these may be 'real' Eocene fault populations. These faults suggest Late Eocene compression, which is compatible with evidence for Late Eocene thrusting along the northern margins of the Bolkardağ and Aladağ (Fig. 7.8).

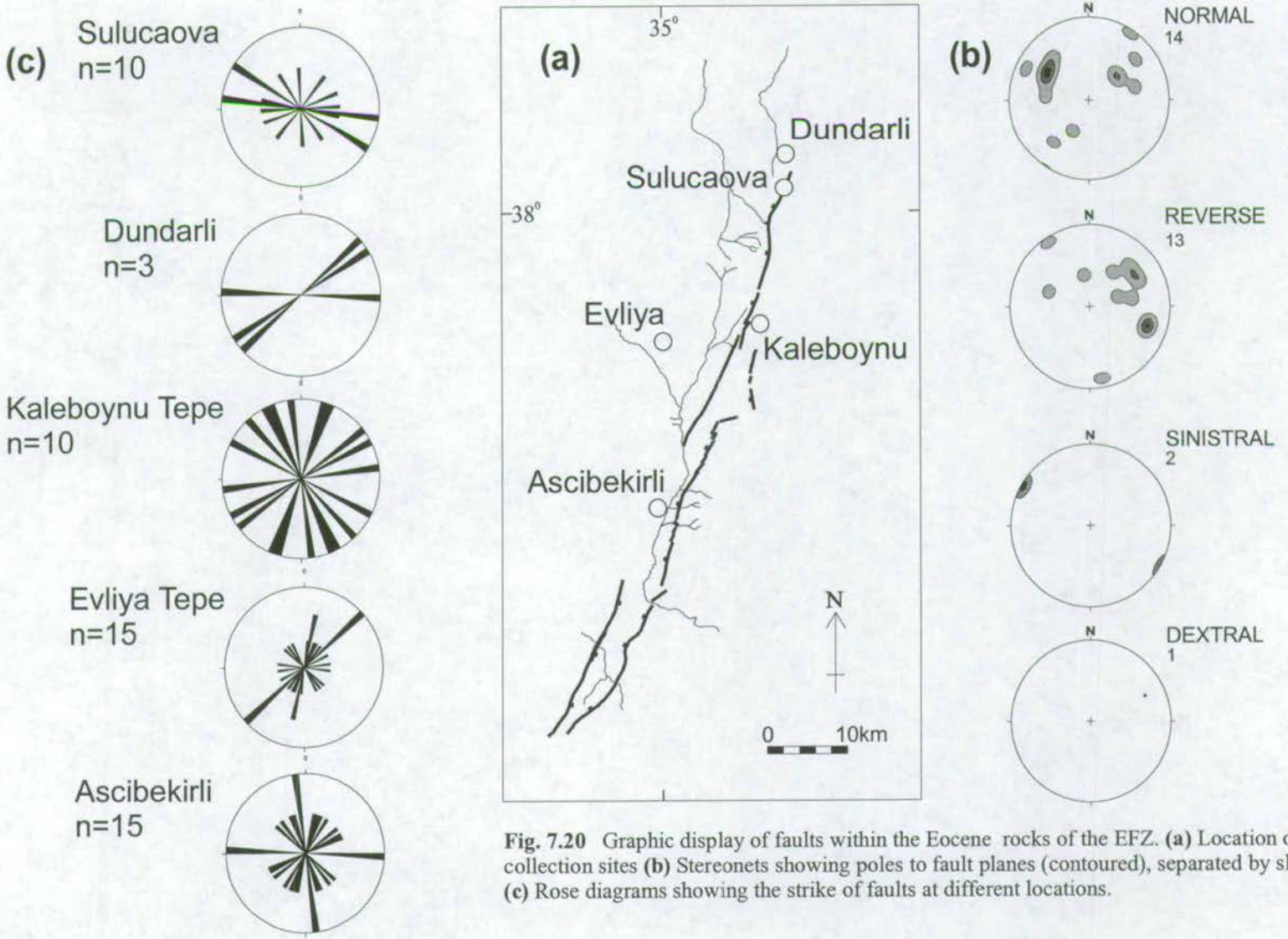

Fig. 7.20 Graphic display of faults within the Eocene rocks of the EFZ. **(a)** Location of data collection sites **(b)** Stereonets showing poles to fault planes (contoured), separated by slip sense, **(c)** Rose diagrams showing the strike of faults at different locations.

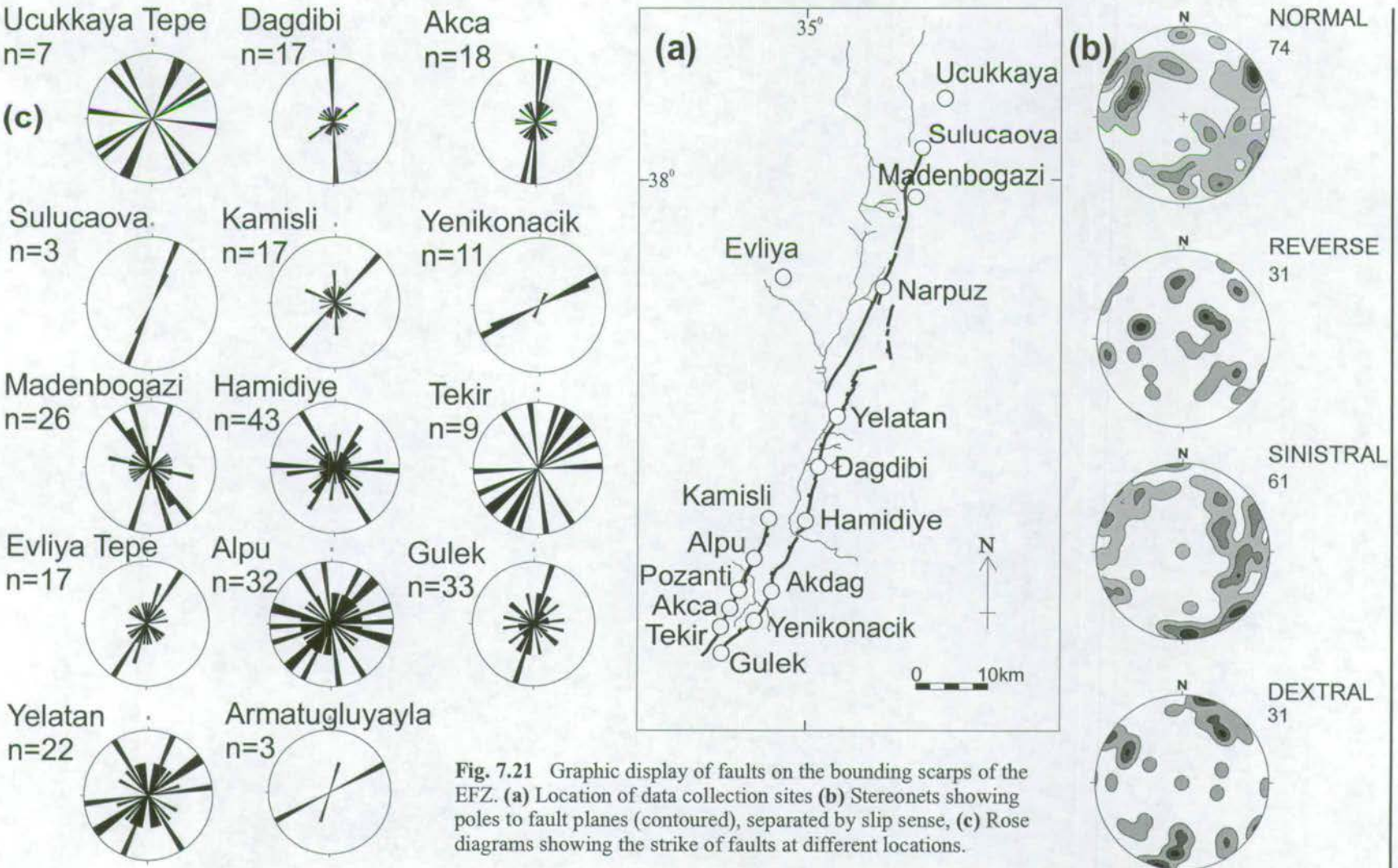

Fig. 7.21 Graphic display of faults on the bounding scarps of the EFZ. **(a)** Location of data collection sites **(b)** Stereonets showing poles to fault planes (contoured), separated by slip sense, **(c)** Rose diagrams showing the strike of faults at different locations.

7.4.2.5 Faulting on the Main Fault Scarps

The best preserved slip faces and slickenlines are exposed along the main scarps bounding the Ecemiş graben and half graben. Mesozoic carbonates are frequently exposed as high (up to 2000m) fault scarps, forming the fault footwalls. Fault orientation and slickenline data were collected from fourteen areas on both sides of the graben (Fig. 7.21).

Contoured poles to fault planes reveal the overall dominance of NNE-SSW striking normal and sinistral faults, and the lower abundance of reverse and dextral faults, which do not show preferred orientations. Rose diagrams by area reveal that in almost all data collection sites, NE-SW striking normal and sinistral faulting is dominant.

Interpretation:
As deduced from sedimentary facies evidence (section 4.4.2.4), it is believed that the present main fault scarps did not appear as topographic entities until Plio-Quaternary time. The dominance of normal and sinistral slip on these scarps indicates that they accommodated mainly extension, with a significant component of sinistral strike-slip. Locally dextral Reidel shears (Fig. 7.16) and restraining bends (Fig. 7.15) in the strike-slip system may account for the presence of small scale dextral and reverse slip.

7.5 Palaeostress

7.5.1 Introduction (after Payne 1996)

Various methods have been devised to determine the stress tensor for observed populations of faults, led by Carey & Brunier (1974). Angelier (1984) provided a review of the development of stress tensor determinations. This thesis uses a program based on the 'right dihedra' method of Angelier & Mechler (1977), although others such

as the 'movement plane' method of Alexandrowski (1985) exist. These methods calculate the principal stress directions involved in faulting. In order to determine the complete stress tensor, which not only describes the magnitudes of the principal stresses (σ^1, σ^2 and σ^3) but six shear stresses, lithostatic pressure in the rocks during faulting must be known. Such information is beyond the scope of this thesis. Instead, the method used calculates the 'reduced' stress tensor, i.e. the three normal stresses, excluding the six remaining shear stresses.

7.5.2 The P-T Dihedra technique, Angelier 1984 (after Payne 1996)

Also known as the 'right dihedra' method, this technique is based on the determination of compressional and extensional dihedra ('diedres droits') on a stereographic projection.

For each fault, the lower hemisphere of the stereographic projection (equal area net) is divided into four equal dihedra by the fault plane and a second plane orthogonal to the slip vector (i.e. the plane on which the pole to the fault and the perpendicular to the slickenside lie, Fig. 7.22a).

Two of these dihedra are compressional (P) dihedra and contain the maximum compressional stress (σ^1) direction for the fault. The other two dihedra are extensional (T) and contain the minimum compressional stress (σ^3) axis. The sense of movement on the slickenside determines which dihedra are which.

When the process is repeated for each fault in the population (Fig. 7.22b), the stereographic projection shows an area enclosed by all the compressional dihedra and an area of entirely extensional dihedra. These areas respectively enclose σ^1 and σ^3 (Fig. 7.22c).

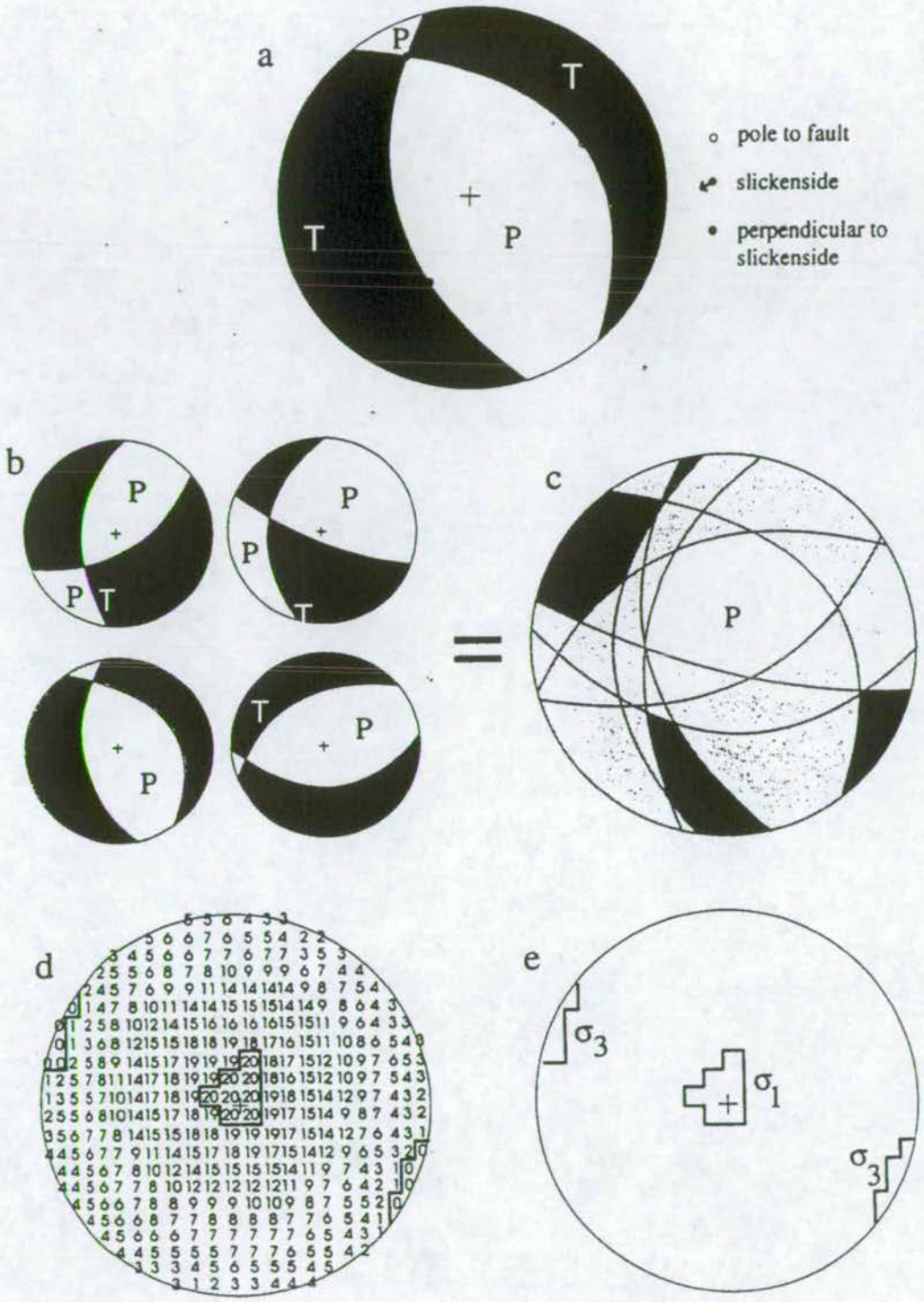

Fig. 7.22 Explanation of the P-T Dihedra method of kinematic analysis (after Angelier &v Mechler 1977). See text for discussion.

For ease of analysis with large numbers of data, the stereographic projection is divided into domains and the frequency of compressional dihedra in each domain is determined (Fig. 7.22d). If there is a restricted area which contains all of the compressional dihedra then the faults are the product of the same stress tensor and the area of 100% compressional dihedra constrains the orientation of σ^1 (Fig. 7.22e).

The disadvantages of this technique are that in most cases it does not give a unique solution for the principal stress orientations, and that sense of movement data are required for all of the slikensides used in the analysis. However, its advantages are that it is computationally very simple and quick to perform.

Assumptions of the method:

A basic assumption is that the fault population under study is the result of a single tectonic event governed by a single stress regime. All faults move independently in response to the same mean stress tensor and that the faults slip in the direction of the slikenside on the fault plane. In a region such as the Ecemiş Fault Zone where more than one tectonic event is responsible for the fault population observed, the faults must be divided into sets caused by single events before they are analysed for principal stresses. The authors of the method recommend that this is done based on field observations (Angelier 1984). For the data sets analysed here different tectonic events can be distinguished by the different ages of the rocks affected and by location.

The relatively small number of fault slip data available for the analysis reduces the reliability of the solutions. However, data sets were chosen that were well grouped; hence, the relatively small sample size does not preclude them from being accurately representative of the local population as a whole.

The principal stress determination method used here does not take into account the magnitude of slip of the faults, and hence does not include any weighting factor for large faults relative to minor ones. The data sets used for kinematic analysis in this study are composed of minor faults (exposed length under 1m long); however, the actual length of each fault may be much larger (if only partially exposed). The absence of a weighting consideration may, therefore, slightly affect the reliability of the result.

Angelier-type palaeostress determination techniques have been criticised by Roberts (1996) who pointed out that slickenlines of several different orientations are produced during the genesis of one simple normal fault, thus any technique reliant on the input of slickenline data should account for this.

7.5.3 Methodology

A version of the P-T Dihedra technique, the INVERS program of Sperner *et al.* (1993) was used (with the assistance of Tobore Orife, Cardiff University) to calculate palaeostress orientations for specific sites where high quality or well grouped slickenline populations have been measured. The aim being to constrain the orientations of σ^1, σ^2 and σ^3 in specific 'problem' areas and to provide a validation of the interpretations made in section 7.4.2 (above). This program was chosen as it quick and simple to use.

The INVERS program requires the input of fault orientation (dip and dip direction), the lineations of slickenlines on these faults (dip and plunge) and the sense of slip on these slickenlines. The output is a 'best fit' σ^1, σ^2 and σ^3 for the fault population used.

7.5.4 Results & Interpretation

7.5.4.1 Plio-Quaternary Çatalca Formation

Analysis of the fault population from Narpuz (Çamardi alluvial fan, Fig. 4.29) resulted in a vertical σ^1 (lineation 276/87), a NE-SW σ^2 (lineation 052/2) and a NW-SE σ^3 (lineation 142/2) (Fig. 7.23a). This confirms the interpretation of a dominantly extensional regime, with maximum extension towards the NW and SE.

Also on the Çamardi alluvial fan, the fault set at Elekgolu was analysed. This fault set outcrops within the Oligo-Miocene Çukurbağ Formation but directly underlies faulted Plio-Quaternary fan material (hence faulting is inferred to be of Plio-Quaternary age). Analysis resulted in a vertical σ^2 (lineation 284/79), an E-W σ^3 (lineation 107/11) and a N-S σ^1 (lineation 016/1) (Fig. 7.23b). A vertical σ^2 indicates strike-slip dominance and an E-W σ^3 is compatible with sinistral strike-slip, as determined in section 7.3.2.3 above.

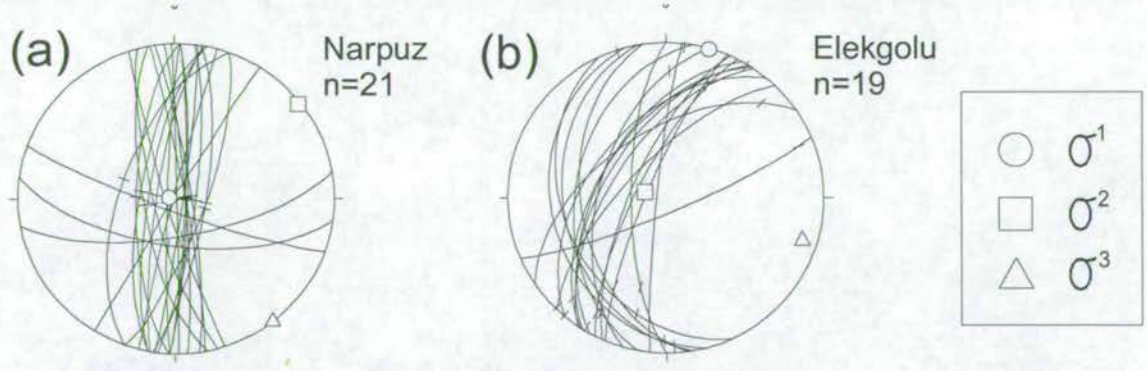

Fig. 7.23 Reduced palaeostress tensors derived from slickenlines in Plio-Quaternary rocks of the EFZ, using the INVERS program of Sperner *et al.* 1993. For locations of sites, see Fig. 7.17. Stereonets show: fault trace orientations (great circles), slickenline orientations (ticks on great circles) and lineations to sigma 1-3 (open symbols).

7.5.4.2 Late Miocene Burç Formation

Late Miocene fault populations are less well clustered than those of the Plio-Quaternary Çatalca Formation. However, a recurring trend in palaeostress results is that of a vertical σ^1. This is seen at Hacibeyli, Kamişli and Daripinari (σ^1 lineations 347/71, 317/84 and 001/90 respectively, Fig. 7.24a-c). This indicates the dominance of extension in the Burç Formation fault populations (in agreement with section 7.4.2.2 above).

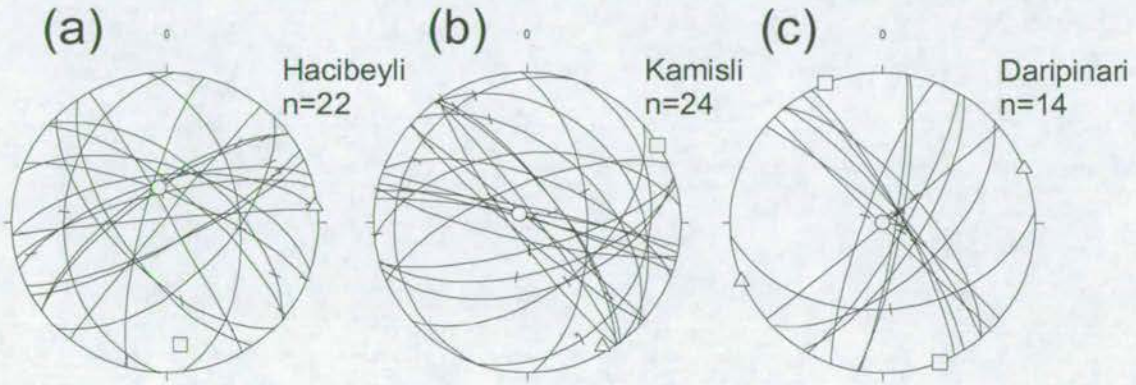

Fig. 7.24 Reduced palaeostress tensor derived from slickenlines in Late Miocene (Burc Fm.) rocks using the INVERS program of Sperner *et al.* 1993. For locations of sites, see Fig. 7.18. Stereonets shows: fault trace orientations (great circles), slickenline orientations (ticks on great circles) and lineations to sigma 1-3 (open symbols).

7.5.4.3 Base of ophiolite structures

A fault population at Hamidiye was analysed, from Mesozoic Tauride units directly below the melange unit at the base of the Pozanti-Karsanti ophiolite (Fig. 7.25). These structures are assumed to be emplacement-related (affecting Tauride units) rather than pre-obduction ocean ridge detachment structures. Results show that σ^3 is vertical (lineation 064/89), and that σ^1 has a N-S orientation (lineation 171/0). This is

compatible with the S-directed compressional structured seen in the field, and with the N to S emplacement model of Lytwyn & Casey (1995).

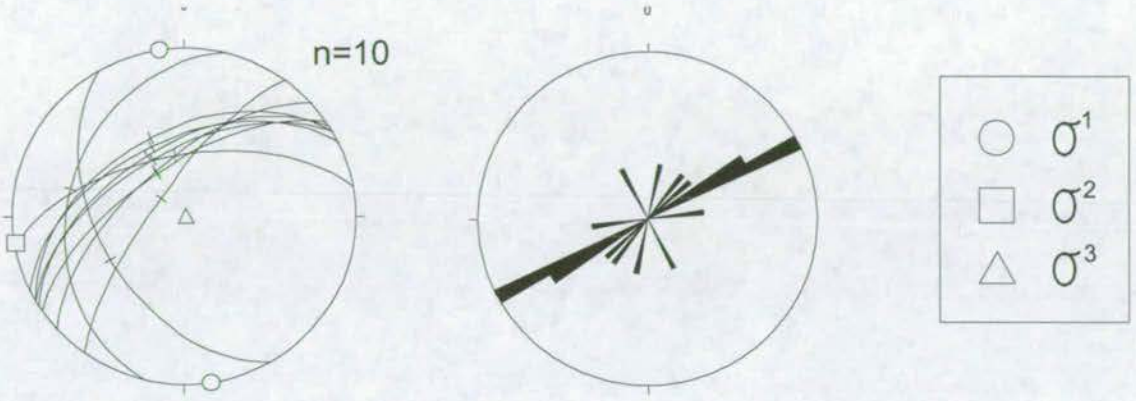

Fig. 7.25 Reduced palaeostress tensor derived from slickenlines in sheared rocks beneath the Pozanti-Karsanti ophiolite at Hamidiye, using the INVERS program of Sperner *et al.* 1993. For locations of site, see Fig. 7.3. Stereonet shows: fault trace orientations (great circles), slickenline orientations (ticks on great circles) and lineations to sigma 1-3 (open symbols). Rose diagram shows striek of fault planes.

7.5.4.4 Main Fault Scarps of the EFZ

Results from the larger fault populations on the bounding scarps of the EFZ, at Dağdibi, Kamişli, Hamidiye, Alpu, and Gülek (Fig. 7.26) all display vertical σ^1 (lineations 240/76, 315/86, 168/76, 017/83 and 217/77 respectively), reflecting the dominance of dip-slip slickenlines seen in the field.

7.5.5 A word of warning

Determination of palaeostress directions from slickenline populations is regarded by many workers as highly problematic due to the commonly wide dispersion of slickenline orientations resulting from a single, simple fault. Palaeostress orientations should only be considered useful when derived from well clustered slickenline populations with consistent senses and directions of slip.

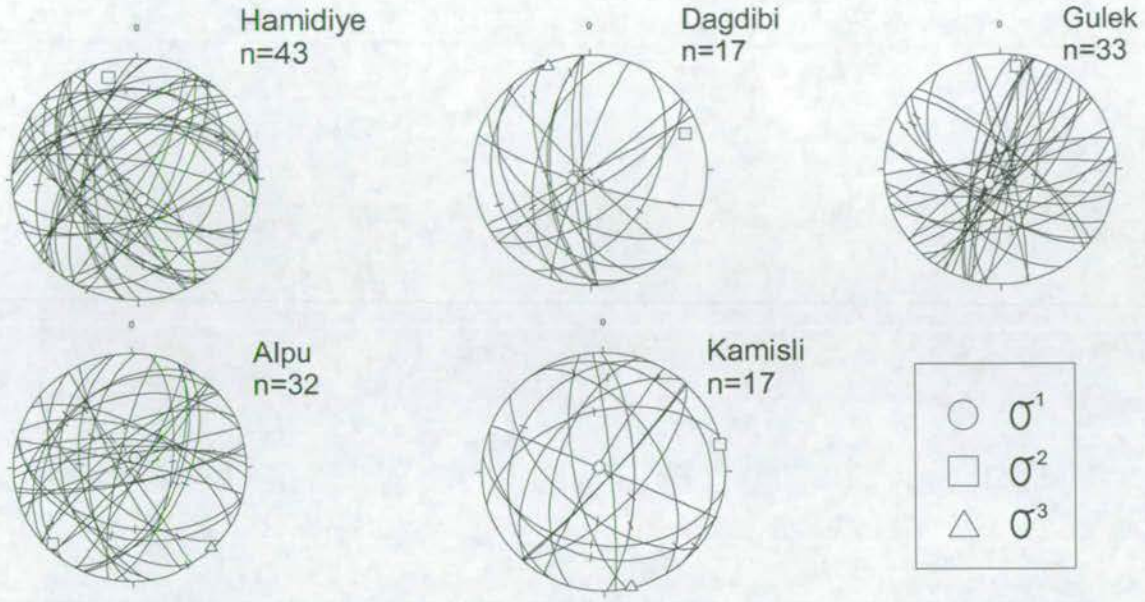

Fig. 7.26 Reduced palaeostress tensors derived from slickenlines on the bounding fault scarps of the EFZ, using the INVERS program of Sperner *et al.* 1993. For locations of sites, see Fig. 7.21. Stereonets show: fault trace orientations (great circles), slickenline orientations (ticks on great circles) and lineations to sigma 1-3 (open symbols).

Palaeostress analysis has been useful here to confirm: (i) the dominantly extensional regime during the Plio-Quaternary, (ii) the north to south thrusting direction below the Pozanti-Karsanti ophiolite and (iii) the dominance of normal slip on the EFZ bounding scarps.

7.6 Modern Stress

The modern version of the World Stress Map (Mueller *et al.* 1997), based on the original stress map of Zoback (1992), has been compiled using several data sources. These include: (i) earthquake focal mechanisms (58%), (ii) well bore breakouts (27%), (iii) *in situ* stress measurements (overcoring and hydraulic fracturing, 11%) and (iv) young geologic data (from fault slip analysis and volcanic vent alignments, 4%). There is very little stress data available for the Central Turkey region but the nearest

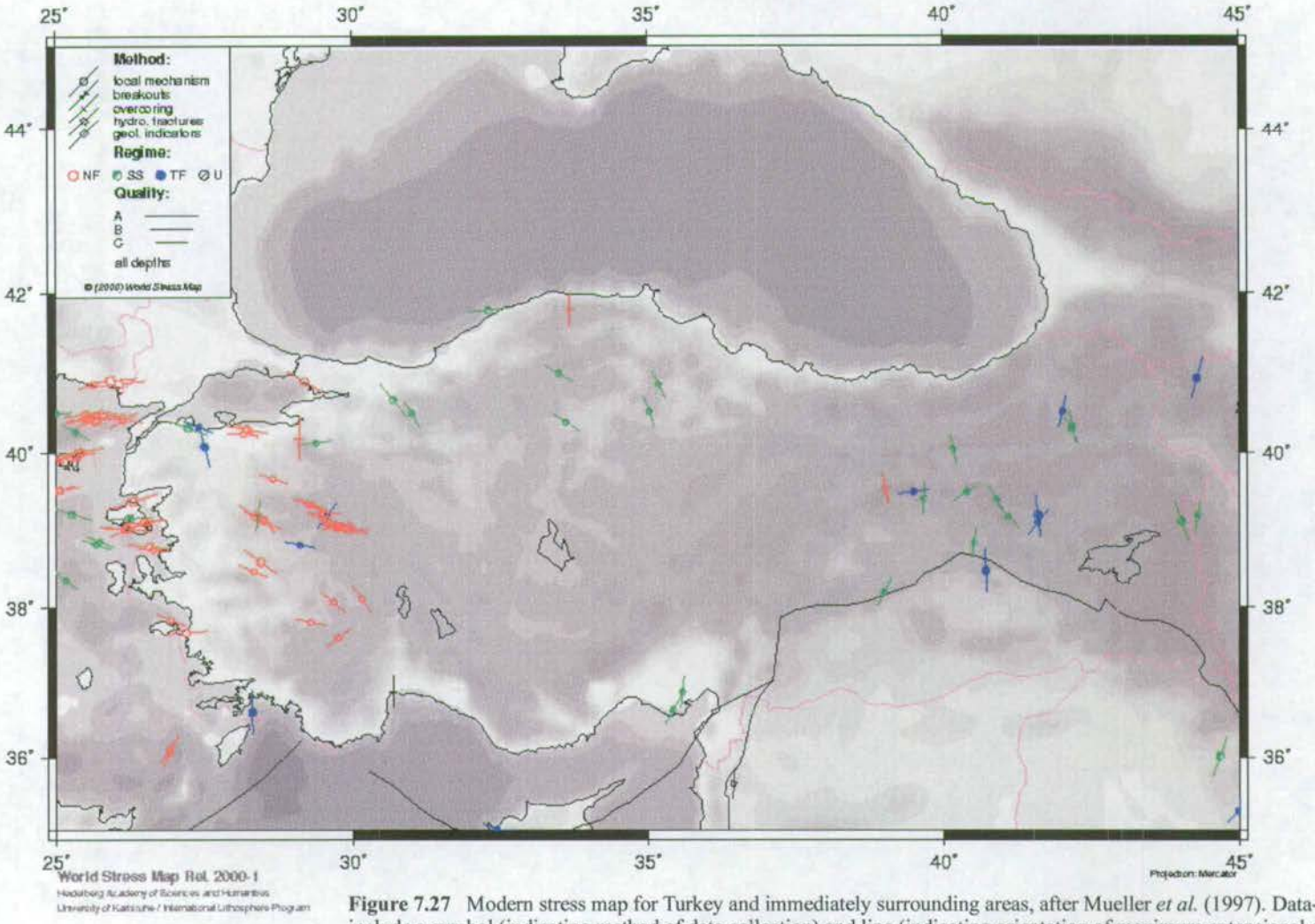

Figure 7.27 Modern stress map for Turkey and immediately surrounding areas, after Mueller *et al.* (1997). Data-points include a symbol (indicating method of data collection) and line (indicating orientation of maximum extensional or compressional stress). Shading indicates topography, light colours indicate high ground, dark indicates low ground. NF = tensional stress, SS = strike-slip stress, TF = compressional stress, U = unknown sense of stress.

datapoints are sinistral strike-slip in the Cayhan/Adana area (associated with movement on the EAFZ), E-W tension in the Maras area and dextral strike-slip in the NAFZ area (Fig. 7.27). None of these bear any direct relevance to the EFZ.

7.7 Conclusions

7.7.1 Deformation

- SE directed folding and thrust faulting during the Late Cretaceous was associated with the N to S obduction of the Pozanti-Karsanti ophiolite. This has caused pervasive SE directed deformation throughout the Aladağ and eastern Bolkardağ.
- A NW-directed thrusting event occurred during the Late Eocene focused on a narrow fold and thrust belt along the N margin of the Aladağ and Bolkardağ. This was possibly associated with the final closure of Neotethys.
- A NW-SE compression event affected the Cenozoic sediments of the EFZ during the Middle Miocene. This was associated with sinistral strike slip faulting and minor compression, and not with large scale west-vergent thrust faulting as described by previous workers.

7.7.2 Fault and slickenline data

- The Plio-Quaternary period appears to have been dominated by E-W extension, with a minor component of sinistral strike-slip, as seen localised on the 'small-graben' of the Çamardi alluvial fan complex.
- During the Late Miocene to earliest Pliocene sinistral trans-tension dominated in the EFZ. This strain was distributed throughout the fault zone.
- Sinistral trans-tension may have been active during the Late Oligocene – Early Miocene period. N-S and E-W extension were certainly active during this period.

- The Eocene period was dominated by compression in the northern EFZ. The orientation of this compression was probably originally parallel to that of the northern Taurus thrust system (section 7.3.4), but exposures may have been subsequently rotated during strike-slip.

7.7.3 Palaeostress

P-T dihedra palaeostress analysis of slickenline data sets provide supporting evidence that:

- The Pozanti-Karsanti Ophiolite was emplaced from N to S and affected underlying Tauride units.
- Faults within the Plio-Quaternary Çatalca Formation are the result of E-W extension.
- Sinistral strike-slip was localised on the small graben (Çamardi fan) during the Plio-Quaternary.
- The main bounding fault scarps are mainly the result of NW-SE extension.

8 Geomorphology

8.1 Introduction

In recent years academic interest has focused on whether the EFZ has been seismically active in the historical past and whether it is likely to be active in the near future. Plans for a new hydroelectric power scheme at Çamardi (pers. com. Yetiş 1999) and the proposed development of a nuclear power plant at Akkuyu (near Anamur, Mediterranean coast) have focused Turkish geologists on dating the last movements on the EFZ and on predicting its future seismicity. Study of the geomorphology of the Ecemiş Fault Zone can shed light on these questions and on its modern tectonic setting.

Recent publications (Koçyiğit & Beyhan 1998, 1999, Westaway 1999) have largely focused on this aspect, but are unresolved on whether the EFZ is a currently or recently active strike-slip fault zone. The two opposing hypotheses are:

(i) The current geomorphology of the EFZ is the result of active faulting (Koçyiğit & Beyhan 1998, 1999).
(ii) The current geomorphology of the EFZ is not the result of active faulting. The EFZ is an ancient fault zone which was last active during the Eocene (Westaway 1999, Yetiş 1984).

This chapter presents geomorphological observations and measurements with the aim of testing the two above hypotheses. Tracings of 1:60,000 aerial photographs, held at MTA (Turkish Geological Survey) in Ankara were used to produce a geomorphological map (Enclosure 2) of the EFZ and to locate sites of geomorphological interest in the field. Unfortunately, the originals of these aerial photographs were not available for reproduction.

8.2 Geometry and segmentation of the EFZ

8.2.1 Aerial Photograph Analysis

Structural mapping and analysis of aerial photographs reveal that the EFZ extends, as a distinct topographic feature, from Gülek in the south to Dundarli in the north; a distance of some 100km (Enclosure 2). The fault zone outcrops as a deep graben in the south (Gülek to Kamişli) with scarps varying from 50 – 1200m in height. This changes to a half-graben morphology in the north (Kamişli to Dundarli) where scarps increase in height to a maximum of 1400m. The graben and half graben are bounded by significant fault scarps, which bring Mesozoic and Palaeozoic platform carbonates (foot-wall) into contact with Tertiary sediments (hanging-wall).

Previous aerial photograph analysis (Fig. 7.2a, Koçyiğit & Beyhan 1998) has divided the EFZ into six fault segments of between 15 and 25km in length. Importantly, they maintain that both eastern and western bounding faults exist along the entire length of the EFZ. The sense of movement is not shown on the majority of these mapped faults.

This study attempted to produce a more detailed geomorphological map of the EFZ, in a limited area of excellent exposure (Enclosure 2). It was found that the main fault scarps are separated into many tens of segments, which are dominantly arranged in an en-echelon pattern, stepping to the west into the hangingwall (Enclosure 2).

In the south of the EFZ (Gülek to Kamişli) an *en echelon* arrangement of scarps is seldom seen. Steep (sometimes vertical) continuous scarps, 2-5km in length, are seen on the eastern side of the EFZ, as at Tekir (Fig. 8.1a). On the western side the fault zone is bounded by high mountain slopes, a continuous break of slope marking the western boundary (Fig. 8.1b), rather than the scarps seen on the eastern side.

Figure 8.1b A continuous break of slope marks the western boundary of the EFZ at Tekir, rather than the scarps seen on the eastern side.

Figure 8.1a Steep, sometimes vertical continuous scarps, 2-5km in length, seen on the eastern side of the EFZ, at Tekir.

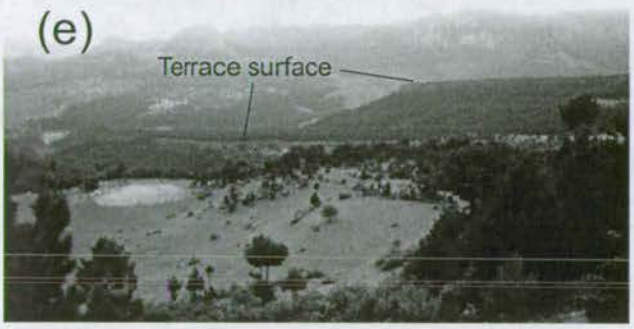

Figure 8.1e Plio-Quaternary alluvial fan material outcrops as several distinct and laterally correlateable surfaces (or terraces) at different topographic heights, seen here at Tekir.

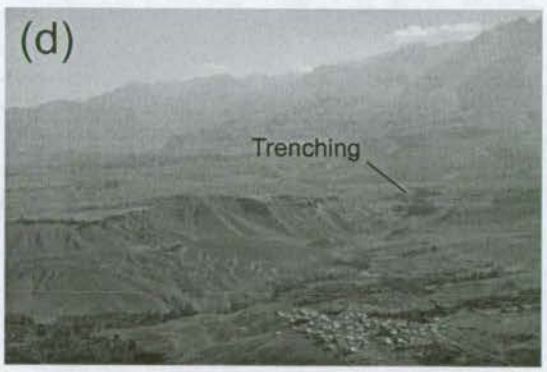

Figure 8.1c & d Plio-Quaternary alluvial fans have undergone extensive 'fan-head trenching', the entrenchment of the trunk channel below the upper part of the fan surface. Trenching is seen here at Elekgolu (Emli stream).

Figure 8.1 Photographs of scarp and alluvial fan morphology along the EFZ.

In the north of the EFZ (Kamişli to Dundarli) the western bounding faults die out altogether; the final western scarps are seen 3km north of Kamişli (Enclosure 2). An *en echelon* arrangement of scarps is much better developed in the north, with shorter segments of 1-2km in length stepping to the west into the hangingwall (Fig. 8.2, Enclosure 2).

The *en echelon* nature of faulting in the north of the EFZ is clearly seen in the Çamardi area (Enclosure 2, Fig. 8.2 & 8.3). Here, normal offset faults can be seen stepping to the west into the hangingwall, resulting in the formation of transfer zones[1] at stepovers[2]. As yet these transfer zones have not been breached at the surface by linking faults[3]. Transfer zones in this area coincide with the passage of major streams from east to west, draining the Aladağ Mountains in the uplifted footwall (Fig. 8.2). Examples of this can be seen at Narpuz and Madenboğazi where these streams pass through the main bounding scarp (Enclosure 2, Fig. 8.2 & 8.3).

8.2.2 Fault growth and linkage in the EFZ

The shape of vertical-offset displacement profiles measured along the strike of fault zones can be used to assess whether fault populations are growing by simple radial propagation, or by segment linkage (Fig. 8.4, Cartwright *et al.* 1995), and also to what degree segments of a fault population have linked. The shape of offset displacement profiles can also be used to locate the area of maximum displacement (Fig. 8.4), which often corresponds to the location of hangingwall sedimentary depocentres.

In the EFZ, the total normal displacement across the main scarps is not easily measured as the stratigraphy is not repeated in hangingwall and footwall. Variations in scarp height were measured, as a proxy for minimum normal offset, on both sides of the graben and half graben. Scarp heights from mean sea level were measured at 1km intervals from Gülek in the south to Dundarli in the north, on both sides of the fault zone using 1:25,000 topographic maps (Fig. 8.5). This technique has the disadvantage

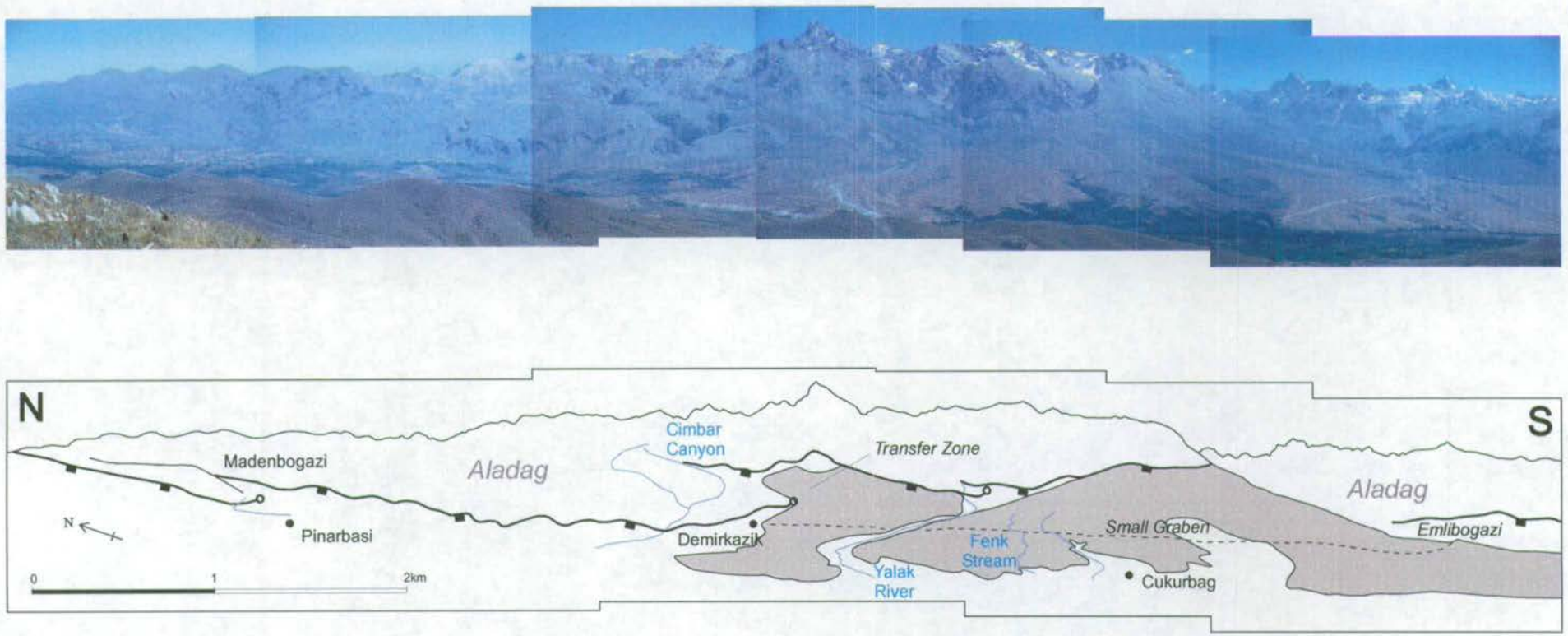

Figure 8.2 Photomontage of the Camardi alluvial fan complex and EFZ as seen from Evliya Tepe (Fig. 8.3 for location and map). The photomontage shows fault segments (heavy lines with filled squares on down-thrown side), rivers and streams (blue lines), outcrop of the Plio-Quaternary Catalca Formation (grey shade), and villages (filled circles). The location of segment tips are represented by open circles.

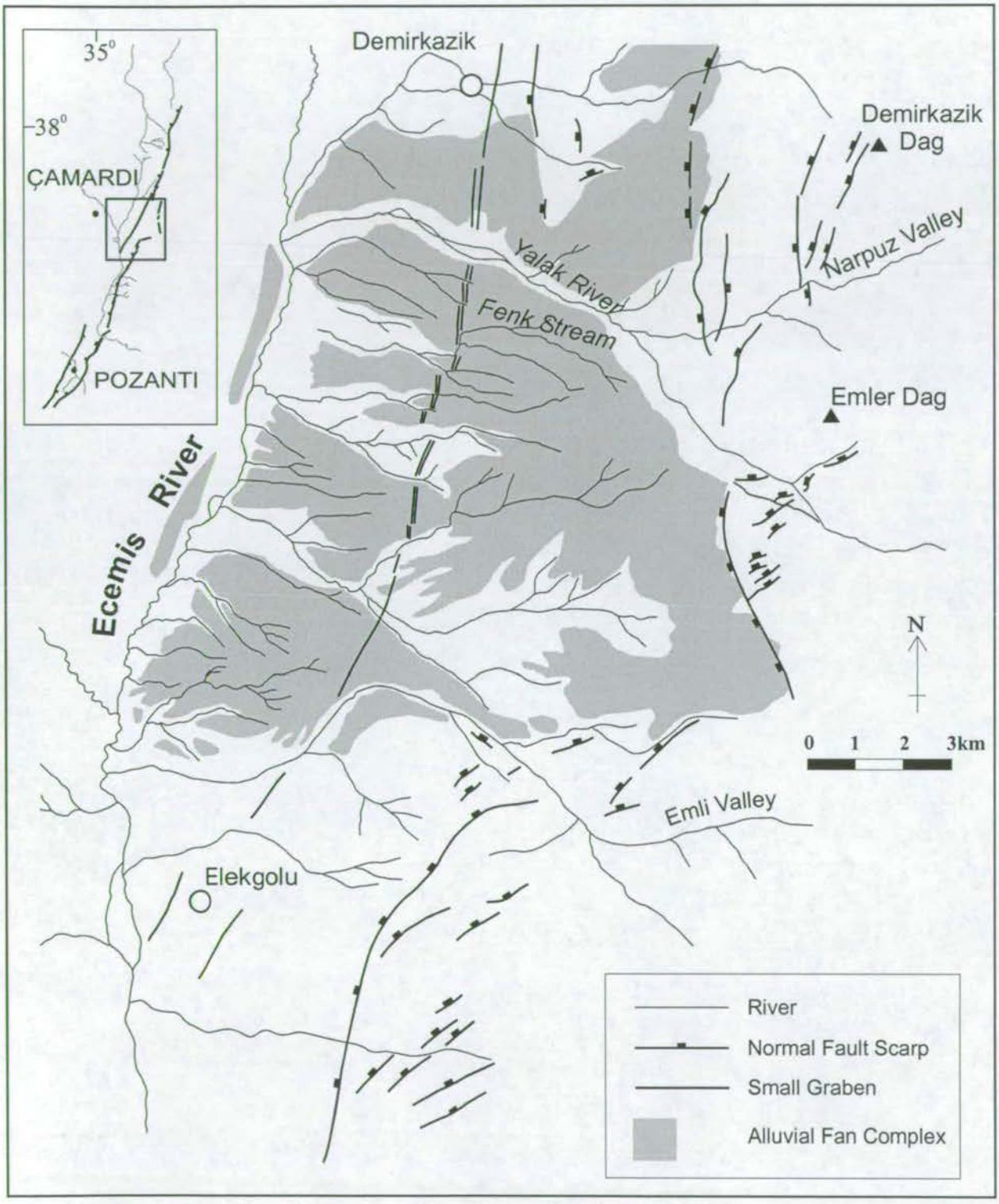

Figure 8.3 Map of the Çamardi fan area compiled from tracings of 1:30,000 aerial photographs and field mapping. Map shows drainage (thin lines), Plio-Quaternary alluvial fan complex (shaded area), main fault scarps (black lines with block symbol on downthrown side) and the 'small graben' feature (thick black line).

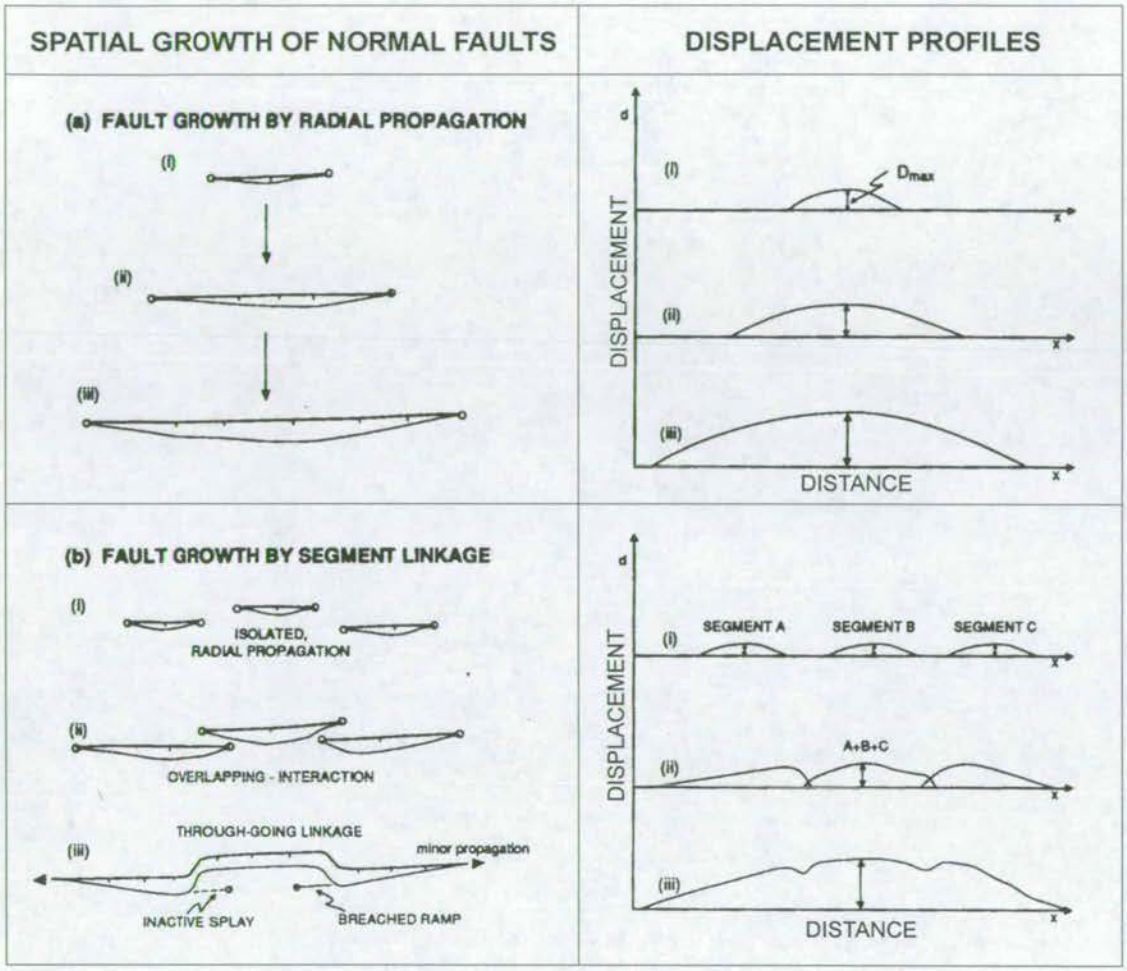

Figure 8.4 How displacement profiles develop in two models of fault growth: **(a)** radial propagation, and **(b)** segment linkage. After Cartwright et al. 1995.

that present scarps may not represent ancient fault displacements; antecedent rivers such as the Ecemiş and Çakit rivers (Enclosure 2) may have incised into these initial fault scarps, reducing their apparent offset. Scarp heights should, therefore, be seen as a minimum of ancient vertical fault displacements.

Results show that in the south of the EFZ maximum displacement is to the W, with scarps approaching 1.6km in the Bolkardağ. There is little segmentation of the main fault in the SW of the EFZ, with continuous scarps up to 10km in length between Tekir

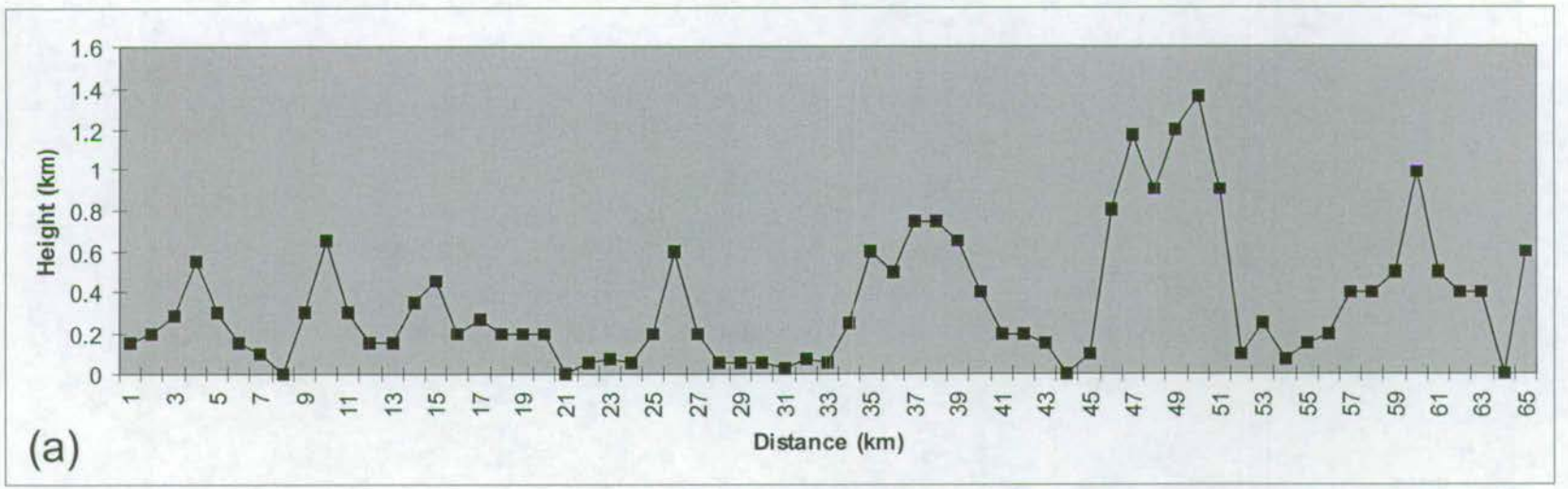

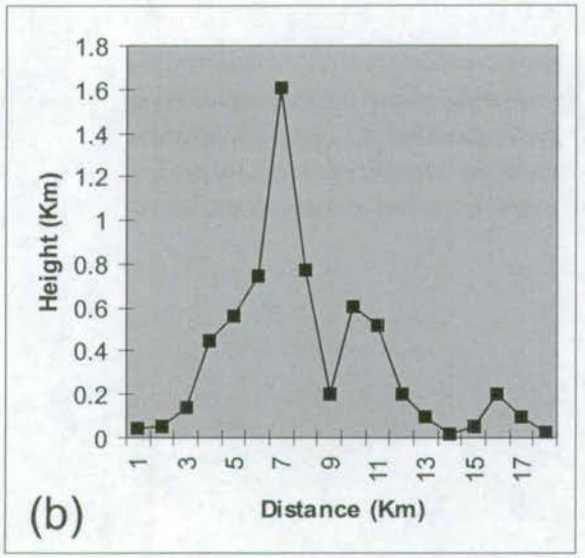

Figure 8.5 Scarp height profiles for **(a)** the eastern scarps of the EFZ, and **(b)** the western scarps of the EFZ. Black squares indicate spot heights of exposed scarps (height above mean sea level), measured at 1km intervals along the EFZ from Gulek. Horizontal scale indicates distance from Gulek. Scarp heights are used as a proxy for vertical fault displacement (see text for explanation), hence the profiles are used as a substitute for displacement

and Alpu (Enclosure 2). Maximum displacement in the southern EFZ is in the Tekir-Akça area, on the western bounding fault, where many Plio-Quaternary alluvial fans are preserved (Fig. 8.5). In the SE of the EFZ scarps are lower, more segmented, and appear to accommodate less displacement (Fig. 8.5, Enclosure 2). The SE of the EFZ appears to be in phase 1 of segment linkage (Fig. 8.4b, Cartwright model), whereas the SW appears to be in phase 3 (Fig. 8.4a & b, Cartwright model).

In the north of the EFZ the maximum displacement is to the east, with offset to the west of the EFZ dying out 3km N of Kamişli (Enclosure 2) as the morphology of the EFZ changes from graben to half-graben. Scarps have a much larger height variation in the north (max. 1.3km variation) and form three distinct segments (Fig. 8.2, 8.5). Maximum scarp height (proxy for normal fault displacement) is located at Demirkazik, which coincides with the largest Plio-Quaternary sedimentary depocentre in the area, the Çamardi alluvial fan complex (Enclosure 2).

Overall it appears that the EFZ is growing by a process of segment linkage rather than radial propagation (Fig. 8.4). The evidence for this is that the majority of the fault zone is composed of several discrete fault segments with Gaussian shaped displacement profiles (Fig. 8.5), resulting in several displacement maxima, rather than a single segment with a single displacement maximum.

8.3 Alluvial Fan Morphology

8.3.1 General Characteristics

The Pliocene – Quaternary Çatalca Formation is preserved as remnants of a previously more extensive alluvial fan complex, as discussed in Section 4.4.4. These remnants are best preserved in the Tekir – Pozanti area in the south of the EFZ, and the Çamardi area in the north (Enclosure 2). These alluvial fans have undergone extensive 'fan-head

trenching', the entrenchment of the trunk channel below the upper part of the fan surface (Summerfield 1991, Fig. 8.1c).

The original (highest) fan surfaces often have a small lateral extent (Enclosure 2), and the remainder of the alluvial fan material outcrop as several distinct and laterally correlateable surfaces (or terraces) at different topographic heights (Enclosure 2, Fig. 8.1e). These terraces are 'unpaired' in all cases (i.e. they do not correlate with terraces of an equal height on the opposite side of the valley, Fig. 8.6a), which suggests that the rate of lateral migration of river channels has been more rapid than that of vertical incision (Summerfield 1991). The terraces have been dated as Holocene by Koçyiğit & Beyhan (1999), without any supporting evidence, and are described as depositional, rather than erosional features. The age of these terraces relative to faulting on the EFZ has not been previously investigated.

The highest terraces are very restricted in outcrop, confined to small outcrops adjacent to the bounding scarps. Lower terraces have an increasingly greater lateral extent (Enclosure 2). The highest terraces are well cemented with calcite spar (Fig. 8.7a & b), whereas lower terraces are composed of unlithified matrix-supported conglomerates (Fig. 8.7c). Lower terraces can also be seen to incise into higher ones (Fig. 8.7d). This suggests that the higher terraces are older and that lower terrace surfaces have been developed subsequently.

An important question is why terraced fans are only preserved in the Pozanti and Çamardi areas, and whether they eroded from-, or were never deposited in other parts of the EFZ. From the displacement profiles (Fig. 8.5) it is inferred that fault scarps (and probably normal displacement) are highest in the Pozanti and Çamardi areas; hence it is expected that maximum accommodation space and maximum fan thickness would be developed in the hanging-walls directly adjacent to these areas. Although there are small remnants of Plio-Quaternary fanglomerates elsewhere in the EFZ (notably 2km

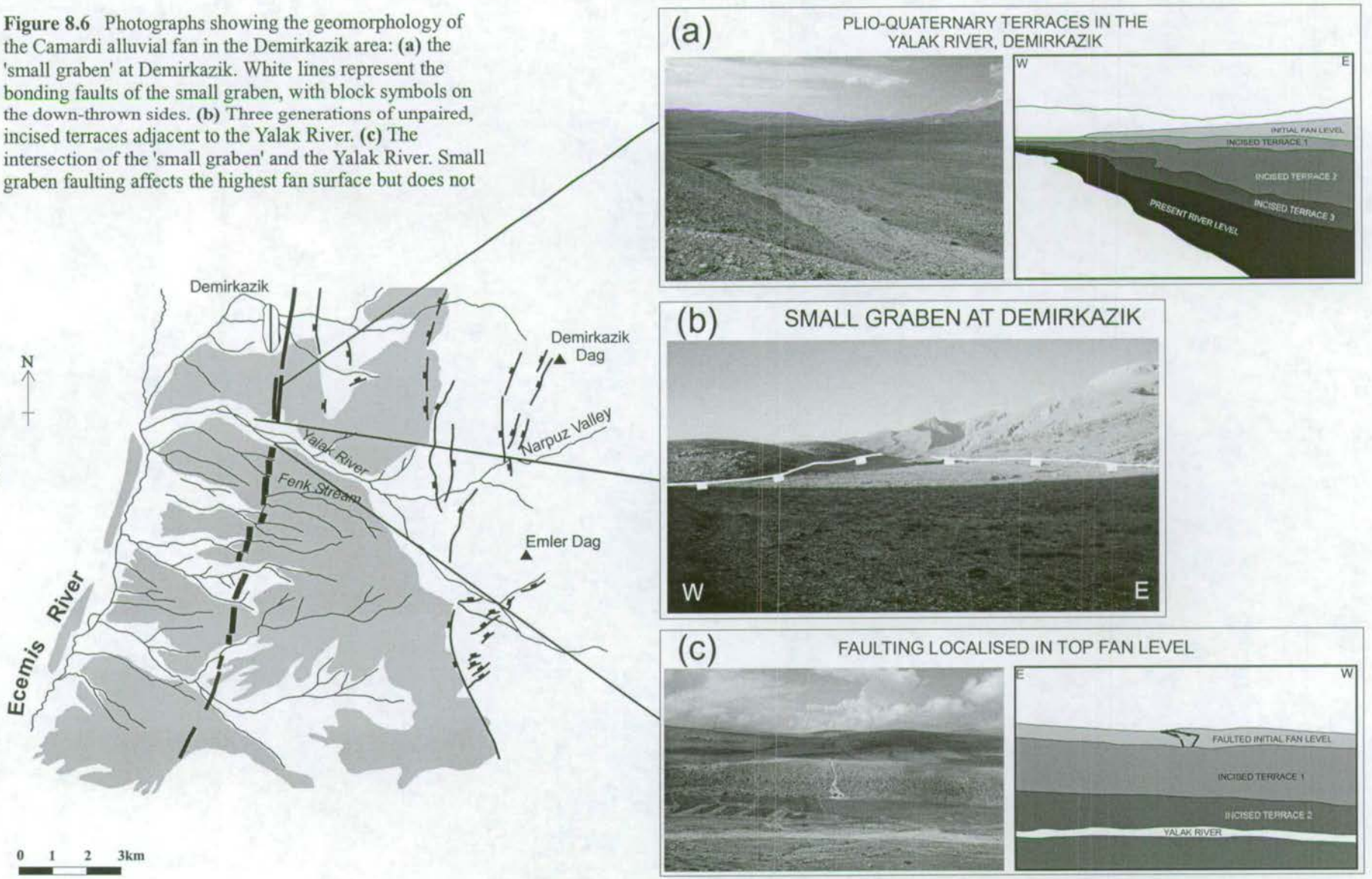

Figure 8.6 Photographs showing the geomorphology of the Camardi alluvial fan in the Demirkazik area: **(a)** the 'small graben' at Demirkazik. White lines represent the bonding faults of the small graben, with block symbols on the down-thrown sides. **(b)** Three generations of unpaired, incised terraces adjacent to the Yalak River. **(c)** The intersection of the 'small graben' and the Yalak River. Small graben faulting affects the highest fan surface but does not

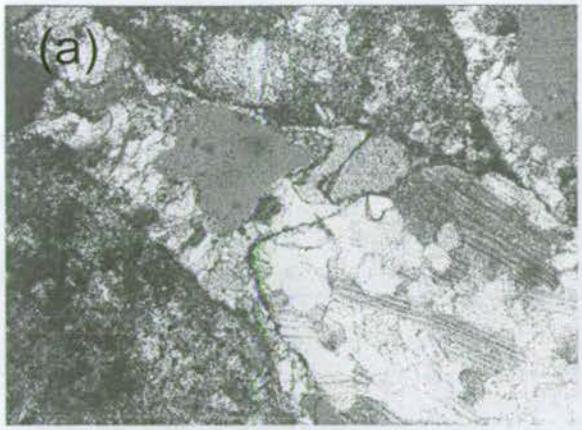

Figure 8.7a Photomicrograph of Plio-Quaternary alluvial fan material (highest fan surface) from the Camardi area. Slide shows marble clast (bottom right), micritic limestone clast (bottom left) and quartz grain (centre left). Clasts are cemented by a calcite spar. Magnification = 4x.

Figure 8.7b Well cemented nature of the highest fan surface, Camardi fan complex.

Figure 8.7c Unconsolidated nature of the first incised terrace material. Yalak River, Camardi fan complex.

Figure 8.7d Highest fan surfaces are incised along modern streams. Terraces develop along the banks of these streams. Camardi fan comlex.

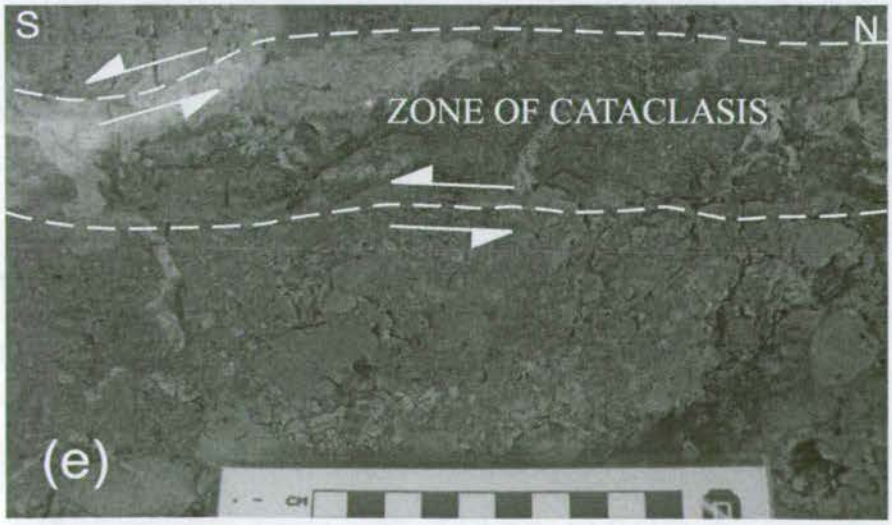

Figure 8.7e Zones of cataclasis are observed at the boundaries of the 'small graben' (Fig. 8.6b), where clast size is reduced from 10-20cm to 0.2-0.3cm diameter. White arrows show kinematics of slip, determined from slikenlines at Elekgolu (Fig. 8.10) and offset of streams on the 'small graben'. There are no kinematic indicators within the fault breccia to indicate direction of slip.

north of Kamişli), there is no evidence that the thick, multi-level alluvial fans of the Pozanti and Çamardi areas were ever developed elsewhere in the EFZ. It seems probable that the largest alluvial fans formed, and were preserved in areas of maximum accommodation space, i.e. locations of fault displacement maxima.

The Pliocene and Pleistocene were periods of extensive fanglomerate deposition and incision throughout Turkey. Early Pleistocene marine and fluvial terraces have been documented at several levels from throughout Turkey (Erol 1991). Deposition of the coastal Kemer fanglomerate (Isparta Angle) took place during the Early-Mid Pliocene (Glover & Robertson 1998), and the Pleistocene was a period of extensive continental fanglomerate deposition in Cyprus (Poole & Robertson 1998).

8.3.2 Controls of terrace formation

It is known from sedimentological and palaeocurrent evidence presented in Section 4.3.8 that the Çatalca Formation is a complex of alluvial fans whose original deposition was controlled by the proximity of fault scarps. The formation of subsequent terraces may be the result of one, or several of the following factors:

- **Tectonic control**. Pulsed uplift of the Taurus mountain range relative to sea level could have resulted in a steepening of local river profiles and an increase in the potential energy of river waters, resulting in river incision into the alluvial fans.
- **Changes in base level**[4]. A fall in relative sea level of the Mediterranean may have caused re-grading of the river long profile, through the head-ward migration of knick-points[5] (Summerfield 1991). This may have caused rivers to repeatedly incise into the alluvial fans, resulting in similar erosional terraces. Such a fall in base level could be due to: (i) fluctuations in the level of the Mediterranean Sea or (ii) the opening of EFZ drainage to the Mediterranean after a period of high enclosed inward drainage.

subsequent down-cutting of rivers. According to Erol (1991) this was synchronous with high rates of fluvial incision and headward erosion throughout the Taurus (Erol 1991). This major change in drainage and base level accounts for the erosive base of the Çatalca Formation and the deposition of the Plio-Quaternary fans; however, it is not temporally related to later terrace formation in the Pozanti and Çamardi areas.

There is currently considerable debate over the distance over which the effects of changing base level can penetrate into a fluvial system. Some authors suggest that the effects of a lowering of sea level can be felt throughout the catchment, via a re-grading of rivers and re-establishment of an equilibrium profile (Posamentier 1988, Posamentier & Vail 1988). Turkish geomorphologists also believe that the pulsed lowering of base level resulted in the incision and stabilisation of at least two erosional terraces, which are visible throughout the EFZ (Erol 1991). Conversely, others believe that the influence of base level change is restricted to coastal lowland areas only (Koss *et al.* 1994, Summerfield 1991). This has become the more popular view in recent years, with results from fluvial terraces of the Rio Cinca river (Spanish Pyrenees) showing that the upper reaches of rivers are heavily influenced by tectonics and climate, and that base level changes are of almost no significance (Jones *et al.* 1999). Recent studies of the incision history of alluvial fans in tectonically active areas (the Dead Sea Basin, Israel) have shown that short-term changes in climate, rather than tectonics or base level is the controlling factor in the modification of fan surfaces (Frostick & Reid 1989). They conclude that the discrete pulses of sedimentation and incision which they document are the result of high magnitude floods, rather than a long periods of re-grading of the river profile, associated with faulting. In the light of these results and the arguments outlined above, it seems unlikely that terrace formation in the uppermost parts of the Ecemiş River are the result of sea level changes in the Mediterranean.

Climatic control

Glaciation

There is evidence for glaciation in the upper valleys of the Aladağ, such as the upper Emli valley, Narpuz and Cimbar valleys (Enclosure 2). These areas display classic U-shaped morphologies (Fig. 8.8a & b), extensive accumulations of unconsolidated recessional and lateral glacial moraine (Fig. 8.8c), mountain cirques (Fig. 8.8d) and glacial striations, which all indicate that mountain glaciation has been active in the recent past (Pleistocene - Holocene). Glacial features are also documented from the Bolkardağ, where lateral and terminal moraine, glacial striations, rock-cut trimlines and hanging cirques were described above 1770m by Birman (1968). He dated this glaciation at Late Pleistocene and Holocene. Using this evidence, the Plio-Quaternary fans of the EFZ are below the lowest evidence for glacial activity (the small graben on the Çamardi fan is at a height of 1750m).

The highest alluvial fan surfaces are formed of well-cemented (pre-Quaternary) material and are interpreted as being deposited prior to the glacial maximum (Late Pleistocene-Holocene). The development of multiple incised terraces along rivers draining the upper Aladağ valleys (e.g. Yalak river, Fig. 8.6a) and the lack of glacial striations on fan surfaces both suggest that the Çamardi fan was not overridden by glaciers and that it was situated beyond the termination of mountain glaciers. The main fault zone is devoid of moraine accumulations, indicating that the main Ecemiş Fault Zone was not the site of extensive glaciation. These lines of evidence indicate that the glacial maximum did not reach as far as the current EFZ bounding faults.

It has been suggested (Hinchliffe, pers. com. 1998) that the formation of the multiple terraces seen in the Yalak river (Fig. 8.6a) may be controlled by glacial retention of sediment (incisional periods) and interglacial release of sediment (fan deposition). Pro-glacial outwash areas, such as the Çamardi fan are prone to large fluctuations in

Figure 8.8a The classically U-shaped upper Emlibogazi (Emli Valley), Camardi area.

Figure 8.8b The U-shaped, glacially scoured uppermost Narpuz Corrie. Recessional moraine covers the corrie floor.

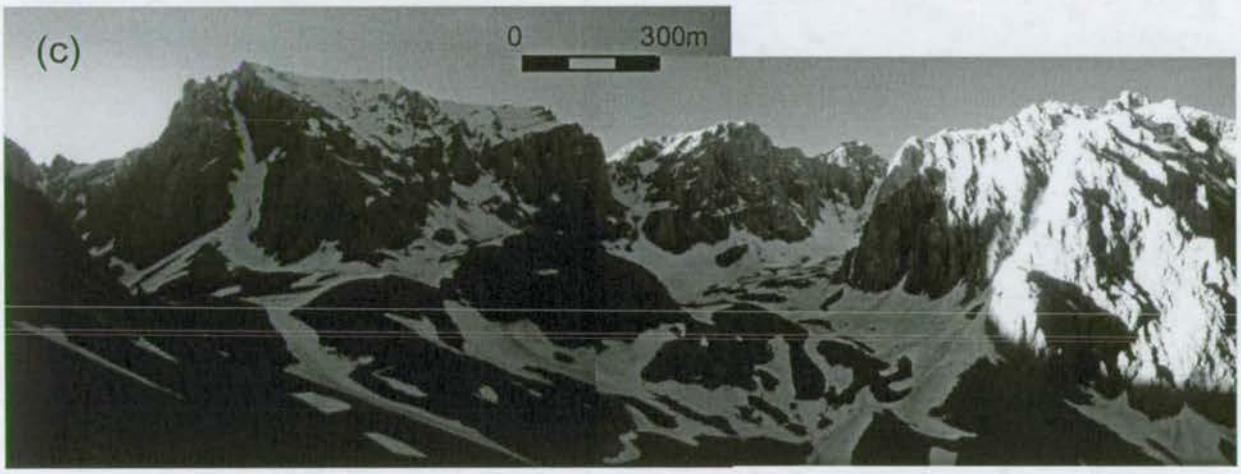

Figure 8.8c The glacially scoured Narpuz Corrie. Recessional moraine covers the corrie floor.

Figure 8.8d Hanging corries and cirques of Kaldi (southern Aladag), indicating intense mountain glaciation.

discharge and sediment supply (Smith 1985), suggesting that such an explanation for terrace formation is likely.

Short term fluctuations in climate – flood events

The effects of flood events on the evolution of alluvial fan systems has been investigated by Frostick & Reid (1989). Their study from the alluvial fans of the west bank of the Dead Sea (Israel) concludes that storm events are mainly responsible for the deposition of pulses of course river gravels; not for incision of the alluvial fan, which is the result of low lake levels (local base level change) during the Holocene.

8.3.3 Evidence for Quaternary faulting in alluvial fan material

Several features associated with the Çamardi fan indicate that it has undergone Quaternary faulting :

- **Normal faulting of fan material**. At the intersection of the Emli Valley and the eastern bounding fault scarp, fan material is seen to be offset by N-S striking normal faults (Fig. 8.9). Normal offset is of the order of 10m.
- **Small Graben.** The Çamardi fan complex is dissected by a 'small graben' (Fig. 8.3, 8.6b), as noted by Koçyiğit & Beyhan (1999), which they infer to mark the site of surface breaks induced by historical earthquakes (<2000 years old). This feature is dextrally offset numerous times (by E-W striking faults), with offsets in the order of hundreds of meters (Fig. 8.3). These offsets suggest that this feature is older than 2000 years (recorded history), as suggested by Koçyiğit & Beyhan 1998. Scarps bounding this graben have minimum vertical offsets of 10-20m (based on current scarp height).
- **Cataclasis of fan material.** In the vicinity of the 'small graben', fan conglomerate clasts are seen so be heavily brecciated and veined (Fig. 8.7e). Outside this area fan conglomerate clasts have uncompacted clast to clast contacts with no brecciation. The

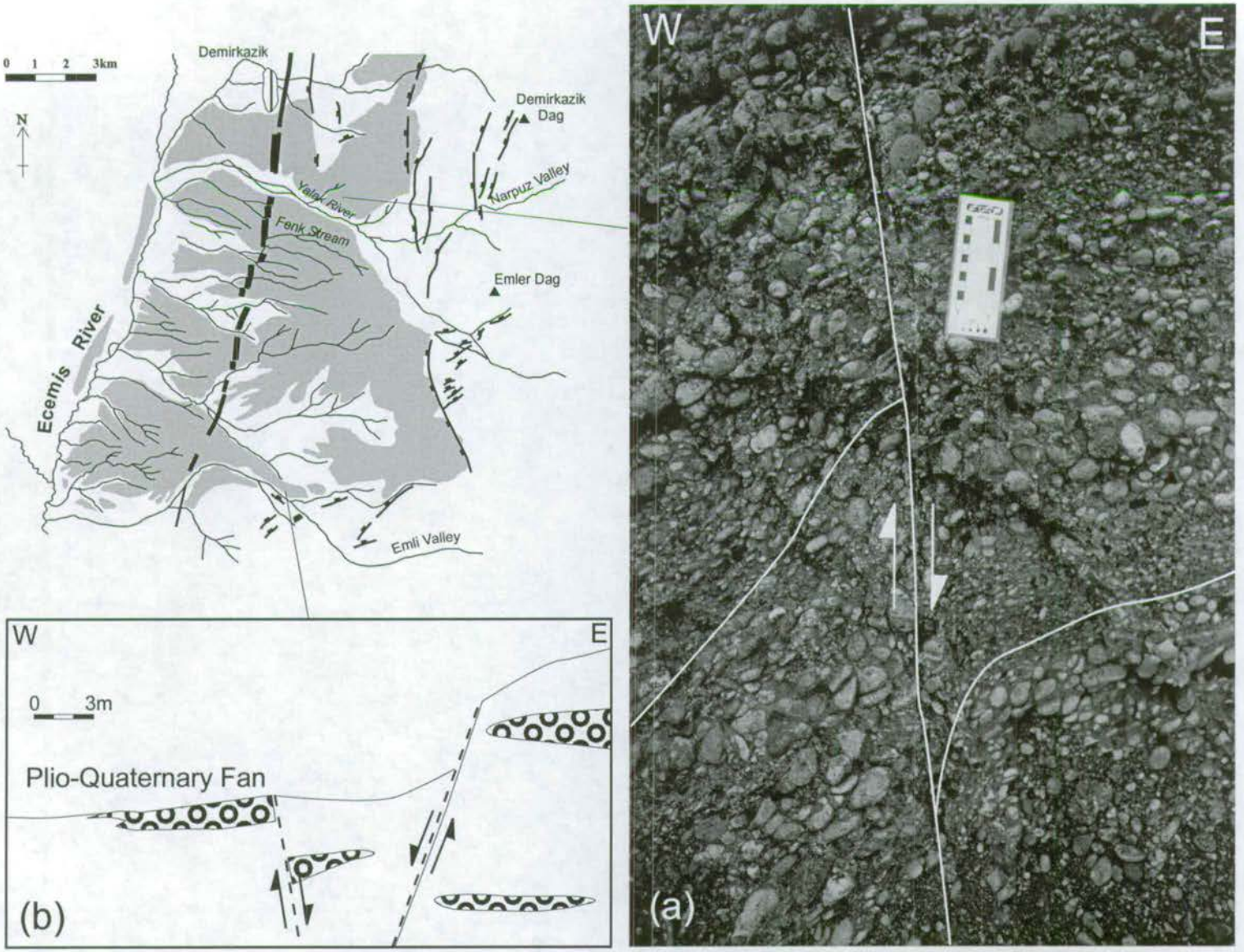

Figure 8.9 Normal faulting on the Camardi alluvial fan complex. **(a)** Normal faulting within the Oligo-Miocene Cukurbag Formation, 500m from the main bounding fault scarp. **(b)** Normal faulting of the Plio-Quaternary Catalca Formation at Emlibogazi, where the Emli River intersects the main bounding fault scarp.

well-cemented nature of the cataclasites (Fig. 8.7e, 8.7b) suggest that faulting occurred at least 1Ma ago.

- **Slickenline clustering below small graben.** Exposures of Oligo-Miocene sediments directly beneath the 'small graben' at Elekgolu display a very well clustered population of almost exclusively sinistral faults (Fig. 8.10). Considering that other exposures of Oligo-Miocene rocks do not display similar (well clustered) fault populations, it is likely that the 'small graben' accommodated sinistral strike-slip offset during Plio-Quaternary time.

8.3.4 Slatted Block Rotation?

The 'small graben' structure which dissects the Çamardi fan (described above) does not follow a straight course. Aerial photographs show that it is offset both dextrally and sinistrally by 10-100m along its course (Enclosure 2, Fig. 8.3). Assuming that the 'small graben' formed as a straight trench, then it appears to have been divided into blocks and offset subsequently. The majority of these offsets are dextral and fit the 'slatted block rotation' model for a sinistral fault zone (Fig. 8.11) which has been documented in the San Andreas Fault (Christie Blick & Biddle 1985), Dead Sea Transform (Freund & Garfunkel 1984) and in Greece (Roberts & Jackson 1991). Other evidence for slatted block rotation, such as deep basins at fault zone margins are not present in the EFZ, therefore the presence of any block rotation should be considered speculative only.

8.4 Drainage Patterns and River Offsets

Recent publications (Koçyiğit & Beyhan 1998, 1999) have placed great importance on the apparent sinistral offset of several rivers and streams along the EFZ, using these as evidence for recent strike-slip. This hypothesis was tested using new observations during this study.

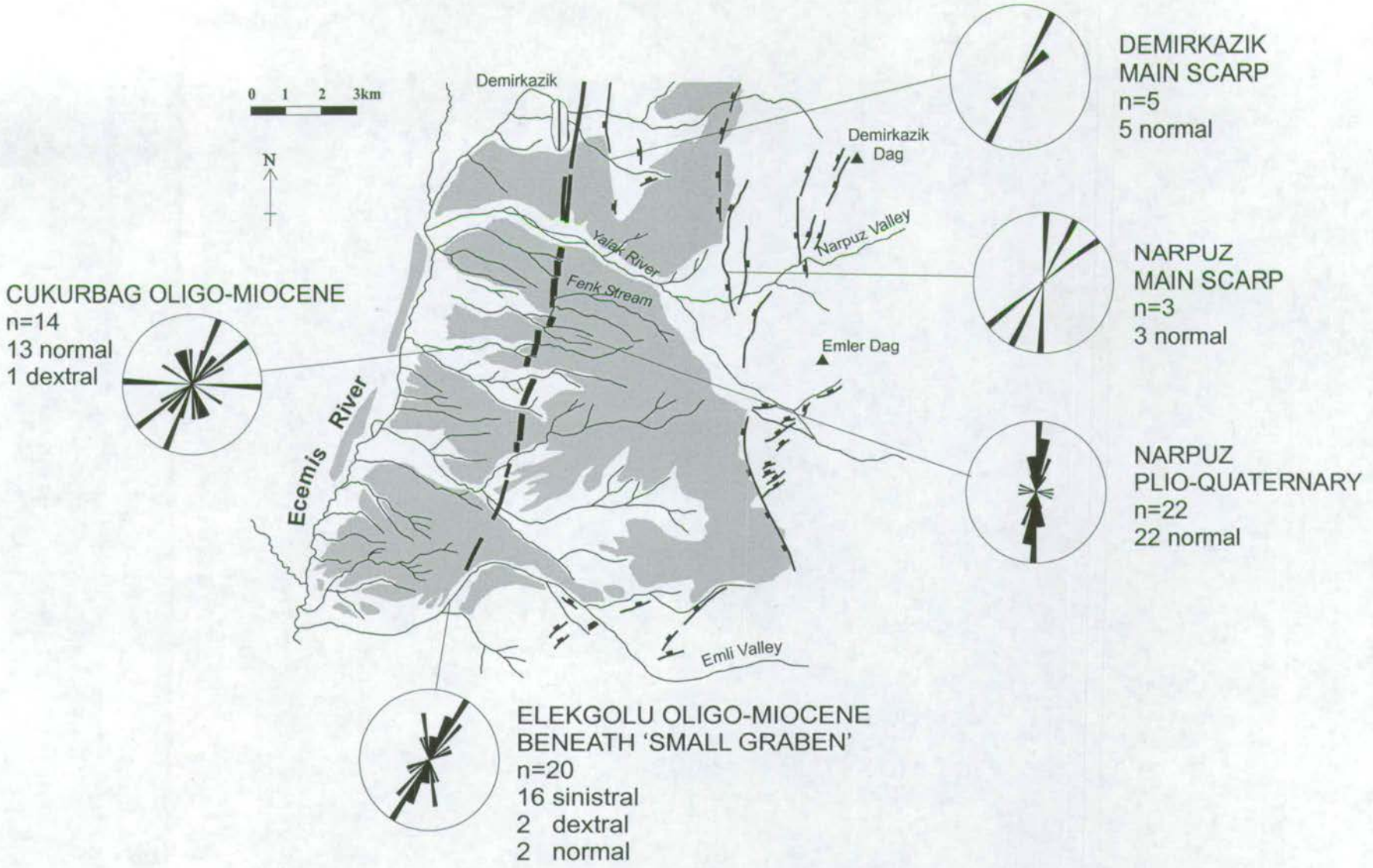

Figure 8.10 Strain partitioning of the normal and strike-slip components of trans-tensional slip in the Camardi area. Normal slikenlines were observed on the main bounding faults at Narpuz and Demirkazik, and on faults within the Catalca Formation at Cukurbag and the Fenk stream (away from the 'small graben'. Strike-slip slikenlines were observed from beneath the 'small graben' at

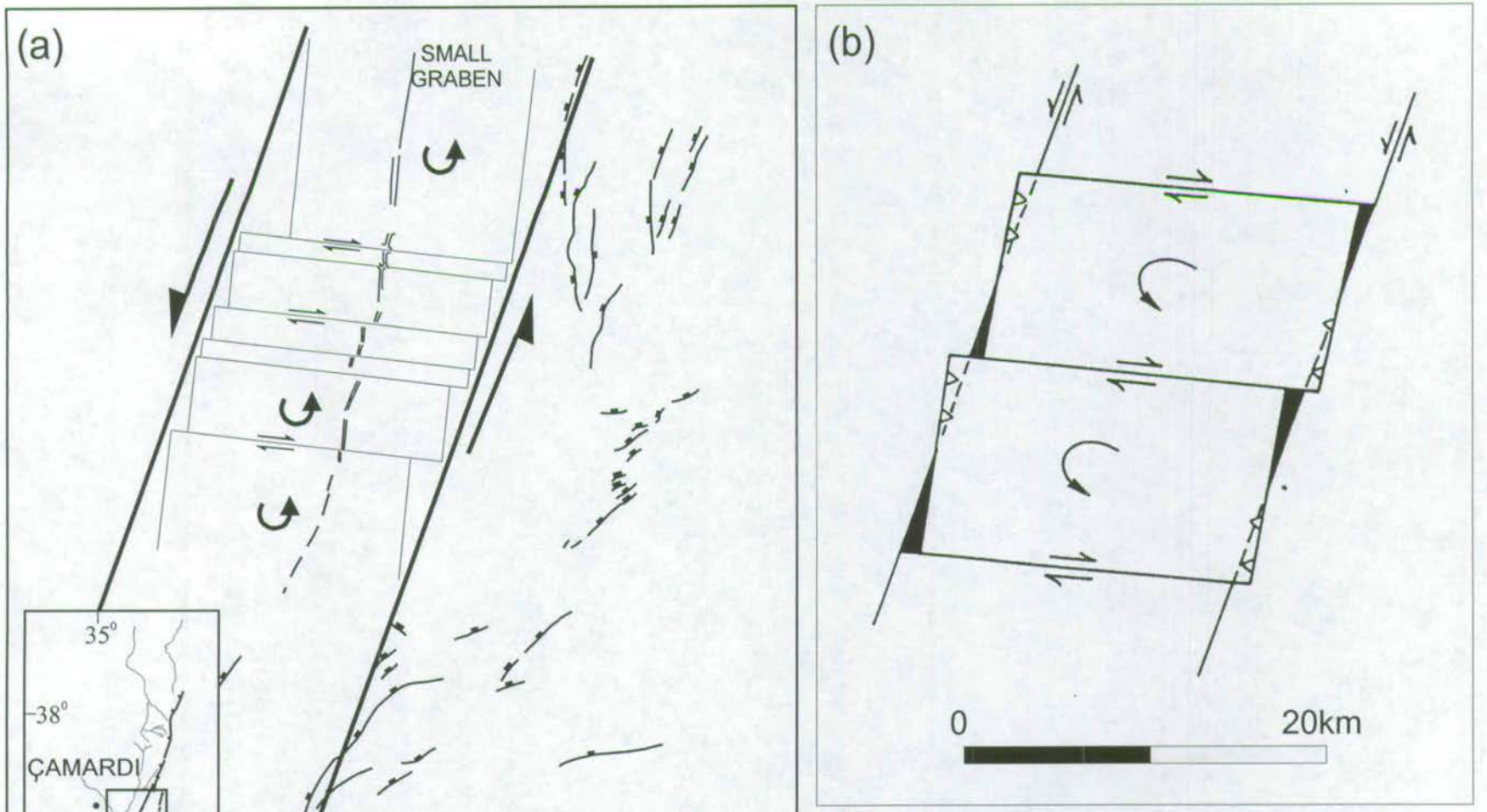

Figure 8.11 **(a)** Line drawing of the 'small graben' (double lines) traced from aerial photographs, Camardi alluvial fan complex. Inferred E-W striking dextral faults and blocks are also shown, which are similar to accepted models of block rotation in strike-slip fault zones. **(b)** A model for the rotation of blocks on the San Andreas fault, California (after Christie-Blick & Biddle 1985).

The majority of drainage from the Taurus Mountains in the Adana region is from north to south. This is seen in the Ecemiş, Çakit and Gokoluk rivers in the south of the EFZ (Enclosure 2). These main rivers have been diverted to a NE to SW flow direction for part of their course as they pass through the EFZ. It is believed that the Ecemiş and Çakit rivers are antecedent, as they persist in their original N-S course by incising into the eastern bounding fault scarps of the EFZ at Hamidiye and Pozanti, respectively (Enclosure 2). The courses of some smaller streams also appear to be controlled by the NE-SW orientation of the fault zone, for example between Kamişli and Alpu where two tributary streams run parallel to the EFZ trend (Enclosure 2).

Some small, ephemeral streams appear to be offset sinistrally by the EFZ. These include the Emliboğazi canyon (4km N of Elekgolu) which appears to be offset sinistrally by 2.4km and the Fenk stream (2.5km E of Cukurbag) with an apparent sinistral offset of 750m (Fig. 8.12, 8.3). Both of these stream offsets occur across the 'small graben' (described above). Koçyiğit & Beyhan 1999 argue that another sinistral stream offset exists 1km N of Akça (near Pozanti). Not all ephemeral streams flowing across the Çamardi fan are offset. The majority of those on the Çamardi fan (6 out of 8 streams, Enclosure 2) are not offset by the 'small graben', suggesting that the two offset ephemeral streams may not have been active since strike-slip offset on the 'small graben'.

The majority of perennial streams (adjacent to apparently offset ones) are not offset. Notably, all of the larger perennial streams in the EFZ such as the Yalak river are not offset (Fig. 8.3). Furthermore, apparently offset streams at Akça and Çukurbag have been found to be the southerly tributaries of converging dendritic streams, rendering interpreted offsets problematic (Enclosure 2). The restriction of sinistral offset to two ephemeral streams and the lack of offset on the majority of streams crossing the EFZ suggest that strike-slip on the EFZ pre-dates the establishment of the modern drainage

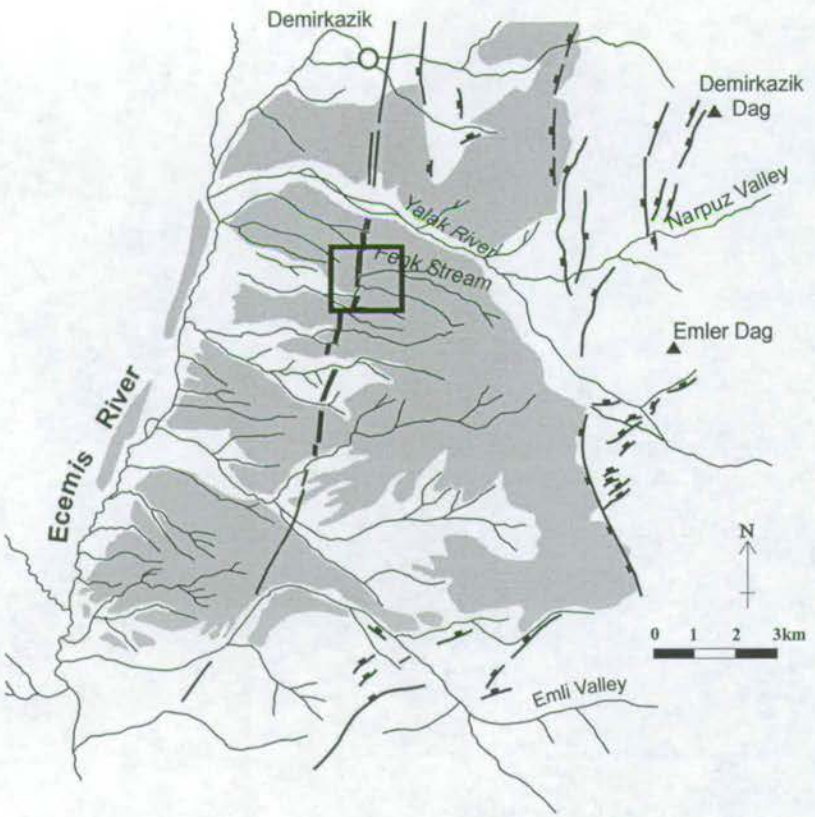

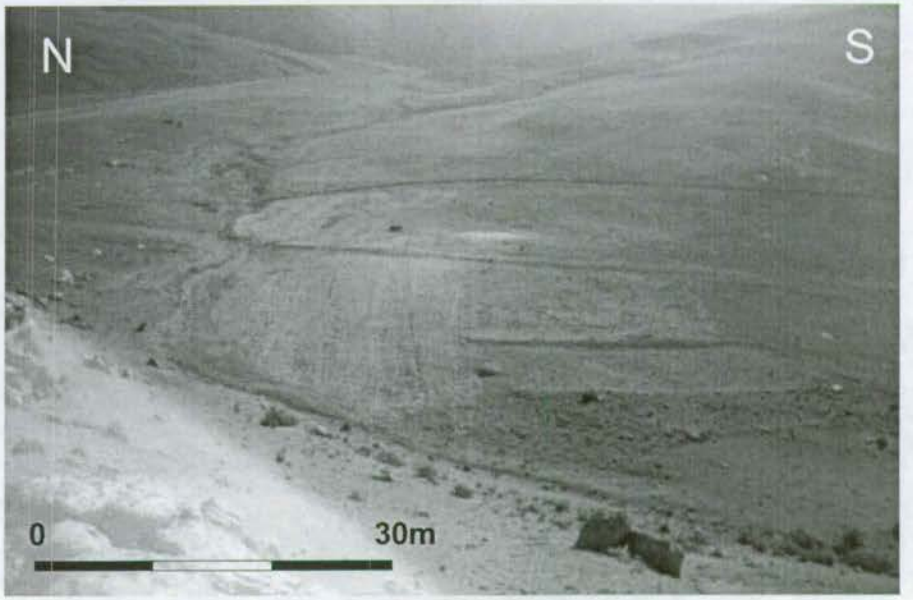

Figure 8.12 The intersection of the Fenk stream and the 'small graben', Camardi alluvial fan complex. The stream from an E-W course to a NNE-SSW course for 750m before resuming an E-W course. This has been used to infer a minimum sinistral offset of 750m on the 'small graben'.

pattern, and that only inactive streams preserve fault offsets, which occurred prior to the establishment of the modern drainage pattern.

No river or stream offsets are seen across the main fault scarps in the N of the EFZ. This suggests that any strike-slip movement which has occurred in the recent past has been focused on the 'small graben', not on main fault scarps (which appear to have accommodated exclusively normal offset, Section 7.4.2.1). This partitioning of trans-tension into normal and strike-slip components is not seen in the south of the EFZ where (if the interpretation of stream offset by Koçyiğit & Beyhan 1999 is correct) the western fault scarp is seen to accommodate normal and sinistral offset at Akça.

The modern Warm Spring Canyon alluvial fan (Death Valley, California) has also undergone strike-slip faulting perpendicular to the drainage direction (Blair 1999). In this example, the main drainage has been dextrally offset several times, resulting in the active depositional lobe being offset. This offset dams the main drainage for a short period, but the main drainage quickly re-established itself, and resumes the original course (Fig. 4.60). This process allows the migration of the active depositional lobe, and the establishment of several streams on the downstream side of the fault, which 'start' at the strike-slip fault. The latter phenomenon can be seen on the Çamardi fan (Enclosure 2) to the south of the Yalak River. The Yalak River (main incised channel) may also have been offset and, then re-established, resulting in several abandoned distal lobes and a series of rivers which apparently start at the 'small graben'.

Compared to other currently active strike-slip faults in zones of crustal extrusion, the geomorphological evidence for recent offset on the EFZ is not compelling. For example, along the Karakoram Fault (SW Tibet), the (SW-directed) course of the Indus river is diverted through 90^0 and follows the (NW-directed) course of the dextral Karakoram Fault for 120km before resuming its original SW course through the Ladakh range

(Searle 1996). Along the same fault, entire alluvial fans have also been displaced on a kilometre scale (Searle 1996).

8.5 Strain Partitioning in the northern EFZ

8.5.1 Definition

Strain partitioning is defined here as deformation accommodated simultaneously by strike-slip (simple shear) and contractional or extensional structures (pure shear) (Teyssier & Tikoff 1998). Partitioning occurs on a range of scales from microscopic grain-scale to global-scale plate boundary movements, and is commonly observed in zones of convergence or divergence. Most orogenic belts shorten obliquely, rather than normal to their length (Woodcock 1990) and outcrop-scale strain partitioning has been observed world-wide along tectonic boundaries where overall motion is oblique to the boundary. It has been documented in both trans-tensional (Rosetti *et al.* in press) and transpressive (Jones & Tanner 1995, Woodcock 1990) regimes.

8.5.2 Evidence for strain partitioning in the EFZ

In the Çamardi area the eastern bounding faults of the EFZ divert from a regional NE-SW strike and assume a strike closer to N-S for ~15km, between Pinarbaşi and Elekgolu (Enclosure 2). This coincides with the maximum normal displacement in the northern EFZ (Fig. 8.5), and an increase in the *en echelon* nature of the main fault scarp (Enclosure 2). Whilst the main bounding scarp changes orientation to a N-S strike, another visible lineament, the 'small graben' (described above) continues south from Pinarbaşi with a NE-SW strike.

Whilst the 'small graben' has taken up at least 10m of normal displacement (vertical offset of fan surface), possible local stream diversions (discussed above) and slickenline

populations associated with the 'small graben' (at Elekgolu, Fig. 8.10) indicate that it has principally taken up sinistral strike-slip displacement.

Conversely, at the main fault scarps, a lack of river offsets (Enclosure 2), exclusively normal slickenline populations (Fig. 8.10) and visible 1400m vertical displacement (Fig. 8.2) indicate that these have principally taken up normal displacement.

Elsewhere in the EFZ bounding fault scarps accommodate both strike-slip and normal offset, as witnessed by (i) oblique-slip slickenline populations along the reminder of the bounding fault scarps (Fig. 7.21) and by (ii) normal displacement (visible scarp) and sinistral displacement (river offsets at bounding fault scarps at Akça village, Section 8.4 above) on the same fault scarp. In the Çamardi area strain is partitioned into normal offset and sinistral offset lineaments. Beyhan (1994) also indicates that normal displacement and strike-slip displacement are partitioned between Sulucaova and Kovali (northernmost EFZ).

It is not possible from available data to determine whether the bounding scarp and the 'small graben' (Çamardi area) were active synchronously (i.e. whether strain was synchronously partitioned or switched from one lineament to another) without knowing the depositional age of the fan surfaces, especially the highest one. Palaeoseismic trenching of the small graben, in progress (H. Çetin pers. com. 1999) could provide data on when this lineament was active.

8.5.3 Controls of strain partitioning

Several hypotheses have been advanced as to why strain is sometimes partitioned into separate strike-slip and dip slip lineaments in zones of transpression and transtension, rather than being accommodated by oblique-slip. These include:

- In the continental upper mantle, a viscous continuum should generate principal stresses and strain rates parallel to, or perpendicular to the Earth's surface (Molnar 1992). Upper crustal vertical axis block rotation is coupled to vorticity fields in the upper mantle, therefore oblique-slip faults should not be stable during bulk finite strain.
- The rate of energy release on oblique-slip faults has been found to be greater than that on pairs of strike-parallel dip-slip and strike-slip faults (Michael 1990). This uses Hamilton's principle that systems choose configurations which minimise work done.

As for the location of strain partitioning, the following hypotheses have been proposed:

- Strain partitioning is facilitated by reactivation of pre-existing structural weaknesses which are in suitable orientations to minimise work done (Jones & Tanner 1995). Put another way, the location of strain partitioning is mainly controlled by competency contrasts within the faulted substrate (Tikoff 2000).
- Partitioning is especially likely where the angle between fault strike and relative plate motion is low ($<20^0$), i.e. in wrench-dominated transtension or transpression (Tikoff & Teyssier 1994).

Strain partitioning within the EFZ is highly localised to the Çamardi area. The controls on this localisation remain poorly resolved. Strain partitioning localisation may be associated with a localised change in orientation of the EFZ from NNE-SSW to more N-S, forming a possible releasing bend. There is little evidence for any pre-existing structural weakness beneath the 'small graben', but a competency contrast between competent Aladağ carbonates and incompetent Ulukişla volcanics may lie beneath this lineament.

8.6 Dating the latest movement on the EFZ

Current academic interest is focused on dating the most recent fault activity on the EFZ. This has been spurred on by plans to construct a hydroelectric power plant on the Ecemiş River at Çamardi and a nuclear power plant at Akkuyu on the Mediterranean coast along the trend of the EFZ.

8.6.1 Dating Methodology

At the intersection of the 'small graben' and the Yalak river (Fig. 8.6c) the topography of the uppermost fan surface is seen to be affected by the N-S striking 'small graben', but lower (erosional terrace) surfaces are not affected (Fig. 8.6c). It is therefore inferred that the oldest (highest) fan level was affected by the latest phase of strike-slip faulting on the 'small graben' (see above), but that younger erosional terraces have not, and that they post-date the last phase of faulting. Therefore, dating the deposition ages of both of these fan surfaces could constrain the timing of the last phase of strike-slip. Dating of the highest fan surface would also enable a minimum strike-slip offset rate to be calculated, using the sinistral offsets of the Fenk and Emli streams (Section 8.4 above).

During this study I attempted to date the ages of deposition of the first (uppermost) and second (first erosional terrace) surfaces. As the Çatalca conglomerate is believed to be devoid of organic material, radiocarbon dating of the surfaces is not possible. The thermoluminescence technique was considered but required lithified samples, and the erosional terrace material is unconsolidated. The cosmogenic isotope technique for exposure dating seemed to be the only technique available.

8.6.2 Cosmogenic exposure age dating

This technique assumes that no burial or disturbance of conglomerate clasts has taken place since original deposition and involves a calculation of the abundance of

cosmogenic ^{36}Cl generated in the surface limestone clasts, hence how long the sample has been exposed at this level (Bierman 1994, Siame et al. 1997, Cockburn 1998).

Unfortunately the expense involved in preparing and analysing samples of micritic limestone for cosmogenic ^{36}Cl, the lack of source material for other cosmogenic isotopes to run in conjunction with ^{36}Cl (i.e. quartz), and the time required for modelling and interpreting results rendered the exercise impractical.

8.6.3 Palaeoseismicity

Workers from Ohio State University (Prof. Larry Mayer *et al.*) are currently involved in trenching across the 'small graben' on the Çamardi fan in order to study the palaeoseismic record and microstructures within the Çatalca conglomerates. Initial results have not yielded any clear evidence of recent palaeoseismicity (H. Çetin pers. com. 1999), in contrast to other nearby faults such as the East Anatolian Fault Zone (Taymaz *et al.* 1991).

8.6.4 Radiometric dating

The northernmost extension of the Ecemiş Fault Zone runs through the Erciyes Basin, part of the Central Anatolian Volcanic Province. As explored in Chapter 9, the timing of faulting in this area can be constrained by $^{40}Ar/^{39}Ar$ radiometric dating of tuffs and lavas which are faulted by, and unconformably drape faults associated with the EFZ. Results from such dating are discussed in Chapter 9.

8.7 Conclusions

- The Ecemiş Fault Zone outcrops as a graben (S) and half graben (N), and is divided into many tens of segments. These generally step to the W into the hanging-wall.
- Maximum vertical displacement (1300m) can be found on faults at Pozanti and Çamardi. These are the locations of the thickest deposits of Plio-Quaternary alluvial fans, and it is inferred that these were also the locations of maximum accommodation space creation during the Plio-Quaternary.

- Plio-Quaternary alluvial fans were originally deposited adjacent to bounding fault scarps, in response to fault activity. These fans were subsequently incised and terraced to several discrete levels. Terracing is probably the result of (i) a gradual decrease in sediment supply from the Aladağ and Bolkardağ as mountain slopes were denuded, and (ii) Glacial-interglacial cyclicity in sediment supply at glacier outflow points. It is not considered likely that sea level changes in the Mediterranean (base level changes) would have affected these upper river courses. Likewise, there is little evidence for widespread tectonic uplift of the Taurus after deposition of the oldest alluvial fans.
- Plio-Quaternary fans have been subject to Quaternary extension and strike-slip. Plio-Quaternary trans-tension has been partitioned in the Çamardi area into sinistral strike slip on the 'small graben' and normal offset at the bounding scarps. Slickenline data suggests that elsewhere in the EFZ strain partitioning does not take place.
- Strike-slip may have resulted in block rotation within the hanging-wall of the half graben at Çamardi, but the evidence is not conclusive.
- Stream offsets are problematic (i.e. not clear 90^0 changes in flow direction), but could suggest a minimum of 2.4km of sinistral displacement on the 'small graben' since the deposition of Plio-Quaternary fans.
- Local stratigraphic relationships at Yalak River (Enclosure 2) enable the relative dating of fault activity on the 'small graben'. In future, fault activity could be chronologically dated using cosmogenic isotopic exposure age dating techniques.

- The current geomorphology of the EFZ was controlled by Plio-Quaternary normal and sinistral strike-slip faulting and was not the result of widespread glacial scouring of an older fault zone.

8.8 Definitions

1 **Transfer Zone**. In a regime of *en echelon* normal faulting, a locality where two discrete faults overlap, forming a ramp between footwall and hanging-wall.

2 **Stepover**. In a regime of *en echelon* normal faulting, where two discrete faults overlap and step towards either the hangingwall or footwall.

3 **Linking faults**. A fault formed where two normal faults grow towards each-other, overlap and join via a short-cut (linking) fault, thereby creating a single fault from two previously discrete ones.

4 **Base level**. The theoretical limit or lowest level to which erosion on the Earth's surface constantly progresses but seldom, if ever, reaches. The level below which a stream cannot erode its bed.

5 **Knick point**. A point of abrupt change or inflection in the longitudinal profile of a stream or of its valley, resulting from rejuvenation (base level fall), glacial erosion or the outcropping of a resistant bed.

9 $^{40}Ar/^{39}Ar$ Radiometric dating of volcanic rocks from the Erciyes (Sultansuz) basin

9.1 Introduction

The Ecemiş Fault Zone *sensu-stricto* (as defined by Yetis 1984) extends as far north as Sulucaova (Fig. 2.4). However, it is now recognised that a northern continuation of the fault zone passes near Dundarli (Beyhan 1994) and into the Central Anatolian Volcanic Province (CAVP, Fig. 9.1, Koçyiğit & Beyhan 1998). The CAVP is recognised as a province of calk-alkaline, continental arc volcanism active during the Neogene, which has given rise to suites of andesites, ignimbrites and andesitic basalts (Pasquare *et al.* 1988). The EFZ intersects the CAVP at the Erciyes Basin, a 30km wide, 60 km-long fault-bounded basin (Fig. 9.2, Koçyiğit & Beyhan 1998). It has been suggested that this basin formed as a pull-apart on the left-lateral Central Anatolian Fault Zone, of which the EFZ is a part (Koçyiğit & Beyhan 1998, 1999).

The Erciyes Basin provides a unique opportunity to constrain the timing of Neogene fault activity on the northern continuation of the EFZ. Poor biostratigraphical control of the Upper Palaeogene and Neogene sediments elsewhere in the EFZ limits the usefulness of these sediments for constraining the timing of faulting. In the Erciyes Basin, however, the EFZ passes through a thick succession of ignimbritic tuffs, andesites and dacites, which are suitable for radiometric dating. A variety of stratigraphic relationships between the faults and these rocks enable temporal constraint on faulting in this area.

The aim of this chapter is to constrain the relative timing of extensional and strike-slip fault generation in the Erciyes Basin. The method of analysis is (a) single crystal $^{40}Ar/^{39}Ar$ dating of feldspars and biotites from tuffs and (b) bulk fusion and $^{40}Ar/^{39}Ar$

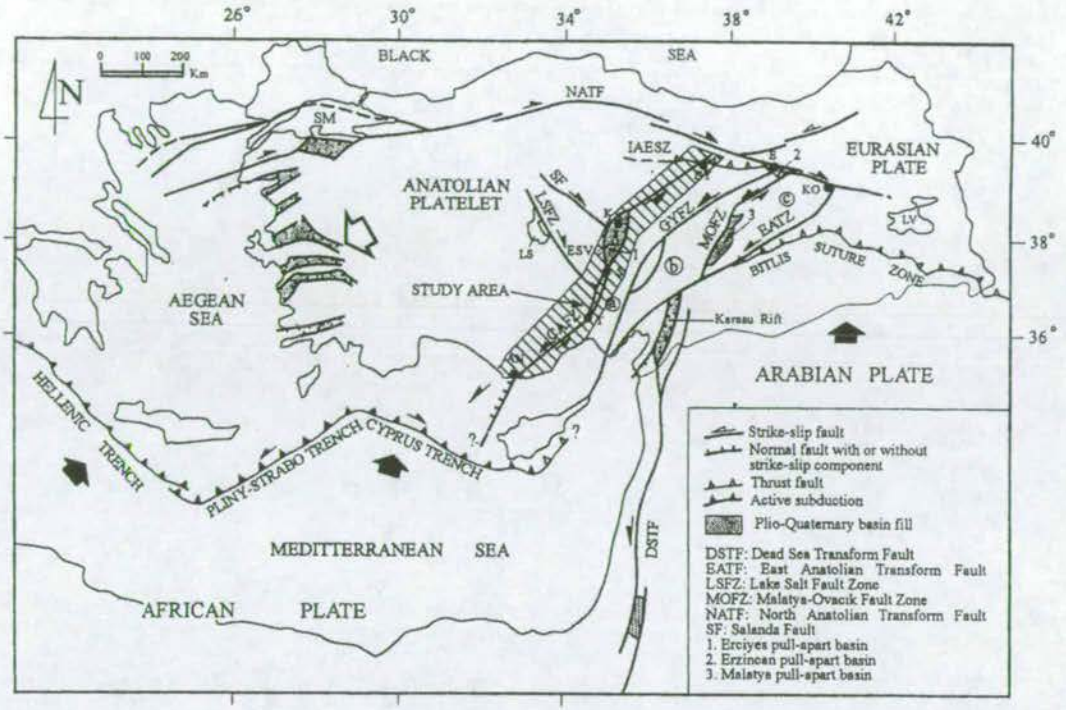

Figure 9.1 Simplified map showing major neotectonic structures of Turkey and adjacent areas, highlighting the Central Anatolian Fault Zone (after Kocyigit & Bayhan 1998). AN=Anamur, DY=Duzyayla, E=Erzincan, K=Kayseri, KO=Karliova, LS=Tuzgolu, LV=Lake Van, S=Sulucaova, SM=Sea of Marmara, T=Takir, a=Adana-Sivas block, b=Munzur block, c=Keban block, CAFZ=Central Anatolian Faut Zone, ESVC=Erciyes Strato-volcano complex, GYFZ=Goksu-Yazyurdu Fault Zone, IAESZ=Izmir-Ankara-Erzincan Suture Zone. Closed black arrows show motion senses of both the African and Arabian plates, large open arrows show escape sense of Anatolian plate.

dating of feldspars from lavas. The approach is to focus on specific localities within the Erciyes Basin where stratigraphic relationships enable the sampling and dating of pre-fault, syn-fault and post-fault volcanic and volcanogenic rocks, and thereby constrain the timing of faulting. Details of previous radiometric dating in this region are given (the results of previous stratigraphic work in the region have been summarised in Chapter 3). A rationale for new radiometric dating is given, techniques and results are described, followed by a discussion of their implications for the evolution of the Ecemiş Fault Zone.

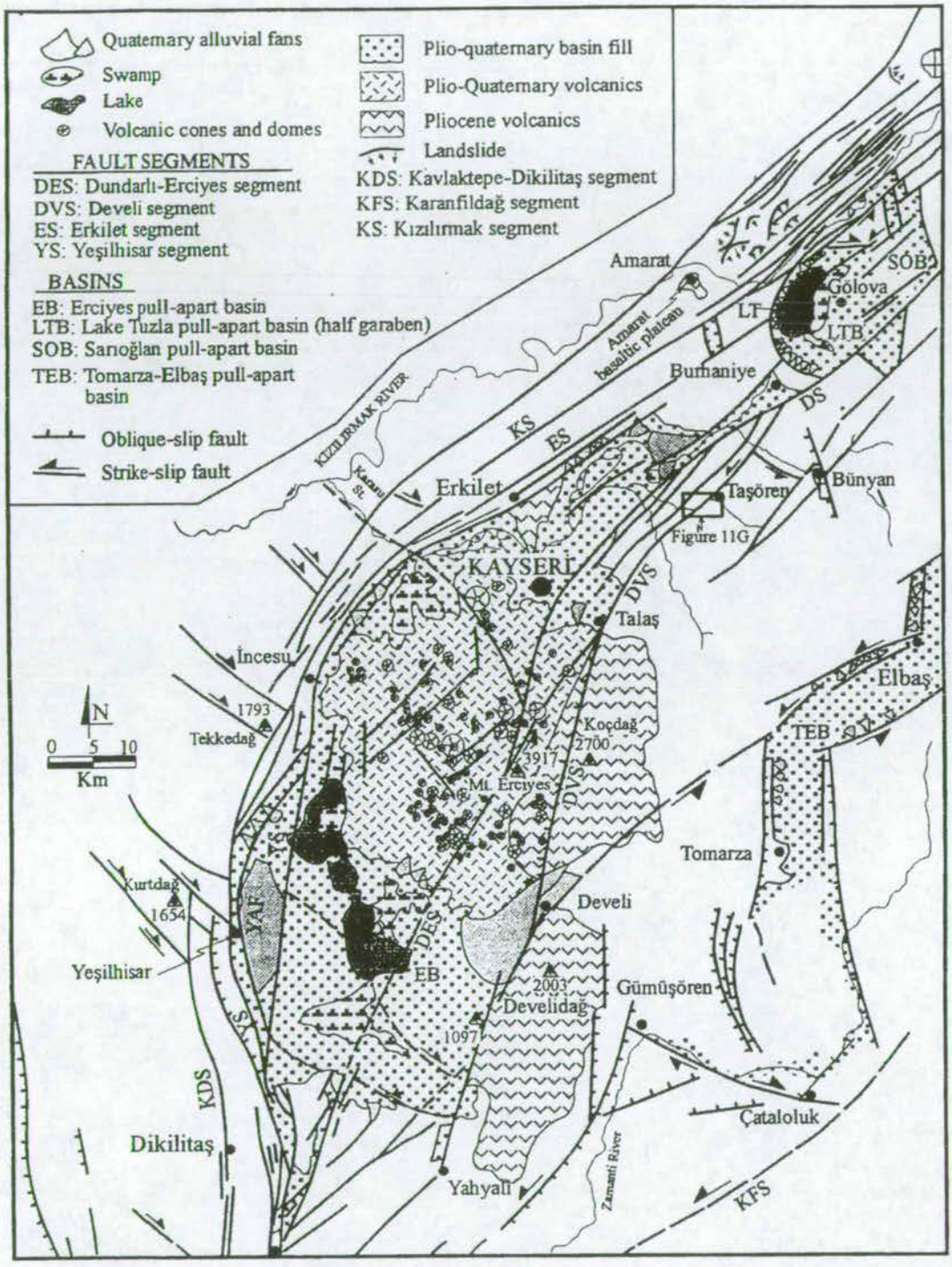

Figure 9.2 Structural map of the Erciyes Basin (after Kocyigit & Beyhan 1998). Normal faults have been inferred along the boundaries of the basin, and strike-slip faults through the centre of the basin.

9.2 Previous radiometric work

$^{40}K/^{40}Ar$ techniques have been used to obtain radiometric ages from tuffs and lavas of the Central Anatolian Volcanic Province, so as to document the timing of volcanic activity (Innocenti *et al.* 1975). The EFZ runs through the Central Anatolian Volcanic Province in the vicinity of the Erciyes Basin. Work by Innocenti *et al.* (1975) dated volcanic rocks throughout the Urgup-Kayseri-Erciyes area (results are tabulated in Fig. 9.3, see Fig. 9.4 for sample location sites). $^{40}K/^{40}Ar$ dating revealed that calk-alkaline volcanism was active in this area from Late Miocene to Holocene times.

Sample	Stratigraphic Unit	Rock Type	K/Ar Age (Ma)
KY1	Akkoy Fm.	Rhyolitic Ignimbrite	8.5±0.2
KY4	-	Andesitic lava	5.0±0.3
U60	-	Andesitic lava	5.1±0.1
U64	-	Andesitic lava	5.0±0.3
U78	-	Andesitic lava	5.5±0.2
U79	Valibaba Tepe Fm.	Ignimbrite	2.7±0.1
U83	-	Dacitic lava	0.9±0.2
U84	-	Andesitic lava	0.3±0.1
U115	Valibaba Tepe	Ignimbrite	2.8±0.1

Figure 9.3 Previous $^{40}K/^{40}Ar$ radiometric ages from volcanic rocks in the Erciyes basin area (after Innocenti et al. 1975). See Fig. 9.4 for location sites of these samples.

However, the previous dating of tuffs and lavas was not carried out with reference to the Ecemiş Fault system, and no attempt was made to constrain the timing of faulting using stratigraphic relationships.

The $^{40}K/^{40}Ar$ technique has been criticised by McDougall & Harrison (1988) as analysis requires the calculation of the absolute abundance of both ^{40}K and ^{40}Ar. The measurement of the absolute abundance these elements is notoriously difficult to

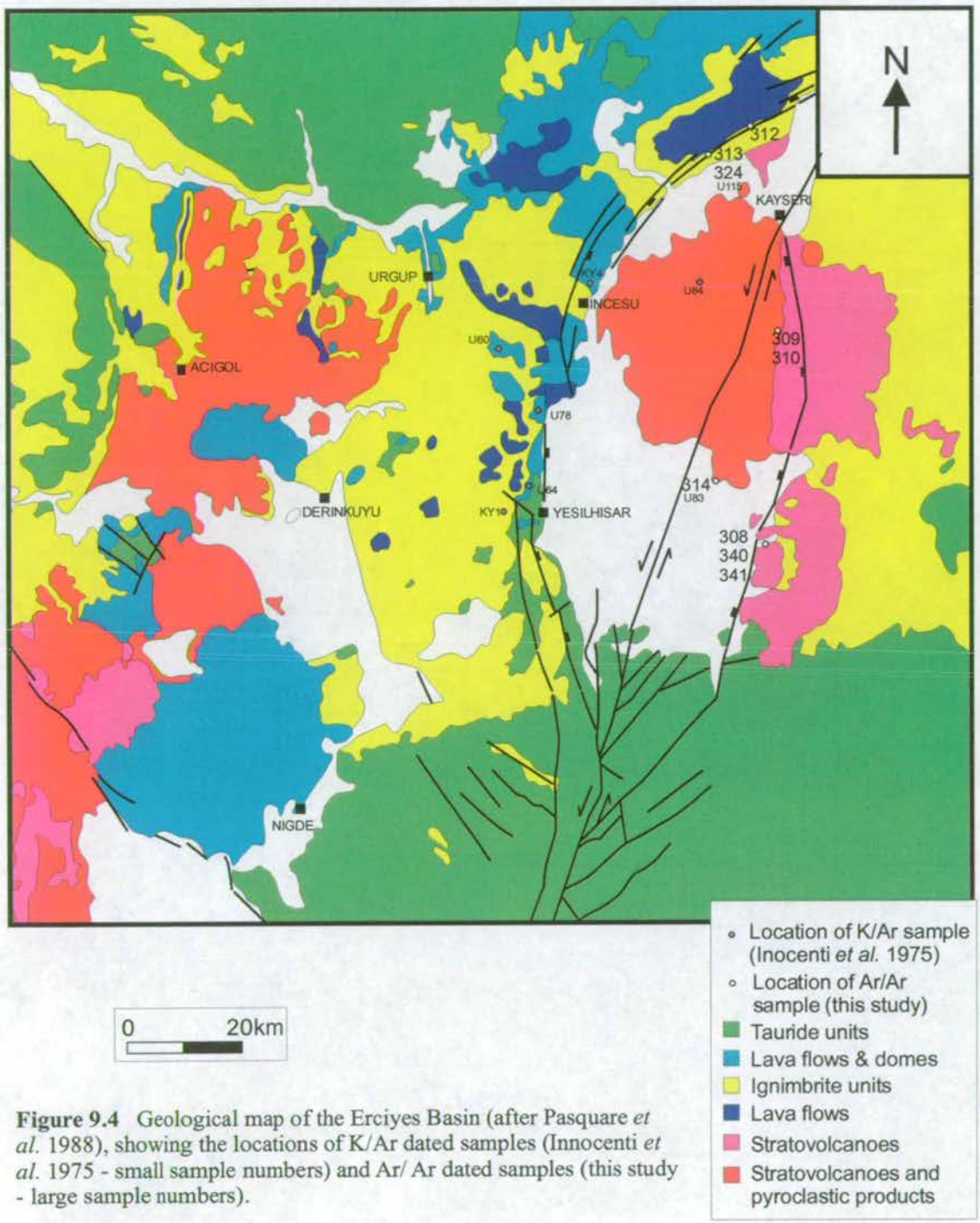

Figure 9.4 Geological map of the Erciyes Basin (after Pasquare *et al.* 1988), showing the locations of K/Ar dated samples (Innocenti *et al.* 1975 - small sample numbers) and Ar/ Ar dated samples (this study - large sample numbers).

calculate as a percentage of the sample is inevitably lost during preparation. Consequently the $^{40}K/^{40}Ar$ technique has tendency to underestimate the abundance of ^{40}K and to give ages which are too young.

Smaller $^{40}K/^{40}Ar$ dating studies have been carried out on the volcanic products of the Central Anatolian Volcanic Province by Besang *et al.* (1977), Batum (1978) and Ercan *et al.* (1990). However, these were not carried out with reference to the Ecemiş fault zone.

More recent work by Toprak & Göncüoğlu (1993) attempted to constrain the timing of faulting within the Central Anatolian Volcanic Province to the west of the Erciyes Basin. Using $^{40}K/^{40}Ar$ data from Besang *et al.* (1977) they constrain the end of NE-SW striking normal faulting (EFZ trend) at 6.5±0.2Ma to 5.5±0.2Ma (Messinian), using overlying relationships of unfaulted- above faulted tuffs. They conclude that all faults other than the EFZ and Tüzgolü Fault were inactive during the Late Pliocene – Quaternary. Evidence cited for the continued activity of these two fault zones during the Quaternary include lines of cinder cones identified using satellite images and inferred to overly deep tension fractures (Dhont *et al.* 1998).

9.3 *Justification for new $^{40}Ar/^{39}Ar$ dating*

Recent structural interpretations of the northern continuation of the EFZ indicate that the fault zone bifurcates as it joins the south of the Erciyes Basin and enters the Central Anatolian Volcanic Province (Fig. 9.1, Koçyiğit & Beyhan 1998). The bounding faults of the Erciyes Basin are interpreted as normal faults, with strike-slip movement partitioned into a fault strand cutting through the centre of the basin which has accommodated very little vertical offset (Fig. 9.2).

There is a consensus amongst previous workers that the Central Anatolian Volcanic Province developed through a three phase history: one of initial andesitic effusive activity (Early Miocene), followed by the deposition of a thick ignimbrite and tuff sequence (Late Miocene) and finally the development of andesitic-basaltic stratovolcanoes (Pliocene - Quaternary) (Innocenti *et al.* 1975, Pasquare *et al.* 1998). A simplified rock relations diagram for the Erciyes Basin is shown in Fig. 9.5. As yet, however, these volcanic products have not been used to constrain the timing of movement on the EFZ. Considerable controversy has surrounded the timing of movement on the EFZ during the Cenozoic (Koçyiğit & Beyhan 1998, Westaway 1999). As the fault zone is mostly exposed in terrestrial red beds throughout its course, it is difficult to use stratigraphic relationships to accurately constrain the timing of faulting. Only here in the Erciyes Basin do the rocks allow the accurate constraint of the timing of motion on the EFZ.

During this study several sites were documented within the Erciyes Basin where faulted (pre-rift) airfall tuffs, tuffaceous sediments and lavas could be separated from overlying un-faulted (syn-rift and post-rift) tuffaceous sediments and lavas. Samples from these sites were used to constrain the timing of initiation and cessation of movement on faults at the margins and in the centre of the Erciyes Basin. The exact field relations are described in section 9.5.

9.4 $^{40}Ar/^{39}Ar$ radiometric dating theory (after Faure 1986)

The $^{40}Ar/^{39}Ar$ technique provides a means of dating the crystallisation ages of igneous minerals based on the decay of ^{40}K to ^{40}Ar. In this study, the technique was used to date the timing of extrusive magmatism in the Erciyes basin. This study was funded by an N.I.G.L. grant awarded to Professor A.H.F. Robertson and N. Jaffey, and carried out in collaboration with Dr. Malcolm Pringle at SUERC, East Kilbride.

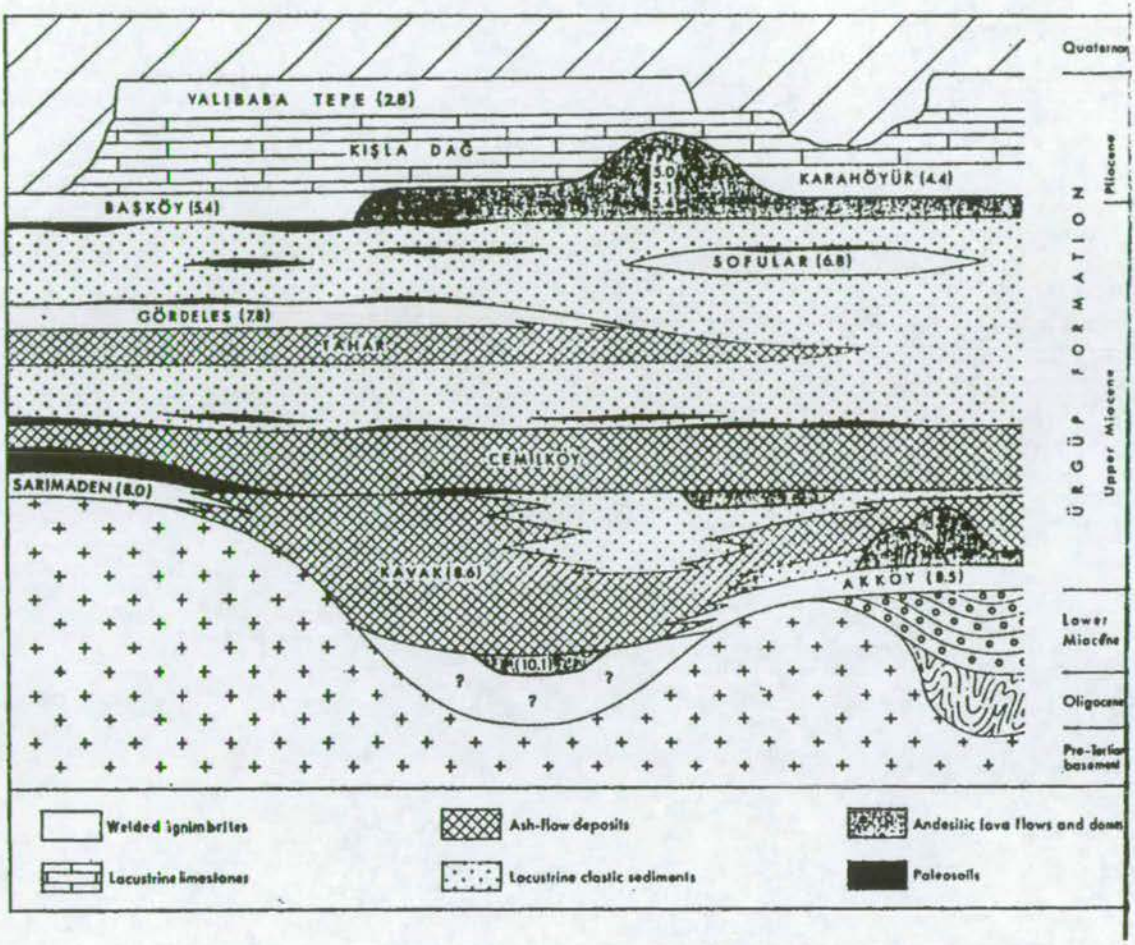

Fig. 9.5 Rock relations diagram for the Oligocene - Recent stratigraphy of the Erciyes Basin area, from west (left) to east (right), after Innocenti *et al.* (1975). Numbers in brackets indicate the age in Ma. Names of members are after Pasquare *et al.* (1988).

^{40}K /^{39}Ar geochronology is based on the decay of radioactive ^{40}K to ^{40}Ar where the age of the rock or mineral can be calculated by measuring the amounts of two Isotopes using equation 1

$$t=1/\lambda \ln[c(^{40}Ar/^{40}K)+1] \quad (1)$$

where λ is the total decay constant of ^{40}K, c is a constant (total decay constant for ^{40}K divided by the decay constant of ^{40}K to ^{40}Ar). It is assumed that no ^{40}Ar or ^{40}K has been lost or added since the system passed through its closure temperature, that no ^{40}Ar was

incorporated into the mineral at the time of formation (Ar is inert) and that corrections are made for atmospheric ^{40}Ar.

$^{40}Ar/^{39}Ar$ geochronology relies on the same decay process and the same assumptions, but has major advantages over $^{40}K/^{40}Ar$. For example, with the $^{40}Ar/^{39}Ar$ technique one measures the ratio of $^{40}Ar/^{39}Ar$ in a mass spectrometer which is more accurate than measuring the amounts of ^{40}K and ^{39}Ar separately. Also $^{40}Ar/^{39}Ar$ dating can be performed on single crystals rather than bulk samples. This has particular advantages in volcanic rocks erupted through and onto older basement where there may be incorporation of xenocrysts, since a number of individual crystals are dated and xenocrysts can be identified by their erroneous ages. Such rocks are common in Central Turkey and the $^{40}Ar/^{39}Ar$ technique was employed to overcome these problems.

The method of $^{40}Ar/^{39}Ar$ geochronology is to bombard the sample with fast neutrons in a nuclear reactor such that $^{39}K(n,p)> {}^{39}Ar$. The ratio of ^{39}K to ^{40}K is a constant such that equation 1 can be modified to

$$t = 1/\lambda \ln[J(^{40}Ar_{rad}/^{39}Ar_k)+1] \qquad (2)$$

$^{40}Ar_{rad}$ = radiogenic ^{40}Ar
$^{39}Ar_k$ = ^{39}Ar derived from ^{39}K

where J is a parameter that relates to the neutron flux density and can be calculated along the length of the irradiated vial including a number of standard crystals of known age. $^{40}Ar_{rad}/^{39}Ar_k$ is calculated from the total $^{40}Ar/^{39}Ar$ measured in the mass spectrometer by making corrections for air, K an Ca.

The $^{40}Ar/^{39}Ar$ technique, using single crystal total laser fusion has the advantage that it allows the elimination of xenocrystic contamination from underlying metamorphic

basement rocks. This is achieved by the fusion of individual grains, which allows erroneously old grains (xenocrysts) to be removed from the age calculation.

9.5 Methodology

Samples were carefully chosen for their ability to constrain the timing of faulting, i.e. pre-rift, syn-rift or post-rift close to identified fault lines. The locations of samples are illustrated in Fig. 9.4 and stratigraphic relations for important sites are shown in Fig. 9.6-9.8. The grid reference and stratigraphical significance of each sample is tabulated in Fig. 9.9. The timing of faulting at the boundaries of the Erciyes Basin is constrained by faulted hangingwall and footwall tuffs (samples 312, 313 and 324) and by overlying (draping) un-faulted lavas at Zile (samples 340, 341, and 314, Fig. 9.4). This relationship is best seen at Zile (Fig. 9.6), but unfortunately faulted tuffs in this area were too altered for analysis. Therefore, tuffs from the eastern side of the basin (Eriklet and Oymagaac) were used, where the same stratigraphic relationship was seen (Fig. 9.7). Material forming the tilted fault blocks and overlying lavas at the basin margins have been mapped as the same units on either side of the basin by Pasquare (1988).

The main strike-slip lineament of the CAFZ is inferred to outcrop on the flanks of Mt. Erciyes, in the centre of the Erciyes Basin (Fig. 9.2). Outcrops of this fault strand were found where the timing of faulting could be constrained by pre-rift (sample 310) and post-rift (sample 309) unconsolidated tuffaceous sediments on the eastern flanks of Mt. Erciyes (Fig. 9.8).

The samples which were finally dated were from silicic airfall tuffs, tuffaceous sediments and dacitic lavas. Samples were crushed using a jaw crusher and ground using a ceramic shaker mill for 30 seconds. Feldspar and biotite crystals were separated using a magnetic separator, feldspars were cleaned in dilute HCl, then large euhedral

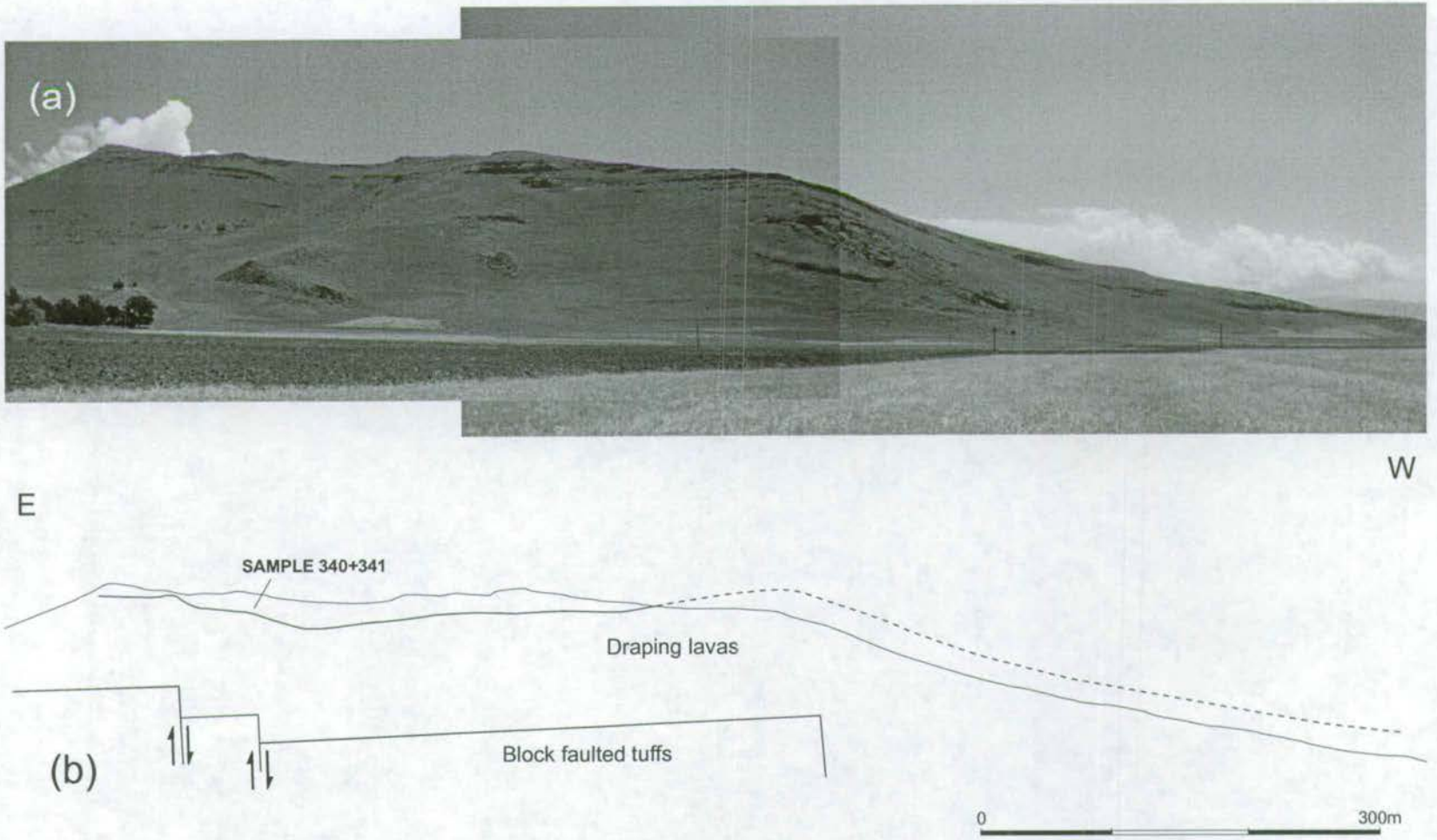

Fig. 9.6 Field observations of the relationship between tilted and faulted underlying tuffs and draping overlying lavas at Zile (eastern margin of the Erciyes basin). **(a)** Photograph looking south. **(b)** line diagram representation of block faulted tuffs and draping dacitic lavas. Samples 340 and 341 were taken from the draping lavas at Zile.

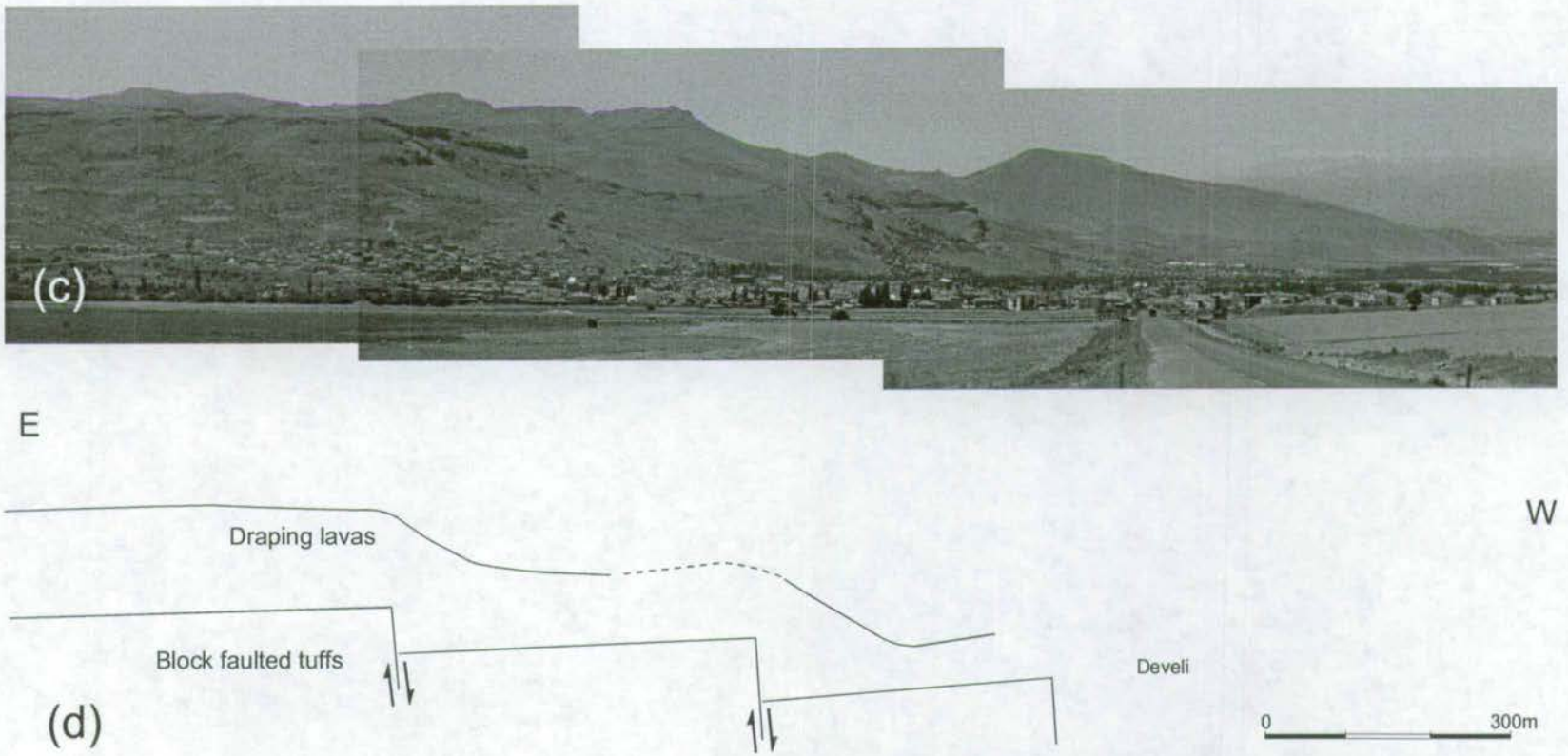

Fig. 9.6 Field observations of the relationship between tilted and faulted underlying tuffs and draping overlying lavas at Develi (eastern margin of the Erciyes basin). **(c)** Photograph looking south. **(d)** line diagram representation of block faulted tuffs and draping dacitic lavas.

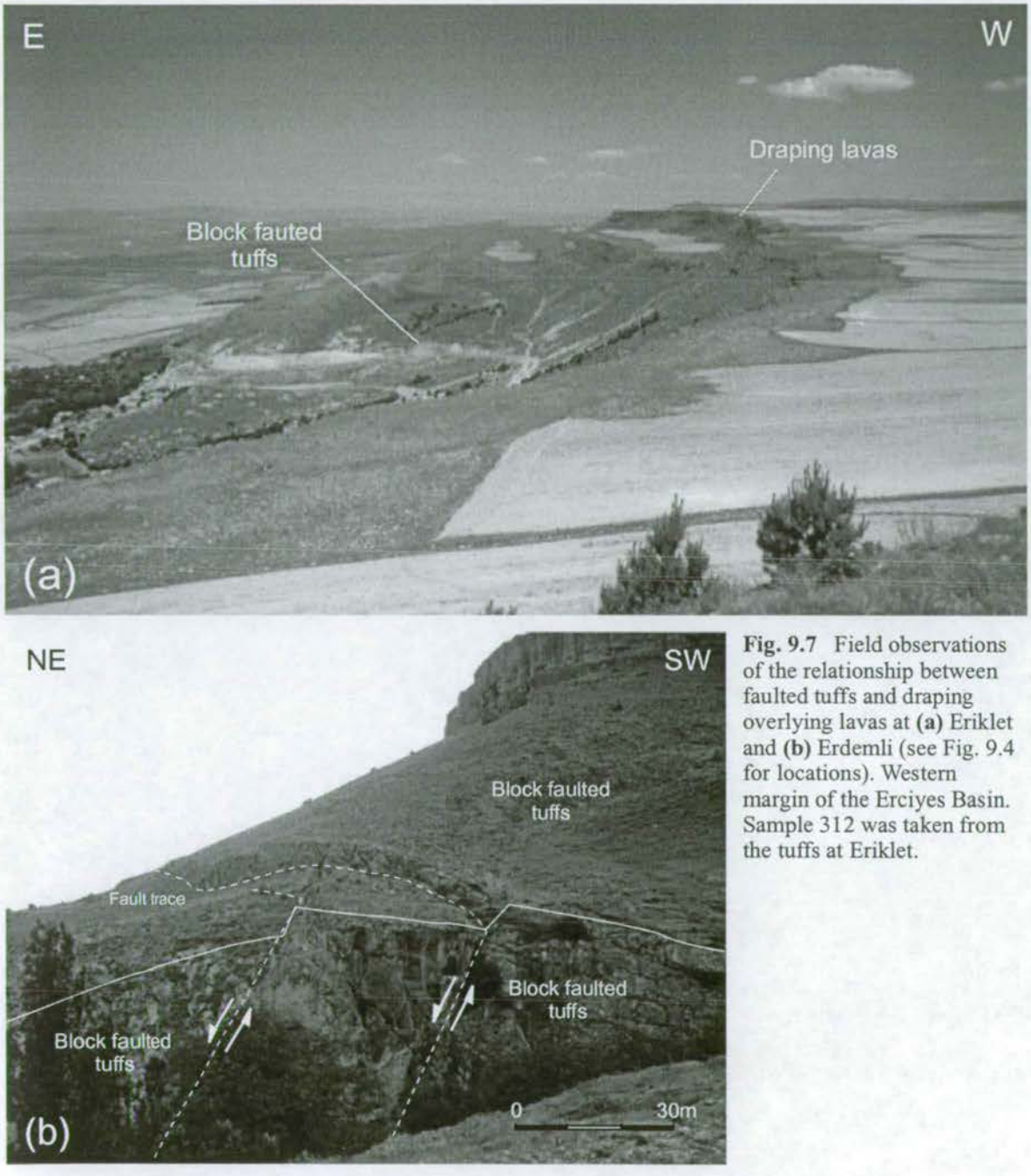

Fig. 9.7 Field observations of the relationship between faulted tuffs and draping overlying lavas at **(a)** Eriklet and **(b)** Erdemli (see Fig. 9.4 for locations). Western margin of the Erciyes Basin. Sample 312 was taken from the tuffs at Eriklet.

Fig. 9.8 **(a)** and **(b)** Normal faulting at Erciyes Dag (central Erciyes Basin, see Fig. 9.4 for location). Underlying tilted fault blocks (pre-rift) and overlying draping unit (post rift) are both composed of tuffaceous sediment **(c)**, comprising clasts of tuff in a tuffaceous sandy matrix. Sample 310 was taken from pre-rift, and sample 309 from the post-rift unit.

feldspars and euhedral biotites were picked under a light microscope. Attempts were made to separate plagioclase from sanidine crystals using a Beckeline test in clove oil, and by identifying lamellar twinning under a light microscope. Feldspars and biotites were then irradiated and single crystals from tuffs were analysed by laser step heating or laser degassing followed by laser fusion. The isotopic ratios of resultant gases were measured using a static vacuum collector mass spectrometer. Feldspar crystals from the dacitic lavas were of a poorer quality and these were analysed by degassing and bulk fusion using a furnace. $^{40}Ar/^{39}Ar$ ages and errors were calculated using standard techniques and corrections after Dalrymple *et al.* (1981).

9.6 Results

The results of the $^{40}Ar/^{39}Ar$ analyses are tabulated in Appendix 5 and summarised in Fig. 9.9 and 9.10.

9.6.1 Consistency of results

Single crystal total fusion of plagioclase crystals from tuffs gave relatively closely grouped age results with the exception of samples 310 and 313. Sample 310 is a tuffaceous sediment and contained three xenocrysts with old ages (11.89, 7.30 and 7.13Ma). Sample 313 contained one old xenocryst (10.58Ma). Single crystal biotites analysed by step heating and by total fusion after degassing generally gave a wider scatter of results and consistently older ages than plagioclase crystals (Fig. 9.10).

9.6.2 Step-heating profiles on single crystal biotites and feldspars

In order to assess the degree of alteration of biotite crystals, two step-heating experiments were carried out on biotites from Sample 313. These resulted in step-heating profiles with a consistent plateau age. The first two to three steps gave young ages, a result of surficial alteration of the biotite crystal. Step-heating on single crystal

Sample	Mineral	Age (Ma)	Location (G.Ref.)	Stratigraphic Significance
217	Feldspar	6.06±0.09	35°08' – 38°02'	Tuff clast in fluvial conglomerate
217	Biotite	7.04±0.16	35°08' – 38°02'	Tuff clast in fluvial conglomerate
309	Feldspar	1.43±0.29	35°33' - 38°32'	Unconsolidated tuffaceous sediment on central fault. Post-rift.
310	Feldspar	1.61±0.24	35°33' - 38°32'	Unconsolidated tuffaceous sediment on central fault. Pre-rift.
312	Feldspar	5.75±0.05	35°27' - 38°49'	Pre-rift airfall tuff. Footwall.
312	Biotite	7.36±0.47	35°27' - 38°49'	Pre-rift airfall tuff. Footwall.
313	Feldspar	7.21±0.13	35°20' - 38°46'	Pre-rift airfall tuff. Hangingwall
313	Biotite	8.08±0.17	35°20' - 38°46'	Pre-rift airfall tuff. Hangingwall
314	Feldspar	1.29±0.05	35°30' - 38°23'	Post-rift draping lavas
324	Feldspar	6.97±0.09	35°20' - 38°46'	Pre-rift airfall tuff. Footwall
340	Feldspar	6.29±0.06	35°27' - 38°16'	Post-rift draping lavas
341	Feldspar	5.80±0.11	35°27' - 38°16'	Post-rift draping lavas

Figure 9.9 Grid references and straitigraphic significance of samples of tuffs and lavas from the Erciyes Basin. See Fig. 9.4 for sample location sites.

biotites shows that the majority of the crystals have undergone minor amounts of alteration, the effects of which can be removed by a 'degassing step'. Simple total fusion experiments on such slightly altered grains would, therefore, have given ages which were too young.

Step heating was also carried out on feldspar crystals. The number of degassing steps required to reach a plateau age was found to be consistently less than that required for biotite crystals, suggesting that biotites had undergone a greater degree of alteration.

Sample No.	Mineral	Location	Lithology	Age (Ma)
217	Feldspar	Hacibeyli	Acidic Tuff	6.06±0.09
217	Biotite	Hacibeyli	Acidic Tuff	7.04±0.16
309	Feldspar	Erciyes Dağ (post-rift)	Tuffaceous Sediment	1.43±0.29
310	Feldspar	Erciyes Dağ (pre-rift)	Tuffaceous Sediment	1.61±0.24
312	Feldspar	Eriklet	Acidic Tuff	5.75±0.05
312	Biotite	Eriklet	Acidic Tuff	7.36±0.47
313	Feldspar	Oymagaac	Acidic Tuff	7.21±0.13
313	Biotite	Oymagaac (hangingwall)	Acidic Tuff	8.08±0.17
314	Feldspar	Develi	Dacitic Lava	1.29±0.05
324	Feldspar	Oymagaac (footwall)	Acidic Tuff	6.97±0.09
340	Felspar	Zile	Dacitic Lava	6.29±0.06
341	Feldspar	Zile	Dacitic Lava	5.80±0.11

Figure 9.10 Results of $^{40}Ar/^{39}Ar$ radiometric dating of tuffs and lavas from the Erciyes Basin. See Fig. 9.4 for sample location sites.

9.6.3 Analysis of Results

Some explanation must be given to explain why single crystal plagioclase ages are consistently younger than single crystal biotite ages from the same sample (Fig. 9.10, samples 217, 312 and 313). Four hypotheses are considered:

Hypothesis A

Biotite crystals are all xenocrysts from underlying rock units which have been incorporated into the erosive pyroclastic flows. Plagioclase crystals are *in situ* and represent the true age of volcanism.

Supporting arguments:

- Biotites show a greater spread of ages than plagioclase crystals.

Conflicting arguments:

- Biotites give relatively consistent ages with a maximum of 1-2 obvious xenocrysts.
- No entrained basement clasts are seen within the tuff units in the field.

Hypothesis B

All crystals are variably altered, giving erroneously young ages. The oldest biotites indicate the age of volcanism most closely.

Supporting arguments:

- Degassing experiments show that all crystals have suffered some alteration.

Conflicting arguments:

- MSWD ('Mean Standard Weighted Deviates', a measure of internal consistency of crystal ages within a sample) indicates that biotites have a wider age scatter than plagioclase crystals, and give generally less reliable ages.
- There are very few old biotites (1-2max. per sample) and these are much older than the majority of biotites, therefore unlikely to represent the true age of volcanism.

Hypothesis C

All plagioclase crystals are altered, giving erroneously young ages. The oldest biotites are xenocrysts. Only the younger biotites record the true age of volcanism.

Supporting arguments:

- Not much.

Conflicting arguments:

- Step-heating experiments suggest that alteration effects are removed by the degassing step.
- Plagioclase crystals give consistent ages.

Hypothesis D

Biotites have acquired excess ^{40}Ar from country rock contamination of the magma chamber. This has biased the Ar ratios, resulting in artificially old biotite ages.

Supporting arguments:

- Biotites crystals are consistently older than plagioclase crystals in all samples.

Conflicting arguments:

- No primary evidence, i.e. magma chamber is not exposed

Hypothesis E

Biotites are more altered than feldspars. This alteration, and the presence of clay minerals has lead to 'Ar recoil' during irradiation, giving the biotites erroneously old ages (McDougall & Harrison 1988).

Supporting arguments:

- Biotites from all samples have a low K/Ca ratio, too low for fresh biotites.
- At least one half of the total gas released from biotites is released during the degassing steps. This indicates that biotites are significantly altered.
- Degassing experiments have shown that biotite crystals are more altered than feldspar crystals.

Conflicting arguments:

- Not much.

I favour a combination of hypotheses D and E, as the consistent difference between biotite and plagioclase ages does not appear to be associated with xenocrysts or alteration. The process of ^{40}Ar acquisition is well documented by McDougall & Harrison (1988). Biotite ages are therefore taken to be less reliable than feldspar ages, which are accepted as the true ages of tuff samples.

Radiometric age results from the Erciyes Basin are summarised in Fig. 9.9, along with the exact location and stratigraphic significance. Samples from the faulted acidic tuff

unit exposed adjacent to the bounding normal faults of the Erciyes Basin (samples 312, 313 and 324) have ages between Late Tortonian and Early Messinian. Samples from Oymagaac (Fig. 9.4) are Tortonian (7.21±0.13 and 6.97±0.09Ma) and samples from Eriklet (Fig. 9.4) are Messinian (5.75±0.05). These disagree with $^{40}K/^{40}Ar$ ages for the same sample sites (Innocenti *et al.* 1975) who give ages of 2.8±0.7Ma (Late Pliocene) for the same rocks (Fig. 9.3). It is, however, in general agreement with the accepted volcanic stratigraphy of the area, which described pyroclastic deposition during the Late Miocene (Pasquare *et al.* 1988, Innocenti *et al.* 1975).

Samples from the overlying (draping), un-faulted lavas at Zile and Develi (samples 340, 341, 308 and 314) have Early Messinian (6.29±0.07 and 5.80±0.11) and Early Pleistocene (1.29±0.05) ages, respectively. These do not conflict with published $^{40}K/^{40}Ar$ ages for the same units (Fig. 9.3), which date the lava flows as Early to Mid-Pliocene (Innocenti *et al.* 1975) despite the fact that they are significantly older, and younger. Combined results indicate that andesitic-basaltic extrusive volcanic activity was occurred between the latest Miocene until the early Pleistocene.

Two samples were taken from the central Erciyes Basin, flanking the Erciyes volcano. These are unconsolidated tuffaceous sediments and constrain the timing of a late phase of normal faulting, in that sample 310 is faulted (pre-rift) and sample 309 is un-faulted (syn-rift and post-rift) (Fig. 9.4, 9.8). The high level of alteration in all crystals, the young age of the samples and the low K composition of the minerals (Ca-rich plagioclase, as opposed to K-rich sanidine) mean that less ^{40}Ar gas was available for analysis and subsequently calculated ages are less accurate than those of other samples. Within error the two samples have a synchronous early Pleistocene crystallisation age (1.61±0.24 pre-rift and 1.43±0.29 post-rift) but this should be seen as a minimum deposition age as the sample is a fluvially transported sediment. These ages (early Pleistocene) are significantly younger than those of the basin bounding tuffs and younger than some lavas, but older than the youngest lavas. They correspond to the

Quaternary volcanic products of the Erciyes strato-volcano described by other workers (Pasquare *et al.* 1988, Innocenti *et al.* 1975).

9.7 *Implications of new ages on the timing of faulting*

New $^{40}Ar/^{39}Ar$ dates from the Erciyes Basin have allowed a more accurate determination of the timing of faulting at the basin margins and on faults in the centre of the basin. Normal faulting appears to have been active along the basin margins (Fig. 9.4), where tilted fault blocks of Late Tortonian to Early Messinian tuff and tuffaceous sediment are draped by un-faulted Early Messinian to Early Pleistocene andesitic-dacitic lava flows (Fig. 9.6). This constrains the timing of normal faulting at the basin margins as Early Messinian (latest Miocene).

The centre of the basin (Mt. Erciyes area) has also been affected by (minor) normal faulting associated with left-lateral strike-slip faulting (Fig. 9.2, Koçyiğit & Beyhan 1998). Both pre-rift and post-rift tuffaceous sediments from this area have an Early Pleistocene crystallisation age. This indicates that tuffs were eroded, re-deposited and then faulted after the early Pleistocene. The small scale of the outcrops limits the extent to which these dates can be used to constrain the timing of faulting within the centre of the Erciyes Basin.

Faults within the Erciyes Basin have been identified as the northern continuation of the EFZ, therefore it is inferred that the timing of faulting here may correspond to periods of faulting further south within the EFZ. Results from new radiometric dating agree with results from slickenline (Chapter 7) and sedimentological analysis (Chapter 4), in that there is evidence for fault activity in the latest Miocene/earliest Pliocene, and also more recently, during the Pleistocene ('small graben' faulting?). Radiometric data does not help to constrain the timing of slip on the EFZ prior to the Neogene.

9.8 Conclusions

- Single crystal $^{40}Ar/^{39}Ar$ dating is able to identify xenocrystic contamination and is, thus, essential for constraining the timing of extrusive volcanism in relation to the timing of offset on the Central Anatolian Fault Zone (the northern continuation of the EFZ).
- Scatter in the data is ascribed to some form of xenocrystic contamination. Differences between the ages of feldspars and biotites from the same sample are ascribed to alteration of biotites leading to '^{40}Ar recoil' and also to excess ^{40}Ar in biotites, acquired by country rock contamination of the magma chamber.
- New $^{40}Ar/^{39}Ar$ dates from feldspars and biotites have yielded reliable Late Miocene to Quaternary ages taken from airfall tuffs, tuffaceous sediments and extrusive lavas.
- The timing of normal faulting along the boundaries of the Erciyes Basin is constrained at Early Messinian (Latest Miocene) in the northern half of the basin.
- Minor normal faulting within the centre of the basin (suggested to be associated with sinistral strike-slip) occurring during the Early Pleistocene. The lack of suitable outcrop in the centre of the basin does not allow the accurate constraint of the timing of faulting in this area prior to the Quaternary.

10 Total offset and piercing points on the Ecemiş Fault Zone

10.1 Introduction

In order to assess the relative importance of the EFZ compared to other regionally significant strike-slip lineaments, its timing and total offset must be measured. This chapter aims to critically assess previously published total offset estimates and to use new structural and sedimentological data to propose new piercing points and estimates of when slip occurred.

10.2 Published estimates

10.2.1 Early estimates of timing and offset

Yetiş (1984) proposed that the maximum of the strike slip offset on the Ecemiş Fault Zone occurred before the Lutetian (Middle Eocene), but after Palaeocene time (i.e. during the Early Eocene) with minor strike-slip and normal offset continuing during the Quaternary. This argument is based on the dissimilarity of the pre-Eocene stratigraphy in the Çamardi area to the east and west of the Ecemiş Fault Zone, and the apparent lack of offset of adjacent Lutetian to Recent deposits in the same area. Pre-Eocene rocks include the Ulukisla volcanic sequence in the western block and Aladağ carbonates in the eastern block (Fig. 10.1). The arguments of Yetiş (1984) are based on the assumption that the Middle Eocene Kaleboynu Formation is not offset by strike-slip across the EFZ. However, as discussed in Section 4.4.1.3, the two Middle Eocene outcrops in question (Evliya Tepe and Kaleboynu Tepe) show widely divergent facies of deposition, palaeocurrents and deformation characteristics (Section 4.3.1). The two outcrops instead, probably originated further apart and underwent separate strain histories prior to final strike-slip juxtaposition. The presence of significant populations

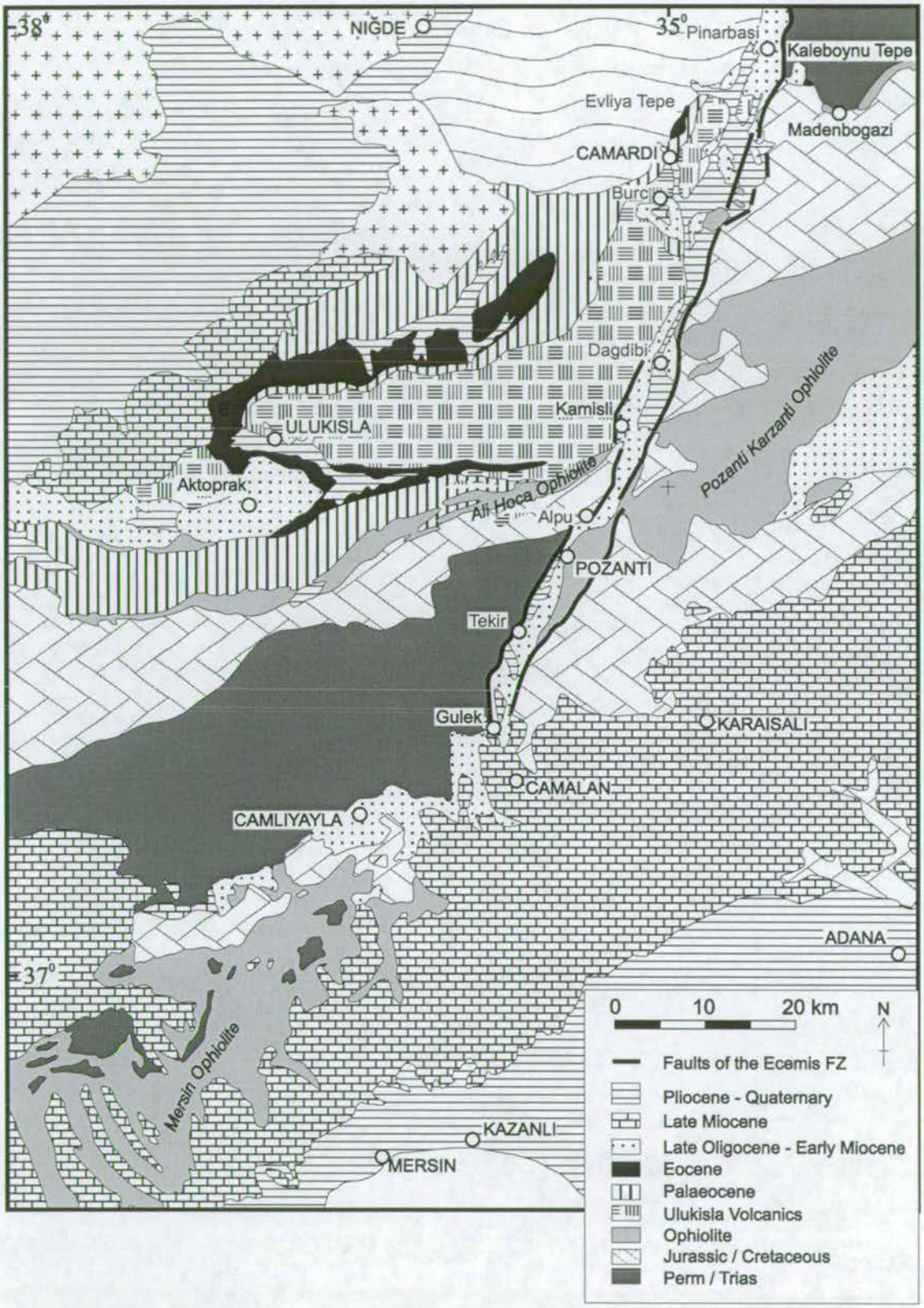

Figure 10.1 Geological map of the Adana region (after Ternek 1962), highlighting the locations of ophiolitic bodies and Tauride units.

of strike-slip faults within the Oligo-Miocene and Late Miocene units (Section 7.4) also indicates that significant strike-slip has occurred since the Middle Eocene.

Yetiş (1978) inferred 80±10km of total sinistral offset during the Early Eocene by correlating the contact between two Mesozoic limestones in the Aladağ (the Late Triassic – Early Jurassic Demirkazik limestone and Early Triassic Maden limestones) with "a possible continuation of this boundary" to the south of the Bolkardağ. The unspecific nature of the contact location does not allow this piercing point to be tested.

10.2.2 Correlation of ophiolites

Early total offset estimates traditionally used the correlation of the Pozanti-Karsanti ophiolite to the east of the Ecemiş Fault Zone with the Mersin ophiolite to the west (Fig. 10.1, Yetiş pers. com. 1997). This would result in a total sinistral offset of 80±10km. It has been proposed that the Late Cretaceous ophiolites of this region, including the Pozanti-Karsanti and Mersin ophiolites, were obducted as a single "continuous ophiolite complex" (Dilek & Moores 1987), ophiolite emplacement being synchronous over the entire area during Latest Cretaceous to Early Palaeocene time (Parlak & Delaloye 1996; Lytwyn & Casey 1995). Therefore, the apparent offset of ophiolite outcrops on either side of the fault zone (Fig. 10.1) may be the result of Tertiary differential uplift and erosion rather than strike-slip offset. Outliers of the Pozanti-Karsanti ophiolite occur in the form of thrusted horses as far north as Madenboğazi (Fig. 10.1) where they have been imbricated with Mesozoic platform carbonates during south-directed thrusting. The presence of these ophiolitic outliers renders a simple correlation of the large ophiolite outcrops across the EFZ problematic.

10.2.3 Recent estimates of timing and offset

Koçyiğit & Beyhan (1998) built on the enigmatic piercing points of Yetiş (1978), proposing a south-directed (north dipping) thrust fault involving Permian over Triassic rocks exposed on both sides of the Ecemiş Fault Zone as a piercing point, giving a total sinistral offset of 75km (Fig. 10.2a). They also made public the results of other workers, from private company reports which are not openly accessible (Gül *et al.* 1984, Fig. 10.3). Unfortunately the locations of the piercing points proposed in these reports were not given in Koçyiğit & Beyhan (1998) and their results remain untested.

The piercing points of Koçyiğit & Beyhan (1998) were criticised by Westaway (1999) who claimed that these thrust faults were previously mapped as conformable contacts (Demirtaşli *et al.* 1984, Tekeli *et al.* 1984). During this study the local geology of the piercing points proposed by Koçyiğit & Beyhan (1998) was examined in detail; the results are summarised in Fig. 10.4. The site at Tekir (west side of EFZ, Fig. 7.4, Section 7.3.3.1) closely matches the description of Koçyiğit & Beyhan (1998). However, their description of the eastern piercing point is less precise, allowing two possible localities: Upper Madenboğazi (Fig. 7.5, Section 7.3.3.2) and Uçukkaya Tepe (Fig. 7.10, Section 7.3.4.2) to be considered as the eastern piercing point (Fig. 10.4 for comparison). Neither of these candidates were found to correlate well with the Tekir site in the west, having different thrust fault geometries, different vergence directions and different rocks in the hanging-and foot-walls (Tekeli *et al.* 1984). These findings render the piercing points of Koçyiğit & Beyhan (1998) unreliable.

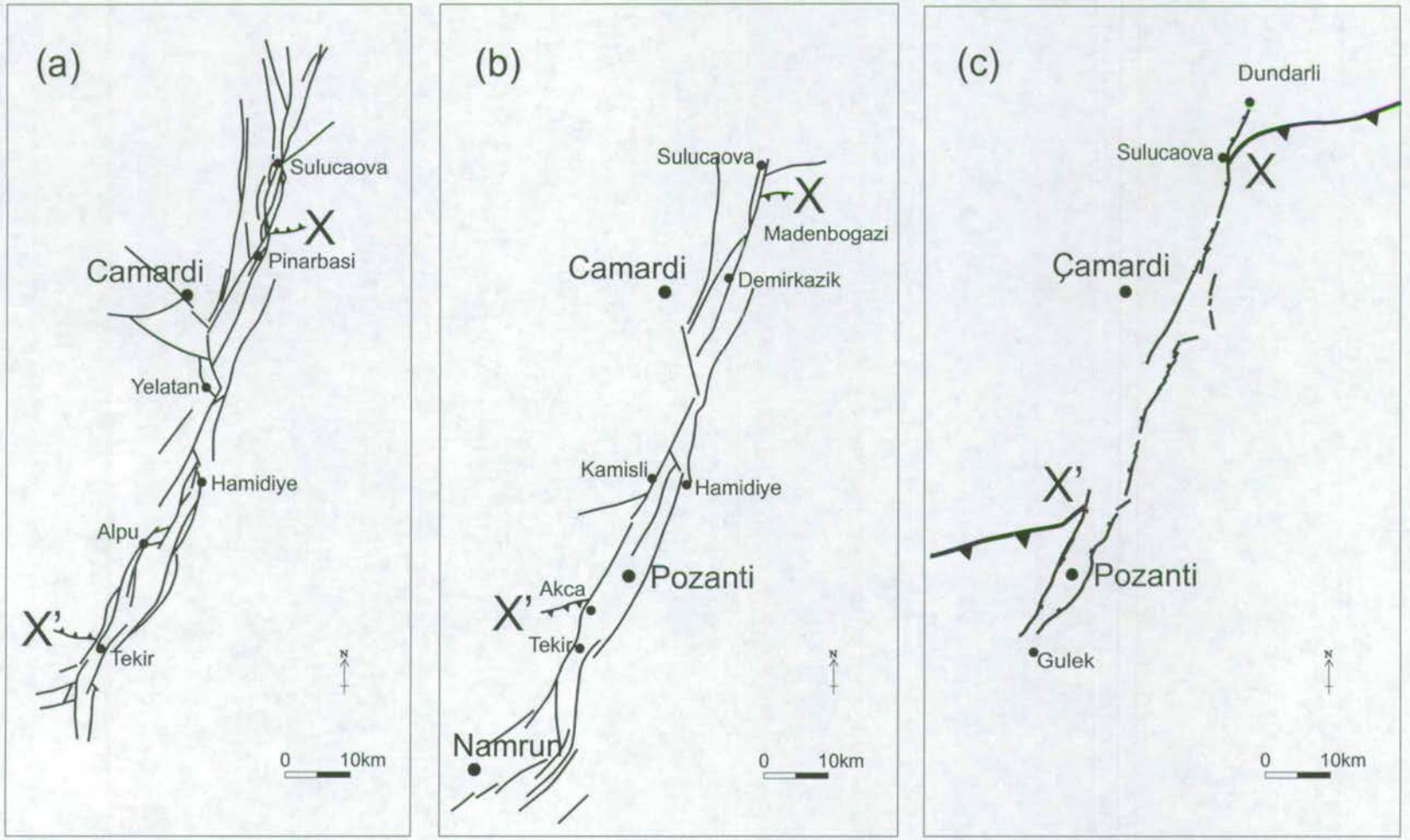

Figure 10.2 Proposed piercing points used to constrain the total offset on the EFZ: **(a)** Kocyigit & Beyhan 1998, **(b)** Kocyigit & Beyhan 1999, **(c)** This study and Westaway 1999.

Author/s	Timing of movement	Offset
Yetiş (1978, 1984)	Two phases of activity: • During Early Eocene • Quaternary	~80±10km total offset
Gül et al. (1984)	Three phases of activity: • Since Mesozoic • Since Miocene • Since Early Quaternary	75km total offset 24km 75m
Ozaner & Tüfekçi (1988)	Since Oligocene	?
Inan (1993)	Two phases of activity: • Since Oligo-Miocene • Since Early Quaternary	4km 0.5km
Koçyiğit & Beyhan (1998)	Three phases of activity: • Since Late Cretaceous • Since Miocene • Since Early Quaternary	75km total sinistral offset 24 km 3.1km
Westaway (1999)	Since Eocene	62km total sinistral offset
Jaffey (2000)	Continuous motion since at least Late Eocene.	60±5km total offset

Figure 10.3 Comparison of the estimates of total offset and timing of activity on the EFZ, made by previous workers.

Side of EFZ	West	East	East
Location of piercing point at EFZ	**Tekir**	Upper Madenboğazi, E of Pinarbaşi	Uçukkaya Tepe, E of Sulucaova
Orientation of thrust	dips to NE	dips to S	dips to S
Tectonic transport direction	to S	to S	to N
Nature of thrust	Simple flat plane thrust	Downward facing thrusted nappe	Simple flat plane thrust
Nature of associated folding	Tight overturned folds in footwall and hangingwall	Open folding in both footwall and hangingwall - no overturning	Tight overturned folds in both footwall and hangingwall
Hangingwall lithology	Highly metamorphosed pelites and marbles Permian (Koçyiğit & Beyhan, 1998)	Unmetamorphosed limestone (no pelitic rocks). Triassic-Jurassic Beyaz Aladağ Fm. (Tekeli, 1984)	Low-grade metamorphosed limestones Devonian - Permian Siyah Aladağ Fm. (Tekeli, 1984)
Footwall lithology	Unmetamorphosed limestones Triassic (Koçyiğit & Beyhan, 1998)	Limestones with bauxite stringers Triassic-Jurassic Beyaz Aladağ Fm. (Tekeli, 1984)	Low-grade metamorphosed limestones Permian-Triassic Yahyali Gp. (Tekeli, 1984)
Presence of ophiolite?	No ophiolite involved	Ophiolite slivers exposed in footwall	Ophiolite exposed in local footwall

Figure 10.4 A comparison of the geological characteristics of the three possible sites of the piercing points proposed by Kocyigit & Beyhan (1998).

10.3 New piercing points

10.3.1 The Late Eocene thrust zone

The candidate which is favoured here as a structural piercing point is the Bolkardağ-Aladağ fold and thrust belt (Section 7.3.4, Figs. 7.8, 7.9 & 7.10). Late Eocene overturned folds and thrusts crop out on both sides of the fault zone, marking the northern margin of the Bolkar Mountains to the west of the Ecemiş Fault Zone (mapped by Demirtaşli *et al.* 1984), and also to the east on Uçukkaya Tepe, NE of Sulucaova (mapped by Tekeli *et al.* 1984). Outcrops on both sides of the Ecemiş Fault Zone exhibit: (a) NW-SE striking fold profile planes, (b) SSE-dipping thrust fault geometries, (c) thrust faults dipping at an angle of 40-50^0, (d) consistent NW-directed kinematic indicators (fold vergence), (e) similar Late Triassic – Early Jurassic Mesozoic platform carbonates in the hangingwall and (f) overturned fold axial planes in thrust hangingwalls and footwalls (Fig. 10.5). Acceptance of the above piercing points yields a total sinistral offset of 60±5km since the Late Eocene; a similar but slightly lower total offset to that proposed by previous workers.

10.3.2 Recent debate over new piercing points

Similar piercing points were recently proposed by Westaway (1999), who described a north-directed (south-dipping) thrust fault ~1km N of Sulucaova and also 5.5km N of Pozanti, which brings Early Permian over Late Permian rocks. Westaway (1999) gives a resultant total sinistral offset of 62km. The position and total offset of these thrust faults are very similar to those of the Bolkardağ-Aladağ backthrust belt.

Koçyiğit & Beyhan (1999), in their reply to Westaway (1999) criticised these piercing points, arguing that thrust faults in these areas dipped in opposite directions and that rock units involved in the hanging- and foot-walls were of different ages either side of

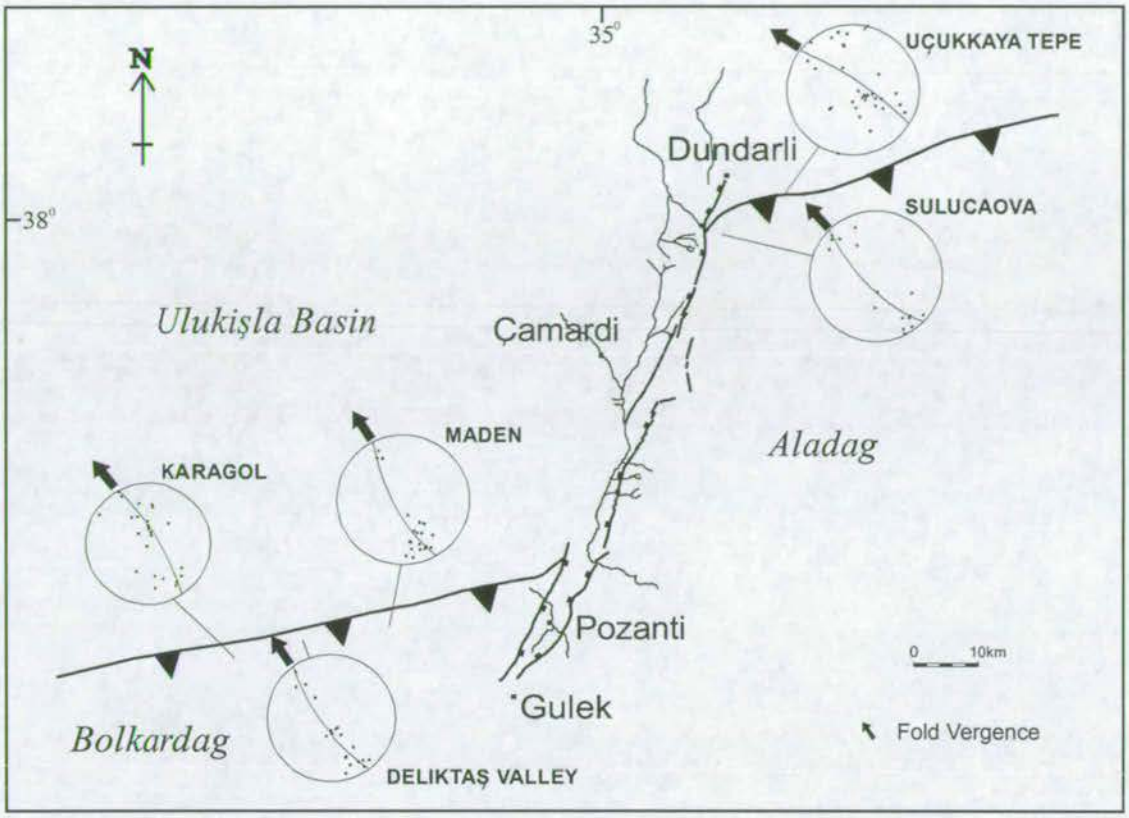

Fig. 10.5 Late Eocene fold and thrust belt along the northern margin of the Bolkardag and Aladag. This is proposed as a piercing point to constrain total offset on the EFZ. Stereoplots show poles to bedding planes (dots), fold profile planes (great circles) and fold vergence (solid arrow). Thrust faults are shown by triangles on the overriding plate. Faults of the current EFZ (thick black lines) and rivers (thin lines) are shown for location purposes only.

the EFZ. Structural evidence provided in this study (Section 7.3.4) and stratigraphic work by Tekeli *et al.* (1984) and Demirtaşli *et al.* (1984) show this to be incorrect. Koçyiğit & Beyhan (1999) then go on to propose two north-directed (south-dipping) thrust faults as piercing points where previously (Koçyiğit & Beyhan 1998) they had interpreted south-directed (north-dipping) ones (Fig. 10.2b). It should be noted that neither Koçyiğit & Beyhan (1998, 1999) nor Westaway (1999) provide any structural or stratigraphic data of their own to back up their piercing point interpretations.

10.3.3 Limitations of new piercing points

There are three potential difficulties with the proposed new piercing points (the Late Eocene Bolkardağ-Aladağ thrust belt). Firstly, different rocks are present in the thrust footwall to the east and west of the Ecemiş Fault Zone. This could be explained by the hypothesis that the Bolkardağ thrust was re-activated by E-W striking (down to N) Oligocene-Quaternary normal faulting and orogenic collapse structures (Fig. 10.6, Dilek *et al.* in press). Structural and palaeocurrent data from Horoz (Figs. 4.56 & 4.32 respectively) indicate that Plio-Quaternary age E-W striking normal faults are well developed in the northern Bolkardağ, but these are not seen to the east of the Ecemiş Fault Zone in the Aladağ. As a result of this normal faulting the Eocene thrust-footwall rocks have been down-thrown to the north and buried beneath sediments of the Late Cenozoic Aktoprak Basin (the upper part of the Ulukişla Basin, Fig. 10.6). By contrast, to the east of the Ecemiş Fault Zone the Late Eocene thrust remains unaffected by normal faulting.

The second potential problem is that the two correlated thrust zones may originally have existed at different structural levels during the Late Eocene, only being brought to the same level later by differential movement across the fault zone. However, the high angle of the backthrusting (40-50°) reduces errors associated with correlating thrusts of originally different structural levels. For example, an original vertical separation of 1 km would result in only a negligible horizontal separation of 1.3-1.5 km. Neither of the above points, therefore, negates the backthrust zones as a suitable piercing point for the Ecemiş Fault Zone.

The third potential problem is that the Mesozoic palaeogeographic setting and Late Cretaceous – Early Tertiary deformation of the Bolkardağ and Aladağ carbonate platforms on either side of the EFZ may have been different (i.e. the northern margin of the Bolkardağ and Aladağ may not have been at the same latitude prior to the closure of

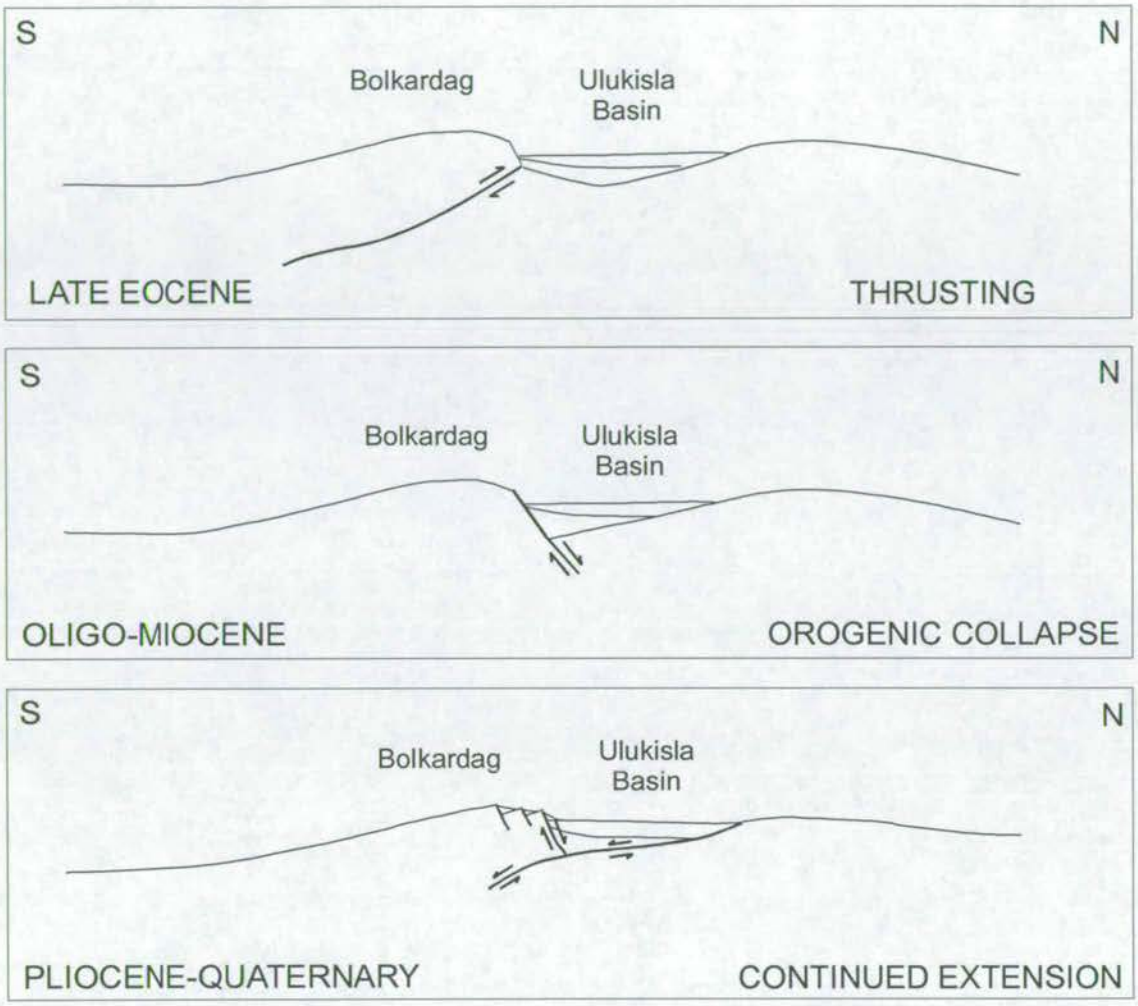

Figure 10.6 Cenozoic evolution of the northern margin of the Bolkardag (after Dilek & Whitney *in press*), including Late Eocene north-directed thrusting followed by Oligo-Miocene normal faulting and continued normal faulting during the Plio-Quaternary.

the Neotethyan seaway). However, in the absence of exhumation history evidence for these bodies we adopt the simplest hypothesis, that the two platform units had a similar (E-W) northern margin during the Mesozoic and underwent a similar deformation history.

There remains however, an element of uncertainty over the exact age of the eastern piercing point (the fold and thrust belt along the northern margin of the Aladağ), due to the lack of stratigraphic control on faulting.

10.4 Conclusions

- Several estimates of the total offset and timing of slip on the EFZ have been made, based on structural and stratigraphic piercing points. Total offset estimates range from 80±10km Yetiş (1978) to 62km (Westaway 1999).
- The original estimates of Yetiş (1978) are rejected, as the validity of the correlation of two Middle Eocene outcrops, apparently unaffected by strike-slip faulting was not confirmed by this study.
- The use of the Pozanti-Karsanti and Mersin ophiolites as piercing points is rejected. The presence of ophiolite outliers suggests that Late Cretaceous ophiolite cover was more extensive than that seen today.
- Recent estimates of Koçyiğit & Beyhan (1998) are rejected as this study has found that correlated thrust faults have different geometries and vergence.
- The Late Eocene Bolkardağ-Aladağ fold and thrust belt is suggested as a new piercing point. This gives a total sinistral offset of 60±5km since the Late Eocene.

11 Geophysical Data

11.1 Introduction

Geophysical techniques can provide accurate and quantitative information on many aspects of extrusion in central Turkey. These include current and historical earthquake activity (seismicity), crustal rotation and movement on a geological timescale (palaeomagnetic data) and on a human timescale (GPS data). In this chapter published data are used to make first order interpretations.

11.2 Seismicity

Macro- and micro-seismic records have been used in the published literature to determine whether the EFZ is a currently active fault zone. Works on the general seismicity of Turkey have largely focused on the Aegean region, North and East Anatolian Faults, portraying central Anatolia as a region of low seismicity (McKenzie 1970, McKenzie 1972, Rotstein 1984, Fig. 11.1). These works show that the EFZ area is much less seismically active than either the NAFZ or the EAFZ. The Harvard Centroid Moment Tensor (CMT) Catalogue is a catalogue of all earthquakes of moment magnitude 0-10, recorded using the moment tensor method (Dziewonski *et al.* 1981) since 1976. Data from this catalogue also shows that there has been no significant seismic activity in Central Anatolia (including the trace of the EFZ) since 1976 (Fig. 11.2).

A recent compilation of seismic data from 1907-1992, focusing on Central Anatolia (Fig. 11.3, Koçyiğit & Beyhan 1998) found that seismicity is concentrated on the Erciyes basin and NAFZ areas, with only one recorded earthquake on the line of the Ecemiş Fault Zone (magnitude 5.2 on 28/6/1944 at Hamidiye). The focal mechanism for

(a)

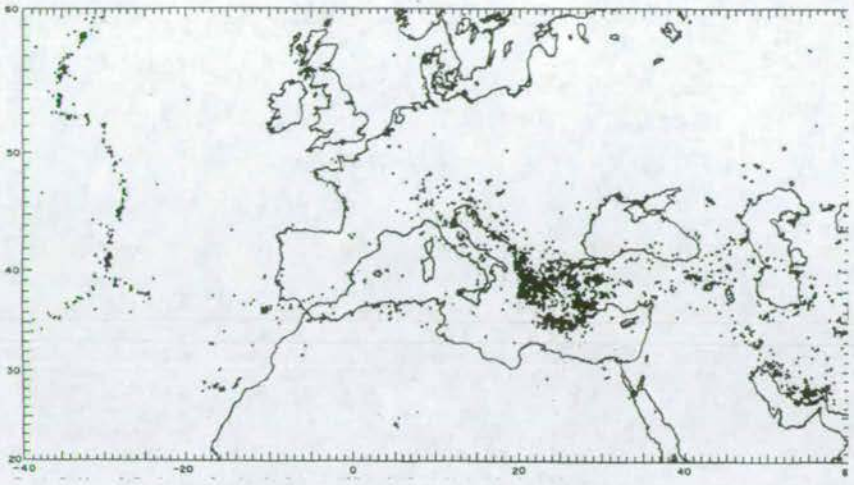

Figure 11.1a Positions of all epicentres of earthquakes between 400W and 600E, 200N to 600N located by the U.S. Coast and Geodetic Survey between 1961 January , and 1970 July 30. After

(b)

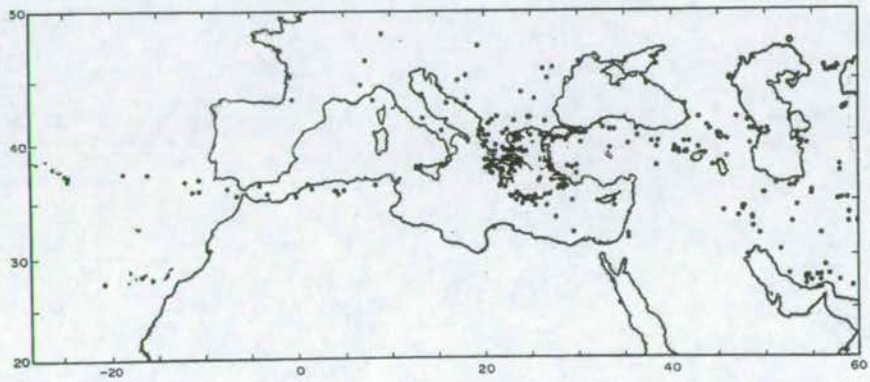

Figure 11.1b Major earthquakes in the Mediterranean area between 1922 and1970. The magnitude of most earthquakes shown is 6 or greater. After McKenzie (1972).

(c)

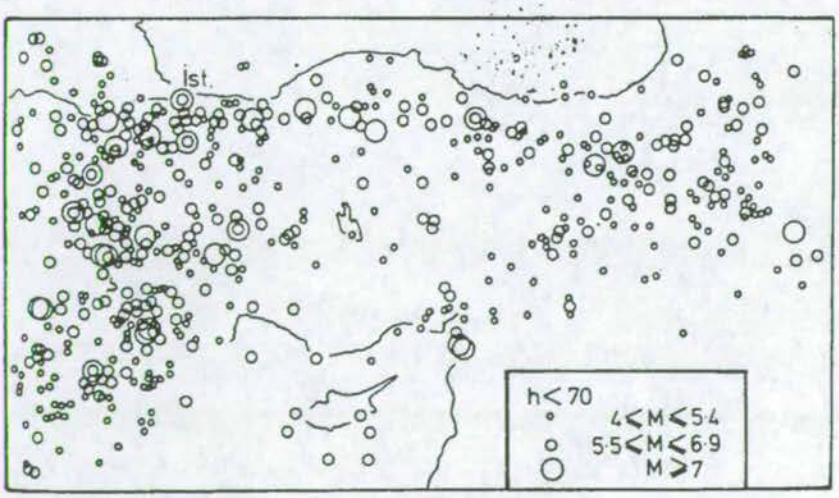

Figure 11.1c Map showing the epicentres of earthquakes less than 70km deep in Anatolia and surrounding regions between 11AD and 1964. After Rotstein(1984).

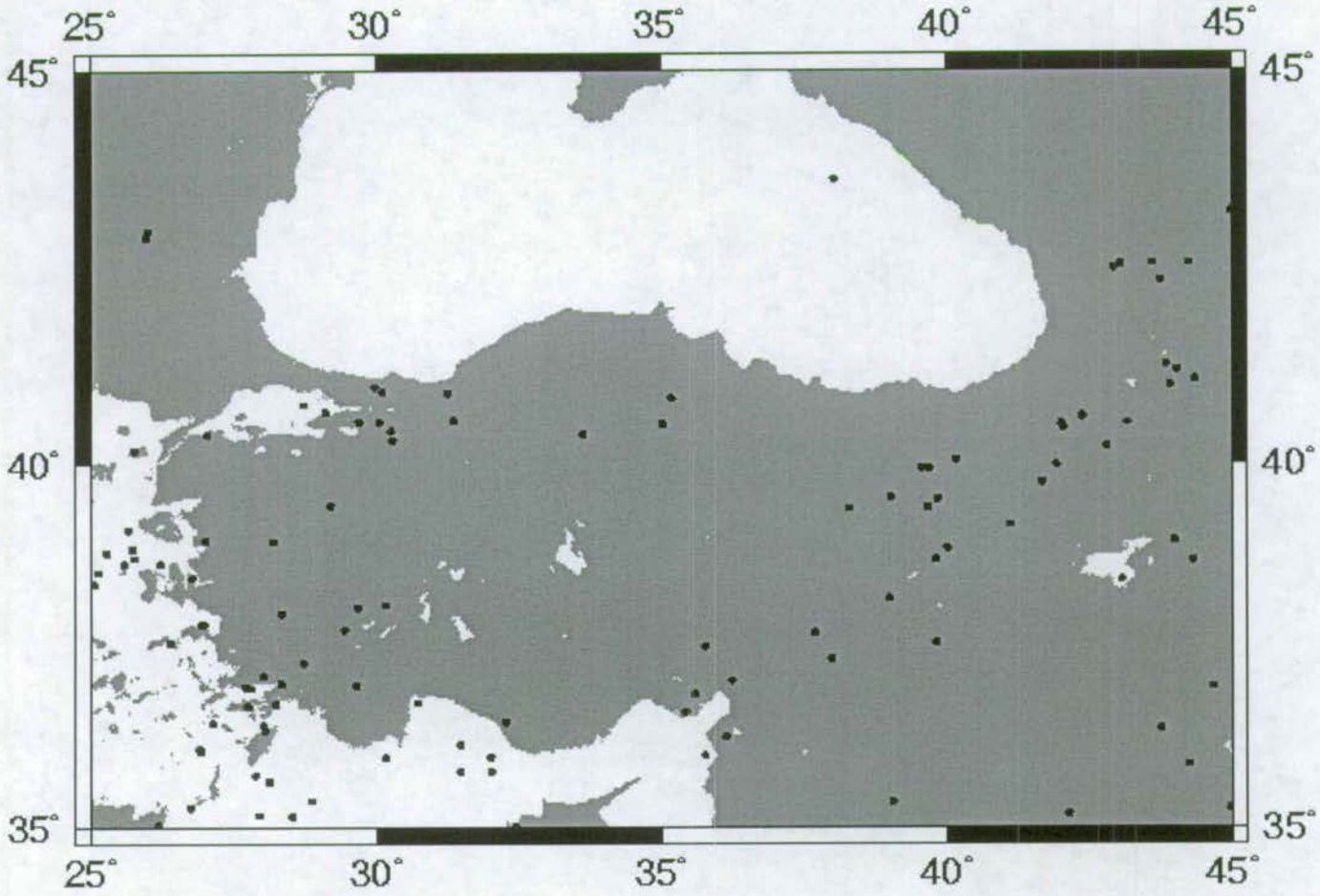

Figure 11.2 Earthquake epicentre locations for earthquakes of moment magnitude 0-10, measured using the centroid moment tensor method (Dziewonski et al. 1981) since 1976. These show that Central Anatolia is relatively seismically inactive compared to the Aegean region North and East Anatolian Faults. Data from the Harvard CMT Catalogue.

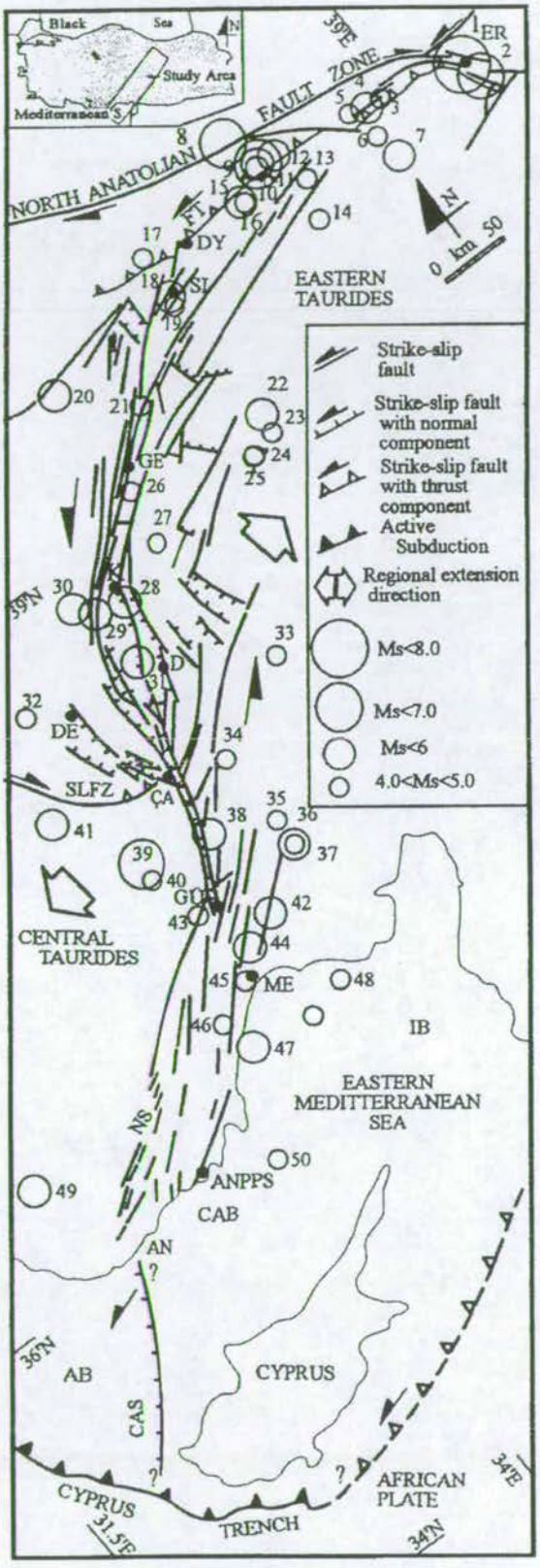

Figure 11.3 Seismicity of the Central Anatolian Fault Zone (after Kocyigit & Beyhan 1998). Numbers 1-50 show epicentres of earthquakes. AB=Antayla basin; AN=Anamur; ANPPS=Akkuyu Nuclear Power Plant Site; CA=Camardi; CAB=Cilicia-Adana basin; CAS=Cyprus-Anamur fault segment; D=Develi; DE= Derinkuyu; DY= Duzyayla; ER=Erzincan; GE=Gemerek; GU=Gulek; IB=Iskenderun basin; k=Kayseri; ME=Mersin; NS=Namrun fault segment; SI=Sivas.

this earthquake was not provided. Koçyiğit & Beyhan 1998 go on to infer the existence of a greater 'Central Anatolian Fault Zone' connecting the EFZ with the NE-SW striking Namrun fault zone, Sivas basin and Erciyes basin, based on this earthquake evidence, and field evidence.

The accuracy of the seismic data presented in Koçyiğit & Beyhan (1998) is contested by Westaway (1999), who argues that (i) the magnitudes of some earthquakes were exaggerated, (ii) that seismicity does not define the trend of the CAFZ but forms a broad zone of seismicity ~200km wide which straddles the boundary zone between African and Arabian plates, and (iii) that there is not enough evidence for major historical earthquakes to account for the 3mm/year slip rate quoted in Koçyiğit & Beyhan (1998).

It is concluded that although there has been some seismicity on the EFZ, that this is very minor compared to that on the North Anatolian and East Anatolian Fault Zones. Considering that the EFZ has an offset comparable with that of the NAFZ and larger than that of the EAFZ, it is suggested that the EFZ is currently less seismically active than it has been in the past.

11.3 Palaeomagnetic Data

The Mediterranean region is one of the most intensely studied segments of the Alpine-Himalayan chain in terms of palaeomagnetism (Morris & Tarling 1996). These data give a unique and quantitative insight into ancient crustal movement and especially into vertical axis rotations.

Four recent papers have shed light on crustal vertical-axis rotations during the Cenozoic in central Anatolia. A regional study of palaeomagnetic rotations from Late Cretaceous and Cenozioic rocks in central Anatolia (Gürsoy *et al.* 1999) found that the area has undergone strong and variable counter-clockwise rotation, with the bulk of the regional

rotation concentrated within the last part of Neotectonic (Late Cenozoic) history (Fig. 11.4 a). They also found that this zone of rotation is bounded by the NAFZ in the north and the EAFZ in the south, and that the degree of counter-clockwise rotation diminishes westwards so that it is near zero by a longitude off 35^0E.

Palaeomagnetic analysis of Eocene volcanics from Central Turkey (Yozgat area, Fig. 11.4d) revealed that the region had undergone an average anticlockwise vertical-axis rotation of ~33° since the Eocene, as well as an ongoing northward movement of a few degrees (Tatar *et al.* 1996). They also conclude that the region affected extends as far west as the Aegean graben system and a far south as the Taurides and that most of this rotation occurred during the Quaternary. Tatar *et al.* (1996) assume that ~33^0 counter-clockwise vertical axis rotation has affected the whole of Central Anatolia (including the EFZ) and is not confined to local, independent block rotations. This conclusion is supported by Gürsoy *et al.* (1999), who provide palaeomagnetic data from throughout central Anatolia.

Palaeomagnetic analysis of samples from the Sivas Basin (NE Anatolia, Fig. 11.4b) revealed that although palaeomagnetic signatures from the early Cenozoic were overprinted, the neotectonic palaeomagnetic record (post-Miocene) was well preserved, and showed regional counter-clockwise rotation (Gürsoy *et al.* 1997). These workers found an absence of perceptible differences between mean rotations from Miocene, Pliocene and Quaternary samples, inferring that the bulk of regional anticlockwise rotation occurred during the Quaternary, at an average rate of 10°/Ma.

Recent palaeomagnetic sampling of Miocene lavas and tuffs from the Erciyes basin (lying directly on the EFZ, Fig. 11.4c) have found that while samples from directly outside the Erciyes Basin display an anticlockwise rotation of ~10^0 during the last 1Ma (typical of most of central Anatolia, Gürsoy *et al.* 1999), that larger differential rotations are identified from within the Erciyes Basin (Tatar *et al.* 2000). Based on samples of

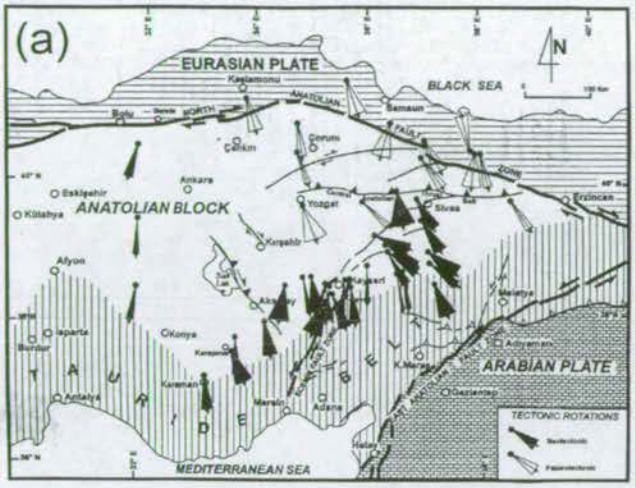

Figure 11.4a Mean palaeomagnetic declination values with 95% confidence limits from Upper Cretaceous (Palaeotectonic) and Cenozoic (Neotectonic) rock units in central Turkey (after Gursoy *et al.* 1999). All vectors are shown as directions of the reversed polarity field, thereby Neotectonic arrows indicate 10-30° counter-clockwise crustal rotations.

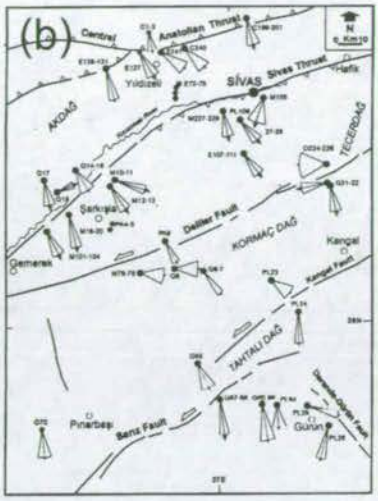

Figure 11.4b Mean palaeomagnetic declination values with 95% confidence limits from Miocene - Quaternary rock units in the Sivas Basin (after Gursoy *et al.* 1997). All vectors are shown as directions of the reversed polarity field, thereby arrows indicate counter-clockwise crustal rotations.

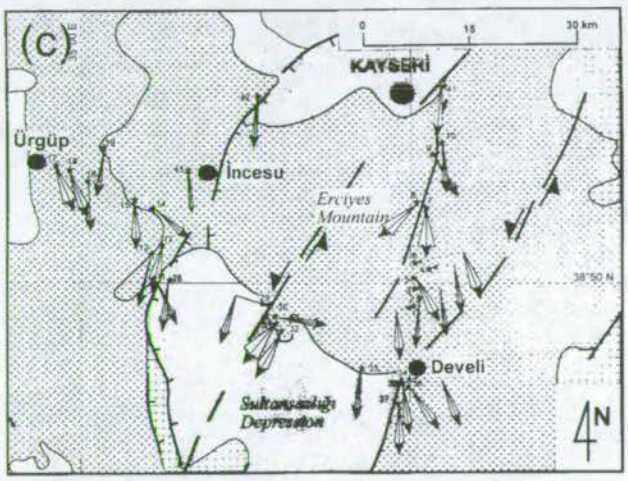

Figure 11.4c Mean palaeomagnetic declination values with 95% confidence limits from Pliocene - Quaternary lavas in the Erciyes Basin (after Tatar *et al.* 2000). All vectors are shown as directions of the reversed polarity field, thereby arrows indicate both clockwise and counter-clockwise block rotations within the Erciyes Basin.

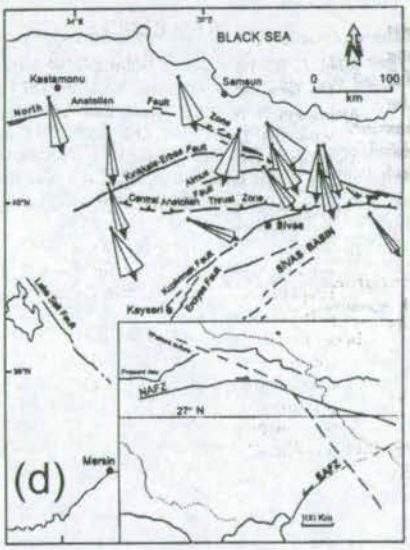

Figure 11.4d Mean palaeomagnetic declination values with 95% confidence limits from Eocene volcanics in the Yozgat area (after Tatar *et al.* 1996). All vectors are shown as directions of the reversed polarity field, thereby arrows indicate counter-clockwise crustal rotations, except for one datapoint.

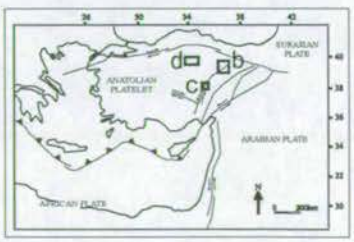

Figure 11.4e Location map for palaeomagnetic sampling sites.

young (1-2Ma) lava flows, they conclude that local vertical-axis rotations within the basin are in both senses (clockwise and counter-clockwise), and reach as much as 25^0. Tatar *et al.* (2000) use these data to infer that local block rotation have occurred within the Erciyes basin (and by implication within the Ecemiş Fault Zone) during the Late Pliocene and Quaternary, although they do not elaborate on the location and size of such 'blocks'.

11.4 Global Positioning System Data

Using an array of 54 GPS sites throughout Turkey, measurements of crustal motions were made for the period 1988-1994 (Reilinger *et al.* 1997). Assuming a static-Eurasia reference frame, these workers found that the northern Arabian platform is currently moving northward at a rate of 20±3mm/year. Eastern Turkey is characterised by distributed deformation, whereas central and western Turkey is characterised by coherent westward plate motion and anticlockwise rotation at a rate of less than 2mm/year (Fig. 11.5). Reilinger *et al.* (1997) conclude that Central and eastern Anatolia are currently undergoing westward extrusion and anticlockwise vertical axis rotation as an internally deforming plate, bounded by the North and East Anatolian Faults. They also conclude that plate motion rates increase toward the Hellenic arc. The scarcity of recording stations in central and southern Anatolia (Fig. 11.5) means that it is not possible to determine whether counter-clockwise rotation is being accommodated by the rotation of a single plate or several independent rotating units.

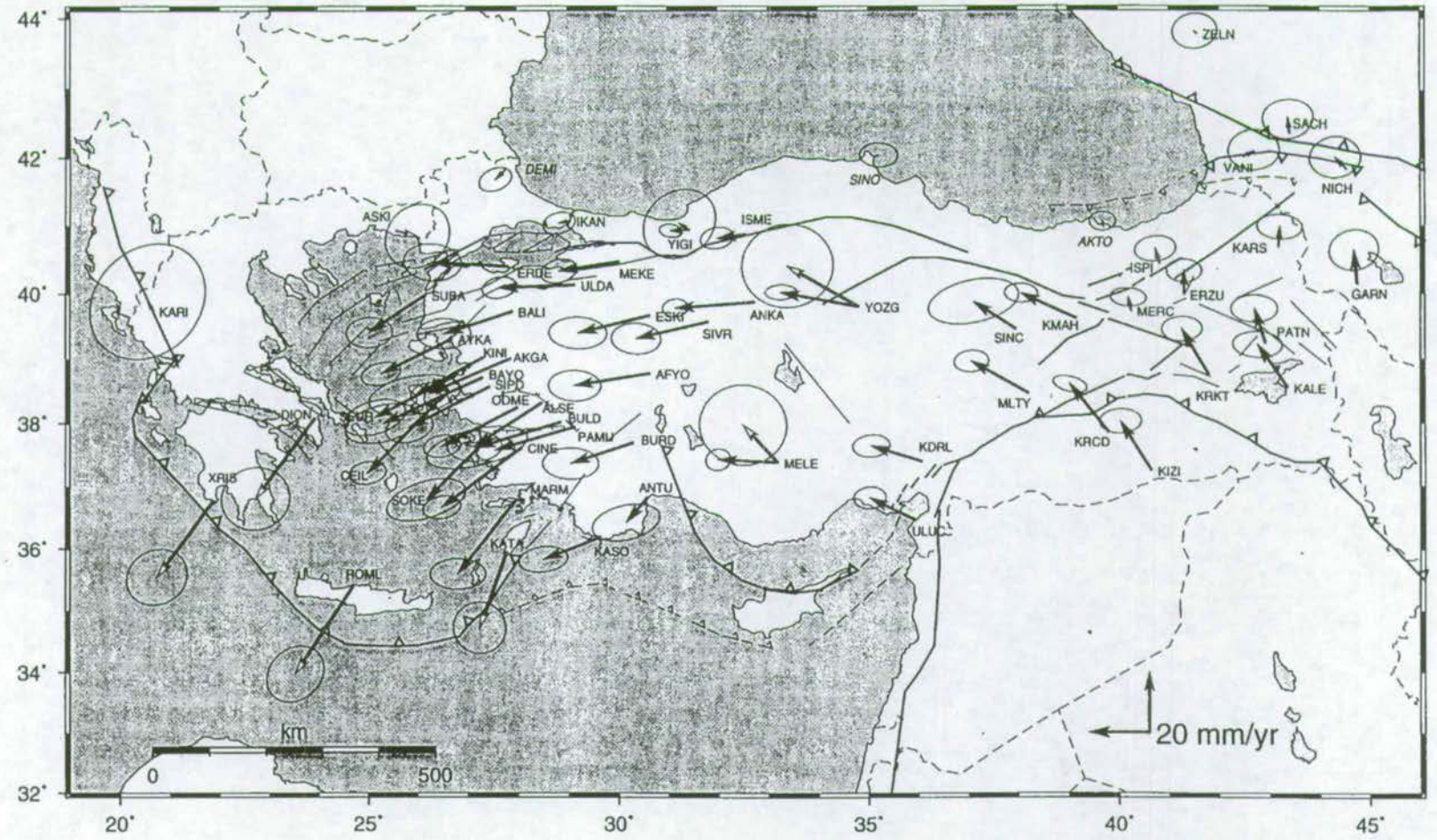

Figure 11.5 Global Positioning System (GPS) (solid arrows) and satellite laser ranging (SLR) (open arrows) horizontal velocities and their 95% confidence ellipses in a Eurasia-fixed reference frame for the period 1988-994. After Reilinger *et al.* 1997.

11.5 Conclusions

- The historical seismicity of central Anatolia is low relative to that of the North Anatolian and East Anatolian Fault Zones and the Aegean region.
- Very little seismicity has been recorded on the EFZ; only one earthquake has been historically recorded on the line of the EFZ, in 1944. The EFZ does not appear to be seismically active at present.
- Central Anatolia has undergone variable counter-clockwise vertical axis rotation since the Eocene (up to ~33^0), of which 10^0 has occurred within the last 1Ma. This area of rotation is bounded by the NAFZ (north) and EAFZ (south) and the degree of rotation decreases away from the Arabian indentor. Regional palaeomagnetic results suggest that the entire EFZ has been rotated counter-clockwise by up to 33^0 during the Neotectonic period.
- Palaeomagnetic evidence exists for block rotation within the EFZ at the Erciyes basin, with vertical axis rotations in both senses, and up to 25^0 since the Late Miocene.
- GPS studies have revealed that central and eastern Anatolia are currently undergoing westward extrusion and counter-clockwise vertical axis rotation as an internally deforming plate, bounded by the NAF and EAF.

Summary of geological events

	Sedimentology	Subsidence	Provenance	Structure
Quaternary	Fault-controlled alluvial fans and debris flows	Renewed local rapid subsidence	Local fault-scarp sources	E-W extension + minor sinistral strike-slip
Pliocene	Uplift - scarp formation		Presnet fault-scarp creation	
Miocene	Gentle topography Pyroclastic activity	Slow subsidence in EFZ	Taurus carbonates main sediment sources	Sinistral trans-tension
	Uplift	Hiatus in subsidence	Nigde massif unroofed to present state	NW-SE compression event. Assoc with strike-slip.
	Inward-draining continental basin. Depocentre in EFZ.	Maximum subsidence Maximum sedimentation rates	Ophiolitic bodies main sediment sources	Probable sinistral trans-tension. Regional N-S orogenic collapse.
Oligocene	Uplift	Hiatus in subsidence	Uplift of Bolkardag and Aladag	Uplift of Taurus Mtns.
Eocene	Marine conditions	Low subsidence rates Low sedimentation rates		NW-directed thrusting, localised on N margin of Taurus Mtns.
Palaeocene			Nigde Massif partially unroofed	
Latest Cretaceous				Ophiolite Obduction (N to S). SE-directed deformation of Taurus Mtns.

	Geomorphology	$^{40}Ar/^{39}Ar$ dating	Piercing points	Geophysical evidence
Quaternary	Terrace deposition Fan incision Strike-slip faulting of alluvial fans. Block rotation?	Strike-slip in Erciyes Basin. Also in EFZ?	2.4km since Pleistocene Based on stream offsets.	10^{0} regional vertical axis rotation since 1Ma.
Pliocene	Oldest alluvial fan deposition	E-W extenion in Erciyes Basin. Fault activity in EFZ?		Block rotation in EFZ since Late Miocene
Miocene				
Oligocene				
Eocene			~60km sinistral offset on EFZ since Late Eocene, based on offset thrust system.	Up to 33^{0} regional vertical axis rotation since Eocene
Palaeocene				
Latest Cretaceous				

12 Discussion

12.1 Introduction

This chapter aims to draw together the multi-disciplinary strands of this study, in order to: (i) establish the timing of activity on the EFZ, (ii) compare the timing and offset of the EFZ with those of other extrusion-related fault zones in the eastern Mediterranean, and thereby evaluate the regional significance of the EFZ, (iii) propose a new mechanism of tectonic escape in Turkey and (iv) compare this mechanism with those proposed for other areas of crustal extrusion.

12.2 Evidence for the timing of activity on the EFZ

Evidence is presented from the previous chapters of this study regarding the timing of fault activity on the EFZ. Periods of inferred fault activity on the EFZ are highlighted in bold.

Sedimentology

- Palaeocurrent and facies data show that an isolated sedimentary basin existed in the location of the EFZ during the **Late Oligocene and Early Miocene** (Section 4.4.2.9). It is likely that this basin was associated with normal fault activity.
- The palaeocurrents, lateral extent and facies of the Plio-Quaternary Çatalca Formation show that they were associated with fault scarps formed during the **latest Miocene - Early Pliocene** (Section 4.4.4.5).
- The dissimilarity and apparent offset between adjacent Lutetian outcrops (Section 4.4.1.3) indicates that strike-slip faulting was active **after the Middle Eocene**.

Subsidence Curves

- Subsidence curves for the EFZ show that rapid subsidence occurred during the **Late Oligocene – Early Miocene**. The shape of this curve suggests that strike-slip faulting may have been involved (Section 5.5.2).
- Renewed subsidence occurred during the **latest Miocene - Early Pliocene**. This was also associated with fault activity (Section 5.5.2).

Provenance

- Both the Aladağ and Bolkardağ were active as sediment sources (areas of high topography) from the **Late Oligocene – Early Miocene** (Fig. 6.11a). It is likely that the uplift of these mountains relative to the EFZ was partly accommodated by the EFZ.

Structure

- The offset of the Late Eocene north-directed fold and thrust belt (Fig. 7.8) indicates that strike-slip faulting was active **after the Late Eocene**.
- The offset of the Ulukişla Volcanics indicates that strike-slip faulting was active **after the Palaeocene** (Fig. 10.1).
- The deformation pattern of the Oligo-Miocene Çukurbağ Formation within the EFZ suggests that strike-slip faulting was active during the **Mid Miocene** (Fig. 7.13).
- The vertical offset of Plio-Quaternary fan material at Emliboğazi (Fig. 8.9) and the presence of sinistral slickenline populations in Plio-Quaternary fan material on the 'small graben' (Fig. 8.10) indicate that faulting was active **after the Pliocene**.

Geomorphology

- River and stream offsets on the Çamardi fan complex suggest that sinistral strike-slip faulting has taken place on the 'small graben' during the **Quaternary** (Fig. 8.12).

$^{40}Ar/^{39}Ar$ radiometric dating

- Dating of tuffs and lavas at the boundaries of the Erciyes Basin indicate that normal faulting occurred there during the **Messinian (latest Miocene)** and by implication, also occurred in the EFZ proper during this period (Section 9.7).
- Dating of tuffaceous sediments in the centre of the Erciyes Basin indicates that strike-slip and (minor) normal faulting occurred there during the **early Pleistocene**, and by implication in the EFZ proper during this period (Section 9.7).

Geophysical Data

- Records of seismicity indicate that the EFZ has not been significantly seismically active during human history (Section 11.2), although microseismicity cannot be ruled out.
- Palaeomagnetic data from the Erciyes Basin indicate that block rotations, associated with strike-slip faulting have taken place within the EFZ during the **Quaternary** (Section 11.3).

Summary

The first indirect evidence for faulting is during the Late Oligocene - Early Miocene (basin formation). There is more direct evidence for faulting during the Mid Miocene, latest Miocene - earliest Pliocene and early Pleistocene. There are no constraints on the timing of fault initiation, prior to the Late Oligocene.

12.3 Regional significance of the EFZ

In order to assess the regional significance of the EFZ, the timing and offset of other extrusion-related fault zones in Turkey must also be examined. The locations of these fault zones are shown in Fig. 12.1 and previous work on their offsets and timing of activity is detailed in Sections 2.5.3 – 2.5.7.

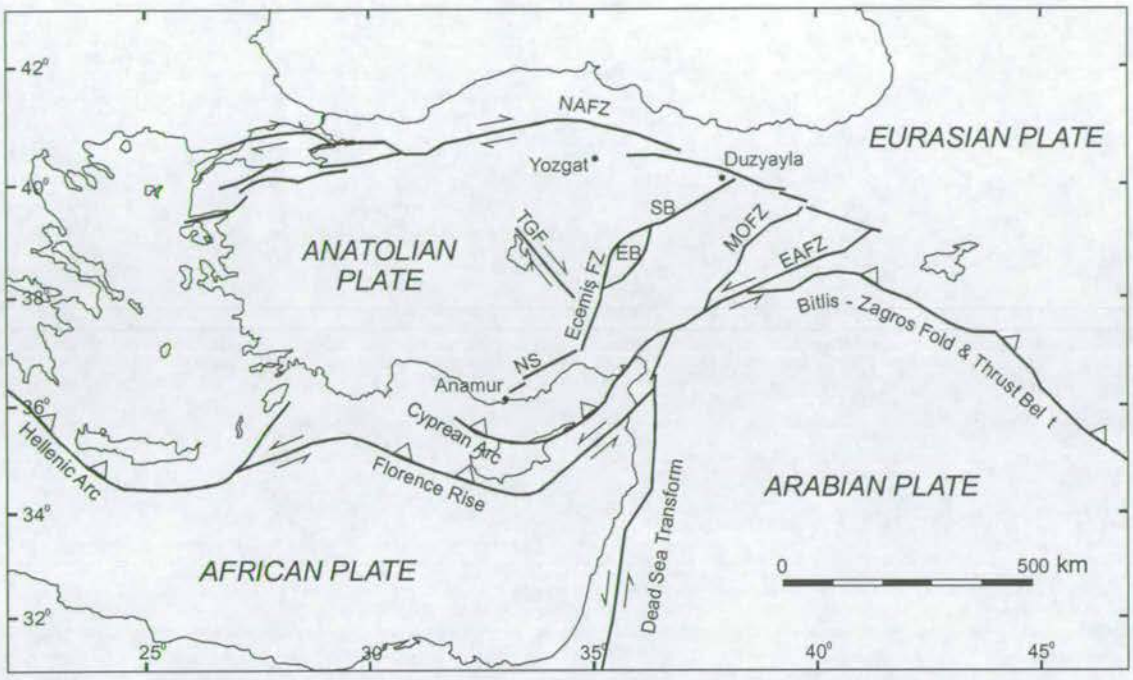

Figure 12.1 Simplified tectonic map of the Eastern Mediterranean (after Şengör *et al.* 1985 and Koçyiğit & Beyhan 1998), highlighting Neotectonic (Late Cenozoic) faults. Solid lines are strike-slip faults or subduction zones with triangles on the overriding block. Abbreviations: EAFZ East Anatolian Fault Zone, EB Erciyes Basin, MOFZ Malatya-Ovacik Fault Zone, NAFZ North Anatolian Fault Zone, NS Namrun Segment, SB Sivas Basin, TGF Tuzgölü Fault.

12.3.1 Ecemiş Fault Zone

New sedimentological data suggest that the EFZ may have been initiated during the Late Oligocene, although other (structural) lines of evidence suggest a Mid – Late Miocene initiation age. Although there is no evidence for activity prior to this, pre-Oligocene faulting is not ruled out. The EFZ remained active through the Pliocene and Early Pleistocene (based on offsets of Plio-Quaternary alluvial fan material). Seismic and geomorphologic evidence suggests that the EFZ is not currently active, but that it was active during the Early Pleistocene.

New piercing points indicate a total sinistral offset of 60±5km, based on the offset of a major north-vergent fold and thrust belt along the northern margin of the Bolkardağ and Aladağ. This is in general agreement with other published total offsets for the EFZ (i.e. Yetiş 1978, Koçyiğit & Beyhan 1998, Westaway 1999).

12.3.2 Comparative Table (Fig. 12.2)

From a comparative table of the timing, offset and slip rates of the major continental neotectonic faults in the Eastern Mediterranean, the following first order inferences can be drawn:

(i) The EFZ has a total offset comparable with that of the North Anatolian Fault Zone and the Dead Sea Fault Zone, and greater than that of the East Anatolian Fault Zone.

(ii) The averaged slip rate on the EFZ (7-8mm yr^{-1}) is comparable with that on the East Anatolian F.Z. (4-10mm yr^{-1}) and Dead Sea Fault Zone (6-8mm yr^{-1}). The slip rate on the North Anatolian Fault Zone (17mm yr^{-1}) is twice as fast as any other neotectonic fault in the region.

(iii) While the North Anatolian Fault Zone and East Anatolian Fault Zone remain active at present, neotectonic faults within Anatolia are currently inactive (or much less active).

(iv) Fault zones within Anatolia (EFZ and Tuzgölü Fault Zone) appear to have been active at an earlier stage than those at its current boundaries (North Anatolian Fault Zone and East Anatolian Fault Zone).

Fault Zone	Timing of slip		Total Offset	Averaged Slip Rate
	Initiation	Cessation		
North Anatolian Fault Zone	End Tortonian as shear zone Pliocene (5Ma) as fault zone	Currently active	85±5km (Westaway 1994) or 30-40km (Barka & Gulen 1989)	17mm/year (Westaway 1994)
East Anatolian Fault Zone	Late Pliocene (2-3Ma)	Currently active	20-21km (Perincek & Cemen 1990)	4-10mm/year (poorly constrained)
Malatya-Ovacik Faiult Zone	Early Pliocene (~5Ma)	Late Pliocene (~3Ma)	~30km (Westaway in press)	10mm/year (Westaway in press)
Tuzgolu Fault Zone	Late Maastrichtian	Unknown	?	?
Dead Sea Transform	Burdigalian (18Ma)	Currently active	~105km (Quennel 1959)	Currently 6-8mm/year (since 5Ma)
Ecemis Fault Zone	Middle Miocene (~8Ma)	Pliocene as a strike-slip fault Quaternary as a normal fault	60±5km (this study)	7-8mm/year (this study)

Fifure 12.2 Comparison of the timing, offset and slip rates of major continental neotectonic faults in the Eastern Mediterranean

12.4 *Mechanism of tectonic escape in Turkey*

A new mechanism is now proposed for how extrusion proceeded in central/eastern Anatolia, based on the integration of new sedimentological, structural, radiometric, and palaeomagnetic data.

12.4.1 New model for extrusion in Turkey

The comparative table of fault timing and offset (Fig. 12.2) indicates that whereas the dextral component of extrusion has been taken up by one lineament throughout the neotectonic period (the North Anatolian Fault Zone), the sinistral component of extrusion has been taken up by at least three distinct fault zones: (i) the Ecemiş Fault Zone, (ii) the Malatya-Ovacik Fault Zone and (iii) the East Anatolian Fault Zone. Timing evidence suggests that of these three lineaments the EFZ was active first (active at least by 12Ma). Slickenline data suggest that the EFZ changed from a dominantly trans-tensional to dominantly normal fault zone (after 3Ma). The sinistral component of extrusion was then transferred to the Malatya-Ovacik Fault Zone, which was active at a later stage, between ~5Ma and ~3Ma (Westaway in press). Finally sinistral slip was transferred to the East Anatolian Fault Zone, which has taken up the sinistral component of extrusion from 3Ma until the present day (Fig. 12.3).

By restoring 33° of regional anti-clockwise crustal rotation, which has been ascribed to a large portion of central Anatolia, including crustal blocks on both sides of the EFZ (Tatar *et al.* 1996, Gürsoy *et al.* 1999, Section 11.3) it is inferred that the Ecemiş Fault Zone was initiated as a strike-slip fault system by Middle Miocene time with an orientation closer to NE-SW (similar to that of the present-day East Anatolian Fault Zone). During Late Miocene, Pliocene and Quaternary it is suggested that the EFZ progressively rotated to its current NNE-SSW orientation within encompassing crustal units. As the EFZ was rotated, it moved out of the optimum orientation for

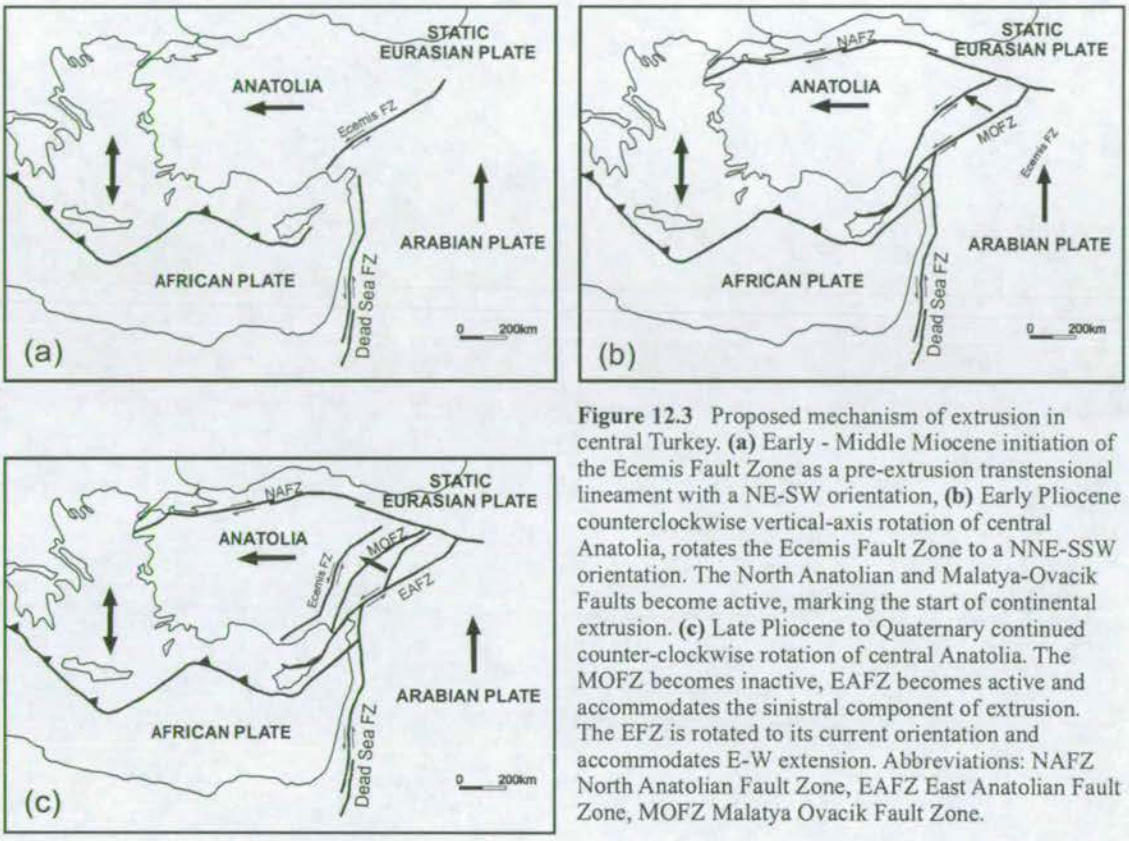

Figure 12.3 Proposed mechanism of extrusion in central Turkey. **(a)** Early - Middle Miocene initiation of the Ecemis Fault Zone as a pre-extrusion transtensional lineament with a NE-SW orientation, **(b)** Early Pliocene counterclockwise vertical-axis rotation of central Anatolia, rotates the Ecemis Fault Zone to a NNE-SSW orientation. The North Anatolian and Malatya-Ovacik Faults become active, marking the start of continental extrusion. **(c)** Late Pliocene to Quaternary continued counter-clockwise rotation of central Anatolia. The MOFZ becomes inactive, EAFZ becomes active and accommodates the sinistral component of extrusion. The EFZ is rotated to its current orientation and accommodates E-W extension. Abbreviations: NAFZ North Anatolian Fault Zone, EAFZ East Anatolian Fault Zone, MOFZ Malatya Ovacik Fault Zone.

accommodating the sinistral component of extrusion, and new sinistral strike-slip lineaments formed with a NE-SW strike further to the east.

This hypothesis accounts for: (i) the sequential initiation of successive sinistral strike-slip fault zones, (ii) the change in sense of slip on the EFZ from dominantly trans-tensional (Late Oligocene - Pliocene) to dominantly normal (Quaternary), and (iii) the fact that the NAFZ has moved faster and further than either the East Anatolian Fault Zone or the EFZ. A discussion of this hypothesis is found in Jaffey & Robertson (in press).

Middle Miocene (Fig. 12.3a)

- Known sinistral offset occurred on the EFZ during this period, which had a NE-SW strike. The EFZ was active as a pre-extrusion fault during this period, possibly accommodating variable crustal shortening during continental collision.
- A tightening of the Neotethys suture resulted in a region-wide unconformity and deformation.
- The North Anatolian Fault Zone initiated as a shear zone, but extrusion was not yet occurring.

Late Miocene

- Continued sinistral offset occurred on the EFZ and dextral shearing on the North Anatolian Fault Zone.

Early Pliocene (Fig. 12.3b)

- The North Anatolian Fault Zone was initiated as a dextral fault zone, marking the start of 'tectonic escape'.
- The EFZ rotated anti-clockwise, and started to accommodate transtension rather than pure strike-slip.
- The Malatya-Ovacik Fault Zone initiated as a sinistral strike-slip fault with a NE-SW strike and formed the boundary of the 'escaping' Anatolia.

Late Pliocene (Fig. 12.3c)

- The EFZ and Malatya-Ovacik Fault Zone rotated anti-clockwise, along with their bounding crustal blocks.
- Fault activity on the Malatya-Ovacik Fault Zone ceased.
- The East Anatolian Fault Zone was initiated as a sinistral strike-slip fault with a NE-SW strike, forming the new SE boundary of Anatolia.
- The EFZ took up normal offset with a minor component of strike-slip.

Quaternary

- The EFZ took up minor sinistral and normal offset.
- The North Anatolian Fault Zone and East Anatolian Fault Zone remained the boundaries of the zone of 'escape'.

12.4.2 Implications of the new mechanism

This mechanism implies that the North Anatolian Fault Zone has been active for longer than the Malatya-Ovacik Fault Zone and the East Anatolian Fault Zone. Evidence for the timing of faulting on both of these two fault zones indicates that this is the case (Şaroğlu 1992, Westaway in press).

The model also implies that the North Anatolian Fault Zone moved at a faster rate than any of the sinistral extrusion-related fault zones. Published evidence indicates that the North Anatolian Fault Zone has moved at an average rate of 17mm $year^{-1}$ (Westaway 1994), whereas the East Anatolian Fault Zone and EFZ have moved at averaged rates of 4-10mm yr^{-1} and 7-8mm yr^{-1} respectively.

12.4.3 Limitations of proposed mechanism

The new mechanism relies heavily on the assumption that the regional 33^0 anti-clockwise vertical axis rotation of the Yozgat-Sivas area (Tatar *et al.* 1996) affected the whole of central Anatolia (the 'escaping' wedge) during the Late Cenozoic. The hypothesis that all of central and eastern Anatolia has undergone distributed anti-clockwise rotation during the Cenozoic is supported by other palaeomagnetic studies carried out throughout central Anatolia (Gürsoy *et al.* 1999, Tatar *et al.* 2000). However, the value of 33^0 anti-clockwise rotation found from volcanics in the Yozgat area only constrains the timing of rotation as post-Eocene, as rocks from overlying and

underlying units were not sampled. Also, an absence of perceptible difference between group mean rotations identified from Miocene, Pliocene and Quaternary units in the Sivas Basin (central Turkey, Gürsoy *et al.* 1997) indicate that the maximum regional rotation was concentrated during the Quaternary (at an average rate of $\sim 10^0$ Ma^{-1}), not steadily since the Middle Miocene, as suggested by the proposed mechanism.

The proposed mechanism also relies on the establishment of the correct timing of slip on the Malatya-Ovacik Fault Zone. The only results available are those of Westaway (in press) and do not provide convincing evidence for the timing of slip on the MOFZ, focusing rather on evidence for total offset.

The new mechanism does not specify the boundaries of the zone of anti-clockwise crustal rotation during extrusion. Tatar *et al.* (1996) propose that it may extend as far west as the Aegean grabens (west coast of Turkey). Other workers have found anti-clockwise vertical axis rotations within the Isparta Angle of 30^0, active since the Middle Miocene (Morris & Robertson 1993) supporting this hypothesis. This, however, is seen as a local effect of the Mid Miocene tightening of the Isparta Angle (Glover & Robertson 1998), rather than part of the regional rotation of Anatolia.

12.4.4 Alternative mechanism for tectonic escape in Turkey

Low rotation extrusion

Palaeomagnetic evidence for the significant anti-clockwise rotation of Central Anatolia prior to the Quaternary is poor (see previous section). If pre-Quaternary rotation did not occur, then the EFZ must have initiated with an orientation similar to that seen today. Evidence still remains, however, that faulting was active sequentially from west (EFZ) to east (East Anatolian Fault Zone). Fault activity may have moved to the SE as the regional stress field changed from N-S compression during continental collision (with

differential compression accommodated by the EFZ, Fig. 12.4a) to westward extrusion (accommodated by the Malatya-Ovacik and East Anatolian Fault Zones, Fig. 12.4b).

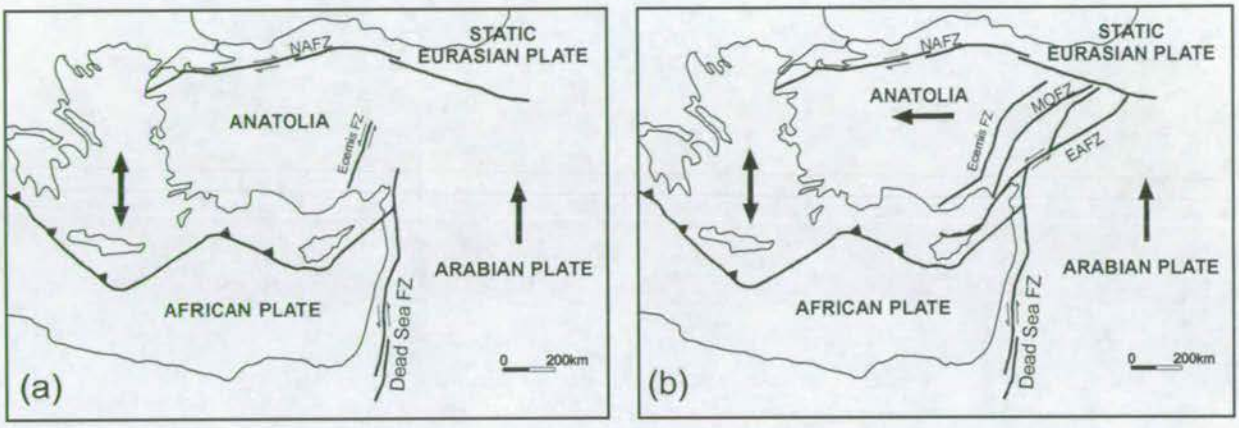

Figure 12.4 Model of low rotation extrusion. **(a)** The EFZ accommodated differential N-S compression during Mid-Miocene final continental collision **(b)** Pliocene and Quaternary westward extrusion is accommodated by the Malatya-Ovacik and East Anatolian Fault Zones.

Distributed faulting

Another possibility is that the age constraints on the timing of the Malatya-Ovacik Fault Zone are incorrect, and that the EFZ, the Malatya-Ovacik Fault Zone and the East Anatolian Fault Zone were all active synchronously. The hypothesis implies that these three faults accommodated the sinistral component of Pliocene and Quaternary extrusion as a wide zone of distributed faulting. This hypothesis is viewed as less likely than those above, as it does not account for the different age constraints on the respective fault zones, or for well established anti-clockwise crustal rotations within central Anatolia.

12.5 Comparison with South-Asian extrusion

It is useful at this stage to take a more global perspective and to test whether the proposed mechanism for tectonic escape in Anatolia can be applied to other extrusion settings. The best known case of continental extrusion is that of South Asia, where the India-Eurasia collision has caused the eastward extrusion of parts of China and SE Asia.

The traditional bounding faults of the South Asian extrusion zone have been the dextral Karakoram Fault (KKF) and the sinistral Altyn Tagh Fault (Fig. 12.5, Tapponnier *et al.* 1982, 1986). The southern limit of extrusion was extended through a zone of dextral strike-slip, linking the Karakoram Fault with the Jiali Fault along the line of the Bangong-Nujiang suture zone to the Red River Fault (Armijo *et al.* 1986, 1989). Initially large offsets were inferred on these extrusion-related faults: 1000km of dextral offset on the Karakoram Fault based on the offset of the Late Cretaceous Gangdese-Ladakh Batholith (Peltzer & Tapponnier 1988), and between 500 and 740km of dextral offset on the Red River Fault (Tapponnier *et al.* 1990). These authors proposed that extrusion was initiated during the Eocene, just after continental collision, and that it has continued until the present day.

More recent workers have contested these large offsets. Only between 10.5 and 15.5km total dextral offset was confirmed on the Haiyuan Fault in northern China (Fig. 12.5, Burchfiel *et al.* 1991), with the authors concluding that it did not accommodate any significant eastward movement of the Tibetan crust. 30km total sinistral offset was found on the Kunlun Fault (Kidd & Molnar 1988) which was initiated during the Late Pliocene. Work on the Karakoram Fault has concluded that the fault was only initiated during the Pliocene (~5Ma) and has taken up a maximum dextral offset of 120km, based on the offsets of the Baltoro batholith, Bangong-Shyok suture zone and Indus river (Searle 1996). Searle (1996) concludes that despite the high slip-rates on many of the long strike-slip faults in the region, that their pre-Holocene offsets are minimal (<150-200km) and that extrusion did not start until the Plio-Pleistocene (younger than ~5Ma). These conclusions are reinforced by recent work on the Red River Fault , Xianshuihe-Xiaojiang Fault and Dali Fault in SE Tibet (Wang *et al.* 1998), which limits these faults to a maximum of ~50km (Red River Fault) and 60km (Xianshuihe-Xiaojiang Fault). They conclude that all of these faults initiated at ~4Ma (Early Pliocene), although they separate this phase of activity from older shearing on the nearby AiloShan Shear Zone.

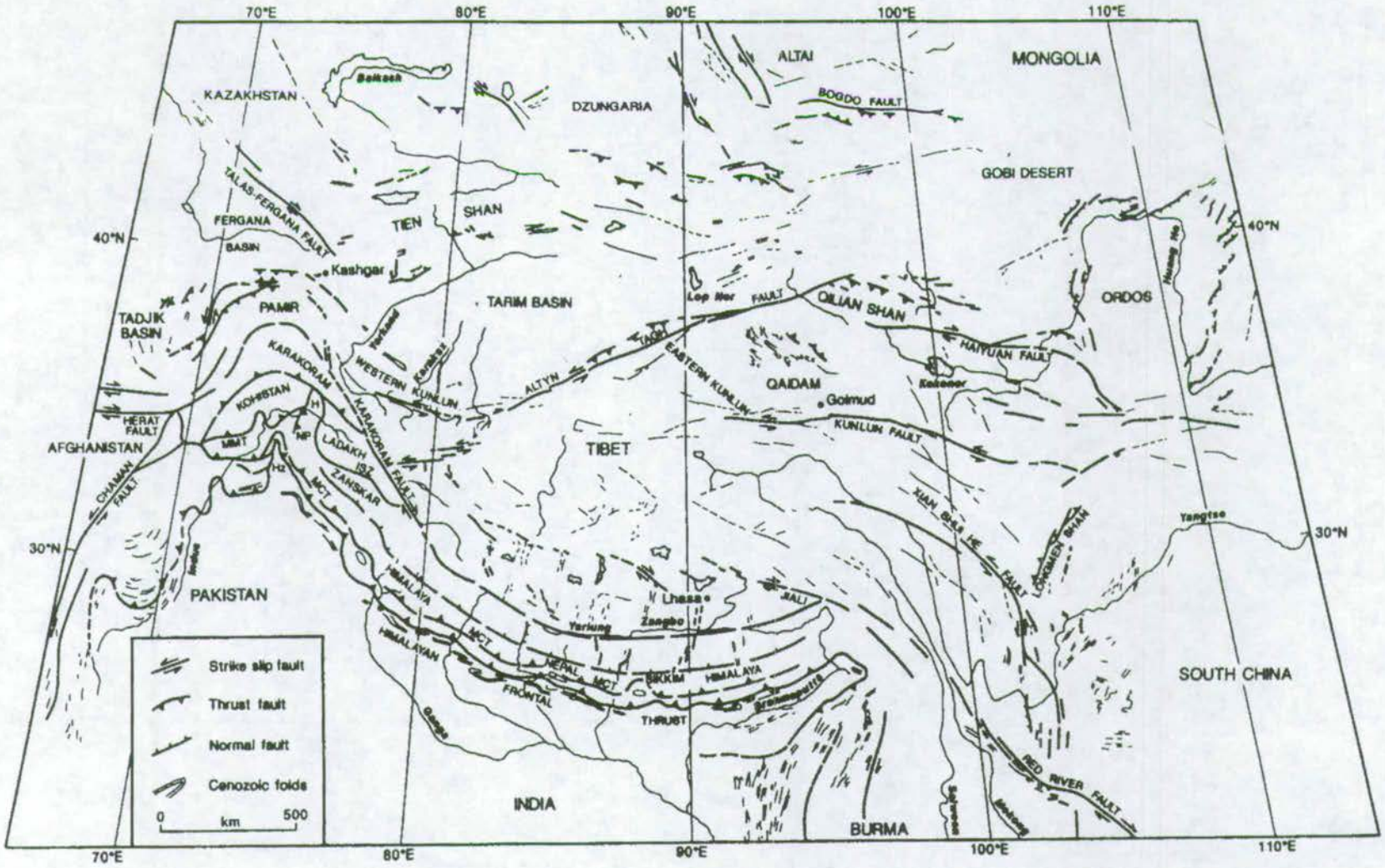

Figure 12.5 Tectonic map of central Asia (after Searle 1996)

The most recent results imply that the South Asian collision system has responded first by crustal thickening and deformation and later by limited extrusion, with a ~35Ma delay between first collision and the start of extrusion. This appears to be similar in Anatolia, where continental collision during the Late Eocene (Robertson 2000, Dercourt *et al.* 1986, Şengor *et al.* 1984), was followed by crustal thickening during the Oligocene (Whitney & Dilek 1997), suture-zone tightening during the Late Miocene (Robertson 2000) and by wholesale extrusion along the North Anatolian and East Anatolian Faults during the Early Pliocene (a delay of ~37Ma between continental collision and extrusion).

Palaeomagnetic and GPS data from South Asia conforms to a picture of rotation away from the zone of indentation. Anti-clockwise vertical axis rotations have been recorded to the west of the indentor (Pakistan): 30^0 in the Fergana basin and 60^0 in the Tajik basin (Thomas *et al.* 1993, 1994) and clockwise rotations to the east of the indentor: 10mm/yr eastward clockwise rotation of all of eastern China has been deduced using GPS station movements (Chen *et al.* 2000). In this respect South Asia has behaved in a similar manner to Anatolia, with variable crustal rotation away from the indentor has being a major feature of extrusion.

Comparison of the sequence of fault initiation and termination between Turkey and South Asia is problematic as the timing of many of the strike-slip faults in Tibet remain unknown (e.g. the Altyn Tagh Fault). Overall, however, the relatively large offsets on extrusion-related faults in Anatolia, and the relatively small confirmed offsets on those in South Asia suggest that the process of extrusion has played a more important role in the evolution of the Eastern Mediterranean than it has in South Asia.

12.6 Suggestions for Future Work

Several unanswered questions have come to light as a result of this thesis. These pertain both to local problems and to wider regional problems.

Local problems of the EFZ

Definitive evidence still does not exist regarding the detailed timing of the latest movement on the Ecemiş Fault Zone *sensu stricto*. This could be established through cosmogenic exposure age dating of the Çamardi fan terraces (Section 8.6.2) and/or palaeoseismic trench studies of the EFZ in the Çamardi area.

Evidence still does not exist for the timing of the initiation of the Ecemiş Fault Zone, which is at best constrained to pre-Mid Miocene at present. Further palaeo-ecological and palaeomagnetic studies of the Aladağ and Bolkardağ Taurus Mountains may shed light on their relative positions during the Mesozoic, and when the EFZ may have initiated as a sinistral strike-slip lineament.

Biostratigraphic control of the ages of Cenozoic non-marine sediments within the Ecemiş Fault Zone and Aktoprak Basin (Ulukişla Basin) remains poor. Useful comparative studies could be made between the ostracod and mamalian faunal records of these basins and the non-marine units of other Cenozoic basins in the area (i.e. the lower sections of the Karsanti Basin, Mut Basin and Adana Basin). A limited amount of heavy mineral analysis of Oligocene – Miocene sediments of the Çukurbağ Formation and Burç Formation may also prove productive in assessing provenance changes.

The problem of whether the EFZ continues in a NNE-SSW trend south of Gülek (C.Yetis pers. com. 1998), or whether it changes to a NE-SW trend and joins the Namrun fault set (Koçyiğit & Beyhan 1998) remains unresolved. The terrestrial

exposure south of Gülek, and shallow seismic data from the offshore Cilicia Basin could be usefully examined to further constrain this.

Wider regional problems

The hypothesis that the EFZ forms part of a larger Central Anatolian Fault Zone (Koçyiğit & Beyhan 1998) remains highly controversial. Further testing of strike-slip offsets and palaeoseismic trenching in the Sivas (north) and Namrun (south) areas should be carried out to test this hypothesis.

The Malatya-Ovacik Fault Zone is a relatively little known lineament and the only work available (Westaway in press) does not constrain the period of its activity with any authority. Further work is necessary in this area to better constrain the timing and offset of this newly described fault zone.

Further palaeomagnetic work from Early Cenozoic rocks is necessary in central and eastern Anatolia in order to verify or disprove the conclusions of Tatar *et al.* (1996), that the whole of central Anatolia has undergone 33^0 of anti-clockwise rotation since the Eocene. It is important to identify whether any rotation took place prior to the Quaternary, and if so, how much. This can be accomplished by comparative palaeomagnetic studies of different aged units from the same locality.

The controversy over the total offset on the North Anatolian Fault remains unresolved. Although outside the scope of this project, whether this fault zone has a total offset of 85±5km (Barka 1992) or 30-40km (Koçyiğit 1988) has major implications for the averaged slip rate and therefore for any proposed mechanism of extrusion.

13 Conclusions

13.1 Chronological evolution of the Ecemiş Fault Zone

Controls on the timing of fault initiation in the EFZ remain poor. It has been demonstrated through structural mapping that strike-slip offset took place after the Lutetian (Middle Eocene), based on the fault juxtaposition of two Lutetian outcrops in the EFZ. Strike-slip faulting also took place after the Late Eocene, based on the offset of the north-vergent Bolkardağ-Aladağ fold and thrust belt.

There is clearer evidence for faulting in the EFZ during the Late Oligocene and Early Miocene. Palaeocurrent and facies data show that an isolated terrestrial basin existed in the EFZ area during this time, and that this basin creation was synchronous with the large-scale extension and unroofing in the Niğde Massif. Subsidence curves have also shown that rapid subsidence took place during this time, with subsidence rates compatible with strike-slip basin formation. Fault slickenline data indicate that sinistral trans-tension was active in the EFZ area, synchronously with N-S extension.

The deformation pattern recorded in Oligo-Miocene sediments indicate that the Middle Miocene was a period of regional N-S compression, associated with final tightening of the Bitlis Suture. Deformation patterns within the Oligo-Miocene sediments of the EFZ suggest that sinistral strike slip may have been occurring in the EFZ during this time.

Slickenline data indicate that the Late Miocene was a period of continued sinistral trans-tension in the EFZ, but that subsidence rates were considerably slower than during the Late Oligocene – Early Miocene. The EFZ was the site of multiple lake-filled basins.

Sedimentological and structural data indicate that a phase of renewed faulting took place during the latest Miocene – Early Pliocene, with the creation of 0.5-1.5km-high scarps and the deposition of the large alluvial fan complexes which characterise the present-day morphology of the EFZ. These faults developed as many tens of discrete fault segments which are arranged in an *en echelon* array. Slickenline data from these scarps indicate that they accommodated significant sinistral trans-tension, but other evidence (scarp heights and sedimentology) suggest that the major component was extensional. Radiometric dating of faulted tuffs from the Erciyes Basin (the northern continuation of the EFZ) shows that the area underwent extensive E-W extension during the Messinian (latest Miocene). This phase of renewed faulting was synchronous with the initiation of the North Anatolian Fault and the start of the westward crustal extrusion of Anatolia.

Radiometric dating of faulted tuffs in the centre of the Erciyes Basin shows that the last phase of strike-slip faulting took place during the late Pleistocene. Normal faulting and minor strike-slip has also dissected the Plio-Quaternary alluvial fans of the northern EFZ, and this is assumed to be of the same age, although the faulted fanglomerate material has not yet been dated accurately. Slickenline data indicate that the most recent (late Pleistocene) faults affecting the EFZ have been dominantly E-W normal faults, with sinistral strike-slip becoming much less important than in previous phases of faulting.

Seismic records and the lack of consistent river offsets on the EFZ suggest that the fault zone is not currently as active as the NAFZ or EAFZ, and that it is less active than it has been in the past.

13.2 Wider conclusions

The Ecemiş Fault Zone is a regionally important transtensional lineament with an inferred total of 60±5 km sinistral offset since Late Eocene time. This estimate is based on the offset of a north-vergent fold and thrust belt along the northern margin of the Bolkardağ and Aladağ. The offset is comparable with that of the North Anatolian Fault Zone (c.80 km), but is larger than that of the East Anatolian Fault Zone (18-22km).

Strike-slip faulting along the Ecemiş Fault Zone probably began in the Mid-Miocene or slightly earlier, as suggested by subsidence analysis; at least 7-10Ma earlier than initiation of the North Anatolian Fault Zone and the East Anatolian Fault Zone. The early history (Middle - Late Miocene) of the Ecemiş Fault Zone was dominated by sinistral strike-slip, whereas the later history (Pliocene and Quaternary) was dominated by E-W extension, with a very much smaller component of strike slip.

The Ecemiş Fault Zone experienced a prolonged tectonic history. In the study area it lay within a transtensional basin during Oligo-Miocene time, accommodating differential along-strike exhumation of the Taurus Mountains. The Ecemiş Fault Zone was active as a through-going left-lateral strike-slip system by Mid-Miocene time, helping to accommodate regional deformation of the orogen, up to 10Ma prior to Plio-Quaternary westward tectonic escape of Anatolia along the North Anatolian and East Anatolian fault systems. During Plio-Quaternary time, slip became mainly extensional with a minor trans-tensional component, creating grabens and half-grabens along the Ecemiş Fault Zone. Left-lateral displacement continued into Late Pliocene-Quaternary time, as shown by river offsets on alluvial fans shed from the footwall of the transtensional half-grabens.

During the Late Miocene-Quaternary the Ecemiş Fault Zone apparently rotated to near its current NNE-SSW orientation within encompassing crustal units, as suggested by palaeomagnetic data, thus accommodating progressively more E-W extension and less strike-slip. The present-day sinistral component of extrusion is accommodated by faults with a NE-SW strike (similar in orientation to the East Anatolian Fault Zone). Assuming the Ecemiş Fault Zone rotated away from an initial NE-SW strike, it later ceased to be in the optimum orientation to accommodate strike-slip and instead experienced dominantly normal offset.

Significant internal fault deformation took place within Anatolia *prior to* the initial stages of westward tectonic escape. Internal deformation was active prior to and during motion on the bounding right-lateral North Anatolian Fault Zone and left-lateral East Anatolian Fault Zone. Internal deformation of Anatolia may, therefore, may have proceeded along multiple, rotating, strike-slip zones rather than by simple extrusion of a coherent Anatolian 'microplate" bounded by strike-slip faults to the north and south.

Comparison with the South Asian extrusion example shows that a period of crustal thickening (lasting up to 37Ma) commonly separates continental collision from the start of extrusion. It has become clear that even with the aid of detailed structural, sedimentological, geomorphological and other data, it is difficult to precisely constrain the timing and offset on strike-slip faults with prolonged histories in continental settings.

References

AIGNER, T. & REINECK, H.E. 1982. Proximality trends in modern storm sands from the Hegoland Bight (North Sea) and their implications for basin analysis. *Senckenbergiana marit.*, **14**, 183-215.

AKSU, A.E., CALON, T.J., PIPER, D.J.W., TURGAT, S. & IZDAR, E. 1992. Architecture of late orogenic Quaternary basins in northeastern Mediterranean Sea. *Tectonophysics*, **210**, 191-213.

AKTAŞ, G. & ROBERTSON, A.H.F. 1984. The Maden Complex, SE Turkey: evolution of a Neotethyan active margin. *In:* DIXON, J.E. & ROBERTSON, A.H.F. (eds.) The geological evolution of the Eastern Mediterranean. *Geological Society Special Publication*, **17**, 375-402.

ALEXANDROWSKI, P. 1985. Graphical determination of principal stress directions for slikenline lineation populations: an attempt to modify Arthaud's method. *Journal of Structural Geology*, **7**, 73-82.

ALLEN, P.A. & ALLEN, J.R. 1990. Basin Analysis, principles and applications. Blackwell Science.

ALLEN, P.A., HOMEWOOD, P. & WILLIAMS, G.D. 1986. Foreland basins: an introduction. *In*: ALLEN, P.A. & HOMEWOOD, P. (eds.) Foreland Basins. *International Assoaciation of Sedimentologists Special Publication*, **8**, 3-12.

ANGELIER, J. & MECHLER, P. 1977. Sur une méthode graphique de recherche des contraintes principales également utilisable en tectonique et en séismologie: la méthode des dièdres droits. *Bulletin de la Societe Geologique de France*, Série 7, **19**, 1309-1218.

ANGELIER, J. 1984. Tectonic analysis of fault slip data sets. *Journal of Geophysical Research*, **89**, 5835-5848.

ARMIJO, R., MEYER, B., HUBERT, A. & BARKA, A. 1999. Westward propagation of the North Anatolian fault into the northern Aegean: Timing and kinematics. *Geology*, **27**, 267-270.

ARMIJO, R., TAPPONNIER, P. & HAN, T. 1989. Late Cenozoic right-lateral strike-slip faulting in southern Tibet. *Journal of Geophysical Research*, **94**, 2787-2838.

ARMIJO, R., TAPPONNIER, P., MERCIER, J.L. & HAN, T. 1986. Quaternary extension in southern Tibet: Field observations and tectonic implications. *Journal of Geophysical Research*, **91**, 13803-13872.

ARPAT, E. & ŞAROGLU, F. 1972. The East Anatolian Fault System: Thoughts on its development. *Bulletin of the Mineral Research and exploration Institute of Turkey, Ankara*, **78**, 33-39.

ARTHAUD, F. 1969. Méthode de determination graphique des directions de raccourcissement d'allongement et intermédiaire d'une population de failles. *Bulletin de le Societe Geologique Francaise*. Série **7**, **11**, 729-737.

ATABEY, E. & AYHAN, A. 1986. Nigde-Ulukişla - Çamardi -Ciftehan Yoresinin Jeolojisi. *MTA report*, **8064** (unpublished), Ankara.

AVSAR, N. 1997. Personal communication, Dr. Niyazi Avsar, Department of Geology, Cukurova Unversity, Adana, Turkey.

BARKA, A.A. 1992. The North Anatolian Fault Zone. *Annales Tectoniicae*, **6**, 164-195.

BARKA, A.A & GULEN, L. 1989. Complex evolution of the Erzincan basin (Eastern Turkey) and its pull apart and continental escape origin. *Journal of Structural Geology*, **11/3**, 275-283.

BARKA, A.A. & HANCOCK, P.L. 1984. Neotectonic deformation patterns in the convex-northwards arc of the North Anatolian Fault Zone. *In* Dixon, J.E. & Robertson, A.H.F. The geological evolution of the eastern Mediterranean. *Geological Society of London Special Publication*, **17**, 763-774.

BAROV, J. 1974. A structural and palaeogeographic study of the central Sinai faults and domes. *PhD Thesis, Hebrew University, Jerusalem*, 143.

BASU, A., YOUNG, S.W., SUTTNER, L.J., JAMES, W.C. & MACK, G.H. 1975. Re-evaluation of the use of undulatory extinction and polycrystallinity in detrital quartz for provenance interpretation. *Journal of Sedimentary Petrology*, **45**, 873-882.

BATUM, I. 1978. Geology and petrography of Acigol and Golludag volcanics at SW of Nevsehir, Central Anatolia, Turkey. *Yeribilimleri*, **4**, 50-69 [in Turkish with English abstract].

BEAUMONT, C., KEEN, C.E. & BOUTILIER, R. 1982. On the evolution of rifted continental margins: comparison of models and observations for the Nova Scotia margin. Geophysical Journal of the Royal Astronomical Society, **70**, 667-715.

BERGOUGNAN, H. 1976. Structure de la Chaine pontique dans le Haut-Kelkit (Nord-Est de l'Anatolie) *Bulletin Societe Geologique Francaise*, **18**, 675-686.

BERNARD, H.F. & MAJOR, C.F.JR. 1963. Recent meander belt deposits of the Brazos River: an alluvial 'sand' model. *Bulletin of the American Association of Petroleum Geologists*, **47**, 350.

BESANG, C., ECKHARDT, F.J., HARRE, W., KREUZER, H. & MULLE, P. 1977. Radiometrische Altersbestimmungen an neogen Eruptivgesteinen der Turkei. *Geologisches Jahrbuch*, **B25**, 3-36.

BEYHAN, A. 1994. Stratigraphic outline and neotectonics of the Sulucaova-Kovali segment of the Ecemiş Fault Zone. MSc thesis (unpublished), Department of Geological Engineering, Middle East Technical University (ODTU), Ankara, Turkey.

BHATIA, M.R. 1983. Plate tectonics and geochemical composition of sandstones. *Journal of Geology*, **91**, 611-627.

BHATIA, M.R. & CROOK, K.A.W. 1986. Trace element characteristics of greywackes and tectonic setting discrimination of sedimentary basins. *Contributions to Mineralogy and Petrology*, **92**, 181-193.

BIERMAN, P.R. 1994. Using in situ produced cosmogenic isotopes to estimate rates of landscape evolution: A review from the geomorphic perspective. *Journal of Geophysical Research*, **99**, 13885-12896.

BIRMAN, J.H. 1968. Glacial reconnaissance in Turkey. *Geological Society of America Bulletin*, **79**, 1009-1026.

BLACK, R.M. 1970. The elements of palaontology. *Cambridge University Press.*

BLAIR, T.C. 1999. Sedimentology of the debris-flow-dominated Warm Spring Canyon alluvial fan, Death Valley, California. *Sedimentology*, **46**, 941-965.

BLUMENTHAL, M.M. 1956. Yuksek Bolkardağinin Kuzey Kenar Bolgelarinin ve Bati Uzantilarinin Jeolojisi, *MTA yayinlari, Series D*, No. **7.**

BOGGS, S.JR. 1987. Principles of sedimetology and stratigraphy. *Prentice Hall, New Jersay, USA.*

BOOTHROYD, J.C. 1972. Coarse grained sedimentation on a braided outwash fan, northeast gulf of Alaska. *Technical Report Number 6*, Coastal Research Division, University of South Carolina, Columbia, 127.

BOUDAGHER-FADEL, M.K., BANNER, F.T. & WHITTAKER, J.E. 1997. The early evolutionary history of planktonic foraminifera. British Micropalaeontological Society Publications Series, Chapman & Hall.

BRASIER, M.D. 1980. Microfossils. George Allen & Unwin, London. 144-146.

BURCHETTE, T.P. & WRIGHT, V.P. 1992. Carbonate ramp depositional systems. *Sedimentary Geology*, **79**, 3-57.

BURCHFIEL, B.C., MOLNAR, P., ZHANG, P., DENG, Q., ZHANG, W. & WANG, Y. 1995. Example of a supra-detachment basin within a pull-apart tectonic setting: Mormon Point, Death Valley, California. *Basin Research*, **7**, 199-214.

BURCHFIEL, B.C. & STEWART, J.H. 1966. 'Pull-apart' origin of the central segment of Death Valley, California. *Bulletin of the Geolgical Society of America*, 77, 439-442.

BURCHFIEL, B.C., PEIZHEN, Z., YIPENG, W., WEIQI, Z., FANGMIN, S., QIDONG, D., MOLNAR, P. & ROYDEN, L. 1991. Geology of the Haiyuan fault zone, Ninxia-Hui autonomous region, China, and its relation to the evolution of the northeastern margin of the Tibetan plateau. *Tectonics*, **10**, 1091-1110.

BURKE, K. & ŞENGOR, C. 1986. Tectonic escape in the evolution of the continental crust. In BARAZANGI & BROWN (eds) Reflection seismolgy: The continental crust. *American Geophysical Union: Geodynamics Series* **14**, 41-53.

BURNE, R.V. & MOORE, L.S. 1987. Microbialites: organosedimentary deposits of benthic microbial communities. *Palaios*, **2**, 241-254.

CAREY, E. & BRUNIER, B. 1974. Analyse théorique d'un modèle mécanique élémentaire appliqué è l'étude d'une population de failles. *Comptes Rendues de 'Academie des Sciences de Paris*, Série D, **279**, 891-894.

CARTWRIGHT, J.A., TRUDGILL, B.D. & MANSFIELD, C.S. 1995. Fault growth by segment linkage: an explanation for scatter in maximum displacement and trace length data from the Canyonlands Grabens of SE Utah. *Journal of Structural Geology*, **17**, 1319-1326.

ÇEMEN, I., GÖNCÜOĞLU, M.C. & DIREK, K. 1999. Structural evolution of the Tuzgölü Basin in Central Anatolia, Turkey. *Journal of Geology*, **107**, 693-706.

ÇETIN, H. 1999. Personal communication. Dr. Hasan Çetin, Department of Geological Engineering, Cukurova University, Adana, Turkey.

ÇEVIKBAŞ, A., BOZTUG, D., DEMIRKOL, C., AKYILDIZ, M., ACLAN, M., DEMIR, M. & TAŞ, R. 1995. Mineralogical and geochemical evidence for the equilibrated hybrid system in the genesis of the Horoz pluton, Ulukişla-Niğde area, Turkey. *Bulletin of the Geological Congress of Turkey*, **10**, 62-77.

CHAIMOV, T.A., BARAZANGI, M., ALSAAD, D. et al. 1993. Mesozoic and Cenozoic deformation inferred from seismic stratigraphy in the southwestern intracontinental Palmyride fold-thrust belt, Syria. *Geological Society of America Bulletin*, **104**, 704-715.

CHEN, Z., BURCHFIEL, B.C., LIU, Y., KING, R.W., ROYDEN, L.H., TANG, W., WANG, E., ZHAO, J. & ZHANG, X. 2000. GPS measurements from eastern Tibet and their implications for India/Eurasia intracontinental deformation. *Journal of Geophysical Research*, **10**, 16215-16227.

CHRISTIE-BLICK, N. & BIDDLE, K.T. 1985. Deformation and basin formation along strike-slip faults. In Christie-Blick, N. Strike-slip deformation, basin formation, and sedimentation: based on a symposium sponsored by the Society of Economic Palaeontologists and Mineralogists. *SEPM Special publication* **37**, 1-33.

CLARK, M. 2000 Personal communication. Matthew Clark, PhD student, Department of Geology & Geophysics, University of Edinburgh, UK.

COCHRAN, J.R. 1983. Effects of finite rifting times on the development of sedimentary basins. *Earth and Planetary Science Letters*, **66**, 289-302.

COCKBURN, H. 1998. Landscape evolution in Namibia and Antarctica: quantifying denudation rates using in-situ cosmogenic isotope analysis. PhD Thesis, Edinburgh University, Scotland, UK.

COLLINS, A.S. & ROBERTSON, A.H.F. 1998. Processes of Late Cretaceous to Late Miocene episodic thrust-sheet translation in the Lycean Taurides, SW Turkey. *Journal of the Geological Society of London*, **155**, 759-772.

DALRYMPLE, G.B., ALEXANDER, E.C., LANPHERE, M.A. & KRAKER, G.P. 1981. Irradiation of samples for $^{40}Ar/^{39}Ar$ dating using the Geological Survey TRIGA reactor. *US Geological Survey Professional Paper*, **1176**, 55.

DE GEER, G. 1912. A geochronology of the last 12,000 years. *Proceedings of the 11th International Congress, Stockholm* 1910, 241-253.

DELLALOGLU, A. & AKSU, R. 1984 Kulu-Sereflikochisar-Aksaray dolayinin jeolojisi ve petrol olanaklari. Unpublished TPAO report **2020**.

DEMIRTAŞLI, E., BILGIN, A.Z., ERENLER, F., ISIKLAR, S., SANLI, D.Y., SELIM, M. & TURHAN, N. 1973. Bolkardağlarinin Jeolojisi. Cumhuriyetin 50. Yili Yerbilimleri Kongresi, Ankara, 42-57.

DEMIRTAŞLI, E., TURHAN, N., BILGIN, A.Z. & SELIM, M. 1984. Geology of the Bolkar Mountains. *In* Tekeli, O. & Göncüoğlu, M.C. (eds.) Geology of the Taurus Belt, *International Symposium on the Geology of the Taurus Belt*, MTA, Ankara, Turkey, 125-141.

DERCOURT, J., ZONENSHAIN, L.P., RICOU, L.E., KAZMIN, V.G., LEPICHON, X., KNIPPER, A.L., GRANDJACQUET, C., SBORTSHHIKOV, I.M., GEYSSANT, J., LEPVRIER, C., PERCHERSKY, D.H., BOULIN, J., SIBUET, J.C., SAVOSTIN, L.A., SOROKHTIN, O., WESTPHAL, M., BAZHRNOV, M.L., LAUER, J.P. & BIJU-DUVAL, B. 1986. Geological evolution of the Tethys belt from the Atlantic to the Pamirs since the Lias. Tectonophysics, **123**, 241-315.

DEWEY, J.F. & ŞENGOR, A.M.C. 1979. Aegean and surrounding regions: complex multiplate and continuum tectonics in a convergent zone. *Geological Society of Amarica Bulletin*, **90**, 84-92.

DEWEY, J.F., HEMPTON, M.R., KIDD, W.S.F., SAROGLU, F. & SENGOR, A.M.C. 1986. Shortening of continental lithosphere: the neotectonics of Eastern Anatolia – a young collision zone. *In:* COWARD, M.P. & RIES, A.C. (eds.) Collision tectonics. *Geological Society of London Special Publication*, **19**, 3-36.

DEWEY, J.F., HELMAN, M.L., TURCO, E., HUTTON, D.H.W. & NOTT, S.D. 1989. Kinematics of the western Mediterranean. *In*: COWARD, M.P., DIETRICH, D. & PARK, R.G. (eds.) *Alpine Tectonics*. Special Publication of the Geological Society of London, **45**, 265-283.

DEWEY, J.F. & WINDLEY, B.F. 1981 Growth and differentiation of the continental crust. *Philosophical Transacions of the Royal Society of London*, Series A, **301**, 189-206.

DHONT, D., CHOROWICZ, J., YURUR, T., FROGER, J.L., KOSE, O. & GUNDOGDU, N. 1998. Emplacement of volcanic vents and geodynamics of Central Anatolia, Turkey. *Journal of Volcanology and Geothermal Research*, **85**, 33-54.

DICKINSON, W.R. & SUCZEC, C. 1979. Plate tectonics and sandstone compositions. *The American Association of Petroleum Geologists Bulletin*, **63**, 2164-2182.

DILEK, Y., GARVER, J.I. & WHITNEY, D.L. 1997. Extensional exhumation, uplift, and crustal cooling in a collisional orogen and the geomorphic response, central Anatolia-Turkey. *Geological Society of America, Abstract with programs*, **29**, A474.

DILEK, Y. & MOORES, E.M. 1990. Regional tectonics of the Eastern Mediterranean ophiolites. In Malpas, J., Moores, E., Panayiotou, A. & Xenophontos, C. (eds), Ophiolites and ocean crustal analogues. *Proceedings of the symposium 'Troodos 1987', Geolgical Survey Department, Nicosia, Cyprus,* 295-309.

DILEK, Y., THY, P., HACKER, B. & GRUNDVIG., S. 1999. Structure and petrology of Tauride ohiolites and mafic dike intrusions (Turkey): Implications for the Neotethyan ocean. *GSA Bulletin*, **111**, 1192-1216.

DILEK Y. & WHITNEY D.L. *in press* Cenozoic crustal extension and its geomorphic expression in a collisional mountain belt in central Anatolia. *In* Proceedings of the Third International Conference on the Geology of the Eastern Mediterranean, Geological Survey Department, Nicosia, Cyprus.

DZIEWONSKI, A., COU, T.A. & WOODHOUSE, J. 1981. Determination of earthquake source parameters from waveform data for studies of global and regional seismicity. *Journal of Geophysical Research*, **86(B4)**, 2825-2852.

EGGLESTON, J.R. & DEAN, W.E. 1976. Freshwater stromatolitic bioherms in Green Lake, New York. *In:* WALTER, M.R. (ed.) Stromatolites. *Developments in Sedimentology*, **20**, 479-488.

ENGLAND, P. & MCKENZIE, D.P. 1982, A thin viscous sheet model for continental deformation. *Geophysical Journal of the Royal Astronomical Society*, **70**, 295-321.

ENGLAND, P. & MCKENZIE, D.P. 1983, Correction to: A thin viscous sheet model for continental deformation. *Geophysical Journal of the Royal Astronomical Society*, **73**, 523-532.

ERCAN, T., FUJITANI, T., MASUDA, J.I., TOKEL, S., NOTSU, K., UI, T., CAN, B., SELVI, Y., YILDIRIM, T., FISEKCI, A., OLMEZ, M. & AKBASLI, A. 1990. The origin and evolution of the Cenozoic volcanism of Hasandagi-Karacadag area (Central Anatolia). *Jeomorpholoji Bulteni Turkey*, **18**, 39-54 [in Turkish with English abstract].

EROL, O. 1991. Geomorphological evolution of the Taurus Mountains, Turkey. *Zeitshrift für Geomorphologie, Neue Folge Suppl.*, **82**, 99-109.

EVANS, J.E. 1999. Recognition and implications of Eocene tufas and travertines in the Chadron Formation, White River Group, Badlands of South Dakota. *Sedimentology*, **46**, 771-789.

FARROW, G.E. (1966). Bathymetric zonation of Jurassic trace fossils from the coast of Yorkshire, England. *Plaeogeography, Palaeoclimatology, Palaeoecology*, **2**, 103-151.

FAURE, G. 1986. Principles of isotope geology. John Wiley, New York, 2nd edition.

FILLMORE, R.P. 1993. Sedimentation and extensional basin evolution in a Miocene metamorphic core complex setting, Alvord Mountain, central Mojave Desert, California, USA. *Sedimentology*, **40**, 721-742.

FITTON, J.G. & DUNLOP, H.M. 1985. The Cameroon line, West Africa, and its bearing on the origin of oceanic and continental alkali basalts. *Earth and Planetary Science Letters*, **72**, 23-38

FITTON, J.G., JAMES, D.E. AND THIRLWALL, M.F. 1984. A users guide to the X-ray fluorescence analysis of rock samples. Unpublished report, 2nd edition, University of Edinburgh.

FLECKER, R., ROBERTSON, A.H.F., POISSON, A. & MULLER, C. 1995. Facies and tectonic significance of two contrasting Miocene basins in south coastal Turkey. *Terra Nova*, **7**, 221-232.

FLECKER, R., ELLAM, R.M., MULLER, C., POISSON, A., ROBERTSON, A.H.F & TURNER, J. 1998. Application of Sr isotope stratigraphy and sedimentary analysis to the origin and evolution of the Neogene basins in the Isparta Angle, southern Turkey. *Tectonophysics*, **298**, 83-101.

FODOR, L. 1995. From transpression to transtension: Oligocene - Miocene structural evolution of the Vienna Basin and the East Alpine - Western Carpathian junction. *Tectonophysics*, **242**, 151-182.

FREUND, R. 1965. A model of the structural development of Israel and adjacent areas since Upper Cretaceous times. *Geological Magazine*, **102**, 189-205.

FREUND, R. & GARFUNKEL, Z. 1984. Block rotation by strike-slip faulting: structural and paleomagnetic evidence. *Journal of Geophysical Research*, **89**, 6256-6270.

FREUND, R., GARFUNKEL, Z., ZAK, I., GOLDBERG, M., DERIN, B. & WEISSBROD, T. 1970. The shear along the Dead Sea Rift. *Philosophical Transactions of the Royal Society of London, Series A*, **267**, 107-130.

FROSTICK, L.E. & REID, I. 1989. Climatic versus tectonic controls of fan sequences: lessons from the Dead Sea, Israel. *Journal of the Geological Society of London*, **146**, 527-538.

GARFUNKEL, Z. 1981. Internal structure of the Dead Sea leaky transform (rift) in relation to plate kinematics. *Tectonophysics*, **80**, 81-108.

GARFUNKEL, Z. & BEN-AVRAHAM, Z. 1994. Guidebook to the Dead Sea field trip. International Lithosphere Program, Fifth workshop: "Origin of Sedimentary Basins", October 2-7, 1994. Tel Aviv University, Israel.

GLOVER, C.P. 1996. *Plio-Quaternary sediments and neotectonics of the Isparta Angle, S.W. Turkey*. PhD thesis, Edinburgh University.

GLOVER, C.P. & ROBERTSON, A.H.F. 1998. Role of extension and uplift in the Plio-Pleistocene evolution of the Aksu Basin, SW Turkey. *Journal of the Geological Society of London*, **155**, 365-387.

GRIFFIN, D.L. 1999. The late Miocene climate of northeastern Africa: unravelling the signals in the sedimentary succession. *Journal of the Geological Society of London*, **156**, 817-826.

GÖNCÜOĞLU, M.C. 1988. Geology of the Niğde Massif. Tubitak Geotraverse Project proceedings (unpublished).

GÖRÜR N., OKTAY F.Y., SEYMEN I & ŞENGÖR A.M.C. 1984 Palaeotectonic evolution of the Tuzgölü basin complex, Central Turkey; sedimentary record of a Neo-Tethyan closure. *In* DIXON, J.E. & ROBERTSON, A.H.F. (eds.) The Geological Evolution of the Eastern Mediterranean. *Geological Society of London Special Publication*, **17**, 467-482.

GROMET, L.P., DYMEK, R.F., HASKIN, L.A. & KOROTEV, R.L. 1984. The "North American Shale Composite": its compilation, major and trace element characteristics. *Geochimica Cosmochimica Acta*, **48**, 2469-2482

GUCCIONE, M.J. 1993. Grain-size distribution of overbank sediment and its use to locate channel positions. *In:* MARZO, M. & PUIDEFABRIGAS, C. (eds.) Alluvial sedimentation. *Special Publication of the International Association of Sedimentologists*, **17**, 185-194.

GÜL, M.A., ÇUHADAR, Ö., ÖZBAŞ, Y., ALKAN, H. & EFEÇINAR, T. 1984. Bolkar-Belemedik yöresinin jeolojisi ve petrol olanaklari. *Turk Petroll. Anonim Ortakligi*, **Rapor 1972**, 159.

GULEN, L., BARKA, A. & TOKSOZ, M.N. 1987. Continental collision and related complex deformation: Maras triple junction and surrounding structures, SE Turkey. *Yerbilimleri*, **14**, 319-336.

GÜRSOY, H., PIPER, J.D.A., TATAR, O. & TEMIZ, H. 1997. A palaeomagnetic study of the Sivas Basin, central Turkey: crustal deformation during lateral extrusion of the Anatolian Block. *Tectonophysics*, **271**, 89-105.

GÜRSOY, H., PIPER, J.D.A. & TATAR, O. 1999. Palaeomagnetic study of the Galatean volcanic province, north-central Turkey: Neogene deformation at the northern border of the Anatolian block. *Geological Journal*, **34**, 7-23.

HALLOCK, P. & GLENN, C.E. 1986. Larger Foraminifera: a tool for palaeoenvironmental analysis of Cenozoic carbonate depositional facies. *Palaios*, **1**, 55-64.

HARDING, T.P., VIERBUCHEN, R.C. & CHRISTIE-BLICK, N. 1985. Structural styles, plate-tectonic settings, and hydrocarbon traps of divergent (transtensional) wrench faults. In Christie-Blick, N. Strike-slip deformation, basin formation, and sedimentation: based on a symposium sponsored by the Society of Economic Palaeontologists and Mineralogists. *SEPM Special publication* **37**, 51-77.

HARLAND, W.B., ARMSTRONG, R.L., COX, A.V., CRAIG, L.E., SMITH, A.G. & SMITH, D.G. 1990. A Geologic Time Scale 1989. *Cambridge University Press*.

HAQ, B.U., HARDENBOL, J. & VAIL, P.R. 1987. Chronology of fluctuating sea-levels since the Triassic. *Science*, **235**, 1153-1165.

HEMPTON, M.R. 1984. Results of detailed mapping near Lake Hazar (eastern Taurus mountains). In Tekeli, O. & Göncüoğlu, M. (eds) Geology of the Taurus Belt. *General Directorate of Mineral Research and Exploration (MTA), Ankara*, 223-228.

HEMPTON, M.R. 1985. Structure and deformation history of the Bitlis suture near Lake Hazar, southeastern Turkey. *Geological Society of America Bulletin*, **96**, 233-243.

HINCHLIFFE, S. 1998. Personal communication, Dr. Simon Hinchliffe, 1 Aston Way, Sheffield, UK.

HOTTINGER, L. 1983. Processes determining the distribution of larger Foraminifera in space and time. *In:* MEULENKAMP, J.E. (ed.) Reconstruction of marine palaeoenvironments. *Bulletin of Utrecht micropalaeotology*, **30**, 239-253.

HSU, K., MONTADERT, L. & BERNOULLI, D. 1978. History of the Mediterranean salinity crisis. *Initial reports of the Deep Sea Drilling Project*, **42**, 1053-1078.

INAN, S. 1993. Kizilirmak fay zonunun yapisal ve morfotektonik özellikleri. *Türk. Jeol. Kurumu Bul.*, **8**, 321-328.

INNOCENTI, F., MAZZUOLI, G., PASQUARE, F., RADICATI DI BROZOLA, F. & VILLARI, L. 1975. The Neogene calkalkaline volcanism of Central Anatolia: geochronological data on Kayseri-Nigde area. *Geological Magazine*, **112**, 349-360.

ISSLER, D.R., MCQUEEN, H. & BEAUMONT, C. 1989. Thermal and isostatic consquences of simple shear extension of continental lithosphere. *Earth and Planetary Science Letters*, **91**, 341-358.

JACKSON, J.A. 1997. Glossary of Geology. *Fourth Edition*, American Geological Institute.

JAFFEY, N. & ROBERTSON, A.H.F. (2001). New sedimentological and structural data from the Ecemiş Fault Zone, southern Turkey; implications for its timing and offset and the Cenozoic Tectonic Escape of Anatolia. *Journal of the Geological Society*,

JONES, D.J. 1956. Introduction to microfossils. Harper & Brothers, New York. 169-177.

JONES, S.J., FROSTICK, L.E. & ASTIN, T.R. 1999. Climatic and tectonic controls on fluvial incision and aggredation in the Spanish Pyrenees. *Journal of the Geological Society of London*, **156**, 761-769.

JONES, R.R. & TANNER, P.W.G. 1995. Strain partitioning in transpression zones. *Journal of Structural Geology*, **17**, 793-802.

KARADENIZLI, L. & KAZANCI, N. 1993. Lithofacies characteristics of the Oligocene-Early Miocene deposits of Pozanti (Adana) area and new comments on the strike-slip Ecemiş Fault. *In* SUAT, A. Erk Jeoloji Simpozyumu (2-5 Eylul 1991), Bildirileri, 83-92.

KARIG, D.E. & KOZLU, H. 1990. Late Palaeogene-Neogene evolution of the triple junction region near Maras, south-central Turkey. *Journal of the Geological Society of London*, **147**, 1023-1034.

KASAPOGLU, K.E. 1984. Stress-strain and displacement distributions in the Taurus Belt. *In* Tekeli, O. & Goncuoglu, M. (eds) Geology of the Taurus Belt. *General Directorate of Mineral Research and Exploration (MTA), Ankara*, 295-301.

KEMPLER, D. & GARFUNKEL, Z. 1991. The Northeast Mediterrannean triple junction from a plate kinematic point of view. *Bulletin of the Technical University of Istanbul*, **44**, 425-454.

KENDALL, A.C. 1984. Evaporites. *In:* Walker, R.G. (ed.) Facies Models. *Geological Association of Canada, Toronto*, 259-296.

KIDD, W.S.F. & MOLNAR, P. 1988. Quaternary and active faulting observed on the 1985 Academia Sinica - Royal Society Geotraverse of Tibet. *In*: Geological evolution of Tibet, *The Royal Society of London*, 337-363.

KOÇYIĞIT, A. 1988. Tectonic setting of the Geyve basin: age and total displacement of the Geyve fault zone. *In*: 1987 Melih Tokay Symposium, Special Publication of the Middle East Technical University, Ankara, Turkey, 81-104.

KOÇYIĞIT, A. & BEYHAN, A. 1998. A new intracontinental transcurrent structure: the Central Anatolian Fault Zone. *Tectonophysics*, **284**, 317-336.

KOÇYIĞIT, A. & BEYHAN, A. 1999. Reply to Rob Westaway's comment on 'A new intracontinental transcurrent structure: the Central Anatolian Fault Zone, Turkey'. *Tectonophysics*, **314**, 481-496.

KOSS, J.E., ETHRIDGE, F.G. & SCHUMM, S.A. 1994. An experimental study of the effects of base level change on fluvial, coastal plain and shelf systems. *Journal of Sedimentary Research*, **B64**, 90-98.

KUSCI, I. 1998. Personal Communication. Ilkay Kuscu, Middle East Technical University (ODTU), Ankara, Turkey.

KUSCU, I. 1992. Geology of the Çamardi, Niğde region and Madsan Antimony deposit. M.Sc. thesis in Geological Engineering Department, Middle East Technical University (O.D.T.U.), Ankara, Turkey.

LEEDER, M.R. 1999. Sedimentology and sedimentary basins, from turbulence to tectonics. *Blackwell Science*, 313.

LIVERMORE, R.A. & SMITH, A.G. 1984. Relative motions of Africa and Europe in the vicinity of Turkey. *In:* Tekeli, O. & Göncüoğlu, M.C. (eds.) Geology of the Taurus Belt, *International Symposium on the Geology of the Taurus Belt*, MTA, Ankara, Turkey. 1-10.

LORD, A. 1999. Personal communication. Professor Alan Lord, Dept. Geology, University College London, Gower St. London, WC1E 6BT.

LOWE, D.R. 1976. Subaqueous liquified and fluidized sediment flows and their deposits. *Sedimentology*, **23**, 285-308.

LYTWYN, J.N. & CASEY, J.F. 1995. The geochemistry of post-kinematic mafic dike swarms and sub-ophiolitic metabasites, Pozanti-Karsanti ophiolite, Turkey: Evidence for ridge subduction. *Geological Society of America Bulletin*, **107**, 830-850.

MACHETTE, M.N. 1985. Calcic soils of the southwestern United States. *Special Paper of the Geological Society of America*, **203**, 1-21.

MACK, G.H. & LEEDER, M.R. 1999. Climatic and tectonic controls on alluvial-fan and axial-fluvial sedimentaion in the Plio-Pleistocene Palomas half graben, southern Rio Grande rift. *Journal of Sedimentary Research*, **69**, 635-652.

MALZ, H. 1999. Personal communication. Dr. Heinz Malz, Neulandstr. 3., D-49565 Bramsche, Germany.

MANN, P. 1997. Model for the formation of large, transtensional basins in zones of tectonic escape. *Geology*, **25**, 211-214.

MANN, P., HEMPTON, M.R., BRADLEY, D.C. & BURKE, K. 1983. Development of pull-apart basins. *Journal of the Geological Society of Chicago*, **91**, 529-554.

MAYER, L. 1999 Personal Communication, Prof. Larry Mayer, Ohio State University, USA.

MCCABE, P.J. 1984. Depositional environments of coal and oal-bearing strata. *In:* RAHMANI, R.A. & FLORES, R.M. (eds) Sedimentology of coal and coal-bearing Sequences, *Special Publication of the International Association of Sedimentologists*, **7**, 13-42.

MCCANN, T. 1991. Petrological and geochemical determination of provenance in the southern Welsh Basin. *In* Morton, A.C., Todd, S.P. & Haughton, P.D.W. (eds), 1991, Developments in sedimentary provenance studies. *Geological Society Special Publication* **No.57**, 215-230.

MCDOUGALL, I. & HARRISON, T.M. 1988. Geochronology and thermochronology by the $^{40}Ar/^{39}Ar$ method. Oxford University Press.

MCKENZIE, D.P. 1968. Speculations on the consequences and causes of plate motions. *Geophysical Journal of the Royal Astronomical Society*, **18**, 1-32.

MCKENZIE, D.P. 1970. Plate tectonics of the Mediterranean region. *Nature*, **226**, 239-243.

MCKENZIE, D.P. 1972. Active tectonics of the Mediterranean region. *Geophysical Journal of the Royal Astronomical Society*, **30**, 109-185.

MCKENZIE, D.P. 1978. Some remarks on the development of sedimentary basins. *Earth and Planetary Science Letters*, **40**, 25-32.

MEYER, L. 1999 Personal communication. Professor Larry Meyer, Department of geology, Ohio State University, USA.

MICHAEL, A.J. 1990. Energy constraints on kinematic models of oblique faulting: Loma Prieta versus Parkfield-Coalinga. *Geophysical Research Letters*, **17**, 1453-1456.

MOLNAR, P. 1992. Brace-Goetze strength profiles, the partitioning of strike-slip and thrust faulting at zones of oblique convergence, and the stress-heat flow paradox of the San Andreas Fault. *In*: EVANS, B. & WONG, T.F. (eds.) *Fault mechanics and transport properties of rocks*. Academic Press, London, 435-459.

MOLNAR, P. & TAPPONIER, P. 1975. Cenozoic tectonics of Asia: Effects of a continental collision. *Science*, **189**, 419-426.

MORRIS, A. & ROBERTSON, A.H.F. 1993. Miocene remagnetisation of carbonate platform and Antalya Complex units within the Isparta Angle, SW Turkey. *Tectonophysics*, **220**, 243-266.

MORRIS, A. & TARLING, D.H. 1996. Palaeomagnetism and tectonics of the Mediterranean region: an introduction. *In:* MORRIS, A. & TARILING, D.H. (eds.) 1996. Palaeomagnetism and tectonics of the Mediterranean region. *Geological Society of London Special Publication*, **105**, 1-18.

MOUNT, V.S. & SUPPE, J. 1987. State of stress near the San Andreas Fault: Implications for wrench tectonics. *Geology*, **15**, 1143-1146.

MUELLER, B., WEHRLE, V. & FUCHS, K. 1997. The 1997 release of the World Stess Map (available on-line at http://www-wsm.physik.uni karlsruhe.de/pub/Rel97/wsm97.html).

MURPHY, D.H. & WILKINSON, B.H. 1980. Carbonate deposition and facies distribution in a central Michigan marl lake. *Sedimentology*, **27**, 123-135.

NAJMAN Y, GARZANTI E 2000. Reconstructing early Himalayan tectonic evolution and paleogeography from Tertiary foreland basin sedimentary rocks, northern India. *Geological Society of America Bulletin* **112**, 435-449

NAZIK, A. 1999. Personal communication. Dr. A. Nazik, Jeoloji Muh. Bolumu, Cukurova Universitesi, Adana.

NAZIK, A. & GOKCEN, N. 1992. Ostracoda genus Zonocypris and its species in Kurtulmus Formation of Ulukişla Basin (Turkey). *Revista Espanola De Micropaleontologia*, **24**, 63-69.

NEMEC, W. 1992. Depositional controls on plant growth and peat accumulation in a braidplain delta environment: Helvetiafjellet Formation (Barremian-Aptian), Svalbard. *In:* MCCABE, P.J. & PARRISH, J.T. (eds.) Controls on the distribution and quality of Cretaceous coals. *Special Paper of the Geological Society of America*, **267**, 209-226.

NEMEC, W. & STEEL, R.J. 1984. Alluvial and coastal conglomerates: their significant feature and some comments on gravelly mass flow deposits. *In:* KOSTER, E.H. & STEEL, R.J. (eds.) Sedimentology of gravels and conglomerates. *Canadian Society of Petroleum Geology Memoir*, **10**, 1-31.

NICHOLSON, C., SEEBER, L., WILLIAMS, P.L. & SYKES, L.R. 1985. Seismic deformation along the southern San Andreas fault, California: implications for conjugate slip rotational block tectonics. *Tectonics*, **5**, 629-648.

NICKEL, E. 1983. Environmental significance of freshwater oncoids, Eocene Guarga Formation, southern Pyrenees, Spain. *In:* PERT, T.M. (ed.) Coated grains. Springer-Verlag, Berlin, 308-329.

OKTAY, F.Y. 1982. Stratigraphy and geological evolution of Ulukisla and its surroundings. *Bulletin of the Gelogical Survey of Turkey*, **25**, 15-23.

ORAL, M.B., REILINGER, R.E. & TOKSOZ, M.N. 1995. Global positioning system offers evidence of plate motions in Eastern Meditteranean. *Eos, Transactions of the American Geophysical Union*, **76**, 1-11.

ORDÓÑEZ, S. & GARCÍA DEL CURA, M.A. 1983. Recent and Tertiary fluvial carbonates in central Spain. *In:* COLLINSON, J.D. & LEWIN, J. (eds.) Modern and ancient fluvial systems. *Special Publication of the International Association of Sedimentologists*, **6**, 485-497.

OZANER, F.S. & TÜFEKÇI, K.D. 1988. Şarkişla-Gemerek dolayarinin jeomorfolojisi ve genç tektoniği. *Jeomorfol. Dergisi*, **16**, 53-60.

PARLAK, O., BOZKURT, E. & DELALOYE, M. 1996. The obduction direction of the Mersin Ophiolite: structural evidence from subophiolitic metamorphics in the Central Tauride Belt, southern Turkey. *International Geology Review*, **38**, 778-786.

PARLAK, O. & DELALOYE, M. 1999. Precise 40Ar/39Ar ages from the metamorphic sole of the Mersin ophiolite (southern Turkey). *Tectonophysics*, **301**, 145-158.

PASQUARE, G. 1968. Geology of the Cenozoic Volcanic area of central Anatolia. *Atti. Accad. Naz. Lincei.*, **9**, 53-204.

PASQUARE, G., POLI, S., VEZZOLI, L. & ZANCHI, A. 1988. Continental arc volcanism and tectonic setting in Central Anatolia, Turkey. *Tectonophysics*, **146**, 217-230.

PAVONI, N. 1961. Die Nordanatolische Horizontal-verschiebung. *Geology Rundschau*, **51**, 122-39.

PAYNE, A.S. 1996. The structural and sedimentary evolution of the Polis graben system, West Cyprus. *Unpublished PhD thesis, Edinburgh University.*

PEDLEY, H.M. 1990. Classification and environmental models of cool freshwater tufas. *Sedimentary Geology*, **68**, 143-154.

PELTZER, G. & TAPPONNIER, P. 1988. Formation and evolution of strike-slip faults, rifts and basins during the India-Asia collision: An experimental approach. *Journal of Geophysical Research*, **93**, 15085-15117.

PERINCEK, D. & ÇEMEN, I. 1990. The structural relationship between the East Anatolian and Dead Sea fault zones in southeastern Turkey. *Tectonophysics*, **172**, 331-340.

PICKERING, K.T., HISCOTT, R.N. & HEIN, F.J. 1989. Deep marine environments: clastic sedimentation and tectonics. Unwin Hyman, London.

PITMAN, W.C. & ANDREWS, J.A. 1985. Subsidence and thermal history of small pull-apart basins. *In:* BIDDLE, K.T. & CHRISTIE-BLICK, N. (eds.) Strike-slip deformation, basin formation and sedimentation. *Society of Economic Palaeontology and Mineralogy Special Publication*, **37**, 45-49.

POOLE, A. & ROBERTSON, A.H.F. 1998. Pleistocene fanglomerate deposition related to uplift of the Troodos ophiolite, Cyprus. *Proceedings of the Ocean Drilling Program, Scientific Results*, **160**, 545-566.

POSAMENTIER, H.W. 1988. Fluvial deposition in a stratigraphic framework. *In:* JAMES, D.P. LECKIE, D.A. (eds.) Sequences, stratigraphy, sedimentology: surface and subsurface. *Canadian Society of Petroleum Geologists Memoirs*, **15**, 582-583.

POSAMENTIER, H.W. & VAIL, P.R. 1988. Eustatic controls on clastic deposition 2: Sequence and systems tract models. *In:* WILGUS, C.K., HASTINGS, B.S., KENDALL, C.G.ST.C., POSAMENTIER, H.W., ROSS, C.A. & VAN WAGONER, C. (eds.) Sea level changes: an integrated approach. *Society of Economic Paleontologists and Mineralogists, Special Publications*, **42**, 125-154.

PRIOR, D.B. & BORNHOLD, B.D. 1988. Submarine morphology and processes of fjord fan deltas and related high-gradient systems: modern examples from British Columbia. *In:* NEMEC, W. & STEEL, R.J. (eds.) Fan deltas: sedimentology and tectonic setting. *Blackie, London*, 125-143.

PURSER, B. & EVANS, G. 1975. Regional sedimentation along the Trucial Coast, SE Persian Gulf. *In:* The Persian Gulf: Holocene carbonate sedimentation and diagenesis in a shallow epicontinental sea. *Springer-Verlag, Berlin*, 211-231.

PURVIS, M. 1998. *The late Tertiary-Recent tectonic-sedimentary evolution of extensional sedimentary basins of the northern Menderes Massif, west Turkey*. PhD thesis, Edinburgh University, UK.

QUENNELL, A.M. 1959. Tectonics of the Dead Sea Rift. *20th International Geology Congress, Mexixo Assoc. Serv. Geol. Afr.*, 385-405.

QUENNELL, A.M. 1984. The western Arabia rift system. *In*: DIXON, J.E. & ROBERTSON, A.H.F. (eds) *The geological evolution of the Eastern Mediterranean*. Geological Societ Special Publication, **17**, 775-788.

RAMOS, A. & SOPEÑA, A. 1983.Gravel bars in low sinuosity streams (Permian and Triassic, central Spain). *In:* COLLINSON, J.D. & LEWIN, J. (eds.) Modern and ancient fluvial systems. *Special Publication of the International Association of Sedimentologists*, **6**, 301-312.

RATSCHBACHER, L., MERLE, O., DAVY, P. & COBBOLD, P. 1991. Lateral extrusion in the eastern Alps, part 1: boundary conditions and experiments scaled for gravity. *Tectonics*, **10**, 245-256.

READING, H.G. 1978. Sedimentary environments, process, facies and stratigraphy. *Blackwell Science*.

REILINGER, R.E., MCCLUSKY, S.C., ORAL, M.B., KING, R.W & TOKAZ, M.N. 1997. Global Positioning System measurements of present-day crustal movements in the Arabia-Africa-Eurasia plate collision zone. *Journal of Geophysical Research*, **102**, 9983-9999.

REINSON, G.E. 1984. Barrier island and associated strand-plain systems. *In:* Walker, R.G. (ed.) Facies models. *Geoscience Canada Reprint Series*, Figure 16, 128.

ROBERTS, G.P. 1996. Variation in fault slip directions along active normal faults. *Journal of Structural Geology*, **18**, 835-845.

ROBERTS, S. & JACKSON, J. 1991. Active normal faulting in central Greece: an overview. *In:* ROBERTS, A.M., YIELDING, G. & FREEMAN, B. (eds.) The geometry of normal faults. *Geological Society of London Special Publication*, **56**, 125-142.

ROBERTSON, A.H.F. 2000. Mesozoic-Tertiary tectonic-sedimentary evolution of a south Tethyan oceanic basin and its margins in southern Turkey. *In:* BOZKURT, E., WINCHESTER, J.A. & PIPER, J.D.A. (eds.) Tectonics and Magmatism in Turkey and the Surrounding Area. *Geological Society of London Special Publication*, **173**, 97-138.

Robertson, A.H.F. 2000a. Outline of the tectonic evolution of te North african/Leant continental margin in relation to the bordering Tethys ocean. Post-meeting abstract – African continental margins of the Mediterrannean Sea, Commission Internationale pour l'exporation de la mer Mediterranee, CIESM Workshop, Djerba, Tunisia.

ROBERTSON, A.H.F. & GRASSO, M. 1995. Overview of the Late Tertiary-Recent tectonic and palaeo-environmental development of the Mediterranean region. *Terra Nova*, **7**, 114-127.

ROBERTSON, A.H.F. & DIXON, J.E. 1984. Introduction: aspects of the geological evolution of the Eastern Mediterranean. *In:* DIXON, J.E. & ROBERTSON, A.H.F. (eds.) The geological evolution of the Eastern Mediterranean. *Geological Society Special Publication*, **17**, 1-74.

ROSER, B.P. & KORSCH, R.J. 1986. Determination of tectonic setting of sandstone-mudstone suites using SiO2 content and K2O/Na2O ratio. *Journal of Geology*, **94**, 635-650.

ROSETTI, F., STORTIAND, F. & SALVINI, F. *in press*. Cenozoic non-coaxial transtension along the western shoulder of the Ross Sea, Antarctica, and the emplacement of McMurdo dyke array. *Terra Nova*, **12**.

ROTSTEIN, Y. 1984. Counter-clockwise rotation of the Anatolian block. *Tectonophysics*, **108**, 71-91.

ŞAROGLU, F. 1992. The East Anatolian Fault Zone of Turkey. *Annales Tectonicae*, **6**, 99-125.

SCLATER, J.G. & CHRISTIE, P.A.F. 1980. Continental stretching: an explanation of the post-mid-Cretaceous subsidence of the continental North Sea Basin. *Journal of Geophysical Research*, **85**, 3711-3739.

SEARLE, M.P. 1996. Geological evidence against large scale pre-Holocene offsets along the Karakoram Fault: Implications for the limited extrusion of the Tibetan plateau. *Tectonics*, **15**, 171-186.

SEEBER, L. & PECHER, A. 1998. Strain partitioning along the Himalayan arc and the Nanga Parbat antiform. *Geology*, **26**, 791-794.

ŞENGOR, A.M.C. 1979. The North Anatolian transform fault: its age. Offset and significance. *Journal of the Geological Society of London*, **136**, 269-282.

ŞENGÖR, A.M.C., YALÇIN, N. & CANITEZ, N. 1980. The origin of the Adana/Cilicia Basin. An incompatibility structure arising at the common termination of the East Anatolian and Dead Sea Transform Faults. *Sedimentary basins of Mediterranean margins, Abstract*, 45-46.

ŞENGOR, A.M.C. & YILMAZ, Y. 1981. Tethyan evolution of Turkey: A plate tectonic approach. *Tectonophysics*, **75**, 181-241.

ŞENGOR, A.M.C., YILMAZ, Y. & SUNGURLU, O. 1984a. Tectonics of the Mediterranean Cimmerides: nature and evolution of the western termination of Palaeo-tethys. *In*: DIXON, J.E. & ROBERTSON, A.H.F. (eds.) *The geological evolution of the Eastern Mediterranean*. Geological Societ Special Publication, 17, 77-112.

ŞENGOR, A.M.C., SATIR, M. & AKKOK, R. 1984b. Timing of tectonic events in the Menderes Massif, western Turkey: implications for tectonic evolution and evidence for Pan-African basement in Turkey. *Tectonics*, **3**, 693-707.

ŞENGOR, A.M.C., GÖRÜR, N. & ŞAROGLU, F. 1985. Strike-slip faulting and related basin formation in zones of tectonic escape: Turkey as a case study. *In* Biddle, K.T. & Christie-Blick, N. (eds.) Strike-slip deformation, basin formation and sedimentation. *Society of Economic Palaeontologists and Mineralogists Special Publication*. **37**, 227-264.

SEYMEN, I. 1975. Kelkit Vadisi Kesiminde Kuzey Anadolu fay zonunum tektonik ozelligi. PhD Thesis (unpublished), Istanbul Technical University.

SHEARMAN, D.J., MCGUGAN, A., STEIN, C. & SMITH, A.J. 1989. Ikaite, $CaCO_3.6H_2O$, precursor of thinolites in the Quaternary tufas and tufa mounds of the Lahontan and Mono Lake basins, western Unites States. *Bulletin of the Geological Society of America*, **101**, 913-917.

SIAME, L.L., BOURLÈS, D.L., SÉBRIER, M., BELLIER, O., CASTANO, J.C., ARAUJO, M., PEREZ, M., RAISBECK, G.M. & YIOU, F. 1997. Cosmogenic dating ranging from 20 to 700ka of a series of alluvial fan surfaces affected by the El Tigre fault, Argentina. *Geology*, **25**, 975-978.

SIGURDSSON, H., SPARKS, R.S.J., CAREY, S.N. & HUANG, T.C. 1980. Volcanogenic sedimentation in the Lesser Antilles arc. *Journal of the Geological Society, London*, **88**, 523-540.

SINCLAIR, H.D. & JAFFEY, N. *In Press*. Sedimentology of the Indus Group, Ladakh, northern India: implications for the timing of initiation of the palaeo-Indus River. *Journal of the Geological Society of London*.

SINCLAIR, H.D., SAYER, Z.R. & TUCKER, M.E. 1998. Carbonate sedimentation during early foreland basin subsidence: the Eocene succession of the French Alps. *In:* WRIGHT, V.P. & BURCHETTE, T.P. (eds.) Carbonate Ramps. *Geological Society, London Special Publication*, **149**, 205-227.

SMITH, A.G. & SPRAY, J.G. 1984. A half-ridge transform model for the Hellenic-Dinaric ophiolites. *In*: DIXON, J.E. & ROBERTSON, A.H.F. (eds.) *The geological evolution of the Eastern Mediterranean*. Geological Societ Special Publication, **17**, 629-644.

SMITH, N.D. 1985. Proglacial fluvial environment. *In:* ASHLEY, G.M., SHAW, J. & SMITH, N,D. (eds.) Glacial sedimentary environments. *Society of Economic Palaeontologists and Mineralogists, Short Course*, **16**, Tulsa, 85-134.

SPEARING, D.R. 1974. Summary sheets of sedimentary deposits, Mc-8, Sheet 1, Fig. 1c. Geological Socity of America.

SPERNER, B., RATSCHBACHER, L. & OTT, R. 1993. Fault-striae analysis: a turbo pascal program package for graphical presentation and reduced stress tensor calculation. *Computers and Geosciences*, **19**, 1361-1388.

STECKLER, M.S. & WATTS, A.B. 1978. Subsidence of the Atlantic-type continental margin of New York. *Earth and Planetary Science Letters*, **41**, 1-13.

SUMMERFIELD, M.A. 1991. Global geomorphology: an introduction to the study of landforms. Longman, London.

TAPPONNIER, P.R., LACASSIN, P.H., LELOUP, U., SCHARER, D., ZHONG, H., WU, L., SHAOCHENG, L., ZHANG, J. & ZHONG. 1990. The Ailo Shan – Red River metamorphic belt: Tertiary left-lateral shear between IndoChina and south China. *Nature*, **343**, 431-437.

TAPPONIER, P., PELTZER, G & ARMIJO, R. 1986. On the mechanics of the collision between India and Asia. In Coward, M.P. & Ries, A.C. (eds.) Collision tectonics. *Geological Society Special Publication*, **19**, 115-157.

TAPPONNIER, P., PELTZER, G., LEDAIN, A.Y., ARMIJO, R. & COBBOLD, P.R. 1982. Propagating extrusion tectonics in Asia: New insights from simple experiments with plasticine, *Geology*, **10**, 611-616.

TATAR, O., PIPER, J.D.A. & GÜRSOY, H. 2000. Palaeomagnetic study of the Erciyes sector of the Ecemiş Fault Zone: neotectonic deformation in the southeastern part of the Anatolian block. *In* BOZKURT, E., WINCHESTER, J.A. & PIPER, J.D.A. (eds.) *Tectonics and magmatism in Turkey and the surrounding area*. Geological Society, London, Special Publication, **173**, 423-440.

TATAR, O., PIPER, J.D.A., GÜRSOY, H. & TEMIZ, H. 1996. Regional significance of Neotectonic counter-clockwise rotation in central Turkey. *International Geology Review*, **38**, 692-700.

TAYMAZ, T., EYIDOGAN, H. & JACKSON, J. 1991. Source parameters of large earthquakes in the East Anatolian Fault Zone (Turkey). *Geophysical Journal International*, **106**, 537-550.

TEKELI, O., AKSAY, A., URGUN, B.M. & ISIK, A. 1984. Geology of the Aladağ Mountains. *In* Tekeli, O. & Göncüoğlu, M.C. (eds.) Geology of the Taurus Belt, *International Symposium on the Geology of the Taurus Belt*, MTA, Ankara, Turkey, 125-141.

TERNEK, Z. 1962. 1:500,000 geological map of the Adana region. Published by the Turkish Geological Survey (MTA), Ankara, Turkey.

TEYSSIER, C. & TIKOFF, B. 1998. Strike-slip partitioned transpression of the San Andreas fault system: a lithospheric-scale approach. *In* Holdworth, R.E, Strachan, R.A. & Dewey, J.F. (eds.) Continental transpressional and transtensional tectonics. *Geological Society of London Special Publication*, **135**, 143-159.

THOMAS, J.C., HAUVIN, C.A., GAPAIS, D., BAZHENOV, M.L., PERROUD, H., COBBOLD, P.R. & BURTMAN, V.S. 1994. Palaeomagnetic evidence for Cenozoic block rotation in the Tadjik depression (central Asia). *Journal of Geophysical Research*, **99**, 141-160.

THOMAS, J.C., PERROUD, H., COBBOLD, P.R., BAZHENOV, M.L., BURTMAN, V.S., CHAUVIN, A. & SADYBAKASOV, E. 1993. A palaeomagnetic study of Tertiary formations from the Kyrgyz Tien Shan and its tectonic implications. *Journal of Geophysical Research*, **98**, 9571-9589.

THUIZAT, R., WHITECHURCH, H., MONTIGNY, R. & JUTEAU, T. 1981. K-Ar dating of some infra-ophiolitic metamorphic sole from the Eastern Mediterranean: New evidence for ocean thrustings before obduction. *Earth and Planetary Science Letters*. **52**, 302-310.

TIKOFF, B. & TEYSSIER, C. 1994. Strain modelling of displacement-field partitioning in transpressional orogens. *Journal of structural Geology*, **16**, 1575-1588.

TOKAY, M. 1973. Kuzey Anadolu fay zonunum Gerede ile Ilgaz arasindaki kisminda jeolojik gozlemler. In: Symposium on the North Anatolian Fault and Earthquake Belt. M.T.A. Enstitüsü, Ankara, 19-29.

TOPRAK, V. & GÖNCÜOĞLU, M.C. 1993. Tectonic control on the development of the Neogene-Quaternary Central Anatolian Volcanic Province, Turkey. *Geological Journal*, **28**, 357-369.

TRIFONOV, V.G., KARAKHANIAN, A.S. & KOZHURIN, A.I. 1994. Major active faults of the collision area between the Arabian and the Eurasian plates. *In* BOLT, B.A. & AMIRBEKIAN, R. (eds.) Continental collision zone earthquakes and seismic hazard reduction. *Proceedings of the International Conference at Yerevan-Sevan, Armenia (1-6 October 1993), IASPEI*, 56-76.

TURNER, J. 1998. The subsidence of sedimentary basins. PhD thesis, Edinburgh University.

UÇAR, L. 1997. Gülek-Pozanti-Kamişli (NW Adana) dolayinin stratigrafisi ve sedimanter petrografik incelemesi. *Cukurova University PhD Thesis, Unpublished*, 472.

ÜNLUGENÇ, U., DEMIRKOL, C. & SAFAK, U. 1993. Startigraphical and sedimentological characteristics of the Karsanti Basin fill to the N-NE of the Adana Basin. A.SUAT ERK JEOLOJI SIMPOZYUMU (2-5 Eylul 1991) BILDIRILERI, 215-227.

VAN HAVER, T. 1984. *Etude stratigraphique, sedimentologique et structural d'un bassin d'avant arc: example du bassin de 'Indus, Ladakh, Himalya*. PhD thesis, University of Grenoble, France.

WANG, E., BURÇHFIEL, B.C., ROYDEN, L.H., LIANGZHONG, C., JISHEN, C., WENXIN, L. & ZHILIANG, C. 1998. Late Cenozoic Xianshuihe-Xiaojiang, Red River, and Dali fault systems of southwestern Sichuan and Central Yunnan, China. *Geological Society of America Special Paper*, **327**.

WERNICKE, B. 1985. Uniform-sense normal, simple shear of the continental lithosphere. *Canadian Journal of Earth Sciences*, **22**, 108-125.

WESTAWAY, R. 1994. Present-day kinematics of the Middle East and eastern Mediterranean. *Journal of Geophysical Research*, **99**, 12071-12090.

WESTAWAY, R. 1999. Comment on A new intracontinental transcurrent structure: the Central Anatolian Fault Zone, Turkey" by A. Koçyiğit and A. Beyhan. *Tectonophysics*, **314**, 469-479.

WESTAWAY, R. *In Press*. Kinematics of the Malatya-Ovacik fault Zone. *Geodynamica Acta* special issue on Neotectonics of Turkey.

WESTAWAY, R. & ARGER, J. 1996. The Golbaşı basin, southeastern Turkey: a complex discontinuity in a major strike-slip fault zone. *Journal of the Geological Society of London*, **153**, 729-744.

WHITNEY, D.L. & DILEK, Y. 1997. Core complex development in central Anatolia, Turkey. *Geology*, **25**, 1023-1026.

WHITNEY, D.L. & DILEK, Y. 1998. Metamorphism during Alpine crustal thickening and extension in central Anatolia, Turkey: the Niğde Metamorphic core complex. *Journal of Petrology*, **39**, 1385-1403.

WILLIAMS, G.D., ÜNLÜGENÇ, U., KELLING, G. & DEMIRKOL, C. 1995. Tectonic control on stratigraphic evolution of the Adana Basin, Turkey. *Journal of the Geological Society, London*, **152**, 873-882.

WOODCOCK, N.H. 1990. Transpressive Acadian deformation across the Central Wales Lineament. *Journal of Structural Geology*, **12**, 329-337.

WRONKIEWICZ, D.J. & CONDIE, K.C. 1987. Geochemistry of Archean shales from the Witwatersrand Supergroup, South Africa: Source area weathering and provenance. *Geochimica et Cosmochimica Acta*, **51**, 2401-2416.

YALCIN, M.N. & GÖRÜR, N. 1984. Sedimentological evolution of the Adana Basin. *In* Tekeli, O. & Göncüoğlu, M.C. (eds.) Proceedings of the international symposium on the Geology of the Taurus belt, MTA, Ankara, 165-172.

YETIŞ, C. 1978. Geology of the Çamardi (Niğde) region and the charachteristics of the Ecemiş Fault Zone between Maden Bogazi and Kamişli. *Istanbul University Fen Fakultesi Mecmuasi, Series B*, **43**, 41-61.

YETIŞ, C. 1984. New observations on the age of the Ecemiş Fault. *In* Tekeli, O. & Göncüoğlu, M.C. (eds.) Proceedings of the international symposium on the Geology of the Taurus belt, MTA, Ankara. 159-164.

YETIŞ, C. 1987. Facies and environmental aspects of the fluvio-lacustrine Oligo-Miocene deposits in the Çamardi (Niğde) area. *Turkiye Jeoloji Bulteni*, **30**, 1-8.

YETIŞ, C. 1999 Personal communication. Professor Cengiz Yetiş, Department of Geological Engineering, Cukurova University, Adana, Turkey.

YILMAZ, Y. 1993. New evidence and model on the evolution of the southeast Anatolian orogen. *Geological Society of America Bulletin*, **105**, 251-271.

ZOBACK, M.L. 1992. First and second order patterns of stress in the lithosphere: The World Stress Map Project. *Journal of Geophysical Research*, **97**, 11703-11728.

The author at work

The Aladağ

APPENDIX 1

Simplified logs for Backstripping

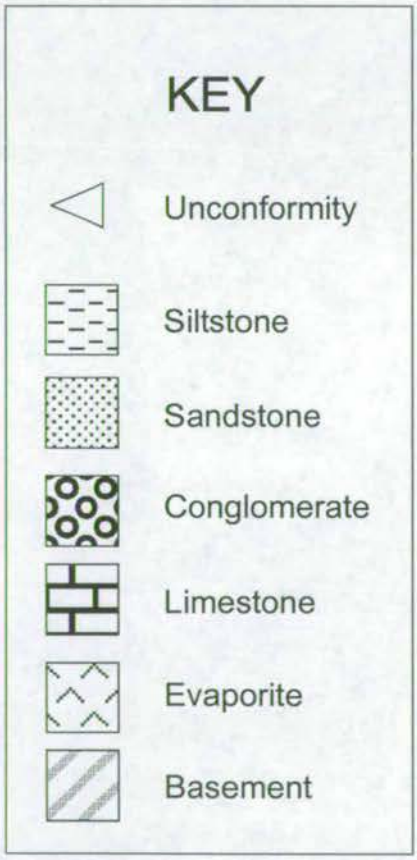

ECEMIS BASIN

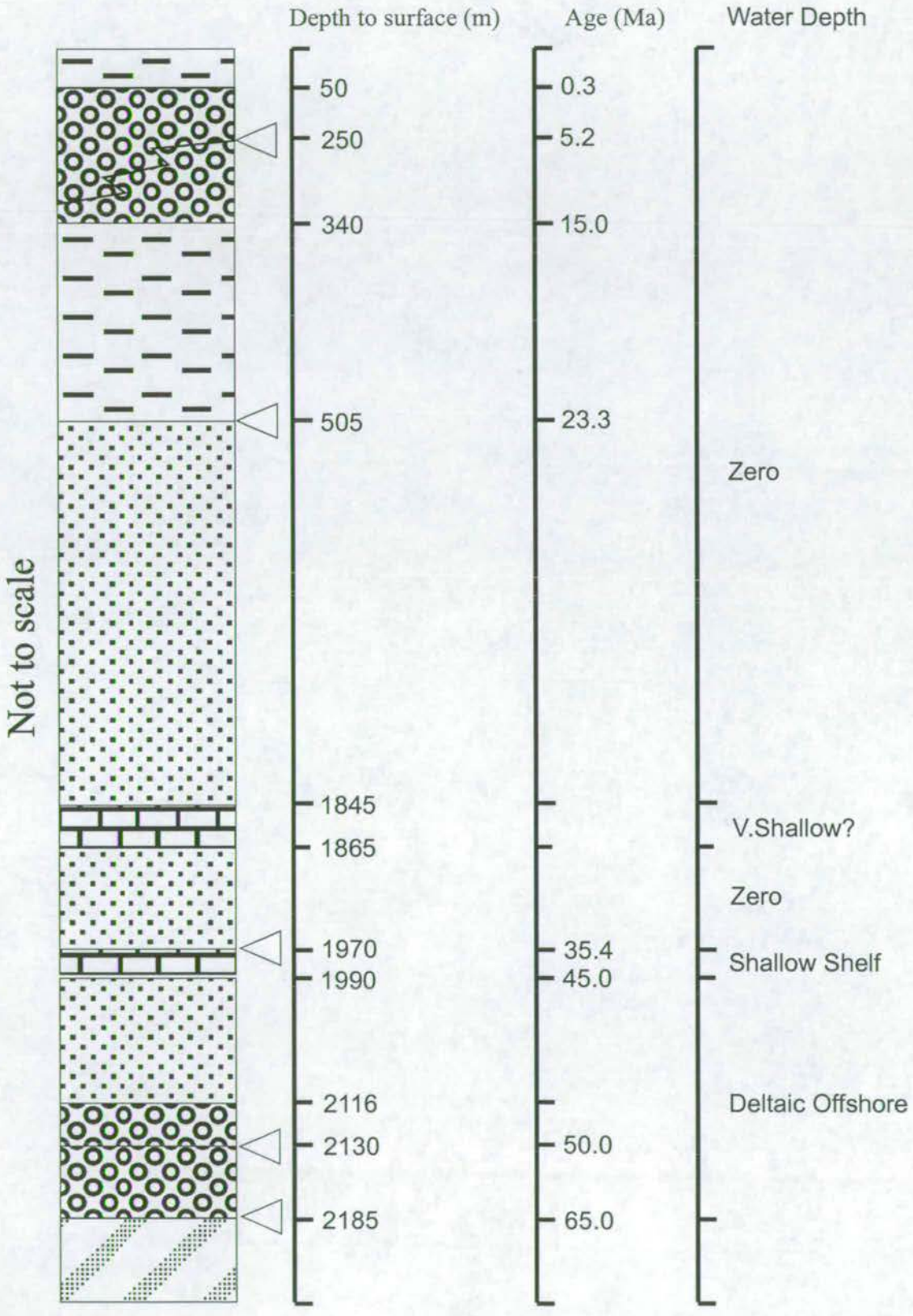

ULUKISLA BASIN

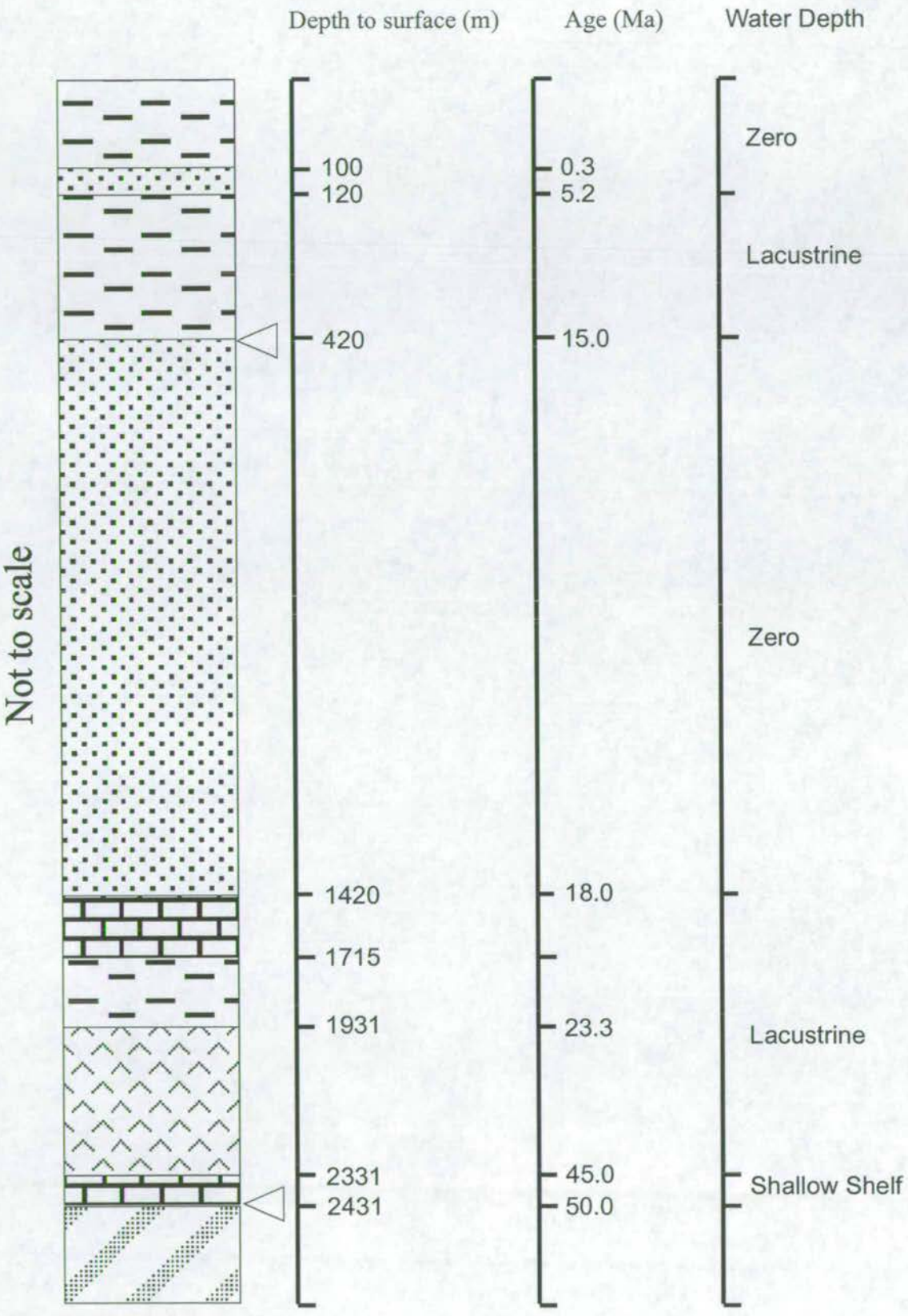

ADANA BASIN

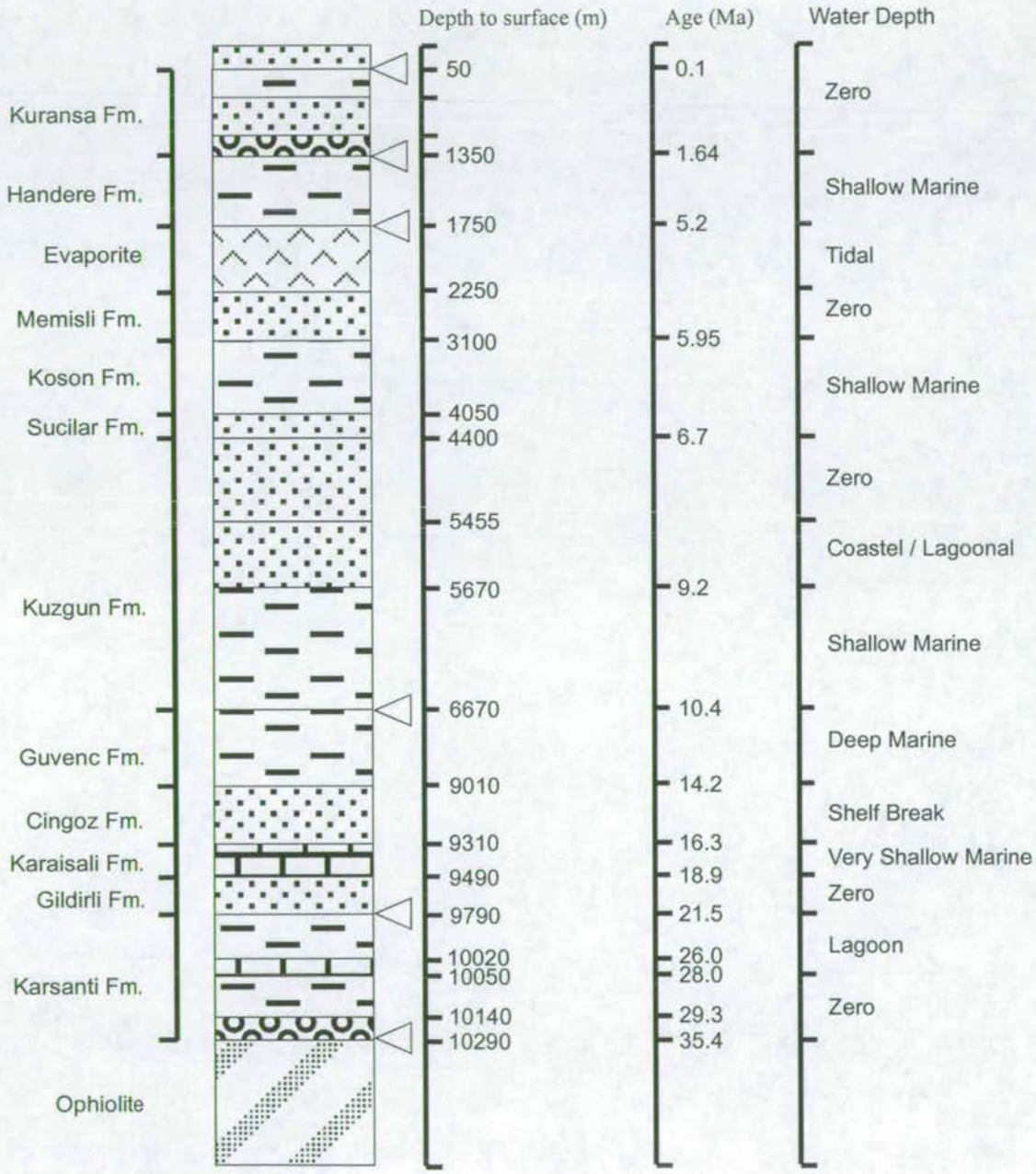
Depth to surface (m)
Age (Ma)
Water Depth
Kuransa Fm.
Handere Fm.
Evaporite
Memisli Fm.
Koson Fm.
Sucilar Fm.
Kuzgun Fm.
Guvenc Fm.
Cingoz Fm.
Karaisali Fm.
Gildirli Fm.
Karsanti Fm.
Ophiolite
50
1350
1750
2250
3100
4050
4400
5455
5670
6670
9010
9310
9490
9790
10020
10050
10140
10290
0.1
1.64
5.2
5.95
6.7
9.2
10.4
14.2
16.3
18.9
21.5
26.0
28.0
29.3
35.4
Zero
Shallow Marine
Tidal
Zero
Shallow Marine
Zero
Coastel / Lagoonal
Shallow Marine
Deep Marine
Shelf Break
Very Shallow Marine
Zero
Lagoon
Zero

APPENDIX 2

Point Counting Data from Sandstones

Sample	Location	Q	Qm	Qu	F	Plag.	Kfeld.	L	Llst	Micrite	Calcite	Lsst	Lign	Micas	Chert
69	Bademdere	6	6	0	2	1	1	72	68	30	38	0	4	0	5
71	Bademdere	9	7	2	0	0	0	221	214	140	74	0	7	3	27
288	Bademdere	65	42	23	13	3	10	115	71	-	-	1	43	3	9
289	Bademdere	12	9	3	2	0	2	227	193	-	-	12	22	0	12
282	Bademdere	43	26	17	14	0	14	170	153	-	-	3	14	2	15
284	Bademdere	41	38	3	30	2	28	159	145	-	-	2	12	1	17
293	Bademdere	67	42	25	18	0	18	94	78	-	-	5	11	6	34
295	Bademdere	6	6	0	0	0	0	254	241	-	-	6	7	2	27
140	Burc	76	38	38	18	0	18	58	46	17	29	0	12	0	18
302	Burc	83	47	36	37	6	31	127	111	-	-	1	15	4	28
189	Burc	91	51	40	26	11	15	97	74	-	-	1	22	5	9
25	Alpu	50	29	21	57	4	53	209	14	-	-	38	157	4	39
26	Alpu	16	9	7	52	3	49	72	21	-	-	0	51	4	48
232	Alpu	13	10	3	13	1	12	205	175	-	-	2	28	1	3
231	Alpu	20	19	1	19	3	16	160	90	-	-	0	70	0	4
230	Alpu	7	7	0	33	0	33	178	97	-	-	6	75	2	15
233	Alpu	8	7	1	58	0	58	121	40	-	-	6	75	0	19
209	Kamisli	13	10	3	16	1	15	180	105	-	-	3	72	0	8
241	Gulek	5	4	1	7	0	7	123	116	-	-	5	2	0	7
254	Kepez Tepe	52	21	31	39	4	35	168	104	43	61	0	64	0	18
255	Kepez Tepe	61	30	31	42	10	32	164	102	40	62	0	62	0	24
157	Kepez Tepe	47	25	22	26	8	18	174	133	32	101	0	41	1	25
120	Hacibekirli	13	9	4	10	0	10	228	208	61	147	0	20	1	11
305	Altay	21	11	10	11	3	8	222	187	28	159	0	35	4	7
307	Altay	8	4	4	8	1	7	220	203	59	144	0	17	5	7
124	Altay	30	13	17	15	5	10	383	291	215	76	0	92	7	26
104	Emirler	8	2	6	0	0	0	197	170	87	83	1	26	0	7
261	Kurtulmus	27	19	8	20	3	17	167	146	55	91	0	21	1	18
105	Aktoprak 95	42	53	65	15	50	118	53	28	25	10	55	7	37	
106	Aktoprak 64	32	32	71	14	57	81	57	21	36	0	24	9	41	
116	Ulukisla	42	23	19	50	13	37	198	95	36	59	24	79	6	77

Appendix 2 Results of point counting (using the techniques of Dickinson & Suczec 1979) of sandstone samples from the EFZ and Ulukisla Basin. Q = total quartz, Qm = monocrystalline quartz, Qu = undulose quartz, F = total feldspars, Plag. = plagioclase feldspar, K.Feld. = potassium feldspar, L = total lithic fragments, Llst = total carbonate grains, Micrite = micritic carbonate, Calcite = calcite grains, Lsst = sandstone grains, Lign = igneous rock grains, Micas = muscovite + biotite, Chert = total chert grains, Haem. = haematite cement, Heavies = Heavy and/or opaque minerals, Cal.cem. = calcite cement, Pores = pore space. Dashes indicate that differentiation was not made between carbonate grains.

Sample	Haem.	Heavies	Cal.cem	Pores	Chlorite	Total counts
69	33	6	0	31	0	300
71	28	7	58	63	0	500
288	0	6	85	4	0	300
289	0	10	31	6	0	300
282	0	8	47	1	0	300
284	0	13	34	5	0	300
293	45	5	0	31	0	300
295	1	2	0	8	0	300
140	7	1	83	10	0	500
302	0	1	10	10	0	300
189	0	2	69	1	0	300
25	0	8	119	0	14	500
26	49	13	0	0	0	500
232	0	26	11	28	0	300
231	0	33	61	3	0	300
230	0	3	50	12	0	300
233	0	5	79	10	0	300
209	0	3	76	4	0	300
241	0	3	136	19	0	300
254	0	2	3	18	0	300
255	0	5	3	1	0	300
157	0	9	5	13	0	300
120	0	2	1	34	0	300
305	16	0	8	11	0	300
307	26	0	15	11	0	300
124	39	0	0	0	0	500
104	67	1	0	0	0	300
261	19	0	38	10	0	300
105	0	16	162	0	0	500
106	39	36	159	0	0	500
116	0	0	120	0	0	500

APPENDIX 3

X-Ray Fluorescence Techniques and Data

Appendix 3 X-Ray Fluorescence techniques

Sample analysis using the X-ray fluorescence technique and results

Standard X-ray fluorescence techniques (XRF) were used to analyse major and minor elements in mudstone samples.

Rock Preparation

Approximately 50g of material was cut from each rock sample to be analysed. The material selected was chosen to be as free from alteration and veining as possible. The cut sample was crushed and the chips ground to a fine powder in a tungsten carbide barrel for roughly one minute.

XRF preparation – major elements

Glass discs formed from the rock powder were used in the analysis of the major elements. Preparation involved firstly drying the rock powders in an oven at 110^0C overnight. Approximately 1g of each powder was placed into a Pt-5%Au crucible. The three modern mudstones (samples 347, 333 & 319) were fired in silica crucibles, as any carbon will react with, and damage platignum. All of the samples were ignited for 20 minutes at 1100^0C and a value for the loss on ignition ($H_2O + CO_2$-O_2) calculated. The ignited powder was then fused for 20 minutes at 1100^0C using a lithium borate flux (Johnson Matthey Spectroflux 105) with a 5:1 flux:sample dilution ratio. The molten material was placed onto a graphite plate and pressed into a disc by lowering an aluminium plunger onto the globule. The casting operation was carried out on a hotplate at 220^0C and the glass disc allowed to anneal at this temperature for 10 minutes before cooling.

Trace elements

Pressed pellets formed from the rock powder were used in the analysis of the trace elements. The pellets were made by mixing ~6g of rock powder with 4 drops of binding agent (2% PVA in distilled water). The mixture was placed in a steel mould, surrounded and backed by boric acid powder and compressed at 8 tons using a hydraulic press to form 40mm diameter pellets.

XRF Analysis

Samples were analysed using standard procedures on the Edinburgh University Philips 1280 wavelength dispersive, sequential X-ray fluorescence spectrometer which is regularly calibrated and monitored for drift using standard samples. Major elements were screened by combining the total of the measured oxides with the loss on ignition. Where the total was outside the range 99.4-100.4 the sample was re-analysed using a new glass disc. In cases where a repeat analysis also resulted in values outside this range (i.e. samples 296, 333 and 347) the second set of results are given.

Errors in XRF analysis

Repeat analysis and regular calibration of standards on the Edinburgh machine shows that major element data has typical errors, incorporating the instrument and sample reproducibility, of for example: SiO_2±0.44wt%, MgO±0.16wt%, K_2O±0.04wt%, Nb±1.2ppm, Zr±2ppm, Rb±0.8ppm (all 2σ errors from James 1995).

Sample	33	161	168	179	191	198	201	238	253	258	259	260	262	263	264	269	271
Formation	Burc	Nigde	Cuk.	Cuk.	Burc	Cuk.	Cuk.	Cuk.	Burc	Cuk.	Cuk.	Cuk.	Cuk.	Cuk.	Cuk.	Bolk.	Bolk.
SiO2	15.52	-	45.88	35.24	10.78	19.31	34.96	30.67	40.17	25.62	26.51	34.98	40.95	43.57	43.62	-	-
Al2O3	5.23	-	11.35	8.06	3.08	2.53	8.07	5.12	9.08	6.13	5.88	6.57	9.97	9.44	8.99	-	-
Fe2O3	2.19	-	7.37	4.72	1.85	2.9	7.53	5.55	6.23	3.92	4.26	5.68	7.05	7.49	6.75	-	-
MgO	1.66	-	9.17	5.78	1.93	2.94	11.32	14.2	10.93	4.53	4.61	14.25	8.59	9.11	9.26	-	-
CaO	40.06	-	9.28	21.52	42.77	38.14	17.22	20.86	10.39	29.62	29.17	13.1	13.46	12.08	12.85	-	-
Na2O	0.27	-	1.34	0.65	0.01	0	0	0.51	0.09	0	0.03	0.47	0.6	1.19	1.21	-	-
K2O	0.35	-	1.52	0.88	0.234	0.14	0.44	0.23	1.17	0.945	0.86	0.776	1.45	1.17	1.15	-	-
TiO2	0.17	-	0.66	0.42	0.11	0.10	0.30	0.24	0.52	0.375	0.274	0.39	0.53	0.55	0.55	-	-
MnO	0.12	-	0.12	0.11	0.13	0.02	0.05	0.13	0.096	0.088	0.077	0.12	0.09	0.10	0.11	-	-
P2O5	0.14	-	0.10	0.09	0.14	0.07	0.05	0.03	0.05	0.078	0.057	0.06	0.09	0.10	0.09	-	-
Subtotal	65.72	-	86.8	77.46	61.0	66.09	79.95	77.54	78.71	71.3	71.73	76.4	82.76	84.81	84.59	-	-
LOI	33.97	-	12.96	23.07	36.47	33.54	19.94	22.5	21.35	28.45	28.11	23.64	17.37	15.11	15.79	-	-
Total	99.69	-	99.76	100.53	97.51	99.63	99.89	100.04	100.06	99.75	99.84	100.04	100.13	99.92	100.38	-	-
Mo	-	7	1	1	-	1	1	0.8	2	2	1	1	0	1	2	1	1
Nb	-	2	10	5	-	3	5.5	1	8	6	3	5.5	8	8	8	2	1
Zr	-	20	86	63	-	27	33	16	69	49	35	44	68	77	74	15	5
Y	-	5	19	14	-	4	7	8	16	13	10	12	15	16	17	3	3
Sr	-	896	243	450	-	1537	206	131	207	303	432	227	204	215	306	1524	576
U	-	13	0	0	-	0	0	0	0	0	0	0	0	0	0	0	0
Rb	-	13	57	32	-	5	17	4	45	34	35	30	54	39	43	1	0
Th	-	1	7	4	-	1	2	0	3	3	2	2	5	5	4	0	0
Pb	-	1	6.5	7	-	0	2	0	10	3	4	3	6	6	4	1	0
Zn	-	24	86	53	-	24	54	34	61	48	46	49	73	71	65	7.5	13.5
Cu	-	38	35.5	51	-	38	77	40	51	47	49	26	32	28	29.5	28	29
Ni	-	75	481	339	-	308	854	929	543	337	380	597	536	511	479.5	19	17
Cr	-	83	529.5	576	-	260	937	1272	522	415	279	779	545	786	720	30	23
Ce	-	55.5	37	49	-	46	19	3.5	30	56	32.5	31.5	35	30	26	65	64
Nd	-	0	18	9.5	-	0	3	0	16	1	2	11	12	13	15	0	0
La	-	0	13.5	12.5	-	4	0	0	16	14	6.5	7	14	11	9	0	0
V	-	71	158	130	-	56	133	117	146	155	97	133	153	158	130	25	6.5
Ba	-	49	265	385	-	160.5	182	19	145	251	123	144.5	206	185	179	36	0
Sc	-	47	28	32	-	42	32	40	27	39	32	27	34	25	23	50	53

Sample	274	283	285	287	290	292	296	297	300	303	304	306	311	316	317A	317B	318A
Formation	Aladag	Cuk.	Cuk.	Cuk.	Cuk.	Cuk.	Cuk.	Cuk.	Burc	Burc	Burc	Burc	basalt	Marble	Schist	Schist	Granite
SiO2	30.04	42.52	43.01	34.54	35.87	44.7	59.07	12.23	38.76	42.24	0.91	35.3	-	-	-	-	-
Al2O3	7.88	9.81	11.15	7.74	7.96	10.97	15.12	2.68	10.87	12.1	0.3	6.06	-	-	-	-	-
Fe2O3	4.95	6.28	6.35	4.7	5.05	6.41	8.48	1.81	5.26	5.92	0.14	9.04	-	-	-	-	-
MgO	2.97	4.28	5.04	6.21	5.95	5.72	4	1.65	3.88	4.44	0.68	12.15	-	-	-	-	-
CaO	27.47	16.78	14.91	21.25	18.52	13.2	2.11	44.11	19.8	15.8	53.99	15.43	-	-	-	-	-
Na2O	0	0.63	1.05	0.45	0.43	0.4	0.19	0	0.8	0.93	0	0.08	-	-	-	-	-
K2O	1.23	1.11	1.20	0.82	0.86	1.23	2.95	0.32	1.03	1.20	0.02	1.07	-	-	-	-	-
TiO2	0.41	0.49	0.5	0.40	0.43	0.50	0.65	0.14	0.49	0.47	0.02	0.36	-	-	-	-	-
MnO	0.07	0.07	0.08	0.10	0.07	0.07	0.03	0.04	0.15	0.10	0.04	0.07	-	-	-	-	-
P2O5	0.08	0.08	0.07	0.08	0.08	0.08	0.02	0.03	0.09	0.08	0.03	0.07	-	-	-	-	-
Subtotal	75.06	82.06	83.37	76.29	75.22	83.28	92.62	62.92	81.12	83.27	56.07	79.63	-	-	-	-	-
LOI	24.92	18.04	16.56	23.7	22.01	16.96	8.53	36.82	19.21	16.44	43.51	20.12	-	-	-	-	-
Total	99.98	100.1	99.93	99.99	97.23	100.24	101.15	99.74	100.33	99.71	99.58	99.75	-	-	-	-	-
Mo	1	1	1	1	1	1	1	1	1	1	1	1	1	1	0	0	0
Nb	10	7	7	5	6	7	13	2	5	5	1	7	5	1	7	18	15
Zr	73	66	64	61	63	67	102	18	62	67	7	45	129	2	144.5	310	159.5
Y	16	14	15	13	14	15.5	14	7	17	18	1	12	23	2	28	39	21
Sr	85	190.5	385.5	324	319	225	55	145	365	347	629	178	404	125	225	141	101
U	0	0	0	0	0	0	0	0	0	0	0	0	0	0	3	1	7
Rb	57	42	47	30	32.5	46	94	9	42.5	53	1	32	3	0	115	166.5	225
Th	6	4	3	3	4	6	13	1	4	5	0	2	3	0	7	17	22
Pb	61	11	9	10	8	10	15	3	9	7.5	0	8.5	3	0	25	25	31
Zn	112	61	64	49	66	59.5	133	28	57.5	63	6	66	71	5	35	96	47
Cu	35	42	44	44	49	39	35	35	46	52	29	26	71	31	2	7	4
Ni	584	400	336	306.5	450	356.5	321	169	123	137	36	1521	126	19	5	32	1
Cr	539	472	476.5	562	643	449	612	459	273	323	25	857	232	17	22	78	6.5
Ce	62	47	35	51	42	40	36	61	34	37.5	59	27	8	55	33	77	70
Nd	10	19	11	13	8	13	17	0	4	14	0	8	18	0	14	39	24
La	20	14	13	13.5	7	10	14	0	4	6	0	5	12	0	12	37	22
V	100	148	106	121	141	140	111	64	156	158	14.5	96	182	5	27	106	19
Ba	83	203	226	307	191	205	144	56.5	164	145	29	101	212	0	497	826	510
Sc	32	31	29	33	33	30	29.5	51	35	36	52	30	27	69	9	17.5	0

Sample	318B	319	322	323	330	333	338	342	343	344	347
Formation	Granite	Modern	Cuk.	basalt	Bolk.	Modern	Aladag	Tuff	Tuff	Tuff	Modern
SiO2	-	71	30.72	-	-	45.48	-	-	-	-	37.94
Al2O3	-	13.02	7.26	-	-	17.92	-	-	-	-	11.15
Fe2O3	-	2.77	5.74	-	-	7.59	-	-	-	-	6.32
MgO	-	1	8.25	-	-	3.84	-	-	-	-	13.61
CaO	-	6	23.37	-	-	20.77	-	-	-	-	27.8
Na2O	-	2.02	0.57	-	-	0.34	-	-	-	-	0.63
K2O	-	3.43	0.477	-	-	2.242	-	-	-	-	1.34
TiO2	-	0.412	0.342	-	-	0.806	-	-	-	-	0.611
MnO	-	0.053	0.098	-	-	0.419	-	-	-	-	0.137
P2O5	-	0.098	0.052	-	-	0.2	-	-	-	-	0.226
Subtotal	-	99.8	76.88	-	-	99.61	-	-	-	-	99.76
LOI	-	6.82	23.25	-	-	27.97	-	-	-	-	29.94
Total	-	100.13	100.23	-	-	127.58	-	-	-	-	129.7
Mo	0	1	1	1	0	8	1	2	2	2	2
Nb	11	11	3	6	2	14	8	12	7	19	8
Zr	80.5	182	30	116	70	117.5	144	141	99	350	78
Y	22.5	22	13	23	4	28	15	19	9	51	18
Sr	80	116	200	392	10	110	366	273	267	224	112
U	4	2	0	0	2	0	0	4	3	9	0
Rb	177	130	14	7	2	68.5	51	8.5	12.5	8	43
Th	11	10	0	5	0	6	5	2	0.5	19	3
Pb	41	30	2	5	0	154.5	8	14	15	13	124
Zn	14	58	67	69	3	367	20	7	8	7	229
Cu	0	17	58	50	0	47	23	17	24	13	46
Ni	0	21	423	80	0	186	20	0	3	0	211
Cr	4	48.5	407	188	6	228	42	98	43	13	344
Ce	23	75	19	23	6	93	77.5	37	42	93	61
Nd	9	22	1	16	0	36	14	15	14	38	18.5
La	5	29	1	9	0	45	20	14	7	43	29
V	6	53	143	164	7	172	45	142	150.5	109	136
Ba	207	539	93	215	10	413	334	491	294	1015	238
Sc	3	8	40	26	0	28	27	10	19	44	31

APPENDIX 4

^{40}Ar / ^{39}Ar Raiometric Dating Results

Ar/Ar laser-fusion ages of minerals from tuffs of the Erciyes Basin

Step (a)	40Ar/39Ar (b)	37Ar/39Ar (b)	36Ar/39Ar (b)	40Ar s.d. (%)	39Ar s.d. (%)	37Ar s.d. (%)	36Ar s.d. (%)	40ArR (mol)	40ArR (c)	40ArK (c)	39ArCa (c)	36ArCa (c)	K/Ca (%)	39Ar (%)	Apparent Age (Ma)	(d)	1 s.d. (Ma)
217		Feldspar		J =	0.00157 +-		3.1E-06 (1 s.d.)			Exp. No.:	nj0l5208.IHD		Total gas age =		6.047	+-	0.077
fs1	2.575	7.082	0.003658	0.6	0.4	0.46	36.16	6.60E-16	79.4	0.03	0.48	51.11	0.069	3.8	5.812	+-	0.524
fs2	2.339	3.576	0.001591	0.57	0.26	0.44	57.18	1.20E-15	91.8	0.04	0.24	59.32	0.137	6.5	6.086	+-	0.3
fs3	2.499	3.706	0.001768	0.38	0.3	0.5	53.44	1.20E-15	90.6	0.03	0.25	55.35	0.132	6.1	6.419	+-	0.341
fs4	3.233	5.218	0.003514	0.76	0.34	0.58	63.05	5.60E-16	80.4	0.03	0.35	39.2	0.094	2.5	7.378	+-	1.085
fs5	9.726	5.271	0.02753	0.38	0.34	0.47	3.35	4.10E-16	20.6	0.01	0.35	5.05	0.093	2.4	5.678	+-	0.724
fs6	2.944	3.882	0.00392	0.5	0.26	0.7	21.73	7.00E-16	70.9	0.03	0.26	26.15	0.126	4	5.918	+-	0.508
fs7	4.651	4.749	0.009504	0.15	0.12	0.37	1.64	2.90E-15	47.6	0.02	0.32	13.19	0.103	15.5	6.274	+-	0.113
fs8	2.601	3.457	0.002392	0.16	0.18	0.26	12.25	3.00E-15	83.2	0.03	0.23	38.15	0.141	16.2	6.129	+-	0.147
fs9	3.413	5.07	0.005809	0.33	0.33	0.41	8.15	1.30E-15	61.3	0.03	0.34	23.04	0.096	7.1	5.934	+-	0.297
fs10	2.868	3.585	0.002843	0.4	0.42	0.36	16.98	1.50E-15	80.4	0.03	0.24	33.29	0.136	7.5	6.537	+-	0.263
fs11	4.175	4.001	0.00827	0.25	0.3	0.49	3.11	1.60E-15	48.9	0.02	0.27	12.77	0.122	9.3	5.79	+-	0.185
fs12	2.593	3.78	0.003013	0.34	0.19	0.69	10.32	1.80E-15	77	0.03	0.25	33.12	0.129	10.6	5.662	+-	0.168
fs13	7.101	4.016	0.018568	0.16	0.32	0.5	2.19	1.40E-15	27.1	0.01	0.27	5.71	0.122	8.3	5.462	+-	0.317
217		biotite		J =	0.00157 +-		3.1E-06 (1 s.d.)			Exp. No.:	nj0l5247.IHD		Total gas age =		7.358	+-	0.148
fs1	44.11	0.06462	0.14006	0.12	0.06	2.48	0.27	5.80E-15	6.2	0	0	0.01	7.58	23.5	7.711	+-	0.389
fs2	26.54	0.12967	0.08119	0.05	0.17	2.99	0.33	3.80E-15	9.6	0	0.01	0.04	3.78	16.6	7.23	+-	0.295
fs3	27.11	0.12152	0.08387	0.09	0.18	4.08	0.91	1.40E-15	8.6	0	0.01	0.04	4.03	6.7	6.593	+-	0.646
fs4	25.27	0.18091	0.07749	0.08	0.23	3.12	0.56	1.40E-15	9.4	0	0.01	0.06	2.71	6.5	6.739	+-	0.423
fs5	30.16	0.09433	0.09372	0.08	0.3	4.58	0.52	1.60E-15	8.2	0	0.01	0.03	5.19	7	6.984	+-	0.535
fs6	21.1	0.13806	0.06335	0.08	0.17	3.62	0.65	2.00E-15	11.3	0	0.01	0.06	3.55	9.4	6.741	+-	0.363
fs7	18.026	0.15364	0.05224	0.12	0.13	3.14	0.85	2.80E-15	14.4	0	0.01	0.08	3.19	12	7.353	+-	0.371
fs8	18.982	0.14847	0.0522	0.11	0.24	2.5	1.17	2.60E-15	18.8	0	0.01	0.08	3.3	8.1	10.079	+-	0.516
fs9	25.32	0.2038	0.0776	0.11	0.34	2.47	0.65	1.30E-15	9.5	0	0.01	0.07	2.4	6.1	6.809	+-	0.529
fs10	20.32	0.15924	0.06211	0.16	0.31	5.11	1.36	7.30E-16	9.8	0	0.01	0.07	3.08	4.1	5.604	+-	0.72
309		Feldspar		J =	0.001567 +-		3.1E-06 (1 s.d.)			Exp. No.:	nj0l5207.IHD		Total gas age =		1.74	+-	0.206
fs1	6.388	7.317	0.02068	0.32	0.43	0.38	4.04	3.00E-16	13.3	0.01	0.49	9.34	0.067	11.2	2.405	+-	0.62
fs2	2.341	7.291	0.010301	0.67	0.39	0.28	6.73	-4.30E-17	-5.8	0.04	0.49	18.68	0.067	9.9	-0.383	+-	0.457
fs3	21.42	14.814	0.07204	0.37	0.43	0.52	2.18	1.50E-16	6	0	1	5.43	0.033	3.6	3.663	+-	1.274
fs4	19.626	8.72	0.06547	0.15	0.28	0.27	1.26	3.00E-16	4.9	0	0.59	3.52	0.056	10	2.721	+-	0.686
fs5	27.65	21.86	0.09467	0.21	0.53	0.45	2.3	1.90E-16	5	0	1.47	6.1	0.022	4.3	3.953	+-	1.769
fs6	8.62	10.869	0.02771	0.5	0.7	0.36	6.24	1.80E-16	14.8	0.01	0.73	10.35	0.045	4.5	3.637	+-	1.275
fs7	1.0452	8.587	0.004186	1.42	0.37	0.37	32.64	1.40E-16	45.7	0.08	0.58	54.16	0.057	9.4	1.357	+-	0.505

fs8	2.338	10.241	0.009711	0.57	0.28	0.2	5.78	1.20E-16	11.4	0.04	0.69	27.84	0.048	14	0.758 +-	0.33
fs9	36.34	6.488	0.12015	0.21	0.51	0.6	1.1	2.50E-16	3.7	0	0.44	1.43	0.075	5.9	3.811 +-	1.303
fs10	0.5136	11.678	0.003674	12.58	0.57	0.94	402.53	3.60E-17	65.9	0.17	0.79	83.93	0.042	3.3	0.963 +-	1.922
fs11	3.047	9.125	0.011885	0.5	0.32	0.23	4.97	1.00E-16	8.1	0.03	0.61	20.27	0.053	13.1	0.7 +-	0.383
fs12	5.896	10.677	0.02069	0.37	0.46	0.31	3.29	2.10E-16	10.4	0.01	0.72	13.62	0.046	10.7	1.75 +-	0.49
310	Feldspar		J =	0.001564 +-			3.1E-06 (1 s.d.)		Exp. No.:	nj0l5206.IHD		Total gas age =			2.109 +-	0.2
fs1	17.101	6.293	0.05829	0.21	0.39	0.77	1.91	6.20E-17	2.1	0.01	0.42	2.85	0.078	3.8	1.04 +-	0.911
fs2	0.4782	6.264	0.002453	7.6	0.53	0.59	249.94	3.10E-17	50.5	0.18	0.42	67.43	0.078	2.9	0.683 +-	1.595
fs3	0.4971	7.179	0.001973	4.94	0.5	0.46	%1631.43	9.20E-17	95.2	0.17	0.48	96.07	0.068	4.4	1.341 +-	1.011
fs4	5.936	17.564	0.010571	1.07	0.7	0.29	49.88	3.20E-16	70.4	0.01	1.18	43.86	0.028	1.7	11.899 +-	2.374
fs5	1.278	7.913	0.003421	3.1	0.38	0.63	137.55	9.80E-17	69.1	0.07	0.53	61.06	0.062	2.5	2.504 +-	1.465
fs6	1.748	6.758	0.006397	2.13	0.7	3.81	49.2	4.50E-17	22	0.05	0.45	27.89	0.072	2.7	1.088 +-	1.813
fs7	4.168	8.821	0.007911	0.76	0.41	0.52	20.72	4.50E-16	60.4	0.02	0.59	29.44	0.055	4	7.131 +-	0.926
fs8	3.995	8.244	0.013393	0.34	0.23	0.45	5.68	2.40E-16	17	0.02	0.55	16.25	0.059	8	1.927 +-	0.512
fs9	0.2831	6.81	0.002273	2.56	0.39	0.26	100.46	8.60E-17	50.1	0.3	0.46	79.11	0.072	13.7	0.402 +-	0.381
fs10	16.084	10.915	0.05356	0.13	0.42	0.14	1.52	8.30E-16	6.9	0.01	0.73	5.38	0.045	17	3.147 +-	0.676
FS11	5.755	9.127	0.01889	0.35	0.43	0.67	3.12	3.00E-16	15.4	0.01	0.61	12.76	0.053	7.7	2.508 +-	0.426
FS12	2.738	8.944	0.009775	1.03	0.65	0.64	9.27	1.40E-16	19.9	0.03	0.6	24.16	0.054	5.6	1.549 +-	0.559
FS13	1.4842	11.642	0.007451	3.53	0.73	0.84	52.51	2.30E-17	12.8	0.06	0.78	41.25	0.042	2.7	0.54 +-	1.845
FS14	2.806	9.279	0.010466	0.66	0.46	0.43	6.61	1.50E-16	15.6	0.03	0.62	23.41	0.052	8	1.24 +-	0.43
FS15	8.159	12.798	0.02229	0.78	1.05	0.66	11.97	2.60E-16	31.5	0.01	0.86	15.16	0.038	2.3	7.297 +-	1.841
fs16	2.734	6.736	0.011999	0.93	0.41	0.63	6.27	-8.30E-17	%-10.5	0.03	0.45	14.82	0.072	6.5	-0.814 +-	0.519
fs17	7.033	8.486	0.02322	0.33	0.28	0.68	3.41	2.40E-16	11.9	0.01	0.57	9.65	0.057	6.4	2.364 +-	0.58
312			J =	0.001564 +-			3.1E-06 (1 s.d.)		Exp. No.:	nj0l5210.IHD		Total gas age =			7.442 +-	0.102
dg1	6.768	2.488	0.013259	0.25	0.28	0.65	3.61	1.20E-15	45	0.01	0.17	4.95	0.197	6.3	8.579 +-	0.371
d2-4	18.526	2.941	0.04229	0.16	0.38	0.55	1.29	2.20E-15	33.8	0	0.2	1.84	0.166	5.7	17.61 +-	0.498
d5-9	17.145	3.28	0.04201	0.13	0.21	0.69	1.16	3.10E-15	29.1	0.01	0.22	2.06	0.149	10.1	14.048 +-	0.406
fs1	2.548	4.276	0.002924	0.34	0.15	0.27	17.46	1.60E-15	79.2	0.03	0.29	38.61	0.114	12.7	5.697 +-	0.252
fs2	2.567	4.563	0.003286	0.4	0.27	0.42	16.77	1.20E-15	76	0.03	0.31	36.66	0.107	10.2	5.512 +-	0.28
fs3	2.416	4.633	0.002332	0.48	0.29	0.29	27.8	1.30E-15	86.4	0.04	0.31	52.45	0.105	10.2	5.897 +-	0.249
fs4	2.7	4.645	0.003435	0.42	0.24	0.52	15.93	1.20E-15	75.8	0.03	0.31	35.7	0.105	9.5	5.782 +-	0.284
fs5	2.699	4.001	0.003387	0.48	0.17	0.33	16.46	1.10E-15	74.5	0.03	0.27	31.19	0.122	9.1	5.676 +-	0.309
fs6	2.719	4.299	0.003282	0.46	0.15	0.29	19.36	1.10E-15	76.6	0.03	0.29	34.58	0.114	8.3	5.887 +-	0.334
fs7	2.501	5.062	0.003037	0.64	0.22	0.47	32.61	8.40E-16	79.9	0.03	0.34	44	0.096	6.7	5.645 +-	0.446
fs8	2.347	4.71	0.002065	0.81	0.29	0.58	62.31	8.00E-16	89.6	0.04	0.32	60.22	0.104	6.1	5.944 +-	0.413
fs9	3.027	4.437	0.004352	0.65	0.24	0.58	21.66	6.80E-16	68.9	0.03	0.3	26.92	0.11	5.2	5.893 +-	0.554
312	BIOTITE		J =	0.00154 +-			0 (1 s.d.)		Exp. No.:	nj0l5245.IHD		Total gas age =			7.419 +-	0.274
tf1	46.5	0.15877	0.14671	0.19	0.21	3.62	0.56	1.90E-15	6.8	0	0.01	0.03	3.09	15.5	8.741 +-	0.803
tf2	44.39	0.08786	0.14093	0.06	0.16	3.76	0.36	2.50E-15	6.2	0	0.01	0.02	5.58	23.7	7.642 +-	0.522

tf3	32.69	0.05599	0.10231	0.18	0.41	31.49	1.21	6.40E-16	7.5	0	0	0.01	8.75	6.9	6.824 +-	1.11
tf4	31.02	0.15914	0.09706	0.12	0.21	2.37	0.34	3.00E-15	7.6	0	0.01	0.04	3.08	33.4	6.507 +-	0.391
tf5	41.52	0.08504	0.12943	0.22	0.27	6.66	0.64	1.80E-15	7.9	0	0.01	0.02	5.76	14.7	9.084 +-	0.824
tf6	47.53	0.12094	0.15511	0.23	0.46	10.93	0.92	3.80E-16	3.6	0	0.01	0.02	4.05	5.8	4.73 +-	1.434
313	Feldspar		J =	0.001558 +-			3.1E-06 (1 s.d.)		Exp. No.:	nj0l5211.IHD		Total gas age =			7.92 +-	0.181
fs1	35.63	6.231	0.1089	0.11	0.25	0.43	1.33	1.40E-15	11.1	0	0.42	1.51	0.078	7.4	11.083 +-	1.196
fs2	33.43	5.655	0.10255	0.1	0.25	0.48	0.68	1.50E-15	10.7	0	0.38	1.46	0.086	8.6	10.052 +-	0.654
fs3	2.949	4.842	0.002694	0.83	0.2	0.49	68.29	6.40E-16	85.8	0.03	0.33	47.45	0.101	5.2	7.118 +-	0.77
fs4	2.831	4.458	0.001406	1.06	0.23	1.04	371.46	6.10E-16	97.6	0.03	0.3	83.73	0.11	4.6	7.771 +-	0.679
fs5	2.773	5.321	0.001557	0.99	0.29	0.74	555.32	6.90E-16	98.3	0.03	0.36	90.23	0.092	5.2	7.675 +-	0.675
fs6	3.026	8.355	0.006269	1.25	0.43	1.3	26.85	3.20E-16	60.3	0.03	0.56	35.18	0.058	3.6	5.148 +-	0.876
fs7	3.073	4.87	0.002819	1.03	0.43	0.68	48	6.50E-16	85.2	0.03	0.33	45.61	0.1	5.1	7.371 +-	0.592
fs8	3.118	5.199	0.003021	9	0.75	1.09	119.48	3.60E-16	84.3	0.03	0.35	45.43	0.094	2.8	7.401 +-	1.752
fs9	2.834	3.606	0.001585	0.58	0.32	0.7	71.19	1.40E-15	93.4	0.03	0.24	60.07	0.136	10.9	7.439 +-	0.356
fs10	2.776	10.556	0.003253	0.69	0.5	0.49	127.99	1.00E-15	95	0.03	0.71	85.68	0.046	7.9	7.451 +-	0.474
fs11	2.612	5.585	0.001897	1.04	0.48	0.79	176.96	6.30E-16	95.2	0.03	0.38	77.72	0.087	5.3	7.001 +-	0.592
fs12	2.705	9.779	0.003122	1.1	0.61	0.46	155.87	5.60E-16	94.1	0.03	0.66	82.68	0.05	4.5	7.183 +-	0.669
fs13	3.067	6.808	0.004523	1.37	0.41	0.43	44.64	3.80E-16	73.7	0.03	0.46	39.74	0.072	3.5	6.372 +-	0.962
tf14	6.138	4.152	0.009124	0.6	0.67	1.17	12.34	1.20E-15	61.3	0.01	0.28	12.01	0.118	6.5	10.58 +-	0.791
tf15	3.653	4.95	0.004819	1.17	0.31	0.63	26.95	6.60E-16	71.6	0.02	0.33	27.12	0.099	5.2	7.356 +-	0.751
tf17	4.719	5.635	0.009133	2.05	0.51	1.04	15.6	4.20E-16	52.1	0.02	0.38	16.29	0.087	3.6	6.924 +-	0.976
tf18	3.847	6.269	0.006548	1.86	0.58	0.59	15.58	5.30E-16	62.4	0.02	0.42	25.27	0.078	4.6	6.762 +-	0.634
tf16	5.339	5.692	0.01095	0.72	0.38	0.42	8.41	7.10E-16	47.7	0.02	0.38	13.72	0.086	5.7	7.17 +-	0.635
313	BIOTITE		J =	0.00154 +-			0 (1 s.d.)		Exp. No.:	nj0l5243.IHD		Total gas age =			7.524 +-	0.135
fs1	10.412	0.05532	0.02575	0.12	0.19	5.29	1.06	2.80E-15	27	0.01	0	0.06	8.86	8.9	7.78 +-	0.229
fs2	7.729	0.12508	0.016724	0.27	0.19	4.28	1.48	2.60E-15	36.2	0.01	0.01	0.2	3.92	8.3	7.751 +-	0.208
d3-5	28.27	0.05006	0.087	0.09	0.09	3.68	0.6	6.20E-15	9.1	0	0	0.02	9.79	21.7	7.102 +-	0.439
d6-9	33.94	0.3432	0.10872	0.07	0.1	0.94	0.31	3.40E-15	5.4	0	0.02	0.08	1.427	16.5	5.111 +-	0.329
fs3	21.11	0.2221	0.05787	0.08	0.27	2.07	0.92	2.40E-15	19.1	0	0.01	0.1	2.21	5.3	11.154 +-	0.467
fs4	25.7	0.3437	0.07776	0.12	0.29	2.13	0.89	1.40E-15	10.7	0	0.02	0.12	1.425	4.5	7.622 +-	0.618
fs5	28.59	0.19269	0.0865	0.11	0.2	3.18	0.53	2.40E-15	10.6	0	0.01	0.06	2.54	7	8.431 +-	0.439
fs6	20.09	0.12055	0.05717	0.07	0.21	2.76	0.71	2.70E-15	15.9	0	0.01	0.06	4.06	7.4	8.88 +-	0.36
fs7	9.185	0.06301	0.02089	0.21	0.22	4.04	1.1	2.90E-15	32.8	0.01	0	0.08	7.78	8.6	8.355 +-	0.201
fs8	25.33	0.4599	0.07572	0.09	0.21	3.32	1.47	1.50E-15	11.8	0	0.03	0.16	1.065	4.5	8.293 +-	0.9
fs9	17.271	0.2482	0.04963	0.11	0.18	2.24	0.68	2.20E-15	15.2	0	0.02	0.13	1.974	7.3	7.272 +-	0.298
313	Biotite		J =	0.001558 +-			3.1E-06 (1 s.d.)		Exp. No.:	nj0l5230.IHD		Total gas age =			6.02 +-	0.378
3.3	37.52	0.16877	0.12065	0.07	0.31	3.48	0.71	1.10E-15	5	0	0.01	0.04	2.9	31.2	5.282 +-	0.83
3.5	30.05	0.10617	0.09702	0.22	0.4	12.64	1.6	2.60E-16	4.6	0	0.01	0.03	4.62	9.8	3.903 +-	1.33
3.7	33.2	0.1747	0.10644	0.2	0.39	5.88	0.99	5.00E-16	5.3	0	0.01	0.04	2.8	15.2	4.955 +-	0.999

3.9	19.433	0.09401	0.05623	0.33	0.49	14.52	1.9	5.30E-16	14.5	0	0.01	0.04	5.21	10.1	7.915 +-	0.934
4.2	11.11	0.08467	0.02964	0.31	0.41	11.89	4.67	5.40E-16	21.2	0.01	0.01	0.08	5.79	12.2	6.615 +-	1.112
12	6.457	0.2278	0.012753	0.32	0.39	3.63	4	1.10E-15	41.9	0.01	0.02	0.47	2.15	21.5	7.588 +-	0.414
313 Pan 4N		biotite		J =	0.00156 +-		0 (1 s.d.)		Exp. No.:		nj0l5231.IHD		Total gas age =		4.66 +-	0.384
3.3	75.25	0.09759	0.2491	0.09	0.18	3.31	0.31	1.80E-15	2.2	0	0.01	0.01	5.02	0	4.6 +-	0.891
3.5	41.23	0.09521	0.13207	0.08	0.29	5.05	0.82	1.60E-15	5.3	0	0.01	0.02	5.15	0	6.195 +-	0.986
3.7	41.17	0.08544	0.13012	0.06	0.32	8.24	0.71	1.10E-15	6.6	0	0.01	0.02	5.73	0	7.647 +-	0.899
3.9	35.9	0.09871	0.11344	0.17	0.4	11.58	0.98	5.20E-16	6.6	0	0.01	0.02	4.96	0	6.691 +-	1.06
4.2	36.17	0.09441	0.11282	0.13	0.44	8.4	1.12	9.10E-16	7.8	0	0.01	0.02	5.19	0	7.97 +-	1.182
4.7	27.94	0.08781	0.08519	0.26	0.2	6.93	1.52	1.20E-15	9.9	0	0.01	0.03	5.58	0	7.785 +-	1.07
12	21.92	0.4159	0.06383	0.12	0.34	1.7	1.04	1.30E-15	14.1	0	0.03	0.17	1.178	0	8.674 +-	0.604
324		Feldspar		J =	0.001554 +-		3.1E-06 (1 s.d.)		Exp. No.:		nj0l5209.IHD		Total gas age =		6.992 +-	0.087
fs1	3.017	3.317	0.002355	0.3	0.29	0.67	23.18	1.70E-15	85.5	0.03	0.22	37.19	0.147	7.7	7.232 +-	0.274
fs2	3.077	3.161	0.002198	0.39	0.4	0.82	41.25	9.80E-16	86.9	0.03	0.21	37.97	0.155	4.3	7.496 +-	0.448
fs3	3.237	3.061	0.003578	2.53	0.29	0.82	16.87	2.00E-15	74.7	0.03	0.21	22.58	0.16	9.8	6.779 +-	0.437
fs4	2.891	3.202	0.0017	0.28	0.12	0.48	38.89	2.00E-15	91.2	0.03	0.22	49.72	0.153	9	7.396 +-	0.265
fs5	3.47	3.155	0.004981	0.31	0.22	0.47	8.16	1.20E-15	64.6	0.02	0.21	16.72	0.155	6.2	6.291 +-	0.271
fs6	2.801	3.157	0.001227	0.57	0.4	0.64	117.58	1.30E-15	95.8	0.03	0.21	67.92	0.155	5.6	7.524 +-	0.371
fs7	3.036	3.121	0.003169	0.63	0.45	1.07	22.24	8.30E-16	77.1	0.03	0.21	26	0.157	4.2	6.567 +-	0.419
fs8	2.71	3.161	0.001925	0.48	0.24	0.43	31.09	1.30E-15	88.1	0.03	0.21	43.35	0.155	6.4	6.693 +-	0.272
tf9	3.259	3.117	0.003319	0.44	0.38	0.71	12.36	1.60E-15	77.3	0.03	0.21	24.79	0.157	7.4	7.067 +-	0.25
tf10	2.85	2.853	0.002343	0.38	0.25	0.55	18.15	1.70E-15	83.5	0.03	0.19	32.15	0.171	8.2	6.67 +-	0.232
tf11	3.054	2.753	0.002815	0.47	0.27	0.44	17.81	1.30E-15	79.8	0.03	0.19	25.81	0.178	6	6.829 +-	0.298
tf12	2.899	3.676	0.002479	0.41	0.18	0.63	23.62	1.50E-15	84.6	0.03	0.25	39.14	0.133	7.3	6.879 +-	0.285
fs13	3.249	4.841	0.003486	0.38	0.26	0.44	16.27	1.40E-15	79.9	0.03	0.33	36.66	0.101	6.5	7.286 +-	0.285
s14a	3.246	2.559	0.003225	0.65	0.41	0.88	28.6	7.50E-16	76.8	0.03	0.17	20.95	0.191	3.5	6.983 +-	0.485
s14b	3.344	3.179	0.00303	1.7	0.68	1.04	42.39	5.60E-16	80.6	0.03	0.21	27.7	0.154	2.4	7.558 +-	0.63
s14c	2.708	3.252	0.001876	1.53	0.37	0.96	125.88	4.30E-16	88.9	0.03	0.22	45.76	0.15	2.1	6.748 +-	0.852
s14d	2.672	3.256	0.001214	0.83	0.23	0.67	194.12	7.60E-16	96	0.03	0.22	70.81	0.15	3.5	7.197 +-	0.458

(a) Steps labeled either as total fusion (tf), fusion of degassed crystals (fs), of individual step-heating (s) analyses.
(b) Corrected for 37Ar and 39Ar decay, half-lives 35.1 days and 259 years, respectively.
(c) Radiogenic (R), calcium-derived (Ca), and potassium-derived (K) argon, respectively (percent).
(d) Ages calculated relative to 85G003 TCR Sanidine at 27.92 Ma with lambda e = 0.581E-10/yr and lambda b = 4.692E-10/yr.

Ar/Ar fusion ages of plagioclase from Zile (Turkey)

Step (a)	40Ar/39Ar (b)	37Ar/39Ar (b)	36Ar/39Ar (b)	40Ar s.d. (%)	39Ar s.d. (%)	37Ar s.d. (%)	36Ar s.d. (%)	40ArR (mol)	40ArR (c)	40ArK (c)	39ArCa (c)	36ArCa (c)	K/Ca (%)	39Ar (%)	Apparent Age (Ma)	(d)	1 s.d. (Ma)
341		feldspar		J =	0.00117	+-	4.7E-06	(1 s.d.)		Exp. No.:	nj0f0078.IHD		Total gas age =		0	+-	0
fuse	10.819	7.638	0.02916	0.03	0.09	0.24	0.72	1.10E-14	25.8	0.01	0.51	6.91	0.064	0	5.924	+-	0.124
340		feldspar		J =	0.001185	+-	4.7E-06	(1 s.d.)		Exp. No.:	nj0f0079.IHD		Total gas age =		0	+-	0
fuse	6.249	7.227	0.013159	0.07	0.09	0.17	0.56	1.70E-14	46.8	0.01	0.49	14.5	0.067	0	6.269	+-	0.044
314		feldspar		J =	0.001195	+-	4.8E-06	(1 s.d.)		Exp. No.:	nj0f0081.IHD		Total gas age =		0	+-	0
fuse	5.943	8.012	0.02021	0.04	0.08	0.12	0.36	4.50E-15	10	0.01	0.54	10.47	0.061	0	1.293	+-	0.048

(a) fuse is 15 min 1300 deg C fusion step after 15 min 700 deg C degassing step.
(b) Corrected for 37Ar and 39Ar decay, half-lives 35.1 days and 259 years, respectively.
(c) Radiogenic (R), calcium-derived (Ca), and potassium-derived (K) argon, respectively (percent).
(d) Ages calculated relative to 85G003 TCR Sanidine at 27.92 Ma with lambda e = 0.581E-10/yr and lambda b = 4.692E-10/yr.

Appendix 5

Published papers

JAFFEY, N. & ROBERTSON, A.H.F. (in press). New sedimentological and structural data from the Ecemiş Fault Zone, southern Turkey; implications for its timing and offset and the Cenozoic Tectonic Escape of Anatolia. *Journal of the Geological Society*.

JAFFEY, N., PRINGLE, M. & ROBERTSON, A.H.F (in preparation) The dating of slip on the Central Anatolian Fault Zone using $^{40}Ar/^{39}Ar$ single crystal ablation: implications for continental extrusion in Turkey.

	Sedimentology	Subsidence	Provenance	Structure
Quaternary	Fault-controlled alluvial fans and debris flows	Renewed local rapid subsidence	Local fault-scarp sources	E-W extension + minor sinistral strike-slip
Pliocene	Uplift - scarp formation		Presnet fault-scarp creation	
Miocene	Gentle topography Pyroclastic activity Uplift Inward-draining continental basin. Depocentre in EFZ.	Slow subsidence in EFZ Hiatus in subsidence Maximum subsidence Maximum sedimentation rates	Taurus carbonates main sediment sources Nigde massif unroofed to present state Ophiolitic bodies main sediment sources	Sinistral trans-tension NW-SE compression event. Assoc with strike-slip. Probable sinistral trans-tension. Regional N-S orogenic collapse.
Oligocene	Uplift	Hiatus in subsidence	Uplift of Bolkardag and Aladag	Uplift of Taurus Mtns.
Eocene	Marine conditions	Low subsidence rates Low sedimentation rates		NW-directed thrusting, localised on N margin of Taurus Mtns.
Palaeocene			Nigde Massif partially unroofed	
Latest Cretaceous				Ophiolite Obduction (N to S). SE-directed deformation of Taurus Mtns.

	Geomorphology	$^{40}Ar/^{39}Ar$ dating	Piercing points	Geophysical evidence
Quaternary	Terrace deposition Fan incision Strike-slip faulting of alluvial fans. Block rotation?	Strike-slip in Erciyes Basin. Also in EFZ?	2.4km since Pleistocene Based on stream offsets.	10° regional vertical axis rotation since 1Ma.
Pliocene	Oldest alluvial fan deposition	E-W extenion in Erciyes Basin. Fault activity in EFZ?		Block rotation in EFZ since Late Miocene
Miocene				
Oligocene				
Eocene			~60km sinistral offset on EFZ since Late Eocene, based on offset thrust system.	Up to 33° regional vertical axis rotation since Eocene
Palaeocene				
Latest Cretaceous				

ENCLOSURE 1: CLAST TYPE VARIATION

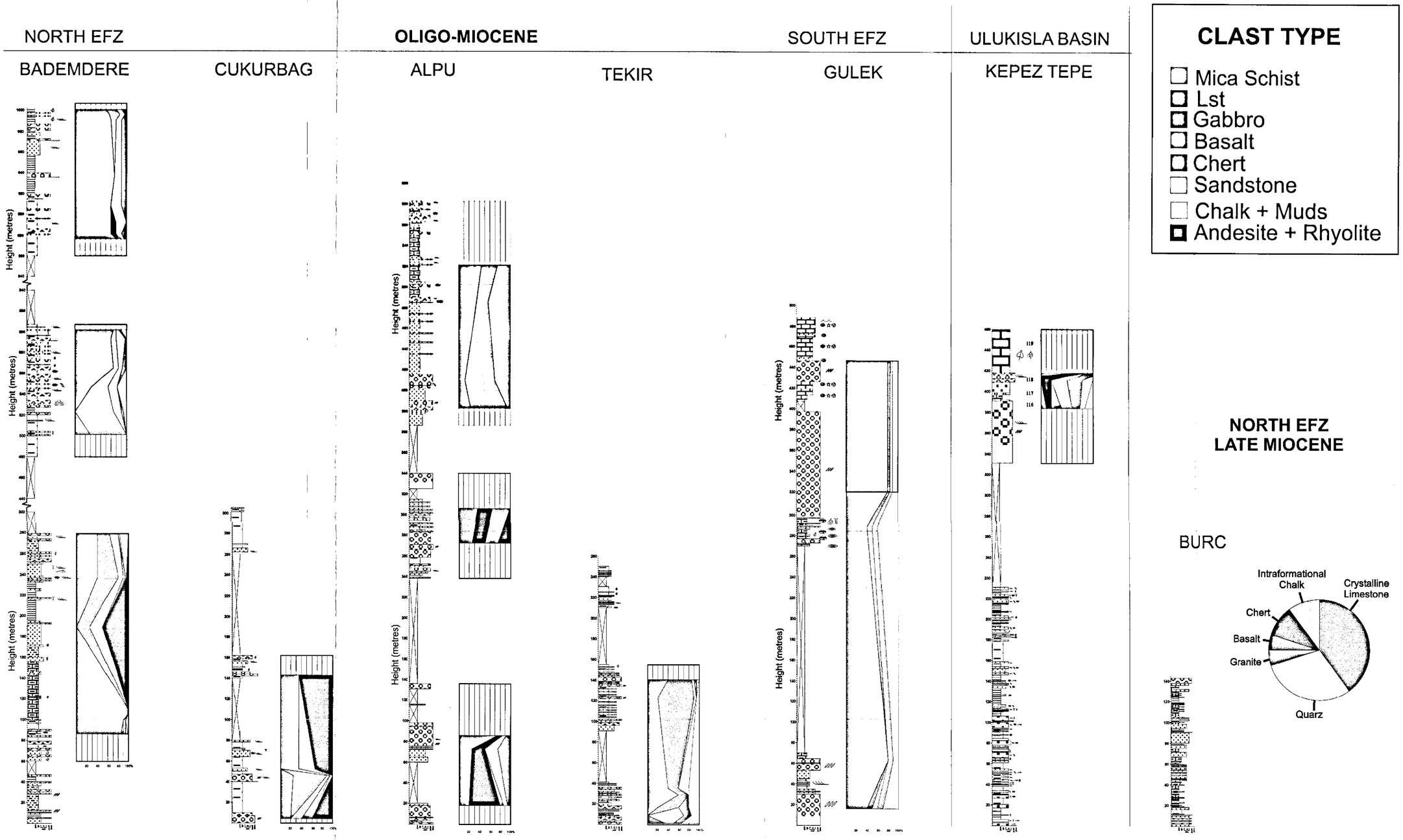

Enclosure 1 Selected Oligo-Miocene (left of diagram) and Late Miocene (right of diagram) logged sections, showing the variation of clast types in conglomerate beds up-section. Logs are arranged with northern EFZ sections to the left and southern EFZ sections to the right. Coloured bands indicate the abundance of each clast type (plotted at % of total clasts). The distance between logs is not to scale.

Geomorphology of the Ecemis Fault Zone

Compiled from aerial photograph tracings and structural mapping